A CRYSTALLOGRAPHIC AND MECHANISTIC INVESTIGATION OF RHENIUM(I) TRICARBONYL COMPLEXES AS MODEL RADIOPHARMACEUTICALS

by

ALICE BRINK

A thesis submitted to meet the requirements for the degree of

PHILOSOPHIAE DOCTOR

In the

DEPARTMENT OF CHEMISTRY

FACULTY OF NATURAL AND AGRICULTURAL SCIENCES

At the

UNIVERSITY OF THE FREE STATE

PROMOTOR: PROF. ANDREAS ROODT

CO-PROMOTOR: PROF. HENDRIK G. VISSER

NOVEMBER 2011

ACKNOWLEDGEMENTS

Firstly, all the glory and honour to my God and Heavenly Father who equipped me with the wisdom, knowledge and insight to complete this work. Thank you for the countless blessings which You have bestowed on me, for I am nothing without You.

Thank you to Prof. André Roodt for all the opportunities, guidance, support and patience in answering numerous questions. It is an honour to be known as your student.

To Prof. Deon Visser, thank you for all your guidance, encouragement and unwavering support. Your willingness to give advice and for always making time for your students is greatly appreciated.

Thank you to all my colleagues in the Inorganic group for all the laughter, jokes, advice and for sharing your knowledge. Thank you to the Crystallographic team, in particular Leo Kirsten, Inus Janse van Rensburg and Theuns Muller.

Thank you also to Prof. Roodt, Prof. Ola Wendt and the SIDA program for the opportunity to study abroad in Sweden.

To my family, Andrew and Jeanita Brink, as well as Jeandrew, Jac, Hestia and the Big B for your never-ending love, support and sacrifices.

Thank you to many who have made this journey easier: Simon Skans Lintlhoane, for taking care of the precious ones; Greg 'Ozzy' Balmer, for keeping us 'of sound foot and therefore of sound mind' and Anita Perrow.

Financial assistance from the University of the Free State, the UFS Biomolecular Cluster, SASOL and the South African National Research Foundation (NRF) is gratefully acknowledged.

For

Lephallo Police Ntsaoana

Jer 33: 1-3

How great the words of a wise man.

They shall be whispered in the grasslands and resonate through halls of knowledge.

TABLE OF CONTENTS

Chapter 3

Synthesis of Free Ligands and Metal Compounds

Chapter 4

X-Ray Crystallographic Study of Free Ligands Containing SalH-Aromatic Functionalities

Chapter 5

X-Ray Crystallographic Study of Free Ligands Containing SalH-Biological Functionalities

Chapter 6

X-Ray Crystallographic Study of fac-[Re(Sal)(CO)$_3$(S)] Complexes

Chapter 7

X-Ray Crystallographic Study of fac-[Re(5Me-Sal)(CO)$_3$(S)] Complexes

Chapter 8

Theoretical Study of Non-Coordinated SalH Ligands and fac-[Re(Sal)(CO)$_3$(S)] Complexes

Chapter 9

Methanol Substitution Kinetic Study of fac-[Re(Sal)(CO)$_3$(S)] Complexes

Chapter 10

In Vitro Cancer Screening of Selected Compounds

ABBREVIATIONS AND SYMBOLS

ABBREVIATION	MEANING
L,L'-Bid	Bidentate ligand
SalH-T	2-("T"-iminomethyl)phenol
T	Coordinated substituent
Z	Number of molecules in a unit cell
Å	Angstrom
NMR	Nuclear magnetic resonance spectroscopy
ppm	(Unit of chemical shift) parts per million
IR	Infrared spectroscopy
υ	Stretching frequency on IR
π	Pi
σ	Sigma
α	Alpha
β	Beta
γ	Gamma
λ	Wavelength
θ	Sigma
°	Degrees
°C	Degrees Celsius
$X^{\neq}$	Activated state
M	$(mol.dm^{-3})$
ΔH	Enthalpy of activation
ΔS	Entropy of activation
CO	Carbonyl
h	Planck's constant
k_B	Boltzman's constant
k_{obs}	Observed pseudo-first-order rate constant
Ph	Phenyl
CyHex	Cyclohexyl
T or temp.	Temperature
UV	Ultraviolet region in light specturm
Vis	Visible region in light spectrum
$CDCl_3$	Deuterated chloroform
C_6D_6	Deuterated benzene
TMS	Tetramethylsilane
DMF	N,N-Dimethylformamide
NC_5H_5 / Py	Pyridine
DFT	Density Functional Theory
RMS	Root Mean Square

1 INTRODUCTION AND AIM

1.1 INTRODUCTION

Cancer is the common term for any group of diseases characterized by abnormal cell growth that typically produces malignant tumors. The close correspondence between normal and abnormal DNA, means that a drug which reacts with a cancer cell will also target a normal cell. This produces enormous difficulties when trying to design cancer chemotherapeutic agents with optimal cancer killing efficiency but minimal toxicity to the rest of the body. Unfortunately cancer is a problem which must be addressed. 1.5 Million new cancer cases in the USA were expected to have been diagnosed in 2010,[1] and cancer accounts for 1 of every 4 deaths in the US. It is the second most common cause of death in the US after heart disease. Statistically, 40.77 % of men and women born today will be diagnosed with cancer at some time during their lifetime based on rates determined during the study period of 2005-2007.[2] An estimated number of deaths, for both sexes, caused by cancer will be due to lung cancer (27.6 %), colon cancer (9 %), breast cancer (7 %) and prostate cancer (5.6 %).[1] The statistics no doubt provides a strong initiative to continually develop new pharmaceutical drugs which can detect and eliminate cancer as well as other diseases. The development of new drugs is unfortunately a time consuming, complicated and very expensive exercise.

The development of one new medical product from its discovery to the time it is made available for the treatment of patients takes on average 10 – 15 years with an average cost of $800 million - $ 1 billion to research and develop each successful drug. For every one drug which receives approval an estimated 10 000 compounds have entered the research and development pipeline.[3,4,5] Four major phases in drug development can be identified:

---

[1] American Cancer Society, *Cancer Facts and Figures 2010*, American Cancer Society, Atlanta, 2010

[2] N. Howlader, A.M. Noone, M. Krapcho, N. Neyman, R. Aminou, W. Waldron, S.F. Altekruse, C.L. Kosary, J. Ruhl, Z. Tatalovich, H. Cho, A. Mariotto, M.P. Eisner, D.R. Lewis, H.S. Chen, E.J. Feuer, K.A. Cronin, B.K. Edwards (Eds). *SEER Cancer Statistics Review, 1975-2008*, National Cancer Institute, Bethesda, MD, http://seer.cancer.gov/csr/1975_2008/, released online 2011

[3] *Drug Discovery and Development*, Pharmaceutical Research and Manufacturers of America, Washington, USA, 2007, http://www.innovation.org/drug_discovery/objects/pdf/RD_Brochure.pdf

1. Pre-discovery of compounds
2. Pre-clinical research and development
3. Clinical research and development
4. Post-marketing phase, which occurs after the compound is on the market

The pre-discovery phase consists of numerous scientists exploring the disease and the underlying cause of conditions. Researchers initially select a "target" for a potential medicine which is generally a single molecule (*e.g.* gene or protein) that is involved in a particular disease. It is important to confirm how the selected target is involved in the disease and whether it can interact and be affected by a drug molecule. The search for a promising molecule, or "lead compound" can now be undertaken with the hope that the disease can be arrested by the molecule. Lead compounds are assessed early for safety according to pharmokinetics or ADME/Tox properties. Successful drugs must adhere to several conditions:

- **A**bsorbed into the bloodstream
- **D**istribution to the correct site of action in the body
- **M**etabolism should be effective and efficient
- **E**xcretion must successfully occur from the body
- Compound must not be **T**oxic

Lead compounds that survive initial screening can then be altered to make them safer and more effective by changing the chemical structure of the compound. The pre-clinical research occurs in the laboratory (*in vitro*) followed by animal testing which includes kinetics, toxicity and carcinogenicity in live organisms (*in vivo*). This concludes the discovery phase of drug development. The initial 5 000 – 10 000 compounds have now been reduced to 1 – 5 promising molecules which will be studied in clinical trials. The clinical research consists of the time from the start of human trials to the new drug application submission when permission to market the new drug is sought. This phase can take 2 – 10 years and is the longest portion of the drug development cycle. The final phase (Phase 4) is set up to evaluate the long term safety of the market approved drug in order to catch any unexpected side effects.

---

[4] J. Eckstein, *Drug Development Tutorial*, in collaboration with Institute for the Study of Aging (ISOA) and Alzheimer Research Foundation, 2005, http://www.alzforum.org/drg/tut/tutorial.asp

[5] R. Tonkens, *An Overview of the Drug Development Process*, The Physician Executive, 2005, May-June, 31(3), 48.

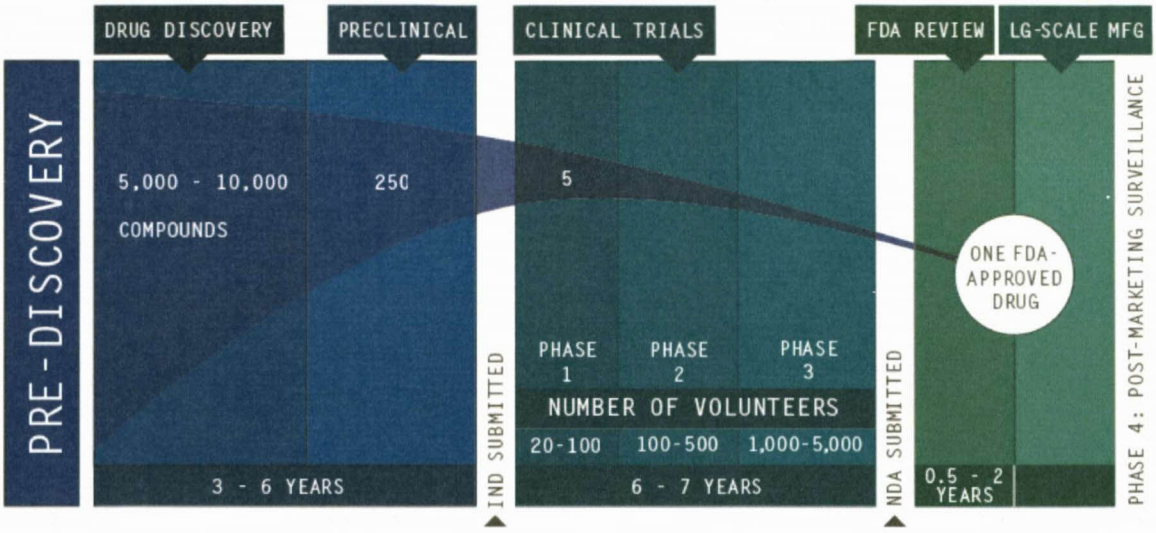

Figure 1.1: **Three major phases in drug development process. (Reproduced with permission from PhRMA: Pharmaceutical Research and Manufacturers of America.)[3]**

1.2 METALS IN MEDICINE AND HISTORY

Despite the enormous odds which researchers face, numerous successful drugs have been synthesized. Traditionally, the kingdom of drug design and medicinal chemistry has belonged to organic and not inorganic chemists. The potential role of organometallic complexes has been relatively neglected. The inclusion of metal atoms significantly increases the variety of building blocks which can be made. Metals perform a wide variety of tasks within the body, 70-80% of all inorganic material in the body is made up of the seven principle mineral macronutrient elements (Ca, Mg, Na, K, P, S, Cl).[6] Calcium plays an important role with its involvement in bone structure. Ca^{2+} is important to electrical transmission within the brain and heart and to muscle contraction in both skeletal and smooth muscle. K^+ and Na^+ ions are essential to the functioning of excitable tissues such as neutral, cardiac and muscle tissues. Iron, in the protein hemoglobin, binds oxygen through its metal atom and transports it throughout the body tissues. Zinc is a component of insulin, used in the regulation of sugar metabolism.[7]

---

[6] T. Nogrady, D.F. Weaver, *Medicinal Chemistry: A Molecular and Biochemical Approach*, 3rd Ed., Oxford University Press, Inc., Oxford, 2005

[7] C. Orvig, M.J. Abrams, *Chem. Rev.*, 1999, 99, 2201

Metals play not only an important role in human biochemistry, but also various disease states are caused from either deficiencies or excess of various metal ions. Patients with cancer spreading to the bones may experience life-threatening hypercalcemia from excess blood concentrations of Ca^{2+}. Iron deficiency leads to anemia while excess concentrations lead to liver and pancreatic damage. Dwarfism resulting from pronounced zinc deficiency has been described in geographical areas with zinc-deficient soil. Excess copper resulting in disordered and abnormal body movement is due to a neurological disease called Wilson's disease. The medicinal use of metal elements has been practiced since antiquity.[8,9] The Egyptians used copper to sterilize water (3000 BC). Zinc was discovered to promote the healing of wounds at around the same time as iron remedies were used in Egypt (1500 BC). The nutritional value of zinc was discovered during the Renaissance era in Europe. The modern research of medicinal inorganic chemistry introduces a metal ion into a biological system either by chance or by choice. The intentional introduction of a metal ion into a biological system will be either for therapeutic or diagnostic purposes. The refinement of the biological properties of metal complexes by ligand modification will provide many new therapeutic and diagnostic agents.

1.3 RADIOPHARMACEUTICALS

Radiopharmaceuticals are drugs containing a radionuclide and are used in nuclear medicine for therapy or diagnosis of various diseases. They are mostly small organic or inorganic compounds with definite chemical composition. The development of radiometal-labeled complexes began prominent in the 1950's where the use of nuclear technology for medical purposes began with nuclear reactors, accelerators and cyclotrons being applied to medical isotope production. The $^{99}Mo/^{99m}Tc$ generator was developed by Brookhaven National Laboratory in 1959 and the first ^{99m}Tc radiotracers were developed at the University of Chicago in 1964.[10] Research into ^{99m}Tc radiopharmaceuticals was the beginning of the study of how coordination chemistry relates to diagnostic imaging and is still the one radionuclide which is used in more than 80% of radiopharmaceuticals.

---

[8] R.H. Holm, E.I. Solomon, Eds., *Chem. Rev.*, 1996, 96, 7

[9] H.E. Howard-Lock, C.J.L. Lock, *Comprehensive Coordination Chemistry*, Eds: G. Wilkinson, R.D. Gillard, J.A. McCleverty, Pergamon, Oxford, 1987, 6, 755

[10] C.J. Anderson, M.J. Welch, *Chem. Rev.*, 1999, 99, 2219

Several factors must be considered when designing a radiopharmaceutical such as the half-life of the radiometal, the mode of decay, the cost and availability of the isotope. The half-life of the radionuclide, for diagnostic imaging, must be long enough to carry out the synthesis of the radiopharmaceutical, then having sufficient time to accumulate in the target tissue of the patient while allowing clearance through the non-target organs. Ideally the radiation dose to the patient must be limited at the same time as achieving the above mentioned goals.

Radiopharmaceuticals can be divided into two primary classes namely diagnostic or therapeutic applications. Diagnostic radiopharmaceuticals are labeled with gamma-emitting isotopes for single photon emission computed tomography (SPECT) or positron-emitting isotopes for positron emission tomography (PET). These compounds are generally used at low concentrations (10^{-6} to 10^{-8} M) and are not intended to have any pharmacological effect. The purpose of diagnostic radiopharmaceuticals is to provide a non-invasive method of assessing the disease or disease infected tissues and for monitoring the effect of treatment.[11] Therapeutic radiopharmaceuticals are designed to deliver therapeutic doses of ionizing radiation to specific diseased sites. The delivery of therapeutic radiation doses can be implemented *via* three methods: external beam irradiation, implantable "seeds" or systematic administration. Brachytherapy uses implantable "seeds" which are physically placed at the tumor site and plays an important role in the treatment of prostate cancer patients. External beam radiation plays a vital role in cancer treatment but it is not effective for treatment of secondary or metastic cancer sites outside the treatment area. Systematic administration of radiopharmaceuticals which are designed for site-specific localization enables the treatment of widely dispersed disease sites. Ideally therapeutic, and to a lesser extent, diagnostic radiopharmaceuticals are designed to locate with high specificity at cancerous sites while preventing excessive radiation damage to normal tissues.[12] To find such a site specific compound is difficult due to a variety of factors which are directly related to the chemical and physical characteristics of the radiopharmaceutical.

[11] S. Liu, *Chem. Soc. Rev.*, 2004, 33, 445
[12] W.A. Volkert, T.J. Hoffman, *Chem. Rev.*, 1999, 99, 2269

1.4 AIM OF THIS STUDY

Considerable interest is being shown to metallic radionuclides, for the development of radiopharmaceuticals, due to the rich coordination chemistry of metal ions and the wide range of nuclear properties which can be found. In particular, the use of the ^{99m}Tc radionuclide, with its desirable properties, is intensively used for diagnostic nuclear medicine. Considerable interest has been paid to organometallic technetium and rhenium complexes in low oxidation states for the development of target specific radiopharmaceuticals.[13,14,15] The rhenium(I) and technetium(I) metal centers possesses a d^6 electronic configuration in an octahedral field, which is generally known to be kinetically inert. The tricarbonyl complexes of technetium and rhenium *fac*-$[Et_4N]_2[M(CO)_3X_3]$ (M = Tc(I) or Re(I), X = halides Cl, Br] can be easily prepared in a one-step synthesis directly from oxometallates, $[MOCl_4]^-$ and $[MO_4]^-$. The halide ligands of *fac*-$[Et_4N]_2[M(CO)_3X_3]$ can be readily substituted by other ligands or solvents such as methanol, acetonitrile or water.[16] The major advantage of *fac*-$[M(CO)_3(H_2O)_3]^+$ complexes is the high stability of the *fac*-$M(CO)_3$ core in water and the potential of exchanging specifically the labile solvent ligands. The *fac*-$[M(CO)_3(H_2O)_3]^+$ core accepts many types of ligands which makes it possible to design complexes whose electronic, steric and biological properties can be adapted by coordinated biomolecules. The diverse coordination chemistry of the *fac*-$[M(CO)_3]^+$ core offers a tremendous opportunity for the development of new biomolecules.

This study was concerned with investigating the coordinative and kinetic behaviour of *fac*-[Re(L,L'-Bid)$(CO)_3$(S)] complexes (L,L'-Bid = mono-negative bidentate ligands, S = coordinated solvent or halide). The use of bidentate ligand systems would leave a third vacant position on the *fac*-$Re(CO)_3$ complex which could be substituted by a variety of incoming mondentate ligands. Few reactivity investigations have been completed on the Re(I) and Tc(I) tricarbonyl complexes, despite numerous synthetic studies, therefore the kinetic behaviour of the complexes were of particular interest during this study. The main objectives

---

[13] A. Egli, R. Alberto, L. Tannahill, R. Schibli, U. Abram, A. Shaffland, R. Waibel, D. Tourwé, L. Jeannin, K. Iterbeke, P.A. Schubiger, *J. Nucl. Med.*, 1999, 40, 1913

[14] R. Alberto, R. Schibli, A.P. Schubiger, U. Abram, H.J. Pietzsch, B. Johannsen, *J. Am. Chem. Soc.*, 1999, 121, 6076

[15] T.W. Spradau, W.B. Edwards, C.J. Anderson, M.J. Welch, J.A. Katzenellenbogen, *Nucl. Med. Biol.*, 1999, 26, 1

[16] R. Alberto, R. Schibli, A. Egli, P.A. Schubiger, W.A. Herrmann, G. Artus, U. Abram, T.A. Kaden, *J. Organomet. Chem.*, 1995, 493, 119

of this study were focused on the synthesis and characterization of some mixed rhenium complexes based on model ligands as well as some derivatized biologically active molecules and the kinetic effects thereof. The objectives are summarized as follows:

1. To synthesize a range of mono-negative bidentate ligands (L,L'-Bid), which would allow convenient coordination of selected aromatic, aliphatic or biologically active molecules to a common coordinative backbone. The backbone was derived from the salicylaldehyde starting reagent. Amine substituents with various steric, electronic and biological properties were coordinated to the backbone to form the salicylidene mono-negative bidentate ligand (**SalH**).
2. To synthesize complexes of the type *fac*-[Re(L,L'-Bid)$(CO)_3$(S)] (S = coordinated solvent or halide) with a variety of mono-negative bidentate ligands. Particular interest in the possible effects which the different molecules, coordinated to the backbone of the bidentate ligand, would have on the rhenium metal centre was expressed.
3. To characterize the complexes with single crystal X-ray diffraction, IR and NMR spectroscopy.
4. To determine the mechanism of substitution and activation parameters of *fac*-[Re(L,L'-Bid)$(CO)_3$(S)] complexes with a variety of ligands by means of a kinetic study. The span of activation introduced by the set of bidendate ligands utilized is of particular importance, to estimate the effects introduced on primary and secondary *in vivo* activity due to the metal centre activation/de-activation reaction.

In the following chapters, a brief literature review of the development of rhenium and technetium chemistry in radiopharmaceuticals is presented, followed by the systematic presentation and discussion of experimental results.

2 LITERATURE STUDY

2.1 INTRODUCTION

The group seven transition metals have an extensive organometallic and coordination chemical history. Rhenium and technetium in particular are often used in nuclear medicine due to their nuclear properties, however they do hold many catalytic capabilities, e.g. for olefin epoxidation, olefin metathesis, oxidation of organic sulphides, arenes, phenols and aldehydes.[1] Both elements are able to form complexes in the oxidation states ranging from –I to VII and because the field of coordination chemistry of rhenium and technetium is very broad, only the relevant aspects of radiopharmaceuticals to this study will be highlighted. A historical view of the influence which these transition metals have had on medicine as well as the general aspects of radiopharmaceutical drug design which can be visualised as a collection of molecular fragments or building blocks will be discussed in this chapter.

2.2 RADIOPHARMACEUTICALS

Drugs containing a radionuclide are known as radiopharmaceuticals and are regularly used in nuclear medicine for diagnosis and / or therapy of diseases.[2] The radionuclides utilized in imaging are photon emitters: gamma (γ) or positron (β^+), where as therapeutic agents are particle emitters: alpha (α), beta (β) or Auger/conversion e^-. The majority of radiopharmaceuticals are administrated via intravenous injection and are mostly small inorganic or organic compounds. Two primary classes can be defined regarding the medical application of the radiopharmaceutical: therapeutic or diagnostic. Target specific radiopharmaceuticals is the term commonly used to describe molecules whose ultimate distribution is determined by their receptor binding capability or other biological interactions.

---

[1] F.A. Cotton, G. Wilkinson, C.A. Murillo, M. Bochmann, *Advanced Inorganic Chemistry*, 6th Ed., John Wiley & Sons, Inc., New York, USA, 1999

[2] S. Liu, *Advanced Drug Delivery Rev.*, 2008, 60, 1347

Another type of bio-distribution is where the distribution of the drug is determined exclusively by the chemical and physical properties of the molecule.

Diagnostic radiopharmaceuticals are labeled with a gamma (γ) -emitting isotope for single photon emission computed tomography (SPECT) or a positron-emitting isotope for positron emission tomography (PET). As the purpose of diagnostic radiopharmaceuticals is to provide a non-invasive method of assessing the disease or disease infected tissues and for monitoring the effect of treatment, the compounds are generally used at low concentrations (10^{-6} to 10^{-8} M) and not intended to have any pharmacological effect.[3] Therapeutic radiopharmaceuticals on the other hand are designed to deliver therapeutic doses of ionizing radiation to specific diseased sites. The ideal therapeutic drug should concentrate in the tumor site with sufficient levels to deliver a cytotoxic radiation dose to tumor cells but at the similar time it should have rapid clearance from normal tissue and blood to prevent excessive damage to healthy organs.

2.3 METHOD IN THE MADNESS – DESIGNING DRUGS

Several aspects should be considered when designing radiopharmaceuticals. Selection of the radionuclide, which is the radiation source, is dependent on the medical application and therefore the nuclear properties. For diagnostic applications the choice for SPECT or PET imaging will preferably be ^{99m}Tc, ^{111}In, $^{62/64}$Cu and $^{67/68}$Ga. Technetium-99m is particularly useful in SPECT imaging due to its ideal nuclear properties, where as ^{64}Cu and ^{68}Ga are more useful in PET imaging. For the development of therapeutic radiopharmaceuticals, β-emitters are more useful, such as ^{90}Y, ^{177}Lu and $^{186/188}$Re. The nuclear properties of the radionuclide play an enormous role in the synthesis and design of the drug.[4,5,6] Factors such as half-life, chemical properties, type of radiation, energy, presence of other particulate radiation emissions, availability and cost of production affects the choice of radionuclide. Other factors which come into play after the potential radiopharmaceutical has been synthesized is tumor

[3] S. Liu, *Chem. Soc. Rev.*, 2004, 33, 445
[4] S. Liu, D.S. Edwards, *Top. Curr. Chem.*, 2002, 222, 259
[5] W.A. Volkert, T.J. Hoffman, *Chem. Rev.*, 1999, 99, 2269
[6] P.A. Schubiger, R. Alberto, A. Smith, *Bioconjug. Chem.*, 1996, 7, 165

uptake, tumor retention, blood clearance, rate of radiation delivery and can large scale production of the radionuclide be conducted within economical constraints.

The half-life is an important factor to consider. It should be as short as possible to minimize the radiation dose to the patient but long enough to prove effective. Sufficient time must be made available for the synthesis of the radiopharmaceutical, purification, transportation, administration to patient, accumulation in the target tissue and should still have optimal clearance from non-target organs. ^{18}F is excellent PET isotope, however the short half-life ($t_{1/2}$ = 110 min) limits the clinical application of synthesizing novel target-specific radiopharmaceuticals.

The chemical properties of the chosen nuclide must be considered. Coordination of the radiometal to an organic chelate ligand may drastically affect the stability, biodistribution, target specificity *etc.* of the final radiopharmaceutical. Radiolabelling should be easily completed, ideally over 10-30 min depending on the radiometal half-life.

The availability and quality of the radionuclide must be sufficient and reproducible. Trace amounts of impurities can affect the purity and labelling of the radiopharmaceutical. Trace metal contaminants should be kept to a minimal as they can compete with the radionuclide for the bifunctional chelator, and metallic complexes may compete for receptor binding. A generator-based isotope would be ideal to achieve high specific activity for target-specific radiopharmaceuticals. Using a generator produced isotope simplifies dose preparation, quality control, transportation and delivery.

The diagnostic radionuclide used in SPECT imaging is often a gamma (γ)-emitting isoptope, whereas PET imaging uses positron-emitters. The use of generator-produced radiometals is advantageous since the daughter radionuclide can be readily separated from the parent isotope by ion exchange chromatography or solvent extraction. Technetium-99m remains the most widely used isotope for SPECT imaging, due to its optimal nuclear properties. ^{111}In is useful in SPECT imaging and as a substitute for ^{90}Y analogs since ^{90}Y is a β-emitter. It is best that radionuclides, used in PET imaging, have no radiation decays other than 511 keV gamma photos from positron annihilation. This reduces impairment of spatial resolution due to high β^+ energy and minimizes the radiation burden on the patient. The choice of beta (β) –emitters for therapy may differ, depending on the tumor size and location. β-emitters have a relatively

long penetration range (2-12 mm) which is important for solid tumors with high heterogeneity. Medium to low β-emitters (e.g. ^{177}Lu) are better for smaller metastases while high energy β-emitters (e.g. ^{90}Y) are used for larger tumors. Properties of selected radionuclides are indicated in Table 2.1.

Table 2.1: Selected radionuclides used in therapeutic or diagnostic radiopharmaceuticals. [2, 7, 8, 9, 10, 11, 12]

Radionuclide	Half-life	Energy	Decay mode	Source
Scintigraphic Imaging		**γ Gamma Energy (keV)**		
^{99m}Tc	6.02 h	141 (89%)	IT	^{99}Mo-^{99m}Tc Generator
^{67}Ga	78.3 h	93 (10%), 185 (24%), 296 (22%)	EC	Cyclotron ^{68}Zn(p,2n)-^{67}Ga
^{111}In	67.9 h	171 (88%), 247 (94%)	EC	Cyclotron, ^{111}Cd(p,n)-^{111}In
PET Imaging	**Half-life**	**β^+ Positron Energy (keV)**	**Decay mode**	**Source**
^{61}Cu	3.3 h	1220, 1150 940, 560 Eγ = 283 (13%), 380 (93%) keV	β^+ (62%) EC (38%)	Cyclotron, ^{61}Ni(p,n)-^{61}Cu
^{62}Cu	0.16 h	2910	β^+ (98%) EC (2%)	^{62}Zn-^{62}Cu Generator
^{64}Cu	12.7 h	656	β^+ (19%) EC (41%) β (40%)	Cyclotron, ^{64}Ni(p, n)-^{64}Cu
^{68}Ga	1.1 h	1880, 770	β^+ (90%) EC (10%)	^{68}Ge-^{68}Ga Generator
^{66}Ga	9.5 h	4150, 935	β^+ (56%)	Cyclotron, ^{63}Cu(α, nγ)-^{66}Ga

[7] R.B. Firestone, *Table of Isotopes*, Eds.: V.S. Shirley, S.B. Baglin, S.Y.F. Chu, J. Zipkin, Wiley, New York, USA, 1996

[8] F.W. Walker, J.R. Parrington, F. Feiner, *Nuclides and Isotopes, Chart of the Nuclides*, 14th Ed., GE Nuclear Energy, General Electric Company, Nuclear Energy Operations, California, USA, 1989

[9] E. Brown, J. Dairiki, R.E. Doebler, A.A. Shibab-Elden, L.J. Jardine, J.K. Tuli, A.B. Byurn, *Table of Isotopes*, 7th Ed., Eds.: C.M. Lederer, V.S. Shirley, Wiley, New York, USA, 1978

[10] C.A. Boswell, M.W. Brechbiel, *Nuclear Medicine and Biology*, 2007, 34, 757

[11] D.A. Weber, L. Eckerman, L.T. Dillman, J.C. Ryman, *MIRD: Radionuclide Data and Decay Schemes*, Society of Nuclear Medicine, New York, USA, 1989

[12] S.Z Lever, J.D. Lydon, C.S. Cutler, S.S. Jurisson, *Comprehensive Coordination Chemistry II*, Eds.: J.A. McCleverty, T.J. Meyer, Pergamon Press, Oxford, UK, Vol. 9, 2004

^{89}Zr	78.5	897	β^+ (23%) EC (77%)	Cyclotron, $^{89}Y(p, n)-^{89}Zr$
Therapeutic Applications	**Half-life**	**β Beta Energy (MeV)**	**Maximum range (mm)**	**Source**
^{67}Cu	62.0 h	0.40 (45%), 0.48 (3%), 0.58 (20%) Eγ = 93 (17%), 185 (48%) keV	1.8	$^{68}Zn(p,2p)-^{67}Cu$ Accelerator
^{90}Y	2.66 days	2.28 (100%) Eγ = -	12.0	$^{90}Sr-^{90}Y$ Generator
^{153}Sm	46.8 h	0.64 (30%), 0.71 (50%), 0.81 (20%) Eγ = 103 (28%) keV	3.0	$^{152}Sm(n, \gamma)-^{153}Sm$ Reactor
^{166}Ho	26.4 h	1.85 Eγ = 80.6 (6.6%) keV, 1.38 (0.9%) MeV	8.0	Reactor
^{177}Lu	6.64 days	0.176 (12%), 0.384 (9%), 0.497 (79%) Eγ = 113 (6.4 %), 208 (11%) keV	1.5	$^{176}Lu(n, \gamma)-^{177}Lu$ Reactor
^{186}Re	3.7 days	1.07 (91%) Eγ = 137 (9%) keV	5.0	$^{185}Re(n, \gamma)-^{186}Re$ Reactor
^{188}Re	17.0 h	2.12 (85%) Eγ = 155 (15%) keV	11.0	$^{188}W-^{188}Re$ Generator

*IT = isomeric transition; EC = electron capture; m = metastable isomer; e = electron

Factors relating to the chemical and biological properties of the possible drug molecule also influence the design of the radiopharmaceutical. In general the molecule should be small enough to be transported throughout the body, contain sufficient hydrophilicity to dissolve in the blood stream and be lipophilic enough to cross the fat barriers in the body. The drug-like molecule must contain sufficient polar groups to bind to the receptor but too many may increase the excretion rate before it can exert any therapeutic effects. Lipinski's Rule of Five is often used to quantify the above mentioned properties.[13,14,15] Other factors in radiopharmaceuticals should also be considered. Can the radionuclide be incorporated in the final molecule with a bifunctional chelator? What are the effects of pharmacokinetic linkers?

[13] T. Nogrady, D.F. Weaver, *Medicinal Chemistry: A Molecular and Biochemical Approach*, 3rd Ed., Oxford University Press, New York, 2005
[14] C.A. Lipinski, F. Lombardo, B.W. Dominy, P.J. Feeney, *Adv. Drug Del. Rev.*, 2001, 46, 3
[15] S. Mather, *Eur. J. Nuclear Medicine*, 2001, 28, 543

The stoichiometric amount of each molecule needed in synthesis and labelling? The charge of the final complex may determine the solubility as well as the bio-distribution of the molecule. The solubility of the molecule in aqueous and non-aqueous medium must be considered. The toxicity of the molecule as well as the stability, both *in vitro* and *in vivo* should be explored.

2.4 LABELLING OF RADIOPHARMACEUTICALS

2.4.1 Target-Specific Radiopharmaceuticals

The development of target-specific radiopharmaceuticals has been the focus of much research. The idea is based on the receptor binding of a radiolabeled receptor ligand in the diseased tissue. The receptor ligand or "targeting biomolecule" serves as a "carrier" to carry the radionuclide to the diseased site which contains a large concentration of the target receptor. The success of these radiopharmaceuticals relies on the receptor ligand coordinating to the bio-receptors with high affinity and specificity. Several target-specific radiopharmaceuticals have been approved and are listed in Table 2.2.

Table 2.2: List of several target-specific therapeutic and diagnostic radiopharmaceuticals.[3]

Radiopharmaceutical	Commercial name	Primary medical application
^{111}Indium capromab pendetide	ProstaScint®	Image of prostate cancer
^{111}Indium pentetreotide	Octreoscan®	Imaging of neuroendocrine tumors
^{111}Indium satumomab pendetide	OncoScint®	Imaging of metastatic disease
^{90}Y Ibitumomab tiuxetan	Zevalin®	Treatment of non-Hodgkin's lymphoma
^{131}I Tositumomab	Bexxar®	Treatment of non-Hodgkin's lymphoma
^{99m}Tc Apcitide	AcuTect®	Imaging of deep vein thrombosis
^{99m}Tc Arcitumomab	CEA-Scan®	Monoclonal antibody for colorectal cancer
^{99m}Tc Depreotide	Neotect®	Somatostatin receptor-bearing pulmonary masses

The development of coordination chemistry still plays as an important role as the biological characterization of radiolabled receptor ligands in the development and synthesis of new target-specific radiopharmaceuticals. Three methods (integrated, bifunctional and hybrid approach) mentioned below (Figure 2.1) may be used to label novel radiopharmaceuticals and utilize inorganic chemistry as the foundation for the drug design. The radiation source for the specific medical application whether it be imaging or design is the radiometal.

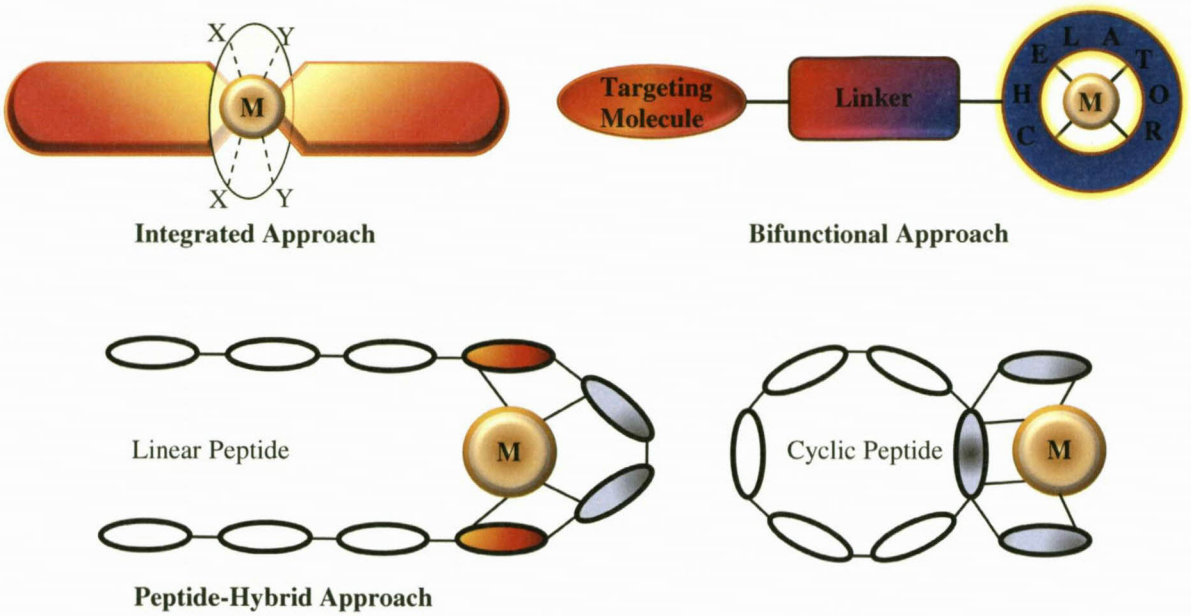

Figure 2.1: **Schematic representation of the integrated, bifunctional and peptide approaches in radiopharmaceutical design.**[3]

2.4.1.1 Integrated Method

This approach consists of replacing part of a known high affinity receptor ligand with a metal chelate, leading to minimal changes in size, conformation and receptor binding affinity. The radionuclide is now an integral part of the receptor binding molecule, with the entire metal complex acting as a high affinity receptor ligand. A disadvantage of this method is the complex synthetic methods and the molecules have lower receptor binding affinity.[16] The introduction of a metal unfortunately does affect the lipophilicity, size and conformation of the original receptor ligand. Several examples will be listed later in the section discussing second generation technetium complexes (§ 2.6.2).

2.4.1.2 Bifunctional Method

The bifunctional method uses a high affinity receptor ligand as the targeting biomolecule. It is bound to the radiometal of choice with a bifunctional chelator. A linker between the chelator and targeting biomolecule can be incorporated for pharmacokinetic modifications. Pharmacokinetic modifying linkers are becoming an important consideration in improving

[16] R.K. Hom, J.A. Katzenellenbogen, *Nucl. Med. Biol.*, 1997, 24, 485

target-to-background noise ratios by modifying excretion kinetics of radiolabeled biomolecules. The linker may improve lipophilicity by using a hydrocarbon chain or a peptide sequence (e.g. polyaspartic acid) to improve hydrophilicity and renal clearance. The biodistribution of ^{99m}Tc and ^{111}In labelled antibodies can be influence by the linker groups.[17,18,19] Tumor to liver ratios of ^{125}I and ^{18}F-labeled cyclic RGD peptides[20] was increased with a sugar moiety.[21,22] Improved tumor uptake and excretion kinetics of ^{125}In and ^{18}F-labeled cyclic RGD monomer has been reported by the introduction of a polyethylene glycol linker.[23] The ideal of pharmacokinetic modifying linkers is to vary the excretion kinetics in order that high amounts of radiopharmaceuticals is absorbed by the tumors while minimal uptake occurs in non-tumor organs.[2]

The bifunctional chelator is selected to complement the nature and oxidation state of the radiometal. This method is popular for the development of target-specific radiopharmaceuticals as it increases the possibility of retaining the original receptor binding affinity. As rhenium and technetium are transition metals, conjugation with a targeting biomolecule is necessary. The metal centre has to be stabilized by chelators containing functionalities with particular and varied physicochemical properties. The resulting metallic biomolecules often vary to a considerable degree in solubility, size and dipole moment from the original biomolecule.

Limited ligands, such as basic frameworks, are available which provide sufficient stability to ^{99m}Tc core under physiological conditions, for example the tetradentate N,S,O chelators for the $[Tc(V)=O]^{3+}$ core.[24] Mixed ligand approaches allow for tuning of the ligand properties and therefore screening of the biological behaviour. The [3+1] mixed ligand approach is well known and contains a constant tridentate ligand linked to a biomolecule while the

---

[17] S.M. Quadri, H.M. Vriesendorp, *J. Nucl. Med.*, 1998, 42, 250
[18] Y. Arano, H. Matsushima, M. Tagawa, M. Koizumi, K. Endo, J. Konish, A. Yokoyama, *Bioconjug. Chem.*, 1991, 2, 71
[19] L.E. Williams, M.R. Lewis, G.G. Bebb, K.G. Clarcke, T.L. Odom-Maryon, J.E. Shively, A.A. Raubitscheck, *Bioconjug. Chem.*, 1998, 9, 87
[20] R. Haubner, H.J. Wester, W.A. Weber, C. Mang, S.J. Ziegler, S.L. Goodman, R. Senekowisch-Schmidtke, H. Kessler, M. Schwaiger, *Cancer Res.*, 2001, 61, 1781
[21] R. Haubner, H.J. Wester, U. Reuning, R. Senekowisch-Schmidtke, B. Diefenbach, H. Kessler, G. Stöcklin, M. Schwaiger, *J. Nucl. Med.*, 1999, 40, 1061
[22] R. Haubner, H.J. Wester, F. Burkhart, R. Senekowisch-Schmidtke, W.A. Weber, S.L. Goodman, H. Kessler, M. Schwaiger, *J. Nucl. Med.*, 2001, 42, 326
[23] X. Chen, R. Park, A.H. Shahinian, J.R. Bading, P.S. Conti, *Nucl. Med. Biol.*, 2004, 31, 11
[24] S.S. Jurisson, J.D. Lydon, *Chem. Rev.*, 1999, 99, 2205

monodentate co-ligand is continuously varied or *vice versa*.[25,26] Umbrella-like tetradentate N,S,S,S ligands and monodentate isocyanides with lipophilic Tc(III) complexes have very good *in vitro* stability towards plasma components.[27,28,29] Another mixed ligand approach utilizes the hynic approach whereby biomolecules are linked to 6-hydrazinonicotinamide[30] and the remaining coordination sites are then occupied by co-ligands. The major advantage of this approach is the variability of the co-ligands that influences the biological properties.

The [2+1] mixed ligand concept suggested by Mundwiler *et al.*[31] for *fac*-$[M(CO)_3(H_2O)_3]^+$ complexes, substitutes the three aqua ligands with one bidentate and one monodentate ligand. The biomolecule can be linked either to the bidentate ($[2_B + 1]$ concept) or to the modentate ($[2 + 1_B]$ concept) (Figure 2.2)

[25] H.J. Pietzsch, H. Spies, S. Hoffmann, *Inorg. Chim. Acta*, 1989, 165, 163
[26] S. Seifert, H.J. Pietzsch, M. Scheunemann, H. Spies, R. Syhre, B. Johannsen, *Appl. Radiat. Isot.*, 1997, 49, 5
[27] H. Spies, M. Glaser, H.J. Pietzsch, F.E. Hahn, O. Kintzel, T. Luegger, *Angew. Chem.*, 1994, 106, 1416
[28] H. Spies, M. Glaser, *Inorg. Chim. Acta*, 1995, 240, 465
[29] H.J. Pietzsch, S. Seifert, R. Syhre, F. Tisato, F. Refosco, P. Leibnitz, H. Spies, *Bioconjugate Chem.*, 2003, 14, 136
[30] M.J. Abrams, M. Juweid, C.L. TenKate, D.A. Schwartz, M.M. Hauser, F.E. Gaul, A.J. Fuccello, R.H. Rubin, H.W. Strauss, A.J. Fischman, *J. Nucl. Med.*, 1990, 31, 2022
[31] S. Mundwiler, M. Kündig, K. Ortner, R. Alberto, *Dalton Trans.*, 2004, 1320

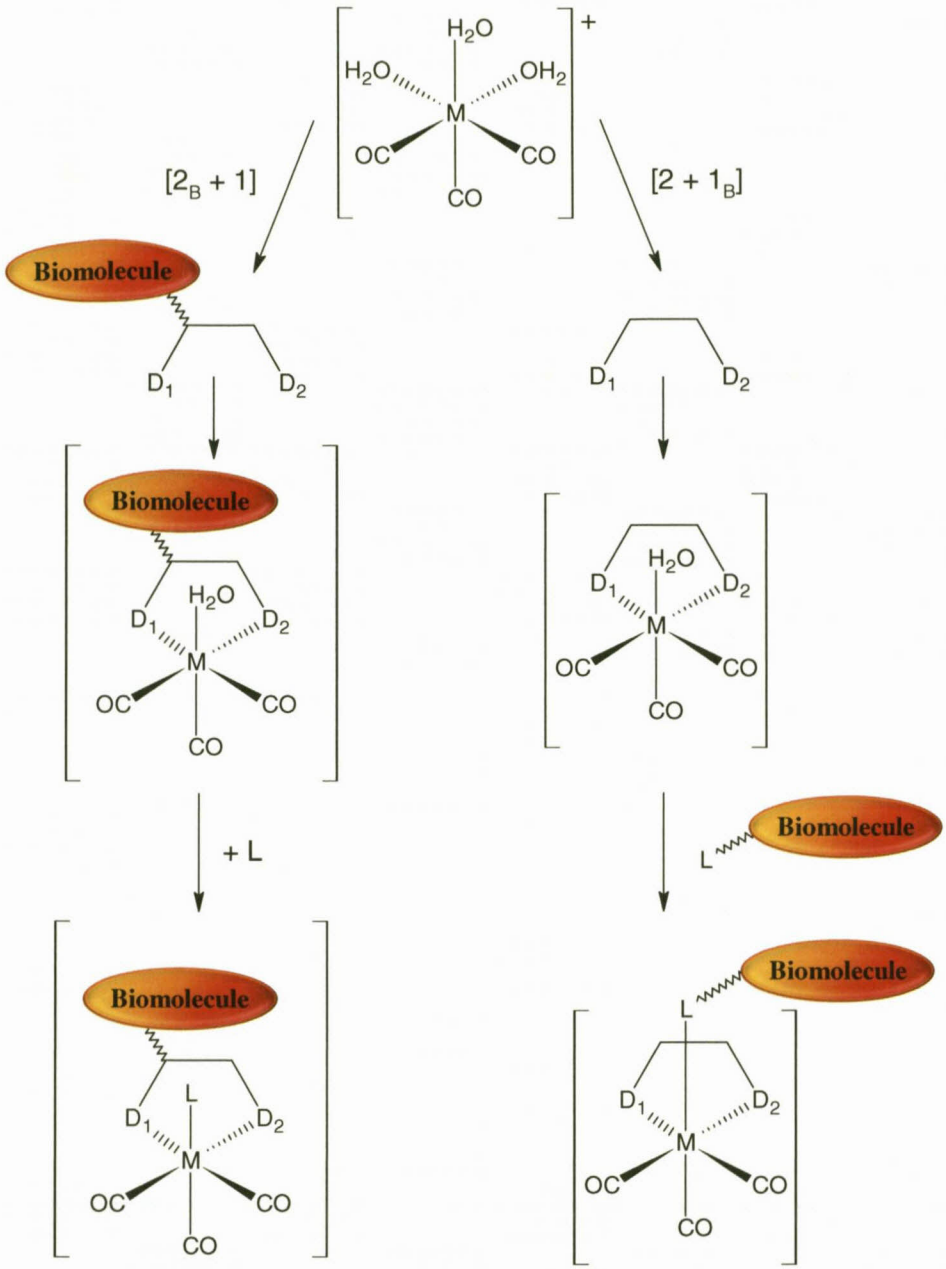

Figure 2.2: **The mixed [2 + 1] ligand concept for *fac*-$[M(CO)_3]^+$ complexes (M = Tc, Re; D_1, D_2 = various donor atoms; L = entering monodentate ligand).[31]**

In the mixed ligand [2 + 1_B] concept, the bidentate ligand is the variable of the radiolabled biomolecule, which fine tunes the physio-chemical properties. The ligand must fulfil two requirements: (1) it should be anionic to leave one labile water at the 3rd coordination site. Neutral bidentate ligands generally contain a Br^-/Cl^- at this position which is more difficult to substitute due to electrostatic reasons. (2) Steric properties must ensure that only one bidentate ligand coordinates. The advantage of the [2 + 1] mixed ligand approach for *fac*-$[M(CO)_3]^+$ complexes is that the synthetic procedure is performed in water and the final

complexes usually have high kinetic stability. This approach increases the range of possible co-ligands and enables fine tuning of the physico-chemical properties of the labelled biomolecules.

2.4.1.3 Peptide Method

The radiometal, in the peptide approach, is chelated by a tripeptide sequence containing a N_4, N_3S, or N_2S_2 donor set. The tripeptide sequence can be part of a cyclic peptide backbone or a linear polypeptide. The bonding of the radiometal increases the receptor binding affinity of the polypeptide which is a significant advantage of this method. One approach in the diagnostic imaging of thrombi is the conjugation of platelet glycoprotein IIb/IIIa antagonists to a Tc chelate. Cyclic peptides containing the Arg-Gly-Asp (RGD) sequence show a high affinity for the glycoprotein receptor. Figure 2.3 illustrates an example of N_2S_2 diamide dithiol chelate ligand coordinated to technetium and linked with a cyclic peptide.

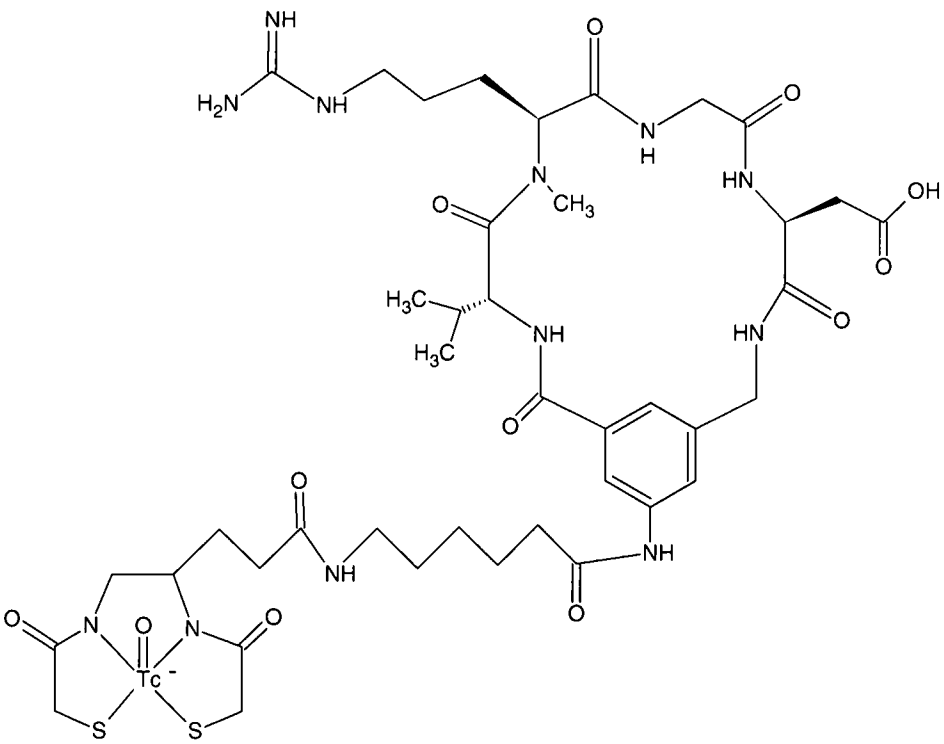

Figure 2.3: **Linkage of cyclic peptide to Tc=O core *via* N_2S_2 chelate ligand.** [32]

[32] S. Liu, D.S. Edwards, R.J. Looby, M.J. Poirier, M. Rajopadhye, J.P. Bourgque, T.R. Carroll, *Bioconj. Chem.*, 1996, 7, 203

The chelate which binds the radiometal to the radiopharmaceutical can have significant impact on the biological properties. Therefore the biodistribution of a target-specific radiopharmaceutical can be systematically altered by either modifying the coordination environment around the radionuclide with a variety of chelating ligands or with the use of various co-ligands if more than one chelate is bound to the metal centre. The intrinsic properties of the radiometal, whether it be nuclear or coordination, also affect the design of radiopharmaceuticals and have been discussed in the sections above. Due to the advantages of working with rhenium and technetium, both with regards to stability and varying coordinative ability, these transition metals were chosen as the focal point of this study in particular the tricarbonyl complexes. The remaining sections will focus on the chemical behavior as well as the current tendencies in radiopharmaceutical design.

2.5 BRIEF GENERAL HISTORY OF RHENIUM AND TECHNETIUM

Rhenium was first detected in 1925 *via* its X-ray spectrum. It occurs with molybdenite minerals (MoS_2) and some copper ores. Rhenium is usually isolated as the perrhenate ion $[ReO_4]^-$ but can be precipitated as slightly soluble $KReO_4$. It occurs in two stable isotopes,[1] ^{185}Re (37.4 %) and ^{187}Re (62.6 %). In nuclear medicine the radioactive isotopes of interest are $^{186/188}Re$, whose nuclear properties are summarized in Table 2.1. Both rhenium isotopes are suitable for therapeutic applications by means of β-irradiation.

In 1937, technetium was the first of the artificially produced elements and was obtained as isotopes ^{95}Tc and ^{97}Tc produced by the bombardment of molybdenum with deuterons.[33] Twenty-one radioactive isotopes are known with mass numbers 90 – 111. ^{98}Tc is the longest lived isotope ($t_{1/2}$ = 4 x 10^6 y) but ^{99}Tc is the most common ($t_{1/2}$ = 2 x 10^5 y). The total amount of this isotope is ~ 78 tons, which exceeds the known amount of rhenium in the earth's crust. ^{99}Tc can be handled with modest precautions as it emits a soft (293.6 keV) β particle. In much of the chemistry, especially in organometallic chemistry, technetium resembles rhenium. Important differences, however do occur. The greater reducibility of the higher oxidation states of Tc is an example. Rhenium complexes are easier to oxidize and are

[33] J.P. Icenhower, N.P. Qafoku, J.M. Zachara, W.J. Martin, *Am. J. Sci.*, 2010, 310, 721

more kinetically inert than the technetium analogues. Rhenium has an extremely high melting point (3180 °C), and both metals burn in air above 400 °C to give heptoxides M_2O_7.

2.6 TECHNETIUM CHEMISTRY DIRECTED TO NUCLEAR MEDICINE

Technetium-99m is a decay product of ^{99}Mo (a fission product with a half-life of 66 hours) in a ^{99}Mo – ^{99m}Tc generator. $^{99}MoO_4^{2-}$ is absorbed to an alumina column and the ^{99m}Tc is formed by the decay of ^{99}Mo. $^{99m}TcO_4^-$ is eluted from the column with saline. Nearly 80% of radiopharmaceuticals currently available in clinical nuclear medicine use ^{99m}Tc because of its ideal nuclear properties. The 6 h half-life provides sufficient time to synthesize, prepare the dosage, administer the drug and collect useful images. The monochromatic 140 keV photons give images of high spatial resolution. ^{99m}Tc is readily obtained at low cost from ^{99}Mo – ^{99m}Tc generators. Several difficulties do arise with synthesizing ^{99m}Tc complexes. The ^{99m}Tc radiopharmaceuticals are used in low concentrations (10^{-8} – 10^{-6} M). Synthesis should be completed under 30 min due to the short half-life and in an aqueous solution. The molecule purity should be greater than 90% because lower organ specificity will be obtained by the injection of ^{99m}Tc-species mixtures. The dilute concentration of $[^{99m}TcO_4]^-$ solutions requires characterisation via HPLC or other chromatographic methods with γ-detection in order to monitor the chemistry. The ^{99}Tc isotope is used to isolate and fully characterise the technetium complexes.

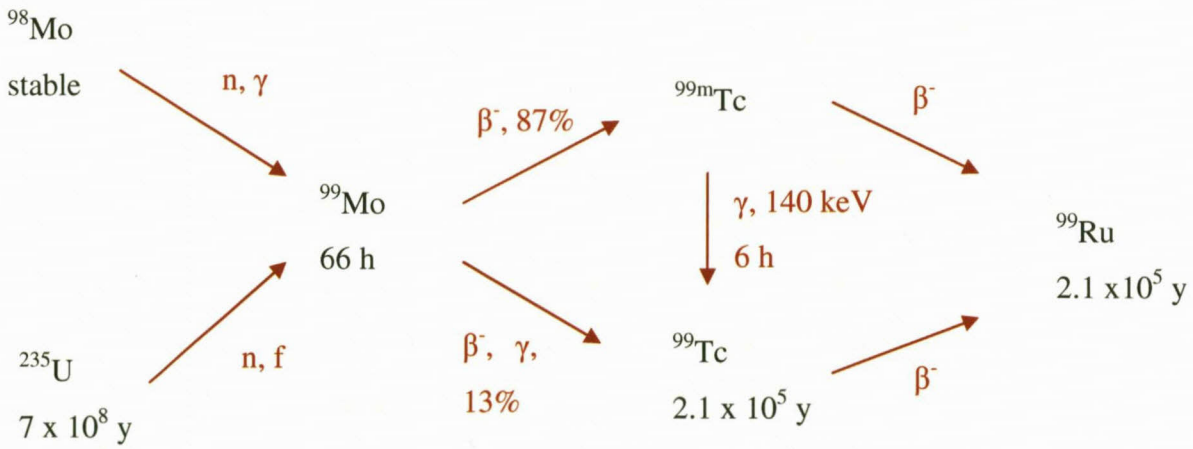

Figure 2.4: Decay sequences related to the ^{99}Mo-^{99m}Tc generator for the production of ^{99m}Tc.[3]

2.6.1 First-generation complexes

The use of $^{99m}TcO_4^-$ for the diagnosis of thyroid disease was the first application of ^{99m}Tc radionuclide for medical imaging. From this starting point, many ^{99m}Tc complexes have been synthesized and studied which led to the development of "technetium essential agents" which is considered as the first generation ^{99m}Tc complex radiopharmaceuticals.[34,35,36] The coordination chemistry of Tc, during this generation of complexes, played an important role. Total dependence on the design of the complexes occurred for the successful development of the ^{99m}Tc imaging agents as the biodistribution was dependant on the lipopholicity, size and charge of the complex.[37]

2.6.1.1 Brain imaging

For a pharmaceutical to accumulate in the brain it must be able to cross the blood-brain barrier. Complexes must therefore be moderately lipophilic with an overall neutral charge. The commercially successful Ceretec® utilises a hexamethylpropyleneamineoxime ligand (HMPAO hexametazime) which loses three protons and forms a neutral, square pyramidal Tc(V) mono-oxo complex. Ceretec® has limited stability in solution and considerable efforts have been made to increase the lifetime of the radiopharmaceutical with the addition of other metallic centres such as Co(II).

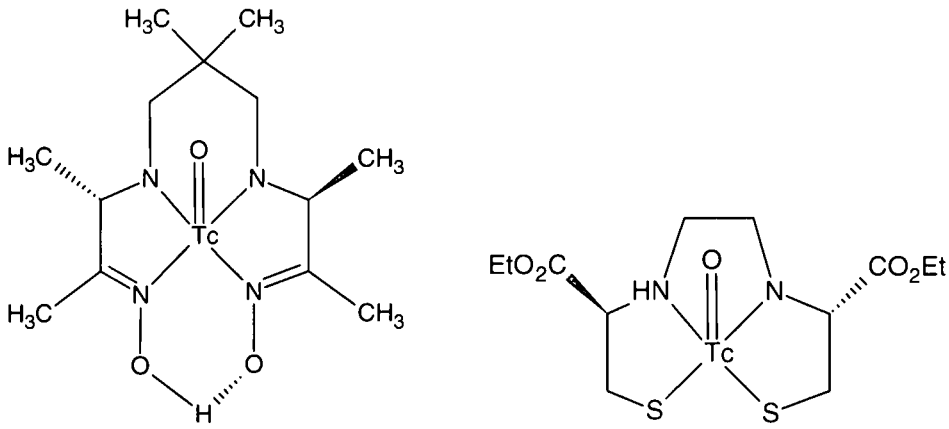

(A) ^{99m}Tc-$_{D,L}$-HMPAO **(B) ^{99m}Tc-Bicisate**

Figure 2.5: Chemical structures of selected technetium radiopharmaceuticals based on small metal complexes.

---

[34] D. Jain, *Semin. Nucl. Med.* 1999, 29, 221
[35] S. Banerjee, M.R.A Pillai, N. Ramamoorthy, *Semin. Nucl. Med.*, 2001, 21, 260
[36] U. Mazzi, R. Schibli, H.J. Pietzsch, J.U. Künstler, H. Spies, *Technetium-99m Pharmaceuticals*, Part 1, 2007, pp 7-58
[37] J.R. Dilworth, S.J. Parrott, *Chem. Soc. Rev.*, 1998, 27, 43

Other brain imaging agents such as Neurolite® (^{99m}Tc-Bicisate) is also commercially available. The ethylenecysteine diester (ECD) complex is formed by the reaction of the ligand with $[TcO_4]^-$ to give a neutral square pyramidal complex. The stereo chemistry of the complex plays an important role in the biochemical behaviour.

2.6.1.2 Heart imaging

The synthesis of the cationic $[^{99m}Tc(dmpe)_2Cl_2]^+$ (dmpe = 1,2-bis(dimethylphosphino)ethane) as a potential myocardial perfusion agent[38] was initiated by the theory that lipophilic mono-positively charged complexes would accumulate in the heart *via* the Na/K ATPase mechanism whereby the Tc complex mimics K^+ ions. However the complex was found to reduce *in vivo* to the neutral Tc(II) complex $[^{99m}Tc(dmpe)_2Cl_2]$ which is rapidly removed from the heart and accumulates in the liver. The approval of Cardiolite® or $[^{99m}Tc(MIBI)_6]^+$ (MIBI = 2-methoxy-2-methylpropylisocyanide) was the result of the further development of cationic complexes as myocardial perfusion agents.[39] Lately it is successfully utilized for tumour imaging and the detection of multidrug resistance.[40, 41] Cardiolite® has an octahedral arrangement around the metal core of isocyanide ligands. It is believed that cations accumulate *via* a diffusion mechanism and electrostatic binding due to a high mitochondrial membrane potential. Cardiotec® (^{99m}Tc-Teboroxime) was the first approved neutral myocardial perfusion agent. It is a Tc(III) seven coordinate complex with three dioxime ligands bound *via* six nitrogens and one chlorido ligand.[42]

---

[38] M.C. Gerson, E.A. Deutsch, H. Nishyama, K.G. Libson, R.J. Adolph, L.W. Grossman, V.J. Sodd, J.L. Fortman, C.C. Vanderhagden, C.C. Williams, E.L. Salinger, *Eur. J. Nucl. Med.*, 1983, 8, 371

[39] B.L. Holman, A.G. Jones, J. Listerjames, A. Davison, M.J. Abrams, J.M. Kirshenbaum, S.S. Tumeh, R.J. English, *J. Nucl. Med.*, 1984, 25, 1350

[40] D. Piwnica-Worms, V.V. Rao, J.F. Kronauge, J.M. Croop, *Biochemistry*, 1995, 34, 12210

[41] L.W. Herman, V. Sharma, J.F. Kronauge, E. Barbarics, L.A. Herman, D. Piwnica-Worms, *J. Med. Chem.*, 1995, 38, 2955

[42] K.E. Linder, M.F. Malley, J.Z. Gongoutas, S.E. Unger, A.D. Nunn, *Inorg. Chem.*, 1990, 29, 2428

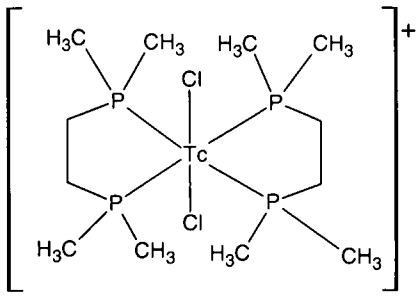

(A) $[^{99m}Tc(dmpe)_2Cl_2]^+$

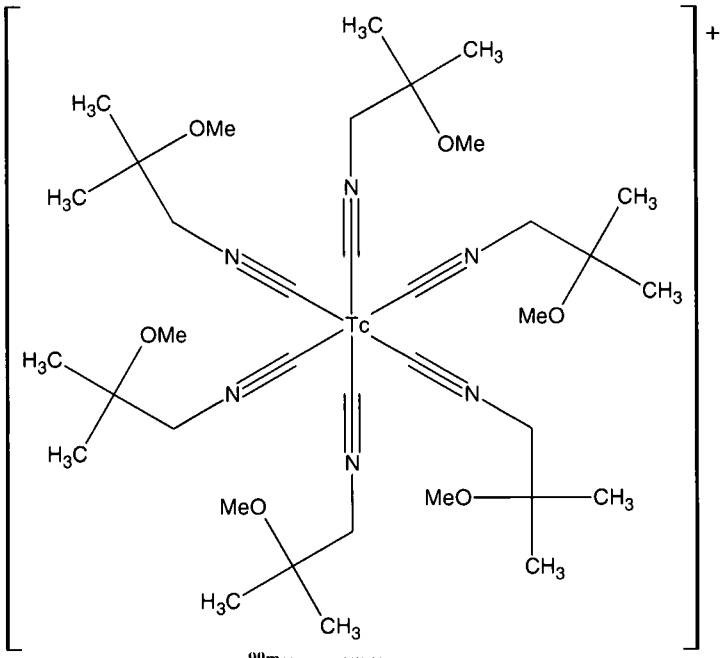

(B) ^{99m}Tc-MIBI

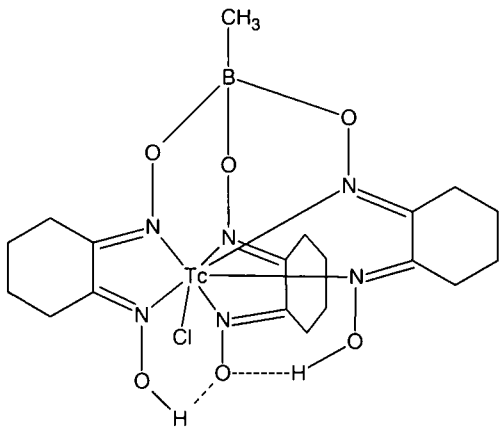

(C) ^{99m}Tc-Teboroxime

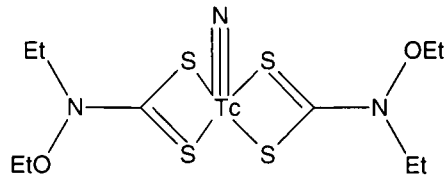

(D) ^{99m}Tc-NOET

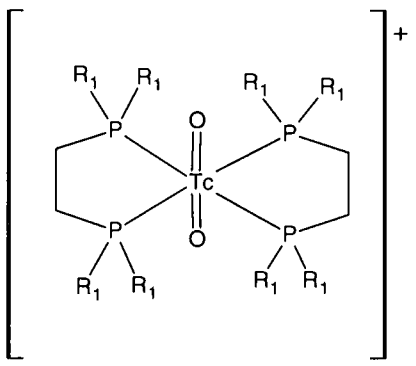

$R_1 = CH_2CH_2OEt$

(E) ^{99m}Tc-Tetrofosmin

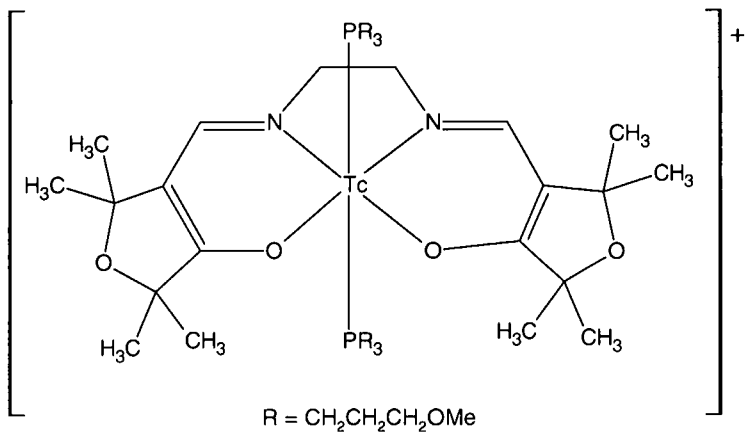

$R = CH_2CH_2CH_2OMe$

(F) ^{99m}Tc-Q12

Figure 2.6: Chemical structures of selected technetium radiopharmaceuticals for heart imaging.

^{99m}Tc-NOET, a neutrally charged myocardial imaging agent, consisting of a $^{99m}TcN^{2+}$ core. The lack of charge is an indication that a cationic charge for myocardial perfusion imaging agents is not an essential requirement. Two other imaging radiopharmaceuticals available, are both cationic and contain coordinated phosphine ligands, ^{99m}Tc-Tetrofosmin (Myoview®) and ^{99m}Tc-Q12 (Technecard®). ^{99m}Tc-Q12 is a Tc(III) metal centre with a mixed N_2O_2-donor Schiff-base and coordinated phosphine.[3] This complex contains fewer phosphine ligands in an attempt to prevent reduction of the metal ion. The Schiff-base ligand contains a furanone group to assist in drug clearance from the blood, lungs and liver.[43]

2.6.1.3 Bone imaging

Several ^{99m}Tc complexes have been developed as bone-imaging radiopharmaceuticals containing phosphonate ligands. The identification of metastasis in bone in cancer patients is one of the main uses of such complexes. The synthesis of ^{99m}Tc-MDP consists of $[^{99m}TcO_4]^-$ with methylenediphosphonate (MDP) and $SnCl_2.H_2O$ which acts as a reductant. Free phosphoryl oxygens are thought to coordinate to the calcium ions on the hydroxyapatite bone surface which could explain the bone absorption mechanism. Images of stressed bones appear as "hot spots" due to the high concentration of calcium ions and therefore greater accumulation of the Tc complex.[37]

2.6.2 Second-generation complexes

Second-generation imaging radiopharmaceuticals are classified according to the biological function which is targeted by the radiopharmaceutical. These complexes are often termed "target-specific radiopharmaceuticals". Various radiolabelling methods are used, such as the bifunctional and integrated method, which have already been discussed (§ 2.4).

2.6.2.1 Steroid receptors

Many breast tumors are estrogen receptor positive, whereas prostate cancers are androgen and progesterone receptor positive. If a complex which binds selectively to these sites could be synthesized, such as a radiolabelled receptor hormone, then it would provide a method by

[43] M.A. DeRosch, J.W. Brodack, G.D. Grummon, M.E. Marmian, D.L. Nosco, K.F. Deutsch, E.A. Deutsch, *J. Nucl. Med.*, 1992, 22, 850

which such tumors could be monitored. The coordination of N_2S_2 ligands to ^{99m}Tc containing a progesterone receptor linked *via* a phenyl spacer has been investigated (Figure 2.7).[44] It is important to find a linking site on the steroid which does not affect the receptor binding.

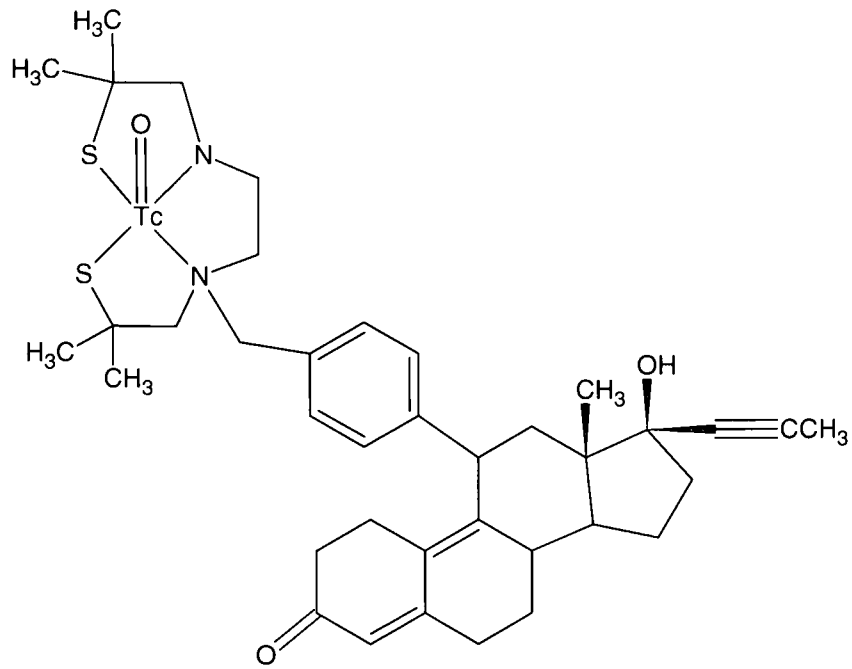

Figure 2.7: Linkage of progesterone receptors *via* N_2S_2 ligands.

The integrated approach towards radiolabelling can be utilized by placing the receptor binding sites onto the periphery of the Tc ligands, such as seen in Figure 2.8 which is structurally similar to progesterone and estradiol.[45]

[44] M.J. Welch, J.B. Downer, J.A. Katzenellenbogen, *Current Directions in Radiopharmaceutical Research and Development*, Eds: S.J. Mather, Kluwer Academic Press, Netherlands, 1996
[45] D.Y. Chi, J.P. O'Neil, C.J. Anderson, M.J. Welch, J.A. Katzenellenbogen, *J. Med. Chem.*, 1994, 37, 928

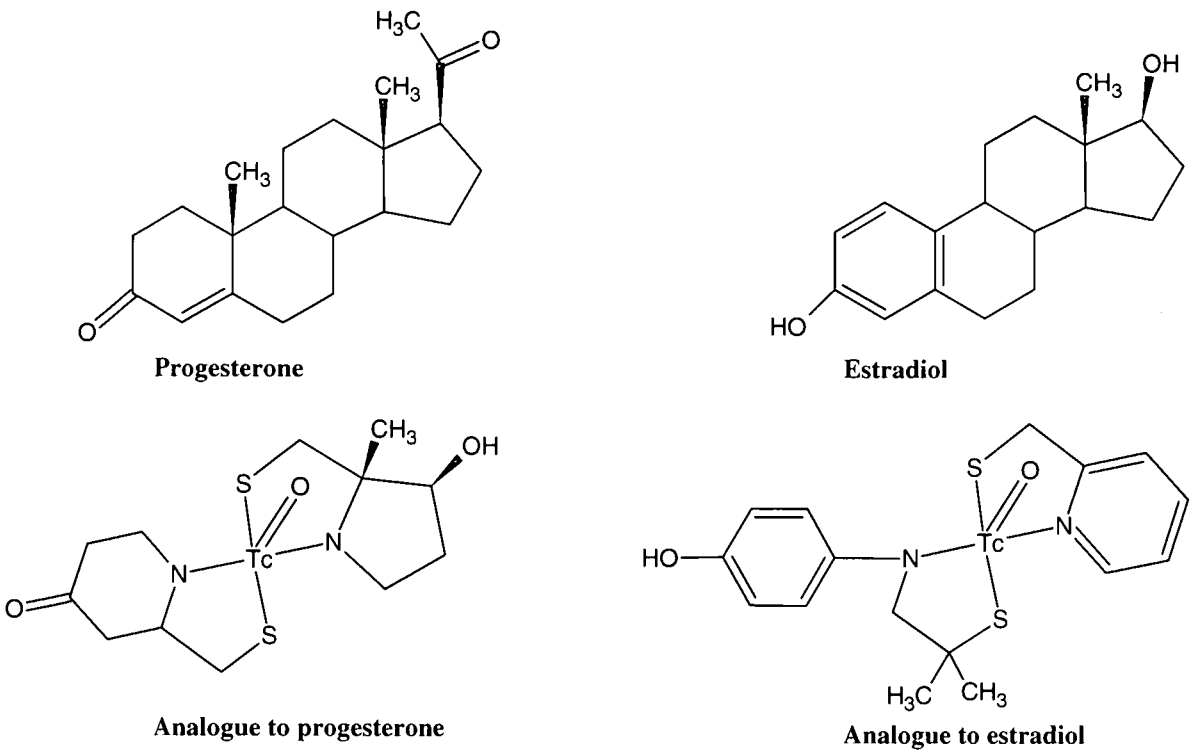

Figure 2.8: **Integrated approach of radiolabelling mimicking related steroid molecules utilizing N_2S_2 ligands.[37]**

2.6.2.2 Central nervous system receptors

Several diseases such as Alzheimer's disease, epilepsy, Parkinson's disease and psychiatric conditions are associated with changes in the densities of neurotransmitter receptor sites in the brain. Initial studies utilized PET imaging however a cyclotron is required in the nearby vicinity. ^{123}Iodine (γ-isotope) has been used for SPECT brain receptor imaging, however the isotope is expensive and not widely available. Ideally the design of ^{99m}Tc complexes would overcome numerous problems. The [M=O] core utilizing NS_2^{2-}, SS_2^{2-} and N_2S_2 chelating ligands can be used to bind receptor active molecules to the radiopharmaceutical such as ketanserin for serotonin receptor sites or cocaine for dopamine transporter sites.[46]

[46] H. Spies, T. Fietz, M. Glacer, H.J. Peitsch, B. Johanssen, *Technetium and Rhenium Chemistry and Nuclear Medicine*, Eds.: M. Nicolini, G. Bandoli, U. Mazzi, Padova, Italy, 1995

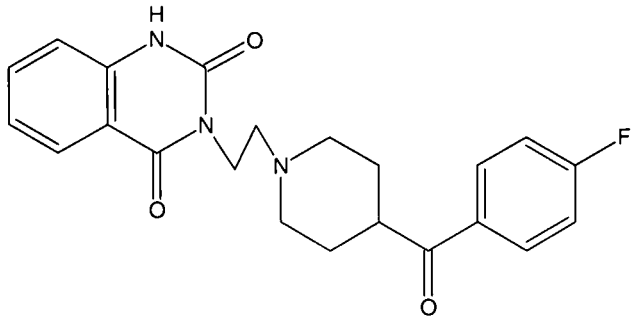

Ketanserin

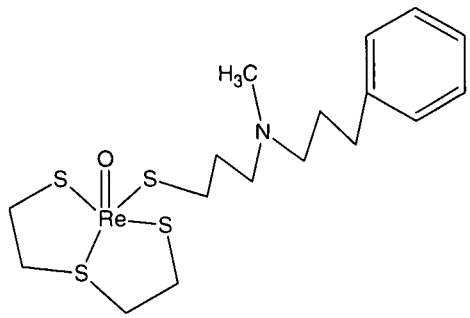

Re=O analogue

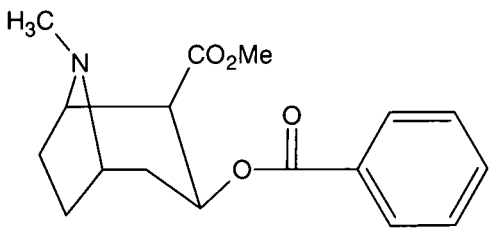

Cocaine

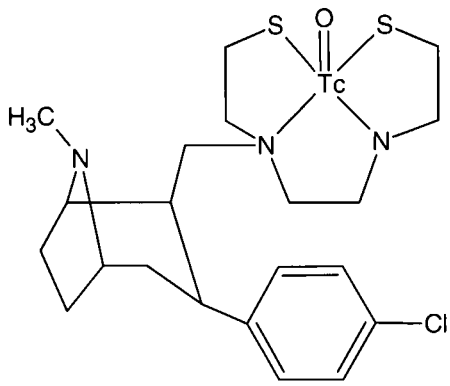

Tc=O analogue (Tc-TRODAT)

Figure 2.9: Bifunctional approach of radiolabelling for CNS receptors.

2.6.2.3 Magic Bullets – Monoclonal antibodies

Monoclonal antibodies are able to transport radionuclides to specific sites in the human body as long as the radiolabel does not interfere with the coordination of the antibody to the receptor site. Fragments, with specific binding characteristics, are being utilized instead of whole antibodies because the biodistribution kinetics is very slow due to their large size. The linkage between the radionuclide and the antibody is vitally important for the development of ^{99m}Tc labelled antibodies as the premature release of the isotope must be prevented. One method of coordination involves linking the antibody to the metal chelation groups followed by the coordination of the radionuclide. Hydrazine nicotinamide derivatives or thiolactone can be used for this approach.[47] Another method initially coordinates the radionuclide to the chelate which contains an activated ester group, followed by linkage of the fragment. The diamidedithiolate ligand containing a pendant tetrafluorophenyl (TFP) activated ester (Figure 2.10) is being investigated as potential melanoma and lung cancer targeting systems.

[47] D.J. Hnatowich, G. Mardirossan, M. Ruscowski, M. Fargarasi, F. Firzi, P. Winnard, *J. Nucl. Med. Chem.*, 1993, 34, 172

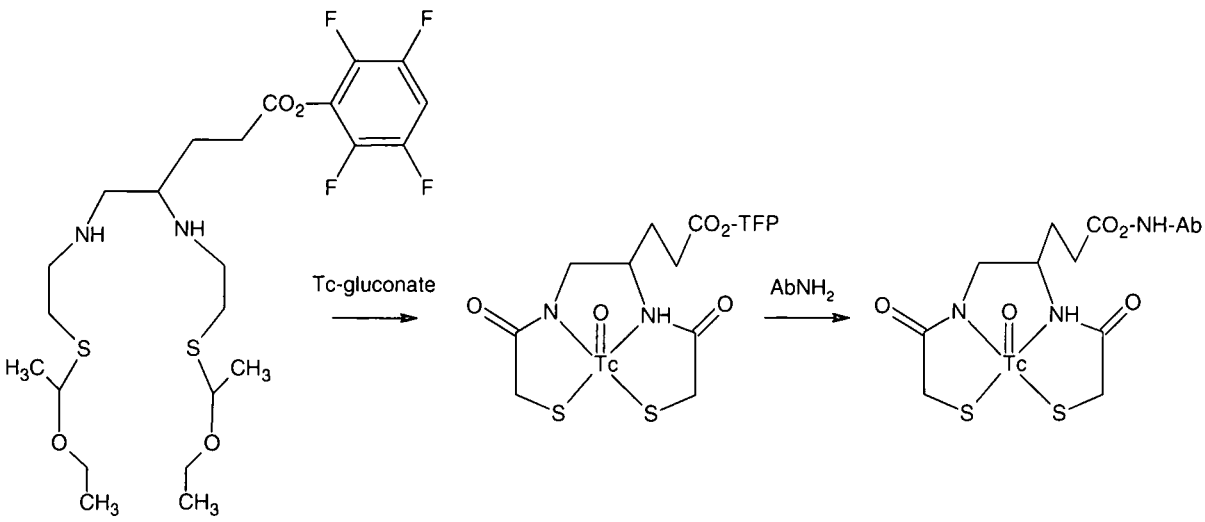

Figure 2.10: **Pre-formed chelation of ^{99m}Tc antibody attachment.**

2.7 RHENIUM CHEMISTRY DIRECTED TO NUCLEAR MEDICINE

Rhenium is a third row transition metal in the same periodic group as Tc and Mn. Due to the periodic relationship, the coordination chemistry of rhenium is similar but not identical to that of technetium. This similarity is advantageous as it allows bifunctional chelating ligands that have been developed for ^{99m}Tc to be used for rhenium as well. The great advantage of working first with rhenium, is that experimental synthesis can be conducted on a non-radioactive "cold" isotope. Two rhenium radionuclides are utilized in therapeutic nuclear medicine, ^{186}Re and ^{188}Re, by means of β-irradiation. Rhenium-186 is generated by neutron radiation of ^{185}Re but contamination of the isotope with ^{185}Re occurs. Rhenium-188 is made from a ^{188}W generator which is commercially available.[48] The short half-life (17 h) and higher β-radiation energy (E_β = 2.12 *vs.* 1.07 MeV for ^{186}Re) makes ^{188}Re more suitable for synthesizing radiopharmaceuticals designed for larger tumors with fast clearance from the blood and other non-cancerous tissues. Radiopharmaceuticals that do not clear rapidly from the blood stream tend to use ^{186}Re, a medium energy β-particle emitter with a long half-life (3.7 day). Rhenium has not been used as extensively as other therapeutic radionuclides (^{131}I or ^{90}Y) partially because more complex labeling chemistry is required for it. More reducing agent (e.g. Sn^{II}) is required to convert the oxidation state of rhenium (Re^{VII} in ReO_4^- to lower

[48] G.J. Ehrhardt, A.R. Ketring, L.M. Ayers, *Appl. Radiat. Isot.*, 1998, 49, 295

oxidation states) since Tc^{VII} is easier to reduce than rhenium.[5,49,50] Various unavoidable aspects influence the design of Re labeled compound with high yields, purity, specific *in vivo* cancer targeting such as the presence of reducing agents may affect synthetic purity of the rhenium biomolecule, rhenium can be less stable in lower oxidation states than technetium, and although the chemistry of Re and Tc is similar it is not identical.

2.7.1 Rhenium Radiopharmaceuticals

Due to the similarities, site specific radiopharmaceuticals of rhenium have run nearly parallel to the development of ^{99m}Tc complexes. Numerous bifunctional chelating molecules coordinated to $^{186/188}Re$ use a triaminothiol N_3S ligand framework.[51,52,53] Ligand systems with diamidodithiol and diaminodithiol (N_2S_2) donor atoms have been made and are more applicable as hydrophobic agents as most N_2S_2 systems form lipophilic Re/Tc complexes.[5,54] MAG3 and MAG2-GABA are two N_3S chelators which are frequently used to link proteins, peptides and other biomolecules to a rhenium metal centre.[55] The technetium-MAG3 system, a square pyramidal oxo complex, is used as an imaging agent for renal function.[56] MAG2-GABA (mercaptoacetylglycylglycyl-γ-aminobutyric acid) differs from MAG3 (mercaptoacetylglycylglycylglycine) by containing a spacer group between the M-N_3S chelate and linked biomolecule. The GABA spacer group is two carbon atoms longer and may reduce steric hinderance which could improve labelling yields and binding affinities by increasing the distance between the M-N_3S chelate and the binding site of the biomolecule. Identical $[^{99m}TcO]^{3+}$ and $[^{186/188}ReO]^{3+}$ structures form with MAG3 and MAG2-GABA which allow for "matched pair" studies during *in vivo* investigation with N_3S bioconjugates.[5]

---

[49] G.L. Griffiths, *Cancer Therapy with Radiolabelled Antibodies*, Eds.: D.M. Goldenberg, CRC Press, Florida, USA, 1995

[50] P.O. Zamora, H. Bender, S. Gulhke, M.J. Marek, F.F. Knapp, B.A. Rhodes, H.J. Biersack, *Anticancer Res.*, 1997, 17, 1803

[51] H. Breitz, B. Ratliff, R. Schroff, J.L. Vanderheyden, A.R. Fritzberg, J. Appelbaum, D.R. Fisher, P. Abrams, P. Weiden, *J. Nucl. Med.*, 1990, 31, 725

[52] C.J. Smith, T.J. Hoffman, C. Higginbotham, E. Wong, D. Esihmia, J.R. Thornback, W.A. Volkert, *J. Nucl. Med.*, 1998, 39, 215

[53] E. Wong, T. Fauconnier, S. Bennet, J. Valliant, T. Nguyen, F. Lau, L.F.L. Lu, A. Pollak, R.A. Bell, J.R. Thornback, *Inorg. Chem.*, 1997, 36, 5799

[54] Y. Sugano, J.A. Katzenellenbogen, *Bioorg. Med. Chem. Lett.*, 1996, 6, 361

[55] T. Kniess, S. Noll, B. Noll, H. Spies, B. Johannsen, *J. Radioanal. Nucl. Chem.*, 1999, 240, 357

[56] A.R. Fritzberg, S. Kasina, D. Eshima, D.L. Johnson, *Eur. J. Nucl. Med.*, 1983, 8, 371

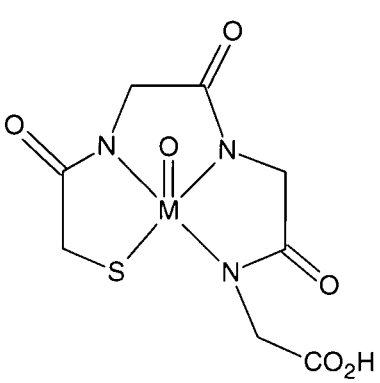

MAG3

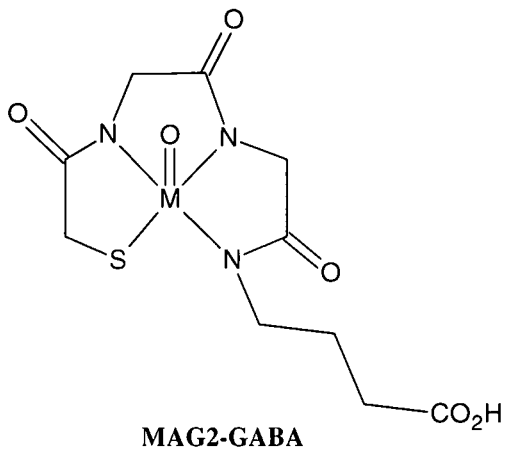

MAG2-GABA

Figure 2.11: M-MAG3 and M-MAG2-GABA ligand framework (M = Tc or Re).

The development of radiopharmaceuticals for the treatment of painful skeletal metastases has prompted the investigation of possible β-emitting radiopharmaceuticals.[5] In 1979, ^{186}Re-HEDP (hydroxyethylidenediphosphonate), was recommended as a possible therapeutic agent and has been successfully used.[57,58,59] The synthesis is similar to ^{99m}Tc-labelled diphosphonates, however the biodistribution of the rhenium complexes differ.

Rhenium complexes which mimic receptor binding molecules have been synthesised (Figure 2.12.), such as a Re(V)=O complex which mimics the molecular parameters of estradiol and progesterone.[60,61,62,63] The linkage of steroids[64] to rhenium *via* various coupling modes are shown in Figure 2.13.

---

[57] L. Mathieu, P. Chevalier, G. Galy, M. Berger, *Int. J. Appl. Radiat. Isot.*, 1979, 30, 725
[58] M.G.E.H. Lam, T.B. Bosma, P.P. van Rijk, B.A. Zonnenberg, *Eur. J. Nucl. Med. Mol. Imaging*, 2009, 36, 1425
[59] K. Liepe, R. Runge, J. Kotzerke, *J. Cancer Res. Clin. Oncol.*, 2005, 131, 60
[60] D.Y. Chi, J.A. Katzenellenbogen, *J. Am. Chem. Soc.*, 1993, 115, 7045
[61] D.Y. Chi, J.P. O'Neil, C.J. Anderson, M.J. Welch, J.A. Katzenellenbogen, *J. Med. Chem.*, 1994, 37, 928
[62] J.P. DiZio, R. Fiaschi, A. Davison, A.G. Jones, J.A. Katzenellenbogen, *Bioconj. Chem.*, 1991, 2, 353
[63] J.P. DiZio, C.J. Anderson, A. Davison, G.J. Ehrhardt, K.E. Carllson, M.J. Welch, J.A. Katzenellenbogen, *J. Nucl. Med.*, 1992, 33, 558
[64] U. Abram, *Comprehensive Coordination Chemistry II*, Eds.: J.A. McCleverty, T.J. Meyer, Elsevier Ltd. Oxford, UK, Vol. 5, 2004

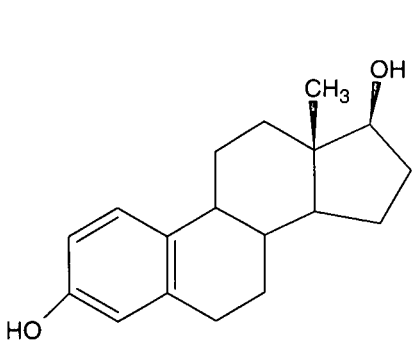

Estradiol

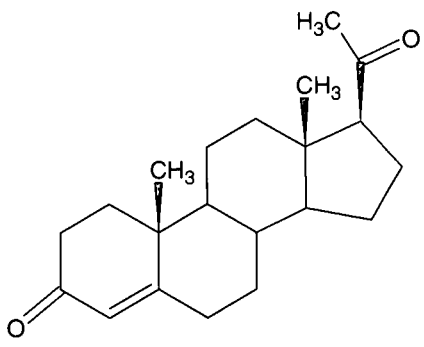

Progesterone

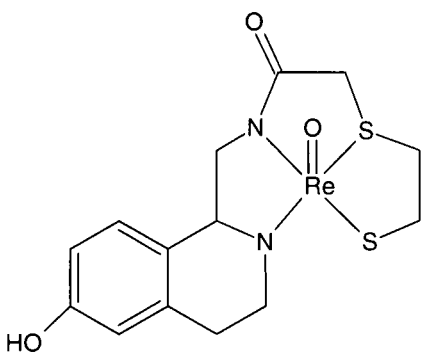

Rhenium analogue of estradiol

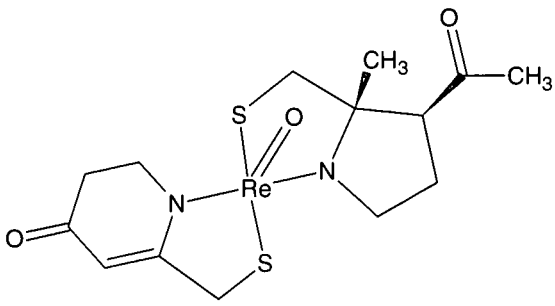

Rhenium analogue of progesterone

Figure 2.12: **Rhenium analogue mimics of receptor binding molecules.**

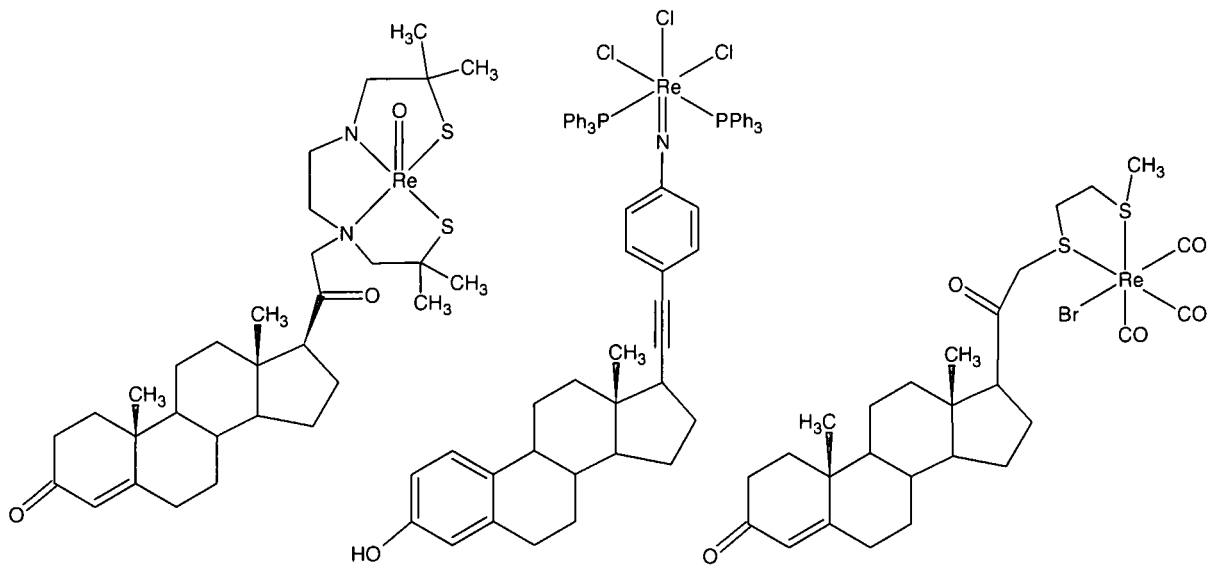

Figure 2.13: **Linkage of steroids to rhenium metal centre *via* various bifunctional chelating agents.**

A promising approach for future rhenium and technetium radiopharmaceuticals is provided by rhenium(I) and technetium(I) tricarbonyl complexes which will be discussed in detail in the following section.

2.8 RHENIUM & TECHNETIUM TRICARBONYL COMPLEXES

2.8.1 Aqueous Chemistry of *fac*-$[M(CO)_3(H_2O)_3]^+$ (M = Re, Tc)

Ideally the metal complex should be kept small in size which will allow the physicochemical properties of the radiopharmaceutical to adopt the properties of the biofunctional label. As the size of the label increases, so should the interference with the bioactivity and physicochemical properties of the biomolecule. Tricarbonyl complexes of rhenium and technetium received little attention from nuclear medical applications due to the unfeasible synthetic procedures, however the novel mild reaction condition described by Alberto *et al.*[65] allowed the synthesis of stable organometallic Tc(I) and Re(I) moieties which are well suitable for medical synthesis. The synthesis of *fac*-$[M(CO)_3(H_2O)_3]^+$ (M = Re, Tc) is readily made from permetallates under mild conditions in aqueous solutions, illustrated in Scheme 2.1 below.[66,67,68,69,70,71]

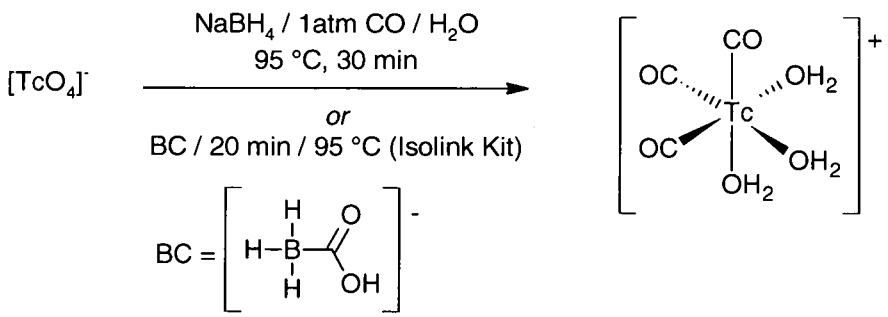

Scheme 2.1: **Two synthetic pathways for *fac*-$[M(CO)_3(H_2O)_3]^+$ from $[MO_4]^-$.**

---

[65] R. Alberto, R. Schibli, R. Waibel, U. Abram, A.P. Schubiger, *Coord. Chem. Rev.*, 1999, 190-192, 901
[66] R. Alberto, *J. Organomet. Chem.*, 2007, 692, 1179
[67] R. Alberto, R. Schibli, A. Egli, P.A. Schubiger, W.A. Herrmann, G. Artus, U. Abram, T.A. Kaden, *J. Organomet. Chem.*, 1995, 493, 119
[68] R. Alberto, R. Schibli, D. Angst, P.A. Schubiger, *Transition Met. Chem.*, 1997, 22, 597
[69] R. Alberto, R. Schibli, A. Egli, A.P. Schubiger, U. Abram, T.A. Kaden, *J. Am. Chem. Soc.*, 1998, 120, 7987
[70] R. Alberto, K. Ortner, N. Wheatley, R. Schibli, A.P. Schubiger, *J. Am. Chem. Soc.*, 2001, 123, 3135
[71] R. Schibli, P.A. Schubiger, *Eur. J. Nucl. Med.*, 2002, 29, 1529

The anionic form of the complex $[NEt_4]_2[M(CO)_3X_3]$ (M = Tc, Re; X = Cl, Br) is soluble in water and the halide ligands are readily substituted by H_2O to form the aqua complex *fac*-$[M(CO)_3(H_2O)_3]^+$. The aqua complex is coordinated by three tightly bound CO ligands and three labilized water ligands. *fac*-$[M(CO)_3(H_2O)_3]^+$ complex is a highly attractive investigative possibility for radiopharmaceutical design due to the high stability of the *fac*-$[M(CO)_3]^+$ core in water and the potential of exchanging the labile solvent ligands. An intriguing feature of the *fac*-$[M(CO)_3]^+$ core is its d^6 low spin configuration in an octahedral field based high kinetic stability with many types of ligands. The *fac*-$[M(CO)_3]^+$ core is nearly spherical in shape and with the use of an appropriate ligand system, such as tridentate ligands or [2+1] ligand systems, the coordination sphere can be "closed" thus protecting the metal centre from further ligand interactions or re-oxidation. Since the *fac*-$[M(CO)_3(H_2O)_3]^+$ accepts many types of ligands it is possible to design complexes whose properties such as hydro/lipophilicity are adapted to those of the biomolecule. The tricarbonyl core was designed as a precursor for simple labeling procedures and was not meant to be a "stand alone" radiopharmaceutical. A variation of the tricarbonyl complexes is the $CpM(CO)_3$ group.[72,73] The versatility of the cyclopentadienyl (Cp) ligand gives the complex much advantages, as it can block three coordination sites (acting as a small "tridentate" ligand), act as a linker and has a low molecular weight (Figure 2.14). Functionalisation of steroids and biomolecules which pass the blood-brain barrier, with this group, should lead to interesting studies as the $CpM(CO)_3$ core is highly lipophilic.[71]

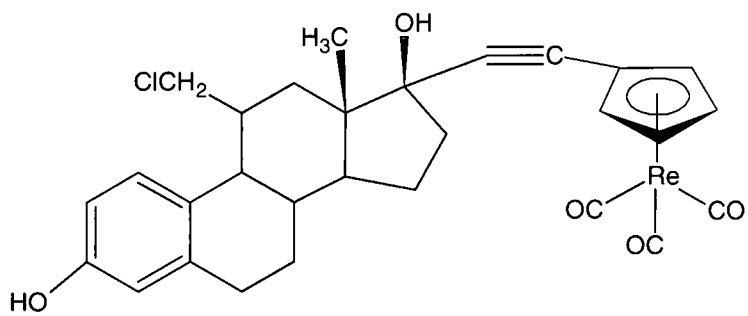

Figure 2.14: Linkage of estradiol derivative to cyclopentadienyltricarbonyl.[74]

[72] J. Wald, R. Alberto, K. Ortner, L. Candreia, *Angew. Chem., Int. Ed.*, 2001, 40, 3062
[73] J. Bernard, K. Ortner, B. Spingler, H.J. Pietzsch, R. Alberto, *Inorg. Chem.*, 2003, 42, 1014
[74] S. Top, M. Elhafa, A. Vessieres, J. Quivy, J. Vaissermann, D.W. Hughes, M.J. McGlinchey, J.P. Mornon, E. Thoreau, G. Jaouen, *J. Am. Chem. Soc.*, 1995, 117, 8372

Special attention has been directed to ligands and ligand systems containing nitrogen, oxygen and sulphur donor atoms which can mimic biological binding sites. Various mono-, bi- and tridentate ligand systems have successfully coordinated to *fac*-$[M(CO)_3]^+$ core containing N-heterocycles such as pyridines, pyrazoles and imidazoles, amines, amides, carboxylic acids, thiols, thio-ethers, phosphines and combinations thereof (Figure 2.15 and 2.16).[71] The variety of ligands can be used as bifunctional chelators for the radionuclide labelling of derivatised biomolecules (e.g. Vitamin B_{12}, estradiol, enkephalin, biotin, histidine, glucose).[3, 31, 65, 66, 71, 75, 76, 77, 78, 79, 80, 81, 82, 83]

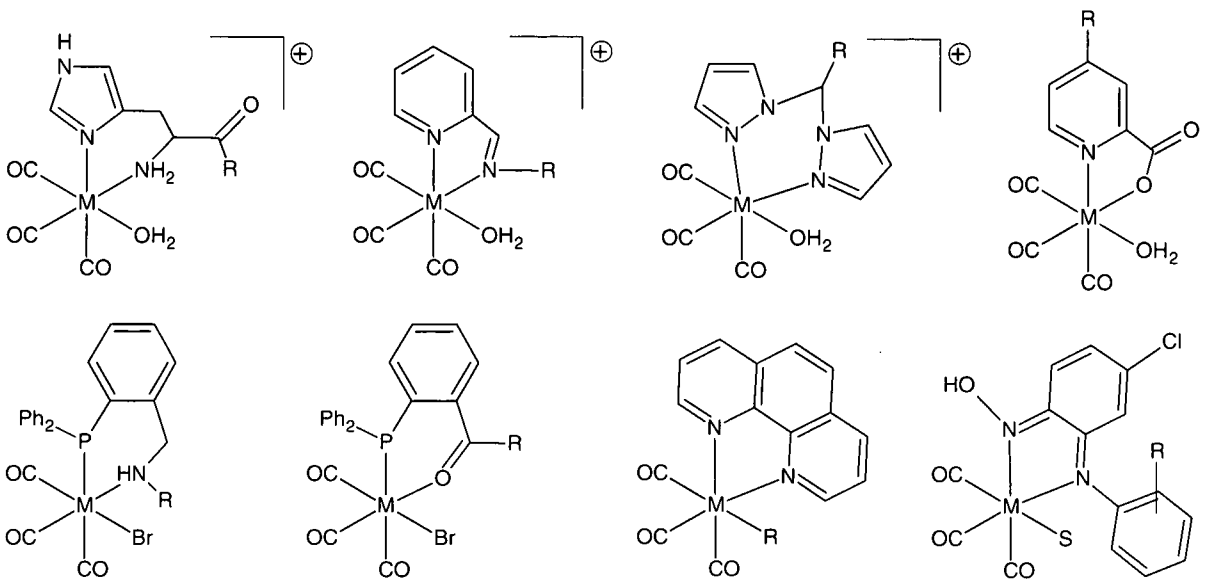

Figure 2.15: **Examples of bidentate chelating systems for the labeling of rhenium and technetium tricarbonyl complexes (R = biomolecule or linker attached to biomolecule, S = coordinated halide/solvent).**

---

[75] L. Maria, S. Cunha, M. Videira, L. Gano, A. Paulo, I.C. Santos, I. Santos, *Dalton Trans.*, 2007, 3010

[76] S. Alves, A. Paulo, J.D.G Correia, L. Gano, C.J. Smith, T.J. Hoffman, I. Santos, *Bioconjugate Chem.*, 2005, 16, 438

[77] C. Xavier, J.K. Pak, I. Santos, R. Alberto, *J. Organomet. Chem.*, 2007, 692, 1332

[78] S. Mundwiler, R. Waibel, B. Spingler, S. Kunze, R. Alberto, *Nucl. Med. Bio.*, 2005, 32, 473

[79] D.R. van Staveren, S. Mundwiler, U. Hoffmanns, J.K. Pak, B. Spingler, N. Metzler-Nolte, R. Alberto, *Org. Biomol. Chem.*, 2004, 2, 2593

[80] E. Palma, J.D.G. Correia, A. Domingos, I. Santos, R. Alberto, H. Spies, *J. Organomet. Chem.*, 2004, 689, 4811

[81] K.K.W. Lo, W.K. Hui, C.K. Chung, K.H.K. Tsang, T.K.M. Lee, C.K. Li, J.S.Y. Lau, D.C.M. Ng, *Coord. Chem. Rev.*, 2006, 250, 1724

[82] S. Wirth, A.U. Wallek, A. Zernickel, F. Feil, M. Sztiller-Sikorska, K. Lesiak-Mieczkowska, C. Bräuchle, I.P. Lorenz, M. Czyz, *J. Inorg. Biochem.*, 2010, 104, 774

[83] J. Petrig, R. Schibli, C. Dumas, R. Alberto, P.A. Schubiger, *Chemistry – a European Journal*, 2001, 7, 1868

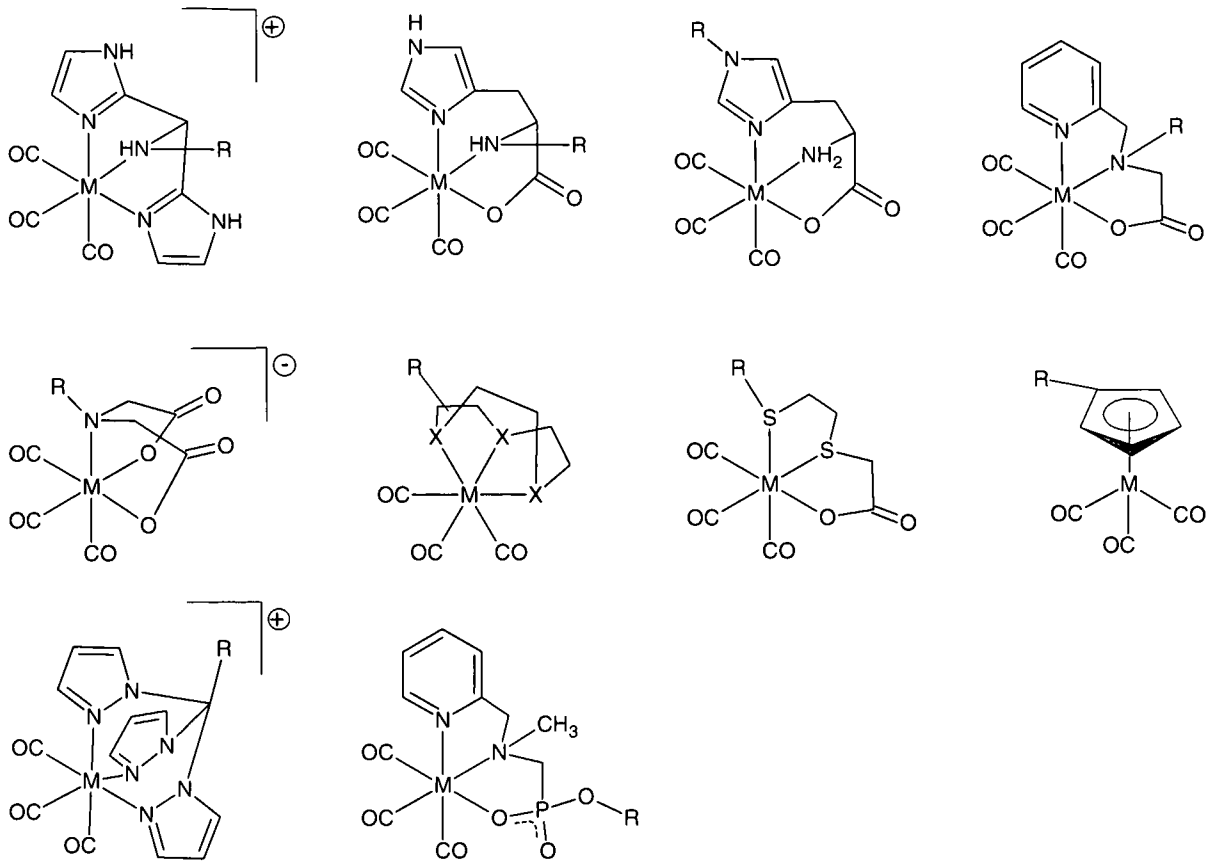

Figure 2.16: **Examples of tridentate chelating systems for the labeling of rhenium and technetium tricarbonyl complexes (R = biomolecule or linker attached to biomolecule, X = N, P, S).**

Diverse coordination chemistry is possible with the tricarbonyl core and offers tremendous development opportunities for new bifunctional chelating agents. However a few limitations with regards to denticity and stability of the chelate have been noted.[71,84] Mono- and bidentate Tc tricarbonyl complexes are significantly retained in the blood stream and in excretion organs (e.g. kidneys and liver) and experience protein binding. The vacant third coordination position, with regards to a bidentate ligand, may play a significant role in the stability of the complexes as it may be readily substituted. It appears that complex charge and lipophilicity play only a minor role in these effects. Technetium tricarbonyl complexes coordinated to tridentate chelators, on the other hand, indicate good stability and rapid clearance from blood and other major organs. It may be a favorable tendency to investigate functionalized biomolecules with either tridentate chelates or bidentate ligands utilizing the [2+1] approach which effectively blocks the labile third position.

---

[84] R. Schibli, R. La Bella, R. Alberto, E. Garcia-Garayoa, K. Ortner, U. Abram, P.A. Schubiger, *Bioconjugate Chem.*, 2000, 11, 345

2.8.2 Substitution and exchange reactions of *fac*-$[M(CO)_3(H_2O)_3]^+$

The potential use of rhenium and technetium complexes, containing the *fac*-$M(CO)_3$ core, as *in vivo* radiotracers in diagnostic and therapeutic medicine, has resulted in much attention and investigation. The advantages of a stable tricarbonyl core and trisolvento ligands, which are readily replaced by incoming ligands has resulted in numerous compounds which have been synthesised and characterized. A variety of ligand atoms (N, P, O and S) can be bound to both Re and Tc metal centres, however the preparation of the complexes must be fast and complete as the half-life of the radioisotopes used in radiopharmaceuticals are generally short. To ensure the development of methods by which these radionuclides (^{99m}Tc, $^{186/188}Re$) can be included into appropriate (and useful) radiopharmaceuticals, a knowledge of kinetics and mechanism of complex formation of the *fac*-$[M(CO)_3(H_2O)_3]^+$ with a diversity of chelating ligands with various binding atoms is important. Just as important is an understanding of reactivity and kinetics of various *fac*-$[M(CO)_3]^+$ complexes which already have a bi- or tridentate ligand coordinated to the metal centre. Understanding the stability and reactivity of these new complexes in a controlled chemical environment may allow better understanding of behaviour patterns in a biological environment.

The first thermodynamic and kinetic data were obtained by Salignac *et. al.* (2003)[85] for **water exchange** on *fac*-$[Re(CO)_3(H_2O)_3]^+$ (**ReAq**) as well as NMR studies (^{17}O, ^{13}C, ^{19}F, ^{1}H) on the water substitution of the rhenium complex using a variety of ligands (CH_3CN, Br^-, DMS, TFA, TU, bipy and phen) at 298 K and ambient pressure. An important property of ReAq is the mean residence time of the coordinated water molecule. The water exchange reaction is a convenient measure for the intrinsic lability of the metal ion. The rate for water exchange process on *fac*-$[Re(CO)_3(H_2O)_3]^+$ (ReAq) was found to be $k_{ex} = 6.3(1) \times 10^{-3}$ s^{-1} and on the monohydroxo species $[Re^I(CO)_3(OH)(H_2O)_2]$, $k_{OH} = 27(1)$ s^{-1}. The basic form only contributed significantly to the kinetic exchange at $[H]^+ < 3 \times 10^{-3}$ M. At higher $[H]^+$ concentrations, the kinetic studies are conducted solely by the ReAq cation. Activation parameters for the water exchange process indicate a dissociative interchange mechanism ($\Delta H^{\neq} = 90(3)$ kJ.mol^{-1}, $\Delta S^{\neq} = 14(10)$ J.K^{-1}.mol^{-1}). Other metals in the group 7 transition metal

[85] B. Salignac, P.V. Grundler, S. Cayemittes, U. Frey, R. Scopelliti, A.E. Merbach, *Inorg. Chem.*, 2003, 42, 3516

elements[86] can be compared using the water exchange reaction as they also form tricarbonyl complexes in aqueous solutions, with three labile water molecules and three inert carbonyl molecules.[87] The water exchange rates for complexes of the type *fac*-$[M(CO)_3(H_2O)_3]^+$ (M = Mn^I, Tc^I, Re^I) vary over several orders of magnitude with Mn reactions being the fastest followed by Tc and then Re. The water exchange rate (k_{ex}) for group 7 and 6 tends to decrease when going down the group. From left to right in the periodic row the decrease of the rate is paralleled by a charge increase of these isoelectronic complexes. Complexes[88,89] of $[Ru(H_2O)_6]^{2+}$ and $[Rh(H_2O)_6]^{3+}$ have a similar trend whereby an increase in bond strength can result in the water exchange mechanism changing from I_d to I_a.[90]

Table 2.3: Mechanisms and kinetic data for water exchange reactions for selected aqua complexes.[86, 92]

	k_{ex} (at 298K) (s^{-1})	$\Delta H^{\neq}$ ($kJ.mol^{-1}$)	$\Delta S^{\neq}$ ($J.K^{-1}.mol^{-1}$)	Mechanism	pK_a
$[Cr(CO)_3(H_2O)_3]$[91]	11×10^{4}	50	+20	-	< 8
$[W(CO)_3(H_2O)_3]$[91]	31	58	-22	-	< 4.5
$[Mn(CO)_3(H_2O)_3]^+$[92]	23	72.5	+24.4	I_d	9-10
$[Tc(CO)_3(H_2O)_3]^+$[92]	0.49	78.3	+11.7	I_d	-
$[Re(CO)_3(H_2O)_3]^+$[85]	6.3×10^{-4}	90.3	+14.5	I_d	7.5
$[Re(CO)_3(OH)(H_2O)_2]$[85]	27	-	-	-	-
$[Ru(H_2O)_6]^{2+}$	1.8×10^{-2}	87.8	+16.1	I_d	6-8
$[Ru(CO)_3(H_2O)_3]^{2+}$[93]	10^{-4}-10^{-3}	-	-	-	-0.14
$[Ru(CO)_3(OH)(H_2O)_3]^+$	5.3×10^{-2}	-	-	-	-
$[Rh(H_2O)_6]^{3+}$	2.2×10^{-9}	131	+29	I_a	3.5
$[Ir(H_2O)_6]^{3+}$	1.1×10^{-10}	130.5	+2.1	I_a	4.45

The **water substitution reactions** indicate that the three coordinated H_2O ligands of $[Re(CO)_3(H_2O)_3]^+$ are readily substituted by unidentate ligands (TFA, CH_3CN, TU, DMS and I^-) to form the mono-, bi- and tricomplexes.[85,86,92] In the cases of CH_3CN and DMS each substitution of an aqua ligand could be identified. The three formation rate constants $k_{+/-i}$ (i =

[86] L. Helm, *Coord. Chem. Rev.*, 2008, 252, 2346
[87] R. Alberto, R. Schibli, R. Waibel, U. Abram, A.P. Schubiger, *Coord. Chem. Rev.*, 1999, 192, 901
[88] G. Laurenczy, I. Rapaport, D. Zbinden, A.E. Merbach, *Magn. Reson. Chem.*, 1991, S45
[89] I. Rapaport, L. Helm, A.E. Merbach, P.Bernhard, A. Ludi, *Inorg. Chem.*, 1988, 27, 873
[90] D. De Vito, E. Sidorenkova, F.P. Rotzinger, J. Weber, A.E. Merbach, *Inorg. Chem.*, 2000, 39, 5547
[91] U. Prinz, *Ph.D. Thesis.*, RWTH Aachen, Aachen, Germany, 2000
[92] P.V. Grundler, L. Helm, R. Alberto, A.E. Merbach, *Inorg. Chem.*, 2006, 45, 10378
[93] U.C. Meier, R. Scopelliti, E. Solari, A.E. Merbach, *Inorg. Chem.*, 2000, 39, 3816

1-3, +/- = forward and reverse reaction) and equilibrium constants K_i ($Ki = k_{+i} / k_{-i}$) can be characterised as below:

$$fac\text{-}[M(CO)_3(H_2O)_3]^+ + L \underset{k_{-1}}{\overset{k_1, K_1}{\rightleftharpoons}} fac\text{-}[M(CO)_3(L)(H_2O)_2]^+ + H_2O$$

$$fac\text{-}[M(CO)_3(L)(H_2O)_2]^+ + L \underset{k_{-2}}{\overset{k_2, K_2}{\rightleftharpoons}} fac\text{-}[M(CO)_3(L)_2(H_2O)]^+ + H_2O$$

$$fac\text{-}[M(CO)_3(L)_2(H_2O)]^+ + L \underset{k_{-3}}{\overset{k_3, K_3}{\rightleftharpoons}} fac\text{-}[M(CO)_3(L)_3]^+ + H_2O$$

Kinetic data for the reaction of *fac*-$[M(CO)_3(H_2O)_3]^+$ complexes (M = Mn, Tc, Re) with DMS and acetonitrile is listed in Table 2.4. [85,92] All three complexes are less stable with CH_3CN than DMS, and have a higher affinity for the S-binding DMS than the N-binding CH_3CN. Several complex formations on *fac*-$[Re(CO)_3(H_2O)_3]^+$ with various ligands have been studied, therefore the majority of data is available for this complex (Table 2.5).[85,92,94] Substitution rates are found to be slightly dependant on the nature of the incoming ligand, with the softer S-bonded ligands coordinating faster than the O- and N-bonded ligands to the Re metal centre. Interestingly, the water exchange rate, k_{ex}, is close to the interchange rate constants, k'_i indicating that the rate of complex formation might be limited by the mechanism which breaks the Re-H_2O bond. The interchange dissociative mechanism (I_d) can be defined[95,96] as the mechanism whereby the leaving group has the greatest influence, whereas the I_a mechanism has the highest sensitivity to the nature of the entering group. Activation volumes, $\Delta V^{\neq}$, can throw more light onto the exact mechanism since negative $\Delta V^{\neq}$ are indicative of an associative activation mode and positive $\Delta V^{\neq}$ are indicative for a dissociative mode. Activation volume parameters for the *fac*-$[Re(CO)_3(H_2O)_3]^+$ complex formation reactions range from negative $\Delta V^{\neq}$ values for S-bonded ligands to positive $\Delta V^{\neq}$ value for N-bonded ligands. The mechanism changes from I_d for the harder ligands to I_a for softer ligands, such as DMS (dimethylsulfide) and THT (tetrahydrothiophene) which are better nucleophiles.

---

[94] P.V. Grundler, B. Salignac, S. Cayemittes, R. Alberto, A.E. Merbach, *Inorg. Chem.*, 2004, 43, 865

[95] R.G. Wilkins, *Kinetics and Mechanism of Reactions of Transition Metal Complexes*, 2nd Ed., VCH Publishers, Inc., New York, 2002

[96] C.H. Langford, H.B. Gray, *Ligand Substitution Processes*, W.A. Benjamin Inc., New York, USA, 1965

Table 2.4: **Kinetic and thermodynamic parameters for water substitution on *fac*-$[M(CO)_3(H_2O)_3]^+$ complexes at 298 K.** [92]

	K_I (M^{-1})	k_I (x 10^{-3} M^{-1} s^{-1})	k'_i (x 10^{-3} s^{-1})	$\Delta H_I^{\neq}$ (kJ mol^{-1})	$\Delta S_I^{\neq}$ (J K^{-1} mol^{-1})	$\Delta V_I^{\neq}$ (cm^3 mol^{-1})
fac-$[Mn(CO)_3(H_2O)_3]^+$						
CH_3CN	4.5(2)	1750(400)	29 000	83.9	+41.3	+4.2
DMS	25.2(5)	5340(2000)	89 000	71.2	+8.1	+11.3
H_2O	-	-	23000(4000)	72.5	+24.4	+7.1
fac-$[Tc(CO)_3(H_2O)_3]^+$						
CH_3CN	2.9(1)	39.9(1)	665	77.8	-10.0	-
DMS	14.9(1)	60.8(8)	1010	70.6	-31.1	-
H_2O	-	-	490(50)	78.3	+11.7	+3.8
fac-$[Re(CO)_3(H_2O)_3]^+$						
Pyrazine (Pyz)	237(15)	1.06(5)	17.7	-	-	+5.4
CH_3CN	4.8(5)	0.76(4)	13	98.6	+26.6	-
DMS	8.3(1)	1.18(6)	20	-	+14.5	-12
H_2O	-	-	5.4(2)	90.3		-

Table 2.5: **Kinetic constants for complex formation of *fac*-$[Re(CO)_3(H_2O)_3]^+$ with various ligands at 298 K.** [85, 94]

Atom bonded	**Nitrogen**		**Sulphur**			**Anionic**	
	CH_3CN	**Pyrazine (Pyz)**	**Dimethyl-sulfide (DMS)**	**Tetrahydro-thiophene (THT)**	**Thiourea (TU)**	**CF_3COO^-**	**Br^-**
k_I (x 10^{-3} M^{-1} s^{-1})	0.76	1.06	1.18	1.28	2.49	0.81	1.6
k_{-I} (x 10^{-5} s^{-1})	16	0.45	14.2	3.05	1.6	99	230
k'_i (x 10^{-3} s^{-1})[a]	12.7	17.7	20	21	41.5	2.9	5.8
K_I (M^{-1})	4.8	237	8.3	41	160	0.82	0.7

[a] Water exchange rate, k_{ex} = 6.3 x 10^{-3} s^{-1}

Substitution of the aqua ligands by CO of *fac*-$[Tc(CO)_3(H_2O)_3]^+$ can occur under CO pressure[97] to form the $[Tc(CO)_6]^+$ ion.[98] Upon release of the CO pressure, mono-, bi- and tri-

[97] N. Aebischer, R. Schibli, R. Alberto, A.E. Merbach, *Angew. Chem. Int. Ed.*, 2000, 39, 254
[98] A.W. Ehlers, Y. Ruiz-Morales, E.J. Baerends, T. Ziegler, *Inorg. Chem.*, 1997, 36, 5031

CO substituted complex[99] returns to the initial *fac*-$[Tc(CO)_3(H_2O)_3]^+$ complex at room temperature.

The carbonyls of the *fac*-$[M(CO)_3(H_2O)_3]^+$ are generally considered inert, however a slow exchange with free CO in solution can be observed. The CO exchange rate constant (k_{CO}), determined at two temperatures for *fac*-$[Tc(CO)_3(H_2O)_3]^+$, are k_{CO} = 10.0(2) x 10^{-4} $s^{-1}M^{-1}$ (310 K) and 0.82(1) x 10^{-4} $s^{-1}M^{-1}$ (277 K). The exchange of carbonyls is 2 – 3 orders of magnitude slower than the exchange of water molecules[86] thus confirming the kinetic inertness of the *fac*-$[Tc(CO)_3]$ moiety.

The water substitution on *fac*-$[Re(L,L'\text{-Bid})(CO)_3(H_2O)]^{n+}$ (L,L'-Bid = N-O, N-N', O-O' bidentate ligands, n = -1, 0, +1) have recently been investigated.[100,101,102] The kinetic reactivity of the axial water substitution of these Re(I) tricarbonyl mono-aqua complexes were evaluated with a variety of neutral and monoanionic, incoming mondentate ligands, ranging from halides to pyridines including S and P donor groups. The use of bidentate ligands allows the blockage of two of the reactive aqua sites, thus leaving one site open for substitution. The kinetic studies were interested in the reactivity effects introduced by the various bidentate ligands on the metal centre due to the influence of the steric and electronic properties of the coordinated ligand. The bidentate ligands were specifically chosen by the authors to investigate complexes with varied Bronsted basicities ranging from a positive charge (N-N' ligand) to a neutral charge (O-O' and N-O ligand) as indicated: 1,10-phenantroline (**Phen**), 2,2'-bipyridine (**Bipy**), 2,4-pyridinedicarboxylic acid (**2,4-PicoH_2**), 2,4-Quinolinedicarboxylic acid (**2,4-QuinH_2**), tribromotropolone (**TropBr_3**) and 3-hydroxyflavone (**Flav**), picolinic acid (**Pico**), quinaldic acid (**Quin**).

The substitution of water in the *fac*-$[Re(L,L'\text{-Bid})(CO)_3(H_2O)]^{n+}$ complexes were studied under pseudo first order conditions defined by the following equilibrium:

$$[Re(L,L'\text{-Bid})(CO)_3(H_2O)]^n + [X]^n \underset{k_{-1}}{\overset{k_1,\ K_1}{\rightleftharpoons}} [Re(L,L'\text{-Bid})(CO)_3(X)]^n + [H_2O] \qquad \text{where n = -1, 0, +1}$$

.. Eq. 2.1

[99] R. Alberto, R. Motterlini, *Dalton Trans.*, 2007, 1651
[100] G. Kemp, *Ph.D. Thesis*, University of Johannesburg, Johannesburg, South Africa, 2006
[101] M. Schutte, *M.Sc. Dissertation*, University of the Free State, Bloemfontein, South Africa, 2008
[102] M. Schutte, G. Kemp, H.G. Visser, A. Roodt, *Inorg. Chem.*, 2011, manuscript accepted.

Table 2.6: **Kinetic constants and activation parameters for *fac*-[Re(L,L')(CO)$_3$(H$_2$O)] complexes with different N-O, N-N', O-O' neutral/monoanionic incoming ligands (methanol; 25°C).**

	k_1 (x 10^{-3} M^{-1} s^{-1})	k_{-1} (x 10^{-3} s^{-1})	K_1 (M^{-1})	$\Delta H_1^{\neq}$ (kJ mol^{-1})	$\Delta S_1^{\neq}$ (J K^{-1} mol^{-1})	$\Delta G_1^{\neq}$ (kJ mol^{-1})
N-N' ligand						
***fac*-[Re(Phen)(CO)$_3$(H$_2$O)]$^+$**						
Br$^-$	50(3)	0.59(3)	84(7)			
I$^-$	53(1)	0.7(1)	76(11)	70(1)	-35(3)	80(2)
Py	0.064(3)	0.0058(4)	11(1)			
***m*-MePy**	0.012(1)	0.005(2)	2.4(9)			
***p*-MePy**	0.014(1)	0.0035(1)	4.0(3)			
PTA	7.9(1)	0.11(1)	70(1)			
Metu	13.7(1)	0.011(1)	1245(122)	80(1)	-9(3)	82(2)
***fac*-[Re(Bipy)(CO)$_3$(H$_2$O)]$^+$**						
Br$^-$	42(7)	0.65(2)	60(10)			
I$^-$	49(3)	0.68(1)	70(10)			
Py	0.096(1)	0.0012(1)	80(7)			
***m*-MePy**	0.025(1)	0.008(1)	3.0(4)			
***p*-MePy**	0.028(1)	0.0047(1)	6.0(2)			
PTA	12.3(1)	0.12(2)	100(20)			
Metu	17.3(1)	0.011(1)	1570(140)			
N-O Ligand						
***fac*-[Re(Pico)(CO)$_3$(H$_2$O)]**						
Br$^-$	11.8(1)	0.8(1)	15(2)			
I$^-$	14(1)	0.64(1)	22(2)	77(1)	-19(3)	82(2)
Py	1.6(1)	0.0084(1)	190(10)	84(1)	-16(4)	89(2)
***m*-MePy**	0.11(1)	0.011(1)	10(1)			
***p*-MePy**	1.39(1)	0.066(1)	21.0(4)			
PTA	5(1)	0.004(1)	1.3(4)			
Metu	25.8(2)	0.006(1)	4300(1)	57(1)	-85(3)	
***fac*-[Re(Quin)(CO)$_3$(H$_2$O)]**						
Br$^-$	29.6(3)	0.7(1)	42(6)			
I$^-$	28.0(1)	0.9(1)	31(4)			
Py	3.9(1)	0.02(1)	195(97)			
***p*-MePy**	3.3(1)	0.11(1)	30(3)			
***fac*-[Re(2,4-PicoH)(CO)$_3$(H$_2$O)]**						
Br$^-$	15.7(2)	0.63(8)	25(3)	80.8(6)	-8(2)	83(1)
Py	1.641(8)	0.030(2)	21(1)	84(2)	-19(4)	90(3)
DMAP	3.21(4)	0.11(1)	292(27)	84.3(3)	-10(1)	87(1)
Pz	2.336(9)	0.016(3)	146(27)	83(1)	-18(5)	88(2)
Im	1.44(4)	0.070(5)	21(2)	85.2(7)	-13(2)	89(1)
***fac*-[Re(2,4-QuinH)(CO)$_3$(H$_2$O)]**						
Py	3.31(2)	0.051(7)	65(9)[b]			
DMAP	6.52(9)	0.025(3)	26(3)[c]			
O-O' Ligand						
***fac*-[Re(TropBr$_3$)(CO)$_3$(H$_2$O)]**						
Br$^-$	70.6(4)	4(1)	18(4)	63(6)	-54(19)	79(6)
Py	20.3(7)	1.6(2)	13(2)[d]	53(5)	-102(17)	83(6)
DMAP	34.5(7)	0.26(2)	133(11)[e]	69(4)	-42(12)	82(5)
***fac*-[Re(Flav)(CO)$_3$(H$_2$O)]**						
Br$^-$	7.2(3)x10^3	3.17(9)x10^3	2.5(2)	52(5)	-52(15)	68(6)
Py	1.38(8)x10^3	0.3(1)	4.6(1)x10^3	54(6)	-60(21)	72(6)
DMAP	5.1(2)x10^3	0.16(4)	3.2(8)x10^4	84(4)	51(14)	69(5)

[a] $K_{eq}=K_1=k_1/k_{-1}$; [b] K_{eq}=17(4) M^{-1} from equilibrium determination of Abs. *vs* [Ligand] data; [c] K_{eq} =47(9) M^{-1}; [d] K_{eq} =5(1) M^{-1}; [e] K_{eq} =31(7) M^{-1}; Metu = methyl-thiourea; Py = pyridine, Pz = pyrazole; Im = Imidazole; DMAP = 4-dimethylaminopyridine; *m*-MePy = *m*-methylpyridine; *p*-MePy = *p*-methylpyridine.

A general trend in the equilibrium constants, K_1, of the *fac*-$[Re(L,L'\text{-}Bid)(CO)_3(H_2O)]^{n+}$ complexes can be found in Table 2.6. Approximate one order-of-magnitude for the cationic complexes Phen and Bipy, for the halide complexes occur as compared with the pyridine complexes. Similar stabilities are found in the N-O ligand complexes for the halide and pyridines, but this was inverted for the O-O' bidentate ligands (halide complexes are *ca.* one order-of-magnitude less stable than the pyridine complexes).

The substitution kinetics of the *fac*-$[Re(L,L'\text{-}Bid)(CO)_3(H_2O)]^{n+}$ complexes indicate interesting variations. The N-N' positively charged metal complex has significant affinity for the negatively charged halido ligands indicative of an associative mode of activation, further confirmed by the negative $\Delta S^{\neq}$ values. The substitution reaction with pyridines indicate the influence of steric effects with *m*-MePy reacting 4 – 6 times slower than the unsubstituted pyridine. For N-O neutrally charged metal complexes the Br^- entering ligand is ~ 5 – 7 times faster than for the neutral entering ligands. For O-O' neutrally charged metal complexes, in particularly the Flav complex, illustrates significant labilizing effects. Great care has been taken by Schutte *et al.*[102] to determine whether the *fac*-$[Re(Flav)(CO)_3(H_2O)]$ complex, which has unusually fast substitution rates, has lost the coordinated water in favour of other solvento ligands. The *fac*-$[Re(Flav)(CO)_3(HOCH_3)]$ crystal structure has been isolated from methanol solution only after several weeks, however the aqua-complex *fac*-$[Re(Flav)(CO)_3(H_2O)]$ can be isolated from a methanol solution and the substitution rates of the aqua complex is nearly identical in various solvents (methanol, acetone and water). The rapid substitution rate of this particular complex plays an interesting role when compared to complexes investigated in this study. In general the O-O' donor ligands activate the metal centre substantially more than the N-O bidentate ligands. The N-N' positively charged complexes have slower aqua substitution rates for the neutral entering ligands.

In summary, the substitution kinetics utilizing the [2+1] approach, irrespective of donor atoms or ligand charge, indicate a decrease in the first-order rate constant, k_1, as follows: Br^-, DMAP, Py, Pz, Im. The decrease is consistent with the nucleophilicity of the entering ligand as indicated by the pKa values. Negative $\Delta S^{\neq}$ values similarly support an associative type mechanism for the complexes studied. The significance of this [2+1] study is the labilization of the metal centre by the bidentate ligands and the increased affinity of the Re(I) for hard nucleophiles such as pyridine which suggests the potential use in radiopharmaceuticals for such [2+1] mixed ligand approaches.

2.9 SCHIFF-BASE LIGAND DESIGN

Schiff-base ligands are one of the most widely utilised ligand systems, due their relative ease of formation and great versatility whereby the individual chemical properties (steric and electronic parameters, denticity, donor atoms, chirality, *etc.*) may be readily altered. Stable complexes are readily formed between the reaction of Schiff-bases and most transition metals and therefore have played an important role in the development of coordination chemistry. The potential and versatility of the ligands has caused their integration into a number of interdisciplinary areas such as bioinorganic chemistry, magnetochemistry, photo-physical chemistry and catalysis.[103,104,105,106] The general synthetic method of the Schiff-bases consists of the condensation reaction with a primary amine and a carbonyl precursor such as an aldehyde of ketone. The reaction may be acid catalyzed but it is not always necessary. Water is a product of the reversible reaction and can be removed to ensure high yields. The resulting compound known as a Schiff-base contains an imine or azomethine functionality (C=N). Depending on the intramolecular hydrogen bonding, Schiff-bases may exhibit tautomerism between the phenol-imine and the keto-amine forms O-H···N ↔ O···H-N. Salicylaldimines often give the enol-imine tautomer in solution (O-H···N). [106,107] One of the best known group of Schiff-base ligands are based on *N,N'*-ethylene-bis(salicylideneiminato) [H_2salen or $(sal)_2$en]. These tetradentate O,N,N,O bis-Schiff base ligands have through convention become known as the salenes.[108]

Several transition metal Schiff-base coordinated complexes have been investigated for biological activities. Gold-199 has nuclear properties suitable for radiotherapeutic applications but has not been pursued extensively. Au(III) is difficult to work with at radiotracer level because it is unstable to reduction, however the radiochemistry of Au(III) complexes with tetradentate $(sal)_2$en and $(sal)_2$pn have been investigated.[12,109] The role of superoxide detoxification in normal cells and tissue is performed by the enzyme superoxide

---

[103] R. Hernández-Molina, A. Merderos, *Comprehensive Coordination Chemistry II*, Eds.: J.A. McCleverty, T.J. Meyer, Pergamon Press, Oxford, UK, Vol. 1, 2004
[104] L. Canali, D.C. Sherrington, *Chem. Soc. Rev.*, 1999, 28, 85
[105] E.A. Ison, J.E. Cessarich, N.E. Travia, P.E. Fanwick, M.M. Abu-Omar, *J. Am. Chem. Soc.*, 2007, 129, 1167
[106] É. Tozzo, S. Romera, M.P. dos Santos, M. Muraro, R.H. de A. Santos, L.M. Lião, L. Vizotto, E.R. Dockal, *J. Mol. Struct.*, 2008, 876, 110
[107] F. Arod, M. Gardon, P. Pattison, G. Chapuis, *Acta Cryst.*, 2005, C61, o317
[108] S.S. Jurisson, K. Dancey, M. McPartlin, P.A. Tasker, E. Deutsch, *Inorg. Chem.*, 1984, 23, 4743
[109] S.L. Barnholtz, J.D. Lydon, G. Huang, M. Venkatesh, C.L. Barnes, A.R. Ketring, S.S. Jurisson, *Inorg. Chem.*, 2001, 40, 972

dismutase (SOD).[110] Superoxide is associated with inflammatory processes and neurological disorders. Manganese chelate compounds based on $(sal)_2en$ and 1,4,8,11-tetraazacyclotetradecane ligands have shown considerable promise as SOD mimics.

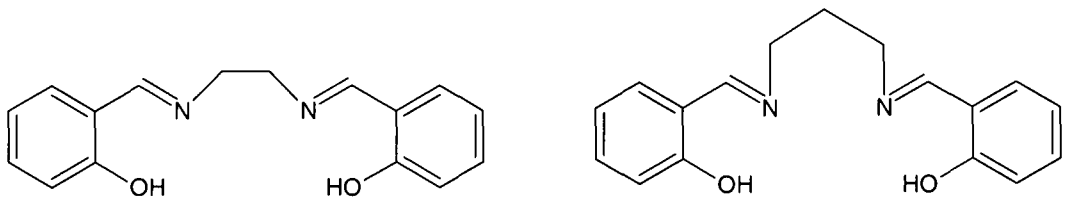

Figure 2.17: Chemical structure of $(sal)_2en$ and $(sal)_2pn$.

Rhenium Schiff-base complexes have been reported since 1979.[111] Numerous Re(V) and (III) Schiff-base species have been synthesised with bi-, tri- and tetra-dentate ligands, some which are soluble in organic and aqueous solvents, that are derivatised from reagents such as salicylaldehyde[112,113,114] or acetylacetone.[115,116,117] A dominant role has been played by the $[M=O]^{3+}$ core in the chemistry of Re(V) and Tc(V) as many radiopharmaceutical agents consist of a multi-dentate ligand coordinated to a metal-oxo core. Schiff-bases provided a convenient manner by which the denticity, steric and electronic properties as well as bonding donor atoms could be tuned and altered.

Over 180 crystal structures incorporating the salicylidene family with rhenium or technetium can be found on the Crystallographic Cambridge Structural Database[118] mostly coordinated to Re(III), (IV), (V), (VII) and Tc(III), (V). To the best of our knowledge the crystal data of

---

[110] N. Farrell, *Comprehensive Coordination Chemistry II*, Eds.: J.A. McCleverty, T.J. Meyer, Pergamon Press, Oxford, UK, Vol. 9, 2004

[111] A.R. Middleton, A.F. Masters, G. Wilkinson, *J. Chem. Soc., Dalton Trans.*, 1979, 542

[112] K.J.C. van Blommel, W. Verboom, H. Kooijman, A.L. Spek, D.N. Reinhoudt, *Inorg. Chem.*, 1998, 37, 4197

[113] K.J.C. van Blommel, W. Verboom, R. Hulst, H. Kooijman, A.L. Spek, D.N. Reinhoudt, *Inorg. Chem.*, 2000, 39, 4099

[114] V.M. Béreau, S.I. Khan, M.M. Abu-Omar, *Inorg. Chem.*, 2001, 40, 6767

[115] P.D. Benny, J.L. Green, H.P. Engelbrecht, C.L. Barnes, S.S. Jurisson, *Inorg. Chem.*, 2005, 44, 2381

[116] A. Sachse, N.C. Mösch-Zanetti, G. Lyashenko, J.W. Wielandt, K. Most, J. Magull, F. Dall' Antonia, A. Pal, R. Herbst-Irmer, *Inorg. Chem.*, 2007, 46, 7129

[117] A. Schröckeneder, P. Traar, G. Raber, J. Baumgartner, F. Belaj, N.C. Mösch-Zanetti, *Inorg. Chem.*, 2009, 48, 11608

[118] Cambridge Structural Database (CSD), Version 5.32, February 2011 update. F.H. Allen, *Acta Cryst.*, 2002, B58, 380

only four Re(I) salicylidene tricarbonyl and three related structures have been reported.[119, 120, 121]

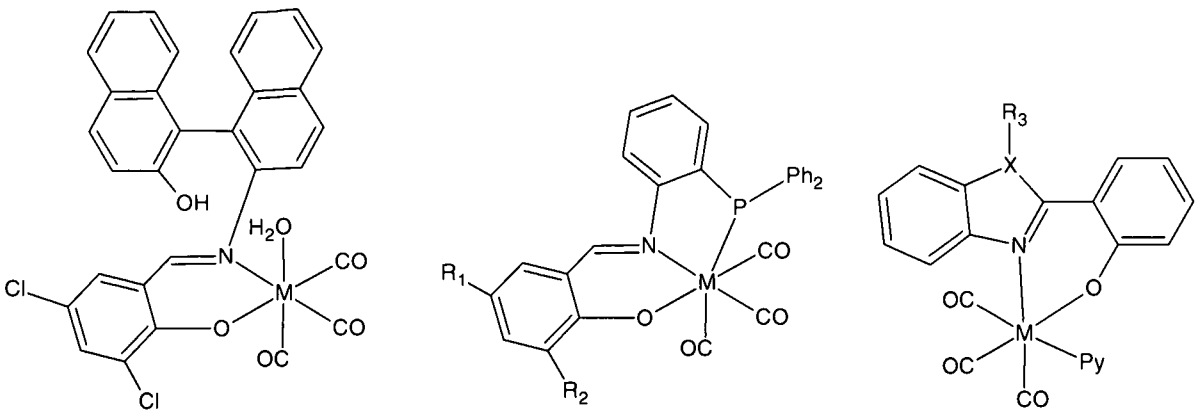

Figure 2.18: **Reported crystal structures of M-salicylidene tricarbonyl complexes (M = Re, Tc; X = N, O, S; R = various substituents).**

Rhenium(I) imine complexes are not common[122,123] and are normally obtained from the reaction of free imine with the appropriate metal starting reagent or via the Schiff-base reaction between the metal coordinated aldehyde/ketone complex and free amine. The formation and stabilization of a rare monosubstitued ArCH=NH imine has been reported with $[Re(CO)_3P_2]^+$ complex.[124] The Schiff-base imine complex in Figure 2.19 was synthesised as part of the development of Tc complexes for early detection and staging of EGFR (epidermal growth factor receptor) positive tumours.[125]

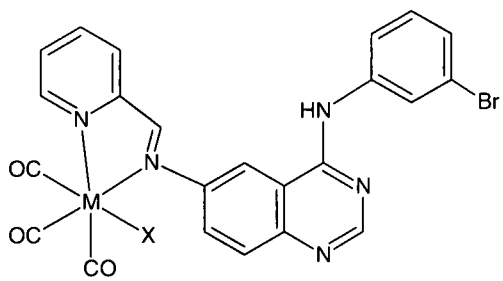

Figure 2.19: **Examples of imine Re/Tc tricarbonyl complexes (M = Re, Tc; X =Br, Cl).**

---

[119] Z.K. Li, Y. Ki, L. Lei, C.M. Che, X.G. Zhou, *Inorg. Chem. Commun.*, 2005, 8, 307
[120] J.W. Faller, G. Mason, J. Par, *J. Organomet. Chem.*, 2001, 626, 191
[121] R. Czerwieniec, A. Kapturkiewicz, R. Anulewicz-Ostrowska, J. Nowacki, *J. Chem. Soc., Dalton Trans.*, 2002, 3434
[122] G. Albertin, S. Antoniutti, A. Bacchi, E. Bordignon, M.T. Giorgi, G. Pelizzi, *Angew. Chem., Int. Ed.*, 2002, 41, 2192
[123] D.A. Knight, M.A. Dewey, G.A. Stark, B.K. Bennet, A.M. Arif, J.A. Gladysz, *Organometallics*, 1993, 12, 4523
[124] G. Albertin, S. Antoniutti, A. Bacchi, A. Celebrin, G. Pelizzi, G. Zanardo, *Dalton Trans.*, 2007, 661
[125] A. Bourkoula, M. Paravatou-Petsotas, A. Papadopoulos, I. Santos, H.J. Pietzsch, E. Livaniou, M. Pelecanou, M. Papadopoulos, I. Pirmettis, *Eur. J. Med. Chem.*, 2009, 44, 4021

Wang *et al.*[126] reported the Schiff-base reaction of *fac*-$[M(CO)_3(H_2O)_3]^+$ whereby Re(I) and Tc(I) coordinated to an aldehyde or ketone was investigated for their reactivity with aliphatic or aromatic amines which would allow a direct labelling of biomolecules with ^{99m}Tc by imine formation. A related method was utilized to synthesize Re/Tc tricarbonyl labelled Lipiodol surrogates for applications in liver cancer imaging and therapy.[127]

2.10 CONCLUSION

A number of limitations have to be considered when designing experimental procedures for radiopharmaceuticals. The restrictions require the synthetic preparations to occur in one step, yield a high purity product (98% yield), preferably 1:1 biomolecule to radionuclide concentration and defined experimental time restrictions dependent of the half-life of the radionuclide. Another important limitation is that any preparation is performed in saline solution (0.9% NaCl in water or buffer).[87] Thus far, the majority of $[M(CO)_3]^+$ complexes synthesized has focused on water as solvent, however the study of various tricarbonyl complexes in other solvents have led to interesting spectroscopic and photochemical results.[128,129,130]

This current study investigated the possible use of Schiff-base ligands in the [2+1] bifunctional labelling approach for *fac*-$[M(CO)_3]^+$ complexes as few salicylidene Re/Tc(I) tricarbonyl complexes have been reported. The coordination chemistry of Schiff-bases has received significant interest due to their ability to form stable complexes with most transition metals.[131] The versatility of the Schiff-bases holds great promise as potential radiopharmaceutical ligands as a variety of mono-, bi- and tri-dentate ligands with varying electronic and steric effects afforded by the substituent on the nitrogen atom can be synthesised.[132] The introduction of a biological active amine on a relatively small backbone holds great promise. This study focused on the effects induced by attaching selected

---

[126] W.Wang, B. Spingler, R. Alberto, *Inorg. Chim. Acta*, 2003, 355, 386
[127] M.M. Saw, P. Kurz, N. Agorastos, T.S.A. Hor, F.X. Sundram, Y.K. Yan, R. Alberto, *Inorg. Chim. Acta.*, 2006, 359, 4087
[128] R. Alberto, A. Egli, U. Abram, K. Hegetschweiler, V. Gramlich, P.A. Schubiger, *J. Chem. Soc. Dalton Trans.*, 1994, 2815
[129] D.H. Gibson, B.A. Sleadd, X. Yin, *Organometallics*, 1998, 17, 2689
[130] R. Czerwieniec, A. Kapturkiewicz, R. Anulewicz-Ostrowska, J. Nowacki, *J. Chem. Soc., Dalton Trans.*, 2001, 2756
[131] G.J.J. Steyn, A. Roodt, I.A. Poletaeva, Y.S. Varshavsky, *J. Organomet. Chem.*, 1997, 536/7, 197
[132] T. Sasamori, T. Matsumoto, N. Takeda, N. Tokitoh, *Organometallics*, 2007, 26, 3621

aromatic, aliphatic or biologically active molecules (such as histamine, carbazole, penicillamine, tryptamine, tyramine and triazole) to a common coordinative backbone and whether the close proximity of the amine tail would stericly prevent the bonding of the salicylidene backbone to the metal centre.

3 SYNTHESIS OF FREE LIGANDS AND METAL COMPOUNDS

3.1 INTRODUCTION

Due to the ideal nuclear properties of ^{99m}Tc, nearly 80% of radiopharmaceuticals currently available in clinical nuclear medicine use compounds containing this radionuclide. The synthesis of Tc(I) and Re(I) complexes *fac*-$[M(CO)_3(H_2O)_3]^+$ (M = ^{99m}Tc, ^{188}Re) by direct reduction of pertechnetate or perrhenate with sodium borohydride in aqueous solution was first reported by Alberto and co-workers.[1,2,3] In *fac*-$[M(CO)_3(H_2O)_3]^+$ complexes, the tricarbonyl core is inert whereas the three water molecules are labile and readily substituted. A variety of bifunctional coupling agents (BFC's) can be used for the radionuclide labelling[4] such as pyridines, pyrazoles, imidazoles, amides, amines, carboxylic acids or combinations thereof as already discussed in Chapter 2. The diverse coordination chemistry of the *fac*-$[M(CO)_3]^+$ core offers a tremendous opportunity for development of new biomolecules. The coordination chemistry of rhenium is similar, but not identical, to the chemistry of technetium due to their periodic relationship. Therefore complexes of similar geometry, size, lipophilicity, dipole moments *etc.* can be formed. As a result, many bifunctional coupling agents developed for Tc can be used to label Re complexes and *vice versa*. It is therefore advantageous to start with rhenium which is non-radioactive in its natural form, whereas technetium does not occur in any stable isotope and requires normal radiation safety procedures during chemical synthesis.

Due to the favourable properties of the *fac*-$[M(CO)_3]^+$ core and promising, yet largely unexplored, O-O' and N-O bidentate ligand systems, it was decided to investigate the

---

[1] R. Alberto, R. Schibli, A. Egli, P.A. Schubiger, U. Abram, T.A. Kaden, *J. Am. Chem. Soc.*, 1998, 120, 7987
[2] R. Alberto, K. Ortner, N. Wheatley, R. Schibli, P.A. Schubiger, *J. Am. Chem. Soc.*, 2001, 123, 3135
[3] R. Schibli, R. Schwarzbach, R. Alberto, K. Ortner, H. Schmalle, C. Dumas, A. Egli, P.A Schubiger, *Bioconjug. Chem.*, 2002, 13, 750
[4] S. Liu, *Advanced Drug Delivery Reviews*, 2008, 60, 1347

coordinative ability of *fac*-$[Re^{I}(CO)_3]^+$ with various bidentate ligands and to establish the kinetic behaviour towards incoming monodenate ligands.

A range of N-O mono-negative bidentate ***SalH*** ligands (2-("T"-iminomethyl)phenol) was synthesized in which the coordinated substituent "T", was systematically changed from one compound to the next. The various substituents consisting of aliphatic and aromatic amines were coordinated to the salicylidene backbone *via* the Schiff-base reaction. The amines were selected for their different electronic and steric parameters. Biological amines were also coordinated to the salicylidene backbone and were selected for the diversity in known biological activity and steric size. The ligands were then coordinated to Re(I) tricarbonyl complexes, to investigate the structural and kinetic effects of the changing substituents of the SalH ligands for the various compounds.

The synthesis of the reagents and final complexes will be discussed in detail in this chapter as well as the characterization of each of the final products using various techniques including nuclear magnetic resonance (NMR), infrared (IR) and ultraviolet-visible spectroscopy (UV-Vis) as well as single crystal X-ray diffraction. Although on the surface, the synthesis of various compounds may appear identical, several important aspects which illustrate the systematic variations in the synthesis are by necessity included, due to their effects on purity, yield, *etc.* of the synthesised compounds.

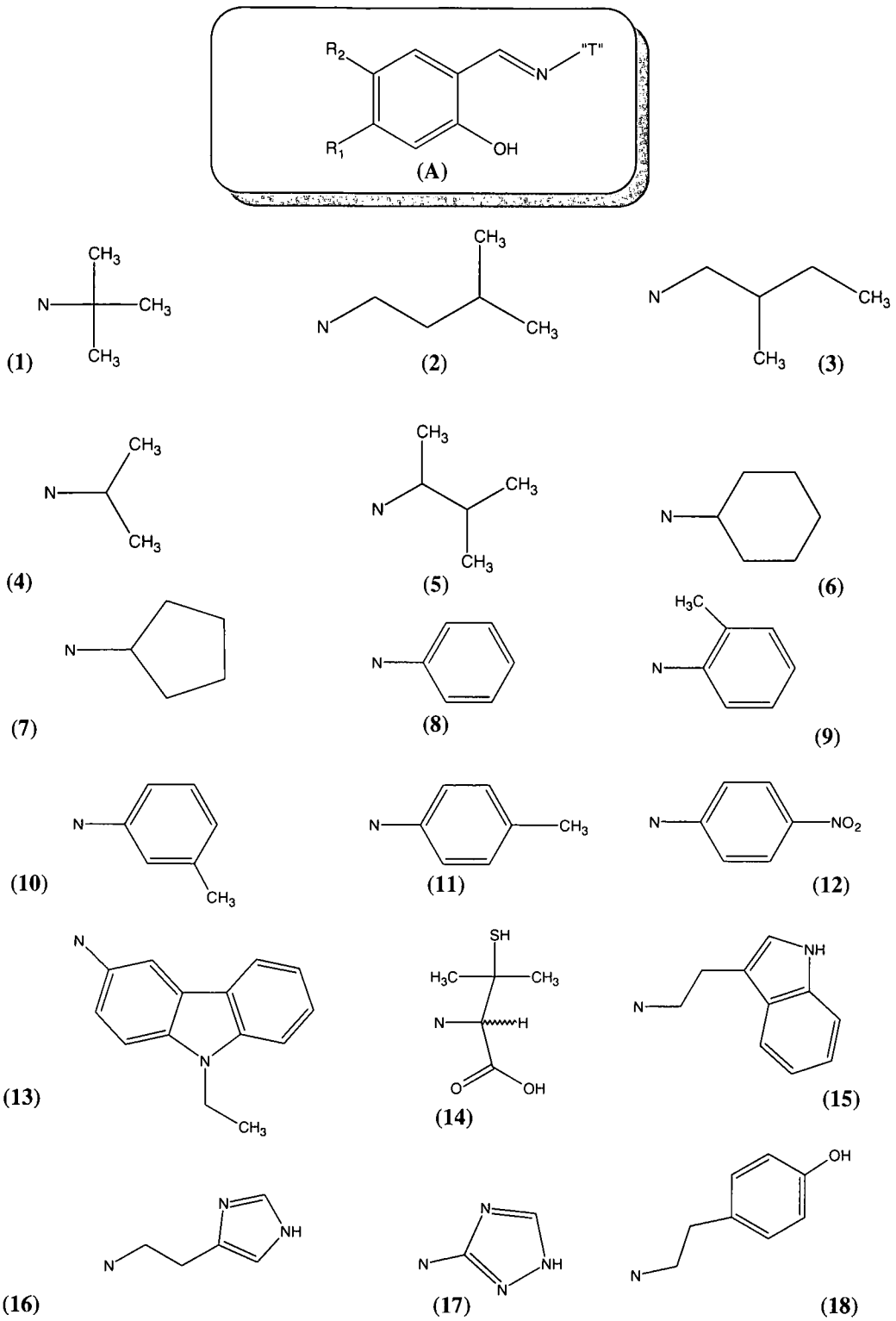

Figure 3.1: **The 2-("T"-iminomethyl)phenol ligands (SalH ligands, T = various substituents) synthesized, characterized and used in this study. (A) SalH-T backbone, T = substituent indicated in 1 – 18, R_1 = H, CH_3, R_2 = H, F. (1) SalH-*t*Bu, (2) SalH-3MeBu, (3) SalH-2MeBu, (4) SalH-*i*Prop, (5), SalH-3Me2Bu, (6) SalH-CyHex, (7) SalH-CyPent, (8) SalH-Ph, (9) SalH-*o*Tol, (10) SalH-*m*Tol, (11) SalH-*p*Tol, (12) SalH-4NitroPh, (13) SalH-Carba, (14) SalH-Pen, (15) SalH-Trypt, (16) SalH-Hist, (17) SalH-Triaz, (18) SalH-Tyra.**

3.2 REAGENTS AND APPARATUS

All reagents used for the synthesis and characterisation were of analytical grade and were purchased from Sigma-Aldrich, unless otherwise stated. Reagents were used as received, without further purification. All solvents used, were of analytical grade and used as received, except where dry conditions were required. In these cases solvents were purified and dried according to literature procedures.[5] Reactions utilizing moisture and oxygen sensitive chemicals / products were performed under argon atmosphere using standard anaerobic conditions. Rhenium pentacarbonyl bromide was purchased from Strem Chemicals, Newburyport (US). *fac*-$[NEt_4]_2[ReBr_3(CO)_3]$ (**ReAA**) was synthesised as described by Alberto *et al.* (1996).[6] The ^{13}C and ^{1}H FT-NMR spectra of the ligand and rhenium compounds were recorded at 150.96 and 600.28 MHz respectively on a Bruker AXS 600 MHz or on a Bruker AXS 300 MHz (75.48 and 300.13 MHz respectively) at 25 °C in CD_3OD (3.31 ppm), C_3H_6O (2.05 ppm) and $CDCl_3$ (7.26 ppm); positive shifts are downfield. All chemical shifts are reported in ppm and coupling constants in Hz. Infrared spectra were recorded on a Bruker Tensor 27 Standard System spectrophotometer with a laser range of 4000 – 370 cm^{-1}, equipped with a temperature cell regulator, accurate within 0.3 °C. Solid samples were analyzed as KBr pellets and liquid samples in methanol solution in a NaCl liquid cell. All data were recorded at room temperature. UV-Vis spectra were collected on a Varian Cary 50 Conc. UV-Visible Spectrophotometer, equipped with a Julabo F12-mV temperature cell regulator (accurate within 0.1 °C) in a 1.000 ± 0.001 cm quartz cuvette cell.

3.3 SYNTHETIC PROCEDURES

The synthesis of ligands and rhenium compounds including the starting reagent *fac*-$[NEt_4]_2[ReBr_3(CO)_3]$ (**ReAA**), were performed under Schlenk conditions to ensure the highest possible yields.

[5] D.D. Perrin, W.L.F. Armarego, *Purification of Laboratory Chemicals*, 3rd Ed., Pergamon Press, 1988
[6] R. Alberto, R. Schibli, P.A. Schubiger, *Polyhedron*, 1996, 15, 1079

3.3.1 Synthesis of SalH ligands

3.3.1.1 General SalH-"T" synthesis

The general synthesis of the SalH ligands are as follows unless otherwise stated. The respective amine was dissolved in methanol and added dropwise to the chosen aldehyde / ketone (1 : 1 mol equivalents) dissolved in methanol. The mixture was refluxed to 80 °C for 3 h. The solvent was carefully removed under vacuum ensuring that the reaction mixture remained at room temperature, as the product is often volatile.

3.3.1.2 2-(*m*-Tolyliminomethyl)phenol – SalH-*m*Tol

The title compound, SalH-*m*Tol, was synthesised according to the procedure described above in § 3.3.1.1 using salicylaldehyde (1.705 g, 1.396 x 10^{-2} mol) and *m*-toluidine (1.507 g, 1.406 x 10^{-2} mol) dissolved in methanol. Anhydrous $MgSO_4$ was added and the reaction was stirred at 80 °C for 3 h. The $MgSO_4$ was filtered and the solvent removed under reduced pressure. The yellow oil product was dissolved in acetone and crystals suitable for X-ray diffraction were obtained by slow evaporation at 0 °C. The title complex[7] crystallized after 2 weeks. (Yield: 2.791 g, 94.6 %).

^{1}H NMR (300 MHz, $CDCl_3$) δ 13.35 (s, 1H, OH), 8.64 (s, 1H, HC=N), 7.32 (m, 3H, Ar), 6.97 (m, 5H, Ar), 2.44 (s, 3H, CH_3). ^{13}C NMR (300 MHz, $CDCl_3$) δ162.47 (C1), 161.25, 148.51, 139.36, 133.10, 132.31, 129.28, 127.76, 122.02, 119.34, 119.08, 118.19, 117.30 (Ar), 21.47 (CH_3).

3.3.1.3 2-(3-Methylbutyliminomethyl)phenol – SalH-3MeBu

The title compound,[8] SalH-3MeBu, was synthesised according to the procedure described in § 3.3.1.1 using salicylaldehyde (1.40 g, 1.15 x 10^{-2} mol), 3-methylbutylamine (1.00 g, 1.40 x 10^{-2} mol) and 3g of anhydrous $MgSO_4$. The reaction was heated to 80 °C and refluxed for 3 h. The $MgSO_4$ was filtered and solvent removed under reduced pressure to yield the yellow oil product. (Yield: 1.611 g, 73.5%).

---

[7] A. Brink, A. Roodt, H.G. Visser, *Acta Cryst.*, 2009, E65, o3175
[8] A. Brink, H.G. Visser, A. Roodt, *J. Coord. Chem.*, 2011, 64, 122

^{1}H NMR (600 MHz, acetone-d_6) δ 8.53 (s, 1H, HC=N), 7.37 (m, 1H, Ar), 7.31 (m, 1H, Ar), 6.87 (m, 2H, Ar) 3.65 (dt, 2H, J = 7.2, 1.3 Hz), 1.72 (m, 1H), 1.58 (q, 2H, J = 7.2 Hz), 0.96 (d, 6H, J = 6.5 Hz). ^{13}C NMR (600 MHz, acetone-d_6) δ 165.43 (C1), 161.25, 131.90, 131.41, 119.10, 118.32, 116.50 (Ar), 57.28, 39.82, 25.69, 21.86 (C24, C25).

3.3.1.4 2-(*tert*-Butyliminomethyl)phenol – SalH-*t*Bu

The title compound, SalH-*t*Bu, was synthesised according to procedure described in § 3.3.1.1 using *tert*-butyl amine (1.002 g, 1.370 x 10^{-2} mol), salicylaldehyde (1.686g, 1.381 x 10^{-2} mol) dissolved in ethanol. The reaction was heated to 80 °C for 3 h. Yellow solution was cooled and solvent removed under reduced pressure to yield a bright yellow oil. (Yield: 2.014 g, 82.3 %).

^{1}H NMR (600 MHz, acetone-d_6) δ 14.05 (s, 1H, OH), 8.55 (s, 1H, HC=N), 7.40 (dd, 1H, J = 1.7, 7.9 Hz), 7.29 (m, 1H, Ar), 6.87 (m, 2H, Ar), 1.34 (s, 9H). ^{13}C NMR (600 MHz, acetone-d_6) δ 162.45 (C1), 161.57, 132.62, 132.53, 120.06, 118.93, 117.45 (Ar), 57.57, 29.79.

3.3.1.5 2-(4-Nitrophenyliminomethyl)phenol – SalH-4NitroPh

The ligand,[9] SalH-4NitroPh, was obtained according to the procedure described for general ligand synthesis, § 3.3.1.1 using 4-nitroaniline (0.5664 g, 4.101 x 10^{-3} mol) and salicylaldehyde (0.5017 g, 4.108 x 10^{-3} mol) at 75 °C for 3 h. Orange crystals were obtained from recrystallizing in acetone. (Yield: 0.7738 g, 77.9 %).

^{1}H NMR (600 MHz, acetone-d_6) δ 12.61 (s, 1H, OH), 9.00 (d, 1H, HC=N, J = 5.2 Hz), 8.35 (m, 2H, Ar), 7.66 (m, 3H, Ar), 7.49 (m, 1H, Ar), 7.02 (m, 2H, Ar). ^{13}C NMR (600 MHz, acetone-d_6) δ 166.90 (d, C1, J = 8.2 Hz), 161.36, 161.03, 154.50, 154.39, 146.18, 134.27 (d, J = 2.8 Hz), 133.59 (d, J = 4.3 Hz), 125.00, 122.39, 119.40 (d, J = 8.9 Hz), 119.14, 116.98 (d, J = 15.3 Hz).

3.3.1.6 2-(Cyclohexyliminomethyl)phenol – SalH-CyHex

The title compound, SalH-CyHex, was obtained according to the procedure described in § 3.3.1.1, using cyclohexylamine (1.510 g, 1.523 x 10^{-2} mol) and salicylaldehyde (1.844 g,

[9] J. Burgess, J. Fawcett, D.R. Russell, S.R. Gilani, V. Palma, *Acta Cryst.*, 1999, C55, 1707

1.510 x 10^{-2} mol). The reaction was stirred at 87 °C for 2.5 h. Product formed a yellow oil. (Yield: 2.931 g, 95.5 %).

^{1}H NMR (300 MHz, $CDCl_3$) δ 13.82 (s, 1H, OH), 8.38 (s, 1H, HC=N), 7.28 (m, 2H, Ar), 6.97 (d, 1H, *J* = 8.3 Hz, Ar), 6.88 (t, 1H, *J* = 7.4 Hz, Ar), 3.26 (m, 1H, C21), 1.86 – 1.27 (m, 10H, Cy). ^{13}C NMR (300 MHz, $CDCl_3$) δ 162.28 (C1), 161.58, 131.99, 131.11, 118.94, 118.32, 117.08 (Ar), 67.39 (CH, C21), 34.32, 25.56, 24.38 (Cy).

3.3.1.7 2-(Phenyliminomethyl)phenol – SalH-Ph

The ligand,[10] SalH-Ph, was synthesised according to procedure described in § 3.3.1.1, using aniline (0.3813 g, 4.094 x 10^{-3} mol) and salicylaldehyde (0.500 g, 4.094 x 10^{-3} mol). The product was obtained as a yellow oil which crystallized after 2 days. (Yield: 0.7180 g, 88.9 %).

^{1}H NMR (600 MHz, acetone-d_6) δ 13.18 (s, 1H, OH), 8.91 (s, 1H, HC=N), 7.60 (d, 1H, *J* = 7.7 Hz, Ar), 7.47 (t, 2H, *J* = 7.7 Hz, Ar), 7.41 (m, 3H, Ar), 7.32 (m, 1H, Ar), 6.97 (m, 2H, Ar). ^{13}C NMR (600 MHz, acetone-d_6) δ 164.72 (C1), 162.08, 161.71, 149.44, 134.03, 133.74, 130.33, 127.81, 122.17, 120.30, 119.88, 117.65, 117.55.

3.3.1.8 2-(*o*-Tolyliminomethyl)phenol – SalH-*o*Tol

The title compound, SalH-*o*Tol, was synthesised according to the procedure described in § 3.3.1.1, using 2-methylaniline (0.439 g, 4.094 x 10^{-3} mol) and salicylaldehyde (0.500 g, 4.094 x 10^{-3} mol). The product was obtained as a yellow oil which crystallized after 2 days. (Yield: 0.7037 g, 81.4 %).

^{1}H NMR (600 MHz, acetone-d_6) δ 13.35 (s, 1H, OH), 8.83 (s, 1H, HC=N), 7.61 (m, 1H, Ar), 7.43 (m, 1H, Ar), 7.31 (m, 3H, Ar), 7.22 (m, 1H, Ar), 6.97 (m, 2H, Ar), 2.38 (s, 3H, CH_3). ^{13}C NMR (600 MHz, acetone-d_6) δ 164.20 (C1), 162.17, 148.37, 133.99, 133.65, 132.86, 131.45, 128.04, 127.74, 120.44, 119.84, 118.81, 117.64 (Ar), 18.23 (CH_3).

[10] F. Arod, M. Gardon, P. Pattison, G. Chapuis, *Acta Cryst.*, 2005, C61, o317

3.3.1.9 2-(*p*-Tolyliminomethyl)phenol – SalH-*p*Tol

The title compound,[11] SalH-*p*Tol, was synthesised according to procedure described in § 3.3.1.1, using *p*-toluidine (0.8778 g, 8.192 x 10^{-3} mol) and salicylaldehyde (1.000 g, 0.873 ml, 8.192 x 10^{-3} mol). The reaction immediately turned yellow and a precipitate formed upon addition of the amine. The reaction was stirred at 70 °C for 3 h. The excess solvent was removed and the yellow crystalline product was washed with minimal acetone. (Yield: 1.962 g, 97.8 %).

^{1}H NMR (600 MHz, acetone-d_6) δ 13.26 (s, 1H, OH), 8.89 (s, 1H, HC=N), 7.57 (dd, 1H, J = 1.7, 7.6 Hz, Ar) 7.40 (m, 1H, Ar), 7.33 (m, 2H, Ar), 7.27 (m, 2H, Ar), 6.96 (m, 2H, Ar), 2.36 (s, 3H, CH_3). ^{13}C NMR (600 MHz, acetone-d_6) δ 163.66 (C1), 162.05, 137.73, 133.79, 133.76, 133.58, 133.54, 130.86, 122.02, 120.37, 119.89, 119.80, 117.61 (Ar), 21.00 (CH_3).

3.3.1.10 2-(2-Chlorophenyliminomethyl)phenol – SalH-2ClPh

The title compound,[12] SalH-2ClPh, was synthesised according to the procedure described in § 3.3.1.1 using 2-chloroaniline (1.045 g, 8.192 x 10^{-3} mol) and salicylaldehyde (1.000 g, 0.873 ml, 8.192 x 10^{-3} mol) in methanol. The yellow coloured reaction was stirred at 75 °C for 3 h. The product was recrystallized from acetone. (Yield: 1.862 g, 98.1 %).

^{1}H NMR (600 MHz, acetone-d_6) δ 13.13 (s, 1H, OH), 8.96 (s, 1H, HC=N), 7.62 (m, 1H, Ar), 7.57 (m, 2H, Ar), 7.45 (m, 2H, Ar), 7.33 (m, 1H, Ar), 7.00 (m, 2H, Ar). ^{13}C NMR (600 MHz, acetone-d_6) δ 165.59 (C1), 162.30, 146.19, 134.62, 134.03, 130.86, 129.94, 129.16, 128.97, 120.63, 120.20, 199.97, 117.86 (Ar).

3.3.1.11 2-(9-Ethylcarbazol-3-yliminomethyl)phenol – SalH-Carba

The title compound, SalH-Carba, was synthesised according to the procedure described in § 3.3.1.1, using 3-amino-9-ethylcarbazole (0.862 g, 4.094 x 10^{-3} mol) and salicylaldehyde (0.500 g, 0.873 ml, 4.094 x 10^{-3} mol) under Schlenck conditions. The reaction was stirred at 80 °C for 3.5 h. The product was washed with cold methanol and filtered. Yellow plate crystals, unsuitable for X-ray diffraction were obtained from acetone. (Yield: 0.9198 g, 71.5 %).

---

[11] S.M. Aldoshin, M.I. Knyazhaniskii, Ya.R. Tymyanskii, L.O. Atovmyan, O.A. D'yachenko, *Khim. Fiz. (Russ) (Sov. J. Chem. Phys.)*, 1982, 1015

[12] J. Bregman, L. Leiserowitz, K. Osaki, *J. Chem. Soc.*, 1964, 2086

^{1}H NMR (300 MHz, $CDCl_3$) δ 13.74 (s, 1H, OH), 8.81 (s, 1H, HC=N), 8.15 (d, 1H, J = 7.8 Hz, Ar), 8.09 (s, 1H, Ar), 7.53-7.26 (m, 7H, Ar), 7.08 (d, 1H, J = 8.3 Hz, Ar), 6.97 (t, 1H, J = 7.4 Hz, Ar), 4.40 (q, 2H, CH_2, J = 7.0 Hz), 1.48 (t, 3H, CH_3, J = 7.0 Hz). ^{13}C NMR (300 MHz, $CDCl_3$) δ 161.14 (C1), 159.85, 140.67, 140.19, 139.18, 132.49, 131.96, 126.23, 123.65, 122.99, 120.72, 119.82, 119.76, 119.22, 119.01, 117.22, 112.72, 109.03, 108.88 (Ar), 37.78 (CH_2), 13.92 (CH_3).

3.3.1.12 2-(Isopropyliminomethyl)phenol – SalH-*i*Prop

The title compound, SalH-*i*Prop, was obtained according to procedure described in § 3.3.1.1 using isopropylamine (0.4846 g, 8.198 x 10^{-3} mol) and salicylaldehyde (1.002 g, 8.205 x 10^{-3} mol) in methanol. The product was obtained as a volatile yellow oil. (Yield: 1.127 g, 84.2 %).
^{1}H NMR (300 MHz, $CDCl_3$) δ 8.36 (s, 1H, HC=N), 7.28 (m, 2H, Ar), 6.95 (d, 1H, J =8.1 Hz, Ar), 6.87 (t, 1H, J = 7.4 Hz, Ar), 6.56 (m, 1H, H21), 1.32 (s, 3H, CH_3), 1.30 (s, 3H, CH_3). ^{13}C NMR (300 MHz, $CDCl_3$) δ 162.11 (C1), 161.45, 132.09, 131.17, 118.87, 118.47, 117.10 (Ar), 60.24 (C21), 24.26 (C22, C23, CH_3).

3.3.2 Synthesis of Substituted Ligands

3.3.2.1 5-Methyl-2-(1,2-dimethylpropyliminomethyl)phenol – 5Me-SalH-3Me2Bu

The title compound, 5Me-SalH-3Me2Bu, was synthesised according to the procedure described in § 3.3.1.1 using 3-methyl-2-butylamine (0.6410 g, 7.354 x 10^{-3} mol) and 2-hydroxy-4-methylbenzaldehyde (1.004 g, 7.374 x 10^{-3} mol) in methanol. The reaction was stirred at 80 °C for 4 h. The product was obtained as a volatile yellow oil. (Yield: 1.349 g, 89.1 %).
^{1}H NMR (300 MHz, $CDCl_3$) δ 8.19 (s, 1H, HC=N), 7.07 (d, 1H, J = 7.8 Hz, Ar), 6.71 (s, 1H, Ar), 6.61 (d, 1H, J = 7.8 Hz, Ar), 3.37 (s, 3H, CH_3), 2.27 (s, 3H, CH_3), 1.75 (m, 1H, CH), 1.49 (m, 1H, CH), 1.01 (s, 3H, CH_3), 0.99 (s, 3H, CH_3). ^{13}C NMR (300 MHz, $CDCl_3$) δ 162.47 (C1), 162.13, 143.15, 131.00, 119.41, 117.61, 116.28 (Ar), 52.34, 34.71, 34.02, 21.80, 19.65, 18.32.

3.3.2.2 5-Methyl-2-(cyclohexyliminomethyl)phenol – 5Me-SalH-CyHex

The title compound, 5Me-SalH-CyHex, was synthesised according to the procedure described in § 3.3.1.1, using cyclohexylamine (0.3642 g, 3.672 x 10^{-3} mol) and 2-hydroxy-4-methylbenzaldehyde (0.500 g, 3.672 x 10^{-3} mol) in methanol. The product was obtained as a yellow powder which was washed with cold methanol and dried. (Yield: 0.6583 g, 82.5 %).

^{1}H NMR (300 MHz, $CDCl_3$) δ 8.35 (s, 1H, HC=N), 7.17 (d, 1H, *J* = 7.8 Hz, Ar), 6.79 (s, 1H, Ar), 6.69 (d, 1H, *J* = 7.8 Hz, Ar), 3.25 (bs, 1H), 2.39 (s, 3H, CH_3), 1.42-1.75(m, 10H, CyHex). ^{13}C NMR (300 MHz, $CDCl_3$) δ 164.12 (C1), 161.98, 143.92, 131.15, 118.98, 118.17, 116.34 (Ar), 50.47 (C21), 34.03 (C141, CH_3), 32.69, 25.32, 24.48, 24.22, 21.67 (CyHex).

3.3.2.3 5-Methyl-2-(2-methylbutyliminomethyl)phenol – 5Me-SalH-2MeBu

The title compound, 5Me-SalH-2MeBu, was synthesised according to the procedure described in § 3.3.1.1, using 2-methylbutylamine (0.640 g, 7.345 x 10^{-3} mol) and 2-hydroxy-4-methylbenzaldehyde (1.000 g, 7.345 x 10^{-3} mol) in methanol. The product was obtained as a yellow oil. (Yield: 1.316 g, 87.3%).

^{1}H NMR (300 MHz, $CDCl_3$) δ 8.26 (s, 1H, HC=N), 7.13 (d, 1H, *J* = 7.8 Hz, Ar), 6.79 (s, 1H, Ar), 6.67 (d, 1H, *J* = 7.8 Hz, Ar), 3.54-3.35 (m, 2H), 2.32 (s, 3H, CH_3), 1.73 (m, 1H), 1.47 (m, 1H), 1.23 (m, 1H), 0.96 (s, 3H, CH_3), 0.93 (s, 3H, CH_3). ^{13}C NMR (300 MHz, $CDCl_3$) δ 164.56 (C1), 161.94, 143.40, 131.13, 119.60, 117.61, 116.32 (Ar), 65.13 (C21), 36.01 (C141, CH_3), 27.31, 21.90 (CH_2), 17.67, 11.47 (CH_3).

3.3.2.4 5-Methyl-2-(3-methylbutyliminomethyl)phenol – 5Me-SalH-3MeBu

The title compound, 5Me-SalH-3MeBu, was synthesised according to the procedure described in § 3.3.1.1, using 3-methylbutylamine (0.640 g, 7.345 x 10^{-3} mol) and 2-hydroxy-4-methylbenzaldehyde (1.000 g, 7.345 x 10^{-3} mol) in methanol. The product was obtained as a yellow oil. (Yield: 1.359 g, 90.1 %).

^{1}H NMR (300 MHz, $CDCl_3$) δ 8.28 (s, 1H, HC=N), 7.11 (d, 1H, *J* = 7.8 Hz, Ar), 6.78 (s, 1H, Ar), 6.66 (d, 1H, *J* = 7.8 Hz, Ar), 3.58 (t, 2H, *J* = 7.0 Hz), 2.32 (s, 3H, CH_3), 1.71 (m, 1H), 1.56 (m, 2H), 0.95 (s, 3H, CH_3), 0.93 (s, 3H, CH_3). ^{13}C NMR (300 MHz, $CDCl_3$) δ 164.16

(C1), 161.76, 143.31, 131.02, 119.56, 117.54, 116.29 (Ar), 57.18 (C21, CH_2), 39.84 (C141, CH_3), 30.96 (CH), 25.77 (CH_2), 22.49, 21.84 (CH_3).

3.3.2.5 5-Methyl-2-(*m*-tolyliminomethyl)phenol – 5Me-SalH-*m*Tol

The title compound, 5Me-SalH-*m*Tol, was synthesised according to the procedure described in § 3.3.1.1, using *m*-toluidine (0.789 g, 7.364 x 10^{-3} mol) and 2-hydroxy-4-methylbenzaldehyde (1.005 g, 7.383 x 10^{-3} mol) in methanol. The reaction was stirred at 80 °C for 4.5 h. The product was obtained as an orange powder and recrystallized from acetone. (Yield: 1.431 g, 86.3 %).

^{1}H NMR (300 MHz, $CDCl_3$) δ 8.58 (s, 1H, HC=N), 7.29 (m, 1H, Ar), 7.09 (bs, 3H, Ar), 6.84 (s, 1H, Ar), 6.74 (d, 1H, J = 7.8 Hz, Ar), 2.40 (s, 3H, CH_3), 2.37 (s, 3H, CH_3). ^{13}C NMR (300 MHz, $CDCl_3$) δ 162.14 (C1), 161.20, 148.47, 144.38, 139.36, 132.14, 129.24, 127.55, 121.92, 120.37, 118.12, 117.59, 116.97 (Ar), 21.96, 21.43 (CH_3).

3.3.2.6 2-[(4-Hydroxyphenyl)iminomethyl]-5-methylphenol - 5Me-SalH-4OHPh

The title compound, 5Me-SalH-4OHPh, was synthesised according to the procedure described in § 3.3.1.1, using 4-hydroxyaniline (0.803 g, 7.354 x 10^{-3} mol) and 2-hydroxy-4-methylbenzaldehyde (1.003 g, 7.367 x 10^{-3} mol) in methanol. The reaction was stirred at 80 °C for 4.5 h. The product was obtained as an orange powder and recrystallized from acetone. (Yield: 1.313 g, 78.6 %).

^{1}H NMR (600 MHz, acetone-d_6) δ 13.36 (bs, 1H, OH), 8.80 (s, 1H, HC=N), 8.58 (bs, 1H, OH), 7.40 (d, 1H, J = 7.2 Hz, Ar), 7.30 (m, 2H, Ar), 6.91 (m, 2H, Ar), 6.78 (s, 1H, Ar), 6.76 (s, 1H, Ar), 2.33 (s, 3H, CH_3). ^{13}C NMR (600 MHz, acetone-d_6) δ 161.90 (C1), 161.24, 157.63, 144.25, 141.34, 133.07, 123.29 (2 x CH), 120.83, 118.19, 117.83, 116.84 (2 x CH), 21.77 (CH_3).

3.3.2.7 5-Methyl-2-(isopropyliminomethyl)phenol – 5Me-SalH-*i*Prop

The title compound, 5Me-SalH-*i*Prop, was synthesised according to the procedure described in § 3.3.1.1, using isopropylamine (0.455 g, 7.699 x 10^{-3} mol) and 2-hydroxy-4-methylbenzaldehyde (1.007 g, 7.396 x 10^{-3} mol) in methanol. The reaction was stirred at 80

°C for 4.5 h. The product was obtained as a yellow powder and recrystallized from acetone. (Yield: 1.202 g, 91.7 %).

^{1}H NMR (300 MHz, $CDCl_3$) δ 8.27 (s, 1H, HC=N), 7.10 (d, 1H, J = 7.8 Hz, Ar), 6.77 (s, 1H, Ar), 6.66 (d, 1H, J = 7.8 Hz, Ar), 3.50 (m, 1H, CH), 2.33 (s, 3H, CH_3), 1.28 (d, 3H, J = 6.4 Hz, CH_3). ^{13}C NMR (300 MHz, $CDCl_3$) δ 161.82 (C1), 161.64, 143.08, 131.04, 119.60, 117.54, 116.46 (Ar), 59.82 (CH), 24.30, 21.89 (CH_3).

3.3.2.8 5-Methyl-2-(cyclopentyliminomethyl)phenol – 5Me-SalH-CyPent

The title compound, 5Me-SalH-CyPent, was synthesised according to the procedure described in § 3.3.1.1, using cyclopentylamine (0.627 g, 7.363 x 10^{-3} mol) and 2-hydroxy-4-methylbenzaldehyde (1.008 g, 7.389 x 10^{-3} mol) in methanol. The product was obtained as a yellow crystalline powder and recrystallized from acetone. (Yield: 1.098 g, 73.1 %).

^{1}H NMR (300 MHz, $CDCl_3$) δ 8.25 (s, 1H, HC=N), 7.06 (d, 1H, J = 7.8 Hz, Ar), 6.72 (s, 1H, Ar), 6.62 (d, 1H, J = 7.8 Hz, Ar), 2.29 (s, 3H, CH_3), 1.92-1.66 (m, 9H, C_5H_9). ^{13}C NMR (300 MHz, $CDCl_3$) δ 162.05 (bs), 143.25, 130.99, 119.54, 117.63, 116.28 (Ar), 69.49 (CH), 34.77, 24.37 (CH_2), 21.84 (CH_3).

3.3.2.9 2-(2-Hydroxy-4-methylphenylmethylene)amino-3-mercapto-3-methylbutanoic acid – 5Me-SalH-Pen

The title compound, 5Me-SalH-Pen, was synthesised according to the procedure described in § 3.3.1.1, using *D*-penicillamine (1.098 g, 7.359 x 10^{-3} mol) and 2-hydroxy-4-methylbenzaldehyde (1.004 g, 7.374 x 10^{-3} mol) in methanol under Schlenk conditions. The reaction was stirred at 80 °C for 4 h. The product was washed with cold methanol to yield a white crystalline powder. The product was recrystallized from acetone. (Yield: 2.365 g, 88.9 %, 50 % racemic mixture indicated by NMR).

^{1}H NMR (600 MHz, acetone-d_6) δ 7.13 (d, 1H, J = 7.9 Hz, Ar), 7.12 (d, 1H, J = 7.9 Hz, Ar), 6.66 (s, 1H, HC=N), 6.55 (s, 1H, HC=N), 6.62 (d, 1H, J = 7.9 Hz, Ar), 6.59 (d, 1H, J = 7.9 Hz, Ar), 6.07 (s, 1H, Ar), 5.83 (s, 1H, Ar), 3.78 (s, 1H, CH), 3.76 (s, 1H, CH), 3.31 (s, 2H, 2x SH), 2.23 (s, 3H, CH_3), 2.22 (s, 3H, CH_3), 1.69 (s, 3H, CH_3), 1.61 (s, 3H, CH_3), 1.42 (s, 3H, CH_3), 1.38 (s, 3H, CH_3). ^{13}C NMR (600 MHz, acetone-d_6) δ 170.84, 170.71, 156.73, 156.47, 140.03, 139.05, 129.05, 128.86, 124.13, 121.83, 120.91, 120.54, 117.66, 117.48 (Ar), 74.48, 73.05, 66.47, 66.03, 58.31, 57.85, 30.37, 28.72, 28.41, 27.23, 21.15, 21.04.

3.3.2.10 2-[(2-Imidazol-4-yl)ethyliminomethyl]-5-methylphenol - 5Me-SalH-Hist

The title compound, 5Me-SalH-Hist, was synthesized according to the procedure described in § 3.3.1.1, using 2-hydroxy-4-methyl benzaldehyde (0.5 g, 3.672 x 10^{-3} mol) and histamine (0.408 g, 3.672 x 10^{-3} mol) dissolved in methanol under Schlenk conditions. The product was dissolved in warm acetone, after which the solvent was partially removed to yield a yellow precipitate. Crystals suitable for X-ray diffraction were grown from methanol at 5 °C. (Yield: 0.808 g, 96.0 %).

^{1}H NMR (600 MHz, acetone-d_6) δ 8.38 (s, 1H, HC=N), 7.53 (s, 1H, Ar), 7.20 (d, 1H, J = 7.9 Hz, Ar), 6.84 (s, 1H, Ar), 6.69 (s, 1H, Ar), 6.68 (s, 1H, Ar), 3.87 (t, 2H, J = 7.0 Hz), 2.94 (t, 2H, J = 7.0 Hz), 2.29 (s, 3H, CH_3). ^{13}C NMR (600 MHz, acetone-d_6) δ 166.31, 162.21, 143.54, 135.50, 132.23, 121.98, 120.24, 117.75, 117.65 (Ar), 59.81, 22.05, 21.68.

3.3.2.11 4-Fluoro-2-(*m*-tolyliminomethyl)phenol – 4F-SalH-*m*Tol

The title compound, 5F-SalH-*m*Tol, was synthesized according to the procedure described in § 3.3.1.1, using 5-fluorosalicylaldehyde (0.5 g, 3.569 x 10^{-3} mol) and *m*-toluidine (0.382 g, 3.569 x 10^{-3} mol) dissolved in methanol. The product was obtained as an orange solid which was washed with cold methanol and filtered. Crystals suitable for X-ray diffraction were grown from the filtrate. (Yield: 0.671 g, 82.1 %).

^{1}H NMR (600 MHz, acetone-d_6) δ 13.04 (s, 1H, OH), 8.90 (s, 1H, HC=N), 7.40 (dd, 1H, J = 3.1, 8.7 Hz, Ar), 7.35 (t, 1H, J = 7.7 Hz, Ar), 7.25 (s, 1H, Ar), 7.24-7.20 (m, 2H, Ar), 7.16 (d, 1H, J = 7.7 Hz, Ar), 6.96 (dd, 1H, J = 4.5, 9.1 Hz, Ar), 2.39 (s, 3H, CH_3). ^{13}C NMR (600 MHz, acetone-d_6) δ 163.43, 158.32, 157.09, 155.34, 149.00, 140.22, 130.20, 128.89, 122.85, 120.80 (d, J = 23.5 Hz), 119.23, 118.97 (d, J = 7.6 Hz), 118.33 (d, J = 23.5 Hz) (Ar), 21.31 (CH_3).

3.3.2.12 2-(9-Ethylcarbazol-3-yliminomethyl)-5-methylphenol - 5Me-SalH-Carba

The title compound, 5Me-SalH-Carba, was synthesized according to the procedure described in § 3.3.1.1, using 2-hydroxy-4-methyl benzaldehyde (1.000 g, 7.345 x 10^{-3} mol) and 3-amino-9-ethyl-carbazole (1.544 g, 7.345 x 10^{-3} mol) in methanol under Schlenk conditions.

The product was obtained as a yellow solid which was washed with cold methanol and filtered. Crystals suitable for X-ray diffraction were grown from a methanol : acetone : benzene (6:2:1) solution at 4 °C. (Yield: 2.145 g, 88.9 %).

^{1}H NMR (600 MHz, acetone-d_6) δ 13.57 (s, 1H, OH), 9.02 (s, 1H, HC=N), 8.26 (m, 1H), 8.21 (d, 1H, J = 7.8 Hz), 7.64 (d, 1H, J = 8.6 Hz), 7.61-7.59 (m, 2H), 7.51-7.47 (m, 2H), 7.24 (m, 1H), 6.81 (m, 2H) (Ar), 4.51 (q, 2H, J = 7.2 Hz, CH_2), 2.36 (s, 3H, CH_3), 1.42 (t, 3H, J = 7.2 Hz, CH_3). ^{13}C NMR (600 MHz, acetone-d_6) δ 161.98, 161.38, 144.22, 141.59, 141.31, 139.97, 133.08, 127.01, 124.41, 123.77, 121.43, 120.87, 120.66, 119.90, 118.42, 117.89, 113.56, 110.32, 110.00 (Ar), 38.19, 21.80, 14.10.

3.3.2.13 2-[(2-Indol-3-yl-ethyl)iminomethyl]-5-methylphenol - 5Me-SalH-Trypt

The title compound, 5Me-SalH-Trypt, was synthesized according to the procedure described in § 3.3.1.1, using 2-hydroxy-4-methyl benzaldehyde (1.000 g, 7.345 x 10^{-3} mol) and tryptamine (1.177 g, 7.345 x 10^{-3} mol) dissolved in methanol under Schlenk conditions. The excess solvent was removed and the yellow solid was filtered, washed with cold methanol and dried. Crystals suitable for X-ray diffraction were obtained from the filtrate. (Yield: 1.712 g, 83.7 %).

^{1}H NMR (600 MHz, acetone-d_6) δ 13.48 (s, 1H, OH), 8.36 (s, 1H, HC=N), 7.63 (d, 1H, J = 7.8 Hz), 7.37 (dt, 1H, J = 0.8, 8.1 Hz), 7.17 (m, 2H), 7.09 (dq, 1H, J = 1.0, 7.0 Hz), 7.02 (dq, 1H, J = 1.0, 7.0 Hz), 6.70 (s, 1H), 6.67 (d, 1H, J = 7.8 Hz) (Ar), 3.91 (dt, 2H, J = 1.0, 7.0 Hz), 3.14 (dt, 2H, J = 1.0, 7.0 Hz), 2.29 (s, 3H, CH_3). ^{13}C NMR (600 MHz, acetone-d_6) δ 166.17, 162.23, 143.49, 137.68, 132.18, 128.45, 123.59, 122.09, 120.21, 119.43, 119.26, 117.73, 117.61, 113.38, 112.16 (Ar), 60.59, 27.77, 21.68.

3.3.2.14 2-[2-(4-Hydroxyphenyl)ethyliminomethyl]-5-methylphenol - 5Me-SalH-Tyra

The title compound, 5Me-SalH-Tyra, was synthesized according to the procedure described in § 3.3.1.1, using 2-hydroxy-4-methyl benzaldehyde (0.500 g, 3.672 x 10^{-3} mol) and tyramine (0.5038 g, 3.672 x 10^{-3} mol) dissolved in methanol. The product was obtained as a

yellow precipitate which was filtered and washed with cold methanol. Crystals suitable for X-ray diffraction were obtained from the filtrate. (Yield: 0.8507 g, 90.7 %).

^{1}H NMR (600 MHz, acetone-d_6) δ 8.34 (s, 1H, HC=N), 7.20 (d, 1H, J = 8.5 Hz, Ar), 7.07 (dt, 1H, J = 2.1, 2.8, 8.5 Hz, Ar), 6.74 (dt, 2H, J = 2.1, 2.8, 8.5 Hz, Ar), 6.68 (d, 2H, J = 7.5 Hz, Ar), 3.80 (dt, 2H, J = 1.2, 7.5 Hz), 2.89 (t, 2H, J = 7.5 Hz), 2.28 (s, 3H, CH_3). ^{13}C NMR (600 MHz, acetone-d_6) δ 166.29 (C1), 162.13, 156.77, 143.55, 132.21, 131.10, 130.70 (3 x CH), 120.26, 117.71, 117.54, 115.97, 61.90, 37.26, 21.67 (CH_3).

3.3.2.15 5-Methyl-2-(1,2,4-triazol-3-yliminomethyl)phenol - 5Me-SalH-Triaz

The title compound, 5Me-SalH-Triaz, was synthesized according to the procedure described in § 3.3.1.1, using 2-hydroxy-4-methyl benzaldehyde (0.500 g, 3.672 x 10^{-3} mol) (placed in an ice-bath) and 3-amino-1,2,4-triazole (0.3088 g, 3.672 x 10^{-3} mol) which was added dropwise to the cold aldehyde. The reaction was gradually heated to room temperature and then stirred at 70 °C for 3 h. The product was obtained as a pale yellow solid. The solid was washed with cold methanol and filtered. Crystals suitable for X-ray diffraction were obtained by the slow evaporation of the filtrate. (Yield: 0.608 g, 81.9 %).

^{1}H NMR (600 MHz, acetone-d_6) δ 9.37 (s, 1H, HC=N), 7.56 (d, 1H, J = 7.9 Hz, Ar), 6.85 (d, 1H, J = 7.9 Hz, Ar), 6.82 (s, 1H, Ar), 3.30 (s, 1H), 2.36 (s, 3H, CH_3). ^{13}C NMR (600 MHz, acetone-d_6) δ 167.05 (C1), 146.37, 134.42 (2 x CH), 121.48 (2 x CH), 118.10 (2 x CH), 117.39, 21.88 (CH_3).

3.3.3 Synthesis of Rhenium(I) Tricarbonyl complexes

3.3.3.1 *fac*-$[Et_4N]_2[Re(Br)_3(CO)_3]$ – [ReAA]

$[Et_4N]Br$ (5.25 g, 0.025 mol) was ground to a fine powder in a mortar and pestle and dried under vacuum overnight. 2,5,8-trioxanone diglyme (150 ml) was added to the $[Et_4N]Br$ under a dry nitrogen atmosphere and slurried on an oil-bath, preheated to 80 °C, for 30 minutes. The system was evacuated and purged with N_2 several times. $[Re(CO)_5Br]$ (5 g, 0.0123 mol) was added and the reaction was stirred at 115 °C for 15 h. Good stirring and ventilation is necessary because of the continuous evolution of CO. The mixture was cooled to room temperature. The precipitate was filtered, washed twice with cold ethanol and then dry, cold

dichloromethane. The product, off-white powder, was dried under vacuum overnight. (Yield: 8.956 g, 94.4%).

IR (KBr, cm^{-1}): $\nu_{(CO)}$ 1996.2, 1867.8. Elemental analysis: calculated C 29.62%, H 5.23%, N 3.64%, found C 29.67 %, H 5.27 %, N 3.61%.

3.3.3.2 *fac*-[Re(Sal-*m*Tol)(CO)$_3$(HOCH$_3$)]

ReAA (0.300 g, 3.894 x 10^{-4} mol) was dissolved in methanol (15 ml). $AgNO_3$ (0.1984 g, 1.168 x 10^{-3} mol, 3eq) was added and the reaction stirred for 26 h at room temperature. AgBr precipitated and filtered off. SalH-*m*Tol (0.0864 g, 4.089 x 10^{-4} mol, 1.05eq) dissolved in methanol (10 ml) was added drop-wise. The reaction was heated to 70 °C and stirred for 14 h. The majority of the solvent was removed under reduced pressure before allowing the yellow solution to evaporate slowly. Crystals suitable for X-ray diffraction were obtained. (Yield crystalline product: 0.0817 g, 40.9 %).

IR (KBr, cm^{-1}): $\nu_{(CO)}$ 2002.0, 1868.8 (bs). UV-Vis (nm, $L.mol^{-1}.cm^{-1}$): λ_{max} = 397.9, ε = 3.139 x 10^3. ^{1}H NMR (600 MHz, acetone-d_6) δ 8.21 (s, 1H, HC=N), 7.37 (m, 5H, Ar), 7.28 (m, 3H, Ar), 2.96 (bs, 3H, OCH_3), 2.40 (s, 3H, CH_3). ^{13}C NMR (600 MHz, acetone-d_6) δ 166.56 (C1), 167.65, 158.66, 137.11, 136.98, 135.30, 129.13, 127.39, 124.53, 123.33, 121.30, 121.12, 114.32 (Ar), 21.44 (CH_3).

3.3.3.3 *fac*-[Re(Sal-*m*Tol)(CO)$_3$(NC$_5$H$_5$)]

$AgNO_3$ (0.0661 g, 3.894 x 10^{-4} mol, 3eq) was added to ReAA (0.100 g, 1.298 x 10^{-4} mol) dissolved in methanol. The reaction was stirred for 26 h at room temperature. AgBr precipitated and filtered. SalH-*m*Tol (0.0288 g, 1.633 x 10^{-4} mol, 1.05 eq) was added and the reaction stirred at 74 °C for 14 h. Pyridine (Py) (0.0103 g, 0.105 ml, 1.298 x 10^{-4} mol) was added to the warm solution and stirred for 1 h. Excess solvent was removed and product crystallized at 4 °C. (Yield: 0.0492 g, 67.7 %).

IR (KBr, cm^{-1}): $\nu_{(CO)}$ 2014.7, 1890.5. UV-Vis (nm, $L.mol^{-1}.cm^{-1}$): λ_{max} = 402.0, ε = 2.345 x 10^3. ^{1}H NMR (600 MHz, acetone-d_6) δ 8.61 (m, 2H, Ar), 8.30 (s, 1H, HC=N), 8.08 (m, 1H, Ar), 7.59 (m, 1H, Ar), 7.38 (m, 1H, Ar), 7.31 (m, 2H, Ar), 7.12 (m, 1H, Ar), 6.90 (d, 1H, Ar), 6.86 (s, 1H, Ar), 6.84 (d, 1H, Ar), 6.58 (m, 1H, Ar), 2.34 (s, 3H, CH_3). ^{13}C NMR (600 MHz, acetone-d_6) δ 168.03 (C1), 166.94, 157.36, 152.89, 140.39, 139.78, 137.24, 136.40, 129.69, 128.13, 126.93, 124.61, 123.43, 121.48, 121.18, 115.91 (Ar), 21.38 (CH_3).

3.3.3.4 *fac*-[Re(Sal-3MeBu)(CO)$_3$(HOCH$_3$)]

SalH-3MeBu (0.0169 g, 8.836 x 10^{-5} mol) dissolved in methanol (5 ml) was added to ReAA (0.0623 g, 8.086 x 10^{-5} mol) in methanol (5 ml). The reaction was stirred for 24 h at room temperature. Yellow crystals suitable for X-ray diffraction were obtained from the slow evaporation of solvent.[8] (Yield: 0.0242 g, 38.0%).

The complex could also be obtained by the following method:

$AgNO_3$ (0.0661g, 3.894 x 10^{-4} mol, 3eq) was added to ReAA (0.100g, 1.298 x 10^{-4} mol) dissolved in methanol (10 ml) and stirred for 26 h at room temperature. The precipitate, AgBr was filtered off. SalH-3MeBu (0.261g, 1.363 x 10^{-4} mol) dissolved in methanol (5 ml) was added and the mixture was heated to 70 °C for 8 h. Excess solvent was removed under reduced pressure. Crystals were obtained from the concentrated methanol solution at 5 °C. (Yield: 0.0434 g, 68.0 %).

IR (KBr, cm^{-1}): $\nu_{(CO)}$ 2001.4, 1876.5. UV-Vis (nm, L.mol^{-1}.cm^{-1}): λ_{max} = 382.9, ε = 1.311 x 10^3. ^{1}H NMR (600 MHz, acetone-d_6) δ 8.22 (s, 1H, HC=N), 7.15 (m, 2H, Ar), 6.65 (d, 1H, *J*= 8.5 Hz, Ar), 6.42 (m, 1H, Ar), 1.68 (m, 5H), 0.99 (d, 3H, *J* = 6.5 Hz), 0.93 (d, 3H, *J* = 6.5 Hz). ^{13}C NMR (600 MHz, acetone-d_6) δ 166.78 (C1), 166.24, 136.23, 134.54, 122.77, 121.53, 113.92 (Ar), 69.14, 41.99, 26.54, 23.12, 22.64.

3.3.3.5 *fac*-[Re(Sal-3MeBu)(CO)$_3$(NC$_5$H$_5$)]

The ligand SalH-3MeBu (0.027g, 1.428 x 10^{-4} mol) dissolved in methanol (5 ml) was added to a methanol (10 ml) solution of ReAA (0.1g, 1.298 x 10^{-4} mol). The reaction was stirred for 6 h at 25 °C before the addition of pyridine (0.015g, 1.950 x 10^{-4} mol), in methanol (5 ml), followed by a further 12 h stirring. The pale yellow precipitate was filtered and dried. Crystals suitable for X-ray diffraction were obtained from the slow evaporation of the filtrate. The addition of pyridine to *fac*-[Re(Sal-3MeBu)(CO)$_3$(HOCH$_3$)], with 6 h stirring also yielded the final complex.[8] (Yield: 0.0152 g, 21.7 %).

IR (KBr, cm^{-1}): $\nu_{(CO)}$ 2013.6, 1904.8, 1878.4. UV-Vis (nm, L.mol^{-1}.cm^{-1}): λ_{max} = 389.0, ε = 2.038 x 10^3. ^{1}H NMR (600 MHz, acetone-d_6) δ 8.69 (m, 2H, Ar), 8.33 (s, 1H, HC=N), 8.03 (tt, 1H, Ar, *J* = 7.8, 3.2, 1.6 Hz), 7.55 (m, 2H, Ar), 7.27 (m, 1H, Ar), 7.14 (dd, 1H, Ar, *J* = 7.8, 1.8 Hz), 6.79 (d, 1H, Ar, *J* = 8.5 Hz) 6.50 (m, 1H, Ar), 4.23-4.04 (m, 2H) 1.62 (m, 1H), 1.80-1.57 (m, 2H), 0.94 (d, 3H, *J* = 6.5 Hz), 0.91 (d, 3H, *J* = 6.5 Hz). ^{13}C NMR (600 MHz,

acetone-d_6) δ 166.75 (C1), 165.41, 152.05, 139.28, 135.46, 134.64, 125.92, 122.09, 120.58, 114.53 (Ar), 68.08, 40.83, 25.71, 22.03, 21.61.

3.3.3.6 *fac*-[Re(Sal-Ph)(CO)$_3$(HOCH$_3$)]

The ligand SalH-Ph (0.0146g, 7.402 x 10^{-5} mol) dissolved in methanol (5ml) was added to ReAA (0.041 g, 5.322 x 10^{-5} mol) in methanol (5 ml). The reaction was heated to 75 °C for 12 hrs. The yellow solution was allowed to evaporate slowly. Crystals suitable for X-ray diffraction were grown from methanol at 5 °C. (Yield: 0.0154 g, 58.0%).

IR (KBr, cm^{-1}): $\nu_{(CO)}$ 2020.5, 1892.5. UV-Vis (nm, L.mol^{-1}.cm^{-1}): λ_{max} = 402.0, ε = 3.717 x 10^3. ^{1}H NMR (600 MHz, acetone-d_6) δ 8.24 (s, 1H, HC=N), 7.40 (m, 2H, Ar), 7.25 (m, 5H, Ar) 6.75 (d, 1H, J = 8.5 Hz, Ar), 6.50 (m, 1H, Ar). ^{13}C NMR (600 MHz, acetone-d_6) δ 165.84 (C1), 166.56, 157.79, 136.13, 134.49, 128.71, 128.45, 125.84, 123.10, 122.45, 120.50, 120.40, 113.47 (Ar).

3.3.3.7 *fac*-[Re(Sal-Ph)(CO)$_3$(NC$_5$H$_5$)]

The ligand SalH-Ph (0.028g, 1.428 x 10^{-4} mol) dissolved in methanol (5 ml) was added to a methanol (10 ml) solution of ReAA (0.1g, 1.298 x 10^{-4} mol). The reaction was stirred for 4 h at 25 °C before the addition of pyridine (0.015g, 1.950 x 10^{-4} mol) followed by a further 12 hrs stirring. The yellow precipitate was filtered and dried. Crystals suitable for X-ray diffraction were obtained from the slow evaporation of the filtrate. (Yield: 0.0458 g, 64.7%).

IR (KBr, cm^{-1}): $\nu_{(CO)}$ 2014.7, 1906.6, 1884.8. UV-Vis (nm, L.mol^{-1}.cm^{-1}): λ_{max} = 407.0, ε = 2.487 x 10^3. ^{1}H NMR (600 MHz, acetone-d_6) δ 8.62 (m, 2H, Ar), 8.32 (s, 1H, HC=N), 8.07 (m, 1H, Ar), 7.58 (m, 3H, Ar), 7.47 (m, 2H, Ar), 7.38 (m, 1H, Ar), 7.31 (m, 2H, Ar), 7.06 (m, 2H, Ar), 6.90 (d, 1H, J = 8.5 Hz, Ar), 6.58 (m, 1H, Ar).^{13}C NMR (600 MHz, acetone-d_6) δ 167.37 (C1), 166.10, 156.61, 154.39, 152.01, 139.47, 139.25, 136.38, 135.57, 129.01, 128.14, 126.60, 126.06, 123.48, 123.14, 122.60, 120.56, 115.02 (Ar).

3.3.3.8 *fac*-[Re(Sal-CyHex)(CO)$_3$(HOCH$_3$)]

The title compound, *fac*-[Re(Sal-CyHex)(CO)$_3$(HOCH$_3$)], was synthesised in a similar fashion as *fac*-[Re(Sal-*m*Tol)(CO)$_3$(HOCH$_3$)] in §3.3.3.2 using ReAA (0.100 g, 1.298 x 10^{-4} mol), $AgNO_3$ (0.0661 g, 3.894 x 10^{-4} mol, 3eq) and SalH-CyHex (0.0277 g, 1.363 x 10^{-4} mol,

1.05eq). Crystals suitable for X-ray diffraction were obtained at 5 °C. (Yield: 0.0582 g, 88. 9%).

IR (KBr, cm^{-1}): $\nu_{(CO)}$ 2014.9, 1871.6. UV-Vis (nm, $L.mol^{-1}.cm^{-1}$): λ_{max} = 293.0, 382.1, ε = 1.421 x 10^4, 5.263 x 10^3. ^{1}H NMR (600 MHz, acetone-d_6) δ 8.30 (s, 1H, HC=N), 7.17 (m, 2H, Ar), 6.63 (d, 1H, J = 8.4 Hz, Ar), 6.41 (m, 1H, Ar), 1.42-1.89 (m, 11H, Cy).^{13}C NMR (600 MHz, acetone-d_6) δ 163.90 (C1), 167.21, 136.47, 134.42, 122.63, 121.99, 113.90 (Ar), 35.04, 34.55, 26.78, 26.31, 25.67, 25.10 (Cy).

3.3.3.9 *fac*-[Re(Sal-*p*Tol)(CO)$_3$(HOCH$_3$)]

The title compound, *fac*-[Re(Sal-*p*Tol)(CO)$_3$(HOCH$_3$)], was synthesised in a similar fashion as *fac*-[Re(Sal-*m*Tol)(CO)$_3$(HOCH$_3$)] in §3.3.3.2 using $AgNO_3$ (0.198 g, 1.168 x 10^{-3} mol, 3eq), ReAA (0.300 g, 3.894 x 10^{-4} mol) and SalH-*p*Tol (0.0864 g, 4.089 x 10^{-4} mol, 1.05 eq). Product crystallized at 4 °C. (Yield: 0.1740 g, 87.2 %).

IR (KBr, cm^{-1}): $\nu_{(CO)}$ 2020.4, 1892.4. UV-Vis (nm, $L.mol^{-1}.cm^{-1}$): λ_{max} = 386.1 ε = 2.032 x 10^3. ^{1}H NMR (600 MHz, acetone-d_6) δ 8.36 (1H, HC=N), 7.35 (m, 2H, Ar), 7.26 (bs, 2H, Ar), 7.19 (m, 2H, Ar), 6.80 (m, 1H, Ar), 6.57 (m, 1H, Ar), 2.39 (s, 3H, CH_3). ^{13}C NMR (600 MHz, acetone-d_6) δ 166.88 (C1), 155.20, 136.20, 135.30, 135.04, 129.29, 129.16, 122.89, 122.80, 122.21, 122.05, 114.73, 114.50 (Ar), 19.99 (CH_3).

3.3.3.10 *fac*-[Re(5Me-Sal-*m*Tol)(CO)$_3$(HOCH$_3$)]

The title compound, *fac*-[Re(5Me-Sal-*m*Tol)(CO)$_3$(HOCH$_3$)], was synthesised in a similar fashion as *fac*-[Re(Sal-*m*Tol)(CO)$_3$(HOCH$_3$)] in § 3.3.3.2 using $AgNO_3$ (0.198 g, 1.168 x 10^{-3} mol, 3eq), ReAA (0.300 g, 3.894 x 10^{-4} mol) and 5Me-SalH-*m*Tol (0.0921 g, 4.089 x 10^{-4} mol, 1.05 eq). The yellow coloured product crystallized at 4 °C. (Yield: 0.2260 g, 59.5 %).

IR (KBr, cm^{-1}): $\nu_{(CO)}$ 2018.5, 1922.5, 1882.9. UV-Vis (nm, $L.mol^{-1}.cm^{-1}$): λ_{max} = 365.1, ε = 2.124 x 10^3. ^{1}H NMR (600 MHz, acetone-d_6) δ 8.28 (s, 1H), 8.14 (s, 1H), 7.31 (m, 1H, Ar), 7.26 (m, 2H, Ar), 7.16-7.03 (m, 7H, Ar), 6.62 (s, 1H, Ar), 6.56 (s, 1H, Ar), 6.44 (m, 1H, Ar), 6.32 (dd, 1H, J = 8.0, 1.5 Hz, Ar), 2.38 (s, 3H, CH_3), 2.35 (s, 3H, CH_3), 2.23 (s, 3H, CH_3), 2.18 (s, 3H, CH_3). ^{13}C NMR (600 MHz, acetone-d_6) δ 167.72 (C1), 165.94, 145.98, 139.02, 136.93, 136.78, 127.23, 124.68, 123.27, 121.44, 119.06, 116.15 (Ar), 21.90, 21.53 (CH_3).

3.3.3.11 *fac*-[Re(5Me-Sal-3Me2Bu)(CO)$_3$(HOCH$_3$)]

The title compound, *fac*-[Re(5Me-Sal-3Me2Bu)(CO)$_3$(HOCH$_3$)], was synthesised in a similar fashion as *fac*-[Re(Sal-*m*Tol)(CO)$_3$(HOCH$_3$)] in §3.3.3.2 using $AgNO_3$ (0.198 g, 1.168 x 10^{-3} mol, 3eq), ReAA (0.300 g, 3.894 x 10^{-4} mol) and 5Me-SalH-3Me2Bu (0.0840 g, 4.089 x 10^{-4} mol, 1.05 eq). The product crystallized at 4 °C. (Yield: 0.1278 g, 64.8 %).

IR (KBr, cm^{-1}): $\nu_{(CO)}$ 2015.6, 1894.8, 1872.1. UV-Vis (nm, $L.mol^{-1}.cm^{-1}$): λ_{max} = 382.0, ε = 1.576 x 10^3. ^{1}H NMR (600 MHz, acetone-d_6) δ 8.19 (d, 1H, *J* = 3.0 Hz), 7.04 (t, 1H, *J* = 8.0 Hz, Ar), 6.47 (bs, 1H), 6.25 (dd, 1H, *J* = 8.0, 1.6 Hz, Ar), 2.20 (s, 3H, CH_3), 1.43 (m, 3H, CH_3), 1.06 (d, 1H, *J* = 6.8 Hz, CH), 1.02 (d, 1H, *J* = 6.8 Hz, CH), 1.00 (m, 3H, CH_3), 0.95 (m, 3H, CH_3). ^{13}C NMR (600 MHz, acetone-d_6) δ 167.41 (C1), 164.20, 144.97, 136.48, 122.69, 115.60, 119.51 (Ar), 34.48, 21.79, 21.13, 21.08, 19.57, 19.13.

3.3.3.12 *fac*-[Re(Sal-4NitroPh)(CO)$_3$(HOCH$_3$)]

$AgNO_3$ (0.0661 g, 3.894 x 10^{-4} mol, 3eq) was added to ReAA (0.100 g, 1.298 x 10^{-4} mol) dissolved in methanol. The reaction was stirred for 24 h at room temperature. AgBr precipitated and filtered. SalH-4NitroPh (0.0314 g, 1.298 x 10^{-4} mol) dissolved in minimal amount of acetone, was added and the reaction stirred at 65°C for 2 h. Two-thirds of the solvent volume was rapidly removed under reduced pressure and the remaining was allowed to evaporate slowly at 4 °C. Red plate crystals formed, unsuitable for X-ray diffraction. (Yield: 0.0505 g, 71.6 %).

IR (KBr, cm^{-1}): $\nu_{(CO)}$ 2021.0, 1883.8. UV-Vis (nm, $L.mol^{-1}.cm^{-1}$): λ_{max} = 367.9, ε = 1.462 x 10^5. ^{1}H NMR (600 MHz, acetone-d_6) δ 9.00 (1H, HC=N), 8.35 (m, 2H, Ar), 7.64 (m, 3H, Ar), 7.49 (m, 1H, Ar), 7.01 (m, 2H, Ar). ^{13}C NMR (600 MHz, acetone-d_6) δ 167.10 (C1), 137.85, 134.51, 126.96, 125.92, 125.58, 125.08, 123.75, 123.33, 120.82, 117.89, 114.61, 113.53.

3.3.3.13 *fac*-[Re(5Me-Sal-Pen)(CO)$_3$(HOCH$_3$)]

The title compound, *fac*-[Re(5Me-Sal-Pen)(CO)$_3$(HOCH$_3$)], was synthesised in a similar fashion as *fac*-[Re(Sal-*m*Tol)(CO)$_3$(HOCH$_3$)] in §3.3.3.2 using $AgNO_3$ (0.0661 g, 3.894 x 10^{-4} mol, 3eq), ReAA (0.100 g, 1.298 x 10^{-4} mol) and 5Me-SalH-Pen (0.0364 g, 1.363 x 10^{-4} mol). The product was obtained as a white powder at 4 °C. (Yield: 0.0738 g, 75.8 %).

IR (KBr, cm^{-1}): $\nu_{(CO)}$ 2020.8, 1894.8. UV-Vis (nm, $L.mol^{-1}.cm^{-1}$): λ_{max} = 262.1, 324.9, ε = 7.467 x 10^3, 2.480 x 10^3. ^1H NMR (600 MHz, acetone-d_6) δ 11.07 (bs, 1H, COOH), 9.97 (s, 1H, HC=N) 7.65 (d, 1H, J = 7.9 Hz, Ar), 6.89 (d, 1H, J = 7.9 Hz, Ar), 6.82 (s, 1H, Ar), 3.30 (s, 1H, CH), 2.36 (s, 3H, CH_3), 2.09 (s, 1H, SH), 3.48 (q, J = 7.2 Hz, Et_4N impurity), 1.37 (tt, J = 1.8, 7.2 Hz, Et_4N impurity). ^{13}C NMR (600 MHz, acetone-d_6) δ 197.03 (COOH), 162.48 (C1), 153.54, 149.55, 134.21, 129.34, 121.89, 120.00, 118.10, 64.61, 23.70 (CH_3), 22.04 (2 x CH_3), 53.00, 7.76 (Et_4N).

3.3.3.14 *fac*-[Re(5Me-Sal-Hist)(CO)$_3$]

The title compound, *fac*-[Re(5Me-Sal-Hist)(CO)$_3$], was synthesised in a similar fashion as *fac*-[Re(Sal-*m*Tol)(CO)$_3$(HOCH$_3$)] in §3.3.3.2 using $AgNO_3$ (0.0992 g, 5.841 x 10^{-4} mol, 3eq), ReAA (0.150 g, 1.947 x 10^{-4} mol) and 5Me-SalH-Hist (0.0469 g, 2.044 x 10^{-4} mol). The reaction stirred at 70°C for 12 h, followed by 24 h at 30 °C. Two-thirds of the solvent volume was removed under reduced pressure and the remaining was allowed to evaporate slowly at 4 °C to yield yellow crystals. (Yield: 0.0638 g, 65.7%).

IR (KBr, cm^{-1}): $\nu_{(CO)}$ 2012.8, 1902.6, 1871.0. UV-Vis (nm, $L.mol^{-1}.cm^{-1}$): λ_{max} = 300.1, 387.9, ε = 5.206 x 10^3, 1.484 x 10^3. ^1H NMR (600 MHz, acetone-d_6) δ 8.08 (s, 1H, HC=N), 7.99 (s, 1H, Ar), 7.14 (s, 1H, Ar), 6.98 (d, 1H, J = 8.0 Hz), 6.45 (s, 1H, Ar), 6.27 (dd, 1H, J = 1.6, 8.0 Hz), 4.43 (m, 1H, CH_2), 4.16 (m, 1H, CH_2), 3.40 (m, 1H, CH_2), 3.12 (m, 1H, CH_2), 2.14 (s, 3H, CH_3). ^{13}C NMR (600 MHz, acetone-d_6) δ 169.78 (C1), 165.61, 145.54, 136.44, 135.01, 122.19, 121.09, 116.77, 61.88 (Ar), 30.35, 28.62 (CH_2), 21.80 (CH_3).

3.3.3.15 *fac*-[Re(5Me-Sal-Trypt)(CO)$_3$(HOCH$_3$)]

The title compound, *fac*-[Re(5Me-Sal-Trypt)(CO)$_3$(HOCH$_3$)], was synthesised in a similar fashion as *fac*-[Re(Sal-*m*Tol)(CO)$_3$(HOCH$_3$)] in §3.3.3.2 using $AgNO_3$ (0.0992 g, 5.841 x 10^{-4} mol, 3eq), ReAA (0.150 g, 1.947 x 10^{-4} mol) and 5Me-SalH-Trypt (0.0569 g, 2.044 x 10^{-4} mol) under Schlenk conditions. Crystallization from methanol at 4 °C was unsuccessful. Product was stored under an argon atmosphere. (Yield: 0.0370 g, 33.0 %).

IR (ATR, cm^{-1}): $\nu_{(CO)}$ 2014.1, 1885.4. UV-Vis (nm, $L.mol^{-1}.cm^{-1}$): λ_{max} = 262.1, 308.1, 399.1, ε = 8.422 x 10^3, 3.176 x 10^3, 6.099 x 10^2. ^1H NMR (600 MHz, acetone-d_6) δ 9.17 (s, 1H), 8.82 (m, 1H, Ar), 8.66 (m, 2H, Ar), 7.60 (m, 2H, Ar), 7.42 (m, 1H, Ar), 7.25 (d, 1H, J = 8.0 Hz, Ar), 6.66 (s, 1H, Ar), 6.42 (dd, 1H, J = 2.0, 8.0 Hz, Ar), 3.44 (m, 2H, CH_2), 3.27 (m, 2H,

CH_2), 2.21 (m, 3H, CH_3). ^{13}C NMR (600 MHz, acetone-d_6) δ 170.51 (C1), 152.65, 151.75, 150.94, 139.67, 139.07, 136.55, 126.12, 125.50, 123.23, 121.47, 118.93, 118.12, 117.87, 111.54, 48.51, 23.48, 21.36 (CH_3).

3.3.3.16 *fac*-[Re(5Me-Sal-Trypt)(CO)$_3$(NC$_5$H$_5$)]

The title compound, *fac*-[Re(5Me-Sal-Trypt)(CO)$_3$(NC$_5$H$_5$)], was synthesised in a similar fashion as *fac*-[Re(Sal-*m*Tol)(CO)$_3$(HOCH$_3$)] in §3.3.3.2 using $AgNO_3$ (0.0992 g, 5.841 x 10^{-4} mol, 3eq), ReAA (0.150 g, 1.947 x 10^{-4} mol) and 5Me-SalH-Trypt (0.0569 g, 2.044 x 10^{-4} mol). Pyridine (0.0231 g, 2.920 x 10^{-4} mol) was added and stirred for 5 min. Two-thirds of the solvent volume was removed under reduced pressure and the remaining was allowed to evaporate slowly at 4 °C to yield yellow crystals. (Yield: 0.1095g, 89.7%).

IR (KBr, cm^{-1}): $\nu_{(CO)}$ 2016.4, 1906.0, 1881.9. UV-Vis (nm, $L.mol^{-1}.cm^{-1}$): λ_{max} = 382.05, ε = 2.112 x 10^3. ^1H NMR (600 MHz, acetone-d_6) δ 8.72 (m, 2H, Ar), 8.01 (m, 1H, Ar), 7.94 (s, 1H, HC=N), 7.67 (d, 1H, J = 8.0 Hz), 7.53 (m, 2H, Ar), 7.40 (m, 1H, Ar), 7.12 (m, 2H, Ar), 7.05 (m, 1H, Ar), 6.77 (d, 1H, J = 8.0 Hz), 6.63 (s, 1H, Ar), 6.26 (dd, 1H, J = 1.6, 8.0 Hz), 4.45 (m, 1H, CH_2), 4.22 (m, 1H, CH_2), 3.35 (m, 1H, CH_2), 3.15 (m, 1H, CH_2), 2.18 (s, 3H, CH_3). ^{13}C NMR (600 MHz, acetone-d_6) δ 167.27 (C1), 166.20, 152.92 (2 x CH), 146.30, 140.15, 137.71, 136.09, 128.20, 126.80 (2 x CH), 124.48, 122.84, 122.30, 119.64, 119.32, 119.08, 117.21, 112.29, 111.91 (Ar), 70.46, 28.59 (CH_2), 21.81 (CH_3).

3.3.3.17 *fac*-[Re(5Me-Sal-Tyra)(CO)$_3$(NC$_5$H$_5$)]

The title compound, *fac*-[Re(5Me-Sal-Tyra)(CO)$_3$(NC$_5$H$_5$)], was synthesised in a similar fashion as *fac*-[Re(5Me-Sal-Trypt)(CO)$_3$(NC$_5$H$_5$)] in §3.3.3.16 using $AgNO_3$ (0.0992 g, 5.841 x 10^{-4} mol, 3eq), ReAA (0.150 g, 1.947 x 10^{-4} mol), 5Me-SalH-Tyra (0.0522 g, 2.044 x 10^{-4} mol) and pyridine (0.0231 g, 2.920 x 10^{-4} mol). The product was obtained as a yellow powder. (Yield: 0.0915 g, 77.9%).

IR (ATR, cm^{-1}): $\nu_{(CO)}$ 2013.8, 1886.4. UV-Vis (nm, $L.mol^{-1}.cm^{-1}$): λ_{max} = 386.1, ε = 2.186 x 10^3. ^1H NMR (600 MHz, acetone-d_6) δ 9.16 (s, 1H, Ar), 8.66 (d, 1H, J = 6.7 Hz, Ar), 7.60 (t, 2H, J = 6.7 Hz, Ar), 7.25 (d, 1H, J = 8.0 Hz, Ar), 7.10 (m, 2H, Ar), 6.89 (d, 1H, J = 8.0 Hz, Ar), 6.76 (d, 1H, J = 6.7 Hz, Ar), 6.66 (s, 1H, Ar), 6.63 (s, 1H, Ar), 6.42 (d, 1H, J = 8.2 Hz, Ar), 6.32 (d, 1H, J = 8.2 Hz, Ar), 4.31 (m, 1H, CH_2), 4.09 (m, 1H, CH_2), 3.11 (m, 1H, CH_2), 2.84 (m, 1H, CH_2), 2.21 (s, 3H, CH_3). ^{13}C NMR (600 MHz, acetone-d_6) δ 171.42, 167.45,

166.27, 152.92, 152.67, 146.44, 140.57, 140.20, 137.46, 131.00, 127.03, 126.85, 122.90, 122.45, 119.12, 118.79, 117.30, 116.24 (Ar), 38.12, 22.30, 21.83 (CH_3).

3.3.3.18 *fac*-[Re(5Me-Sal-Carba)(CO)$_3$(NC$_5$H$_5$)]

The title compound, *fac*-[Re(5Me-Sal-Carba)(CO)$_3$(NC$_5$H$_5$)], was synthesised in a similar fashion as *fac*-[Re(5Me-Sal-Trypt)(CO)$_3$(NC$_5$H$_5$)] in §3.3.3.16 using $AgNO_3$ (0.0992 g, 5.841 x 10^{-4} mol, 3eq), ReAA (0.150 g, 1.947 x 10^{-4} mol), 5Me-SalH-Carba (0.0671 g, 2.044 x 10^{-4} mol) and pyridine (0.0231 g, 2.920 x 10^{-4} mol). The product was obtained as orange crystals suitable for X-ray diffraction at 4 °C. (Yield: 0.0.0872 g, 66.1 %).

IR (ATR, cm^{-1}): $\nu_{(CO)}$ 2010.4, 1902.2 . UV-Vis (nm, $L.mol^{-1}.cm^{-1}$): λ_{max} = 286.0, 350.1, 371.0, ε = 3.096 x 10^4, 2.895 x 10^4, 2.885 x 10^4. ^{1}H NMR (600 MHz, acetone-d_6) δ 8.68 (m, 2H, Ar), 8.38 (s, 1H, HC=N), 8.11 (tt, 1H, J = 1.5, 7.6 Hz, Ar), 8.07 (d, 1H, J = 7.6 Hz, Ar), 7.72 (d, 1H, J = 2.1 Hz, Ar), 7.63-7.60 (m, 4H, Ar), 7.50 (m, 1H, Ar), 7.25 (dd, 1H, J = 2.1, 7.6 Hz, Ar), 7.22 (s, 1H, Ar), 7.21 (s, 1H, Ar), 6.77 (s, 1H, Ar), 6.45 (dd, 1H, J = 1.5, 7.6 Hz, Ar), 4.52 (q, 2H, J = 7.1 Hz, CH_2), 2.26 (s, 3H, CH_3), 1.42 (t, 3H, J = 7.1 Hz, CH_3). ^{13}C NMR (600 MHz, acetone-d_6) δ 167.83 (C1), 166.88, 153.03 (2 x CH), 150.51, 147.22, 141.74, 140.32, 139.21, 136.97, 127.11, 126.94 (2 x CH), 123.65, 123.58, 123.28, 122.69, 121.35, 119.87, 119.57, 117.76, 114.98, 110.05, 109.66 (Ar), 38.25 (CH_2), 21.99 (CH_3), 14.15 (CH_3).

3.3.3.19 *fac*-[Re(5Me-Sal-Triaz)(CO)$_3$(NC$_5$H$_5$)]

The title compound, *fac*-[Re(5Me-Sal-Triaz)(CO)$_3$(NC$_5$H$_5$)], was synthesised in a similar fashion as *fac*-[Re(5Me-Sal-Trypt)(CO)$_3$(NC$_5$H$_5$)] in §3.3.3.16 using $AgNO_3$ (0.0992 g, 5.841 x 10^{-4} mol, 3eq), ReAA (0.150 g, 1.947 x 10^{-4} mol), 5Me-SalH-Triaz (0.0413 g, 2.044 x 10^{-4} mol) and pyridine (0.0231 g, 2.920 x 10^{-4} mol). The product was obtained as a yellow solid. (Yield: 0.0528 g, 49.3 %).

IR (ATR, cm^{-1}): $\nu_{(CO)}$ 2008.1, 1870.6. UV-Vis (nm, $L.mol^{-1}.cm^{-1}$): λ_{max} = 343.0, ε = 2.938 x 10^3. ^{1}H NMR (600 MHz, acetone-d_6) δ 9.95 (s, 1H, NH), 8.83 (m, 1H, Ar), 8.34 (m, 1H, Ar), 8.14 (m, 1H, Ar), 7.87 (m, 2H, Ar), 7.64 (d, 1H, J = 7.4 Hz, Ar), 6.90 (m, 1H, Ar), 6.81 (s, 2H, Ar), 3.30 (s, 1H, CH), 2.37 (s, 3H, CH_3). ^{13}C NMR (600 MHz, acetone-d_6) δ 197.31, 162.38, 154.28, 153.79, 149.60, 146.29, 134.55, 127.20, 126.78, 121.96, 121.32, 119.88, 118.06 (Ar), 49.99, 22.01 (CH_3).

3.3.3.20 *fac*-[Et_4N][Re(*o*Tol)$(CO)_3Br_2$]

ReAA (0.100 g, 1.298 x 10^{-4} mol) was dissolved in methanol. SalH-*o*Tol (0.0302 g, 1.428 x 10^{-4} mol), containing 10 % *o*-toluidine as byproduct, was added to the reaction. The reaction was stirred for 2 h at room temperature. Crystals of the title complex[13] whereby the Re bonded preferentially to the amine were obtained by the slow evaporation of the solvent at 4 °C.

IR (KBr, cm^{-1}): $\nu_{(CO)}$ 2012.6, 1894.3, 1877.7. ^1H NMR (600 MHz, acetone-d_6) δ 7.34 (m, 1H, Ar), 7.00 (m, 1H, Ar), 6.70 (m, 1H, Ar), 6.43 (m, 1H, Ar), 2.50 (s, 3H, CH_3). ^{13}C NMR (600 MHz, acetone-d_6) δ 167.26, 135.06, 126.42, 126.11, 123.77, 113.43 (Ar), 18.02, 53.09, 7.76 (Et_4N).

3.3.3.21 *fac*-[Et_4N][Re(acac)$(CO)_3Br$]

ReAA (0.100 g, 1.298 x 10^{-4} mol) was dissolved in methanol. Acetylacetone (0.0143 g, 1.428 x 10^{-4} mol) dissolved in methanol was slowly added. The reaction was stirred at 56 °C for 24 h. Crystals of the title complex[14] were obtained by the slow evaporation of the solvent. (Yield: 0.0328 g, 56.3 %).

IR (KBr, cm^{-1}): $\nu_{(CO)}$ 2005.1, 1901.7, 1857.8. ^1H NMR (600 MHz, acetone-d_6) δ 5.33, (s, 1H, CH), 1.82 (s, 6H, CH_3), 3.50 (q, 8H, J = 7.3 Hz), 1.40 (tt, 12H, J = 7.3, 1.9 Hz) (Et_4N). ^{13}C NMR (600 MHz, acetone-d_6) δ 186.91, 101.71, 27.29, 53.09, 7.76 (Et_4N).

[13] A. Brink, H.G. Visser, A. Roodt, *Acta Cryst.*, 2011, E67, m32
[14] A. Brink, H.G. Visser, A. Roodt, *Acta Cryst.*, 2011, E67, m34

3.4 CONCLUSION

One of the objectives of this study was to investigate the substitution behaviour of the rhenium aqua species, *fac*-[Re(Sal-T)$(CO)_3$(**H_2O**)]. However due to several reasons listed below, this complex has not yet been made, at least not by a direct synthetic method.

Initially the attempts to synthesize the bromido complex *fac*-[Et_4N][Re(Sal-T)$(CO)_3$(Br)] in methanol was unsuccessful and yielded impure oils. In several reactions with ligands (such as SalH-3MeBu, SalH-Ph, SalH-Cy, SalH-*m*Tol) the bidentate ligand activated the Re metal centre to such a degree that the 3rd bromido ligand was replaced by methanol to form pure crystalline *fac*-[Re(Sal-T)$(CO)_3$(**$HOCH_3$**)] product, although in very low yields. It is not yet known whether this is due to steric or electronic effects.

The synthesis of the mono-aqua complexes (addition of 3 equivalents of $AgNO_3$ for 24 hours in H_2O (pH = 2.2) to ensure complete removal of all bromide anions, followed by filtration) yielded very poor results. Impure oils, with several products, were obtained as indicated by NMR. All attempts to recrystallize these complexes from the water medium were unsuccessful and the addition of a range of organic solvents in an attempt to induce crystallization of these products yielded poor results. Due to the low solubility of certain ligands in water, a small amount of methanol was added. In general, dominant formation of the *fac*-[Re(Sal-T)$(CO)_3$(**$HOCH_3$**)] species occurred and not *fac*-[Re(Sal-T)$(CO)_3$(**H_2O**)], however no product with high purity was ever obtained.

The decision to use methanol as solvent in the synthesis of Re(I)-tricarbonyl complexes with SalH ligands proved to be a successful one for several reasons. Firstly, it was possible to obtain crystallographically pure materials from methanol as opposed to the impure oils obtained from water. In terms of the [2 +1] approach we have shown here that the coordinated methanol is easily substituted to yield a pure product in satisfactory yield. This certainly creates yet another exciting prospect for the development of a radiopharmaceutical kit using the [2+1] approach with these ligand systems.

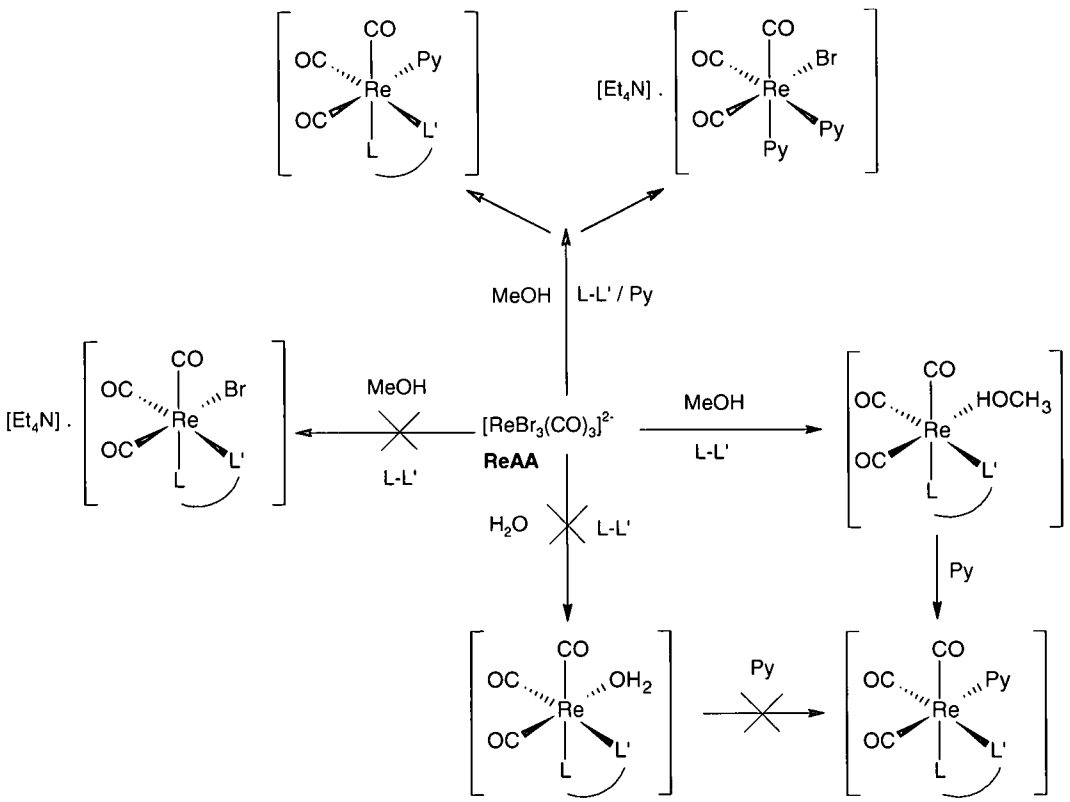

Scheme 3.1: **General reaction scheme of *fac*-[Re(L,L'-Bid)(CO)$_3$(S)] synthesis (L,L'-Bid = mono-anionic bidentate ligand, Py = pyridine, S = coordinating ligand).**

All methanol compounds were synthesized by first subjecting *fac*-$[Et_4N]_2^{2+}[Re(CO)_3Br_3]^{2-}$ to 3 equivalents of $AgNO_3$, after 26 hours of stirring at room temperature all three bromido ligands are replaced by methanol determined by mass analysis of the precipitated AgBr. Attempts to crystallize the *fac*-$[Re(CO)_3(HOCH_3)_3]^+$ complex were unsuccessful. The formation of the *fac*-[Re(Sal-T)(CO)$_3$(HOCH$_3$)] complexes were confirmed by IR, ^{1}H and ^{13}C NMR as well as X-ray diffraction. The Re complexes yield pure crystalline product at low temperature and are stable for several months when stored under an inert atmosphere. The majority lose crystallinity at temperatures above 35 °C to form oils, however the purity of the complexes are unaffected.

Carbonyl stretching frequencies, $\nu_{(CO)}$ of the synthesized complexes are summarised in Table 3.1 together with related bidentate complexes. IR spectroscopy is not an effective analytical method when utilized alone, however the carbonyl stretching frequency is often used for complex characterisation and is a good indication of the electron density surrounding the metal centre. As the electron density on the metal centre increases, the electron back-donation from the metal to the anti-bonding orbital on the C atom increases. This strengthens the Re-

CO bond and thus weakens the C≡O bond which results in a decrease in the $\nu_{(CO)}$ stretching frequency.

Table 3.1: Carbonyl stretching frequencies of *fac*-[Re(L,L'-Bid)(CO)$_3$(S)]^n complexes with L,L'-Bid = N-O, O-O', N-N' bidentate ligands and S = coordinated ligands.

Complex	Carbonyl stretching frequency, $\nu_{(CO)}$, (cm^{-1})			Ref
$[Et_4N]_2[Re(CO)_3Br_3]$	1996.2		1867.8	
N-O ligand				
[Re(Sal-*m*Tol)(CO)$_3$(HOCH$_3$)]	2002.0		1868.8	[a]
[Re(Sal-*m*Tol)(CO)$_3$(Py)]	2014.7		1890.5	[a]
[Re(Sal-3MeBu)(CO)$_3$(HOCH$_3$)]	2001.4		1876.5	[a]
[Re(Sal-3MeBu(CO)$_3$(Py)]	2013.6	1904.8	1878.4	[a]
[Re(Sal-Ph)(CO)$_3$(HOCH$_3$)]	2020.5		1892.5	[a]
[Re(Sal-Ph)(CO)$_3$(Py)]	2014.7	1906.6	1884.8	[a]
[Re(Sal-Cy)(CO)$_3$(HOCH$_3$)]	2014.9		1871.6	[a]
[Re(Sal-*p*Tol)(CO)$_3$(HOCH$_3$)]	2020.4		1892.4	[a]
[Re(Sal-4NitroPh)(CO)$_3$(HOCH$_3$)]	2021.0		1883.8	[a]
[Re(5Me-Sal-*m*Tol)(CO)$_3$(HOCH$_3$)]	2018.5	1922.5	1882.9	[a]
[Re(5Me-Sal-3Me2Bu)(CO)$_3$(HOCH$_3$)]	2015.6	1894.8	1872.1	[a]
[Re(5Me-Sal-Pen)(CO)$_3$(HOCH$_3$)]	2020.8		1894.8	[a]
[Re(5Me-Sal-Hist)(CO)$_3$]	2012.8	1902.6	1871.0	[a]
[Re(5Me-Sal-Trypt)(CO)$_3$(HOCH$_3$)]	2014.1		1885.4	[a]
[Re(5Me-Sal-Trypt)(CO)$_3$(Py)]	2016.4	1906.0	1881.9	[a]
[Re(5Me-Sal-Tyra)(CO)$_3$(Py)]	2013.8		1886.4	[a]
[Re(5Me-Sal-Carba)(CO)$_3$(Py)]	2010.4	1902.2		[a]
[Re(5Me-Sal-Triaz)(CO)$_3$(Py)]	2008.1		1870.6	[a]
[Re(2AcPy)(CO)$_3$Br]	2022	1929	1897	[d]
[Re(2PyAl)(CO)$_3$Br]	2012	1893	1876	[d]
[Re(imc)(CO)$_3$(H$_2$O)]	2039	1936		[e]
[Re(2,4-dipic)(CO)$_3$(H$_2$O)]	2036	1920		[e]
[Re(pico)(CO)$_3$(H$_2$O)]	2022	1908	1874	[c]
O-O' Bidentate ligand				
[Et$_4$N][Re(acac)(CO)$_3$Br]	2005.1	1901.7	1857.8	[a]
[Et$_4$N][Re(Flav)(CO)$_3$Br]	1999		1863	[b]
[Re(Flav)(CO)$_3$(H$_2$O)]	2013		1885	[b]
[Re(Flav)(CO)$_3$(Py)]	2012	1897	1860	[b]
N-N' Bidentate ligand				
[Re(2PyMePh)(CO)$_3$Br]	2024	1926	1897	[d]
[Re(2PyPh)(CO)$_3$Br]	2021	1915	1884	[d]
[Re(2PyProp)(CO)$_3$Br]	2018	1934	1889	[d]

[a] This study; [b] Synthesized by M. Schutte[15]; [c] Synthesised by G. Kemp[16]; [d] Synthesised by Wang *et. al.*[17]; [e] Synthesised by Mundwiler *et. al.*[18] (Py) = pyridine; (Flav) = anion of 3-hydroxyflavone; (2AcPy) = 2-acetyl-pyridine; (2PyAl) = 2-pyridine-aldehyde; (2PyMePh) = N-(2-pyridinylmethylmethylene)phenylamine; (2PyPh) = N-(2-pyridinylmethylene)phenylamine; (2PyProp) = N-(2-pyridinylmethylene)propylamine; (imc) = 4-imidazolcarboxylic acid; (2,4-dipic) = pyridine-2,4-dicarboxylic acid; (pico) = 2-pyridinecarboxylic acid.

[15] M. Schutte, *M.Sc. Dissertation*, University of the Free State, Bloemfontein, South Africa, 2008
[16] G. Kemp, *Ph.D. Thesis*, University of Johannesburg, Johannesburg, South Africa, 2006
[17] W. Wang, B. Springler, R. Alberto, *Inorg. Chim. Acta*, 2003, 355, 386
[18] S. Mundwiler, M. Kündig, K. Ortner, R. Alberto, *Dalton Trans.*, 2004, 1320

The IR spectra of *fac*-[Re(Sal-3MeBu)$(CO)_3(HOCH_3)$ / (Py)] and *fac*-[Re(Sal-*m*Tol)$(CO)_3(HOCH_3)$ / (Py)] show an increase in $\nu_{(CO)}$ stretching frequency from the MeOH to pyridine product indicating the lower electron density present on the Re(I) metal centre for the pyridine compound.[19,20,21,22] All the ^{1}H NMR spectra exhibit a strong peak at approximately 8 ppm for the imine proton. The ^{1}H NMR spectra of *fac*-[Re(Sal-*m*Tol)$(CO)_3(HOCH_3)$], *fac*-[Re(Sal-Ph)$(CO)_3(HOCH_3)$], *fac*-[Re(Sal-3MeBu)$(CO)_3(HOCH_3)$ /Py], *fac*-[Re(5Me-Sal-*m*Tol)$(CO)_3(HOCH_3)$] and [Re(5Me-Sal-3Me2Bu)$(CO)_3(HOCH_3)$] indicate rotamers for the nitrogen coordinated tail. The imine carbon (C1) is situated around 170-160 ppm in ^{13}C NMR spectra.

The single crystal X-ray diffraction study of the crystals obtained from procedures mentioned above are discussed in detail in the following chapters and clearly indicates the coordination of the methanol to the rhenium metal centre which is among the first published crystal structure of this type.[8] A kinetic study is included in later chapters as the effect of various bonded ligands on the reactivity of the normally inert Re(I) tricarbonyl complex should be investigated and understood as this synthon may possibly be used as a therapeutic or diagnostic tool in radiopharmacy.

[19] G.J.J. Steyn, A. Roodt, J.G. Leipoldt. *Inorg. Chem.*, 1992, 31, 3477
[20] S. Otto, A. Roodt. *Inorg. Chim. Acta*, 2004, 1
[21] A. Roodt, S. Otto, G. Steyl. *Coord. Chem. Rev.*, 2003, 245, 125
[22] A. Brink, H.G. Visser, A. Roodt, G. Steyl. *Dalton Trans.*, 2010, 1246

4 X-RAY CRYSTALLOGRAPHIC STUDY OF FREE LIGANDS CONTAINING SalH-AROMATIC FUNCTIONALITIES

4.1 INTRODUCTION

The salicylidene ligand systems (SalH or SalenH ligands) have played a significant role in the development of Schiff-base ligands in several interdisciplinary areas such as catalysis, biomedical and photo-physical chemistry.[1,2,3] The Schiff-base ligands provide a convenient manner in which the steric and electronic properties may be altered and allows easy labelling of biological functionalities.

Due to our interest in *fac*-$[M(CO)_3(H_2O)_3]^+$ complexes and the labelling possibilities which can occur on these complexes, a series of SalH compounds have been synthesised and X-ray single crystal studies initiated to further evaluate the coordination mode. A comparison of the crystallographic data of a variety of non-coordinated SalH-ligands with various aromatic, aliphatic and biological amine substituents coordinated to the salicylidene backbone will be made and discussed in Chapters 4 and 5. The various molecular interactions and crystal packing modes are described in the following paragraphs. The SalH-ligands which are evaluated in this crystallographic chapter are illustrated in Figure 4.1.

---

[1] R. Hernández-Molina, A. Merderos, *Comprehensive Coordination Chemistry II*, Eds.: J.A. McCleverty, T.J. Meyer, Pergamon Press, Oxford, UK, Vol. 1, 2004

[2] É. Tozzo, S. Romera, M.P. dos Santos, M. Muraro, R.H. de A. Santos, L.M. Lião, L. Vizotto, E.R. Dockal, *J. Mol. Struct.*, 2008, 876, 110

[3] A. Bourkoula, M. Paravatou-Petsotas, A. Papadopoulos, I. Santos, H.J. Pietzsch, E. Livaniou, M. Pelecanou, M. Papadopoulos, I. Pirmettis, *Eur. J. Med. Chem.*, 2009, 44, 4021

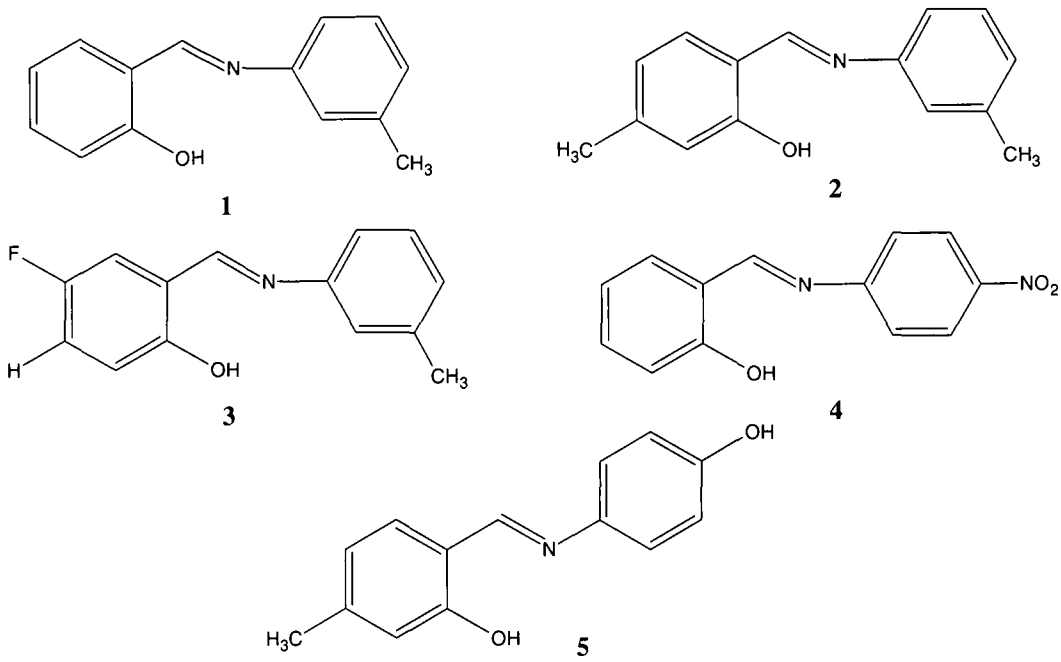

Figure 4.1: **The 2-(T-iminomethyl)phenol ligands (SalH-ligands, T = substituent) discussed in this single crystal X-ray diffraction chapter. (1) 2-(*m*-Tolyliminomethyl)phenol (SalH-*m*Tol), (2) 5-Methyl-2-(*m*-tolyliminomethyl)phenol (5Me-SalH-*m*Tol), (3) 4-Fluoro-2-(*m*-tolyliminomethyl)phenol (4F-SalH-*m*Tol), (4) 2-(4-Nitrophenyliminomethyl)phenol (SalH-4NitroPh), (5) 2-[(4-Hydroxyphenyl)iminomethyl]-5-methylphenol (5Me-SalH-4OHPh).**

An interesting aspect of the non-coordinated salicylidene ligands is the different possible conformations it can adopt in the solid state. Tautomerism between the phenol-imine (O-H···N) and the keto-amine (O···H-N) forms can occur depending on the intramolecular hydrogen bonding. Salicylaldimines tend to give the enol-imine tautomer in solution, whereas 2-hydroxy-1-naphthaldimines predominantly yield keto-amine tautomers and 3-hydroxy-2-naphthaldimines yields enol-imine tautomers.[4] Tautomerism also occurs in the solid state. An increase in the C=N bond distance is observed from X-ray structural analyses when the phenol-imine form is transformed to the keto-amine tautomer.[5] The aromatic Schiff-base group, 2-(phenyliminomethyl)phenol, are a typical class of photochromic materials involving both excited state intramolecular proton transfer (e.g. by photoexcitation with UV light whereby an ultrafast H-atom transfer from the hydroxyl group to the N atom occurs) and *cis-trans* isomerisation to form an orange-red photoproduct from the colourless crystal. The *trans*-enol isomer with intramolecular hydrogen bonding between the hydroxyl group and the

[4] J.D. Crane, *Annu. Rep. Prog. Chem., Sect. A: Inorg. Chem.*, 1995, 91, 205
[5] R. Hernández-Molina, A. Merderos, *Comprehensive Coordination Chemistry II*, Eds.: J.A. McCleverty, T.J. Meyer, Pergamon Press, Oxford, UK, Vol. 1, 2004

nitrogen atom is the generally accepted form of 2-(phenyliminomethyl)phenol in the ground state. Due to electronic redistribution in the excited states, the two aromatic rings rotate around the -C=N- bond axis. Studies on thermochromic and photochromic Schiff-base compounds has resulted in the proposal that rotation around the -C=N- bond influences the specific properties, with planar molecules exhibiting thermochromism and non-planar molecules exhibiting photochromism. The various polymorphs of 2-(phenyliminomethyl)phenol have been isolated and reported.[6,7]

The planarity and rotation of the -C=N- bond of each of the free salicylidene ligands in solid state will be further discussed in following paragraphs.

4.2 EXPERIMENTAL

The reflection data was collected on a Bruker X8 ApexII 4K CCD diffractometer[8] using Mo *K*α radiation with ω-and-φ-scans at 100 K. COSMO[9] was utilized for optimum collection of more than a hemisphere of reciprocal space. Frame integration and data reduction were performed using the Bruker SAINT-Plus[10] and XPREP[10] software packages, respectively. Data was corrected for absorption effects using the multi-scan technique SADABS.[11] The data for the compounds 5Me-SalH-*m*Tol and 5Me-SalH-4OHPh were collected on a Oxford Diffraction Xcalibur 3 Crysalis CCD system[12] using Mo Kα (0.71073 Å) and ω-scans. Intensity data were extracted and integrated using Crysalis RED.[13] The structures were solved by direct methods package SIR97[14] and refined using the software package WinGX,[15] incorporating SHELXL.[16] All non-hydrogen atoms were refined with anisotropic displacement parameters, while the methyl, methane and aromatic H atoms were placed in geometrically idealized positions and constrained to ride on their parent atoms, with (C-H =

---

[6] F. Arod, M. Gardon, P. Pattison, G. Chapuis, *Acta Cryst.*, 2005, C61, o317
[7] F. Arod, P. Pattison, K.J. Schenk, G. Chapuis, *Crystal Growth and Design*, 2007, 7, 1679
[8] Bruker, APEX2 (Version 1.0-27), Bruker AXS Inc., Madison, Wisconsin, USA, 2005
[9] Bruker, COSMO, Version 1.48, Bruker AXS Inc., Madison, Wisconsin, USA, 2003.
[10] Bruker, SAINT-Plus (Version 7.12) (including XPREP), Bruker AXS Inc., Madison, Wisconsin, USA, 2004
[11] Bruker, SADABS, Version 2004/1, Bruker AXS Inc., Madison, Wisconsin, USA,1998.
[12] Crysalis CCD. Oxford Diffraction Ltd., Abingdon, Oxfordshire, U.K., 2005.
[13] Crysalis RED. Oxford Diffraction Ltd., Abingdon, Oxfordshire, U.K., 2005.
[14] A. Altomare, M.C. Burla, M. Camalli, G.L. Cascarano, C. Giacovazzo, A. Guagliardi, A.G.G. Moliterni, G. Polidori, R. Spagna, *J. Appl. Cryst.* 1999, 32, 115.
[15] L.J. Farrugia, *J. Appl. Cryst.*, 1999, 32, 837
[16] G.M. Sheldrick, SHELXL97, *Program for Solving Crystal Structures*, University of Göttingen, Germany, 1997

0.98-0.95 Å and $U_{iso}(H) = 1.5U_{eq}(C)$ and $1.2U_{eq}(C)$), respectively. The methyl protons were located from a difference Fourier map and the group was refined as a rigid motor. The absolute structure parameter of compounds in non-centrosymmetric space groups, analyzed with Mo radiation, is meaningless as the compound is a weak anomalous scatterer (i.e. no atom heavier than Si is present). Therefore the absolute structure parameter (Flack parameter) was removed from the CIF. The program DIAMOND[17] was used for all graphical representation of the crystal structures. All structures are shown with thermal ellipsoids drawn at 50% probability level unless otherwise stated. Graphical representations of overlays of selected complexes are obtained with Hyperchem 7.52.[18]

A summary of the general crystal data and refinement parameters is given in Table 4.1, for all five aromatic salicylidene molecules. Supplementary data for the atomic coordinates, bond distances and angles and anisotropic displacement parameters are given in the Appendix A for each individual dataset.

[17] K. Brandenburg, H. Putz, DIAMOND, Release 3.0c, Crystal Impact GbR, Bonn, Germany, 2005
[18] Hyperchem™ Release 7.52, Windows Molecular Modeling System, Hypercube, Inc., 2002

Table 4.1: **General X-ray crystallographic data and refinement parameters for aromatic salicylidene ligands.**

Compound	SalH-*m*Tol (1)	5Me-SalH-*m*Tol (2)	4F-SalH-*m*Tol (3)	SalH-4NitroPh (4)	5Me-SalH-4OHPh (5)
Empirical Formula	$C_{14}H_{13}NO$	$C_{15}H_{15}NO$	$C_{14}H_{12}FNO$	$C_{13}H_{10}N_2O_3$	$C_{14}H_{13}NO_2$
Formula weight	211.25	225.28	229.25	242.23	227.25
Temperature (K)	100(2)	298(2)	100(2)	100(2)	298(2)
Wavelength (Å)	0.71073 Å	0.71073	0.71073	0.71073	0.71073
Crystal System	Orthorhombic	Orthorhombic	Monoclinic	Monoclinic	Monoclinic
Space Group	$P2_12_12_1$	$P2_12_12_1$	Pc	$P2_1/c$	$P2_1/c$
Unit Cell Dimensions					
a (Å)	7.4946(4)	5.9067(4)	10.2655(6)	12.417(7)	13.3314(6)
b (Å)	11.8669(6)	7.6913(6)	4.6738(2)	5.7016(4)	12.0865(5)
c (Å)	12.2970(6)	27.179(2)	12.3561(8)	15.374(1)	7.2705(3)
α (°)	90	90	90	90	90
β (°)	90	90	112.331(3)	97.570(4)	100.908(4)
γ (°)	90	90	90	90	90
Volume (Å^3)	1093.7(1)	1234.8(2)	548.37(5)	1079.0(1)	1150.4(1)
Z	4	4	2	4	4
Density$_{calc.}$ (g.cm^{-1})	1.283	1.212	1.388	1.491	1.312
μ (mm^{-1})	0.081	0.076	0.099	0.108	0.088
F(000)	448	480	240	504	480
Crystal Colour	Red	Yellow	Yellow	Red	Orange
Crystal Morphology	Plate	Cuboid	Plate	Cuboid	Needle
Crystal Size (mm)	0.35x0.22x0.08	0.20x0.15x0.10	0.19x0.10x0.06	0.32x0.29x0.11	0.31x0.08x0.08
Theta Range (°)	2.39 to 28.30	2.75 to 27.99	3.39 to 27.99	1.65 to 28.00	2.29 to 28.00
Completeness (%)	100.0	99.9	99.6	99.2	99.5
Index Ranges	h = -9 to 9 k = -15 to 12 l = -13 to 16	h = -7 to 7 k = -9 to 10 l = -21 to 35	h = -13 to 13 k = -5 to 6 l = -16 to 16	h = -14 to 16 k = -7 to 7 l = -20 to 20	h = -17 to 17 k = -15 to 15 l = -5 to 9
Reflections Collected	11293	9912	7009	16744	9011
Independent Reflections	1572	1758	1319	2592	2768
R_{int}	0.0548	0.1133	0.0275	0.0441	0.0574
Refinement method	Full-matrix least-squares on F^2	Full-matrix least-squares on F^2	Full-matrix least-squares on F^2	Full-matrix least-squares on F^2	Full-matrix least-squares on F^2
Data / restraints / parameters	1572 / 0 / 150	1758 / 0 / 154	1319 / 2 / 156	2592 / 0 / 163	2768 / 0 / 155
Goodness-of-fit on F^2	1.093	0.780	1.062	1. 057	0.747
Final R indices [I>2sigma(I)]	R1 = 0.0434, wR2 = 0.0937	R1 = 0.0413, wR2 = 0.0668	R1 = 0.0343, wR2 = 0.0915	R1 = 0.0500, wR2 = 0.1239	R1 = 0.0484, wR2 = 0.1195
R indices (all data)	R1 = 0.0604 wR2 = 0.1021	R1 = 0.1999, wR2 = 0.0929	R1 = 0.0386, wR2 = 0.0954	R1 = 0.0700, wR2 = 0.1448	R1 = 0.1212, wR2 = 0.1361
ρ_{max} and ρ_{min} (e.Å^{-3})	0.214 and -0.209	0.100 and -0.117	0.189 and -0.189	0.572 and -0.246	0.270 and -0.219

(SalH-*m*Tol) = 2-(*m*-tolyliminomethyl)phenol; (5Me-SalH-*m*Tol) = 5-methyl-2-(*m*-tolyliminomethyl)phenol; (4F-SalH-*m*Tol) = 4-fluoro-2-(*m*-tolyliminomethyl)phenol; (SalH-4NitroPh) = 2-(4-nitrophenyliminomethyl) phenol; (5Me-SalH-4OHPh) = 2-[(4-hydroxyphenyl)iminomethyl]-5-methylphenol.

4.3 CRYSTAL STRUCTURE OF SalH-*m*Tol

The compound 2-(*m*-tolyliminomethyl)phenol (SalH-*m*Tol) (**1**) crystallizes in a orthorhombic crystal system in the $P2_12_12_1$ space group with four formula units per unit cell (Z = 4).[19] The asymmetric unit contains one complete molecule. The molecular structure of (**1**) is represented in Figure 4.2 along with the atom numbering scheme.

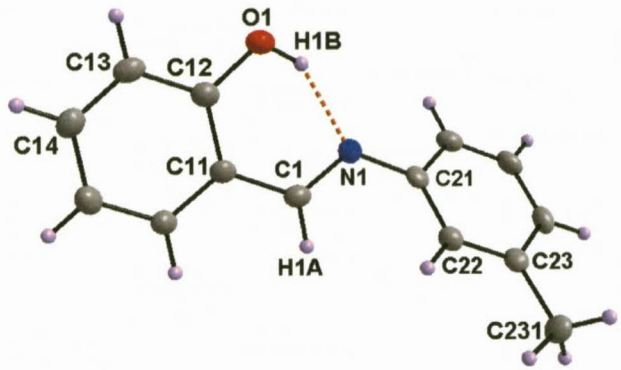

Figure 4.2: **Molecular structure of SalH-*m*Tol showing atom numbering system. For the aromatic rings, the first digit refers to the ring number, while the second digit refers to the specific C-atom in the ring. Hydrogen bond interaction indicated by orange dotted line. Displacement ellipsoids are drawn at 50% probability level.**

Table 4.2: **Selected bond distances and angles for the compound SalH-*m*Tol [Å and °].**

Atoms	Distance	Atoms	Angle
C1-N1	1.289(3)	N1-C1-C11	121.2(2)
N1-C21	1.426(3)	C1-N1-C21	119.5(2)
C1-C11	1.444(3)	N1-C21-C22	122.2(2)
C11-C12	1.415(3)	C12-O1-H1B	109.5*
C12-O1	1.355(2)	C11-C12-O1	120.9(1)
C21-C22	1.392(3)	C22-C23-C231	121.0(1)
C23-C231	1.509(3)	C26-C21-C22	120.1(2)
N1-H1B	1.848(2)		

*No e.s.d. as H-atoms were placed as riding

The molecule crystallizes as the *trans* phenol-imine tautomer with one strong intramolecular hydrogen bond occurring between the O1-H1B...N1 atoms (Table 4.3). The O1...N1 distance (2.595(2) Å) is significantly shorter than the sum of the van der Waals radii for N and O (3.07 Å)[20] and is comparable for other similar compounds.[6] The C1-N1 bond distance of 1.289(3) Å is indicative of a double bond whereas the N1-C21 (1.426(3) Å) and C12-O1 (1.355(2) Å) bond distances are consistent with single bonds. All bond angles and lengths in

[19] A. Brink, A. Roodt, H.G. Visser, *Acta Cryst.*, 2009, E65, o3175
[20] A. Bondi, *J. Phys. Chem.*, 1964, 68, 441

(**1**) are within normal ranges.[21] No classical intermolecular hydrogen interactions occur for this compound in the unit cell. Rotation around the -C=N- causes non-planar packing of the ligand as indicated by the angle between the planes (47.03(8)°) drawn through the aromatic rings (Plane 1: C11, C12, C13, C14, C15, C16 and Plane 2: C21, C22, C23, C24, C25, C26). The nitrogen atom is bent slightly below Plane 1 as indicated by the small torsion angle (O1-C12-C11-N1 = 3.2(2)°). The SalH-*m*Tol molecules pack in a horizontal line along the *c*-axis to form a pseudo herring-bone cross packing.

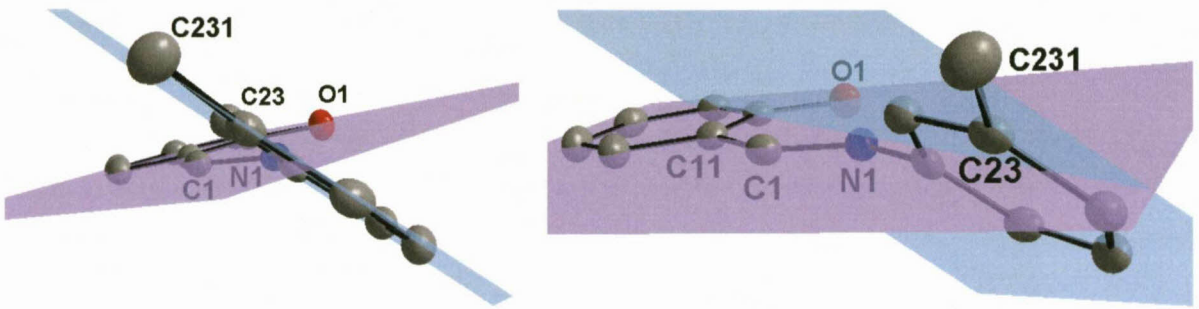

Figure 4.3: **Twisting of aromatic rings as indicated by planes 1 and 2. H atoms have been omitted for clarity.**

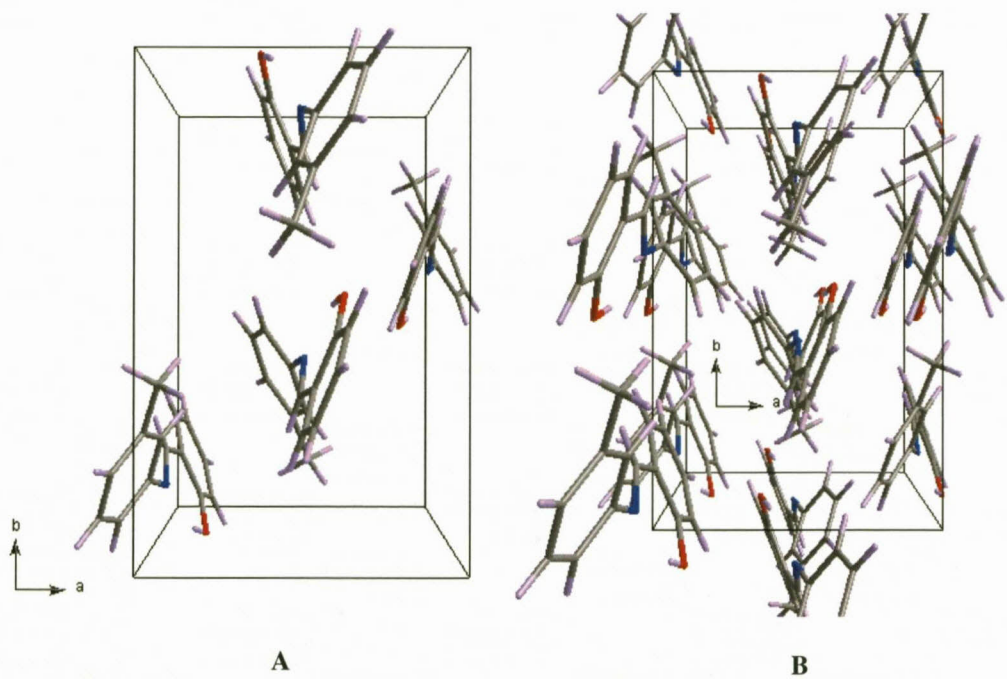

Figure 4.4: **Molecular packing of (1) in the unit cell viewed along the *c*-axis. (A) Single unit cell. (B) Herring-bone packing of molecules.**

[21] F.H. Allen, O. Kennard, D.G. Watson, L. Brammer, A.G. Orpen, R. Taylor, *J. Chem. Soc., Perkin Trans.* II, 1987, S1

Table 4.3: Hydrogen bonds for SalH-*m*Tol [Å and °].

D-H...A	d(D-H)	d(H...A)	d(D...A)	<(DHA)
O(1)-H(1B)...N(1)#1	0.84	1.85	2.595(2)	146.8

Symmetry transformations used to generate equivalent atoms:
#1 x,y,z

4.4 CRYSTAL STRUCTURE OF 5Me-SalH-*m*Tol

The free 5-methyl-2-(*m*-tolyliminomethyl)phenol ligand (5Me-SalH-*m*Tol) (**2**) crystallizes in a orthorhombic crystal system in the $P2_12_12_1$ space group with four formula units per unit cell (Z = 4) at 298 K. Due to the diffraction data being collected at room temperature, larger thermal vibrations along the bond axes are found with R_{int} = 0.1133, GOOF = 0.780; therefore all thermal ellipsoids are drawn at 30% probability level. The molecular structure of (**2**) is represented in Figure 4.5 along with the atom numbering scheme.

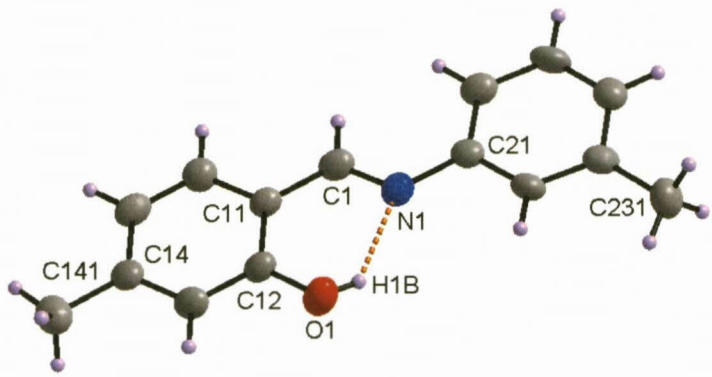

Figure 4.5: Molecular structure of 5Me-SalH-*m*Tol showing atom numbering system. For the aromatic rings, the first digit refers to the ring number, while the second digit refers to the specific C-atom in the ring. Hydrogen bond interaction indicated by orange dotted line. Displacement ellipsoids are drawn at 30% probability level.

Table 4.4: Selected bond distances and angles for the compound 5Me-SalH-*m*Tol [Å and °].

Atoms	Distance	Atoms	Angle
C1-N1	1.282(3)	N1-C1-C11	121.6(4)
N1-C21	1.425(4)	C1-N1-C21	122.1(3)
C1-C11	1.451(4)	N1-C21-C22	115.1(4)
C11-C12	1.399(4)	C12-O1-H1B	109.5*
C12-O1	1.350(4)	C11-C12-O1	120.9(4)
C21-C22	1.390(4)	C22-C23-C231	120.8(4)
C23-C231	1.510(4)	C26-C21-C22	119.1(4)
C14-C141	1.499(4)		
N1-H1B	1.923(3)		

*No e.s.d. as H-atoms were placed as riding

The molecule crystallizes as the *trans* phenol-imine tautomer and only one intramolecular hydrogen bond interaction occurs between the O1-H1B...N1 atoms (Table 4.5). No classical intermolecular hydrogen interactions occur for this compound in the unit cell. As opposed to the crystal structure of SalH-*m*Tol, there is no rotation around the -C=N- bond, resulting in a near planar molecule (Figure 4.6) with the molecules stacking to form a sinusoidal-type wave.

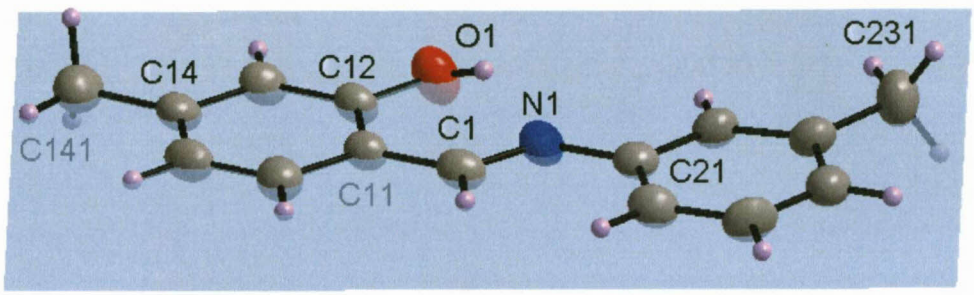

Figure 4.6: **Graphical representation of the 5Me-SalH-*m*Tol ligand indicating co-planarity of aromatic rings.**

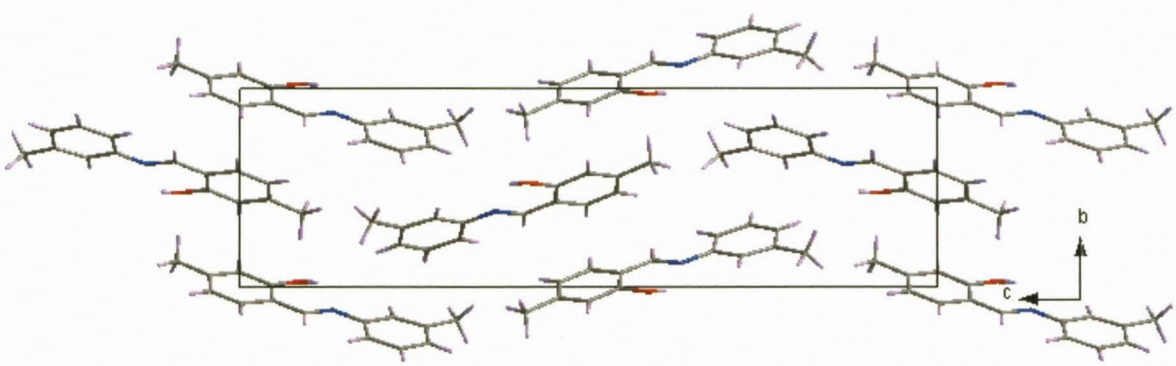

Figure 4.7: **Sinusoidal packing of 5Me-SalH-*m*Tol molecules as viewed along the *a*-axis.**

Table 4.5: **Hydrogen bonds for 5Me-SalH-*m*Tol [Å and °].**

D-H...A	d(D-H)	d(H...A)	d(D...A)	<(DHA)
O(1)-H(1B)...N(1)#1	0.82	1.92	2.591(4)	137.9

Symmetry transformations used to generate equivalent atoms:
#1 x,y,z

4.5 CRYSTAL STRUCTURE OF 4F-SalH-*m*Tol

The molecule, 4-fluoro-2-(*m*-tolyliminomethyl)phenol (4F-SalH-*m*Tol) (**3**) crystallizes in a monoclinic crystal system in the *Pc* space group with two molecules per unit cell (Z = 2). The molecular structure of (**3**) is represented in Figure 4.8 along with atom numbering scheme.

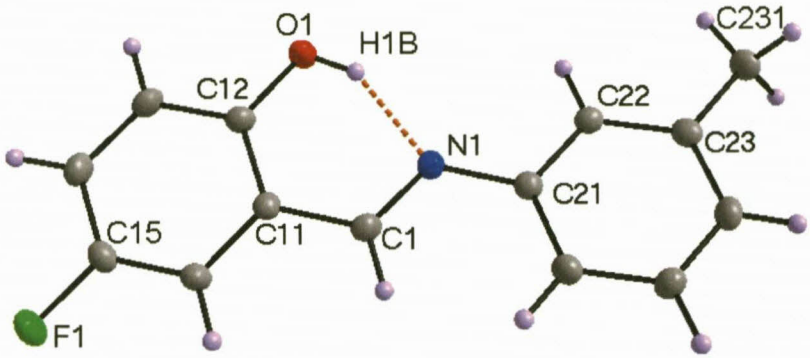

Figure 4.8: **Molecular structure of 4F-SalH-*m*Tol showing atom numbering system. For the aromatic rings, the first digit refers to the ring number, while the second digit refers to the specific C-atom in the ring. Hydrogen bond interaction indicated by orange dotted line. Displacement ellipsoids are drawn at 50% probability level.**

Table 4.6: **Selected bond distances and angles for the compound 4F-SalH-*m*Tol [Å and °].**

Atoms	Distance	Atoms	Angle
C1-N1	1.287(3)	N1-C1-C11	121.2(2)
N1-C21	1.422(3)	C1-N1-C21	120.7(2)
C1-C11	1.450(3)	N1-C21-C22	116.3(2)
C11-C12	1.407(3)	C12-O1-H1B	109.5*
C12-O1	1.353(3)	C11-C12-O1	121.3(2)
C21-C22	1.395(3)	C22-C23-C231	120.9(2)
C23-C231	1.499(3)		
F1-C15	1.361(2)		
N1-H1B	1.855(2)		

*No e.s.d. as H-atoms were placed as riding

The molecule crystallizes as the *trans* phenol-imine tautomer and only one intramolecular hydrogen bond interaction occurs between the O1-H1B...N1 atoms (H1B...N1 distance of 1.855(2) Å and angle of 147.2(1)°). The *m*-tolyl ring is twisted slightly out of the horizontal plane with a dihedral angle of 9.28(7)° between the two aromatic planes (Figure 4.9). Multiple chelated hydrogen bond interaction occurs between the two independent molecules namely C1-H1A...O1 and C16-H16...O1 (symmetry operation: x, 1-y, -0.5+z; D...A = 3.467(3) Å and 3.495(3) Å; C1-H1A...O1 bond angle of 151.0(1)° and C16-H16...O1 bond angle of 149.1(1)°). The two independent molecules pack nearly perpendicular to each other

as indicated by the dihedral angle (88.01(5)°) between planes drawn through the C1 and C1' aromatic rings. The hydrogen interaction bite angle (H1A-O1-H16) is 55.27(3)° (Figure 4.10A).

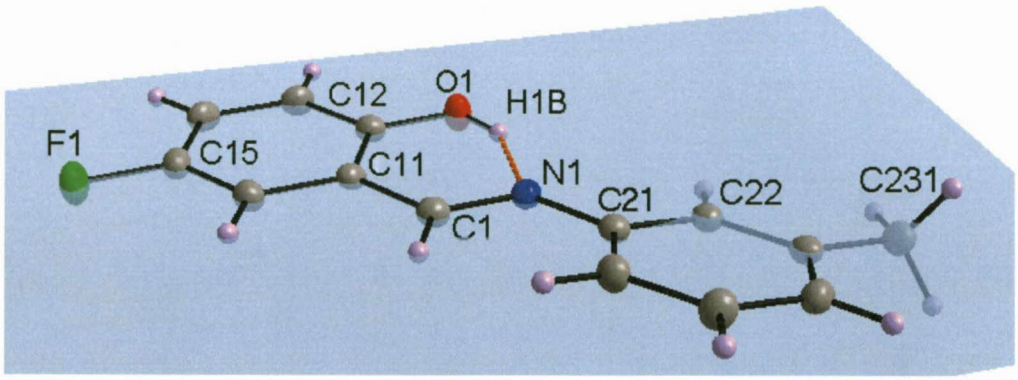

Figure 4.9: **Graphical representation of the 4F-SalH-*m*Tol ligand indicating slight twisting of the C=N bond and general co-planarity of phenyl rings.**

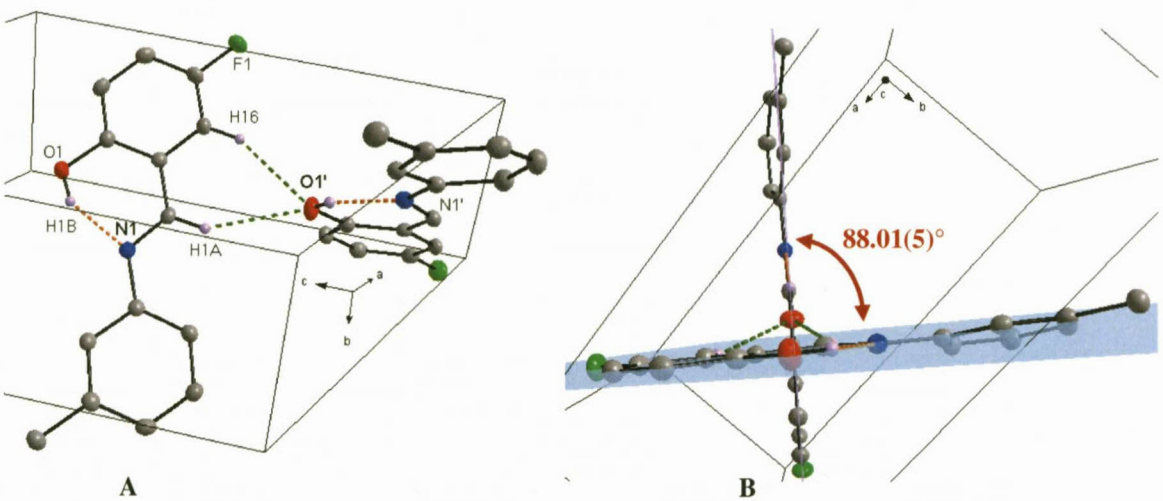

Figure 4.10: **Molecular packing of the unit cell viewed indicating (A) intra- (orange line) and inter-molecular (green line) hydrogen bond interaction and (B) perpendicular orientation of molecules. Some H-atoms are omitted for clarity.**

Other stabilizing soft contacts are formed between H...F with C13-H13...F1' = 152.8(1)°, H...F = 2.600(1) Å (symmetry operation F1' = x, -y, 0.5+z) and with C231-H23C...F1" = 113.9(1)°, H...F = 2.668(2) Å (symmetry operation F1" = -1+x, 2+y, z) to form horizontal linear packing (Figure 4.11 A) parallel to the *ac*-axis plane. Some π-pseudo chelate interactions are observed in the crystal packing between the aromatic ring and the N1-C1-C11-C12-O1 plane with a dihedral angle of only 0.86(6)° (distance between centroids

3.4523(1) Å) (Figure 4.11 B). The molecules pack in a cross-hatching manner to form cubic tunnels when viewed along the *c*-axis (Figure 4.12).

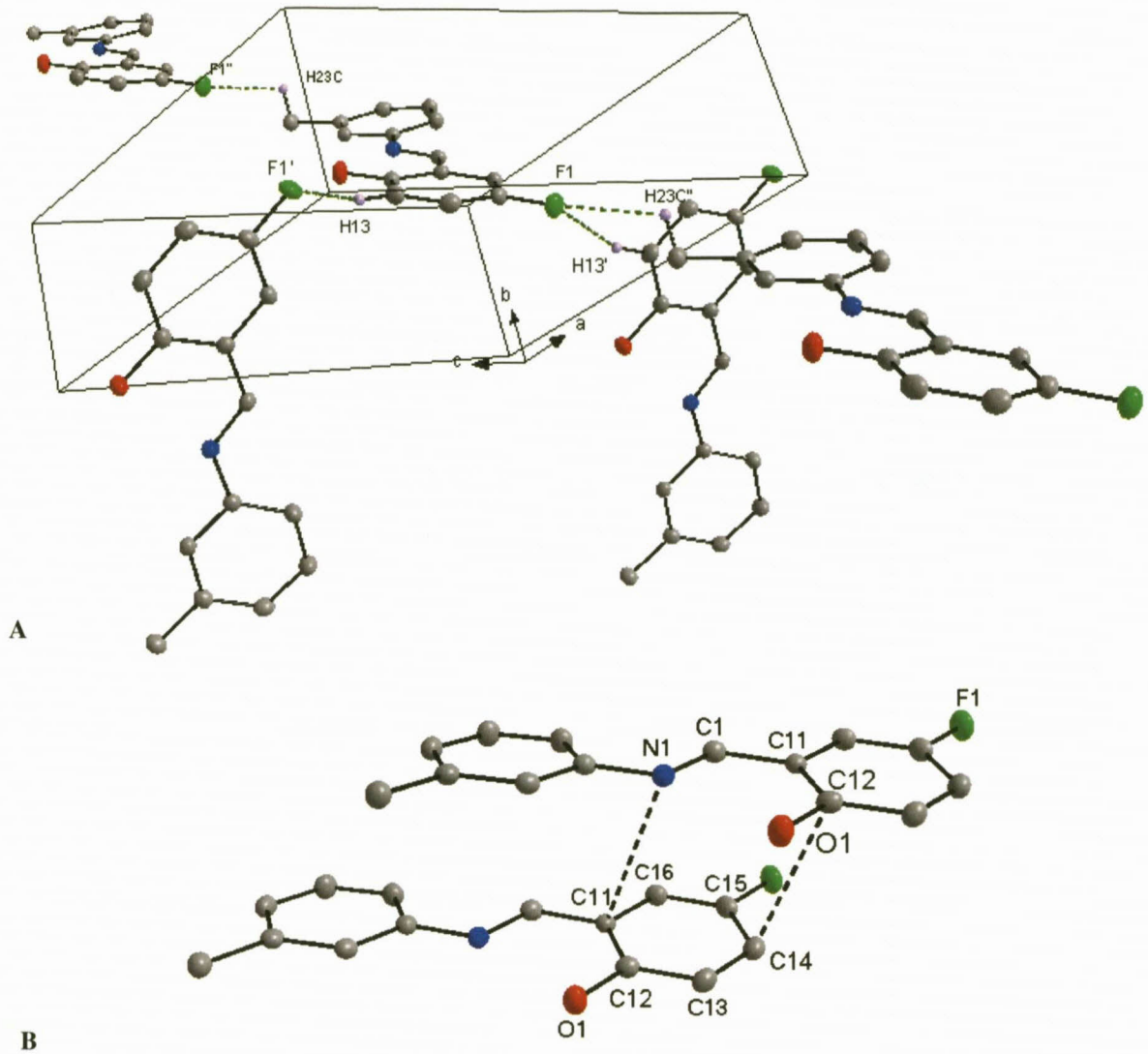

Figure 4.11: **Molecular packing of the unit cell indicating (A) C-H…F intermolecular interaction, (B) π-pseudo chelate ring interaction.**

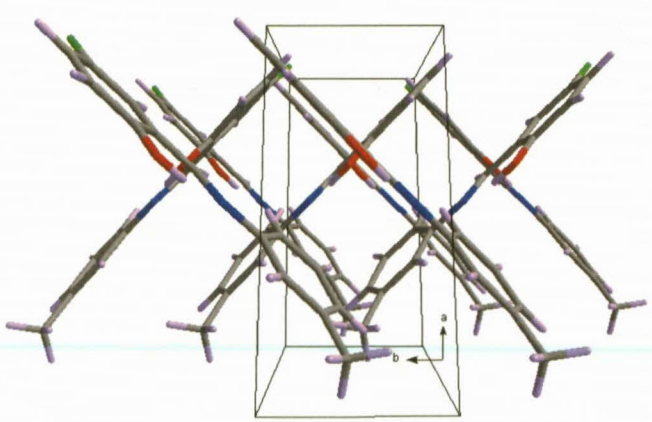

Figure 4.12: **Molecular packing to form cube-like tunnels as viewed along the *c*-axis.**

4.6 CRYSTAL STRUCTURE OF SalH-4NitroPh

The compound 2-(4-nitrophenyliminomethyl)phenol (SalH-4NitroPh) (**4**) crystallized in the monoclinic space group $P2_1/c$, with four molecules in the unit cell (Z = 4). The asymmetric unit contains one complete molecule. This compound has previously been reported by Burgess *et al.*[22] at 190(2) K. The redetermination of the crystal structure was performed at 100 K for the sake of completion and no significant deviations were obtained except for shortening of the *b* and *c* unit cell axes as compared to the collection examined at 190(2) K (*b* = 5.7016(4) Å *vs.* 5.744(2) Å; *c* = 15.374(1) Å *vs.* 15.597(3) Å; β = 97.570(4)° *vs.* 97.69(2)°). The molecular structure of (**4**) is represented in Figure 4.13 along with the atom numbering scheme and important bond distances and angles are shown in Table 4.7.

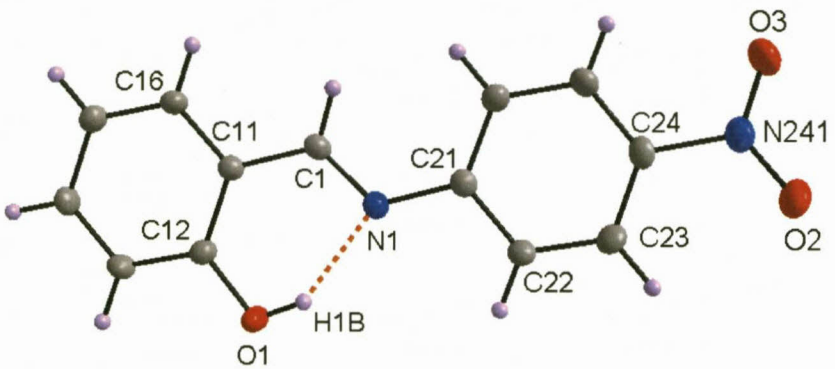

Figure 4.13: **Molecular structure of SalH-4NitroPh showing atom numbering system. For the aromatic rings, the first digit refers to the ring number, while the second digit refers to the specific C-atom in the ring. Hydrogen bond interaction indicated by orange dotted line. Displacement ellipsoids are drawn at 50% probability level.**

Table 4.7: **Selected bond distances and angles for the compound SalH-4NitroPh [Å and °].**

Atoms	Distance	Atoms	Angle
C1-N1	1.289(2)	N1-C1-C11	121.9(2)
N1-C21	1.418(2)	C1-N1-C21	121.1(2)
C1-C11	1.445(2)	N1-C21-C22	115.9(1)
C11-C12	1.414(2)	C12-O1-H1B	109.5*
C12-O1	1.353(2)	C11-C12-O1	121.6(1)
C21-C22	1.391(2)	O3-N241-O2	123.5(2)
C24-N241	1.462(2)	O3-N241-C24	117.9(2)
N241-O2	1.230(2)	O2-N241-C24	118.6(2)
N241-O3	1.229(2)	O1-C12-C11-N1	4.3(2)
N1-H1B	1.900(2)	C1-N1-C21-C26	7.1(3)

*No e.s.d. as H-atoms were placed as riding

[22] J. Burgess, J. Fawcett, D.R. Russell, S.R. Gilani, V. Palma, *Acta Cryst.*, 1999, C55, 1707

The molecule crystallizes as the *trans* phenol-imine tautomer with the expected intramolecular hydrogen bond occuring between the O1-H1B...N1 atoms. All bond angles and lengths are within normal range,[21] with the C1-N1 bond distance of 1.289(2) Å typical of a double bond and C21-N1 (1.418(2) Å), C1-C11 (1.445(2) Å) and C12-O1 (1.353(2) Å) bond distances typical of single bonds for the respective atoms. Intermolecular hydrogen bonding occurs between C14-H14...O2 (symmetry operation: -1+x, -0.5-y, -0.5+z; D...A = 3.331(3) Å). The compound is essentially planar with minimal rotation around the –C1=N1- double bond with dihedral angle between the two aromatic rings (Plane 1: C11, C12, C13, C14, C15, C16 and Plane 2: C21, C22, C23, C24, C25, C26) of 3.02(5)°.

Table 4.8: Hydrogen bonds for SalH-4NitroPh [Å and °].

D-H...A	d(D-H)	d(H...A)	d(D...A)	<(DHA)
O(1)-H(1B)...N(1)#1	0.84	1.90	2.639(2)	146.2
C(14)-H(14)...O(2)#2	0.95	2.56	3.331(3)	138.6

Symmetry transformations used to generate equivalent atoms:
#1 x,y,z #2 x-1,-y-1/2,z-1/2

Two ring π-π interactions exist between neighbouring molecules as indicated by Figure 4.14A (green dotted line). The interactions occur between C1 and C2 aromatic rings which cause the molecules to pack in a "head-to-tail" fashion, with a centroid to centroid distance of 3.563(3) Å for both interactions (symmetry operation: 1-x, -y, -z) and a dihedral angle of 3.02(5)°. A few soft contacts *via* van der Waals interactions are observed in the crystal packing between aromatic carbon atoms and hydrogen atoms: C16-H16...C11 = 136.6(1)°, H16...C11 = 2.727(2) Å and C26-H26...C14 = 137.1(1)°, H26...C14 = 2.816(2) Å (symmetry operation: 1-x, -0.5+y, -0.5-z) (Figure 4.14A, orange dotted line). An O...O' soft contact also assists in stabilising the molecular packing *via* C12-O1...O1'-C12' (O1...O1' bond distance = 2.892(2) Å, C12-O1...O1' = 163.5(1)°, symmetry operation: 1-x, -1-y, -z) (Figure 4.14B, orange dotted line).

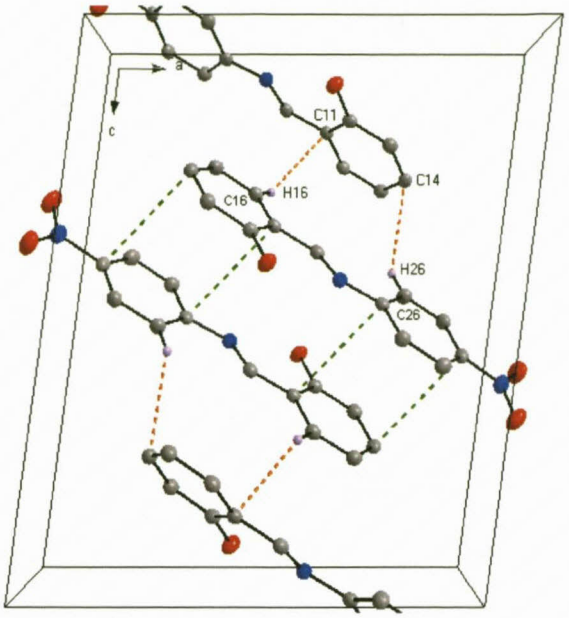

Figure 4.14 A: **Graphical representation of π-π interaction (green line) and C-H...C intermolecular interaction (orange line) between related molecules. Certain H atoms are omitted for clarity.**

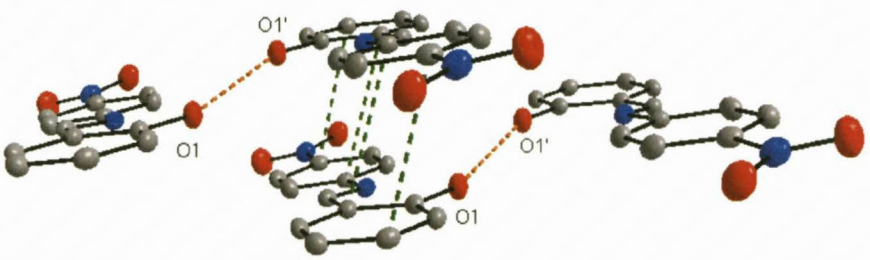

Figure 4.14 B: **Graphical representation of π-π interaction (green line) and C-O...O-C intermolecular interaction (orange line) between related molecules. Certain H atoms are omitted for clarity.**

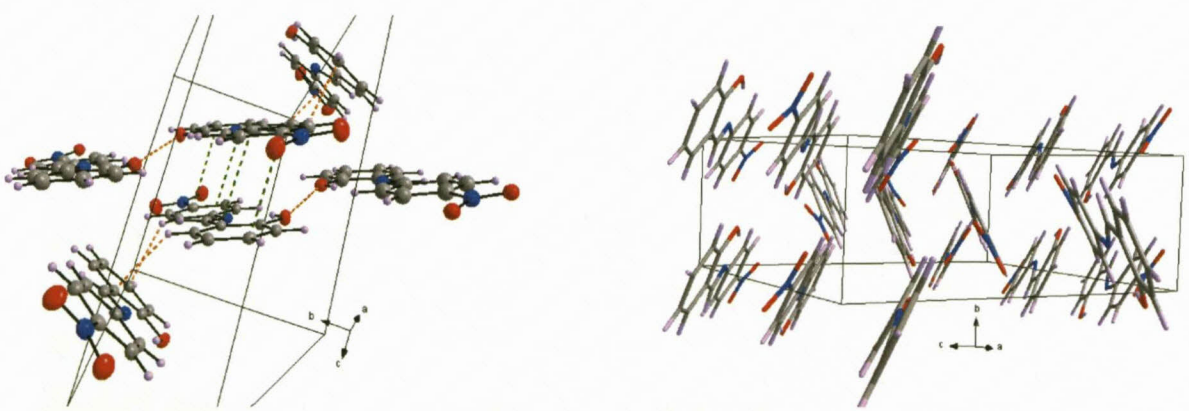

A **B**

Figure 4.15: **Graphical representation (A) of all soft molecular interactions in the unit cell. (B) Zig-zag packing of molecules in unit cell. Certain atoms are omitted for clarity.**

4.7 CRYSTAL STRUCTURE OF 5Me-SalH-4OHPh

The compound, 2-[(4-hydroxyphenyl)iminomethyl]-5-methylphenol (5Me-SalH-4OHPh) (**5**), crystallized in the monoclinic space group $P2_1/c$, with four molecules in the unit cell (Z = 4) at 298 K. Due to the diffraction data being collected at room temperature, larger thermal vibrations along the bond axes are found with a GOOF value of 0.747. All thermal ellipsoids are therefore drawn at 30% probability level. The molecular structure of (**5**) is represented in Figure 4.16 along with the atom numbering scheme and important bond distances and angles are given in Table 4.9.

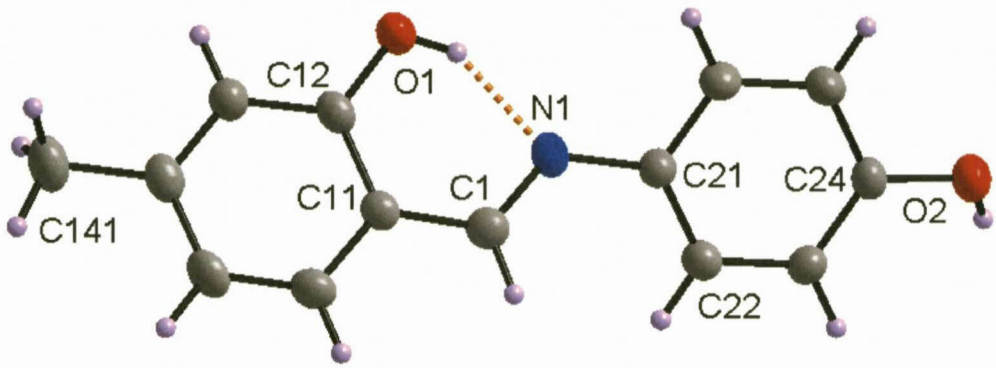

Figure 4.16: **Molecular structure of 5Me-SalH-4OHPh showing atom numbering system. For the aromatic rings, the first digit refers to the ring number, while the second digit refers to the specific C-atom in the ring. Hydrogen bond interaction indicated by orange dotted line. Displacement ellipsoids are drawn at 30% probability level.**

Table 4.9: **Selected bond distances and angles for the compound 5Me-SalH-4OHPh [Å and °].**

Atoms	Distance	Atoms	Angle
C1-N1	1.297(2)	N1-C1-C11	121.8(2)
N1-C21	1.423(2)	C1-N1-C21	124.8(2)
C1-C11	1.420(3)	N1-C21-C22	124.1(2)
C11-C12	1.421(3)	C12-O1-H1B	109.5*
C12-O1	1.331(2)	C11-C12-O1	120.5(2)
C21-C22	1.374(3)	O2-C24-O23	123.7(2)
C24-O2	1.365(2)	O2-C24-O25	117.3(2)
N1-H1B	1.795(2)	O1-C12-C11-N1	1.7(2)
		C1-N1-C21-C22	27.0(3)

*No e.s.d. as H-atoms were placed as riding

The molecule crystallizes as the *trans* phenol-imine tautomer with the expected intramolecular hydrogen bond occuring between the O1-H1B...N1 atoms. All bond angles and lengths are within normal range,[21] with the C1-N1 bond distance of 1.297(2) Å which is typical of a double bond and C21-N1 (1.423(2) Å), C1-C11 (1.420(3) Å) and C12-O1

(1.331(2) Å) bond distances typical of single bonds for the respective atoms. The compound is non-planar with a dihedral angle between the two aromatic rings (Plane 1: C11, C12, C13, C14, C15, C16 and Plane 2: C21, C22, C23, C24, C25, C26) of 31.9(6)°. Intermolecular hydrogen bonding occurs between O2-H2...O1 (symmetry operation: 1-x, -0.5+y, 1.5-z; D...A = 2.685(2) Å).

Table 4.10: Hydrogen bonds for 5Me-SalH-4OHPh [Å and °].

D-H...A	d(D-H)	d(H...A)	d(D...A)	<(DHA)
O(1)-H(1B)...N(1)#1	0.82	1.79	2.535(2)	149.3
O(2)-H(2)...O(1)#2	0.82	2.02	2.685(2)	137.7

Symmetry transformations used to generate equivalent atoms:
#1 x,y,z #2 -x+1,y-1/2,-z+3/2

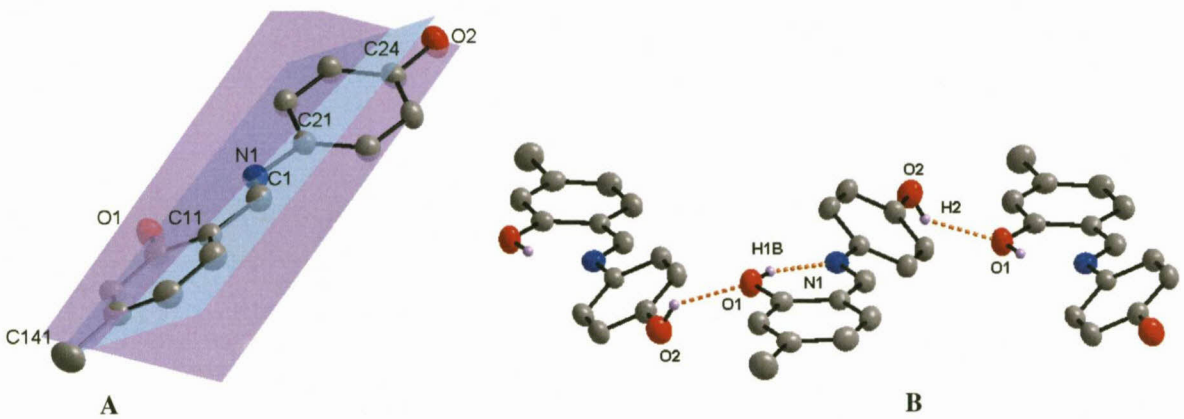

Figure 4.17: Graphical representation of 5Me-SalH-4OHPh (A) indicating twisting of aromatic rings as indicated by planes 1 (blue) and 2 (purple). (B) Intra- and inter-molecular hydrogen bonding. Certain H atoms have been omitted for clarity.

Molecular packing is also stabilized by the formation of ligand to ligand π-stacking in which the ligands pack in a twisted "head-to-tail" mode whereby three π-π interactions are shared between four ligands. Table 4.11 below lists the various centroid to centroid distances and Figure 4.18B illustrates the π-interaction by green dotted lines.

Table 4.11: π-π Interaction between aromatic rings of ligand molecule.

Centroid atom	Centroid atom	Distance between centroid atoms (Å)	Interplanar angle (°)
Cg1	Cg1#1	3.644(3)	1.12(7)
Cg1	Cg1#2	3.644(3)	0
Cg2	Cg2#3	4.096(3)	1.12(7)

Symmetry transformations used to generate equivalent atoms:
#1 x, 0.5-y, -0.5+z; #2 x, 0.5-y, 0.5+z; #3 1-x, 1-y, 1-z
Cg1 = centroid atom of C11, C12, C13, C14, C15, C16; Cg2 = centroid atom of C21, C22, C23, C24, C25, C26

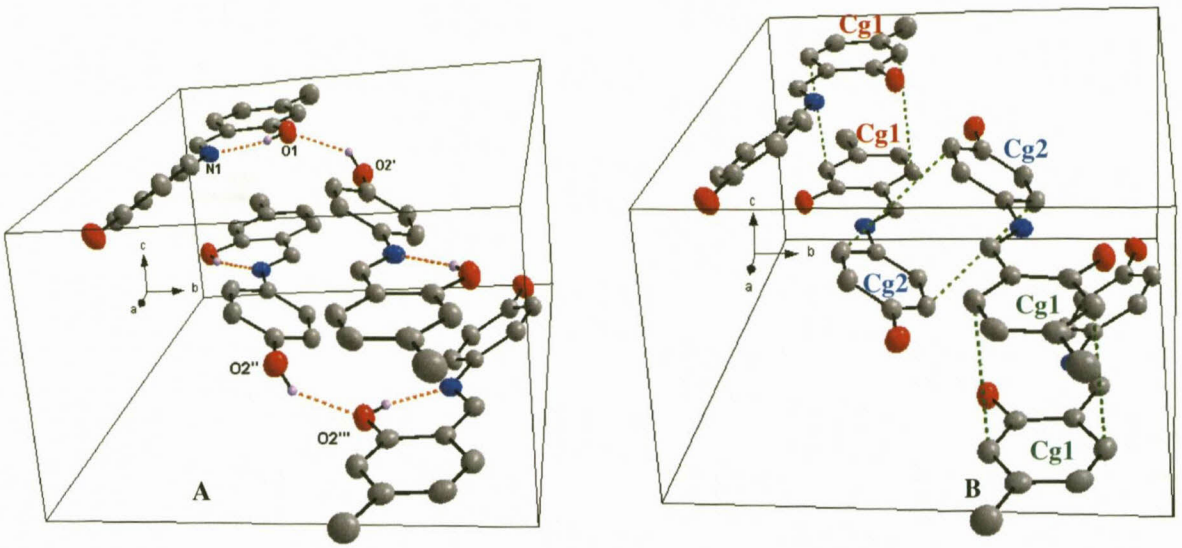

Figure 4.18: **Graphical representation of 5Me-SalH-4OHPh (A) Intra- and inter-molecular hydrogen bonding between molecules in unit cell (B) π-π interaction (green dotted line) between molecules in unit cell (Cg = centroid atom of aromatic ring). H atoms have been omitted for clarity.**

Molecular packing is further stabilized by C-H…π interactions which occurs between C26-H26…Cg2' (symmetry operation: x, 0.5-y, 0.5+z) with an angle of 144.6(1)° and H26… Cg2' distance of 2.7180(1) Å (Figure 4.19A). The molecules stack in the form of a sinusoidal wave when viewed along the *a*-axis (Figure 4.19B).

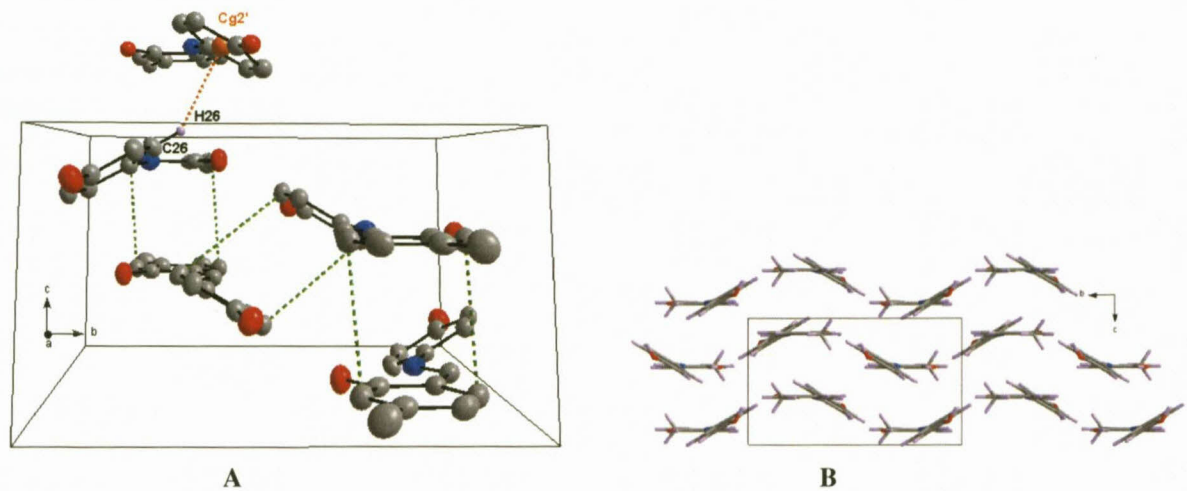

Figure 4.19: **(A) Graphical representation of the C-H…π interaction (orange dotted line) in the crystal packing of the molecule. (B) Sinusoidal packing of 5Me-SalH-4OHPh molecules as viewed along the *a*-axis.**

4.8 INTERPRETATION AND CORRELATION OF STRUCTURAL PARAMETERS

The following subsection correlates structural data from the different aromatic salicylidene compounds as described above. Table 4.13 gives the general bond distances and angles of the crystal structures under discussion.

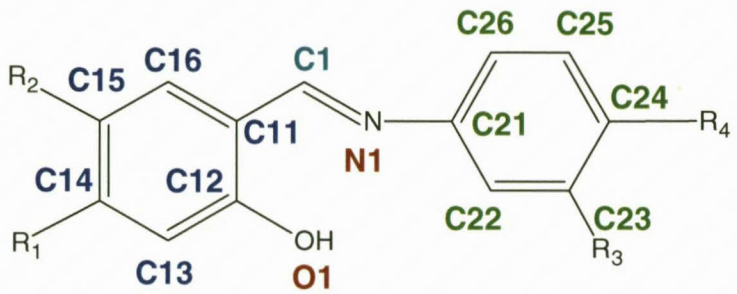

R_1 = H, CH_3; R_2 = H, F; R_3 = H, CH_3; R_4 = H, NO_2

Figure 4.20: **Atom numbering scheme of the aromatic 2-("T"-iminomethyl)phenol ligands (SalH-"T" ligands, where T = various substituents).**

Table 4.12: **Cell dimension overview of presented salicylidene derivatives.**

Compound	**SalH-*m*Tol** **(1)**	**5Me-SalH-*m*Tol** **(2)**	**4F-SalH-*m*Tol** **(3)**	**SalH-4NitroPh** **(4)**	**5Me-SalH-4OHPh** **(5)**
Crystal System	Orthorhombic	Orthorhombic	Monoclinic	Monoclinic	Monoclinic
Space Group	$P2_12_12_1$	$P2_12_12_1$	Pc	$P2_1/c$	$P2_1/c$
Temperature (K)	100(2)	298(2)	100(2)	100(2)	298(2)
Unit Cell Dimensions					
a (Å)	7.4946(4)	5.9067(4)	10.2655(6)	12.417(7)	13.3314(6)
b (Å)	11.8669(6)	7.6913(6)	4.6738(2)	5.7016(4)	12.0865(5)
c (Å)	12.2970(6)	27.179(2)	12.3561(8)	15.374(1)	7.2705(3)
α (°)	90	90	90	90	90
β (°)	90	90	112.331(3)	97.570(4)	100.908(4)
γ (°)	90	90	90	90	90
Volume (Å^3)	1093.7(1)	1234.8(2)	548.37(5)	1079.0(1)	1150.4(1)
Z	4	4	2	4	4

Table 4.13: **Selected geometrical parameters of the presented salicylidene derivatives, tabulated for comparison [Å and °].**

Compound	SalH-*m*Tol (1)	5Me-SalH-*m*Tol (2)	4F-SalH-*m*Tol (3)	SalH-4NitroPh (4)	5Me-SalH-4OHPh (5)
Bonds Distance (Å)					
N1-C1	1.289(3)	1.282(3)	1.287(3)	1.289(2)	1.297(2)
N1-C21	1.426(3)	1.425(4)	1.422(3)	1.418(2)	1.423(2)
C1-C11	1.444(3)	1.451(4)	1.450(3)	1.445(2)	1.420(3)
C12-O1	1.355(2)	1.350(4)	1.353(3)	1.353(2)	1.331(2)
N1...H1B	1.848(2)	1.923(3)	1.855(2)	1.900(2)	1.795(2)
Bond angle (°)					
O1-C12-C11	120.9(1)	120.9(4)	121.3(2)	121.6(1)	120.5(2)
N1-C1-C11	121.2(2)	122.1(3)	121.2(2)	121.9(2)	121.8(2)
C1-N1-C21	119.5(2)	122.1(3)	120.7(2)	121.1(2)	124.8(2)
N1-C21-C22	122.2(2)	115.1(4)	116.3(2)	115.9(1)	124.1(2)
Torsion angle (°)					
O1-C12-C11-N1	3.2(2)	1.5(3)	1.1(2)	4.3(2)	1.7(2)
C1-N1-C21-C22	42.7(3)	1.1(5)	10.4(3)	7.1(3)	27.0(3)
Dihedral angle through Ring 1 and Ring 2 (°)	47.03(8)	1.8(1)	9.28(7)	3.02(5)	31.9(6)

The salicylidene molecules of (**1**), (**2**) and (**3**) all contain the same coordinated *m*-tolyl substituent bonded to the N atom. The differences between these three molecules are the atoms or functionalities bonded to the salicylaldehyde backbone namely, H, CH_3 and F. Despite molecules (**1**) and (**2**) crystallising in the same crystal system (orthorhombic) and space group, $P2_12_12_1$, they are not isomorphic as the unit cell parameters show significant deviations.

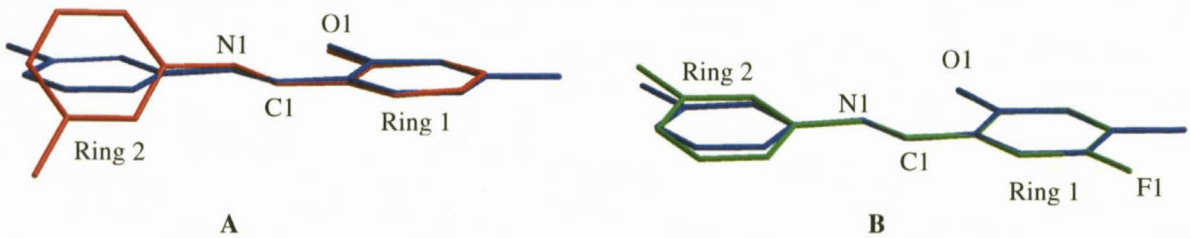

A B

Figure 4.21: **An overlay of crystal structures to indicate the variation of rotation between the two aromatic rings. (A) An overlay of SalH-*m*Tol (1) (indicated in red) and 5Me-SalH-*m*Tol (2) (indicated in blue). Overlay drawn only through atoms C11, C12, C13, C14, C15, C16 to allow free rotation of the *m*-tolyl substituent; RMS = 5.39 x 10^{-2} Å. (True overlay through all atoms, RMS = 1.28 Å). (B) An overlay of 5Me-SalH-*m*Tol (2) (blue) and 4F-SalH-*m*Tol (3) (green). Overlay drawn only through atoms C11, C12, C13, C14, C15, C16 to allow free rotation of the *m*-tolyl substituent; RMS = 1.80 x 10^{-2} Å. (True overlay through all atoms, RMS = 0.100 Å).**

Similarly the molecules (**4**) and (**5**) crystallise in the same spacegroup $P2_1/c$ but are not isomorphic. All molecules crystallise with four independent molecules in the unit cell (Z=4) except for (**3**) which only contains two molecules (Z=2).

The bond angles and distances of the five salicylidene molecules are within normal range,[21] and are comparable to crystal structure determinations of analogous salicylidene compounds.[7,23,24,25,26,27,28,29] The salicylidene molecules crystallize as the *trans* phenol-imine tautomer with strong intramolecular O-H...N hydrogen bond to form a pseudo six membered aromatic ring. The bond distance of C1=N is typical of a double bond for the respective atoms. Significant interest in the planarity of the salicylidene molecules has been expressed in literature due to their photochromic and thermochromic potential (§ 4.1). The crystal structures of molecules (**2**), (**3**) and (**4**) are nearly planar with minimal rotation of the C1=N1 double bond and similar N1-C21-C22 bond angles. Compound (**1**) and (**5**) indicate significant non-planarity in the solid state, with a dihedral angle of 47.03(8)° and 31.9(6)° respectively. It is not yet fully understood what may be the cause of the rotation of the second aromatic ring (for example: steric / electronic parameters of ligand, crystallizing solvent properties, reaction to heat or light).

4.9 CONCLUSION

The crystal structures of five aromatic salicylidene derivatives were analysed and discussed in this section. The five neutral compounds, which will be utilised as coordinating ligands for *fac*-$[M(CO)_3]^+$ moieties (M = Re, Tc), crystallise mainly in two space groups, however this is likely a coincidence and is not a tendency noted in literature of other reported salicylidene compounds. The crystal structure of all five compounds display molecular packing, stabilized by a variety of intra- and intermolecular hydrogen bonding, "head-to-tail" ligand π-stacking and soft van der Waal interactions.

---

[23] A. Karakaş, A. Elmali, H. Ünver, I. Svoboda, *J. Mol. Struct.*, 2004, 702, 103
[24] M.D. Cohen, G.M.J. Schmidt, S. Flavian, *J. Chem. Soc.*, 1964, 2041
[25] E. Hadjoudis, M. Vitterakis, I. Moustakali, I. Mavridis, *Tetrahedron*, 1987, 43, 1345
[26] D.K. Dey, S.P. Dey, A. Elmah, Y. Elerman, *J. Mol. Struct.*, 2001, 562, 177
[27] Z.S. Gül, F. Ersahin, E. Agar, S. Isik, *Acta Cryst.*, 2007, E63, o2854
[28] H.J. Xu, X.X. Gong, H. Wang, *Acta Cryst.*, 2008, E64, o638
[29] S. Gakias, C. Rix, A. Fowless, G. Wills-Johnson, K. Latham, J. White, *J. Mol. Struct.*, 2005, 737, 69

CHAPTER 4

Attempts to crystallize aliphatic salicylidene derivatives, synthesised as mentioned in Chapter 3, proved to be unsuccessful. The majority of the compounds are oils at room temperature whereas some are crystalline at -40 °C but melt too rapidly for successful mounting of the crystal for data collection. A computational study of the molecules in the gas phase, was conducted to better understand the variation of planarity of the two aromatic rings. The theoretical optimized structures with the lowest relative energy shall be compared to the crystal structures of the corresponding SalH ligand. This study is presented and discussed in Chapter 8. The salicylidene crystal structures containing biological active derivatives, bonded to the N atom, will be discussed in the following chapter.

5 X-RAY CRYSTALLOGRAPHIC STUDY OF FREE LIGANDS CONTAINING SalH-BIOLOGICAL FUNCTIONALITIES

5.1 INTRODUCTION

An important part of this investigation is concerned with the synthesis and evaluation of the solid state characteristics of the SalH ligand and whether this ligand system can be used to successfully coordinate to the *fac*-$[M(CO)_3]^+$ moiety. Another focus point is whether biological active derivatives such as amines could be linked to the salicylidene backbone with ease, in order for the organic molecule to be used as a radiolabelled functionality for the medical application in therapy and diagonistic imaging. Numerous bifunctional chelators have been explored for simple attachment of a biological directing molecule. The various methods which have been utilised were discussed in Chapter 2 with particular reference to chelators used for rhenium(I) and technetium(I) tricarbonyl precursors.

The importance of understanding the exact structural nature of a molecule should not be underestimated, particularly when its application is aimed for the medical field. The stereochemical properties of a molecule can affect the biological behaviour of the compound as illustrated by Louis Pasteur (1860) who was the first to demonstrate that molds and yeasts are able to differentiate between (+)- and (-)-tartarates, utilizing only one of the two isomers.[1] The compound *E*-triprolidine (Figure 5.1) was found to have a 1000-fold greater antihistamine activity than its corresponding *Z*-isomer.

[1] T. Nogrady, D.F. Weaver, *Medicinal Chemistry: A Molecular and Biochemical Approach*, 3rd Ed., Oxford University Press, Inc., Oxford, 2005

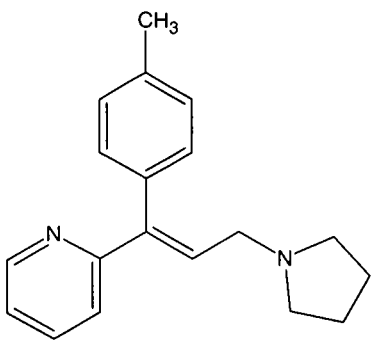

(*E*)-triprolidine

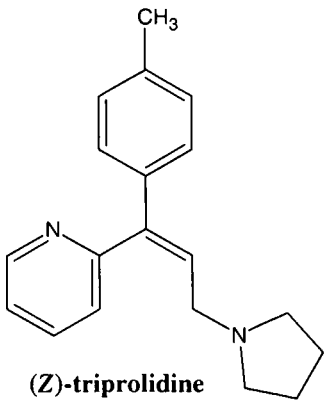

(*Z*)-triprolidine

Figure 5.1: Chemical structure of triprolidine.

The *Z*-isomer of the antipsychotic drug chlorprothixene (Taractan) has 12 times more neuroleptic potency than the corresponding *E*-isomer (Figure 5.2).

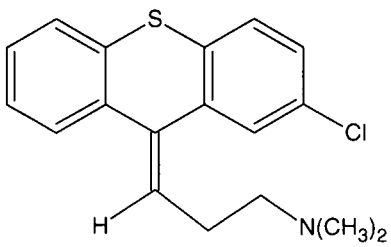

(*Z*)-chloroprothixene

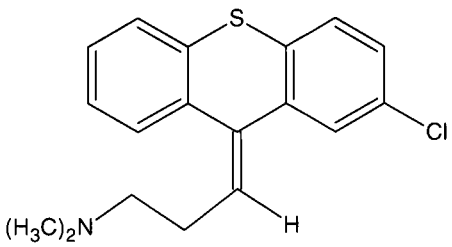

(*E*)-chloroprothixene

Figure 5.2: Chemical structure of chloroprothixene.

The *E*-isomer of the anticancer drug diethylstilbestrol has 14 times greater estrogenic activity than the *Z*-isomer which is possibly caused by the structural resemblance to estradiol, whose interatomic distance between the two hydroxyl functionalities are similar (Figure 5.3).[2]

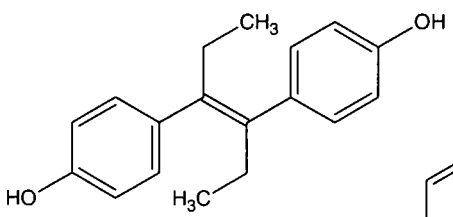

(*E*)-diethylstilbestrol

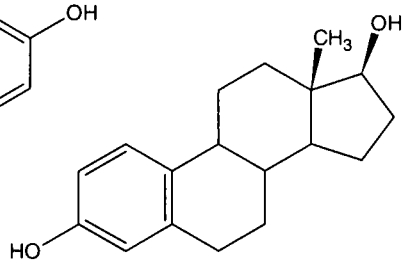

Estradiol

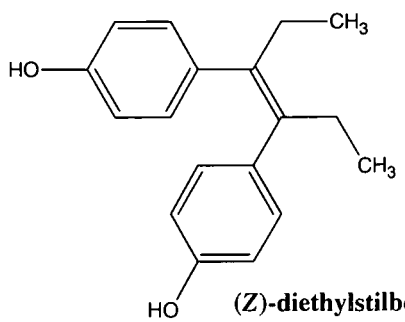

(Z)-diethylstilbe

Figure 5.3: Chemical structure of diethylstilbestrol.

[2] R.B. Silverman, *The Organic Chemistry of Drug Design and Drug Action*, 2nd Ed., Elsevier Academic Press, London, 2004

X-ray crystallography still remains as "the gold standard" when trying to determine the geometry and absolute configuration of a potential drug molecule. Not only can it provide structural insights into small drug molecules, X-ray crystallography can also provide data concerning drug-macromolecule interactions (if a drug and its receptor are co-crystallised). While X-ray crystallography provides structural information about the solid-state form of possible drug molecules it should be remembered that the geometry and conformation may not necessarily bear any resemblance to the solution phase structure of the molecule.

The synthesis of various functionalized salicylidene ligands whereby biologically active amines were attached to the ligand backbone *via* the N atom was described in Chapter 3. These biological amines were selected for the diversity in known biological activity and steric size. The biological activity of the utilized amines is briefly described below:

- **Histamine** - An antibody is produced when a sensitized person is exposed to an allergen, resulting in an antigen-antibody reaction and histamine is released. Histamine binds to the H_1 receptor and causes allergic and hypersensitivity reactions, such as hay fever, itching, urticaria (edematous patches of skin) and anaphylactic shock. Antihistamine compounds are antagonists of histamine receptors and are widely used to treat the above mentioned symptoms.[2]
- **3-Amino-9-ethylcarbazole** - 3-Amino-9-ethylcarbazole (AEC) is used as a substrate for a variety of enzymes and is a suspected carcinogen. It is used to detect cytochrome oxidase[3] and in the AEC staining kit for immunohistochemistry and immunoblotting.[4] The interest in using 3-amino-9-ethylcarbazole was to determine whether the close proximity of a stericly bulky amine would prevent ligand coordination to the Re/Tc metal centre.
- **Tryptamine** - Tryptamine contains the indole ring structure and is classified as a neurotransmitter.[5] It occurs as an endogenous constituent of mammalian brain at very low concentrations. It can be synthesized by the decarboxylation of the amino acid L-tryptophan[6,7] and has played a foundational role as a prototypical flexible biomolecule. Serotonin (5-hydroxytryptamine, 5-HT), a close analogue of tryptamine,

[3] M.S. Burstone, *Enzyme Histochemistry*, Academic Press, New York, 1962
[4] Sigma-Aldrich, Material Safety Data Sheet, www. sigma-aldrich.com, Version 4.0, Revision Date 2010
[5] A.L. Nicely, J.M. Lisy, *J. Phys. Chem. A*, 2011, 115, 2669
[6] R.S.G. Jones, *Progress in Neurobiology*, 1982, 19, 117
[7] R.A. Abramovitch, D. Shapiro, *J. Chem. Soc.*, 1956, 4589

is an important neurotransmitter and regulatory molecule[8] which is involved in a wide variety of physiologic functions and behaviours such as sleep, mood, appetite, muscle and gastrointestinal functions.[9] The biological activity, in particular the hallucinogenic effects, of various tryptamine derivatives have been investigated.[8,10]

- **Tyramine** - The adrenergic system produces neurotransmitters belonging to the chemical class of substances known as catecholamines. Compounds such tyrosine, dopamine, norepinephrine, epinephrine (adrenaline), tyramine and octopamine are biogenetically related catecholamines. The various pathways leading to their biosynthesis are well-studied biochemical pathways.[11] Tyramine binds to a receptor that triggers the release of norepinephrine, which can raise the systemic blood pressure and can cause a hypertensive episode.[2]
- **3-Amino-1,2,4-triazole** - A new generation of fungicides is based on five-membered rings containing three nitrogen atoms – the triazole ring. These compounds are able to inhibit an enzyme present in fungi but not in plants or animals. The 1,2,4-triazole is the basis of modern agricultural fungicides as well as drugs for fungal diseases in humans. A triazole agent which is used against human fungal infections is fluconazole (Figure 5.4) which contains two triazoles.[12] Aminotriazoles are used in herbicides and can occur as food contaminants which suppress thyroid function.[13] *In vivo* tests of 3-amino-1,2,4-triazole indicate mutagenic effects (*i.e.* effects which cause genetic changes) and is a suspected human reproductive toxicant.[4] It is an inhibitor of mitochondrial and chloroplast function.

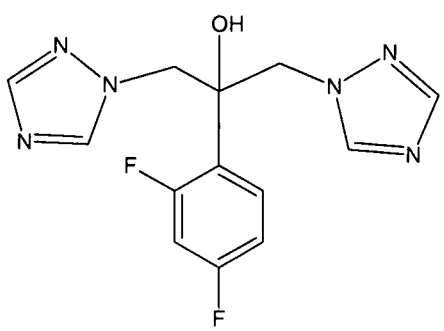

Figure 5.4: Chemical structure of fluconazole.

[8] E.M. Adkins, E.L. Barker, R.D. Blakely, *Mol. Pharmacol.*, 2001, 59, 514
[9] T.A. LeGreve, E.E. Baquero, T.S. Zwier, *J. Am. Chem. Soc.*, 2007, 129, 4028
[10] L.A. Faillace, A. Vourlekis, S. Szara, *J. Nerv. Ment. Dis.*, 1967, 145, 306
[11] T. Nogrady, D.F. Weaver, *Medicinal Chemistry: A Molecular and Biochemical Approach*, 3rd Ed., Oxford University Press, Inc., Oxford, 2005
[12] J. Clayden, N. Greeves, S. Warren, P. Wothers, *Organic Chemistry*, Oxford University Press, Oxford, 2001
[13] J.B. Freeman Clark, S.F. Queener, V. Burke Karb, *Pharmacologic Basis of Nursing Practice*, 4th Ed., Mosby, Missouri, 1993

Several crystal structures were obtained and a comparison of the crystallographic data of a variety of non-coordinated SalH-ligands will be made and discussed in this chapter. The various molecular interactions and crystal packing modes are described. The SalH-ligands which are described in this section are illustrated in Figure 5.5.

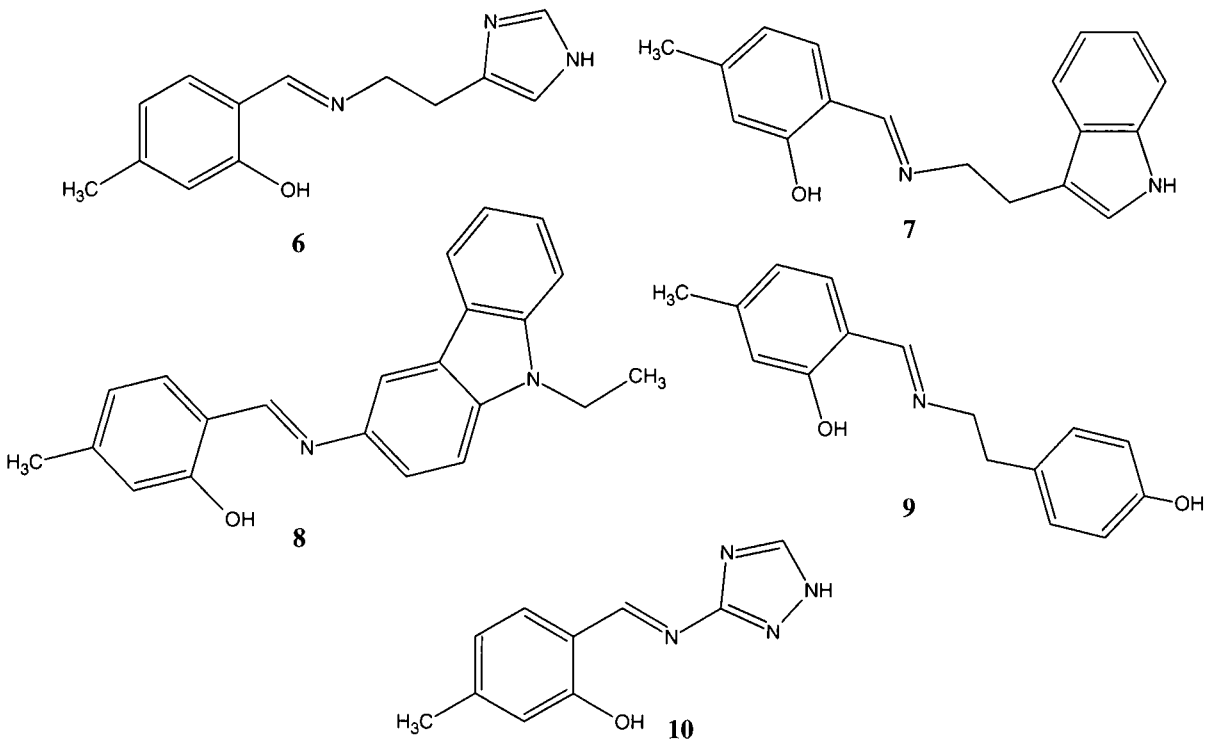

Figure 5.5: **The 2-(iminomethyl)phenol ligands (SalH-ligands) discussed in this chapter. (6) 2-[(2-Imidazol-4-yl)ethyliminomethyl]-5-methylphenol (5Me-SalH-Hist), (7) 2-[(2-Indol-3-yl-ethyl)iminomethyl]-5-methylphenol (5Me-SalH-Trypt), (8) 2-(9-Ethylcarbazol-3-yliminomethyl)-5-methylphenol (5Me-SalH-Carba), (9) 2-[2-(4-Hydroxyphenyl)ethyl iminomethyl]-5-methylphenol (5Me-SalH-Tyra), (10) 5-Methyl-2-(1,2,4-triazol-3-yliminomethyl)phenol (5Me-SalH-Triaz). Please note: crystal numbering is a continuation from Chapter 4 as listed in Section 4.1.**

5.2 EXPERIMENTAL

The reflection data was collected on a Bruker X8 ApexII 4K diffractometer[14] using Mo $K\alpha$ radiation with ω-and-φ-scans at 100 K. COSMO[15] was utilized for optimum collection of more than a hemisphere of reciprocal space. Frame integration and data reduction were performed using the Bruker SAINT-Plus[16] and XPREP[16] software packages, respectively. Data was corrected for absorption effects using the multi-scan technique SADABS.[17] The structures were solved by direct methods package SIR97[18] and refined using the software package WinGX,[19] incorporating SHELXL.[20] All non-hydrogen atoms were refined with anisotropic displacement parameters, while the methyl, methane and aromatic H atoms were placed in geometrically idealized positions and constrained to ride on their parent atoms, with (C-H = 0.98-0.95 Å and U_{iso}(H) = 1.5U_{eq}(C) and 1.2U_{eq}(C)), respectively. The methyl protons were located from a difference Fourier map and the group was refined as a rigid motor. The absolute structure parameter of compounds in non-centrosymmetric space groups, analyzed with Mo radiation, is meaningless as the compound is a weak anomalous scatterer (i.e. no atom heavier than Si is present). Therefore the absolute structure parameter (Flack parameter) was removed from the CIF. The program DIAMOND[21] was used for all graphical representation of the crystal structures. All structures are shown with thermal ellipsoids drawn at 50% probability level. Graphical representations of overlays of selected complexes are obtained with Hyperchem 7.52.[22]

A summary of the general crystal data and refinement parameters is given in Table 5.1 for all five salicylidene ligand molecules. Supplementary data for the atomic coordinates, bond distances and angles and anisotropic displacement parameters are given in the Appendix A for each individual dataset.

---

[14] Bruker, APEX2 (Version 1.0-27), Bruker AXS Inc., Madison, Wisconsin, USA, 2005
[15] Bruker, COSMO, Version 1.48, Bruker AXS Inc., Madison, Wisconsin, USA, 2003.
[16] Bruker, SAINT-Plus (Version 7.12) (including XPREP), Bruker AXS Inc., Madison, Wisconsin, USA, 2004
[17] Bruker, SADABS, Version 2004/1, Bruker AXS Inc., Madison, Wisconsin, USA,1998.
[18] A. Altomare, M.C. Burla, M. Camalli, G.L. Cascarano, C. Giacovazzo, A. Guagliardi, A.G.G. Moliterni, G. Polidori, R. Spagna, *J. Appl. Cryst.* 1999, 32, 115.
[19] L.J. Farrugia, *J. Appl. Cryst.*, 1999, 32, 837
[20] G.M. Sheldrick, SHELXL97, *Program for Solving Crystal Structures*, University of Göttingen, Germany, 1997
[21] K. Brandenburg, H. Putz, DIAMOND, Release 3.0c, Crystal Impact GbR, Bonn, Germany, 2005
[22] Hyperchem™ Release 7.52, Windows Molecular Modeling System, Hypercube, Inc., 2002

Table 5.1: **General X-ray crystallographic data and refinement parameters for salicylidene ligands.**

Compound	5Me-SalH-Hist (6)	5Me-SalH-Trypt (7)	5Me-SalH-Carba (8)	5Me-SalH-Tyra (9)	5Me-SalH-Triaz (10)
Empirical Formula	$C_{13}H_{15}N_3O$	$C_{18}H_{18}N_2O$	$C_{22}H_{20}N_2O$	$C_{16}H_{17}NO_2$	$C_{10}H_{10}N_4O$
Formula weight	229.28	278.34	328.40	255.31	202.22
Temperature (K)	100(2)	100(2)	100(2)	100(2)	100(2)
Wavelength (Å)	0.71073	0.71073	0.71073	0.71073	0.71073
Crystal System	Monoclinic	Triclinic	Orthorhombic	Triclinic	Orthorhombic
Space Group	$P2_1/c$	$P\bar{1}$	$P2_12_12_1$	$P\bar{1}$	$Pca2_1$
Unit Cell Dimensions					
a (Å)	10.4959(3)	6.0722(3)	7.9040(2)	7.3079(5)	21.079(3)
b (Å)	9.9047(3)	8.3073(3)	10.5709(3)	11.7966(8)	4.4677(5)
c (Å)	23.1897(6)	14.1215(6)	20.3219(6)	15.5593(11)	10.0801(12)
α (°)	90	98.482(2)	90	89.413(4)	90
β (°)	106.365(2)	96.914(2)	90	77.258(3)	90
γ (°)	90	94.487(2)	90	80.098(4)	90
Volume (Å^3)	2313.10(11)	696.07(5)	1697.94(8)	1288.28(15)	949.3(2)
Z	8	2	4	4	4
Density$_{calc.}$ (g.cm^{-1})	1.317	1.328	1.285	1.316	1.415
μ (mm^{-1})	0.087	0.083	0.079	0.087	0.098
F(000)	976	296	696	544	424
Crystal Colour	Yellow	Yellow	Yellow	Yellow	Colourless
Crystal Morphology	Cuboid	Plate	Plate	Needle	Needle
Crystal Size (mm)	0.41x0.17x0.14	0.39x0.12x0.07	0.40x0.18x0.06	0.33x0.09x0.08	0.39x0.06x0.04
Theta Range (°)	3.19 to 27.99	2.68 to 28.00	3.22 to 28.00	1.34 to 28.00	3.87 to 28.00
Completeness (%)	99.8	99.4	99.8	98.3	99.5
Index Ranges	h = -13 to 13 k = -13 to 13 l = -30 to 29	h = -7 to 8 k = -10 to 10 l = -18 to 18	h = -10 to 7 k = -13 to 13 l = -26 to 26	h = -9 to 9 k = -15 to 15 l = -20 to 20	h = -27 to 27 k = -5 to 3 l = -13 to 13
Reflections Collected	23821	12530	30092	24644	11211
Independent Reflections	5567	3315	2344	6114	1201
R_{int}	0.0435	0.0243	0.0323	0.0415	0.0572
Refinement method	Full-matrix least-squares on F^2	Full-matrix least-squares on F^2	Full-matrix least-squares on F^2	Full-matrix least-squares on F^2	Full-matrix least-squares on F^2
Data / restraints / parameters	5567 / 0 / 311	3315 / 0 / 192	2344 / 0 / 230	6114 / 0 / 345	1201 / 1 / 137
Goodness-of-fit on F^2	1.043	1.074	1.049	1.086	1.125
Final R indices [I>2sigma(I)]	R1 = 0.0449, wR2 = 0.1023	R1 = 0.0436, wR2 = 0.1148	R1 = 0.0333, wR2 = 0.0858	R1 = 0.0547, wR2 = 0.1445	R1 = 0.0427, wR2 = 0.1022
R indices (all data)	R1 = 0.0700, wR2 = 0.1151	R1 = 0.0518, wR2 = 0.1222	R1 = 0.0366, wR2 = 0.0884	R1 = 0.0776, wR2 = 0.1629	R1 = 0.0515, wR2 = 0.1080
ρ_{max} and ρ_{min} (e.Å^{-3})	0.236 and -0.235	0.393 and -0.400	0.208 and -0.226	0.787 and -0.691	0.395 and -0.401

(5Me-SalH-Hist) = 2-[(2-imidazol-4-yl)ethyliminomethyl]-5-methylphenol; (5Me-SalH-Trypt) = 2-[(2-indol-3-yl-ethyl)iminomethyl]-5-methylphenol; (5Me-SalH-Carba) = 2-(9-ethylcarbazol-3-yliminomethyl)-5-methyl phenol; (5Me-SalH-Tyra) = 2-[2-(4-hydroxyphenyl)ethyliminomethyl]-5-methylphenol; (5Me-SalH-Triaz) = 5-methyl-2-(1,2,4-triazol-3-yliminomethyl)phenol.

5.3 CRYSTAL STRUCTURE OF 5Me-SalH-Hist

The compound 2-[(2-imidazol-4-yl)ethyliminomethyl]-5-methylphenol, (5Me-SalH-Hist) (**6**), crystallizes in a monoclinic crystal system in the $P2_1/c$ space group with eight formula units per unit cell (Z = 8). The asymmetrical unit thus contains two independent molecules. The molecular structure of (**6**) is represented in Figure 5.6 along with the atom numbering scheme and important bond lengths and angles are given in Table 5.2.

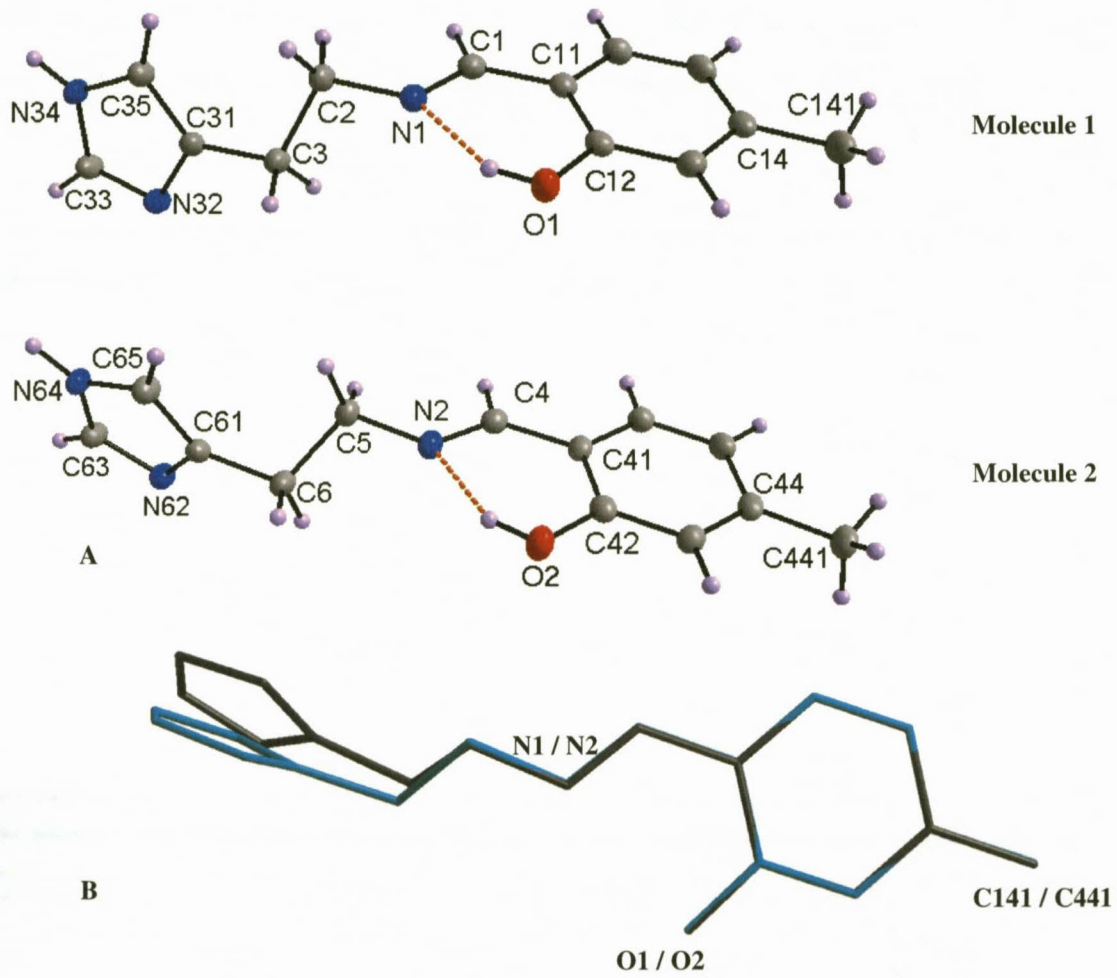

Figure 5.6: **(A) Molecular structure of 5Me-SalH-Hist showing the atom numbering system. For the aromatic rings, the first digit refers to the ring number, while the second digit refers to the specific C-atom in the ring. Hydrogen bond interaction indicated by orange dotted line. Displacement ellipsoids are drawn at 50% probability level.**

(B) Overlay of the two molecules found in the asymmetric unit of the crystal structure to indicate variation of orientation. Overlay drawn through the salicylidene backbone only, to allow free rotation of histamine substituent. (True overlay through all atoms yields an RMS value of 0.336 Å).

Table 5.2: Selected bond distances and angles for 5Me-SalH-Hist [Å and °].

Molecule 1		Molecule 2		Molecule 1		Molecule 2	
Atoms	Distance	Atoms	Distance	Atoms	Angle	Atoms	Angle
C1-N1	1.282(2)	C4-N2	1.280(2)	N1-C1-C11	122.0(1)	N2-C4-C41	122.2(1)
N1-C2	1.459(2)	N2-C5	1.461(2)	C1-N1-C2	117.9(2)	C4-N2-C5	118.3(1)
C1-C11	1.453(2)	C4-C41	1.455(2)	C11-C12-O1	121.4(1)	C41-C42-O2	121.1(1)
C12-O1	1.357(2)	C42-O2	1.362(2)	N32-C31-C35	109.4(1)	N62-C61-C65	109.1(1)
C2-C3	1.526(2)	C5-C6	1.522(2)	C33-N34-C35	106.9(1)	C63-N64-C65	106.7(1)
C31-N32	1.383(2)	C61-N62	1.381(2)				
C31-C35	1.365(2)	C61-C65	1.364(2)	O1-C12-C11-N1	1.6(2)	O2-C42-C41-N2	1.4(2)
N32-C33	1.323(2)	N62-C63	1.327(2)	C1-N1-C2-C3	114.8(1)	C4-N2-C5-C6	134.8(1)
N34-C33	1.341(2)	N64-C63	1.339(2)	C2-C3-C31-C35	15.0(2)	C5-C6-C61-C65	54.8(2)
N1-H1B	1.856(1)	N2-H2B	1.866(2)				

The two molecules in the asymmetric unit, both crystallize as the *trans* phenol-imine tautomer with the expected intramolecular hydrogen bond occurring between the O1-H1B...N1 and O2-H2B...N2 atoms. The O...N distances (2.602(2) Å and 2.613(2) Å) are significantly shorter than the sum of the van der Waals radii for N and O (3.07 Å)[23] and is comparable for related salicylidene compounds.[24] The C1-N1 and C4-N2 bond distances of 1.282(2) Å and 1.280(2) Å are indicative of double bonds. The N1-C2, N2-C5 (1.459(2) Å, 1.461(2) Å) and C12-O1, C42-O2 (1.357(2) Å, 1.362(2) Å) bond distances are consistent with single bonds. All bond angles and lengths in (**6**) are within normal ranges.[25] The bond lengths of the two nitrogen atoms in the histamine 5-membered cyclic ring N32-C33, N62-C63 and N34-C33, N64-C63 are consistent for double and single bonds respectively.

Significant differences in the two independent molecules are manifested in the torsion angles defining the imidazole linker and differ by approximately 20° and 40° respectively as listed in Table 5.2. Intermolecular hydrogen bonding occurs between N34-H34...N32' and N64-H64...N62" (Figure 5.7 and Table 5.3). Generation of symmetry related molecules results in the formation of infinite one dimensional chains along the [010] vector for both independent molecules in the unit cell.

[23] A. Bondi, *J. Phys. Chem.*, 1964, 68, 441
[24] F. Arod, M. Gardon, P. Pattison, G. Chapuis, *Acta Cryst.*, 2005, C61, o317
[25] F.H. Allen, O. Kennard, D.G. Watson, L. Brammer, A.G. Orpen, R. Taylor, *J. Chem. Soc., Perkin Trans.* II, 1987, S1

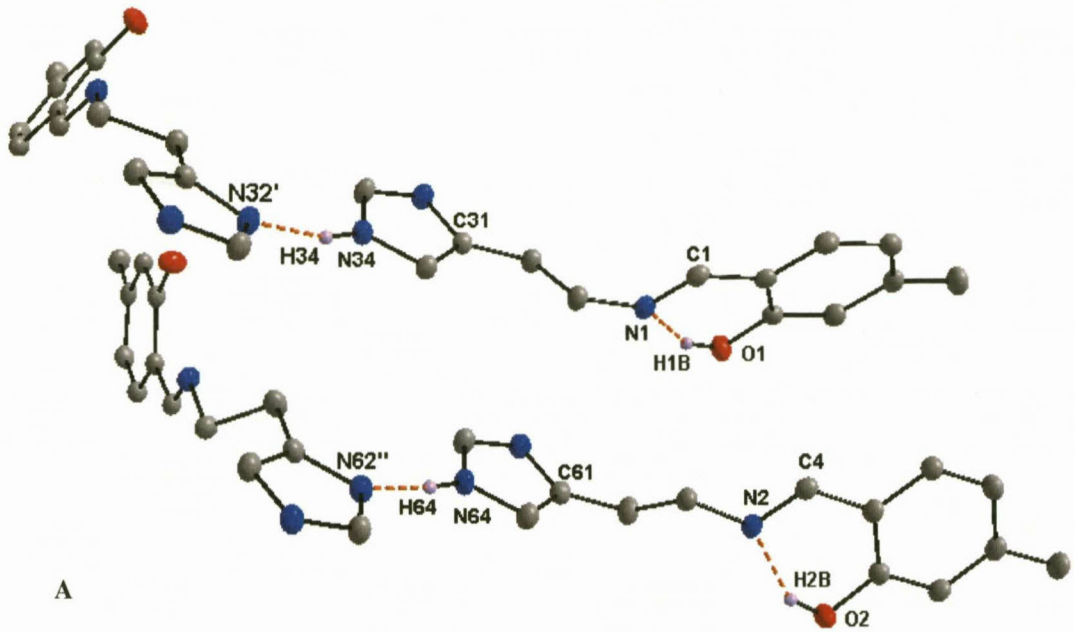

A

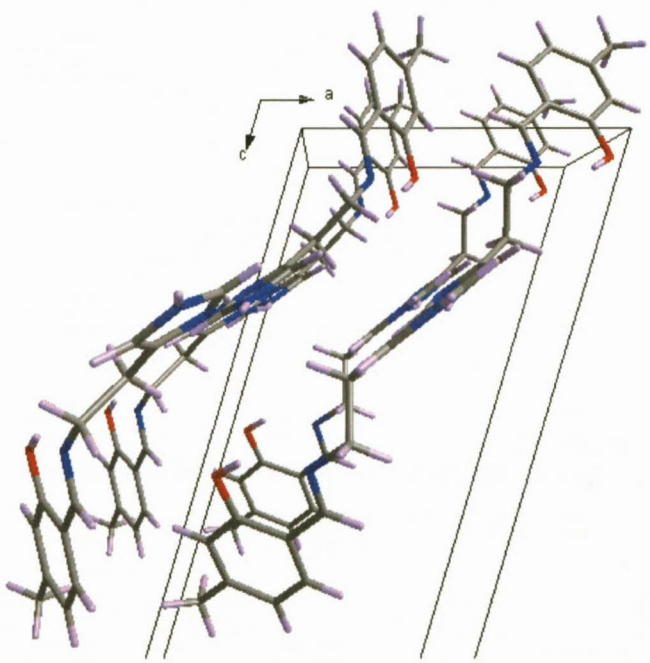

B

Figure 5.7: **(A) Intra- and intermolecular hydrogen bond interactions of (6). (Symmetry operations N32' = -x, y+1/2, -z+1/2 and N62'' = -x+1, y+1/2, -z+1/2). Certain H-atoms are omitted for clarity. (B) Graphical representation of infinite one dimensional chains formed by the generation of symmetry related molecules along the [010] vector.**

Table 5.3: Hydrogen bonds for 5Me-SalH-Hist [Å and °].

D-H...A	d(D-H)	d(H...A)	d(D...A)	<(DHA)
O(1)-H(1B)...N(1)#1	0.84	1.86	2.602(2)	147.2
O(2)-H(2B)...N(2)#1	0.84	1.87	2.613(2)	147.3
N(34)-H(34)...N(32)#2	0.88	2.04	2.896(2)	163.3
N(64)-H(64)...N(62)#3	0.88	1.99	2.860(2)	167.8

Symmetry transformations used to generate equivalent atoms:
#1 x,y,z #2 -x,y+1/2,-z+1/2 #3 -x+1,y+1/2,-z+1/2

The compound is non-planar with dihedral angle between the two aromatic rings (Plane 1: C11, C12, C13, C14, C15, C16; Plane 2: C31, N32, C33, N34, C35 for Molecule 1 and Plane 3: C41, C42, C43, C44, C45, C46; Plane 4: C61, N62, C63, N64, C65 for Molecule 2, respectively) of 77.72(5)° and 77.70(5)° (Figure 5.8).

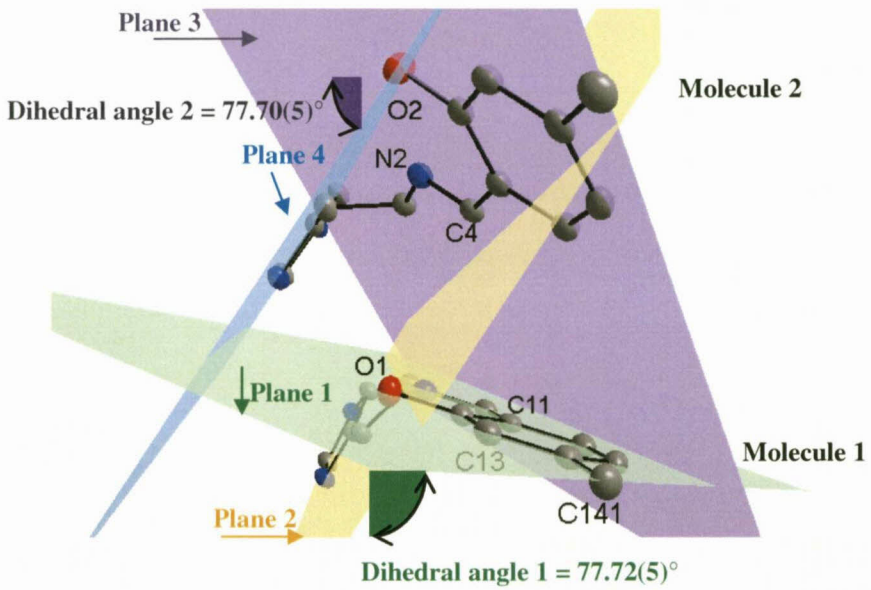

Figure 5.8: Twisting of aromatic rings as indicated by planes 1 (green) and 2 (yellow) for Molecule 1 and planes 3 (purple) and 4 (blue) for Molecule 2. H atoms have been omitted for clarity.

The two molecules in the asymmetric unit are stabilized by C-H...π interactions. The observed interactions are found between several C-H atoms and both the six-membered aromatic salicylidene backbone and the five-membered histamine ring as illustrated in Figure 5.9 and Table 5.4.

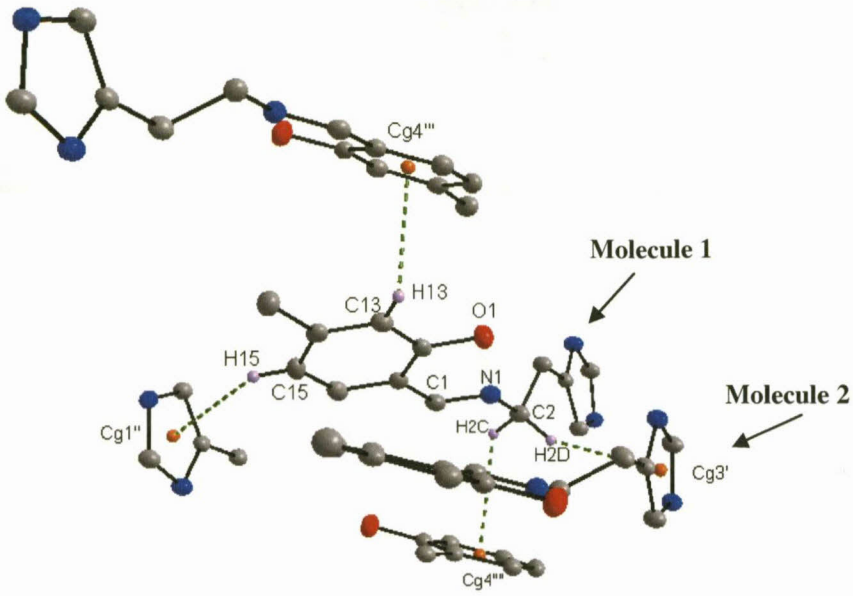

Figure 5.9: **An illustration of C-H…π interactions (green line). Centroid atoms (Cg) of each aromatic ring is indicated in orange. Only the necessary atoms are illustrated for the sake of clarity.**

Table 5.4: **C-H…π Interaction between aromatic rings of ligand molecule.**

C-H...Cg	Centroid atom (Cg)	d(H...Cg) (Å)	d(C...Cg) (Å)	< (C-H...Cg) (°)
C2-H2D	Cg3#1	2.8417(1)	3.751(2)	153.2(9)
C15-H15	Cg1#2	2.9093(1)	3.707(1)	142.3(8)
C13-H13	Cg4#3	2.9067(1)	3.320(2)	107.6(9)
C2-H2C	Cg4#4	2.9417(1)	3.548(2)	120.5(1)

Symmetry transformations:
#1 x, y, z; #2 –x, 1-y, -z; #3 1-x, -y, -z; #4 1-x, 1-y, -z
Cg1 = centroid atom of C31, N32, C33, N34, C35; Cg2 = centroid atom of C11, C12, C13, C14, C15, C16
Cg3 = centroid atom of C61, N62, C63, N64, C65; Cg4 = centroid atom of C41, C42, C43, C44, C45, C46

Structural comparisons and illustrative overlays between the various functionalized salicylidene crystal structures are discussed in Section 5.8.

5.4 CRYSTAL STRUCTURE OF 5Me-SalH-Trypt

The compound, 2-[(2-indol-3-yl-ethyl)iminomethyl]-5-methylphenol, (5Me-SalH-Trypt) (**7**), crystallizes in a triclinic space group $P\bar{1}$, with two molecules in the unit cell (Z = 2). The asymmetrical unit contains one independent molecule. The molecular structure of (**7**) is represented in Figure 5.10 along with the atom numbering scheme. Important bond lengths and angles are given in Table 5.5.

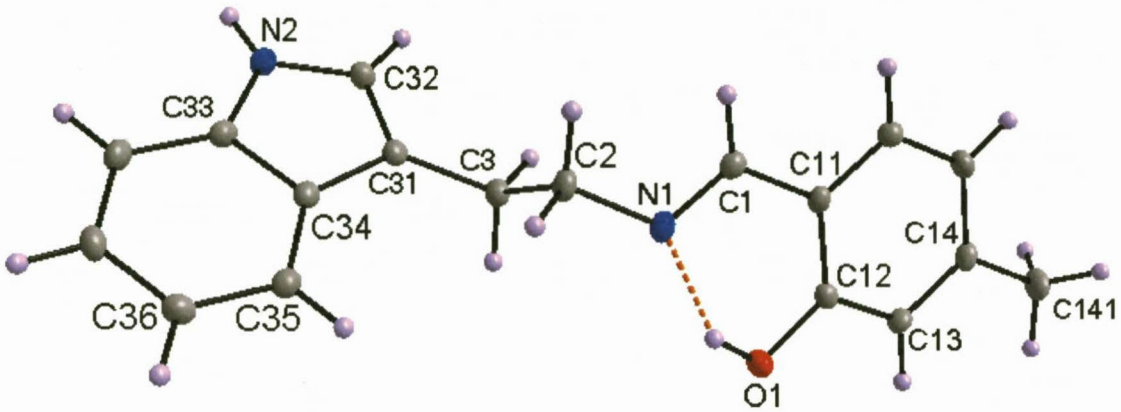

Figure 5.10: **Molecular structure of 5Me-SalH-Trypt showing the atom numbering system. For the aromatic rings, the first digit refers to the ring number, while the second digit refers to the specific C-atom in the ring. Intramolecular hydrogen bond indicated by orange line. Displacement ellipsoids are drawn at 50% probability level.**

Table 5.5: **Selected bond distances and angles for the compound 5Me-SalH-Trypt [Å and °].**

Atoms	Distance	Atoms	Angle
C1-N1	1.282(2)	N1-C1-C11	120.9(1)
N1-C2	1.462(1)	C1-N1-C2	118.5(1)
C1-C11	1.462(2)	N1-C2-C3	107.0(1)
C11-C12	1.411(2)	C12-O1-H1B	109.5*
C12-O1	1.346(2)	C11-C12-O1	121.6(1)
C2-C3	1.533(2)	C32-C31-C34	106.2(1)
C31-C32	1.366(1)	C32-N2-C33	108.9(1)
C32-N2	1.377(1)	O1-C12-C11-N1	2.5(1)
N1-H1B	1.827(1)	C1-N1-C2-C3	103.9(1)
		C2-C3-C31-C32	114.3(1)

*No e.s.d. as H-atoms were placed as riding

The molecule crystallizes as the *trans* phenol-imine tautomer with the intramolecular hydrogen bond occurring between the O1-H1B...N1 atoms. All bond angles and lengths are within normal range,[25] with the C1-N1 bond distance of 1.282(2) Å typical of a double bond and N1-C2 (1.462(1) Å), C1-C11 (1.462(2) Å) and C12-O1 (1.346(2) Å) bond distances typical of single bonds for the respective atoms. The indole aromatic ring system is planar

with no deviations from typical bond angles and lengths. The compound is non-planar with a dihedral angle between the two aromatic ring systems of 48.44(3)° (Plane 1 = C11, C12, C13, C14, C15, C16 and Plane 2: C31, C32, N2, C33, C34, C35, C36, C37, C38).

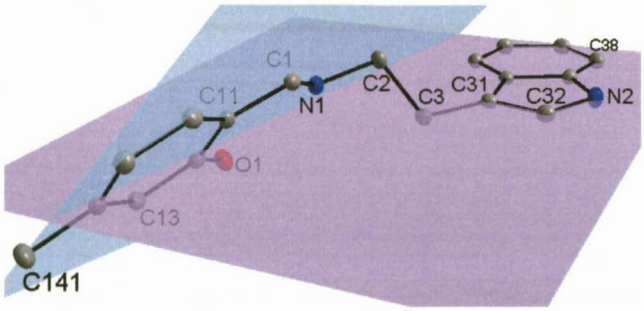

Figure 5.11: **Rotation of aromatic ring systems as indicated by planes 1 and 2. H atoms have been omitted for clarity.**

Table 5.6: **Hydrogen bonds for 5Me-SalH-Trypt [Å and °].**

D-H...A	d(D-H)	d(H...A)	d(D...A)	<(DHA)
O(1)-H(1B)...N(1)#1	0.84	1.83	2.576(1)	147.5

Symmetry transformations used to generate equivalent atoms:
#1 x,y,z

A few soft contacts *via* van der Waals interactions are observed in the crystal packing between the N-H atoms of the indole ring and the aromatic carbons of the salicylidene backbone to form a weak *tridentate* hydrogen interaction. The interactions occur between N1-H2C...C12', C13' and C14'. Similar interactions occur for C12, C13 and C14 to H2C'-N1' (Figure 5.12). Soft C-H...H-C interactions occur between C3-H3A and C3'-H3A' of the same molecule.

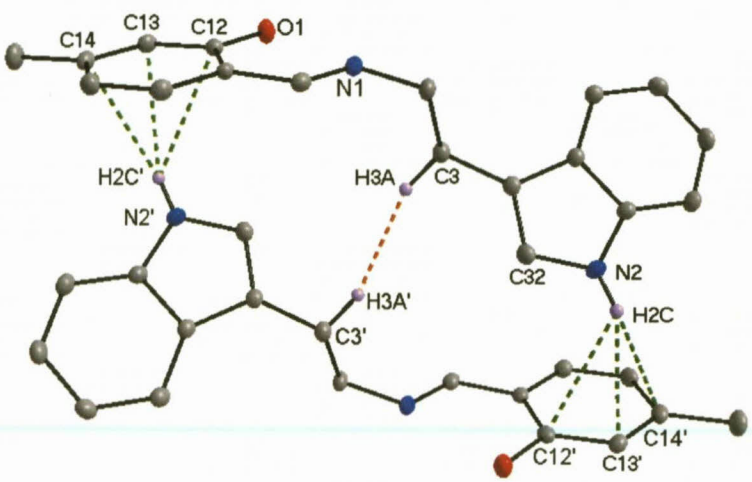

Figure 5.12: **Graphical representation of N-H...π interaction (green line) and C-H...H-C interaction (orange line) between related molecules. Certain H atoms are omitted for clarity.**

Table 5.7: N-H…π and C-H…H-C interactions for the compound 5Me-SalH-Trypt [Å and °].

D-H...A	d(H...A)	d(D...A)	< (D-H...A)
N2-H2C...C12#1	2.890(1)	3.425(2)	120.8(8)
N2-H2C...C13#1	2.650(1)	3.423(2)	147.2(8)
N2-H2C...C14#1	2.801(1)	3.502(2)	137.7(8)
C-H...H-C	d(H...H)	d(C...H)	< (D-H...H)
C3-H3A...H3A#1	2.308(1)	3.223(1)	153.3(7)

Symmetry transformations used to generate equivalent atoms: #1 –x, -y, 1-z

Molecular packing is further stabilized by C-H…π interactions (Figure 5.13) which occur between atoms C1, C13, C141 and C36 to various centroid atoms as listed in Table 5.8 below.

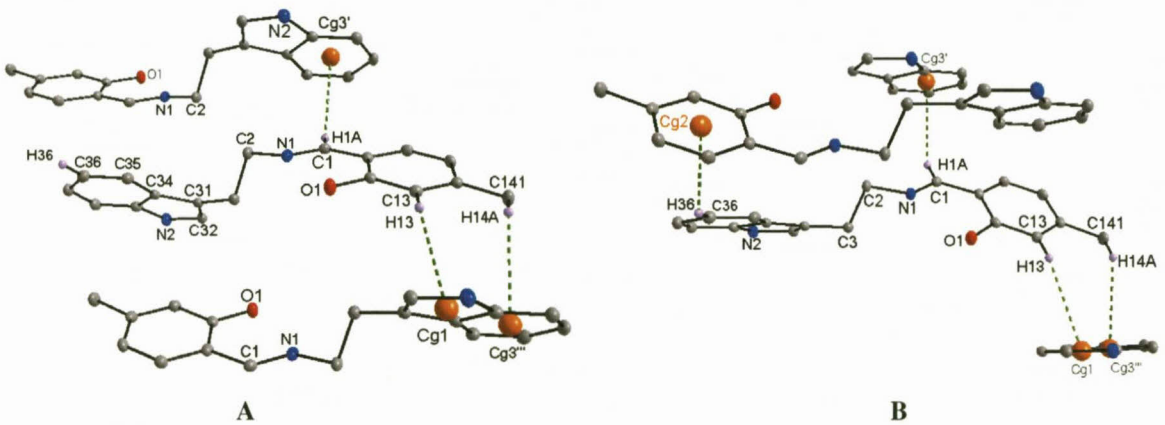

A B

Figure 5.13: Graphical representation of the C-H…π interactions (green line) to (A) centroid atoms Cg3', Cg1 and Cg3''' and (B) to centroid atom Cg2. Certain atoms have been omitted for clarity.

Table 5.8: C-H…π Interaction between aromatic rings of ligand molecule.

C-H...Cg	Centroid atom (Cg)	d(H...Cg) (Å)	d(C...Cg) (Å)	< (C-H...Cg) (°)
C1-H1A	Cg3' #1	2.8529(1)	3.569(1)	133.0(8)
C13-H13	Cg1 #2	2.9570(1)	3.792(1)	147.4(8)
C141-H14A	Cg3''' #3	2.9299(1)	3.529(2)	120.5(8)
C36-H36	Cg2 #4	2.8162(1)	3.483(1)	128.1(1)

Symmetry transformations:
#1 –x, 1-y, 1-z; #2 1-x, -y, 1-z; #3 1-x, -y, 1-z ; #4 1-x, 1-y, 1-z
Cg1 = centroid atom of C31, C32, N2, C33, C34; Cg2 = centroid atom of C11, C12, C13, C14, C15, C16
Cg3 = centroid atom of C33, C34, C35, C36, C37, C38

Structural comparison and illustrative overlays between the various functionalized salicylidene crystal structures are discussed in Section 5.8.

5.5 CRYSTAL STRUCTURE OF 5Me-SalH-Carba

The yellow compound, 2-(9-ethylcarbazol-3-yliminomethyl)-5-methylphenol, (5Me-SalH-Carba) (**8**), crystallizes in an orthorhombic crystal system in the $P2_12_12_1$ space group with four molecules in the units cell (Z = 4). The asymmetrical unit contains one independent molecule. The molecular structure of (**8**) is represented in Figure 5.14 along with the atom numbering scheme and important bond lengths and angles are given in Table 5.9.

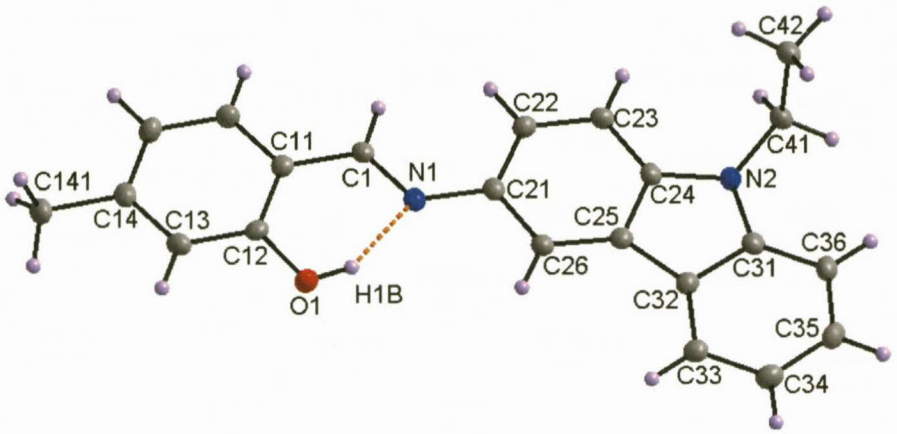

Figure 5.14: **Molecular structure of 5Me-SalH-Carba showing the atom numbering system. For the aromatic rings, the first digit refers to the ring number, while the second digit refers to the specific C-atom in the ring. Intramolecular hydrogen bond indicated by orange line. Displacement ellipsoids are drawn at 50% probability level.**

Table 5.9: **Selected bond distances and angles for the compound 5Me-SalH-Carba [Å and °].**

Atoms	Distance	Atoms	Angle
C1-N1	1.290(2)	N1-C1-C11	121.2(1)
N1-C21	1.422(2)	C1-N1-C21	122.6(1)
C1-C11	1.453(2)	N1-C21-C22	124.1(1)
C11-C12	1.409(2)	C12-O1-H1B	109.5*
C12-O1	1.355(2)	C11-C12-O1	121.7(1)
C14-C141	1.508(2)	C24-N2-C31	108.5(1)
C21-C22	1.415(2)	N2-C41-C42	111.7(1)
N2-C24	1.385(2)		
N2-C31	1.388(2)	O1-C12-C11-N1	3.1(2)
N2-C41	1.457(2)	C1-N1-C21-C22	0.6(2)
C41-C42	1.524(2)	C24-C25-C32-C31	0.8(2)
N1-H1B	1.864(1)		

*No e.s.d. as H-atoms were placed as riding

The molecule crystallizes as the *trans* phenol-imine tautomer with the expected intramolecular hydrogen bond occurring between the O1-H1B...N1 atoms. The O1...N1 distance (2.607(2) Å) is significantly shorter than the sum of the van der Waals radii for N and O (3.07 Å).[23] All bond angles and lengths in (**8**) are within normal range.[24] The C1-N1

bond distance of 1.290(2) Å is indicative of a double bond whereas the N1-C21 (1.422(2) Å), N2-C41 (1.457(2) Å), C12-O1 (1.355(2) Å) and C41-C42 (1.524(2) Å) bond distances are consistent with single bonds for the respective atoms.

Despite the steric bulk of the coordinated amine the compound is essentially planar with minimal rotation around the -C1=N1- double bond with a dihedral angle between the two aromatic rings (Plane 1: C11, C12, C13, C14, C15, C16 and Plane 2: C21, C22, C23, C24, C25, C26) of 4.37(4)°. The carbazole substituent lies below Plane 1 with a C1-N1-C21-C22 torsion angle of 0.6(2)° as indicated in Figure 5.15 below. The ethyl functionality lies above plane 1 with a N2-C41-C42 bond angle of 111.7(1)°.

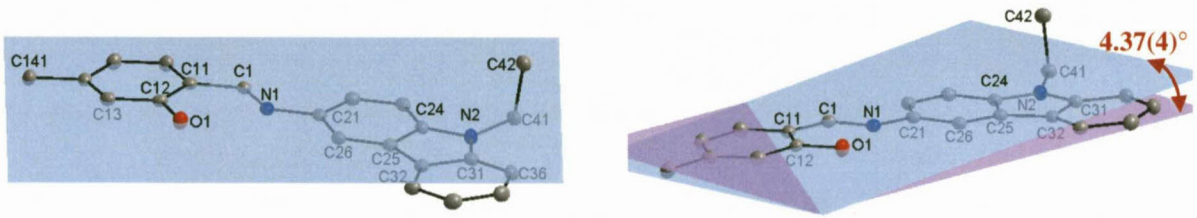

A B

Figure 5.15: **(A) Graphical representation of the 5Me-SalH-Carba indicating co-planarity of the crystal structure. (B) Graphical representation indicating angle between Plane 1 (blue) and Plane 2 (purple). H atoms are omitted for clarity.**

Few classic hydrogen bonding occurs in the crystal structure. Aside from the intramolecular interaction, only one other intermolecular hydrogen bonding occurs between C41-H14A...O1" (C41...O1" = 3.407(2) Å) (Figure 5.16 and Table 5.10).

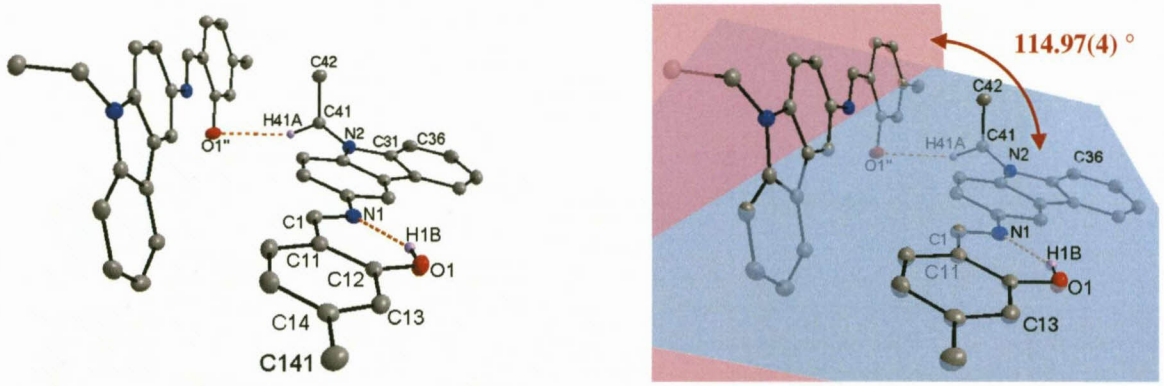

A B

Figure 5.16: **(A) Graphical representation of the 5Me-SalH-Carba indicating H-bond interaction. (B) Molecular packing of molecules due to H-bond interaction with near perpendicular orientation. Plane 1 (blue) drawn through C1 aromatic ring (atoms = C11, C12, C13, C14, C15, C16); Plane 3 (pink) drawn through C1" aromatic ring (Symmetry operation: 2-x, 0.5+y, 0.5-z). Certain H atoms omitted for clarity.**

Table 5.10: Hydrogen bonds for 5Me-SalH-Carba [Å and °].

D-H...A	d(D-H)	d(H...A)	d(D...A)	<(DHA)
O(1)-H(1B)...N(1)#1	0.84	1.86	2.607(2)	146.7
C(41)-H(41A)...O(1)#2	0.99	2.47	3.407(2)	158.0

Symmetry transformations used to generate equivalent atoms:
#1 x,y,z #2 -x+2,y+1/2,-z+1/2

Molecular packing is stabilized by the formation of ring to ring π-π stacking interactions in which the ligands pack in a "head to tail" mode (Figure 5.17). π-π Interactions occur between the C1 aromatic ring (C11, C12, C13, C14, C15, C16) and the carbazole aromatic ring system indicated by green and orange dotted lines. The list of various centroid to centroid distances are given in Table 5.11 below.

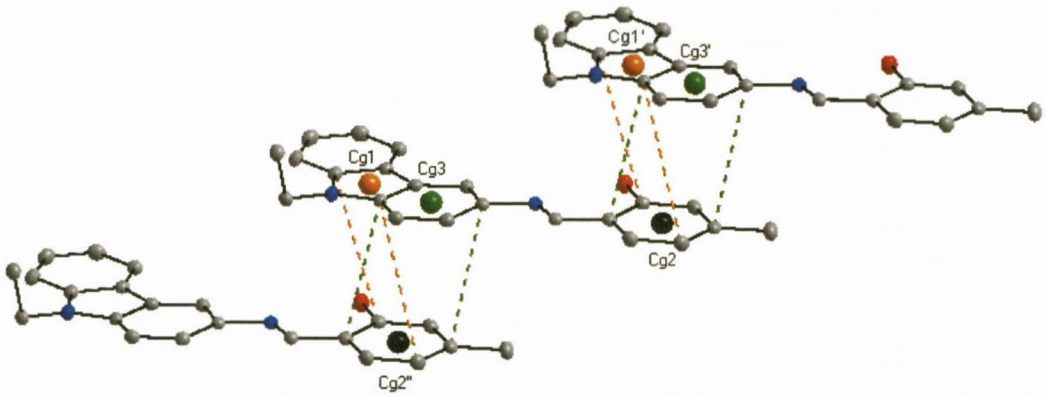

Figure 5.17: Graphical representation of the two π-π interactions indicated by green and orange dotted lines (Cg = centroid of aromatic rings). H atoms have been omitted for clarity.

Table 5.11: π-π Interaction between aromatic rings of ligand molecule.

Centroid atom	Centroid atom	Distance between centroid atoms (Å)	Interplanar angle (°)
Cg2	Cg1' #1	4.5080(9)	2.69(4)
Cg2	Cg3' #1	3.8145(9)	4.37(4)
Cg1	Cg2" #2	4.5080(9)	2.69(4)
Cg3	Cg2" #2	3.8145(9)	4.37(4)

Symmetry transformations used to generate equivalent atoms:
#1 -1+x, y, z; #2 1+x, y, z
Cg1 = centroid atom of N2, C24, C25, C32, C31; Cg2 = centroid atom of C11, C12, C13, C14, C15, C16;
Cg3 = C21, C22, C23, C24, C25, C26

The last set of soft contacts which were observed are illustrated in Figure 5.18 by orange dotted lines. These C-H...π ring interactions are observed in the crystal packing between the aromatic ring systems and are listed in Table 5.12. The contacts further stabilize the near perpendicular manner of packing, which was first illustrated in Figure 5.16, as the result of the classic intermolecular hydrogen bonding occurring between C41-H14A...O1". The unit

cell (Figure 5.19A) illustrates the open packing manner with molecules lying "head-to-tail" with respect to each other. Expansion of the unit cell clearly indicates the zig-zag packing mode of the crystal structure.

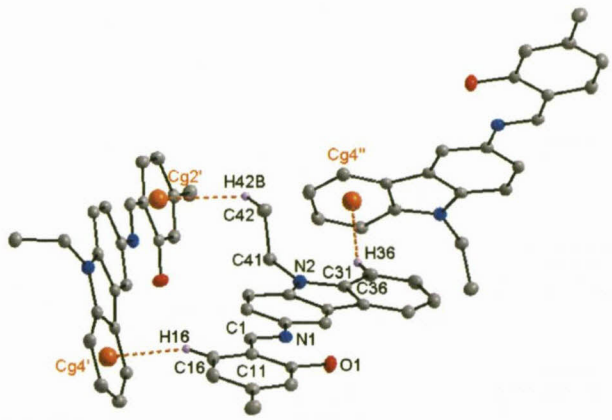

Figure 5.18: **Graphical representation of the C-H...π ring interactions indicated by orange lines. Certain H atoms are omitted for clarity.**

Table 5.12: **C-H...π Interaction between aromatic rings of ligand molecule.**

C-H...Cg	Centroid atom (Cg)	d(H...Cg) (Å)	d(C...Cg) (Å)	< (C-H...Cg) (°)
C16-H16	Cg4' #1	2.682(2)	3.579(2)	157.6(1)
C36-H36	Cg4" #2	2.870(2)	3.751(2)	154.8(1)
C42-H42B	Cg2' #1	2.824(1)	3.625(2)	139.4(1)

Symmetry transformations:
#1 2-x, 0.5+y, 0.5-z; #2 0.5+x, 1.5-y, 1-z
Cg2 = centroid atom of C11, C12, C13, C14, C15, C16; Cg4 = centroid atom of C31, C32, C33, C34, C35, C36

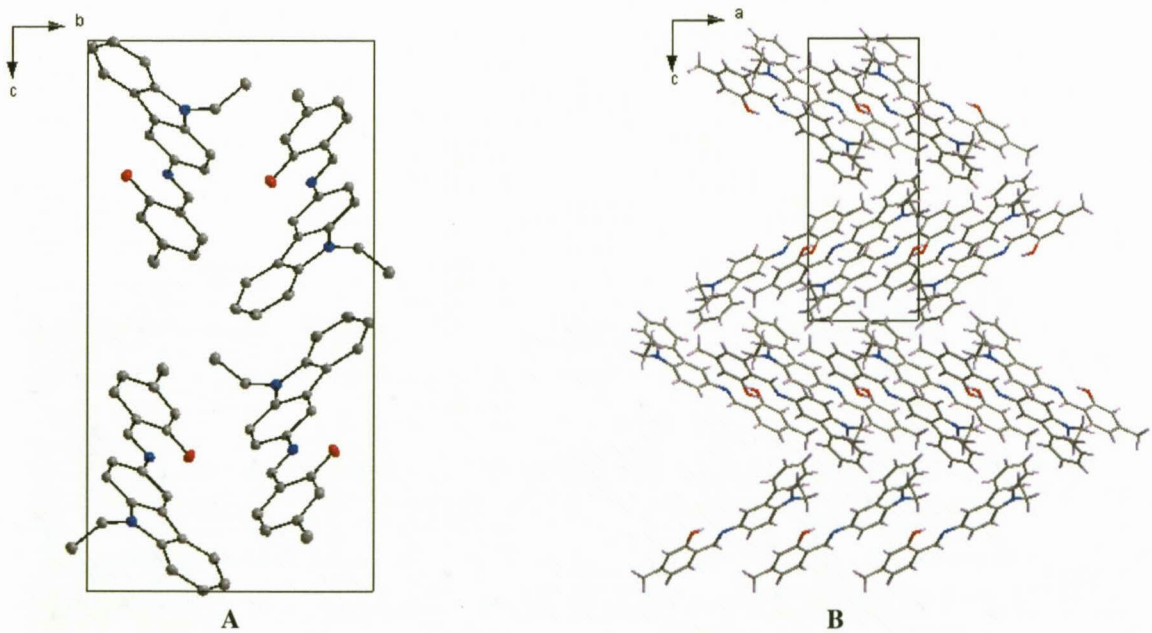

A B

Figure 5.19: **(A) Molecular packing of the unit cell as viewed along the *a*-axis. (B) Zig-zag packing of molecules in the unit cell as viewed along the *b*-axis.**

5.6 CRYSTAL STRUCTURE OF 5Me-SalH-Tyra

The compound 2-[2-(4-hydroxyphenyl)ethyliminomethyl]-5-methylphenol, (5Me-SalH-Tyra) (**9**), crystallized in the triclinic space group, $P\bar{1}$, with four molecules per unit cell (Z = 4). The asymmetric unit thus contains two independent molecules. The molecular structure of (**9**) is illustrated in Figure 5.20 along with the atom numbering scheme. Significant bond distances and angles are shown in Table 5.13.

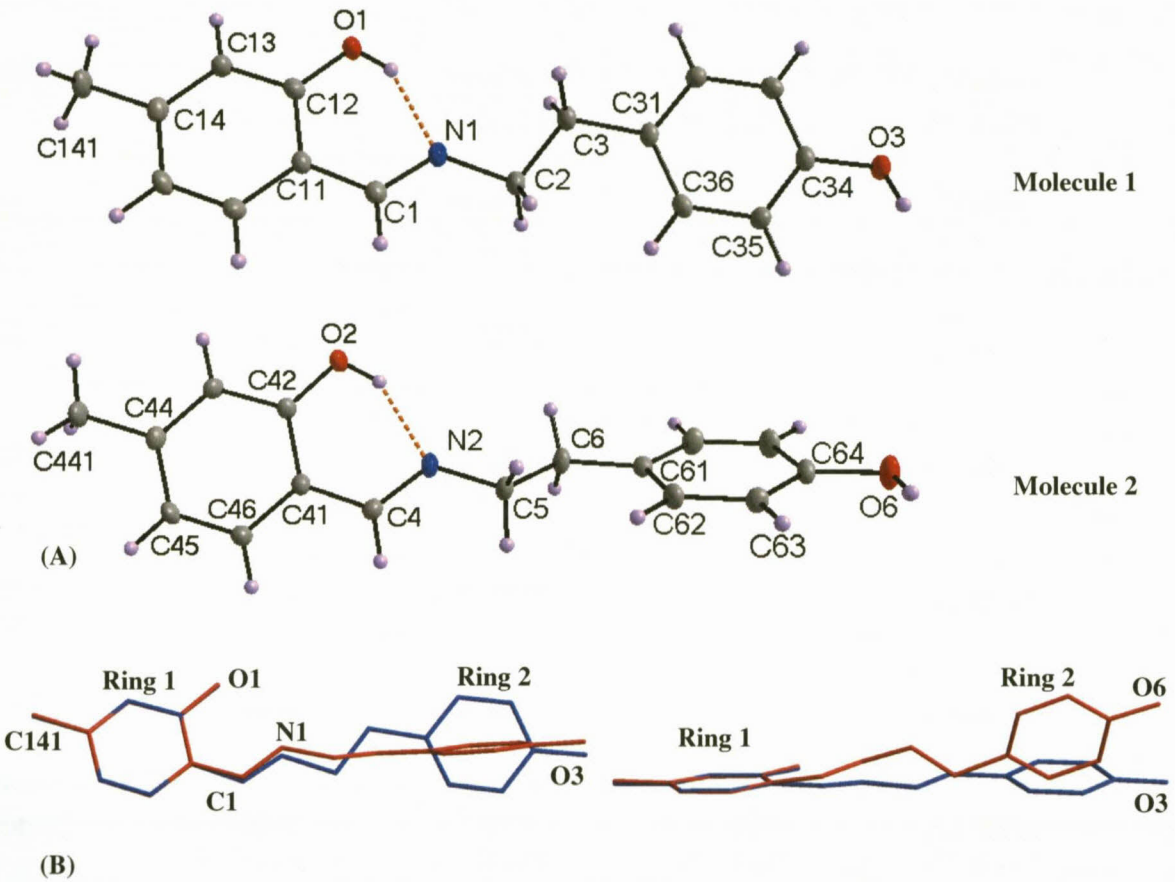

Figure 5.20: **(A) Molecular structures of 5Me-SalH-Tyra indicating atom numbering system. For the aromatic rings, the first digit refers to the ring number, while the second digit refers to the specific C-atom in the ring. Hydrogen bond interaction indicated by orange dotted line. Displacement ellipsoids are drawn at 50% probability level.**

(B) Graphical overlay of the two molecular structures in the asymmetric unit from two different viewing angles. Molecule 1 indicated in blue; Molecule 2 in red. The variation of orientation between the two aromatic rings is indicated. Overlay is drawn through atoms of the C1 and C4 aromatic rings only, namely atoms C11, C12, C13, C14, C15, C16 and C41, C42, C43, C44, C45, C46; RMS = 1.17 x 10^{-2} Å, to allow free rotation of the tyramine substituent. (True overlay through all atoms yields an RMS value of 0.588 Å).

Table 5.13: Selected bond distances and angles for the compound 5Me-SalH-Tyra [Å and °].

Molecule 1		Molecule 2		Molecule 1		Molecule 2	
Atoms	Distance	Atoms	Distance	Atoms	Angle	Atoms	Angle
C1-N1	1.296(2)	C4-N2	1.298(2)	N1-C1-C11	122.5(2)	N2-C4-C41	123.9(2)
N1-C2	1.464(2)	N2-C5	1.461(2)	C1-N1-C2	125.4(2)	C4-N2-C5	124.9(2)
C1-C11	1.415(2)	C4-C41	1.415(2)	C11-C12-O1	120.9(2)	C41-C42-O2	120.9(2)
C12-O1	1.296(2)	C42-O2	1.297(2)	N1-C2-C3	107.5(1)	N2-C5-C6	111.1(2)
C2-C3	1.513(3)	C5-C6	1.514(2)	C33-C34-O3	117.7(2)	C63-C64-O6	123.7(2)
C31-C32	1.397(2)	C61-C62	1.390(3)				
C31-C36	1.394(3)	C61-C66	1.392(3)	O1-C12-C11-N1	3.2(2)	O2-C42-C41-N2	6.5(2)
C34-O3	1.363(2)	C64-O6	1.355(2)	C1-N1-C2-C3	173.1(2)	C4-N2-C5-C6	129.9(2)
C14-C141	1.507(2)	C44-C441	1.501(2)	C2-C3-C31-C36	3.0(2)	C5-C6-C61-C62	0.6(3)
N1-H1A	1.809(2)	N2-H2	1.884(1)				

Both molecules in the asymmetric unit crystallise as the *trans* phenol-imine tautomer with intramolecular hydrogen bonding occurring between O1-H1A...N1 (Molecule 1) and O2-H2...N2 (Molecule 2) atoms. The O...N distances (2.566(2) Å and 2.627(2) Å) are significantly shorter than the sum of the van der Waals radii for N and O (3.07 Å).[23] All bond angles and lengths in (**9**) are within normal ranges. Significant differences in the two independent molecules are manifested in the torsion angles defining the tyramine linker and differ by approximately 40° as listed in Table 5.13.

The two independent molecules in the asymmetric unit, both lie in a "head-to-head" orientation with respect to each other, however the rotation of the two aromatic rings differ, resulting in the two molecules having different planarity (Figure 5.20B).

Molecule 1 (indicated in blue in Figure 5.20B) is essentially co-planar with a dihedral angle between the two aromatic rings of 10.43(5)° (Plane 1: C11, C12, C13, C14, C15, C16 and Plane 2: C31, C32, C33, C34, C35, C36). Molecule 2 is significantly non-planar with a dihedral angle between the two aromatic rings of 59.00(6)° (Plane 3: C41, C42, C43, C44, C45, C46 and Plane 4: C61, C62, C63, C64, C65, C66) (Figure 5.21).

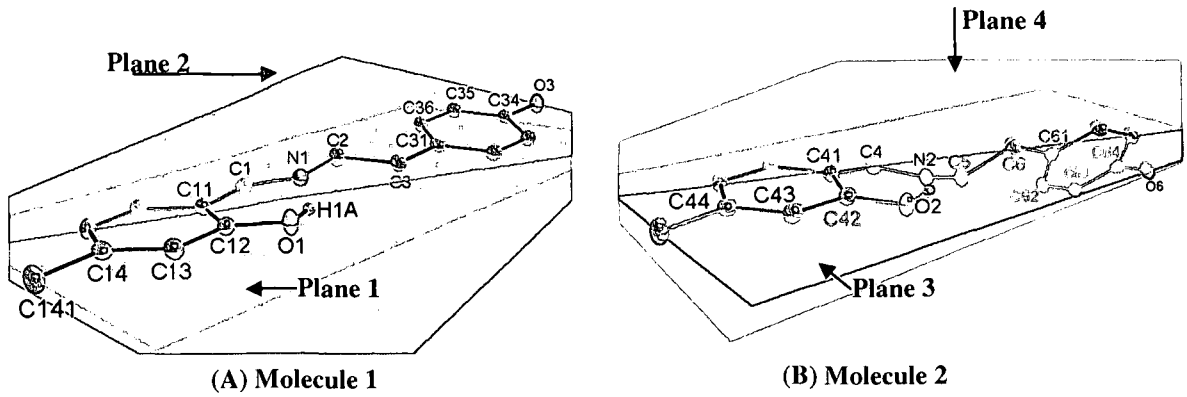

(A) Molecule 1 (B) Molecule 2

Figure 5.21: **Graphical representation of the different planarity of the two molecular structures in the asymmetric unit. (A) Molecule 1 with minimal rotation (Plane 1 drawn in blue, Plane 2 drawn in purple). (B) Molecule 2 with significant rotation of the two aromatic ring systems (Plane 3 indicated in green, Plane 4 indicated in yellow).**

Several intermolecular hydrogen bond interactions occur between O-H...O and C-H...O atoms between neighbouring molecules as listed in Table 5.14. Molecule 1 experiences classical H-bonding between atoms O3-H3...O2$^{\#2}$, C35-H35...O2$^{\#5}$ and C15-H15...O3$^{\#4}$ (orange dotted line). An unusual close H...H contact occurs due to the close proximity of the molecule at symmetry position #5 (symmetry operation: x, y-1, z) between atoms O3-H3...H5B$^{\#5}$-C5$^{\#5}$ with a H...H distance of 2.0468(1) Å, a O3...C5$^{\#5}$ distance of 3.531(1) Å and a O3-H3...H5B$^{\#5}$ angle of 131.49(9)° as illustrated in Figure 5.22A by the green dotted line.

Molecule 2 experiences only two classical intermolecular hydrogen bond interactions between atoms C45-H45...O6$^{\#4}$ and O6-H6C...O1$^{\#3}$ as indicated in Figure 5.22B by the orange dotted lines.

Table 5.14: **Hydrogen bonds for 5Me-SalH-Tyra [Å and °].**

D-H...A	d(D-H)	d(H...A)	d(D...A)	<(DHA)
O(1)-H(1A)...N(1)#1	0.84	1.81	2.566(2)	149.1
O(2)-H(2)...N(2)#1	0.84	1.88	2.627(2)	146.7
O(3)-H(3)...O(2)#2	0.84	1.97	2.6111(18)	132.4
O(6)-H(6C)...O(1)#3	0.84	1.74	2.5778(18)	174.2
C(15)-H(15)...O(3)#4	0.95	2.44	3.387(2)	178.0
C(35)-H(35)...O(2)#5	0.95	2.60	3.514(2)	162.3
C(45)-H(45)...O(6)#4	0.95	2.53	3.408(2)	154.3

Symmetry transformations used to generate equivalent atoms:
#1 x,y,z #2 -x+1,-y+1,-z+1 #3 -x+1,-y+2,-z+1
#4 x,y,z-1 #5 x,y-1,z

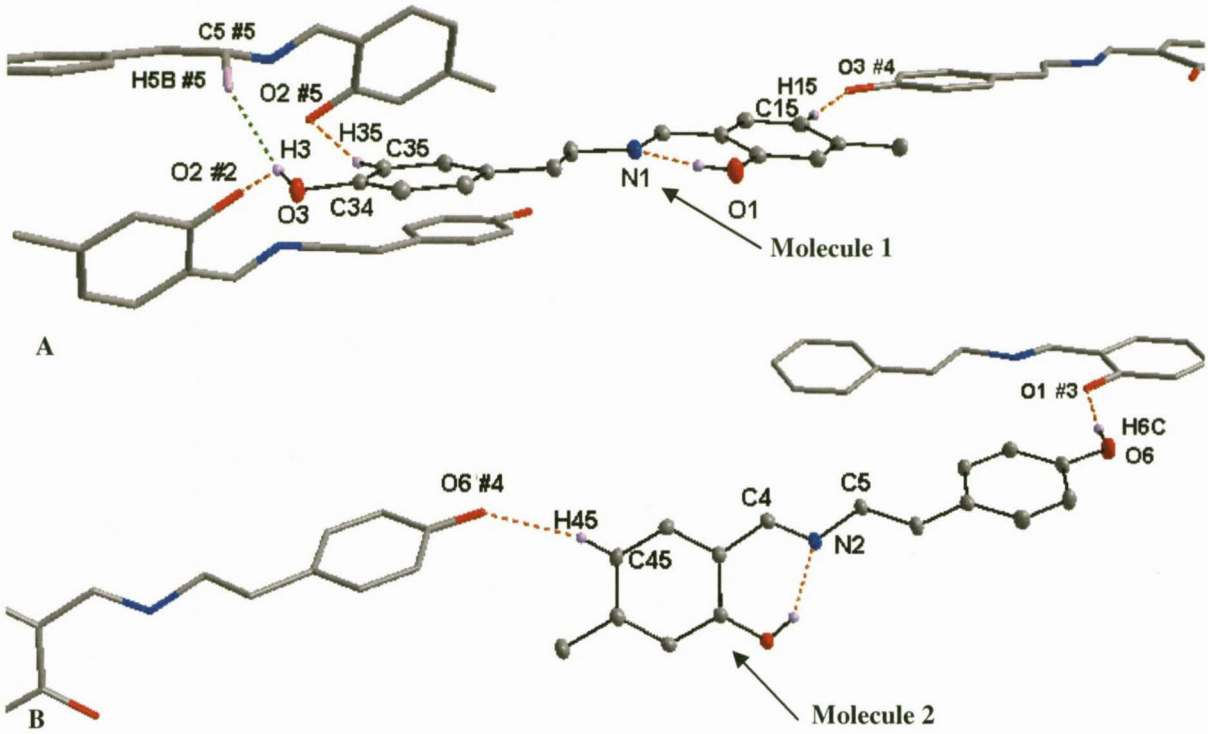

Figure 5.22: **(A) Graphical representation of the intermolecular hydrogen bond interactions experienced by Molecule 1, indicated by orange lines.**
(B) Graphical representation of the intermolecular hydrogen bond interactions experienced by Molecule 2, indicated by orange lines. Certain atoms are omitted for clarity.

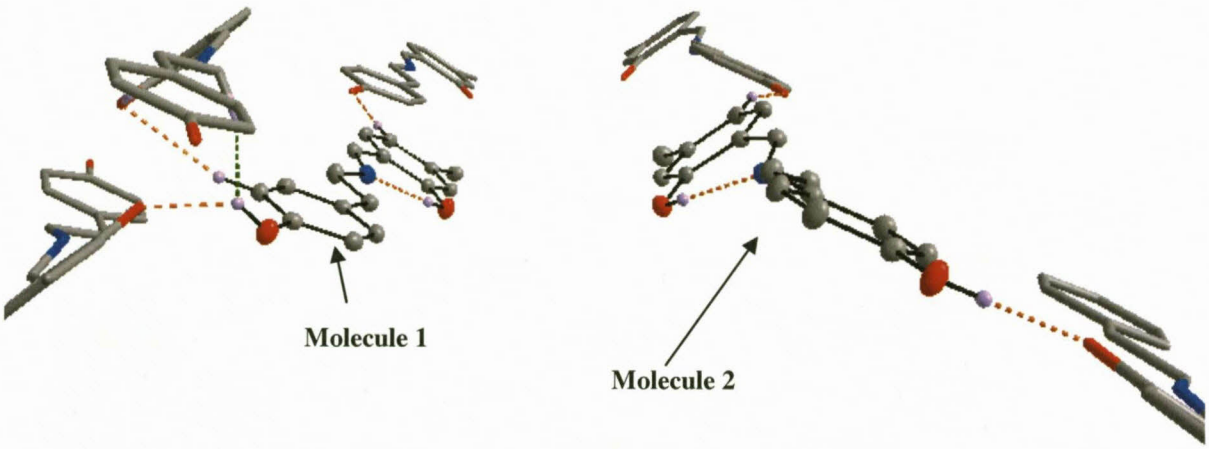

Figure 5.23: **Graphical representation of all intermolecular hydrogen bond interactions for both molecules in the asymmetric unit. Certain atoms are omitted for clarity.**

Only one π-π interaction occurs (Figure 5.24) between aromatic ring C1 (Cg1 = centroid atom of ring C11, C12, C13, C14, C15, C16) and aromatic ring C6 (Cg4' = centroid atom of ring C61, C62, C63, C64, C64, C65, C66; symmetry operation: 1+x, -1+y, -1+z) with a

centroid to centroid distance of 4.002(1) Å and an interplanar angle of 10.76(5)°. The resultant packing of the unit cell forms rectangular tunnels when viewed along the *c*-axis (Figure 5.25).

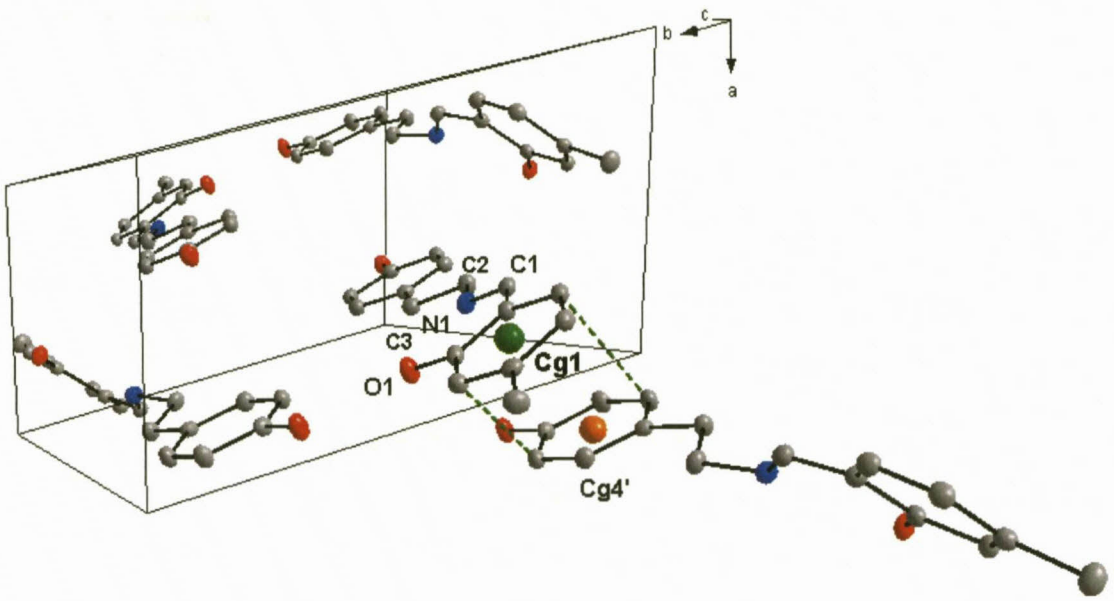

Figure 5.24: **Graphical representation of the unit cell indicating π-π interaction between neighboring molecules. H atoms are omitted for clarity.**

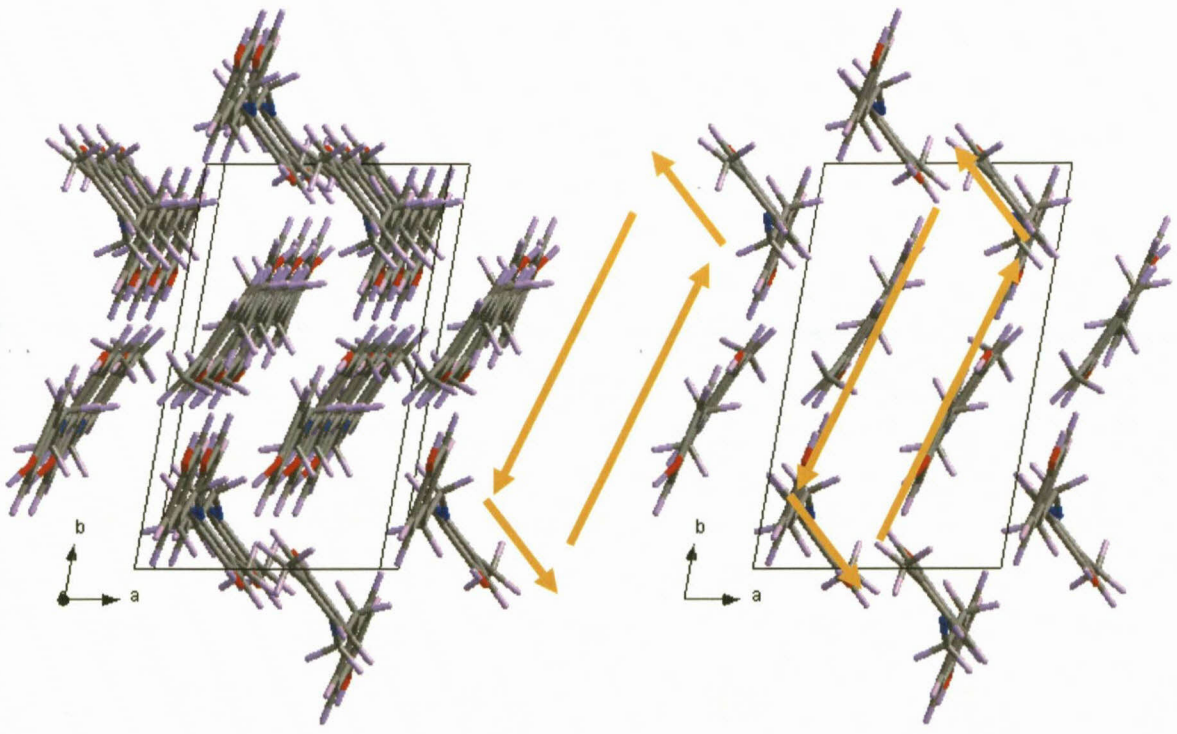

Figure 5.25: **Rectangular packing of the unit cell as viewed along the *c*-axis.**

Structural comparisons and illustrative overlays between the various functionalized salicylidene crystal structures are discussed in Section 5.8.

5.7 CRYSTAL STRUCTURE OF 5Me-SalH-Triaz

The compound, 5-methyl-2-(1,2,4-triazol-3-yliminomethyl)phenol, (5Me-SalH-Triaz) (**10**), crystallizes in a orthorhombic crystal system in the $Pca2_1$ space group with four formula units per unit cell (Z = 4). The asymmetrical unit contains one independent molecule. The molecular structure of (**10**) is represented in Figure 5.26 along with the atom numbering scheme. Significant bond lengths and angles are found in Table 5.15.

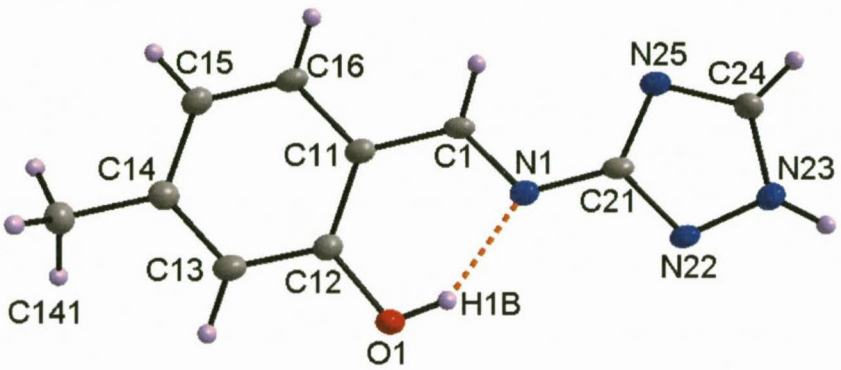

Figure 5.26: **Molecular structure of 5Me-SalH-Triaz indicating the atom numbering system. For the aromatic rings, the first digit refers to the ring number, while the second digit refers to the specific C-atom in the ring. Hydrogen bond interaction indicated by orange dotted line. Displacement ellipsoids are drawn at 50% probability level.**

Table 5.15: **Selected bond distances and angles for the compound 5Me-SalH-Triaz [Å and °].**

Atoms	Distance	Atoms	Angle
C1-N1	1.294(3)	N1-C1-C11	121.3(2)
N1-C21	1.388(3)	C1-N1-C21	120.0(2)
C1-C11	1.440(4)	N1-C21-N22	119.4(2)
C11-C12	1.418(4)	C11-C12-O1	121.6(2)
C12-O1	1.348(3)	C12-O1-H1B	109.5*
C14-C141	1.508(4)	C21-N22-N23	109.8(2)
C21-N22	1.337(4)	C21-N25-C24	101.9(2)
N22-N23	1.364(3)		
N23-C24	1.323(4)	O1-C12-C11-N1	1.7(3)
C24-N25	1.371(4)	C1-N1-C21-N22	178.4(2)
N25-C21	1.335(4)	C1-N1-C21-N25	1.5(4)
N1-H1B	1.863(2)	C21-N22-N23-C24	0.5(3)

*No e.s.d. as H-atoms were placed as riding

The molecule crystallises in a similar fashion to the other salicylidene ligands already discussed, namely the *trans* phenol-imine tautomer with the O1-H1B...N1 intramolecular hydrogen bond. All bond angles and distances found in the salicylidene backbone are within normal range for related compounds.[24] The triazole ring which is bonded *via* the C1=N1 double bond consists of a five-membered ring containing three nitrogen atoms. The bond

distances in the triazole ring are all consistent with average interatomic distances in crystalline organic compounds[25,26] *i.e.* C21-N22 and N25-C21 (1.337(4) Å and 1.335(4) Å *vs.* 1.336 Å for a C*ar*-N*ar* bond; *ar* = aromatic bond), N22-N23H (1.364(3) Å *vs.* 1.366 Å for a N-NH bond), N23H-C24H (1.323(4) Å *vs.* 1.329 Å for a CH-NH bond) and C24H-N25 (1.371(4) Å *vs.* 1.371 Å for a CH-N bond). The molecule is essentially co-planar with minimal rotation around the -C1=N1- double bond with a dihedral angle of 4.58(8)° between the two aromatic rings (Plane 1: C11, C12, C13, C14, C15, C16 and Plane 2: C21, N22, N23, C24, N25) as indicated in Figure 5.27.

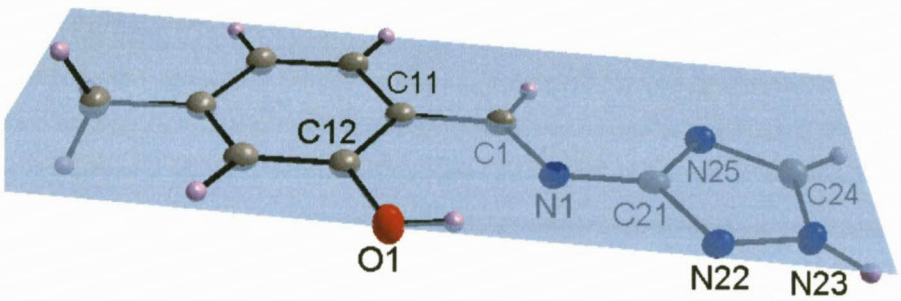

Figure 5.27: **Co-planarity of 5Me-SalH-Triaz indicated by Plane 1 (drawn in blue) through the C1 aromatic ring system.**

Two intermolecular hydrogen bond interactions occur between atoms C16-H16...N23$^{\#2}$ and C24-H24...O1$^{\#3}$ which results in the two symmetry generated molecules lying nearly perpendicular to the molecule at position x, y, z (Figure 5.28). Plane 1 (defined through atoms C11, C12, C13, C14, C15, C16 indicated in blue) lies at an angle of 77.41(6)° to both Plane 2$^{\#2}$ (indicated in yellow) and Plane 3$^{\#3}$ (indicated in pink) (Plane 2$^{\#2}$: C11, C12, C13, C14, C15, C16, symmetry operation #2. Plane 3$^{\#3}$: C11, C12, C13, C14, C15, C16, symmetry operation #3). Plane 2 and 3 are parallel with respect to each other at a distance of 6.971(2) Å. A second intramolecular bond occurs between C1-H1A and N25 of the triazole ring.

Table 5.16: **Hydrogen bonds for 5Me-SalH-Triaz [Å and °].**

D-H...A	d(D-H)	d(H...A)	d(D...A)	<(DHA)
O(1)-H(1B)...N(1)#1	0.84	1.86	2.606(3)	146.8
C(1)-H(1A)...N(25)#1	0.95	2.57	2.892(4)	99.9
C(16)-H(16)...N(23)#2	0.95	2.60	3.423(4)	145.8
C(24)-H(24)...O(1)#3	0.95	2.38	3.255(4)	152.1

Symmetry transformations used to generate equivalent atoms:
#1 x,y,z #2 -x+3/2,y-1,z+1/2 #3 -x+3/2,y+1,z+1/2

[26] D.R. Lide, Editor., *CRC Handbook of Chemistry and Physics*, Version 2008, 88th Ed. (CD-ROM), CRC Press/Taylor and Francis, Boca Raton, Florida, USA

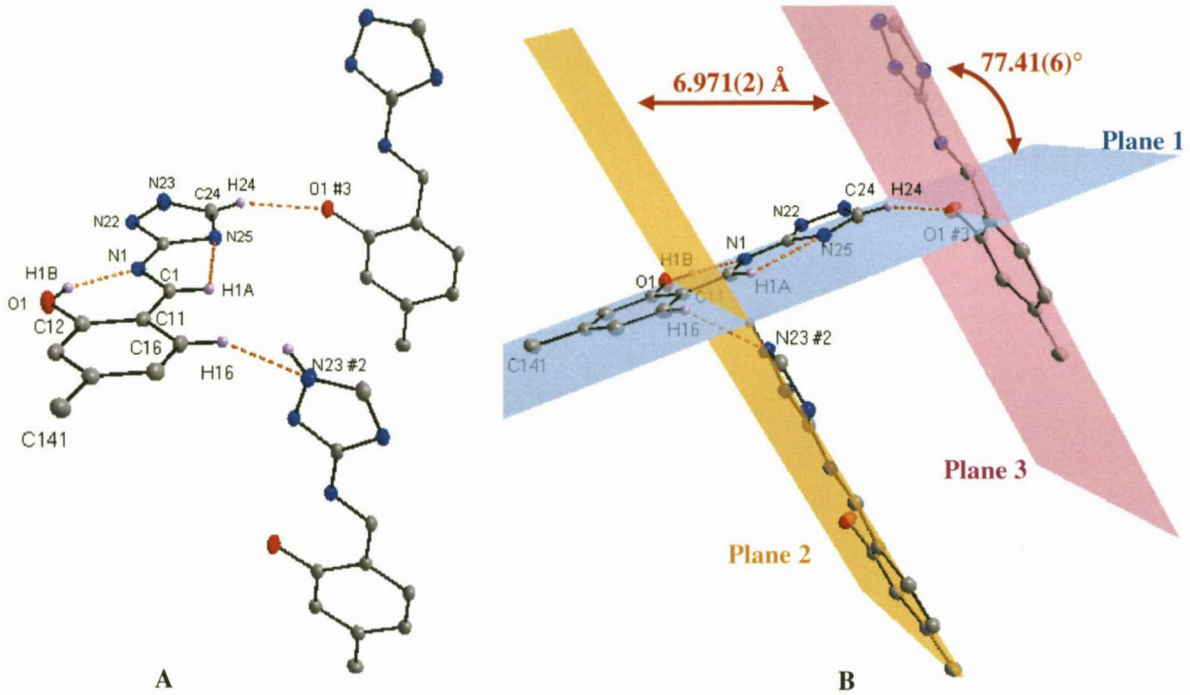

Figure 5.28: **Graphical representation of intra- and intermolecular bonding. (A) Hydrogen bonding indicated by orange dotted lines. (B) Near perpendicular orientation of molecules. H atoms are omitted for clarity.**

Due to the intermolecular H-bond interaction between H16 and $N23^{\#2}$ (sym. op. 1.5-x, -1+y, 0.5+z), an unusually short intermolecular H...H interaction occurs between atoms H16 and $H23^{\#2}$-$N23^{\#2}$ (H16...H23; d = 1.8916(2) Å).

The crystal packing in the unit cell is stabilized by a C-H...π interaction between C141-H14C and the salicylidene C1 aromatic ring system of neighbouring molecules, to form horizontal layers as indicated in Figure 5.29 and Table 5.17.

Table 5.17: **C-H…π Interaction between aromatic rings of ligand molecule.**

C-H...Cg	Centroid atom (Cg)	d(H...Cg) (Å)	d(C...Cg) (Å)	< (C-H...Cg) (°)
C141-H14C	Cg1 #1	2.7281(3)	3.568(3)	144.02(2)

Symmetry transformations:
#1 x, -1+y, z
Cg1 = centroid atom of C11, C12, C13, C14, C15, C16

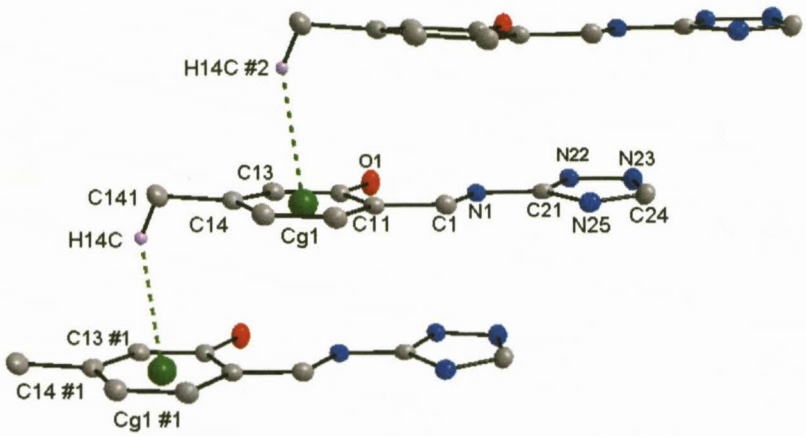

Figure 5.29: **Crystalline packing of molecules due to C-H…π interactions to form horizontal layers. H-atoms are omitted for clarity.**

The crystal packing in the unit cell is further stabilized by soft van der Waal, N...N interactions between N25...N22$^{\#1}$ and N22…N25$^{\#2}$ (N...N = 2.910(3) Å) to form near perpendicular packing to the molecule positioned at x, y, z. The angle between planes (drawn through atoms C11, C12, C13, C14, C15, C16) is identical to that formed from the intermolecular hydrogen bonding, namely 77.41(6)° (Figure 5.30).

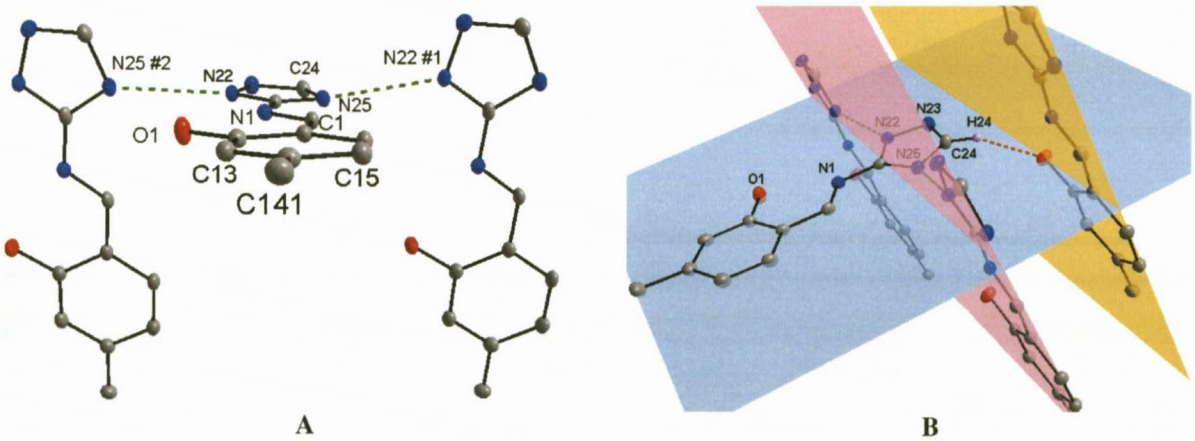

Figure 5.30: **N…N interactions between neighbouring atoms to form near perpendicular layers. (A) N…N interactions indicated by green dotted lines. (B) Near perpendicular planes formed from N…N interactions (green line; pink plane) and H intermolecular bonding (orange line; yellow plane). Certain H-atoms are omitted for clarity. (Symmetry operation: #1 1.5-x, y, 0.5+z; #2 1.5-x, y, -0.5+z)**

The molecules pack in a "head-to-head" manner along the *ac*-axis plane and in horizontal layers parallel to the *b*-axis (Figure 5.31). The sum of the total packing within the unit cell forms herring-bone packing, as illustrated in Figure 5.32.

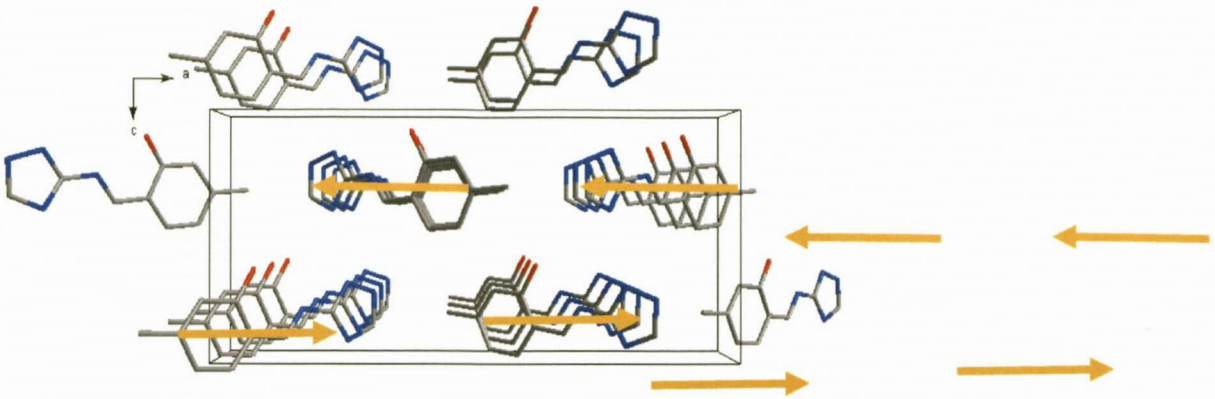

Figure 5.31: **Molecular packing of unit cell as viewed along the *b*-axis.**

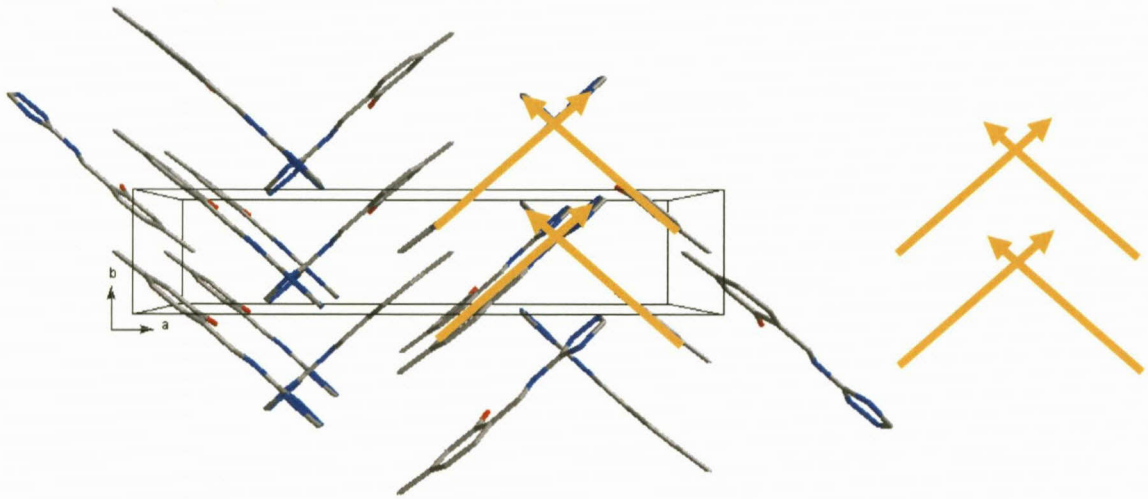

Figure 5.32: **Molecular packing of unit cell as viewed along the *c*-axis.**

Structural comparison and illustrative overlays between the various functionalized salicylidene crystal structures are discussed in Section 5.8.

5.8 INTERPRETATION AND CORRELATION OF STRUCTURAL PARAMETERS

The following subsection correlates structural data from the various functionlized salicylidene compounds as described above. The general bond distances and angles of interest of the crystal structures are given in Table 5.19.

Table 5.18: Cell dimension overview of presented functionalized salicylidene ligands.

Compound	5Me-SalH-Hist (6)	5Me-SalH-Trypt (7)	5Me-SalH-Carba (8)	5Me-SalH-Tyra (9)	5Me-SalH-Triaz (10)
Crystal System	Monoclinic	Triclinic	Orthorhombic	Triclinic	Orthorhombic
Space Group	$P2_1/c$	$P\bar{1}$	$P2_12_12_1$	$P\bar{1}$	$Pca2_1$
Unit Cell Dimensions					
a (Å)	10.4959(3)	6.0722(3)	7.9040(2)	7.3079(5)	21.079(3)
b (Å)	9.9047(3)	8.3073(3)	10.5709(3)	11.7966(8)	4.4677(5)
c (Å)	23.1897(6)	14.1215(6)	20.3219(6)	15.5593(11)	10.0801(12)
α (°)	90	98.482(2)	90	89.413(4)	90
β (°)	106.365(2)	96.914(2)	90	77.258(3)	90
γ (°)	90	94.487(2)	90	80.098(4)	90
Volume (Å^3)	2313.10(11)	696.07(5)	1697.94(8)	1288.28(15)	949.3(2)
Z	8	2	4	4	4

Table 5.19: Selected geometrical parameters of the presented functionalized salicylidene ligands, tabulated for comparison [Å and °].

Compound	5Me-SalH-Hist (6)		5Me-SalH-Trypt (7)	5Me-SalH-Carba (8)	5Me-SalH-Tyra (9)		5Me-SalH-Triaz (10)
Molecule	**1**	**2**			**1**	**2**	
Bonds Distance (Å)							
N1-C1	1.282(2)	1.280(2)	1.282(2)	1.290(2)	1.296(2)	1.298(2)	1.294(3)
N1-C2/C5	1.459(2)	1.461(2)	1.462(1)	-	1.464(2)	1.461(2)	-
N1-C21	-	-	-	1.422(2)	-	-	1.388(3)
C1-C11	1.453(2)	1.455(2)	1.462(2)	1.453(2)	1.415(2)	1.415(2)	1.440(4)
C12-O1	1.357(2)	1.362(2)	1.346(2)	1.355(2)	1.296(2)	1.297(2)	1.348(3)
N1...H1B	1.856(1)	1.866(2)	1.827(1)	1.864(1)	1.809(2)	1.884(1)	1.863(2)
Bond angle (°)							
O1-C12-C11	121.4(1)	121.1(1)	121.6(1)	121.7(1)	120.9(2)	120.9(2)	121.6(2)
N1-C1-C11	122.0(1)	122.2(1)	120.9(1)	121.2(1)	122.5(2)	123.9(2)	121.3(2)
C1-N1-C2/C5	117.9(2)	118.3(1)	118.5(1)	-	125.4(2)	124.9(2)	-
C1-N1-C21	-	-	-	122.6(1)	-	-	120.0(2)
N1-C2-C3	109.6(1)	110.9(1)	107.0(1)	-	107.5(1)	111.1(2)	-
Torsion angle (°)							
O1-C12-C11-N1	1.6(2)	1.4(2)	2.5(1)	3.1(2)	3.2(2)	6.5(2)	1.7(3)
C1-N1-C21-C22	-	-	-	0.6(2)	-	-	1.5(4)
C1-N1-C2-C3	114.8(1)	134.8(1)	103.9(1)	-	173.1(2)	129.9(2)	-
Dihedral angle through Ring 1 and Ring 2 (°)	77.25(5)	77.70(5)	48.44(3)	4.37(4)	10.43(5)	59.00(6)	4.58(8)

The salicylidene compounds (**6**), (**7**) and (**9**) all have -CH_2CH_2-R chain bonded to the N atom of the salicylaldehyde backbone, where R = aromatic functionalities such as histamine, tryptamine and tyramine. None of these molecules are planar as indicated by the dihedral angles. Interestingly compound 5Me-SalH-Tyra (**9**), which contains two independent molecules in the asymmetric unit, has one molecule that is more planar than the other. 5Me-SalH-Hist (**6**) also containing two molecules in the asymmetric unit, both have similar dihedral angles. Molecules (**7**) and (**9**) crystallise in the same space group $P\bar{1}$ but are not isomorphic due to significant variations in the unit cell parameters.

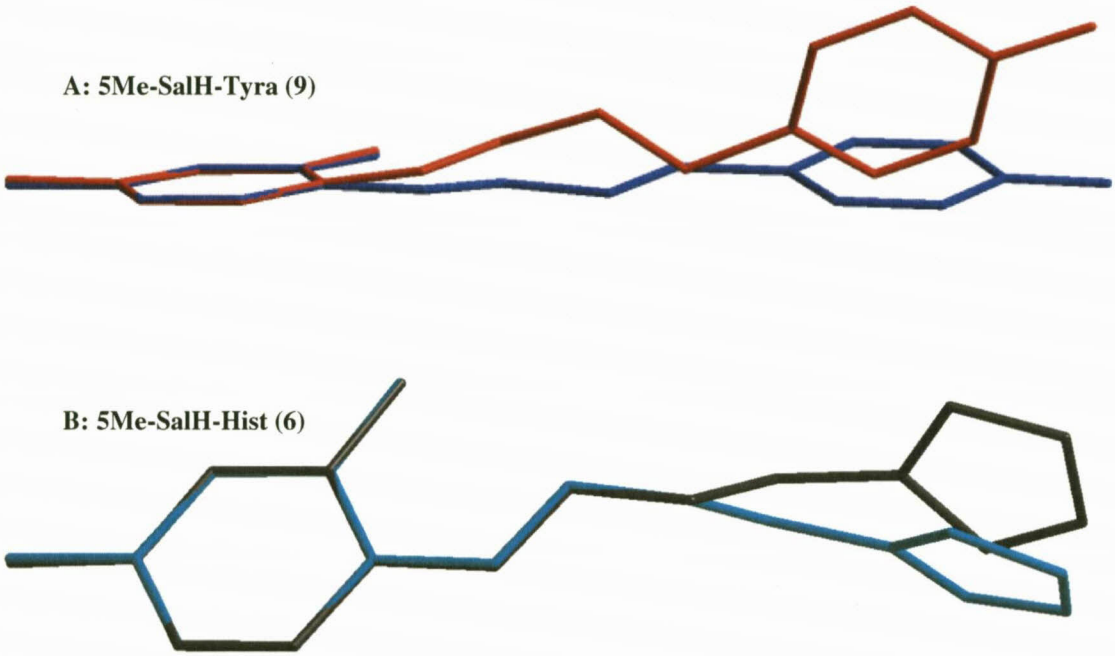

Figure 5.33: **An overlay of the two molecules found in the asymmetric unit of the crystal structures. (A) 5Me-SalH-Tyra (RMS = 1.172 x 10^{-2} Å) and (B) 5Me-SalH-Hist (RMS = 8.169 x 10^{-3} Å) to show variation of orientation. Overlay drawn only through atoms C11, C12, C13, C14, C15, C16 of the respective compounds to allow free rotation of imine substituent, therefore low RMS values are indicated. (True overlay through all atoms yields an RMS value of 0.588 Å for (9) and 0.336 Å for (6)).**

Compounds (**8**) and (**10**) have the aromatic functionality bonded directly to the N atom. Both compounds are planar with minimal rotation around the C1=N1 double bond. Despite the large size of the carbazole functionality (13 member aromatic ring system) bonded to the N atom of compound (**8**), it has a smaller dihedral angle than compound (**10**), which only has a cyclopentyl ring system.

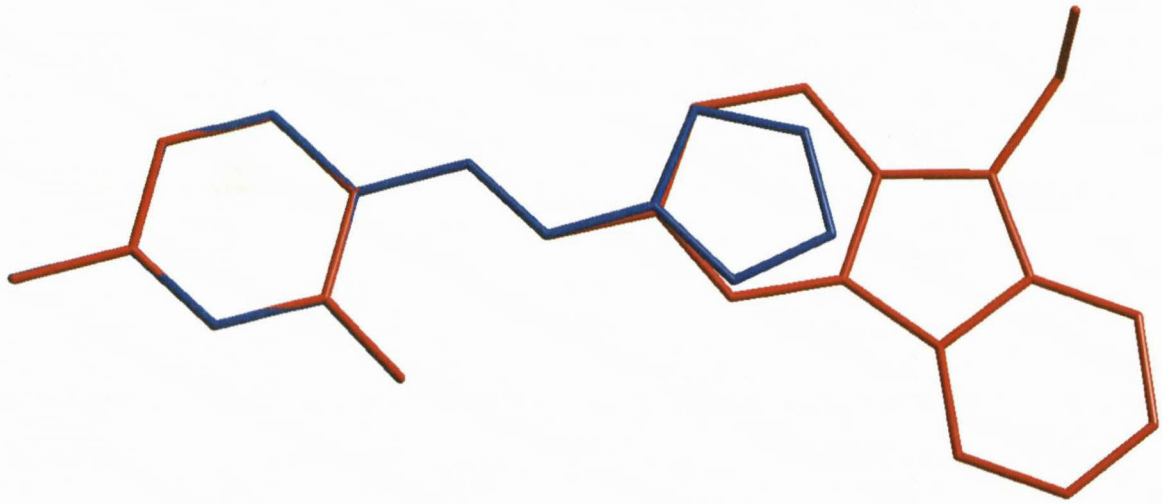

Figure 5.34: **An overlay of crystal structures 5Me-SalH-Carba (drawn in red) and 5Me-SalH-Triaz (drawn in blue) to indicate similarity in aromatic ring orientation. Overlay drawn only through atoms C11, C12, C13, C14, C15, C16 of the respective compounds.**

The bond distances and angles of the five salicylidene molecules are all within normal range and the molecules all crystallize in the *trans* phenol-imine tautomeric form with strong intramolecular O-H...N hydrogen bond to form a pseudo six-membered aromatic ring.

5.9 CONCLUSION

The crystal structures of five salicylidene derivatives, containing various coordinated biological amines, were analysed and discussed in this section. The crystal structures of the five ligands display various molecular packing, intra- and intermolecular hydrogen bonding as well as π-π stacking. These neutral compounds were used in conjunction with the previously discussed aromatic salicylidene compounds, as coordinating ligands for *fac*-$[M(CO)_3]^+$ moieties (M = Re, Tc). The advantages of the salicylidene compounds synthesised, is the ability to lose the proton on the phenol group to become a mono-negatively charged bidentate ligand. This satisfies the electronic requirements of the *fac*-$[M(CO)_3]^+$ moiety while still leaving the third position on the tricarbonyl system open for substitution. The synthetic procedure whereby the salicylidene organic compounds were coordinated to the Re-tricarbonyl metal centre was discussed in Chapter 3. The various *fac*-$[Re(L,L'\text{-Bid})(CO)_3(S)]$ crystal structures (L,L'-Bid = N,O bidentate ligand, S = coordinated solvent / neutral ligand) obtained from the synthesis will be discussed in the following chapters.

6 X-RAY CRYSTALLOGRAPHIC STUDY OF *fac*-[Re(Sal)(CO)$_3$(S)] COMPLEXES

6.1 INTRODUCTION

A large number of rhenium tricarbonyl crystal structures as well as rhenium Schiff-base crystalline complexes have been reported in literature as discussed in Chapter 2. The coordination of the Schiff-base ligands to Re(V) and Re(III) species is prominent in the literature, in particular with regards to Re(V) and Tc(V) due to the importance which the $[M=O]^{3+}$ core has influenced the design of radiopharmaceutical agents. The salicylidene backbone has regularly been used in the coordination with rhenium and technetium with over 180 crystal structures found in the Crystallographic Cambridge Structural Database[1] coordinated to $Re^{III-VII}$ and $Tc^{III, V}$. However the coordination of salicylidene to rhenium(I) tricarbonyl complexes is rare and the crystal structural data of only four Re(I) salicylidene tricarbonyl (**A** and **B**) and three related structures (**C**) have been reported, to the best of our knowledge.[2,3,4]

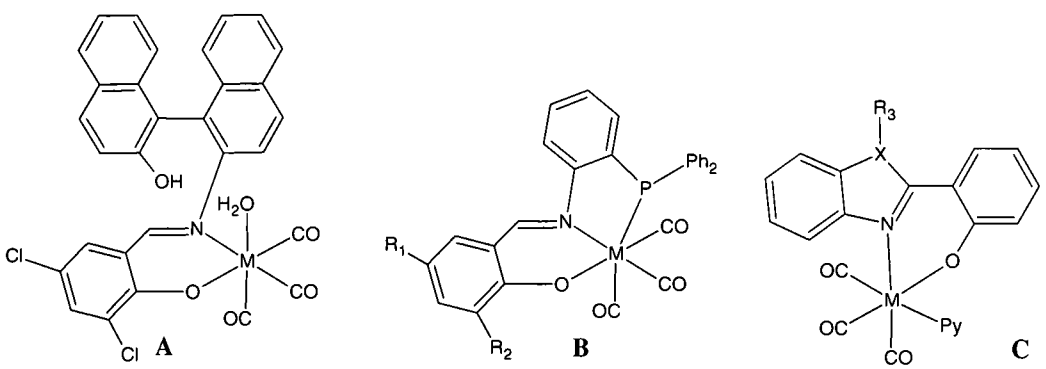

Figure 6.1: **Reported crystal structures of M-salicylidene tricarbonyl complexes (M = Re; X = N, O, S; R = various substituents).**

---

[1] Cambridge Structural Database (CSD), Version 5.32, February 2011 update. F.H. Allen, *Acta Cryst.*, 2002, B58, 380

[2] Z.K. Li, Y. Ki, L. Lei, C.M. Che, X.G. Zhou, *Inorg. Chem. Commun.*, 2005, 8, 307

[3] J.W. Faller, G. Mason, J. Par, *J. Organomet. Chem.*, 2001, 626, 191

[4] R. Czerwieniec, A. Kapturkiewicz, R. Anulewicz-Ostrowska, J. Nowacki, *J. Chem. Soc., Dalton Trans.*, 2002, 3434

The crystallized rhenium tricarbonyl complexes were not all directly related to medical research. Complex **A** is a chiral mononuclear complex of Re(I)-NOBIN tricarbonyl (NOBIN = 1 amino-1'-hydroxylbinaphthyl)[2] which contains a coordinated water in the third position. The complex has shown some catalytic ability in asymmetric epoxidation and aziridination. Complexes of the type **B** were reported by Faller *et al.*[3] who investigated the coordination of hetero- (P, N, O) tridentate ligands to various transition metals including Re(I) tricarbonyl complexes. Finally, complexes of the type **C** formed part of a study[4] investigating whether the primary formation of Re(N-O) species is more likely in a dimeric than a monomeric form.

A primary aim of this investigation was the design of organic ligands and potential radiopharmaceuticals utilizing the [2+1] approach proposed by Mundwiler *et al.*[5] The synthesised bidendate ligand, coordinated to the metal centre and containing an attached directing ligand, could allow the third position on the metal centre to remain "open" for increased reactivity. Alternatively the third position could be occupied which may act as a "blocker" protecting the metal centre from nucleophilic attack. A final option is to coordinate a directing ligand to the third position and utilise the bidentate ligand as a constant stabilization chelator. The salicylidene backbone coordinated to Re(I) and Tc(I) tricarbonyl complexes has rarely been used and therefore it was considered a worthwhile study to pursue as the salicylaldehyde starting reagent is readily able to react with a variety of directing ligands.

From a synthetic viewpoint, we were unable to directly synthesize the rhenium aqua species, *fac*-[Re(L,L'-Bid)$(CO)_3$($\mathbf{H_2O}$)] (L,L'-Bid = N,O mono-negative salicylidene bidentate ligand) from a water medium as impure oils were consistently obtained. It was however, possible to obtain crystallographicly pure complexes from methanol in the form of *fac*-[Re(L,L'-Bid)$(CO)_3$($\mathbf{HOCH_3}$)]. Utilizing the [2+1] approach, it can be shown that methanol is readily substituted to yield pure product in good yield and several complexes which are soluble in water. These complexes create another interesting prospect for the development of radiopharmaceutical kits using the [2+1] approach. To the best of our knowledge, the crystal structures reported here are the first published crystal structures of *fac*-$[Re(CO)_3]^+$ containing a coordinated methanol solvent ligand.[6] A *fac*-$[Tc(CO)_3]$-complex containing a coordinated

[5] S. Mundwiler, M. Kündig, K. Ortner, R. Alberto. *Dalton Trans.*, 2004, 1320
[6] A. Brink, H.G. Visser, A. Roodt, *J. Coord. Chem.*, 2011, 64, 122

methanol solvent ligand has been published by Zobi *et al.*[7] in 2003 and Schutte *et al.* has recently reported the structure of *fac*-[Re(Flav)(CO)$_3$(HOCH$_3$)].CH$_3$OH (Flav = 3-hydroxyflavonate) which was grown by dissolving *fac*-[Re(Flav)(CO)$_3$(H$_2$O)] in methanol and leaving for a period of 21 days for crystals to form.[8] The coordination chemistry of the salicylidene ligands, synthesized in Chapter 3, with *fac*-[Re(CO)$_3$]$^+$ were investigated with single crystal X-ray diffraction. Several crystal structures were obtained and a comparison of the crystallographic data of a variety of coordinated Re-Sal complexes will be made and discussed in this chapter. The various molecular interactions and crystal packing modes are described. The Re-Sal complexes which are described in this chapter are illustrated in Figure 6.2.

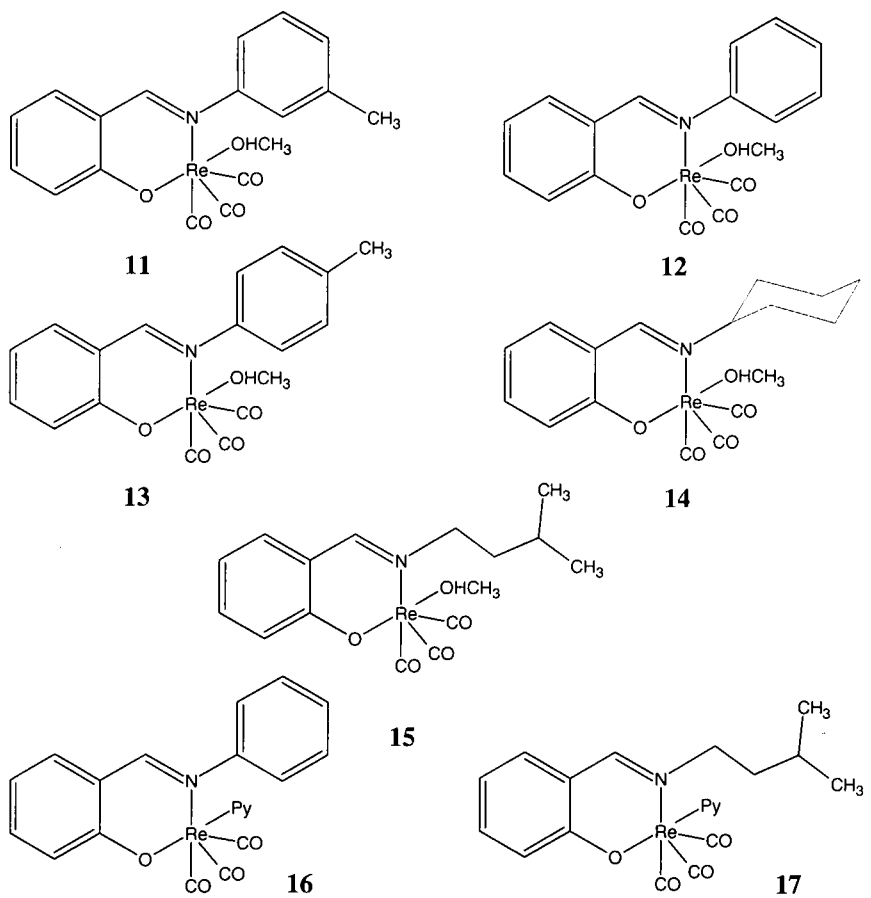

Figure 6.2: **The *fac*-[Re(L,L'-Bid)(CO)$_3$(S)] complexes (L,L'-Bid = mono-negatively charged N-O Sal bidentate ligand; S = coordinated methanol or pyridine) discussed in this chapter. (11) [Re(Sal-*m*Tol)(CO)$_3$(HOCH$_3$)], (12) [Re(Sal-Ph)(CO)$_3$(HOCH$_3$)], (13) [Re(Sal-*p*Tol)(CO)$_3$(HOCH$_3$)], (14) [Re(Sal-CyHex)(CO)$_3$(HOCH$_3$)], (15) [Re(Sal-3MeBu)(CO)$_3$(HOCH$_3$)], (16) [Re(Sal-Ph)(CO)$_3$(NC$_5$H$_5$)], (17) [Re(Sal-3MeBu)(CO)$_3$(NC$_5$H$_5$)] (Structures 1-10 were reported in Chapters 4 and 5).**

[7] F. Zobi, B. Spingler, T. Fox, R. Alberto. *Inorg. Chem.*, 2003, 42, 2818
[8] M. Schutte, G. Kemp, H.G. Visser, A. Roodt, *Inorg. Chem.*, 2011, publication accepted

6.2 EXPERIMENTAL

The reflection data was collected on a Bruker X8 ApexII 4K diffractometer[9] using Mo *K*α radiation with ω-and-φ-scans at 100 K. COSMO[10] was utilized for optimum collection of more than a hemisphere of reciprocal space. Frame integration and data reduction were performed using the Bruker SAINT-Plus[11] and XPREP[11] software packages, respectively. Data was corrected for absorption effects using the multi-scan technique SADABS.[12] The data for the complexes *fac*-[Re(Sal-Ph)$(CO)_3(NC_5H_5)$] and *fac*-[Re(Sal-3MeBu)$(CO)_3(NC_5H_5)$] were collected on a Oxford Diffraction Xcalibur 3 Crysalis CCD system[13] using Mo Kα (0.71073 Å) and ω-scans. Intensity data were extracted and integrated using Crysalis RED.[14] The structures were solved by direct methods package SIR97[15] and refined using the software package WinGX,[16] incorporating SHELXL.[17] All non-hydrogen atoms were refined with anisotropic displacement parameters, while the methyl, methane and aromatic H atoms were placed in geometrically idealized positions and constrained to ride on their parent atoms, with (C-H = 0.98-0.95 Å and $U_{iso}(H) = 1.5U_{eq}(C)$ and $1.2U_{eq}(C)$), respectively. The methyl protons were located from a difference Fourier map and the group was refined as a rigid motor. A large electron density peak/hole is found approximately 0.8 Å from the Re1 metal centre for most structures and is thought to be related to the decomposition of the crystal structure. The program DIAMOND[18] was used for all graphical representation of the crystal structures. All structures are shown with thermal ellipsoids drawn at 50% probability level unless otherwise stated. Graphical representations of overlays of selected complexes are obtained with Hyperchem 7.52.[19] A summary of the general crystal data and refinement parameters is given in Table 6.1 and 6.2 for all seven rhenium tricarbonyl salicylidene complexes. Supplementary data for the atomic coordinates, bond distances and angles and anisotropic displacement parameters are given in the Appendix B for each individual dataset.

---

[9] Bruker, APEX2 (Version 1.0-27), Bruker AXS Inc., Madison, Wisconsin, USA, 2005
[10] Bruker, COSMO, Version 1.48, Bruker AXS Inc., Madison, Wisconsin, USA, 2003.
[11] Bruker, SAINT-Plus (Version 7.12) (including XPREP), Bruker AXS Inc., Madison, Wisconsin, USA, 2004
[12] Bruker, SADABS, Version 2004/1, Bruker AXS Inc., Madison, Wisconsin, USA,1998.
[13] Crysalis CCD. Oxford Diffraction Ltd., Abingdon, Oxfordshire, U.K., 2005.
[14] Crysalis RED. Oxford Diffraction Ltd., Abingdon, Oxfordshire, U.K., 2005.
[15] A. Altomare, M.C. Burla, M. Camalli, G.L. Cascarano, C. Giacovazzo, A. Guagliardi, A.G.G. Moliterni, G. Polidori, R. Spagna, *J. Appl. Cryst.* 1999, 32, 115.
[16] L.J. Farrugia, *J. Appl. Cryst.*, 1999, 32, 837
[17] G.M. Sheldrick, SHELXL97, *Program for Solving Crystal Structures*, University of Göttingen, Germany, 1997
[18] K. Brandenburg, H. Putz, DIAMOND, Release 3.0c, Crystal Impact GbR, Bonn, Germany, 2005
[19] Hyperchem™ Release 7.52, Windows Molecular Modeling System, Hypercube, Inc., 2002

Table 6.1: **General X-ray crystallographic data and refinement parameters for *fac*-[Re(L,L'-Bid)(CO)$_3$(S)] (L,L'-Bid = Sal-T, T = coordinated substituent, S = coordinated methanol or pyridine).**

L,L'-Bid	Sal-*m*Tol (11)	Sal-Ph (12)	Sal-*p*Tol (13)	Sal-CyHex (14)	Sal-3MeBu (15)
S	$HOCH_3$	$HOCH_3$	$HOCH_3$	$HOCH_3$	$HOCH_3$
Empirical Formula	$C_{18}H_{16}NO_5Re$	$C_{17}H_{14}NO_5Re$	$C_{18}H_{16}NO_5Re$	$C_{17}H_{20}NO_5Re$	$C_{16}H_{20}NO_5Re$
Formula weight	512.53	498.49	512.52	504.55	492.53
Temperature (K)	100(2)	100(2)	100(2)	100(2)	100(2)
Wavelength (Å)	0.71069	0.71073	0.71073	0.71073	0.71073
Crystal System	Monoclinic	Monoclinic	Monoclinic	Monoclinic	Monoclinic
Space Group	*C2/c*	*C2/c*	*C2/c*	*C2/c*	*C2/c*
Unit Cell Dimensions					
a (Å)	18.513(6)	18.4769(7)	19.370(4)	18.096(4)	19.3075(8)
b (Å)	13.598(6)	13.4830(7)	14.027(3)	14.441(3)	13.8078(6)
c (Å)	14.294(5)	13.9281(7)	14.002(3)	13.753(3)	13.7882(6)
α (°)	90	90	90	90	90
β (°)	106.443(2)	108.988(3)	112.41(3)	107.18(3)	110.299(2)
γ (°)	90	90	90	90	90
Volume (Å^3)	3451(2)	3281.0(3)	3517(1)	3433.6(1)	3447.6(3)
Z	8	8	8	8	8
Density$_{calc.}$ (g.cm^{-1})	1.973	2.018	1.936	1.952	1.898
μ (mm^{-1})	7.070	7.433	6.938	7.104	7.072
F(000)	1968	1904	1968	1952	1904
Crystal Colour	Yellow	Yellow	Yellow	Colourless	Yellow
Crystal Morphology	Needle	Needle	Cuboid	Cuboid	Plate
Crystal Size (mm)	0.24x0.07x0.06	0.38x0.09x0.07	0.16x0.15x0.14	0.24x0.16x0.16	0.34x0.10x0.08
Theta Range (°)	1.89 to 28.00	1.91 to 28.00	2.69 to 28.00	1.84 to 28.00	1.85 to 28.00
Completeness (%)	99.7	100.0	98.6	99.1	100.0
Index Ranges	h = -24 to 21 k = -17 to 17 l = -18 to 18	h = -22 to 24 k = -17 to 17 l = -17 to 18	h = -21 to 25 k = -18 to 18 l = -18 to 18	h = -22 to 23 k = -18 to 19 l = -17 to 18	h = -25 to 23 k = -18 to 16 l = -18 to 17
Reflections Collected	25419	28593	37821	14839	20559
Independent Reflections	4159	3973	4199	4107	4179
R_{int}	0. 0611	0. 0805	0. 0958	0. 0963	0. 0412
Refinement method	Full-matrix least-squares on F^2	Full-matrix least-squares on F^2	Full-matrix least-squares on F^2	Full-matrix least-squares on F^2	Full-matrix least-squares on F^2
Data / restraints / parameters	4159 / 0 / 227	3973 / 0 / 217	4199 / 22 / 249	4107 / 0 / 217	4179 / 3 / 221
Goodness-of-fit on F^2	1.073	1.083	1.210	1.027	1.048
Final R indices [I>2sigma(I)]	R1 = 0.0356, wR2 = 0.0610	R1 = 0.0429, wR2 = 0.0957	R1 = 0.1073, wR2 = 0.2046	R1 = 0.0760, wR2 = 0.1850	R1 = 0.0379, wR2 = 0.0698
R indices (all data)	R1 = 0.0536, wR2 = 0.0671	R1 = 0.0548, wR2 = 0.1022	R1 = 0.1657, wR2 = 0.2575	R1 = 0.0983, wR2 = 0.2056	R1 = 0.0496, wR2 = 0.0740
ρ_{max} and ρ_{min} (e.Å^{-3})	3.382 (1.03 Å from Re1) and -1.157 (1.36 Å from Re1)	2.641 (0.87 Å from Re1) and -1.860 (0.84 Å from Re1)	5.895 (0.86 Å from Re1) and -5.899 (1.04 Å from Re1)	7.337 (0.88 Å from Re1) and -5.607 (0.79 Å from Re1)	1.891 (0.73 Å from Re1) and -2.780 (0.75 Å from Re1)

(Sal-*m*Tol) = 2-(*m*-tolyliminomethyl)phenolato; (Sal-Ph) = 2-(phenyliminomethyl)phenolato; (Sal-*p*Tol) = 2-(*p*-tolyliminomethyl)phenolato; (Sal-CyHex) = 2-(cyclohexyliminomethyl)phenolato; (Sal-3MeBu) = 2-(3-methylbutyliminomethyl)phenolato.

Table 6.2: **General X-ray crystallographic data and refinement parameters for *fac*-[Re(L,L'-Bid)(CO)$_3$(S)] (L,L'-Bid = Sal-T, T = coordinated substituent, S = coordinated methanol or pyridine).**

L,L'-Bid	**Sal-Ph (16)**	**Sal-3MeBu (17)**
S	**Pyridine**	**Pyridine**
Empirical Formula	$C_{21}H_{15}N_2O_4Re$	$C_{20}H_{21}N_2O_4Re$
Formula weight	545.55	539.60
Temperature (K)	100(2)	100(2)
Wavelength (Å)	0.71073	0.71073
Crystal System	Monoclinic	Monoclinic
Space Group	$P2_1/c$	$P2_1/c$
Unit Cell Dimensions		
a (Å)	10.2910(2)	12.9051(4)
b (Å)	9.8280(2)	8.6642(3)
c (Å)	18.9306(3)	18.6961(5)
α (°)	90	90
β (°)	97.023(2)	105.279(3)
γ (°)	90	90
Volume (Å^3)	1900.27(6)	2016.6(1)
Z	4	4
Density$_{calc.}$ (g.cm^{-1})	1.907	1.777
μ (mm^{-1})	6.424	6.052
F(000)	1048	1048
Crystal Colour	Yellow	Yellow
Crystal Morphology	Plate	Plate
Crystal Size (mm)	0.20x0.10x0.05	0.36x0.20x0.15
Theta Range (°)	2.34 to 27.00	2.26 to 28.00
Completeness (%)	98.2	99.7
Index Ranges	h = -13 to 13 k = -12 to 5 l = -24 to 24	h = -17 to 15 k = -11 to 11 l = -14 to 24
Reflections Collected	13509	15447
Independent Reflections	4074	4867
R_{int}	0. 0309	0.0226
Refinement method	Full-matrix least-squares on F^2	Full-matrix least-squares on F^2
Data / restraints / parameters	4074 / 0 / 254	4867 / 0 / 244
Goodness-of-fit on F^2	1.022	0.983
Final R indices [I>2sigma(I)]	R1 = 0.0352, wR2 = 0.0887	R1 = 0.0208, wR2 = 0.0455
R indices (all data)	R1 = 0.0442, wR2 = 0.0925	R1 = 0.0331, wR2 = 0.0500
ρ_{max} and ρ_{min} (e.Å^{-3})	5.054 (0.87 Å from Re1) and -1.001 (0.95 Å from O1)	0.787 (0.32 Å from H31) and -0.761 (0.84 Å from Re1)

(Sal-Ph) = 2-(phenyliminomethyl)phenolato; (Sal-3MeBu) = 2-(3-methylbutyliminomethyl)phenolato.

Note: The following general planes are defined and are consistently used throughout the text. Partial rhenium complexes are indicated on the right with necessary atom labeling.

Plane 1

= Salicylidene C1 aromatic backbone.

The plane is drawn through atoms C11, C12, C13, C14, C15, C16. Indicated in blue.

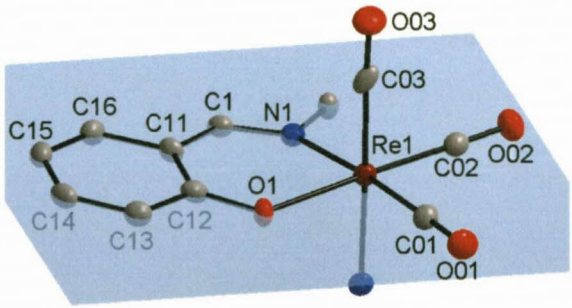

Plane 2

= Re1 equatorial plane.

Plane is drawn through atoms Re1, N1, O1, C01, C02. Indicated in purple.

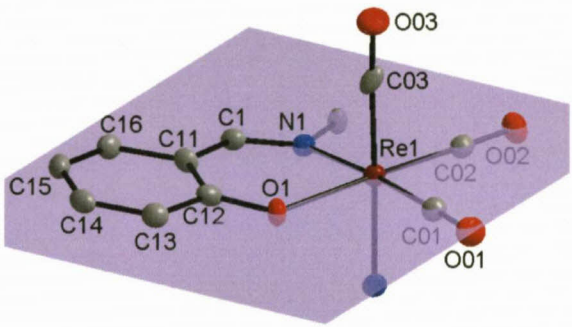

Plane 3

= Imino substituent plane.

Consists of any planar aromatic system bonded to the imine N1-atom. Indicated in green.

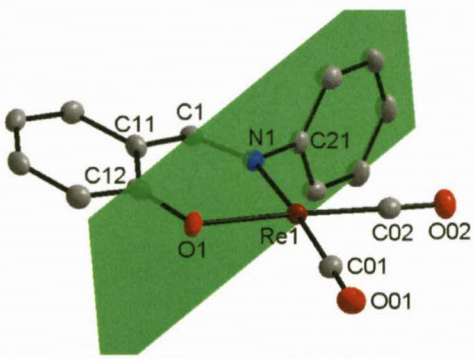

Plane 4

= Pyridine plane.

Plane drawn through the pyridine aromatic ring bonded to the Re metal centre in the 3rd position. Indicated in yellow.

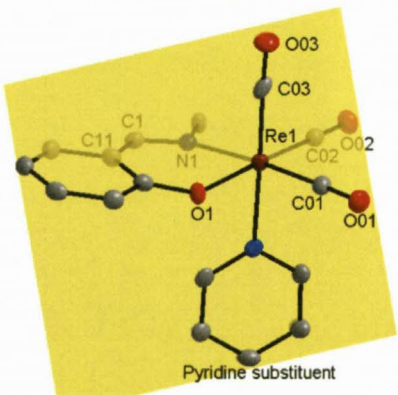

6.3 CRYSTAL STRUCTURE OF

fac-[Re(Sal-*m*Tol)(CO)$_3$(HOCH$_3$)]

The complex, *fac*-[Re(Sal-*m*Tol)(CO)$_3$(HOCH$_3$)] (**11**), (Sal-*m*Tol = 2-(*m*-tolyliminomethyl) phenolato) crystallizes in a monoclinic crystal system in the *C*2/c space group with eight formula units per unit cell (Z = 8). The asymmetric unit contains one independent molecule. The molecular structure of (**11**) is represented in Figure 6.3 along with the atom numbering scheme. Important bond lengths and angles are given in Table 6.3.

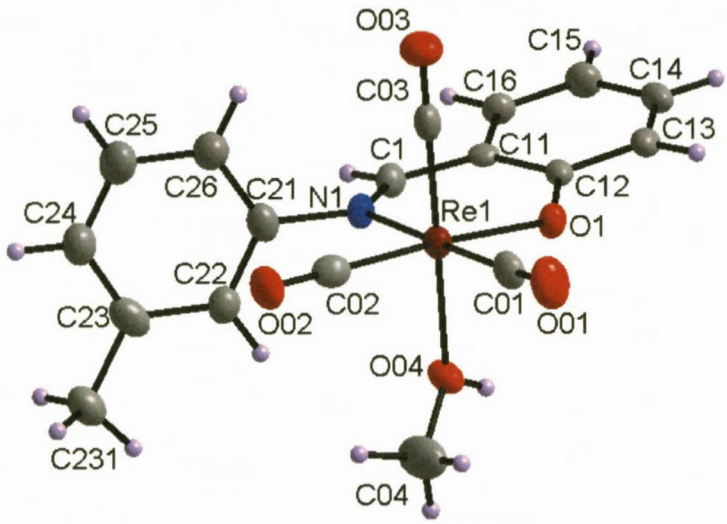

Figure 6.3: **Molecular structure of *fac*-[Re(Sal-*m*Tol)(CO)$_3$(HOCH$_3$)] (11) showing the atom numbering system. For the aromatic rings, the first digit refers to the ring number, while the second digit refers to the specific C-atom in the ring. Displacement ellipsoids are drawn at 50% probability level.**

Table 6.3: **Selected bond distances and angles of *fac*-[Re(Sal-*m*Tol)(CO)$_3$(HOCH$_3$)] (11) [Å and °].**

Atoms	Distance	Atoms	Angle
Re1-N1	2.157(4)	N1-Re1-O1	84.6(1)
Re1-O1	2.119(3)	O04-Re1-C03	175.4(2)
Re1-C01	1.913(6)	N1-Re1-C02	93.7(2)
Re1-C02	1.919(6)	O1-Re1-C01	93.4(2)
Re1-C03	1.890(6)	O1-Re1-C02	175.1(2)
Re1-O04	2.179(3)	Re1-O04-C04	122.1(4)
N1-C1	1.290(6)	Re1-C02-O02	179.4(5)
C1-C11	1.449(7)	C1-N1-C21	115.7(4)
N1-C21	1.456(6)	N1-C1-C12-O1	11.7(4)
O1-C12	1.339(6)	C26-C21-N1-C1	90.9(6)

The central rhenium metal coordinates with the nitrogen atom of the imine and the oxygen atom of the phenol group, from the salicylidene backbone, to form a six-membered ring.

Three carbonyl ligands are facially coordinated to the metal centre with the final position occupied by a methanol molecule. The octahedron around the Re(I) centre is distorted as indicated by the N1-Re1-O1 bite angle of 84.6(1)° and C03-Re1-O04 angle of 175.4(2)°. The Re-N1 and Re-O1 bond distances (2.157(4) Å and 2.119(3) Å) are comparable to related salicylidene structures which range from 2.152 - 2.199 Å for Re-N and 2.093 – 2.156 Å for Re-O,[2,3,4] as well as to other N,O ligand-to-metal bond distances which are in the range of 2.162 – 2.186 Å for Re-N and 2.099 – 2.184 Å for Re-O.[5,20,21]

The bond angle of the coordinated methanol molecule was found to be 122.1(4)° for Re1-O04-C04. The bond distance of rhenium to O04, the methanol oxygen, was calculated as 2.179(3) Å, which is slightly longer than that found for Re-OH_2 bonds, where the distances to the water oxygen range between 2.153 – 2.170 Å [8,20,22] for related Re(N-O) complexes. The bond distance is shorter than the Re-OH_2 bond distance in *fac*-$[Re(CO)_3(H_2O)_3]^+$ (2.201(14) Å).[23] Zobi *et al.*[7] reported a *fac*-$Tc(CO)_3$ complex containing a coordinated methanol with a Tc-OH-CH_3 bond angle of 128.7(3)° and a Tc-O bond distance of 2.177(3) Å.

The plane formed by the salicylidene C1 aromatic backbone (Plane 1: C11, C12, C13, C14, C15, C16) is tilted with respect to the Re1 equatorial plane (Plane 2: Re1, N1, O1, C01, C02) with a dihedral angle of 14.9(2)° (Figure 6.4).

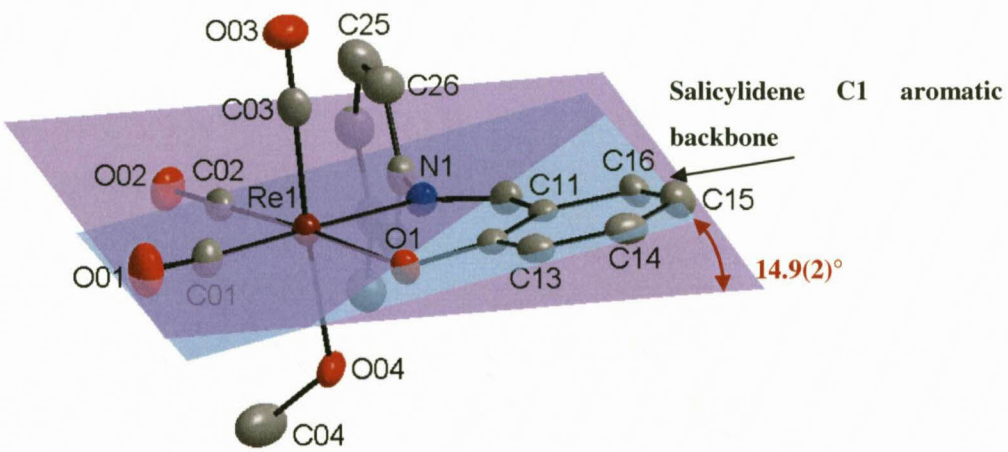

Figure 6.4: **Graphical representation of the bending aromatic backbone (Plane 1 indicated in blue, Plane 2 indicated in purple). H atoms are omitted for clarity.**

[20] M. Schutte, H.G. Visser, *Acta Cryst.*, 2008, E64, m1226
[21] R. Czerwieniec, A. Kapturkiewicz, R. Anulewicz-Ostrowska, J. Novacki, *J. Chem. Soc., Dalton Trans.*, 2001, 2756
[22] M. Schutte, H.G. Visser, A. Roodt, *Acta Cryst.*, 2008, E64, m1610
[23] R.S. Herrick, C.J. Ziegler, A. Cetin, B.R. Franklin, *Eur. J. Inorg. Chem.*, 2007, 1632

The *m*-tolyl substituent bonded to the imine N atom is rotated significantly to the C1 aromatic ring as compared to the non-coordinated free ligand. The dihedral angle between the C1 backbone ring (Plane 1) and the *m*-tolyl ring (Plane 3: C21, C22, C23, C24, C25, C26) is 81.9(2)° compared to the related dihedral angle (47.03(8)°) for the free ligand. The *m*-tolyl ring is rotated nearly perpendicular to the Re1 equatorial plane (Plane 2) with a dihedral angle of 86.7(2)°. The methyl moiety points below the plane in the same direction as the coordinated methanol molecule (Figure 6.5).

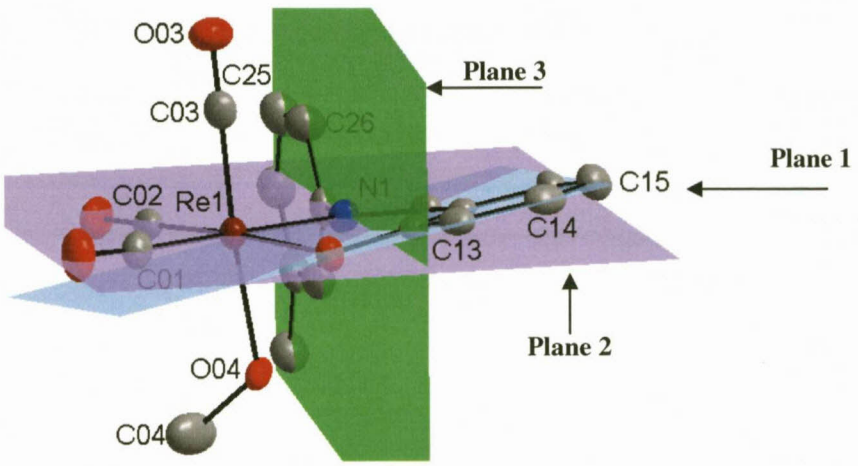

Figure 6.5: **Graphical representation of the rotation of the *m*-tolyl substituent (Plane 1 indicated in blue, Plane 2 indicated in purple, Plane 3 indicated in green). H atoms are omitted for clarity.**

Several intermolecular hydrogen C-H...O and O-H...O bond interactions are observed between neighbouring molecules as listed in Table 6.4 and illustrated in Figure 6.6 by orange dotted lines. The hydrogen interactions occur between the *m*-tolyl moiety and $O01^{\#1}$. A three-centred, bifurcated hydrogen bond interaction[24] occurs between C1-H1...$O02^{\#1}$ and $O03^{\#2}$ (Figure 6.6 A) and the coordinated methanol molecule experiences two hydrogen bonds between O04-H04...$O1^{\#4}$ and C04-H04B...$O03^{\#3}$ (Figure 6.6 B).

[24] G. Gilli, P. Gilli, *The Nature of the Hydrogen Bond*, Oxford University Press, Oxford, UK, 2009

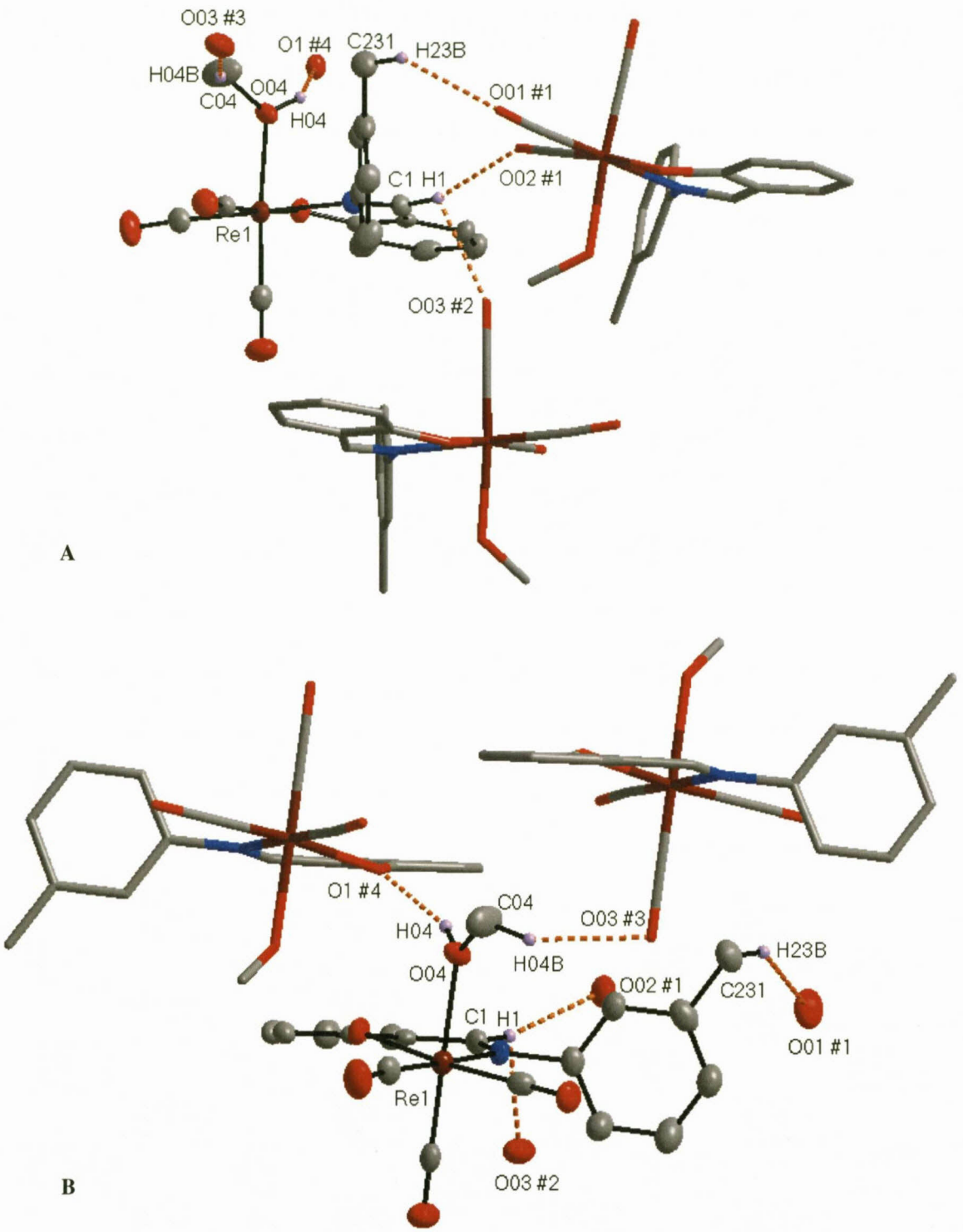

Figure 6.6: **Graphical representation of intermolecular hydrogen bond interactions. (A) Hydrogen bond interaction indicated between C1-H1...O02$^{\#1}$ and O03$^{\#2}$ and C231-H23B...O01$^{\#1}$. (B) Hydrogen bond interaction indicated between O04-H04...O1$^{\#4}$ and C04-H04B...O03$^{\#3}$. Hydrogen interaction indicated by orange dotted lines. Due to the complexity of the image, symmetry generated molecules are illustrated in "stick" format. Certain H atoms omitted for the sake of clarity. (Symmetry operation: #1 -x+3/2, y-1/2, -z+1/2; #2 -x+3/2, -y+1/2, -z; #3 x, -y+1, z+1/2; #4 -x+2, y, -z+1/2)**

Table 6.4: **Hydrogen bonds for *fac*-[Re(Sal-*m*Tol)(CO)$_3$(HOCH$_3$)] [Å and °].**

D-H...A	d(D-H)	d(H...A)	d(D...A)	<(DHA)
C(1)-H(1)...O(02)#1	0.95	2.47	3.387(7)	162.8
C(1)-H(1)...O(03)#2	0.95	2.60	3.019(7)	107.4
C(04)-H(04B)...O(03)#3	0.98	2.46	3.384(8)	157.8
C(231)-H(23B)...O(01)#1	0.98	2.56	3.399(8)	143.3
O(04)-H(04)...O(1)#4	0.95	1.80	2.595(5)	139.0

Symmetry transformations used to generate equivalent atoms:
#1 -x+3/2,y-1/2,-z+1/2 #2 -x+3/2,-y+1/2,-z #3 x,-y+1,z+1/2
#4 -x+2,y,-z+1/2

Short O...O intermolecular contacts between O1...O04$^{\#4}$ and O04...O1$^{\#4}$ (d = 2.596(5) Å; symmetry operation: #4 2-x, y, 0.5-z) occur to form a six-membered ring with a boat conformation as indicated by the green dotted lines (Figure 6.7). A π-π interaction between the C1 aromatic rings of the salicylidene backbone, is observed between the same two molecules as indicated in Figure 6.8.

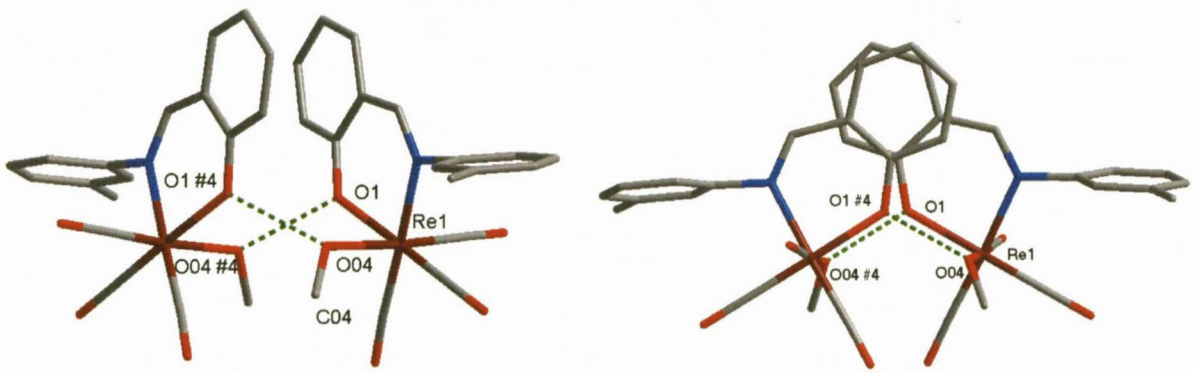

Figure 6.7: **Graphical representation of boat conformation formed by O...O interaction between neighboring molecules from two viewing directions. H atoms are omitted for the sake of clarity.**

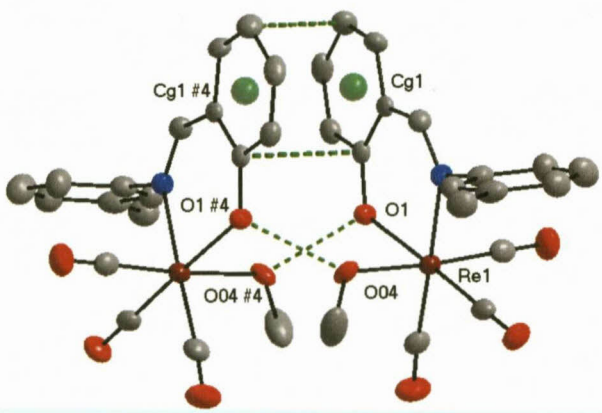

Figure 6.8: **Graphical representation of the π-π interactions indicated by green dotted lines (Cg = centroid atom of aromatic rings). H atoms omitted for clarity.**

Table 6.5: **π-π Interaction between aromatic rings of rhenium complexes.**

Centroid atom	Centroid atom	Distance between centroid atoms (Å)	Interplanar angle (°)
Cg1	Cg1 #4	3.627(3)	0.8(2)

Symmetry transformations used to generate equivalent atoms:
#4 2-x, y, 0.5-z
Cg1 = centroid atom of C11, C12, C13, C14, C15, C16

Molecular packing is further stabilised by the formation of two C-O...π interactions between C02-O02 and the *m*-tolyl aromatic ring as indicated by Figure 6.9 by orange dotted lines. Expansion of the unit cell with the overlaying π-π interactions is illustrated in Figure 6.10.

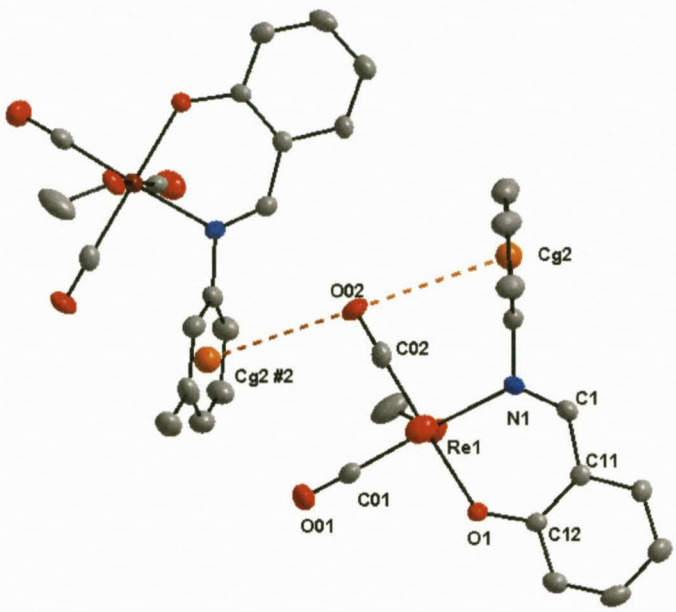

Figure 6.9: **Graphical representation of the C-O…π ring interactions indicated by orange dotted lines (Cg = centroid atom of aromatic rings). H atoms omitted for clarity.**

Table 6.6: **C-O…π Interaction between aromatic rings of rhenium complex.**

C-O...Cg	Centroid atom (Cg)	d(O...Cg) (Å)	d(C...Cg) (Å)	< (C-O...Cg) (°)
C02-O02	Cg2 #1	3.578(5)	3.534(6)	78.5(3)
C02-O02	Cg2 #2	3.940(5)	4.284(6)	99.5(4)

Symmetry transformations:
#1 x, y, z; #2 1.5-x, 0.5+y, 0.5-z
Cg2 = centroid atom of C21, C22, C23, C24, C25, C26

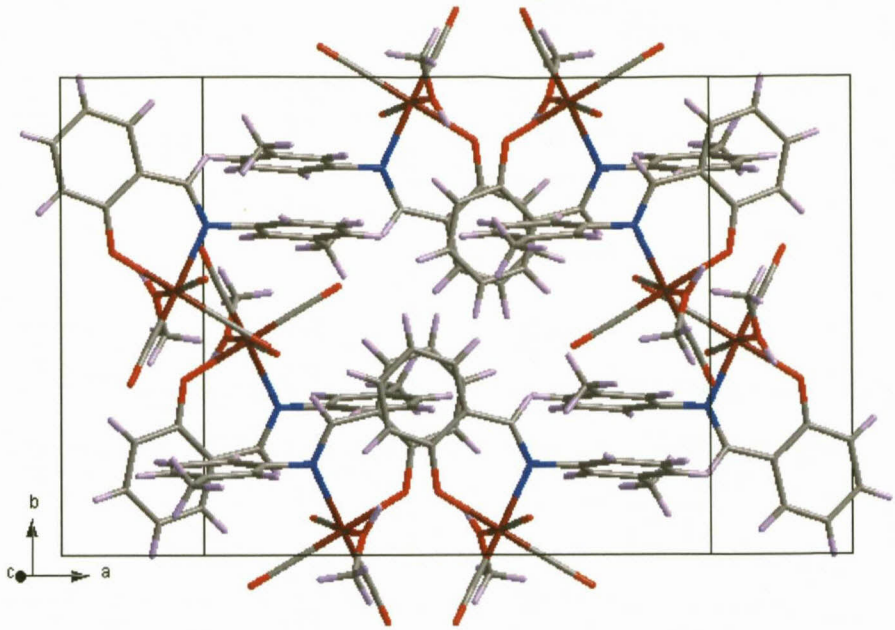

Figure 6.10: Molecular packing of π-π interactions in the unit cell.

Structural comparisons and illustrative overlays between the various coordinated rhenium tricarbonyl complex crystal structures are discussed in Section 6.10.

6.4 CRYSTAL STRUCTURE OF

fac-[Re(Sal-Ph)(CO)$_3$(HOCH$_3$)]

The complex, *fac*-[Re(Sal-Ph)(CO)$_3$(HOCH$_3$)] (**12**), (Sal-Ph = 2-(phenyliminomethyl) phenolato) crystallizes in a monoclinic crystal system in the *C*2/c space group with eight formula units per unit cell (Z = 8). The asymmetric unit contains one independent molecule. The molecular structure of (**12**) is represented in Figure 6.11 along with the atom numbering scheme and important bond lengths and angles are given in Table 6.7.

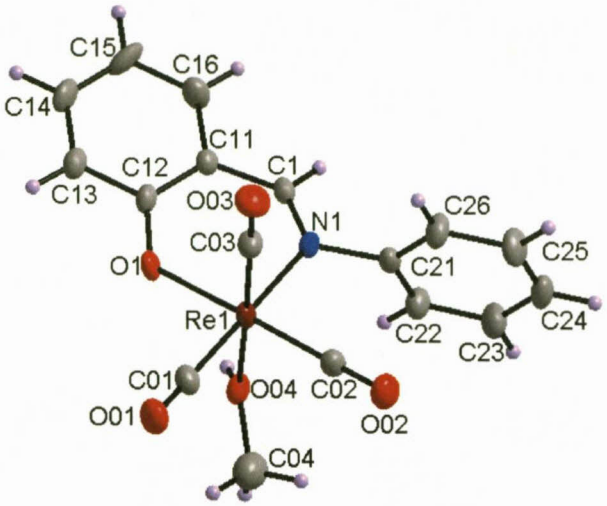

Figure 6.11: **Molecular structure of *fac*-[Re(Sal-Ph)(CO)$_3$(HOCH$_3$)] (12) showing the atom numbering system. For the aromatic rings, the first digit refers to the ring number, while the second digit refers to the specific C-atom in the ring. Displacement ellipsoids are drawn at 50% probability level.**

Table 6.7: **Selected bond distances and angles of *fac*-[Re(Sal-Ph)(CO)$_3$(HOCH$_3$)] (12) [Å and °].**

Atoms	Distance	Atoms	Angle
Re1-N1	2.164(6)	N1-Re1-O1	84.4(2)
Re1-O1	2.121(5)	O04-Re1-C03	174.9(3)
Re1-C01	1.920(7)	N1-Re1-C02	94.6(3)
Re1-C02	1.909(7)	O1-Re1-C01	94.0(3)
Re1-C03	1.895(7)	O1-Re1-C02	176.5(3)
Re1-O04	2.188(5)	Re1-O04-C04	121.2(5)
N1-C1	1.288(9)	Re1-C02-O02	178.4(6)
C1-C11	1.460(9)	C1-N1-C21	115.6(6)
N1-C21	1.459(9)	N1-C1-C12-O1	13.7(6)
O1-C12	1.326(8)	C26-C21-N1-C1	100.6(8)

The central rhenium metal coordinates with the nitrogen atom of the imine and the oxygen atom of the phenol group to form a six-membered ring. Three carbonyl ligands are facially coordinated to the metal centre with the final position occupied by a methanol molecule. The octahedron around the Re(I) centre is distorted as indicated by the N1-Re1-O1 bite angle of 84.4(2)° and C03-Re1-O04 angle of 174.9(3)°. The Re-N1 and Re-O1 bond distance (2.164(6) Å and 2.121(5) Å) are comparable to other N,O ligand-to-metal bond distances which are in the range of 2.162 – 2.186 Å for Re-N and 2.099 – 2.184 Å for Re-O.[5,20,22] The bond angle of the coordinated methanol molecule was found to be 121.2(5)° for Re1-O04-C04. The bond distance of rhenium to O04, the methanol oxygen, was calculated as 2.188(5) Å, which is slightly longer than that found for Re-OH$_2$ bonds, where the distances to the water oxygen range between 2.153 – 2.170 Å [8,20] for related Re(N-O) complexes.

The plane formed by the salicylidene C1 aromatic backbone (Plane 1: C11, C12, C13, C14, C15, C16) is tilted relative to the Re1 equatorial plane (Plane 2: Re1, N1, O1, C01, C02) with a dihedral angle of 18.5(2)° (Figure 6.12 A). The phenyl substituent bonded to the imine N atom is rotated to the C1 aromatic plane with a dihedral angle of 88.5(3)° (Plane 3: C21, C22, C23, C24, C25, C26) but has less rotation relative to the Re1 plane (Plane 2) with a dihedral angle of 77.5(2)°.

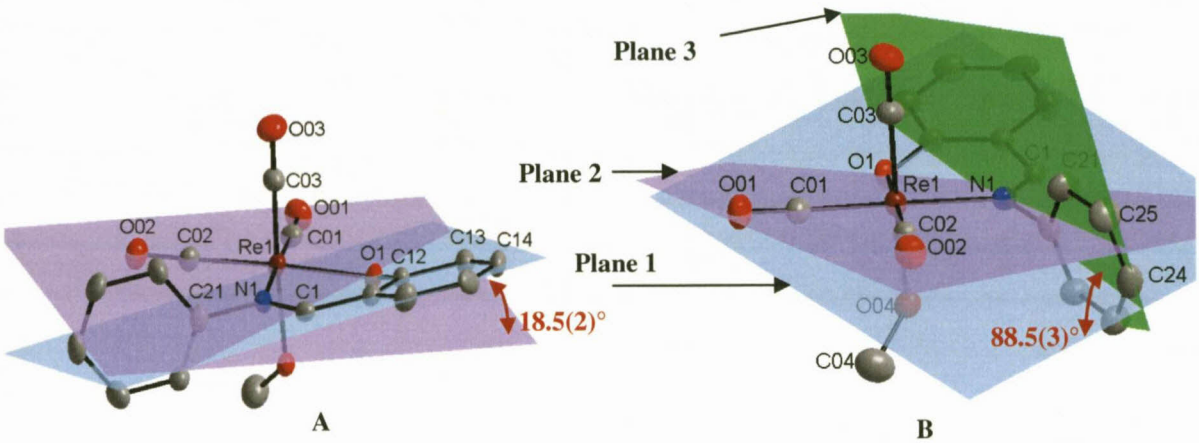

Figure 6.12: **(A) Graphical representation of the bending aromatic backbone. (B) Graphical representation of the rotation of the phenyl substituent. (Plane 1 indicated in blue, Plane 2 indicated in purple, Plane 3 indicated by green). H atoms are omitted for clarity.**

Several intermolecular hydrogen C-H...O and O-H...O bond interactions are observed between neighbouring molecules as listed in Table 6.8 and illustrated in Figure 6.13 by orange dotted lines. No hydrogen bond interactions occur between the aromatic phenyl moiety as compared to the *m*-tolyl moiety which was discussed in § 6.3 for the structure *fac*-[Re(Sal-*m*Tol)$(CO)_3(HOCH_3)$]. A three-centred, bifurcated hydrogen bond interaction occurs between C1-H1...O02$^{\#2}$ and O03$^{\#3}$ (Figure 6.13 A) and the coordinated methanol molecule experiences two hydrogen interactions between O04-H04...O1$^{\#1}$ and C04-H04C...O03$^{\#4}$ (Figure 6.13 B).

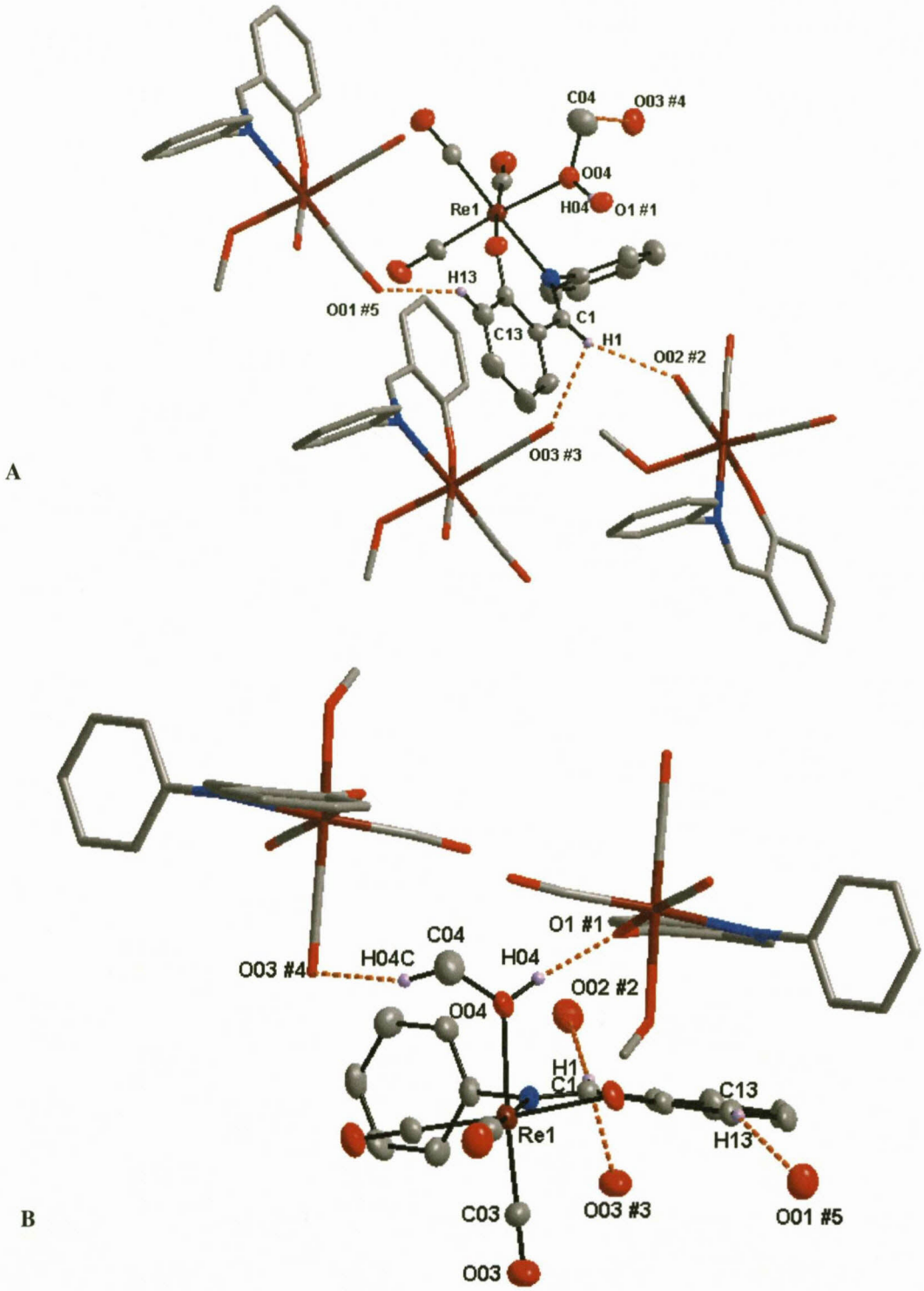

Figure 6.13: **Graphical representation of intermolecular hydrogen bond interaction. (A) Hydrogen bond interaction indicated between C1-H1...O02$^{\#2}$ and O03$^{\#3}$ and C13-H13...O01$^{\#5}$. (B) Hydrogen bond interaction indicated between O04-H04...O1$^{\#1}$ and C04-H04B...O03$^{\#4}$. Hydrogen interaction indicated by orange dotted lines. Due to the complexity of the image, symmetry generated molecules are illustrated in "stick" format. Certain H atoms omitted for the sake of clarity. (Symmetry operation: #1 -x+1, y, -z+3/2; #2 -x+1/2, y+1/2, -z+3/2; #3 -x+1/2, -y+3/2, -z+1; #4 x, -y+1, z+1/2; #5 -x+1, -y+1, -z+1.)**

Table 6.8: **Hydrogen bonds for *fac*-[Re(Sal-Ph)(CO)$_3$(HOCH$_3$)] [Å and °].**

D-H...A	d(D-H)	d(H...A)	d(D...A)	<(DHA)
O(04)-H(04)...O(1)#1	0.95	1.89	2.619(7)	131.0
C(1)-H(1)...O(02)#2	0.95	2.58	3.492(9)	161.1
C(1)-H(1)...O(03)#3	0.95	2.53	3.033(9)	113.1
C(04)-H(04C)...O(03)#4	0.98	2.46	3.368(12)	153.4
C(13)-H(13)...O(01)#5	0.95	2.48	3.288(10)	142.2

Symmetry transformations used to generate equivalent atoms:
#1 -x+1,y,-z+3/2 #2 -x+1/2,y+1/2,-z+3/2 #3 -x+1/2,-y+3/2,-z+1
#4 x,-y+1,z+1/2 #5 -x+1,-y+1,-z+1

Short O...O intermolecular contacts between O1...O04$^{\#1}$ and O04...O1$^{\#1}$ (d = 2.619(7) Å; symmetry operation: #1 1-x, y, 1.5-z) occurs to form a six-member ring with a boat conformation as indicated by the green dotted lines (Figure 6.14). Due to this interaction as well as the hydrogen bond interaction between O04-H04...O1$^{\#1}$, an unusually short H...H contact occurs between H04 and H13$^{\#1}$ as indicated by the orange dotted line (d = 2.0859(1) Å). A π-π interaction is clearly seen between the C1 aromatic rings of the salicylidene backbone of the same two molecules (Figure 6.14 and Table 6.9).

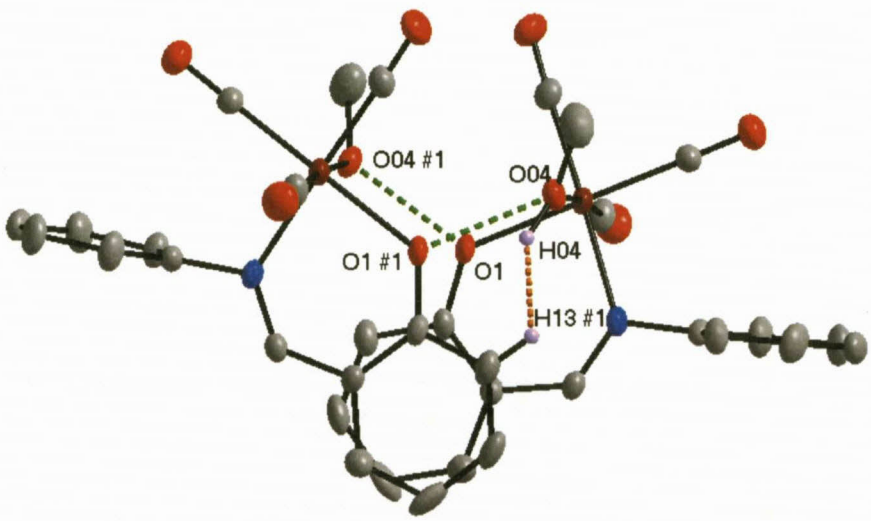

Figure 6.14: **Graphical representation of boat conformation formed by O...O interaction between neighboring molecules. Short H...H interaction is indicated by orange dotted line. H atoms are omitted for clarity.**

Table 6.9: **π-π Interaction between aromatic rings of rhenium complexes.**

Centroid atom	Centroid atom	Distance between centroid atoms (Å)	Interplanar angle (°)
Cg1	Cg1 #1	3.648(4)	2.0(2)

Symmetry transformations used to generate equivalent atoms:
#1 1-x, y, 1.5-z
Cg1 = centroid atom of C11, C12, C13, C14, C15, C16

Molecular packing is stabilised by the formation of two C-O...π interactions between C02-O02 and the phenyl aromatic ring as indicated by Figure 6.15 by orange dotted lines. Molecular packing of the unit cell is similar to the packing found in the previous structure *fac*-[Re(Sal-*m*Tol)$(CO)_3(HOCH_3)$]. Molecules in the unit cell pack in a "head-to-head" manner when viewed along the *a*-axis (Figure 6.16).

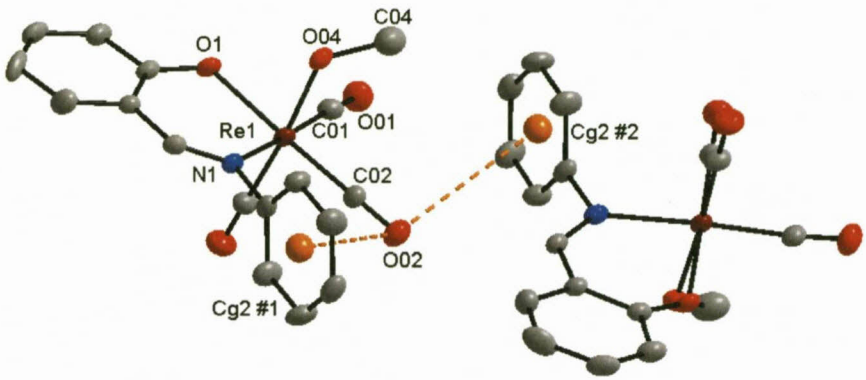

Figure 6.15: **Graphical representation of the C-O...π ring interactions indicated by orange dotted lines (Cg = centroid atom of aromatic rings). H atoms omitted for clarity.**

Table 6.10: **C-O...π Interaction between aromatic rings of rhenium complex.**

C-O...Cg	Centroid atom (Cg)	d(O...Cg) (Å)	d(C...Cg) (Å)	< (C-O...Cg) (°)
C02-O02	Cg2 #1	3.709(6)	3.616(8)	76.3(4)
C02-O02	Cg2 #2	3.877(6)	4.208(7)	98.6(5)

Symmetry transformations:
#1 x, y, z; #2 0.5-x, -0.5+y, 1.5-z
Cg2 = centroid atom of C21, C22, C23, C24, C25, C26

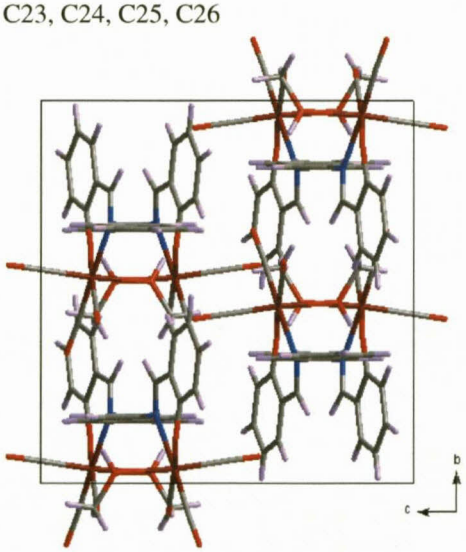

Figure 6.16: **Molecular packing of the unit cell as viewed along the *a*-axis.**

Structural comparisons and illustrative overlays between the various coordinated rhenium tricarbonyl complex crystal structures are discussed in Section 6.10.

6.5 CRYSTAL STRUCTURE OF

fac-[Re(Sal-*p*Tol)(CO)$_3$(HOCH$_3$)]

The complex, *fac*-[Re(Sal-*p*Tol)(CO)$_3$(HOCH$_3$)] (**13**), (Sal-*p*Tol = 2-(*p*-tolyliminomethyl) phenolato) crystallizes in a monoclinic crystal system in the *C*2/c space group with eight formula units per unit cell (Z = 8). The asymmetric unit contains one independent molecule. The yellow crystals were obtained with great difficulty as the complex looses crystallinity rapidly as soon as the crystals are removed from the mother liquid. Even with rapid harvesting, mounting of the crystal and preserving the crystal under a stream of liquid nitrogen, decomposition of the crystal structure could be visually observed. As a result, the crystal structure of **13** is disordered and contains large thermal ellipsoids. The crystallographic parameters are barely within acceptable levels with R_{int} = 0.0958, $R1_{all}$ = 0.1657, $R1_{obs}$ = 0.1073, GOOF = 1.210 with the highest electron density peak (5.895 e.A^{-3}) at a distance of 0.86 Å from Re1. The crystal structure is discussed for the sake of completeness and to assist in the explanation of any structural influences which may affect the kinetic investigation. The molecular structure of (**13**) is represented in Figure 6.17 along with the atom numbering scheme and important bond lengths and angles are given in Table 6.11.

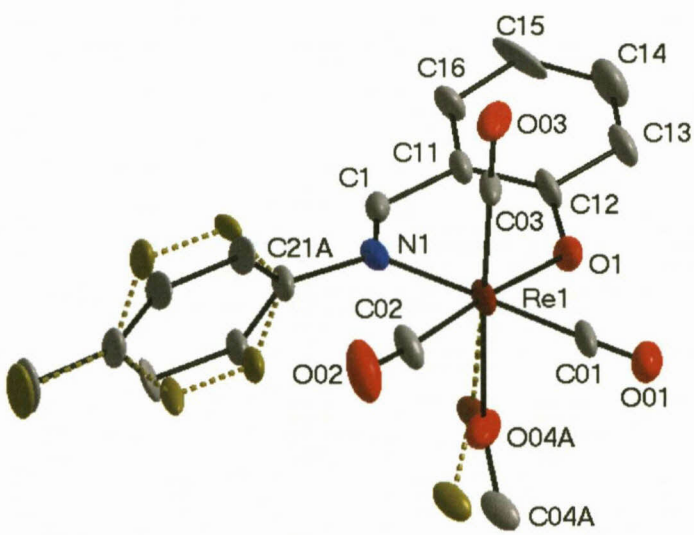

Figure 6.17: **Molecular structure of *fac*-[Re(Sal-*p*Tol)(CO)$_3$(HOCH$_3$)] (13) showing the atom numbering system. For the aromatic rings, the first digit refers to the ring number, while the second digit refers to the specific C-atom in the ring. Displacement ellipsoids are drawn at 30% probability level. H atoms are omitted for clarity.**

Table 6.11: Selected bond distances and angles of *fac*-[Re(Sal-*p*Tol)(CO)$_3$(HOCH$_3$)] (13) [Å and °].

Atoms	Distance	Atoms	Angle
Re1-N1	2.15(2)	N1-Re1-O1	84.8(7)
Re1-O1	2.133(16)	O04A-Re1-C03	176(3)
Re1-C01	1.90(3)	O04B-Re1-C03	173.0(12)
Re1-C02	1.95(2)	N1-Re1-C02	96.4(9)
Re1-C03	1.89(2)	O1-Re1-C01	91.9(9)
Re1-O04A	2.24(10)	O1-Re1-C02	175.5(8)
Re1-O04B	2.17(3)	Re1-O04A-C04A	119(8)
N1-C1	1.28(3)	Re1-O04B-C04B	123.6(19)
C1-C11	1.50(3)	Re1-C02-O02	176(3)
N1-C21A	1.45(2)	C1-N1-C21A	112(2)
O1-C12	1.34(3)	N1-C1-C12-O1	15(2)

The *p*-tolyl substituent is substitutionally disordered over two positions with a 0.57(6) : 0.43(6) ratio (Figure 6.18). The aromatic ring is disordered (*i.e* rotating back and forward) along the axis made by the N1-C21A-C24A line with these three atoms found in both disorders with a 100% occupancy. The dihedral angle between the aromatic rings is 35(2)° (Ring 1: C21A, C22A, C23A, C24A, C25A, C26A; Ring 2: C21A, C22B, C23B, C24A, C25B, C26B).

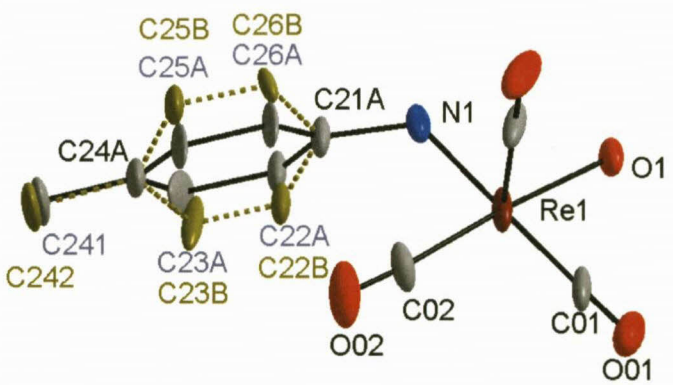

Figure 6.18: Molecular structure of the disordered *p*-tolyl substituent of 13 showing the atom numbering system. For the aromatic rings, the first digit refers to the ring number, while the second digit refers to the specific C-atom in the ring. Displacement ellipsoids are drawn at 30% probability level. H atoms are omitted for clarity.

The coordinated methanol solvent is also substitutionally disordered over two positions with a 0.69(5) : 0.31(5) ratio (Figure 6.19). O04B is lies behind O04A indicating greater deviation from an ideal octahedron with a C03-Re1-O04B angle of 173.0(12)° *vs.* C03-Re1-O04A angle of 176(3)°.

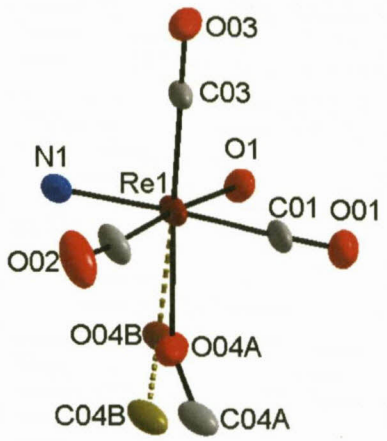

Figure 6.19: **Molecular structure of the disordered methanol ligand of 13 showing the atom numbering system. Displacement ellipsoids are drawn at 30% probability level.**

The octahedron around the Re(I) centre is distorted as indicated by the N1-Re1-O1 bite angle of 84.8(7)° and N1-Re1-C01 angle of 175.6(9)° which is nearly identical to the O1-Re1-C02 angle of 175.5(8)°. The Re-N1 and Re-O1 bond distances (2.15(2) Å and 2.133(16) Å) are comparable to other N,O ligand-to-metal bond distances. Only two intermolecular hydrogen bonding occurs in the molecular structure between atoms O04B-H04I...O1 and C1-H1...O03 as illustrated in Figure 6.20.

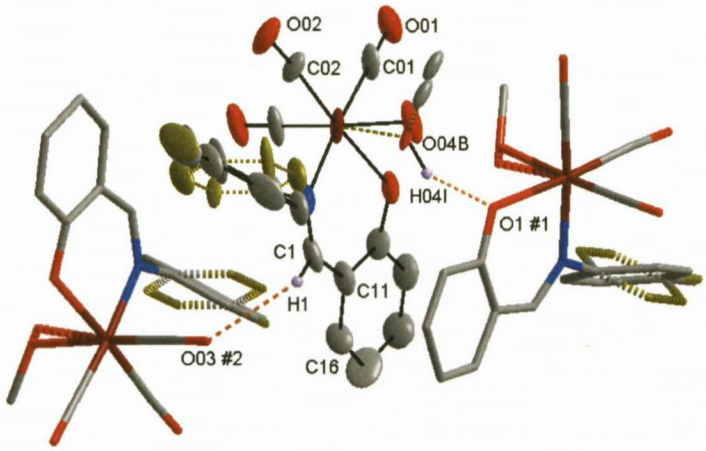

Figure 6.20: **Intermolecular hydrogen bond interaction of 13. Only necessary H atoms are indicated.**

Table 6.12: **Hydrogen bonds for *fac*-[Re(Sal-*p*Tol)(CO)$_3$(HOCH$_3$)] [Å and °].**

D-H...A	d(D-H)	d(H...A)	d(D...A)	<(DHA)
O(04B)-H(04I)...O(1)#1	0.95	1.76	2.59(3)	144.4
C(1)-H(1)...O(03)#2	0.95	2.53	3.13(3)	121.4

Symmetry transformations used to generate equivalent atoms:
#1 -x+1,y,-z+3/2 #2 -x+3/2,-y+1/2,-z+2

6.6 CRYSTAL STRUCTURE OF

fac-[Re(Sal-CyHex)(CO)$_3$(HOCH$_3$)]

The complex, *fac*-[Re(Sal-CyHex)(CO)$_3$(HOCH$_3$)] (**14**), (Sal-CyHex = 2-(cyclohexylimino-methyl)phenolato) crystallizes in a monoclinic crystal system in the *C*2/c space group with eight formula units per unit cell (Z = 8). The asymmetric unit contains one independent molecule. The colourless crystal contains a large electron density peak (7.337 e.Å^{-3}) which lies 0.88 Å from the Re1 metal centre and a R_{int} value of 0.0963. The molecular structure of (**14**) is represented in Figure 6.21 along with the atom numbering scheme and important bond lengths and angles are given in Table 6.13.

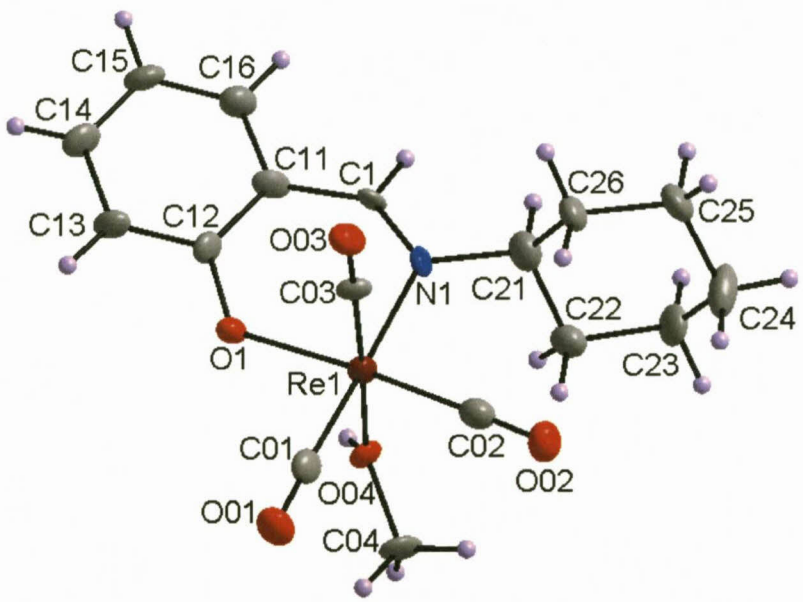

Figure 6.21: **Molecular structure of *fac*-[Re(Sal-CyHex)(CO)$_3$(HOCH$_3$)] (14) showing the atom numbering system. For the aromatic rings, the first digit refers to the ring number, while the second digit refers to the specific C-atom in the ring. Displacement ellipsoids are drawn at 50% probability level.**

Table 6.13: **Selected bond distances and angles of *fac*-[Re(Sal-CyHex)(CO)$_3$(HOCH$_3$)] (14) [Å and °].**

Atoms	Distance	Atoms	Angle
Re1-N1	2.202(9)	N1-Re1-O1	84.6(3)
Re1-O1	2.131(7)	O04-Re1-C03	174.9(3)
Re1-C01	1.896(11)	N1-Re1-C02	97.8(4)
Re1-C02	1.894(13)	O1-Re1-C01	92.3(4)
Re1-C03	1.869(10)	O1-Re1-C02	176.0(4)
Re1-O04	2.172(8)	Re1-O04-C04	123.8(7)
N1-C1	1.282(12)	Re1-C02-O02	175.8(10)
C1-C11	1.453(14)	C1-N1-C21	113.6(9)
N1-C21	1.502(12)	N1-C1-C12-O1	12.8(9)
O1-C12	1.324(12)	C26-C21-N1-C1	107.6(11)

The rhenium metal centre is octahedrally coordinated to the O and N donor atoms of the bidentate ligand, three carbonyl ligands with facial coordination and to the oxygen atom of methanol ligand. The nitrogen imine atom is bonded to the cyclohexyl substituent which has a chair conformation. The bidentate ligand forms a six-membered ring with the Re1 metal centre. The octahedron around the rhenium metal centre is distorted as indicated by the N1-Re1-O1 bite angle of 84.6(3)° and C03-Re1-O04 angle of 174.9(3)°.

The Re1-N1 bond distance (2.202(9) Å) is longer than for related salicylidene structures (2.152 - 2.199 Å) as well as for other N,O ligand to metal bond distances[4,5,8,20] which are in the range of 2.162 – 2.186 Å for Re-N. This may be caused by the steric bulk of the cyclohexyl substituent. The Re-O1 bond distance (2.131(7) Å) falls comfortably in range for related Sal structures (2.093 – 2.156 Å) for Re-O.[2,3,4] The Re1-O04-C04 bond angle of the coordinated methanol is 123.8(7)° with a Re1-O04 bond distance of 2.172(8) Å. The bond is longer than the Re-OH_2 bond distances (2.153 – 2.170 Å) found for related Re(N-O) complexes which coordinate to form five membered rings. The six membered bidentate rhenium complex [Re(Sal-NOBIN)$(CO)_3(H_2O)$] (NOBIN = 1 amino-1'-hydroxylbinaphthyl)[2] however has a even longer Re-OH_2 bond distance of 2.194 Å.

The plane of the salicylidene C1 aromatic backbone (Plane 1: C11, C12, C13, C14, C15, C16) is tilted relative to the Re1 equatorial plane (Plane 2: Re1, N1, O1, C01, C02) with a dihedral angle of 20.0(3)° (Figure 6.22).

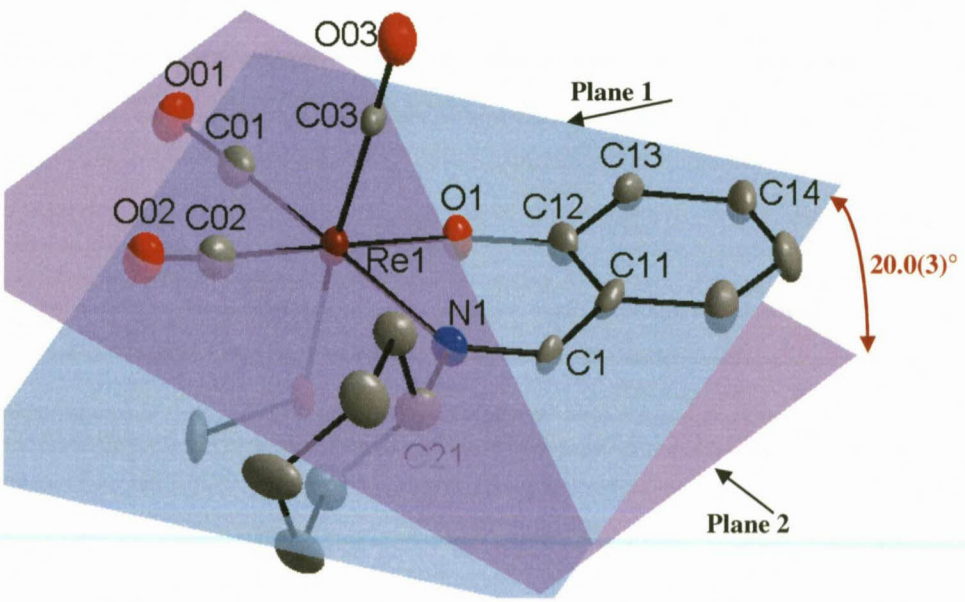

Figure 6.22: **Graphical representation of the bending aromatic ring backbone (Plane 1 indicated in blue, Plane 2 indicated in purple). H atoms are omitted for clarity.**

The non-planar cyclohexyl substituent, bonded to the imine N atom, is rotated to the C1 aromatic plane with a dihedral angle of 72.4(4)° (Plane 3: C21, C22, C23, C24, C25, C26) and has greater rotation relative to the Re1 plane (Plane 2) with a dihedral angle of 86.7(3)°. Due to the orientation of the cyclohexyl ring, a short H...H interaction occurs (Figure 6.23) between atoms C1-H1...H21-C21 (d = 1.9397(4) Å) with a torsion angle of 3.5(7)°.

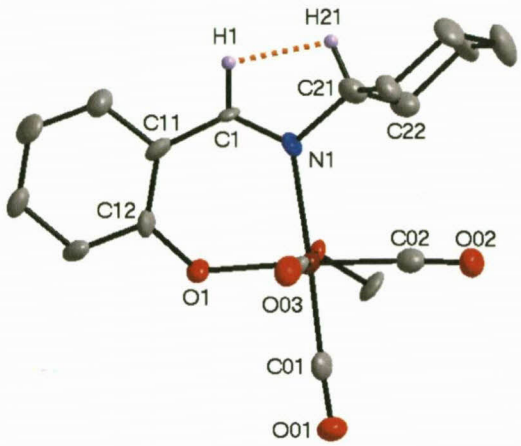

Figure 6.23: **Graphical representation H...H short contact indicated by orange dotted line. H atoms omitted for clarity.**

Two intermolecular hydrogen bond interactions occur of the type C-H...O while one O-H...O hydrogen bond occurs between neighbouring molecules in the unit cell, as indicated in Figure 6.24 and Table 6.14. No classical hydrogen bonding occurs with the cyclohexyl moiety.

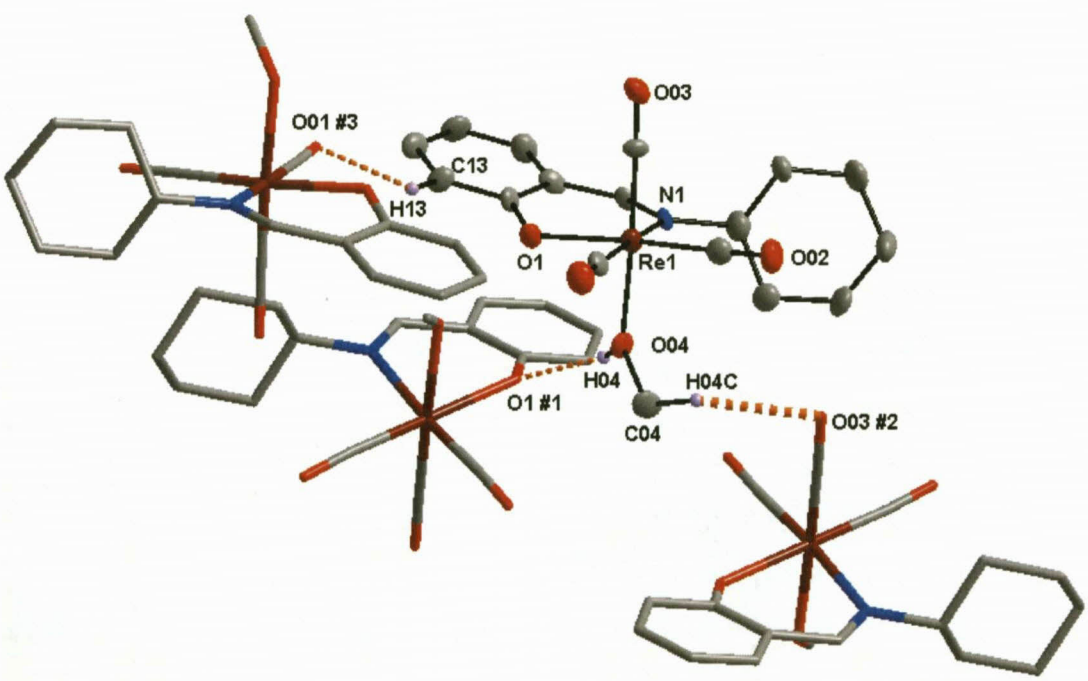

Figure 6.24: **Intermolecular hydrogen bonding of Complex 14. H atoms are omitted for clarity.**

Table 6.14: Hydrogen bonds for *fac*-[Re(Sal-CyHex)(CO)$_3$(HOCH$_3$)] [Å and °].

D-H...A	d(D-H)	d(H...A)	d(D...A)	<(DHA)
O(04)-H(04)...O(1)#1	0.84	1.89	2.586(11)	139.7
C(04)-H(04C)...O(03)#2	0.98	2.46	3.416(15)	165.7
C(13)-H(13)...O(01)#3	0.95	2.50	3.329(12)	146.3

Symmetry transformations used to generate equivalent atoms:
#1 -x+1,y,-z+3/2 #2 x,-y+1,z-1/2 #3 -x+1,-y+1,-z+2

A short intermolecular O...O contact occurs between O1...O04$^{\#1}$ (symmetry operation: #1 1-x, y, 1.5-z; d = 2.59(1) Å) and the symmetry related O04...O1$^{\#1}$ atoms to form a 6 membered cyclic ring in a boat conformation as indicated in Figure 6.25. A π-π ring interaction occurs between the same neighboring molecules between the C1 salicylidene backbone.

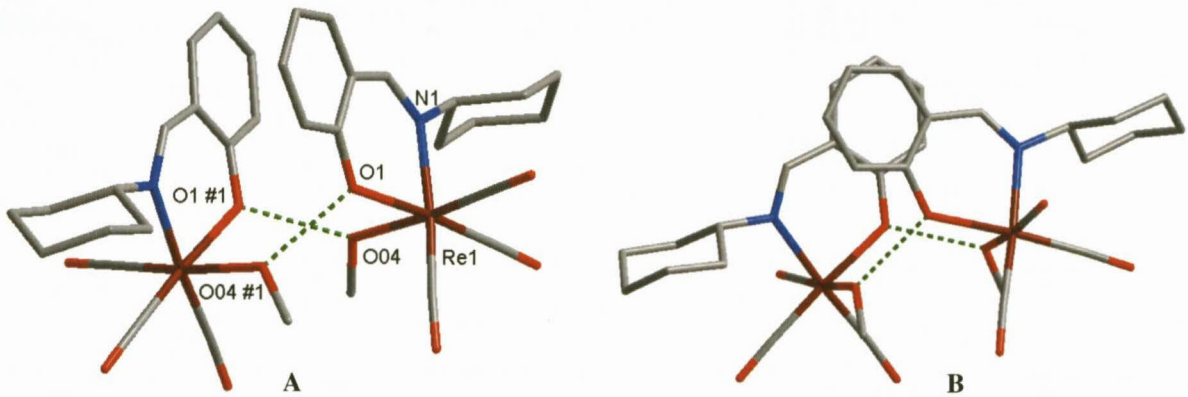

Figure 6.25: Graphical representation of (A) boat conformation formed by O...O interaction. (B) π-π Interaction between neighboring molecules. H atoms are omitted for clarity.

Table 6.15: π-π Interaction between aromatic rings of rhenium complexes.

Centroid atom	Centroid atom	Distance between centroid atoms (Å)	Interplanar angle (°)
Cg1	Cg1 #1	3.8104(10)	2.6(4)

Symmetry transformations used to generate equivalent atoms:
#1 1-x, y, 1.5-z
Cg1 = centroid atom of C11, C12, C13, C14, C15, C16

Structural comparisons and illustrative overlays between the various coordinated rhenium tricarbonyl complex crystal structures are discussed in Section 6.10.

6.7 CRYSTAL STRUCTURE OF

fac-[Re(Sal-3MeBu)(CO)$_3$(HOCH$_3$)]

The complex, *fac*-[Re(Sal-3MeBu)(CO)$_3$(HOCH$_3$)] (**15**), (Sal-3MeBu = 2-(3-methylbutyl iminomethyl)phenolato) crystallizes in a monoclinic crystal system in the *C*2/c space group with eight formula units per unit cell (Z = 8). The asymmetric unit contains one independent molecule.[6] The molecular structure of (**15**) is represented in Figure 6.26 along with the atom numbering scheme. Important bond lengths and angles are given in Table 6.16.

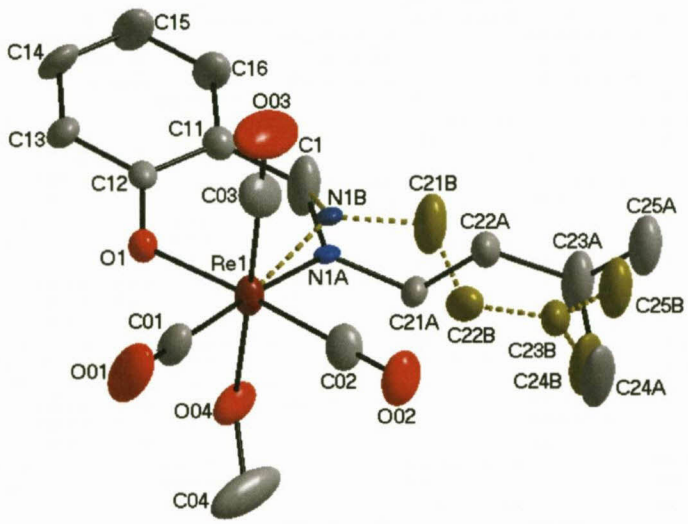

Figure 6.26: **Molecular structure of *fac*-[Re(Sal-3MeBu)(CO)$_3$(HOCH$_3$)] (15) showing the atom numbering system. For the aromatic rings, the first digit refers to the ring number, while the second digit refers to the specific C-atom in the ring. Displacement ellipsoids are drawn at 50% probability level. H atoms are omitted for clarity.**

Table 6.16: **Selected bond distances and angles of *fac*-[Re(Sal-3MeBu)(CO)$_3$(HOCH$_3$)] (15) [Å and °].**

Atoms	Distance	Atoms	Angle
Re1-N1A	2.148(7)	N1A-Re1-O1	84.0(2)
Re1-N1B	2.219(16)	N1B-Re1-O1	83.5(4)
Re1-O1	2.117(4)	O04-Re1-C03	175.1(2)
Re1-C01	1.900(6)	N1A-Re1-C02	95.7(3)
Re1-C02	1.902(6)	O1-Re1-C01	93.4(2)
Re1-C03	1.891(8)	O1-Re1-C02	176.2(2)
Re1-O04	2.179(4)	Re1-O04-C04	124.5(4)
N1A-C1	1.346(11)	Re1-C02-O02	178.1(5)
N1B-C1	1.212(18)	C1-N1A-C21A	115.7(7)
C1-C11	1.447(9)	C1-N1B-C21B	116.1(15)
N1A-C21A	1.469(10)	N1A-C1-N1B	28.3(9)
N1B-C21B	1.54(3)	N1A-C1-C12-O1	3.4(6)
O1-C12	1.331(7)	N1B-C1-C12-O1	32.1(9)

The 3MeBu amino group is substitutionally disordered over two positions with a 0.669(7) : 0.331(7) ratio. The torsion angles show significant displacement of the N1B atom relative to the N1A atom as indicated by the N1A-C1-C12-O1 and N1B-C1-C12-O1 torsion angles (3.4(6)° *vs.* 32.1(9)°). The thermal ellipsoids of the disordered N1A and N1B atoms are smaller than expected. Characterization by NMR, IR and elemental analysis all confirm the coordination of the **N**-3MeBu substituent. Refinement of the crystal structure assuming 100% occupancy of the N-atom increases the goodness of fit value (GOOF = 1.048 for N-atom disordered *vs.* 1.069 for N-atom with 100% occupancy). The disorder of the coordinated substituent is illustrated in Figure 6.27.

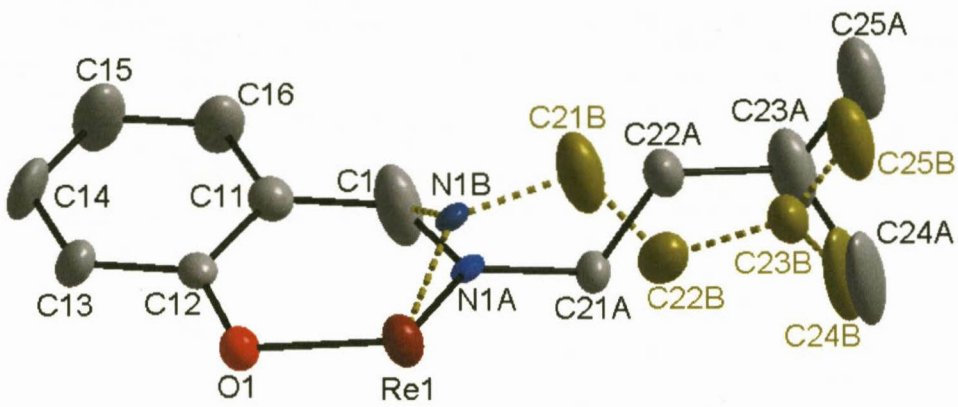

Figure 6.27: **Molecular structure indicating the disorder on the 3MeBu substituent of 15. H atoms are omitted for clarity.**

The central rhenium metal coordinates with the nitrogen atom of the imine and the oxygen atom of the phenol group, from the salicylidene backbone, to form a six-membered ring. Three carbonyl ligands are facially coordinated to the metal centre with the finally position occupied by a methanol molecule. The octahedron around the Re(I) centre is distorted as indicated by the N1A-Re1-O1 bite angle of 84.0(2)° and C03-Re1-O04 angle of 175.1(2)°. The Re-N1A, Re-N1B and Re-O1 bond distances (2.148(7) Å, 2.219(16) Å and 2.117(4) Å) are comparable to related salicylidene structures which range from 2.152 - 2.199 Å for Re-N and 2.093 – 2.156 Å for Re-O. The Re1-O04-C04 bond angle of the coordinated methanol was found to be 124.5(4)° with a Re-O04 bond length of 2.179(4) Å. The C1-N1A and C1-N1B bond distances (1.346(11) Å and 1.212(18) Å) are indicative of double bonds. The O1-C12 (1.331(7) Å), N1A-C21A (1.469(10) Å and N1B-C21B (1.54(3) Å) are consistent with single bonds for the respective atoms.[25]

[25] F.H. Allen, O. Kennard, D.G. Watson, L. Brammer, A.G. Orpen, R. Taylor, *J. Chem. Soc., Perkin Trans.* II, 1987, S1

The plane formed by the salicylidene C1 aromatic backbone (Plane 1: C11, C12, C13, C14, C15, C16) is tilted relative to the Re1 equatorial plane (Plane 2: Re1, N1A, O1, C01, C02) with a dihedral angle of 22.8(2)° (Figure 6.28). The N1B atom of the 3MeBu substituent lies 0.49(2) Å above Plane 2. The 3MeBu substituent is rotated to the C1 aromatic plane (Plane 1) with a dihedral angle of 76.7(3)° relative to the line drawn through atoms N1A and C21A. The substituent has less rotation to the Re1 plane (Plane 2) with a dihedral angle of 70.1(4)°.

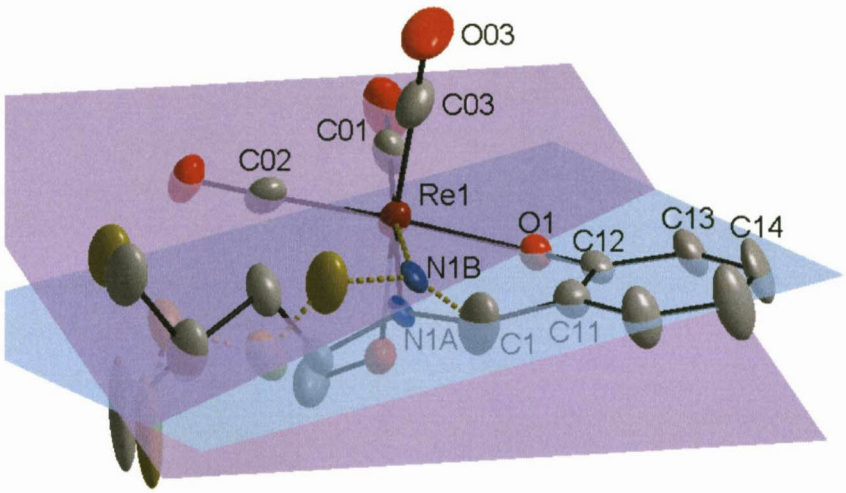

Figure 6.28: **Graphical representation of the bending aromatic C1 backbone as well as the placement of the 3MeBu substituent. (Plane 1 indicated in blue, Plane 2 indicated in purple.) H atoms are omitted for clarity.**

Intermolecular hydrogen bond interactions occur between C1-H1...O03$^{\#2}$ and C13-H13...O01$^{\#3}$ atoms respectively as indicated in Table 6.17 and Figure 6.29 A. An O-H...O interaction occurs between atoms O04-H04...O1$^{\#1}$ of neighbouring molecules as illustrated in Figure 6.29 B.

Table 6.17: **Hydrogen bonds for *fac*-[Re(Sal-3MeBu)(CO)$_3$(HOCH$_3$)] [Å and °].**

D-H...A	d(D-H)	d(H...A)	d(D...A)	<(DHA)
O(04)-H(04)...O(1)#1	0.84	1.85	2.578(5)	143.4
C(1)-H(1)...O(03)#2	0.95	2.51	3.125(11)	122.4
C(13)-H(13)...O(01)#3	0.95	2.48	3.317(8)	146.8

Symmetry transformations used to generate equivalent atoms:
#1 -x+1,y,-z+3/2 #2 -x+1/2,-y+3/2,-z+1 #3 -x+1,-y+1,-z+1

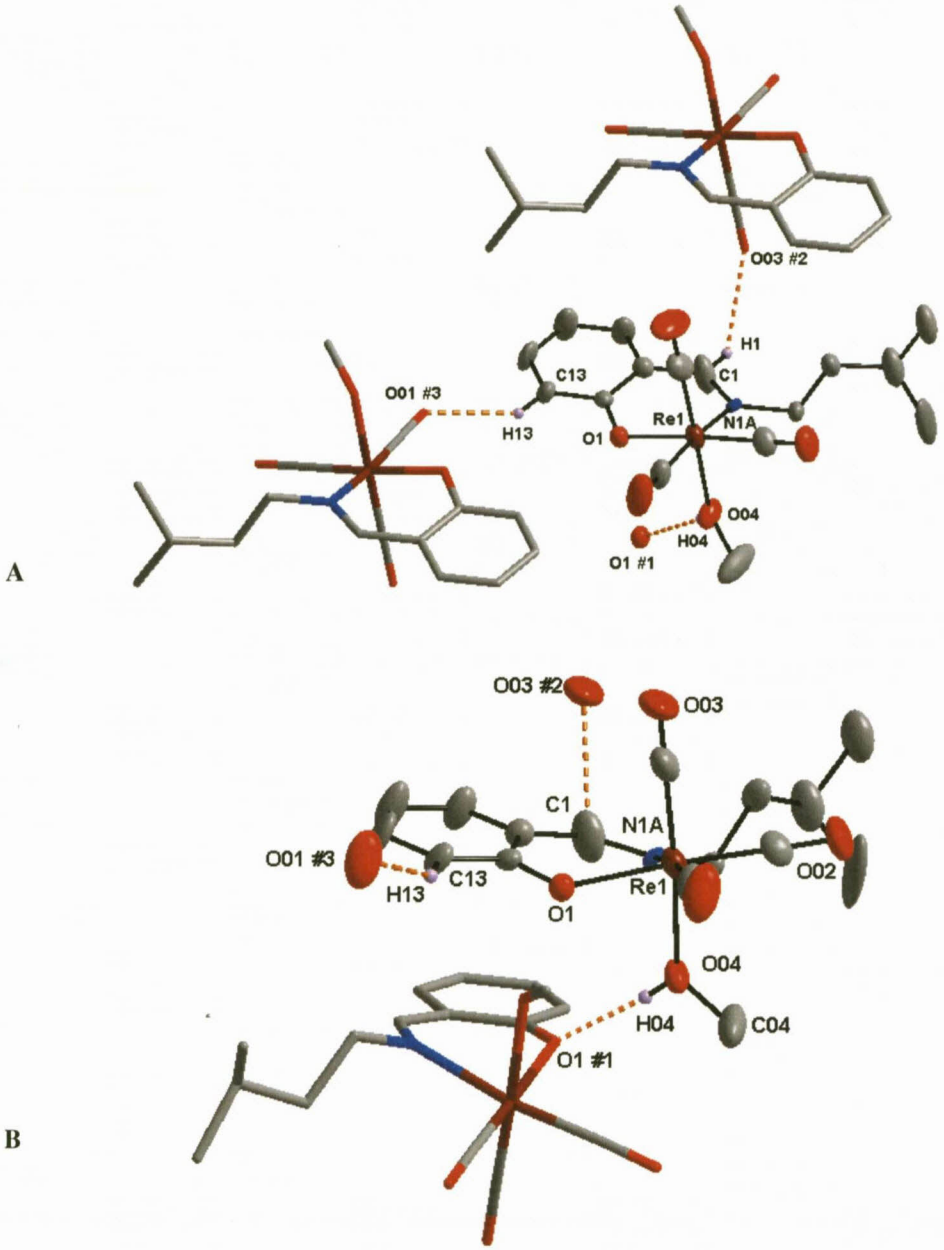

Figure 6.29: **Graphical representation of intermolecular hydrogen bond interaction. (A) Hydrogen bond interaction indicated between C1-H1...O03$^{\#2}$ and C13-H13...O01$^{\#3}$. (B) Hydrogen bond interaction indicated between O04-H04...O1$^{\#1}$. Hydrogen interaction indicated by orange dotted lines. Due to the complexity of the image, symmetry generated molecules are illustrated in "stick" format and only the one section of the 3MeBu substituent (Disorder A) is indicated. Certain H atoms omitted for the sake of clarity. (Symmetry operation: #1 -x+1, y, -z+3/2; #2 -x+1/2, -y+3/2, -z+1; #3 -x+1, -y+1, -z+1)**

Similar interactions are found in this structure, as discussed in previous *fac*-[Re(Sal-T)$(CO)_3(HOCH_3)$] complexes. A short intermolecular O…O contact occurs between O1…O04$^{\#1}$ (symmetry operation: #1 1-x, y, 1.5-z; d = 2.577(5) Å) and the related O04…O1$^{\#1}$ atoms to form a 6 membered cyclic ring in a boat conformation as indicated in

Figure 6.30 by green dotted lines. A π-π interaction occurs between the C1 salicylidene aromatic backbone of the same molecules (Table 6.18).

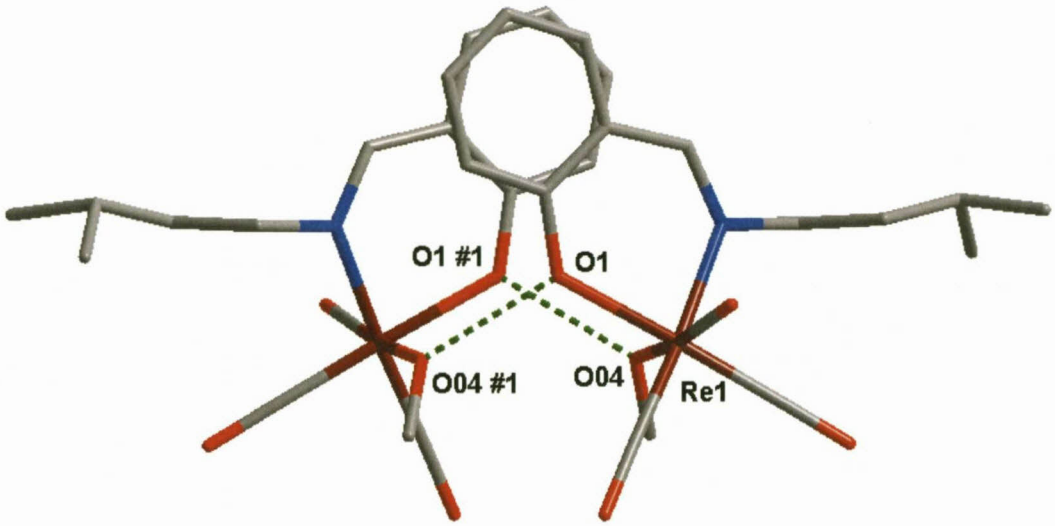

Figure 6.30: **Graphical representation of the boat conformation formed by O…O interaction as well as the π-π interaction between neighboring molecules. To prevent complexity, only one arm of the 3MeBu disorder (Disorder A) is indicated. H atoms are omitted for clarity.**

Table 6.18: **π-π Interaction between aromatic rings of rhenium complexes.**

Centroid atom	Centroid atom	Distance between centroid atoms (Å)	Interplanar angle (°)
Cg1	Cg1 #1	3.7756(2)	5.7(2)

Symmetry transformations used to generate equivalent atoms:
#1 1-x, y, 1.5-z
Cg1 = centroid atom of C11, C12, C13, C14, C15, C16

Structural comparisons and illustrative overlays between the various coordinated rhenium tricarbonyl complex crystal structures are discussed in Section 6.10.

6.8 CRYSTAL STRUCTURE OF

fac-[Re(Sal-Ph)(CO)$_3$(NC$_5$H$_5$)]

The complex, *fac*-[Re(Sal-Ph)(CO)$_3$(NC$_5$H$_5$)] (**16**), (Sal-Ph = 2-(phenyliminomethyl) phenolato) crystallizes in a monoclinic crystal system in the $P2_1/c$ space group with four formula units per unit cell (Z = 4). The asymmetric unit contains one independent molecule. The yellow crystal contains a large electron density peak (5.054 e.Å^{-3}) which lies 0.87 Å from the Re1 metal centre. The molecular structure of (**16**) is represented in Figure 6.31 along with the atom numbering scheme and important bond lengths and angles are given in Table 6.19.

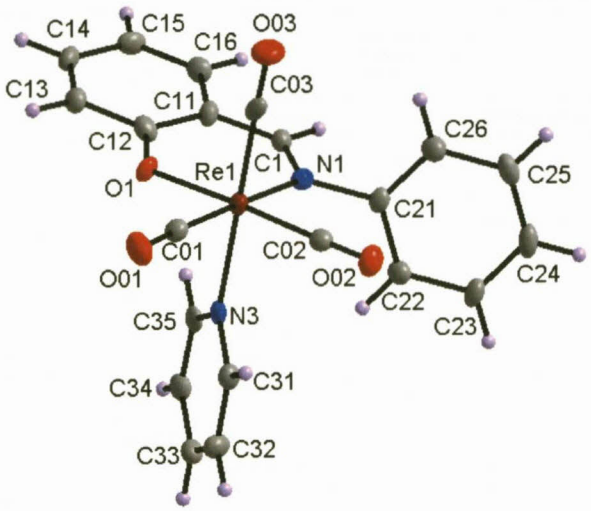

Figure 6.31: **Molecular structure of *fac*-[Re(Sal-Ph)(CO)$_3$(NC$_5$H$_5$)] (16) showing the atom numbering system. For the aromatic rings, the first digit refers to the ring number, while the second digit refers to the specific C-atom in the ring. Displacement ellipsoids are drawn at 50% probability level.**

Table 6.19: **Selected bond distances and angles of *fac*-[Re(Sal-Ph)(CO)$_3$(NC$_5$H$_5$)] (16) [Å and °].**

Atoms	Distance	Atoms	Angle
Re1-N1	2.152(5)	N1-Re1-O1	84.54(16)
Re1-O1	2.114(3)	N3-Re1-C03	178.44(19)
Re1-C01	1.925(5)	N1-Re1-C02	94.8(2)
Re1-C02	1.910(5)	O1-Re1-C01	92.72(19)
Re1-C03	1.904(6)	O1-Re1-C02	176.97(19)
Re1-N3	2.207(5)	N1-Re1-N3	85.23(17)
N1-C1	1.298(7)	Re1-C02-O02	178.9(5)
C1-C11	1.428(7)	C1-N1-C21	114.4(5)
N1-C21	1.448(7)	N1-C1-C12-O1	2.8(5)
O1-C12	1.302(6)	C26-C21-N1-C1	78.2(7)

The central rhenium metal coordinates with the nitrogen atom of the imine and the oxygen atom of the phenol group to form a six-membered ring. Three carbonyl ligands are facially coordinated to the metal centre while the finally position is occupied by a pyridine ligand. The octahedron around the Re(I) centre is distorted as indicated by the N1-Re1-O1 bite angle of 84.54(16)° and C03-Re1-N3 angle of 178.44(19)°. The Re1-N1 and Re1-O1 bond distance (2.152(5) Å and 2.114(3) Å) are comparable to other N,O ligand-to-metal bond distances which are in the range of 2.162 – 2.186 Å for Re-N and 2.099 – 2.184 Å for Re-O.[5,20,22] The Re1-N3 bond distance, of the coordinated pyridine, is 2.207(5) Å and compares well with similar complexes where bond distances between 2.203 – 2.230 Å were observed.[4,21] The C1-N1 bond distance (1.298(7) Å) is indicative of a double bond. The O1-C12 (1.302(6) Å), N1-C21 (1.448(7) Å) and C1-C11 (1.428(7) Å) are consistent for single bonds for the respective atoms.[25] The plane formed by the salicylidene C1 aromatic backbone (Plane 1: C11, C12, C13, C14, C15, C16) is tilted relative to the Re1 equatorial plane (Plane 2: Re1, N1, O1, C01, C02) with an dihedral angle of 12.0(2)° (Figure 6.32 A). The phenyl substituent bonded to the imine N atom is rotated to the C1 aromatic plane with a dihedral angle of 75.1(2)° (Plane 3: C21, C22, C23, C24, C25, C26) and has near perpendicular orientation relative to the Re1 equatorial plane (Plane 2) with a dihedral angle of 86.7(2)°. The final plane, through the atoms of the pyridine aromatic ring (Plane 4: N3, C31, C32, C33, C34, C35) has a dihedral angle of 68.4(2)° relative to phenyl substituent (Plane 3) and is perpendicular (89.0(1)°) to the Re1 plane (Plane 2) (Figure 6.32 B).

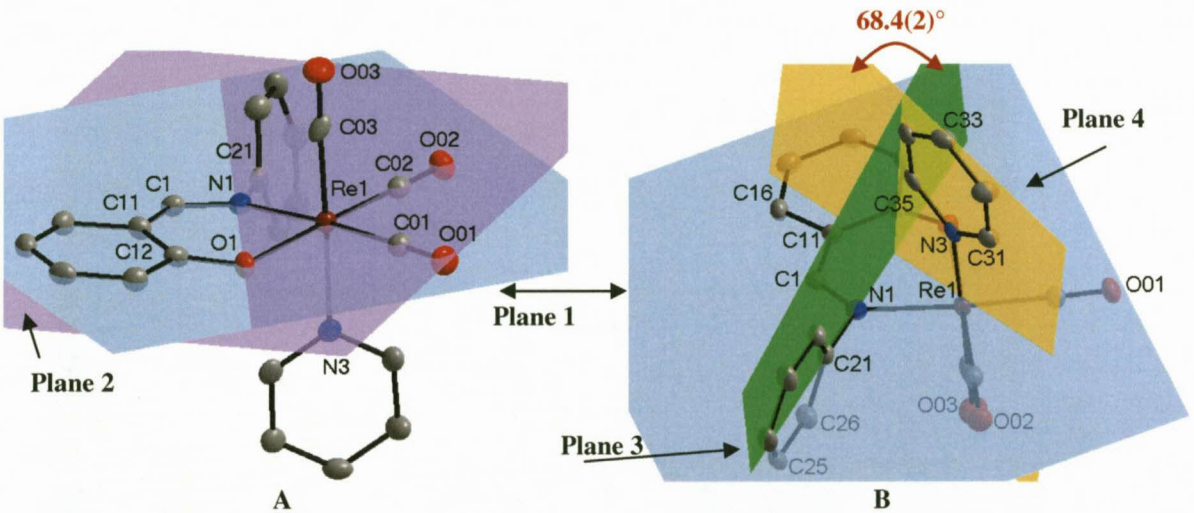

Figure 6.32: **(A) Graphical representation of the tilting C1 aromatic backbone. (B) Graphical representation of the rotation of the phenyl substituent and coordinated pyridine ligand. (Plane 1= blue, Plane 2 = purple, Plane 3 = green, Plane 4 = yellow). H atoms are omitted for clarity.**

One intramolecular hydrogen bond interaction is found between the pyridine atoms C35-H35 and O1 of the phenolato oxygen bonded to the Re(I) metal centre as indicated by the orange dotted line (Table 6.20). The interaction forms a pseudo tridentate ligand with a five-membered ring system (Figure 6.33).

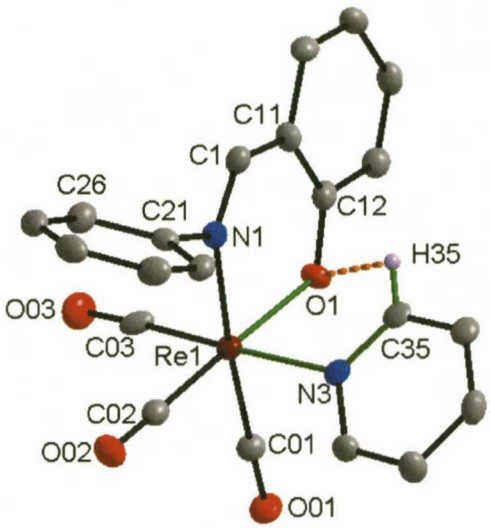

Figure 6.33: **Intramolecular hydrogen bond between the pyridine ligand and O1 atom (orange dotted line). Green coloured bonds indicate the coordination of the pseudo-tridentate ligand. H atoms are omitted for clarity.**

Table 6.20: **Hydrogen bonds for *fac*-[Re(Sal-Ph)(CO)$_3$(NC$_5$H$_5$)] [Å and °].**

D-H...A	d(D-H)	d(H...A)	d(D...A)	<(DHA)
C(35)-H(35)...O(1)#1	0.95	2.56	3.014(7)	109.8

Symmetry transformations used to generate equivalent atoms:
#1 x,y,z

An intramolecular C-O...π interaction occurs between atoms C02-O02 and the phenyl ring bonded to the imine N atom of the salicylidene backbone with a O02...π distance of 3.758(4) Å and a C02-O02...π angle of 77.1(3)° as illustrated in Figure 6.34 by the green dotted line.

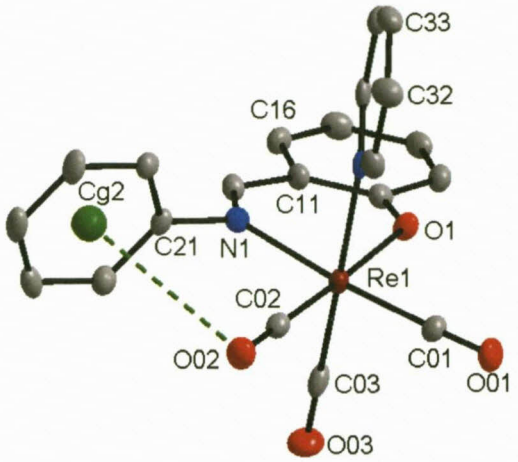

Figure 6.34: **Graphical representation of the C-O…π interaction within the molecule of the asymmetrical unit. Centroid atom (Cg) is indicated in green. H atoms are omitted for clarity.**

The molecular structure of the unit cell is further stabilized by C-H…π interactions. The observed interactions are found between two C-H atoms and both the pyridine and the imine substituted phenyl ring as illustrated in Figure 6.35 and Table 6.21 below.

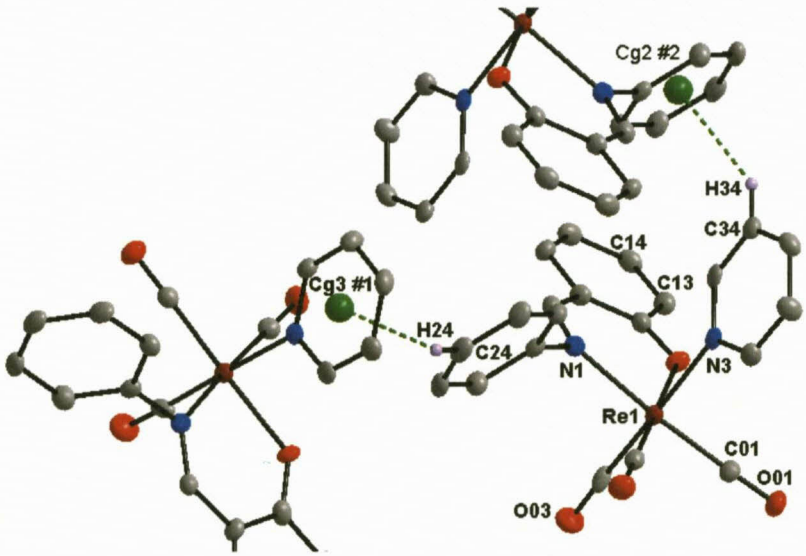

Figure 6.35: **Graphical representation of C-H…π interactions (green dotted line). Centroid atoms (Cg) of each aromatic ring are indicated in green. Only necessary atoms are illustrated for the sake of clarity.**

Table 6.21: **C-H…π Interaction between aromatic rings of rhenium complex.**

C-H...Cg	Centroid atom (Cg)	d(H...Cg) (Å)	d(C...Cg) (Å)	< (C-H...Cg) (°)
C24-H24	Cg3 #1	2.6479(1)	3.524(6)	153.5(3)
C34-H34	Cg2 #2	2.6142(1)	3.435(5)	144.9(4)

Symmetry transformations:
#1 x, 0.5-y, 0.5+z; #2 1-x, 1-y, 2-z
Cg2 = centroid atom of C21, C22, C23, C24, C25, C26; Cg3 = centroid atom of N3, C31, C32, C33, C34, C35

The molecules in the unit cell pack in a "head-to-head" manner when viewed along both the *a*- and the *c*-axis as indicated in Figure 6.36. Structural comparisons and illustrative overlays between the various coordinated rhenium tricarbonyl complex crystal structures are discussed in Section 6.10.

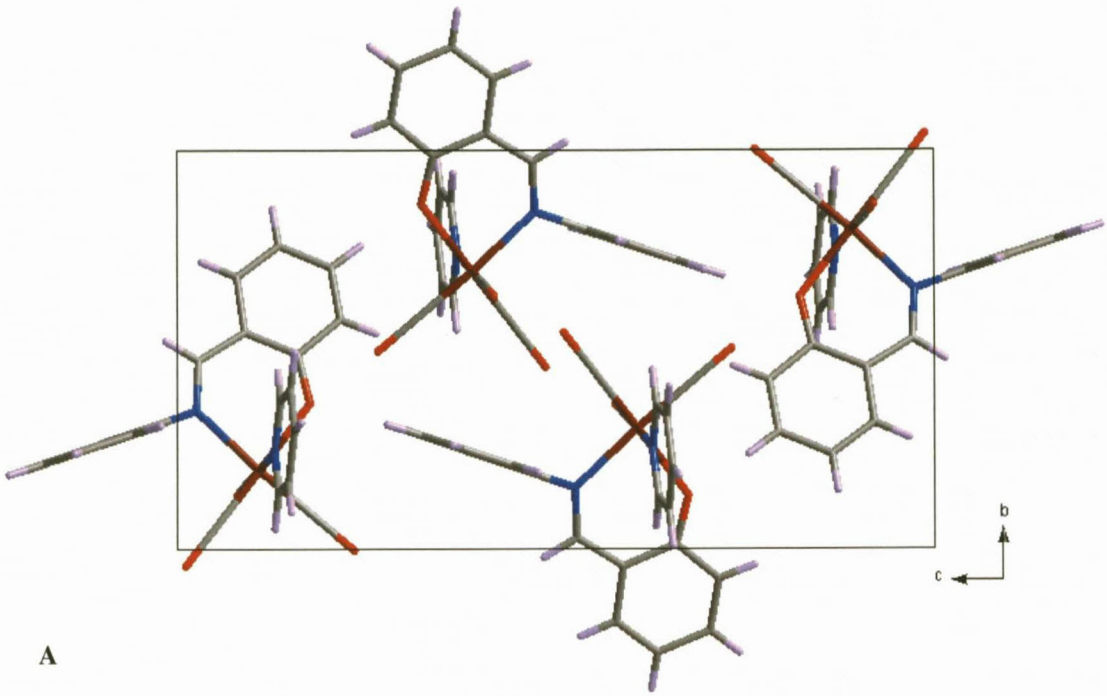

A

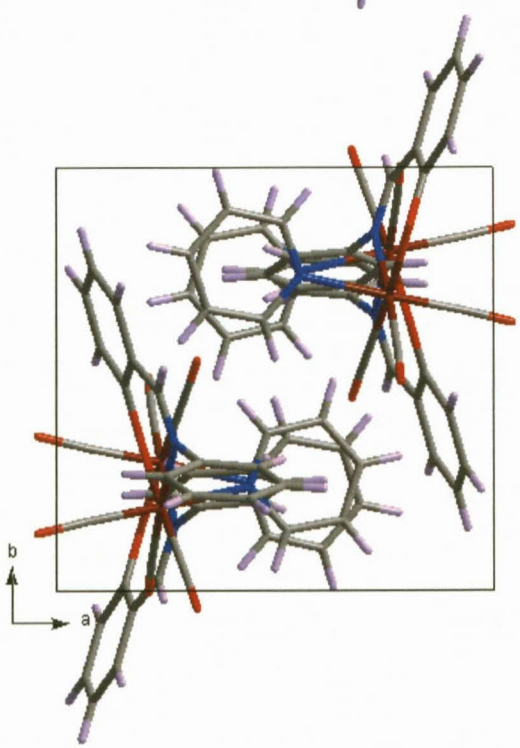

B

Figure 6.36: Molecular packing of the unit cell as viewed along the (A) *a*-axis and (B) the *c*-axis.

6.9 CRYSTAL STRUCTURE OF

fac-[Re(Sal-3MeBu)(CO)$_3$(NC$_5$H$_5$)]

The complex, *fac*-[Re(Sal-3MeBu)(CO)$_3$(NC$_5$H$_5$)] (**17**), (Sal-3MeBu = 2-(3-methylbutyl-iminomethyl)phenolato) crystallizes in a monoclinic crystal system in the $P2_1/c$ space group with four formula units per unit cell (Z = 4). The asymmetric unit contains one independent molecule. The molecular structure of (**17**) is illustrated in Figure 6.37 along with the atom numbering scheme and important bond lengths and angles are given in Table 6.22.

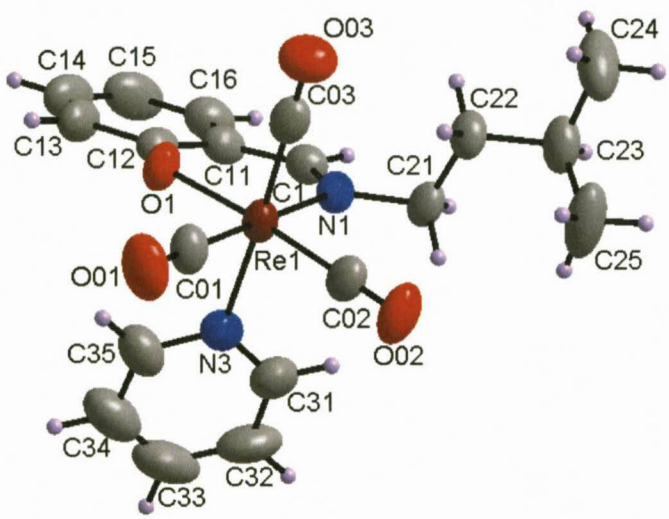

Figure 6.37: **Molecular structure of *fac*-[Re(Sal-3MeBu)(CO)$_3$(NC$_5$H$_5$)] (17) showing the atom numbering system. For the aromatic rings, the first digit refers to the ring number, while the second digit refers to the specific C-atom in the ring. Displacement ellipsoids are drawn at 50% probability level.**

Table 6.22: **Selected bond distances and angles of *fac*-[Re(Sal-3MeBu)(CO)$_3$(NC$_5$H$_5$)] (17) [Å and °].**

Atoms	Distance	Atoms	Angle
Re1-N1	2.172(2)	N1-Re1-O1	86.35(8)
Re1-O1	2.1075(19)	N3-Re1-C03	174.62(10)
Re1-C01	1.919(3)	N1-Re1-C02	94.29(10)
Re1-C02	1.901(3)	O1-Re1-C01	91.07(10)
Re1-C03	1.917(4)	O1-Re1-C02	175.50(12)
Re1-N3	2.213(3)	N1-Re1-N3	84.27(9)
N1-C1	1.290(4)	Re1-C02-O02	179.2(3)
C1-C11	1.433(4)	C1-N1-C21	115.8(2)
N1-C21	1.482(4)	N1-C1-C12-O1	3.1(2)
O1-C12	1.305(3)	C22-C21-N1-C1	102.3(3)

The rhenium metal centre coordinates with the N,O atoms of the salicylidene bidentate ligand to form a six-membered ring. The 3-methylbutyl substituent is bonded to the imine nitrogen atom and unlike the crystal structure of the methanol analogue (**15**), the substituent is not disordered. The pyridine ligand coordinates via the N atom, below the plane of the bidentate ligand. The last three position of the octahedron are occupied by carbonyl ligands coordinated in a facial manner. The octahedron around the Re(I) centre is slightly distorted as indicated by the N1-Re-O1 bite angle of 86.35(8)°, C01-Re1-C03 angle (90.04(13)°) and N3-Re1-C03 angle of 174.62(10)°. The Re-N1 and Re-O1 bond distance (2.172(2) Å and 2.1075(19) Å) are comparable to other N,O ligand-to-metal bond distances which are in the range of 2.162 – 2.186 Å for Re-N and 2.099 – 2.184 Å for Re-O.[5,20,22] The Re-N3 bond distance, of the coordinated pyridine, is 2.213(3) Å and compares well with similar complexes where bond distances between 2.203 – 2.230 Å were observed.[4,21] The C1-N1 bond distance (1.290(4) Å) is indicative of a double bond. The O1-C12 (1.305(3) Å), N1-C21 (1.482(4) Å) and C1-C11 (1.433(4) Å) are consistent for single bonds for the respective atoms.[25]

The plane formed by the salicylidene C1 aromatic backbone (Plane 1: C11, C12, C13, C14, C15, C16) is tilted relative to the Re1 equatorial plane (Plane 2: Re1, N1, O1, C01, C02) with a dihedral angle of 10.12(9)° (Figure 6.38 A). The 3MeBu substituent bonded to the imine N atom lies above both Plane 1 and 2 with a N1-C21-C22 bond angle of 112.2(2)°. The coordinated pyridine (Plane 4: N3, C31, C32, C33, C34, C35) is not orientated perpendicular to neither Plane 1 nor Plane 2 with dihedral angles of 69.2(1)° and 79.3(1)° (Figure 6.38 B).

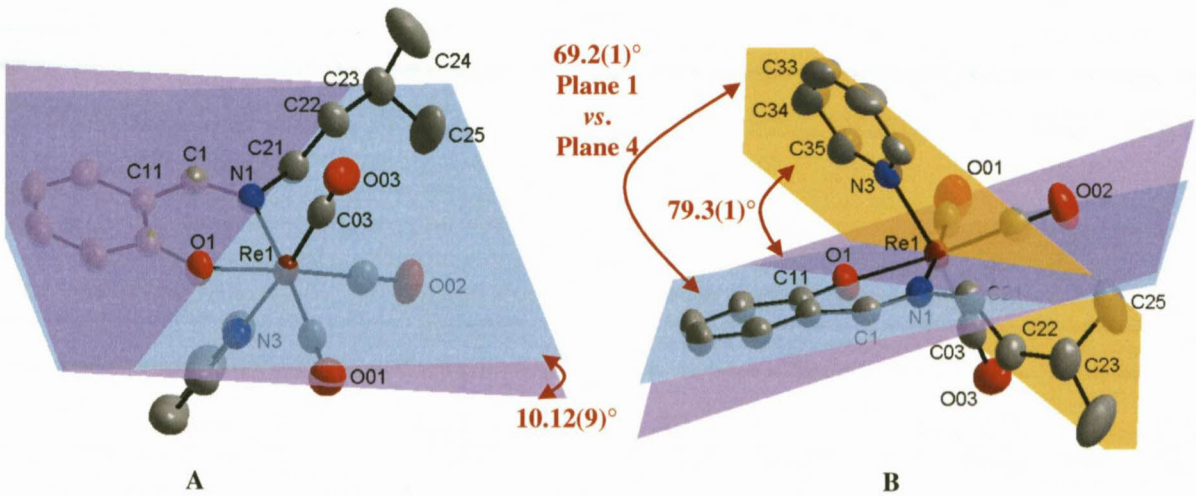

Figure 6.38: **(A) Graphical representation of the tilting C1 aromatic backbone. (B) Graphical representation of the rotation of the coordinated pyridine ligand. (Plane 1= blue, Plane 2 = purple, Plane 4 = yellow). H atoms are omitted for clarity.**

No classical hydrogen bonding is found between neighbouring molecules in the unit cell. A weak π-π interaction occurs between two pyridine molecules as indicated by Figure 6.39 below.

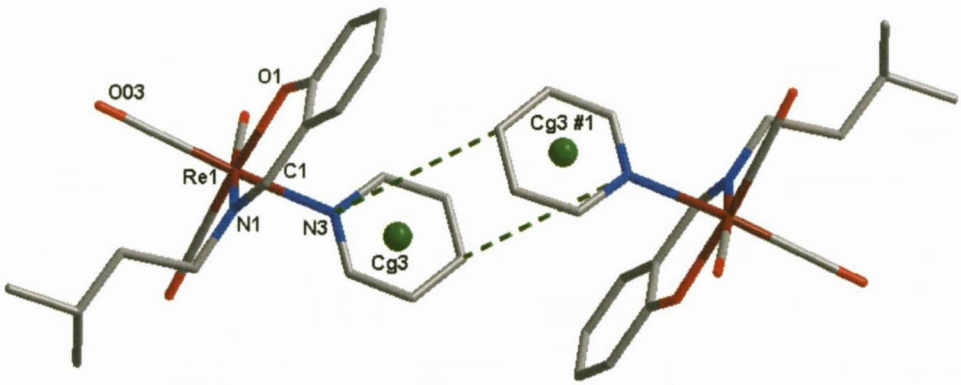

Figure 6.39: **Graphical representation of the π-π interaction between neighbouring pyridine moieties. The centroid atom (Cg) of each aromatic ring is indicated in green.**

Table 6.23: **π-π Interaction between aromatic rings of rhenium complexes.**

Centroid atom	Centroid atom	Distance between centroid atoms (Å)	Interplanar angle (°)
Cg3	Cg3 #1	4.4758(1)	0.0(1)

Symmetry transformations used to generate equivalent atoms:
#1 1-x, 1-y, 2-z
Cg3 = centroid atom of N3, C31, C32, C33, C34, C35

A weak van der Waal interaction occurs between O02...O03$^{\#2}$ as well as the symmetry related atoms (Table 6.24). In the process, the interaction forms a closed six-membered cyclic ring as indicated in Figure 6.40, which is orientated in a chair conformation.

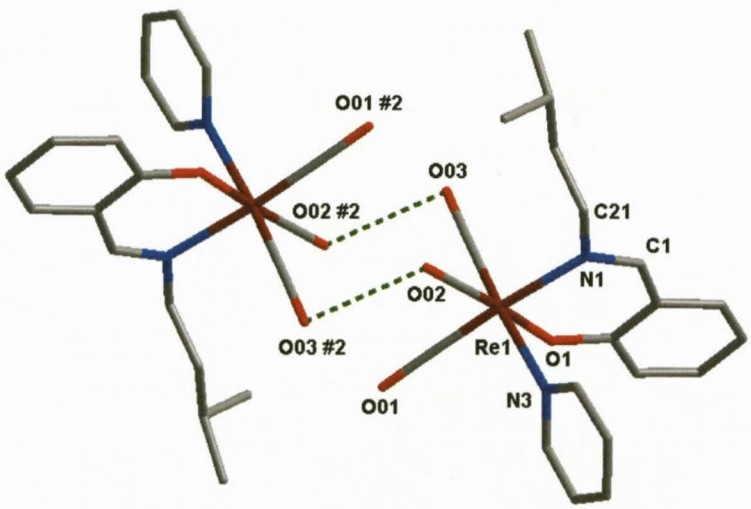

Figure 6.40: **Graphical representation of O…O interactions (green dotted line). H atoms are omitted for the sake of clarity. (Symmetry operation: #2 -x, -y, 2-z)**

Table 6.24: O...O Interaction between the rhenium complexes.

C-O...O	d(O...O) (Å)	d(C-O...O) (Å)	< (C-O...O) (°)
O02...O03#2	2.967(4)	3.229(5)	92.4(2)

Symmetry transformations:
#2 -x, -y, 2-z

A few C-H...π interactions assist in stabilizing the molecular packing. One such interaction occurs between C33-H33...Cg2$^{\#1}$ and the symmetry related atoms to form a pseudo rectangle between neighbouring molecules (Figure 6.41). The packing is further stabilized by the weak π-π interaction between the pyridine rings as already discussed.

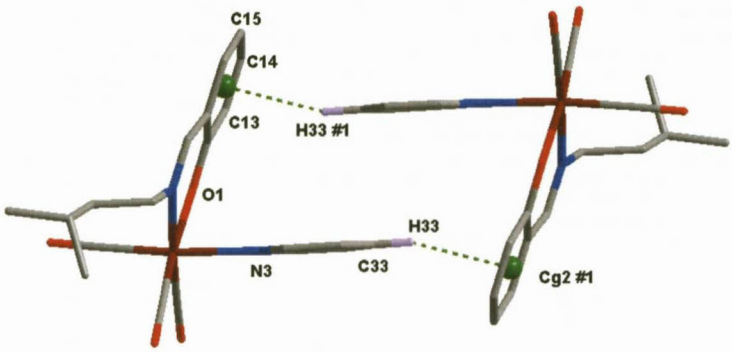

Figure 6.41: Graphical representation of C-H...π interactions (green dotted line). The centroid atom (Cg) of the aromatic rings are indicated in green. (Symmetry operation: #1 1-x, 1-y, 2-z)

Table 6.25: C-H...π Interaction between aromatic rings of the rhenium complex.

C-H...Cg	Centroid atom (Cg)	d(H...Cg) (Å)	d(C...Cg) (Å)	< (C-H...Cg) (°)
C33-H33	Cg2 #1	2.5694(4)	3.485(5)	161.7(3)
C23-H23	Cg1 #4	2.8833(1)	3.788(4)	150.8(2)
C25-H25A	Cg2 #4	2.9313(1)	3.772(4)	144.4(3)

Symmetry transformations:
#1 1-x, 1-y, 2-z; #4 -x, 0.5+y, 1.5-z
Cg1 = centroid atom of Re1, N1, C1, C11, C12, O1; Cg2 = centroid atom of C11, C12, C13, C14, C15, C16

Several weak van der Waal interactions of the type X-H...Y also stabilize the molecular packing. Interactions between C31-H31...O02$^{\#3}$ occur which also form pseudo rectangles with the generation of symmetry equivalent atoms (Figure 6.42 and Table 6.26).

A C-H...H-C interaction occurs between C21-H21A...H22B-C22$^{\#4}$ (symmetry operation: -x, 0.5+y, 1.5-z) (Figure 6.43). The same symmetry generated molecule experiences the remaining C-H...π interactions from the 3MeBu substituent (Figure 6.43 and Table 6.25).

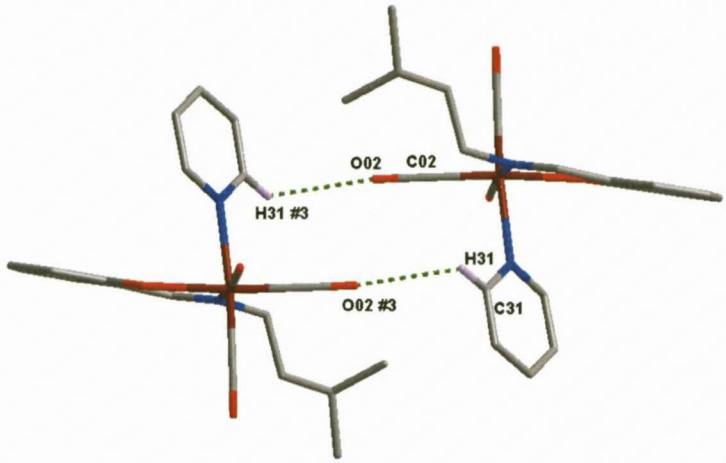

Figure 6.42: **Graphical representation of C-H…O interactions (green dotted line). H atoms are omitted for clarity.**

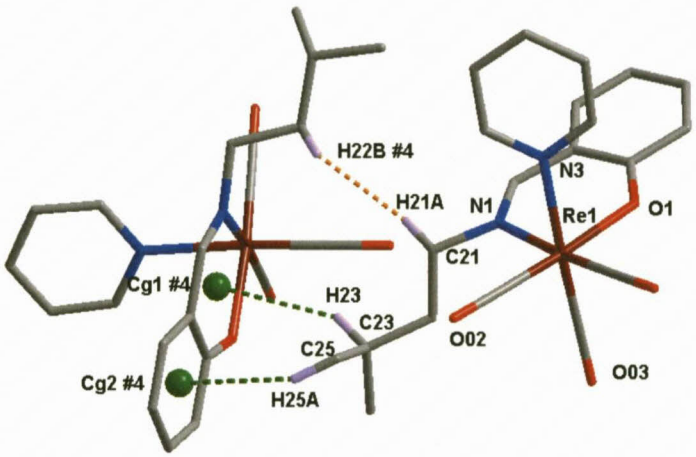

Figure 6.43: **Graphical representation of C-H…H-C interactions (orange dotted line) as well as the C-H…π interactions (green dotted lines). H atoms are omitted for clarity.**

Table 6.26: **X-H…Y Interaction between aromatic rings of rhenium complex.**

X-H...Y	d(H...Y) (Å)	d(X...Y) (Å)	< (X-H...Y) (°)
C31-H31...O02-C02 #3	2.656(3)	3.305(5)	126.0(2)
C21-H21A...H22B-C22 #4	2.358(1)	3.240(3)	147.8(2)

Symmetry transformations:
#3 -x, 1-y, 2-z; #4 -x, 0.5+y, 1.5-z

Structural comparisons and illustrative overlays between the various coordinated rhenium tricarbonyl complex crystal structures are discussed in Section 6.10.

6.10 INTERPRETATION AND CORRELATION OF STRUCTURAL PARAMETERS

The following subsection correlates structural data from the various functionalized *fac*-$[Re(CO)_3]^+$ complexes as described. The general structural parameters, bond distances and angles of the crystal structures are given in Tables 6.27 and 6.28.

Table 6.27a: **Cell dimension overview of presented functionalized *fac*-[Re(L,L'-Bid)$(CO)_3$(S)] complexes (L,L'-Bid = Sal-T, T = coordinated substituent, S = coordinated methanol or pyridine).**

L,L'-Bid	Sal-*m*Tol (11)	Sal-Ph (12)	Sal-*p*Tol (13)	Sal-CyHex (14)	Sal-3MeBu (15)
S	$HOCH_3$	$HOCH_3$	$HOCH_3$	$HOCH_3$	$HOCH_3$
Crystal System	Monoclinic	Monoclinic	Monoclinic	Monoclinic	Monoclinic
Space Group	*C2/c*	*C2/c*	*C2/c*	*C2/c*	*C2/c*
Unit Cell Dimensions					
a (Å)	18.513(6)	18.4769(7)	19.370(4)	18.096(4)	19.3075(8)
b (Å)	13.598(6)	13.4830(7)	14.027(3)	14.441(3)	13.8078(6)
c (Å)	14.294(5)	13.9281(7)	14.002(3)	13.753(3)	13.7882(6)
α (°)	90	90	90	90	90
β (°)	106.443(2)	108.988(3)	112.41(3)	107.18(3)	110.299(2)
γ (°)	90	90	90	90	90
Volume ($Å^3$)	3451(2)	3281.0(3)	3517(1)	3433.6(1)	3447.6(3)
Z	8	8	8	8	8

Table 6.27b: **Cell dimension overview of presented functionalized *fac*-[Re(L,L'-Bid)$(CO)_3$(S)] complexes (L,L'-Bid = Sal-T, T = coordinated substituent, S = coordinated methanol or pyridine).**

L,L'-Bid	Sal-Ph (16)	Sal-3MeBu (17)
S	Pyridine	Pyridine
Crystal System	Monoclinic	Monoclinic
Space Group	$P2_1/c$	$P2_1/c$
Unit Cell Dimensions		
a (Å)	10.2910(2)	12.9051(4)
b (Å)	9.8280(2)	8.6642(3)
c (Å)	18.9306(3)	18.6961(5)
α (°)	90	90
β (°)	97.023(2)	105.279(3)
γ (°)	90	90
Volume ($Å^3$)	1900.27(6)	2016.6(1)
Z	4	4

Seven salicylidene rhenium tricarbonyl complexes were presented in this chapter. Five of the complexes contain a methanol solvent coordinated to the rhenium metal centre of which three of the structures (**11** – **13**) contain aromatic substituents bonded to the N atom of the imine. The other two rhenium-methanol complexes (**14**, **15**) contain aliphatic groups. The last two rhenium tricarbonyl complexes (**16**, **17**) have successfully substituted the methanol for pyridine.

The five rhenium-methanol complexes (**11** – **15**) all have the same crystal system and space group, *C*2/*c*, with eight molecules per unit cell (Z = 8). The unit cell parameters are within similar range with a maximum difference between the highest and lowest values of 1.274 Å for *a*-axis, 0.958 Å for *b*-axis, 0.541 Å for *c*-axis and 5.967° for the β-angle. However, despite the similarities of structural parameters, only *fac*-[Re(Sal-3MeBu)$(CO)_3$($HOCH_3$)] (**15**) and *fac*-[Re(Sal-Ph)$(CO)_3$($HOCH_3$)] (**12**) meet all the requirements for isomorphism as the metal centers are in the exact same symmetry position.

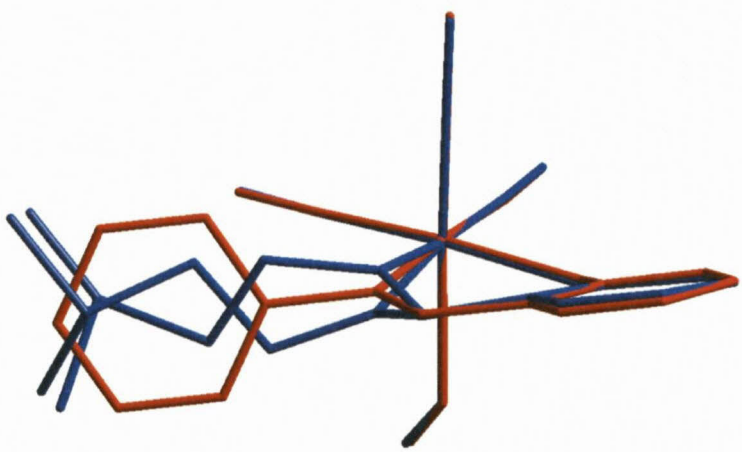

Figure 6.44: **An overlay of the isomorphic complexes 12 (indicated in red) and 15 (indicated in blue). Overlay was not drawn through the substituent bonded to the N atom to allow free rotation of the disorder in 15, RMS = 7.276 x 10^{-2} Å.**

The overlay of the X-ray crystal structures is a graphical representation of the pair-wise differences of related structures. The structural differences can be mathematically described by the root mean square (RMS) value, which is a measure of how far the average is from zero, providing information on the variations of bond lengths and angles. Overlay structures of the rhenium-methanol complexes have been drawn to indicate the similarity in coordination between the various complexes. (Please note that several of the illustrated overlays are only drawn through the salicylidene backbone to allow free rotation of the substituent bonded to the imine N atom and thus have low RMS values). It is interesting to

note that the orientation of the substituent bonded to imine nitrogen atom is in nearly identical positions in all structures. In particular the comparison between *fac*-[Re(Sal-Ph)$(CO)_3(HOCH_3)$] (**12**) and *fac*-[Re(Sal-3MeBu)$(CO)_3(HOCH_3)$] (**15**) (Figure 6.44) or *fac*-[Re(Sal-Ph)$(CO)_3(HOCH_3)$] (**12**) and *fac*-[Re(Sal-*p*Tol)$(CO)_3(HOCH_3)$] (**13**) (Figure 6.45), the phenyl ring lies nearly in the centre of the disorder in both the 3MeBu and *p*-tolyl substituent.

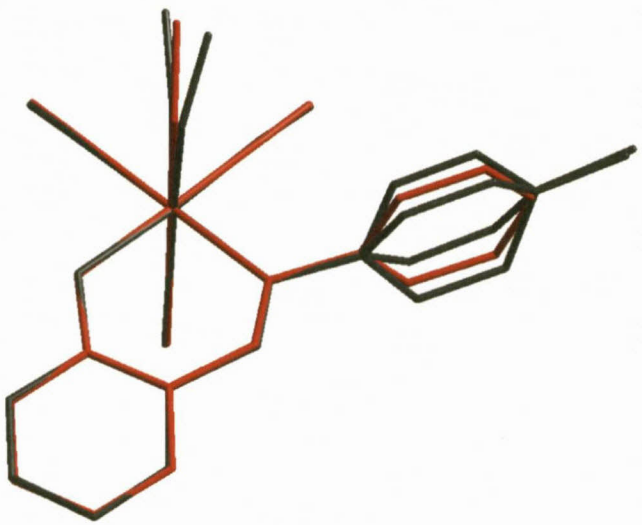

Figure 6.45: **An overlay of complexes 12 (indicated in red) and 13 (inverted crystal structure, indicated in black) (RMS = 6.205 x 10^{-2} Å). Overlay was not drawn through the disordered substituent to allow free rotation of the coordinated N bonded substituents.**

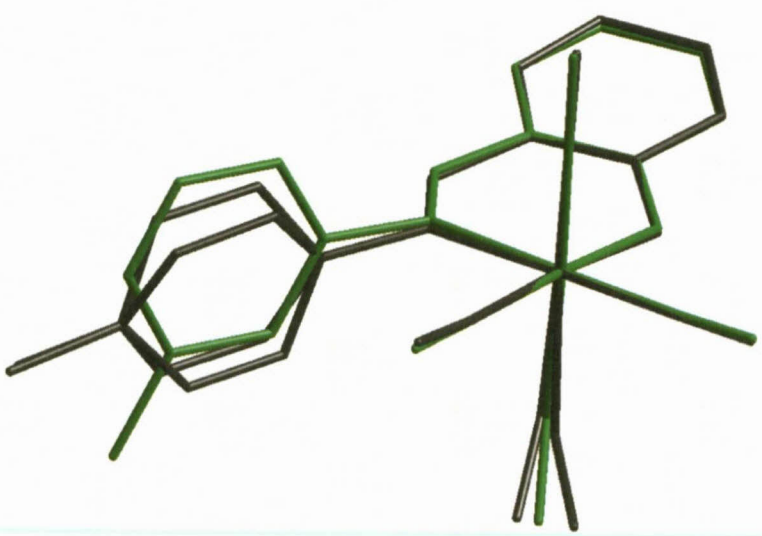

Figure 6.46: **An overlay of complexes 11 (indicated in green) and 13 (indicated in black) (RMS = 7.504 x 10^{-2} Å). Overlay was not drawn through the disordered atoms to allow free rotation of the coordinated N bonded substituents.**

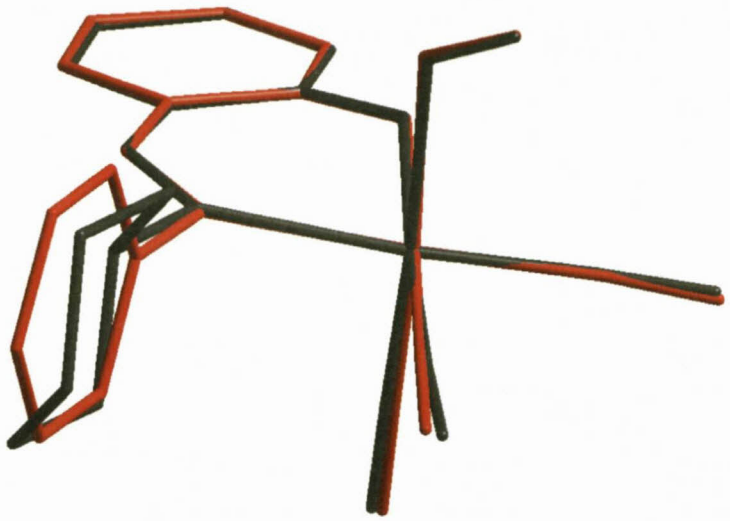

Figure 6.47: **An overlay of complexes 12 (indicated in red) and 14 (indicated in black) (RMS = 7.327 x 10^{-2} Å). Overlay was not drawn through the phenyl / cyclohexyl ring to allow free rotation of the coordinated N bonded substituents.**

Two rhenium tricarbonyl complexes (**16**, **17**) have successfully substituted the coordinated methanol solvent for pyridine, a neutral N-donor monodentate, aromatic ligand. Both complexes crystallize in the same crystal system and space group, $P2_1/c$, with four molecules per unit cell (Z = 4). The unit cell parameters are within similar range with a maximum difference between the highest and lowest values of 2.6141 Å for *a*-axis, 1.1638 Å for *b*-axis, 0.2345 Å for *c*-axis. Unlike the situation for the methanol analogues, these two complexes, *fac*-[Re(Sal-3MeBu)$(CO)_3(NC_5H_5)$] (**17**) and *fac*-[Re(Sal-Ph)$(CO)_3(NC_5H_5)$] (**16**), cannot be classified as isomorphic. The metal centers are in the same symmetry position, however the β-angle shows significant differences between the two structures (Δ β-angle = 8.256°). The overlay diagram of the two structures (Figure 6.48) indicates the near perpendicular orientation of the pyridine moieties relative to each other. The 3MeBu substituent is orientated below the phenyl ring.

A comparison between the methanol / pyridine coordinated complexes of *fac*-[Re(Sal-3MeBu)$(CO)_3$(S)] (**15** *vs.* **17**) and *fac*-[Re(Sal-Ph)$(CO)_3$(S)] (**12** *vs.* **16**) is found in Figure 6.49. Interestingly the *fac*-[Re(Sal-Ph)$(CO)_3$(S)] complexes have only slight difference in the angle of the phenyl substituent, even the coordinated methanol lies in the same plane as the pyridine ligand.

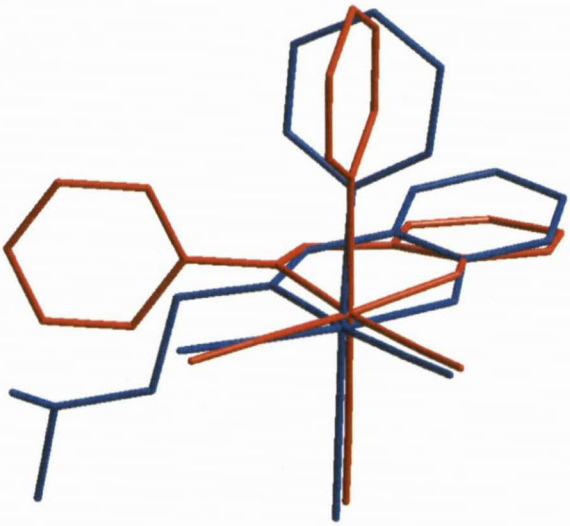

Figure 6.48: An overlay of the isostructural complexes 16 (indicated in red) and 17 (indicated in blue) (RMS = 0.862 Å). Overlay was not drawn through the substituent bonded to the N atom to allow free rotation.

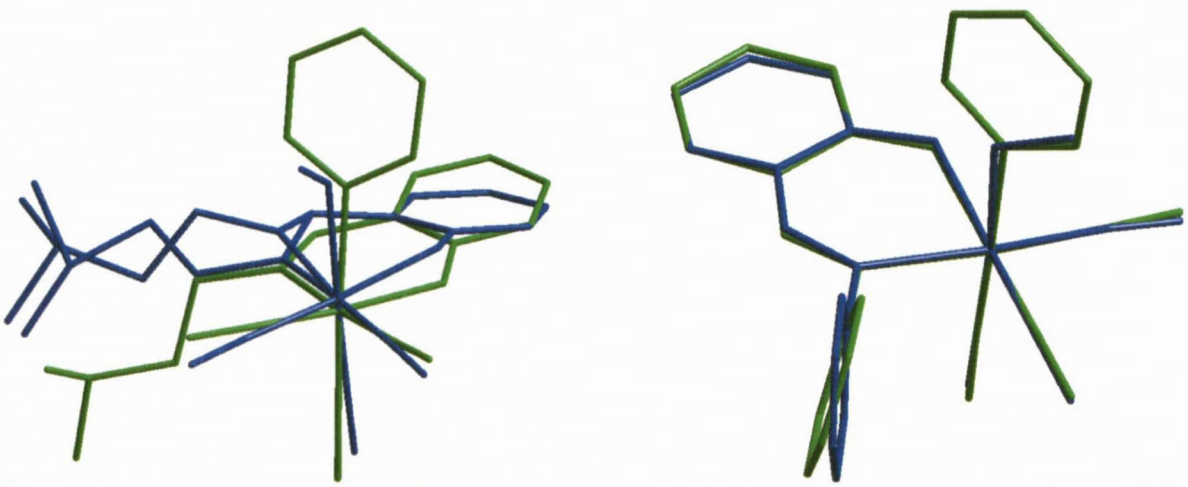

A B

Figure 6.49: A overlay comparison between the methanol and pyridine substituted complexes of *fac*-[Re(Sal-3MeBu)$(CO)_3$(S)] and *fac*-[Re(Sal-Ph)$(CO)_3$(S)]. (A) An overlay of the complexes 15 (indicated in blue) and 17 (indicated in green) (RMS = 0.396 Å). Overlay was not drawn through the substituent bonded to the N atom to allow free rotation of the disorder in 15. (B) An overlay of the complexes 12 (indicated in blue) and 16 (indicated in green) (RMS = 0.115 Å). Overlay was not drawn through the substituent bonded to the N atom to allow free rotation of the coordinating amine.

Table 6.28a: **Selected geometrical parameters of the presented *fac*-[Re(L,L'-Bid)(CO)$_3$(S)] complexes (S = coordinated methanol or pyridine) tabulated for comparison [Å, °].**

L,L'-Bid	Sal-*m*Tol (11)	Sal-Ph (12)	Sal-*p*Tol (13)		Sal-CyHex (14)	Sal-3MeBu (15)	
S	$HOCH_3$	$HOCH_3$	$HOCH_3$		$HOCH_3$	$HOCH_3$	
Bonds Distance (Å)							
Re1-N1	2.157(4)	2.164(6)	2.15(2)		2.202(9)	2.148(7)[a]	2.219(16)[b]
Re1-O1	2.119(3)	2.121(5)	2.133(16)		2.131(7)	2.117(4)	
Re1-C01	1.913(6)	1.920(7)	1.90(3)		1.896(11)	1.900(6)	
Re1-C02	1.919(6)	1.909(7)	1.95(2)		1.894(13)	1.902(6)	
Re1-C03	1.890(6)	1.895(7)	1.89(2)		1.869(10)	1.891(8)	
Re1-O04	2.179(3)	2.188(5)	2.24(10)[a]	2.17(3)[b]	2.172(8)	2.179(4)	
N1-C1	1.290(6)	1.288(9)	1.28(3)		1.282(12)	1.346(11)[a]	1.212(18)[b]
Bond angle (°)							
N1-Re1-O1	84.6(1)	84.4(2)	84.8(7)		84.6(3)	84.0(2)[a]	83.5(4)[b]
O04-Re1-C03	175.4(2)	174.9(3)	176(3)		174.9(3)	175.1(2)	
Re1-O04-C04	122.1(4)	121.2(5)	119(8)[a]	123.6(19)[b]	123.8(7)	124.5(4)	
Re1-C02-O02	179.4(5)	178.4(6)	176(3)		175.8(10)	178.1(5)	
C1-N1-C21	115.7(4)	115.6(6)	112(2)[a]		113.6(9)	115.7(7)[a]	116.1(15)[b]
Torsion angle (°)							
N1-C1-C12-O1	11.7(4)	13.7(6)	15(2)		12.8(9)	3.4(6)[a]	32.1(9)[b]
C26-C21-N1-C1	90.9(6)	100.6(8)	-		107.6(11)	-	

[a/b] = disordered atoms

Table 6.28b: **Selected geometrical parameters of the presented *fac*-[Re(L,L'-Bid)(CO)$_3$(S)] complexes (S = coordinated methanol or pyridine) tabulated for comparison [Å, °].**

L,L'-Bid	Sal-Ph (16)	Sal-3MeBu (17)
S	Pyridine	Pyridine
Bonds Distance (Å)		
Re1-N1	2.152(5)	2.172(2)
Re1-O1	2.114(3)	2.1075(19)
Re1-C01	1.925(5)	1.919(3)
Re1-C02	1.910(5)	1.901(3)
Re1-C03	1.904(6)	1.917(4)
Re1-N3	2.207(5)	2.213(3)
N1-C1	1.298(7)	1.290(4)
Bond angle (°)		
N1-Re1-O1	84.54(16)	86.35(8)
N3-Re1-C03	178.44(19)	174.62(10)
N1-Re1-N3	85.23(17)	84.27(9)
Re1-C02-O02	178.9(5)	179.2(3)
C1-N1-C21	114.4(5)	115.8(2)
Torsion angle (°)		
N1-C1-C12-O1	2.8(5)	3.1(2)
C26-C21-N1-C1	78.2(7)	102.3(3)[c]

[c] Torsion angle C22-C21-N1-C1

Bond distances and angles of the respective rhenium tricarbonyl complexes are all within normal range. Few differences are found within the tabulated values as expected from the similarity which was seen in the structural overlays.

6.11 CONCLUSION

The crystal structures of seven rhenium tricarbonyl complexes containing various coordinated imino substituents bonded to the imine N atom, were analyzed and discussed in this section. The crystal structures are iso-structural and display similar unit cell parameters, molecular packing, intermolecular hydrogen bonding as well as π-π stacking.

The salicylidene bidentate ligands were successfully coordinated to the *fac*-rhenium tricarbonyl moieties and interesting crystallographic similarities were found. The crystallographic study will significantly contribute to the available data in the Crystallographic Cambridge Structural Database as thus far, only one rhenium(I) tricarbonyl crystal structure containing the salicylidene bidentate ligand has been reported.[2]

This chapter describes the first half of the rhenium complex crystallographic study. The second part of the study will be discussed in Chapter 7, where crystal structures of the functionalized salicylidene aromatic backbone are compared. The analysis of rhenium complexes containing the salicylidene bidentate ligand and three different biological amines coordinated to the backbone, will also be mentioned.

7 X-RAY CRYSTALLOGRAPHIC STUDY OF *fac*-[Re(5Me-Sal)(CO)$_3$(S)] COMPLEXES

7.1 INTRODUCTION

The crystallographic analysis discussed in this section is a continuation of the work described in Chapter 6 whereby salicylidene bidentate ligands, containing various substituents, is coordinated to the *fac*-$[Re(CO)_3]^+$ metal centre. Chapter 6 described the packing effects of various complexes containing either an aromatic or aliphatic substituent bonded to the N atom of the **Sal** backbone.

In this chapter, the effects of a small change to the salicylidene backbone (**5Me-Sal**) will be explored (*i.e.* the addition of a methyl moiety in the fifth position). In addition, the coordination mode and packing effects induced by three ligands containing bulky biological active amines bonded *via* the N atom, is discussed.

A comparison of the crystallographic data of the variety of coordinated Re(5Me-Sal) complexes will be made and presented in this chapter. The various molecular interactions and crystal packing modes are described. The Re(5Me-Sal) complexes examined in this section are illustrated in Figure 7.1.

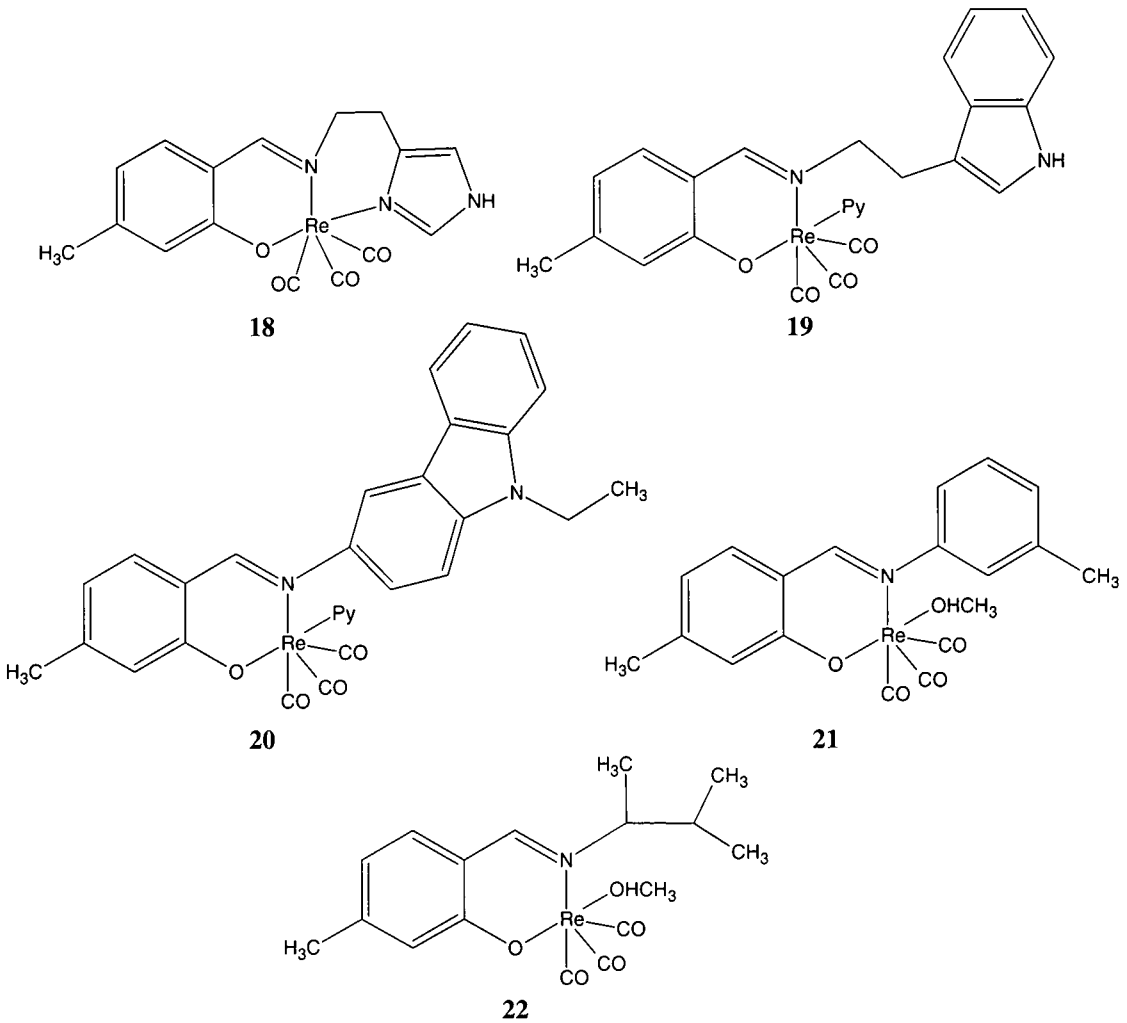

Figure 7.1: **The *fac*-[Re(L,L'-Bid)(CO)$_3$(S)] complexes (L,L'-Bid = mono-negatively charged N-O Sal bidentate ligand; S = coordinated methanol or pyridine) discussed in this chapter. (Note: Crystal structures 1 – 10 are described in Chapters 4 - 5. Structures 11 – 17 described in Chapter 6).**

(18) [Re(5Me-Sal-Hist)(CO)$_3$], (19) [Re(5Me-Sal-Trypt)(CO)$_3$(NC$_5$H$_5$)],

(20) [Re(5Me-Sal-Carba)(CO)$_3$(NC$_5$H$_5$)], (21) [Re(5Me-Sal-*m*Tol)(CO)$_3$(HOCH$_3$)],

(22) [Re(5Me-Sal-3Me2Bu)(CO)$_3$(HOCH$_3$)].

7.2 EXPERIMENTAL

The reflection data was collected on a Bruker X8 ApexII 4K diffractometer[1] using Mo $K\alpha$ radiation with ω-and-φ-scans at 100 K. COSMO[2] was utilized for optimum collection of more than a hemisphere of reciprocal space. Frame integration and data reduction were performed using the Bruker SAINT-Plus[3] and XPREP[3] software packages, respectively. Data was corrected for absorption effects using the multi-scan technique SADABS.[4] The structures were solved by direct methods package SIR97[5] and refined using the software package WinGX,[6] incorporating SHELXL.[7] All non-hydrogen atoms were refined with anisotropic displacement parameters, while the methyl, methane and aromatic H atoms were placed in geometrically idealized positions and constrained to ride on their parent atoms, with (C-H = 0.98-0.95 Å and $U_{iso}(H) = 1.5U_{eq}(C)$ and $1.2U_{eq}(C)$), respectively. The methyl protons were located from a difference Fourier map and the group was refined as a rigid motor. The program DIAMOND[8] was used for all graphical representation of the crystal structures. All structures are shown with thermal ellipsoids drawn at 50% probability level. Graphical representations of overlays of selected complexes are obtained with Hyperchem 7.52.[9]

A summary of the general crystal data and refinement parameters is given in Table 7.1 for all five rhenium tricarbonyl salicylidene complexes. Supplementary data for the atomic coordinates, bond distances and angles and anisotropic displacement parameters are given in the Appendix B for each individual dataset.

---

[1] Bruker, APEX2 (Version 1.0-27), Bruker AXS Inc., Madison, Wisconsin, USA, 2005
[2] Bruker, COSMO, Version 1.48, Bruker AXS Inc., Madison, Wisconsin, USA, 2003.
[3] Bruker, SAINT-Plus (Version 7.12) (including XPREP), Bruker AXS Inc., Madison, Wisconsin, USA, 2004
[4] Bruker, SADABS, Version 2004/1, Bruker AXS Inc., Madison, Wisconsin, USA,1998.
[5] A. Altomare, M.C. Burla, M. Camalli, G.L. Cascarano, C. Giacovazzo, A. Guagliardi, A.G.G. Moliterni, G. Polidori, R. Spagna, *J. Appl. Cryst.* 1999, 32, 115.
[6] L.J. Farrugia, *J. Appl. Cryst.*, 1999, 32, 837
[7] G.M. Sheldrick, SHELXL97, *Program for Solving Crystal Structures*, University of Göttingen, Germany, 1997
[8] K. Brandenburg, H. Putz, DIAMOND, Release 3.0c, Crystal Impact GbR, Bonn, Germany, 2005
[9] Hyperchem™ Release 7.52, Windows Molecular Modeling System, Hypercube, Inc., 2002

Table 7.1: **General X-ray crystallographic data and refinement parameters for *fac*-[Re(L,L'-Bid)(CO)$_3$(S)] (L,L'-Bid = 5Me-Sal-T, T = coordinated substituent, S = coordinated methanol or pyridine).**

L,L'-Bid	5Me-Sal-Hist (18)	5Me-Sal-Trypt (19)	5Me-Sal-Carba (20)	5Me-Sal-*m*Tol (21)	5Me-Sal-3Me2Bu (22)
S	-	Pyridine	Pyridine	$HOCH_3$	$HOCH_3$
Empirical Formula	$C_{16}H_{14}N_3O_4Re$	$C_{26}H_{22}N_3O_4Re$	$C_{30}H_{24}N_3O_4Re$	$C_{19}H_{18}NO_5Re$	$C_{17}H_{22}NO_5Re$
Formula weight	498.50	626.67	676.72	526.54	506.56
Temperature (K)	100(2)	100(2)	100(2)	100(2)	100(2)
Wavelength (Å)	0.71073	0.71073	0.71073	0.71073	0.71073
Crystal System	Triclinic	Monoclinic	Triclinic	Orthorhombic	Monoclinic
Space Group	*P*$\bar{1}$	*C2/c*	*P*$\bar{1}$	*Pbcn*	*C2/c*
Unit Cell Dimensions					
a (Å)	7.3705(1)	23.5078(7)	10.705(5)	18.9720(7)	18.1040(4)
b (Å)	9.1241(2)	10.9385(3)	10.711(5)	14.2191(5)	15.1508(4)
c (Å)	12.8797(2)	18.4481(5)	13.305(5)	14.2316(5)	13.8715(4)
α (°)	107.597(1)	90	66.469(5)	90	90
β (°)	103.111(1)	95.355(2)	67.663(5)	90	102.896(2)
γ (°)	94.297(1)	90	72.708(5)	90	90
Volume (Å^3)	794.43(2)	4723.0(2)	1274.6(1)	3839.2(2)	3708.8(2)
Z	2	8	2	8	8
Density$_{calc.}$ (g.cm^{-1})	2.084	1.763	1.763	1.822	1.814
μ (mm^{-1})	7.674	5.183	4.809	6.358	6.577
F(000)	476	2448	664	2032	1968
Crystal Colour	Yellow	Yellow	Brown	Yellow	Yellow
Crystal Morphology	Cuboid	Plate	Needle	Cuboid	Cuboid
Crystal Size (mm)	0.17x0.16x0.12	0.33x0.17x0.09	0.27x0.07x0.03	0.41x0.16x0.15	0.30x0.17x0.15
Theta Range (°)	3.43 to 27.99	2.06 to 28.00	2.26 to 28.00	1.79 to 28.00	1.77 to 28.00
Completeness (%)	98.6	100.0	98.6	99.9	100.0
Index Ranges	h = -8 to 9 k = -12 to 11 l = -17 to 17	h = -30 to 29 k = -14 to 14 l = -24 to 24	h = -13 to 14 k = -13 to 14 l = -17 to 16	h = -23 to 25 k = -18 to 18 l = -18 to 16	h = -23 to 23 k = -20 to 20 l = -18 to 18
Reflections Collected	9819	80218	22776	51881	29957
Independent Reflections	3777	5705	6062	4643	4479
R_{int}	0. 0203	0. 0407	0. 0282	0. 0538	0. 0338
Refinement method	Full-matrix least-squares on F^2	Full-matrix least-squares on F^2	Full-matrix least-squares on F^2	Full-matrix least-squares on F^2	Full-matrix least-squares on F^2
Data / restraints / parameters	3777 / 0 / 218	5705 / 0 / 308	6062 / 0 / 345	4643 / 0 / 218	4479 / 0 / 240
Goodness-of-fit on F^2	1.043	1.067	1.086	1.168	1.295
Final R indices [I>2sigma(I)]	R1 = 0.0153, wR2 = 0.0323	R1 = 0.0150, wR2 = 0.0360	R1 = 0.0210, wR2 = 0.0531	R1 = 0.0353, wR2 = 0.0996	R1 = 0.0195, wR2 = 0.0645
R indices (all data)	R1 = 0.0166, wR2 = 0.0328	R1 = 0.0166, wR2 = 0.0368	R1 = 0.0240, wR2 = 0.0545	R1 = 0.0714, wR2 = 0.1466	R1 = 0.0259, wR2 = 0.0947
ρ_{max} and ρ_{min} (e.Å^{-3})	0.737 and -0.584	1.124 and -0.605	1.202 and -0.721	1.703 and -2.365	0.996 and -1.183

(5Me-Sal-Hist) = 2-[(2-imidazol-4-yl)ethyliminomethyl]-5-methylphenolato; (5Me-Sal-Trypt) =[(2-indol-3-yl-ethyl)iminomethyl]-5-methylphenolato; (5Me-Sal-Carba) = 2-(9-ethylcarbazol-3-yliminomethyl)-5-methyl phenolato; (5Me-Sal-*m*Tol) = 5-methyl-2-(*m*-tolyliminomethyl)phenolato; (5Me-Sal-3Me2Bu) = 5-methyl-2-(1,2-dimethylpropyliminomethyl)phenolato.

7.3 CRYSTAL STRUCTURE OF

fac-[Re(5Me-Sal-Hist)(CO)$_3$]

The complex, *fac*-[Re(5Me-Sal-Hist)(CO)$_3$] (**18**), (5Me-Sal-Hist = 2-[(2-imidazol-4-yl)ethyl iminomethyl]-5-methylphenolato) crystallizes in a triclinic crystal system in the $P\bar{1}$ space group with two formula units per unit cell (Z = 2). The asymmetric unit contains one independent molecule. The molecular structure of (**18**) is represented in Figure 7.2 along with the atom numbering scheme. Important bond lengths and angles are given in Table 7.2.

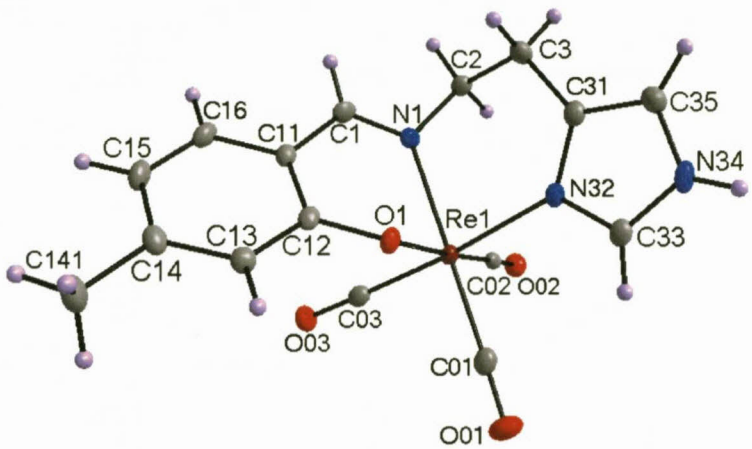

Figure 7.2: **Molecular structure of *fac*-[Re(5Me-Sal-Hist)(CO)$_3$] (18) showing the atom numbering system. For the aromatic rings, the first digit refers to the ring number, while the second digit refers to the specific C-atom in the ring. Displacement ellipsoids are drawn at 50% probability level.**

Table 7.2: **Selected bond distances and angles of *fac*-[Re(5Me-Sal-Hist)(CO)$_3$] (18) [Å and °].**

Atoms	Distance	Atoms	Angle
Re1-N1	2.1599(19)	N1-Re1-O1	80.11(7)
Re1-O1	2.1454(16)	N32-Re1-C03	174.63(9)
Re1-N32	2.1875(19)	N1-Re1-C02	97.31(8)
Re1-C01	1.924(2)	O1-Re1-C01	95.38(8)
Re1-C02	1.905(2)	O1-Re1-C02	177.41(7)
Re1-C03	1.911(2)	N1-Re1-N32	81.85(7)
N1-C1	1.285(3)	Re1-C02-O02	178.64(19)
C1-C11	1.446(3)	C1-N1-C2	117.91(19)
N1-C2	1.467(3)	N1-C1-C12-O1	19.5(2)
O1-C12	1.334(3)	C3-C2-N1-C1	95.2(2)
		N1-C2-C31-N32	35.7(2)

The central rhenium metal atom coordinates with the nitrogen atom of the imine and oxygen atom of the phenol group, from the salicylidene backbone, to form a six-membered ring. Three carbonyl ligands are facially coordinated to the metal centre with the final position

occupied by the N32 atom from the histamine substituent. Unlike the previous *fac*-[Re(L,L'-Bid)$(CO)_3$(S)] complexes described in Chapter 6, this ligand coordinates in a tridentate fashion by replacing the coordinated methanol solvent.

The octahedron around the Re(I) centre is distorted as indicated by the N1-Re1-O1, N1-Re1-N32 bite angles (80.11(7)°, 81.85(7)°) and the C03-Re1-N32 angle of 174.63(9)°. The Re1-N1 and Re1-O1 bond distances (2.1599(19) Å and 2.1454(16) Å) are comparable to related salicylidene structures which range from 2.152 - 2.199 Å for Re-N and 2.093 – 2.156 Å for Re-O.[10,11,12] Similarly, the bond distances are comparable to other N,O ligand-to-metal bond distances which are in the range of 2.162 – 2.186 Å for Re-N and 2.099 – 2.184 Å for Re-O.[13,14,15] The Re1-N32 bond distance (2.1875(19) Å) is significantly longer than the Re1-N1 bond distance with the N32 atom coordinating *trans* to C03 atom.

The plane formed by the salicylidene C1 aromatic backbone (Plane 1: C11, C12, C13, C14, C15, C16) is tilted relative to the Re1 equatorial plane (Plane 2: Re1, N1, O1, C01, C02) with a dihedral angle of 49.89(7)° (Figure 7.3).

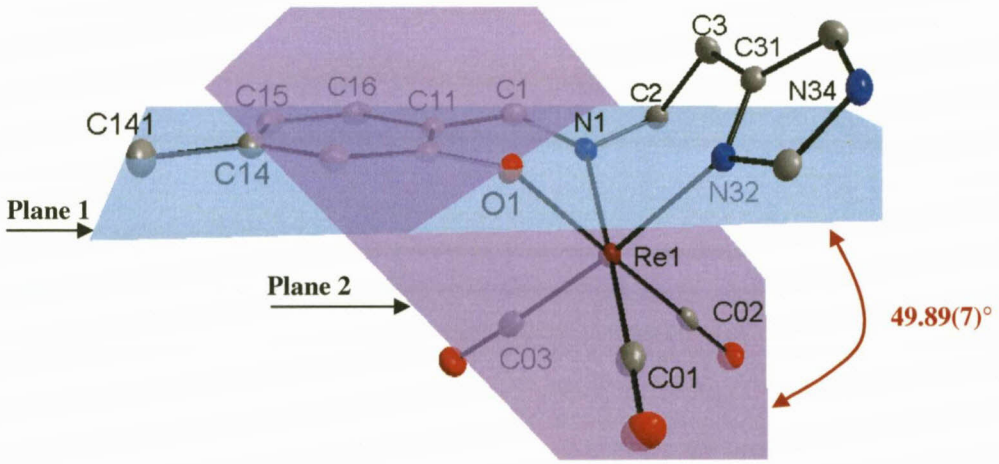

Figure 7.3: **Graphical representation of the bending salicylidene aromatic backbone (Plane 1 indicated in blue, Plane 2 indicated in purple). H atoms are omitted for clarity.**

[10] Z.K. Li, Y. Ki, L. Lei, C.M. Che, X.G. Zhou, *Inorg. Chem. Commun.*, 2005, 8, 307
[11] J.W. Faller, G. Mason, J. Par, *J. Organomet. Chem.*, 2001, 626, 191
[12] R. Czerwieniec, A. Kapturkiewicz, R. Anulewicz-Ostrowska, J. Nowacki, *J. Chem. Soc., Dalton Trans.*, 2002, 3434
[13] S. Mundwiler, M. Kündig, K. Ortner, R. Alberto. *Dalton Trans.*, 2004, 1320
[14] M. Schutte, H.G. Visser, *Acta Cryst.*, 2008, E64, m1226
[15] R. Czerwieniec, A. Kapturkiewicz, R. Anulewicz-Ostrowska, J. Novacki, *J. Chem. Soc., Dalton Trans.*, 2001, 2756

The histamine substituent bonded to the imine N atom is rotated less significantly to the C1 aromatic ring as compared to the non-coordinated free ligand. The dihedral angle between the C1 backbone (Plane 1) and the histamine 5-membered ring (Plane 3: C31, N32, C33, N34, C35) is 51.31(9)° compared to the related dihedral angle (77.72(5)°) for the free ligand. The histamine ring is orientated nearly perpendicular to the Re1 equatorial plane (Plane 2) with a dihedral angle of 86.21(8)° (Figure 7.4).

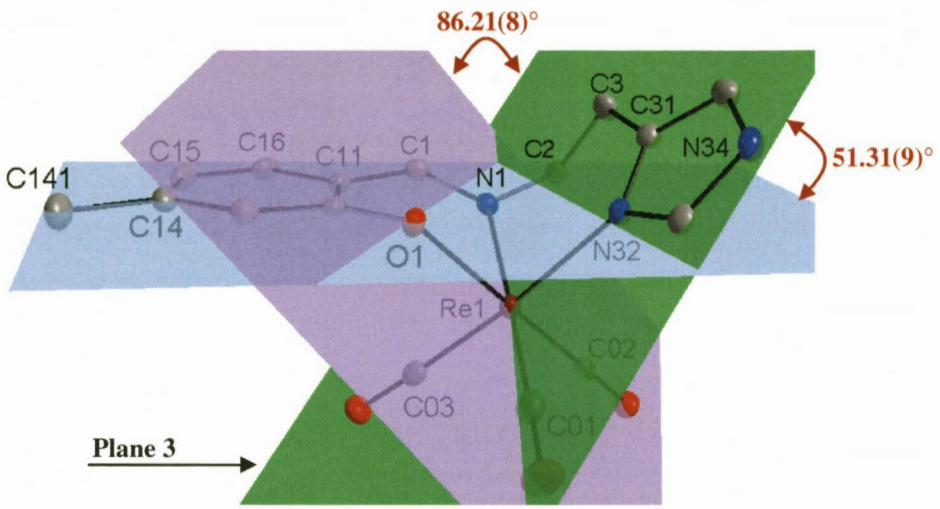

Figure 7.4: **Graphical representation of the orientation of the histamine substituent (Plane 1 indicated in blue, Plane 2 indicated in purple, Plane 3 indicated in green). H atoms are omitted for clarity.**

Two classic intermolecular hydrogen bond interactions, respectively occurs between the histamine substituent and a neighbouring molecule (N34-H34...O1$^{\#1}$) and the methyl moiety on the salicylidene backbone, C141-H14B...O03$^{\#2}$, as indicated in Table 7.3 and Figure 7.5. The N34-H34...O1$^{\#1}$ hydrogen interaction with the neighbouring molecule pack in an inverted "head-to-head" manner to form a closed cube with the facially coordinated tricarbonyl ligands lying in opposite directions (Figure 7.5 B).

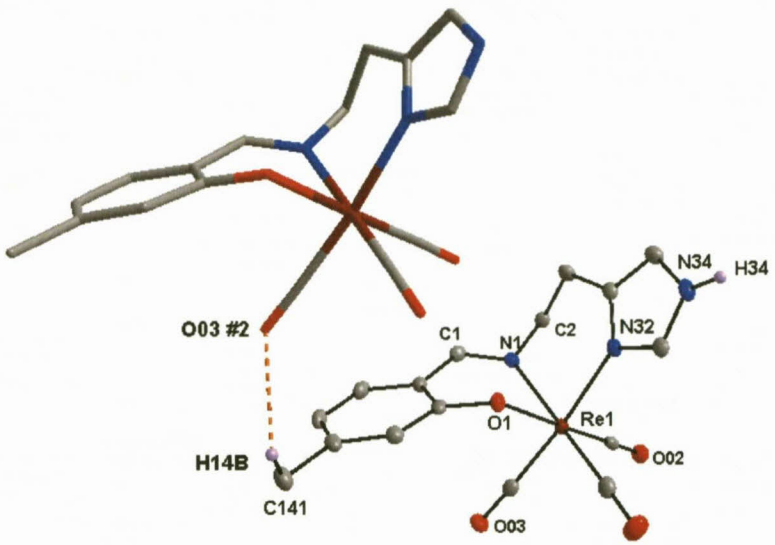

A

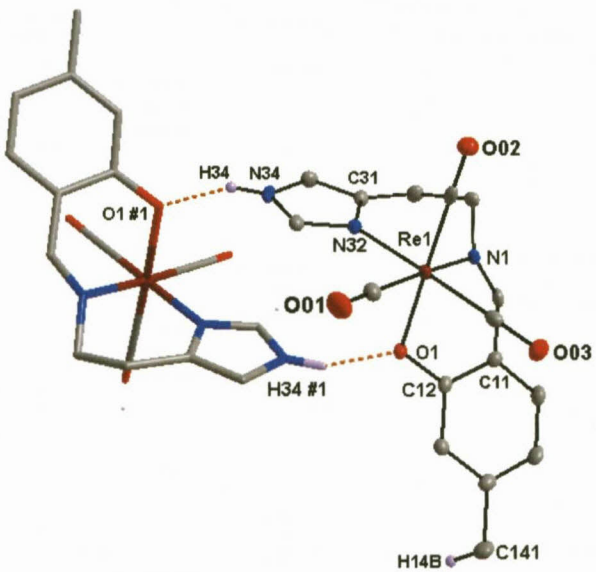

B

Figure 7.5: **Graphical representation of intermolecular hydrogen bond interaction. (A) Hydrogen bond interaction indicated between molecules C141-H14B...O03$^{\#2}$. (B) Hydrogen bond interaction indicated between molecules N34-H34...O1$^{\#1}$. Hydrogen interaction indicated by orange dotted lines. Due to the complexity of the image, symmetry generated molecules are illustrated in "stick" format. Certain H atoms omitted for the sake of clarity. (Symmetry operation: #1 -x+1, -y+2, -z+2; #2 x-1, y, z)**

Table 7.3: **Hydrogen bonds for *fac*-[Re(5Me-Sal-Hist)(CO)$_3$] [Å and °].**

D-H...A	d(D-H)	d(H...A)	d(D...A)	<(DHA)
N(34)-H(34)...O(1)#1	0.88	1.90	2.698(2)	149.8
C(141)-H(14B)...O(03)#2	0.98	2.56	3.143(3)	117.8

Symmetry transformations used to generate equivalent atoms:
#1 -x+1,-y+2,-z+2 #2 x-1,y,z

A π-π interaction occurs between the five-membered histamine rings of the same molecules which experience intermolecular hydrogen bonding. The ring interaction is indicated in Figure 7.6 by green dotted lines and in Table 7.4.

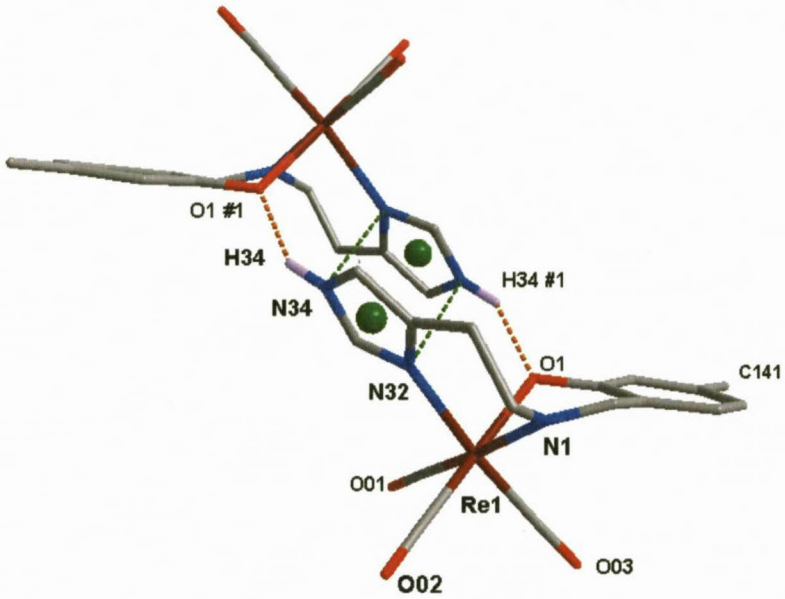

Figure 7.6: **Graphical representation of the π-π interaction indicated by green dotted lines (Cg = centroid atom of aromatic rings). Hydrogen bonding indicated by orange dotted lines. H atoms omitted for clarity.**

Table 7.4: **π-π Interaction between aromatic rings of rhenium complexes.**

Centroid atom	Centroid atom	Distance between centroid atoms (Å)	Interplanar angle (°)
Cg2	Cg2 #1	3.8260(15)	0.0(1)

Symmetry transformations used to generate equivalent atoms:
#1 1-x, 2-y, 2-z
Cg2 = centroid atom of C31, N32, C33, N34, C35

The molecular packing is further stabilised by the formation of two C-O...π interactions between C01-O01...Cg2$^{\#3}$, the histamine ring, and C03-O03...Cg1 of the salicylidene C1 aromatic ring as indicated in Figure 7.7 by orange dotted lines and Table 7.5. The molecules in the unit cell pack in a "head-to-head" manner to form cubic tunnels when viewed along the *c*-axis (Figure 7.8).

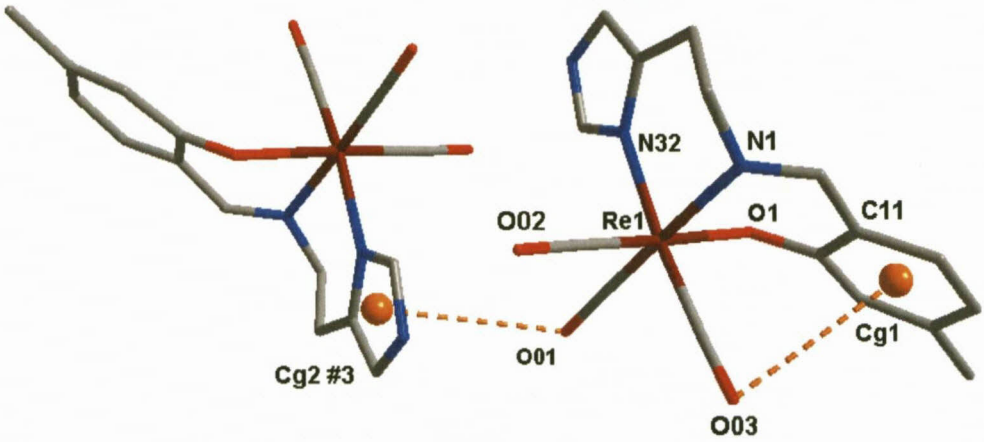

Figure 7.7: **Graphical representation of the C-O…π ring interactions indicated by orange dotted lines (Cg = centroid atom of aromatic rings). H atoms omitted for clarity.**

Table 7.5: **C-O…π Interaction between aromatic rings of rhenium complex.**

C-O...Cg	Centroid atom (Cg)	d(O...Cg) (Å)	d(C...Cg) (Å)	< (C-O...Cg) (°)
C01-O01	Cg2 #3	3.604(2)	4.100(3)	107.5(2)
C03-O03	Cg1 #4	3.815(2)	3.698(2)	75.4(2)

Symmetry transformations:
#3 2-x, 2-y, 2-z; #4 x, y, z
Cg1 = centroid atom of C11, C12, C13, C14, C15, C16; Cg2 = centroid atom of C31, N32, C33, N34, C35

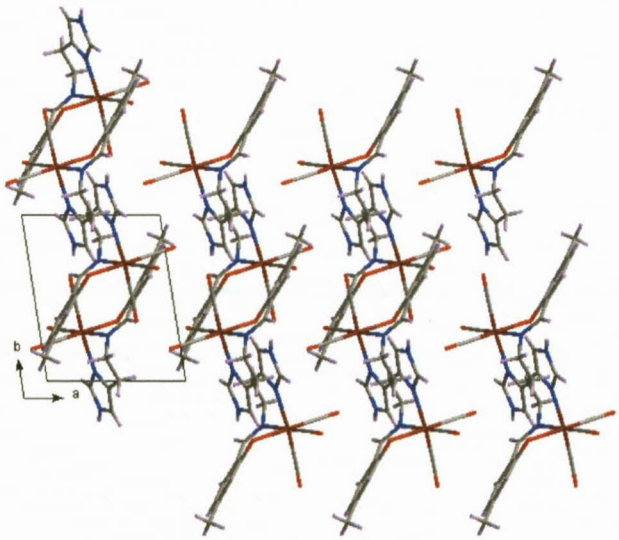

Figure 7.8: **Molecular packing of the unit cell as viewed along the *c*-axis.**

Structural comparisons and illustrative overlays between the various rhenium tricarbonyl complex crystal structures are discussed in Section 7.8.

7.4 CRYSTAL STRUCTURE OF

fac-[Re(5Me-Sal-Trypt)(CO)$_3$(NC$_5$H$_5$)]

The complex, *fac*-[Re(5Me-Sal-Trypt)(CO)$_3$(NC$_5$H$_5$)] (**19**), (5Me-Sal-Trypt =[(2-indol-3-yl-ethyl)iminomethyl]-5-methylphenolato) crystallizes in a monoclinic crystal system in the *C*2/*c* space group with eight formula units per unit cell (Z = 8). The asymmetric unit contains one independent molecule. The molecular structure of (**19**) is represented in Figure 7.9 along with the atom numbering scheme. Important bond lengths and angles are given in Table 7.6.

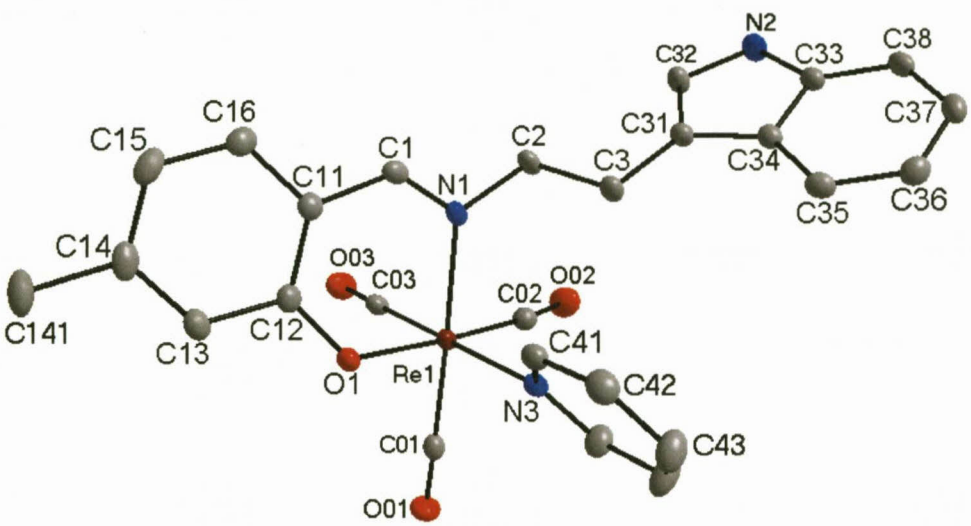

Figure 7.9: **Molecular structure of *fac*-[Re(5Me-Sal-Trypt)(CO)$_3$(NC$_5$H$_5$)] (19) showing the atom numbering system. For the aromatic rings, the first digit refers to the ring number, while the second digit refers to the specific C-atom in the ring. Displacement ellipsoids are drawn at 50% probability level. H atoms are omitted for the sake of clarity.**

Table 7.6: **Selected bond distances and angles of *fac*-[Re(5Me-Sal-Trypt)(CO)$_3$(NC$_5$H$_5$)] (19) [Å and °].**

Atoms	Distance	Atoms	Angle
Re1-N1	2.1795(16)	N1-Re1-O1	84.47(6)
Re1-O1	2.1232(13)	N3-Re1-C03	178.86(7)
Re1-N3	2.2267(16)	N1-Re1-C02	92.60(7)
Re1-C01	1.929(2)	O1-Re1-C01	92.12(7)
Re1-C02	1.906(2)	O1-Re1-C02	117.05(7)
Re1-C03	1.907(2)	N1-Re1-N3	87.19(6)
N1-C1	1.289(2)	Re1-C02-O02	174.31(18)
C1-C11	1.443(3)	C1-N1-C2	115.35(16)
N1-C2	1.483(2)	N1-C1-C12-O1	13.4(2)
O1-C12	1.325(2)	C3-C2-N1-C1	114.7(2)

The central rhenium atom coordinates with the nitrogen of the imine and the oxygen atom of the phenol group to form a six-membered ring. The three carbonyl ligands are facially coordinated to the metal centre with the final position occupied by the pyridine molecule. The Re(I) octahedron is distorted as indicated by the N1-Re1-O1 bite angle of 84.47(6)° and the C03-Re1-N3 bond angle of 178.86(7)°. The N1-Re1-N3 bond angle is nearly perpendicular with an angle of 87.19(6)°. The Re1-N1 and Re1-O1 bond distances (2.1795(16) Å and 2.1232(13) Å) are comparable to other N,O ligand-to-metal bond distances which are in the range of 2.162 – 2.186 Å for Re-N and 2.099 – 2.184 Å for Re-O.[10,13,14,15] The bond distance of rhenium to N3, the coordinated pyridine molecule, is 2.2267(16) Å and compares well with similar complexes where bond distances between 2.203 – 2.230 Å were observed.[12,15] The C1-N1 bond distance (1.289(2) Å) is indicative of a double bond. The O1-C12 (1.325(2) Å), N1-C2 (1.483(2) Å) and C1-C11 (1.443(3) Å) are consistent for single bonds for the respective atoms.[16]

The plane formed by the salicylidene C1 aromatic backbone (Plane 1: C11, C12, C13, C14, C15, C16) is tilted relative to the Re1 equatorial plane (Plane 2: Re1, N1, O1, C01, C02) with a dihedral angle of 30.15(5)° (Figure 7.10). Both the pyridine molecule and the tryptamine substituent lies above Plane 1.

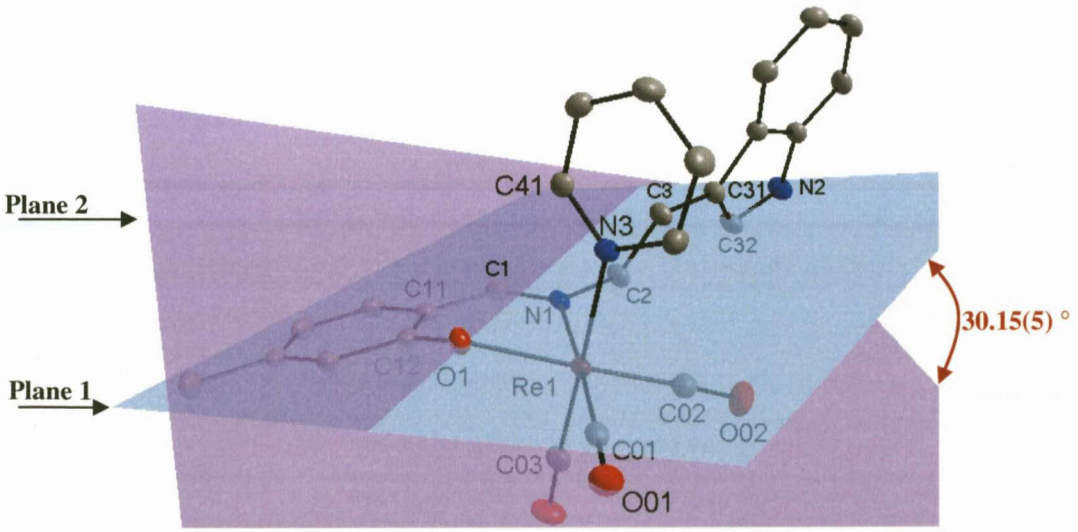

Figure 7.10: **Graphical representation of the bending salicylidene aromatic backbone (Plane 1 indicated in blue, Plane 2 indicated in purple). H atoms are omitted for clarity.**

[16] F.H. Allen, O. Kennard, D.G. Watson, L. Brammer, A.G. Orpen, R. Taylor, *J. Chem. Soc., Perkin Trans.* II, 1987, S1

The indole ring structure of the tryptamine substituent shows no deviation from planarity. It is rotated more significantly to the C1 aromatic ring as compared to the non-coordinated free ligand. The dihedral angle between the C1 backbone (Plane 1) and the tryptamine 9-membered ring (Plane 3: C31, C32, N2, C33, C34, C35, C36, C37, C38) is 60.89(5)° compared to the related dihedral angle (48.44(3)°) for the free ligand.

The tryptamine ring is orientated nearly perpendicular to the Re1 equatorial plane (Plane 2) with a dihedral angle of 87.81(4)° (Figure 7.11). The pyridine molecule (Plane 4: N3, C41, C42, C43, C44, C45) is nearly perpendicular to the Re1 equatorial plane (Plane 2) (88.32(6)°) compared to the typtamine Plane 3 (81.89(6)°)

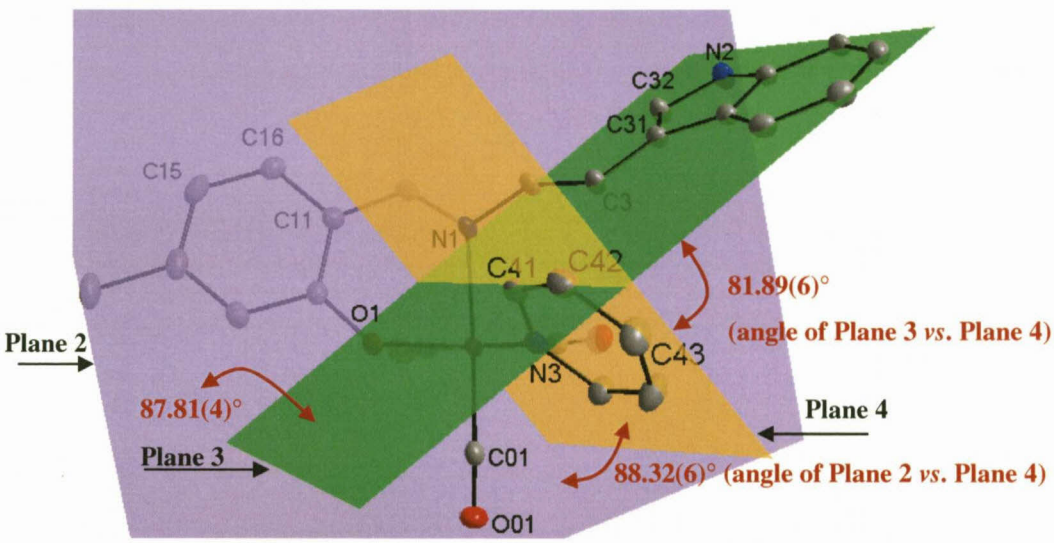

Figure 7.11: **Graphical representation of the orientation of the tryptamine substituent (Plane 3 - indicated in green), the Re1 equatorial plane (Plane 2 - indicated in purple) and pyridine ring (Plane 4 - indicated in yellow). H atoms are omitted for clarity.**

Several intermolecular hydrogen bonds occur between neighbouring molecules of the type N-H...O and C-H...O. The interaction between N2-H2...O1$^{\#1}$, indicated in Figure 7.12A, forms infinite one dimensional chains along the [010] vector as illustrated in Figure 7.12B.

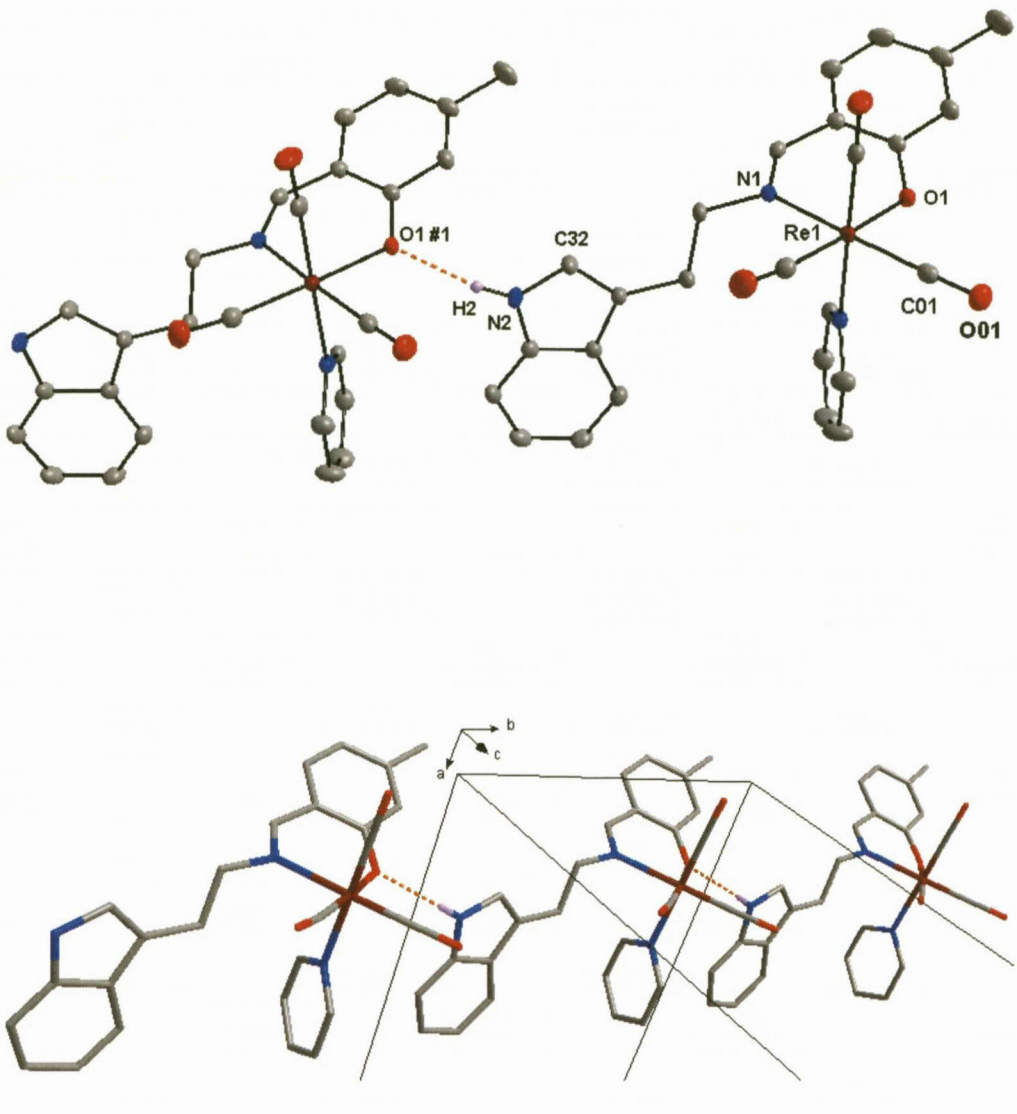

Figure 7.12: **Graphical representation of intermolecular hydrogen bond interaction between (A) N2-H2...O1$^{\#1}$ and (B) infinite one dimensional chain formed by the generation of symmetry related molecules along the [010] vector. Hydrogen interaction indicated by orange dotted lines. Due to the complexity of the image, symmetry generated molecules are illustrated in "stick" format. Certain H atoms omitted for the sake of clarity. (Symmetry operation: #1 x, y-1, z.)**

Intermolecular hydrogen bonds occur between the methyl moiety of the C1 salicylidene aromatic ring with atoms C141-H14C...O01$^{\#2}$ (symmetry operation: x, 2-y, -0.5+z). Expansion of symmetry related molecules also results in an infinite one dimensional chain parallel to the *c*-axis (Figure 7.13).

A

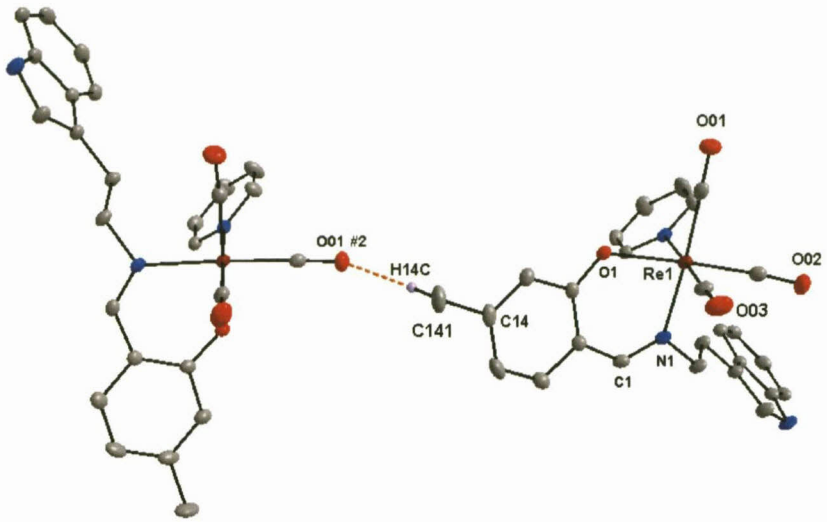

B

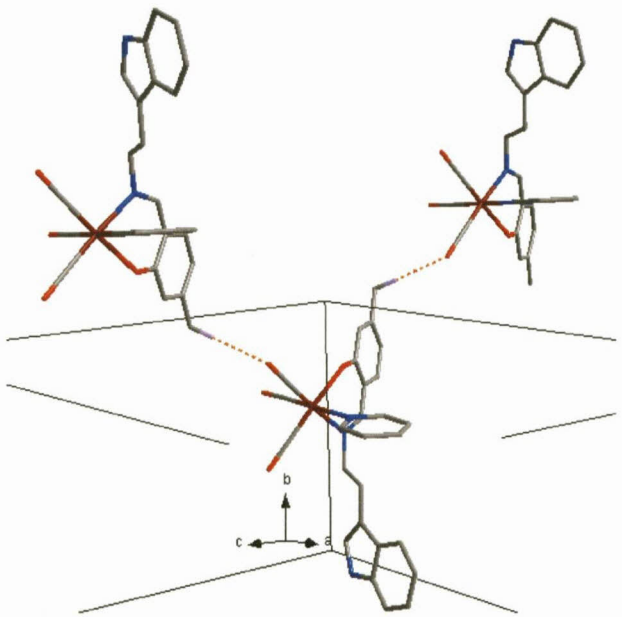

Figure 7.13: **Graphical representation of intermolecular hydrogen bond interaction between (A) C141-H14C...O01$^{\#2}$ and (B) infinite one dimensional chain formed by the generation of symmetry related molecules along the [001] vector. Hydrogen interaction indicated by orange dotted lines. Due to the complexity of the image, symmetry generated molecules are illustrated in "stick" format. Certain H atoms omitted for the sake of clarity. (Symmetry operation: #2 x, 2-y, -0.5+z.)**

The last two intermolecular hydrogen bonds occur between atoms found in the indole ring structure and the carbonyl ligands, namely C36-H36...O03$^{\#3}$ and C37-H37...O02$^{\#4}$ as illustrated in Figure 7.14 A. As with the previous hydrogen bond interactions, generation of symmetry equivalent molecules leads to the formation of one dimensional chains as indicated in Figure 7.14 B & C.

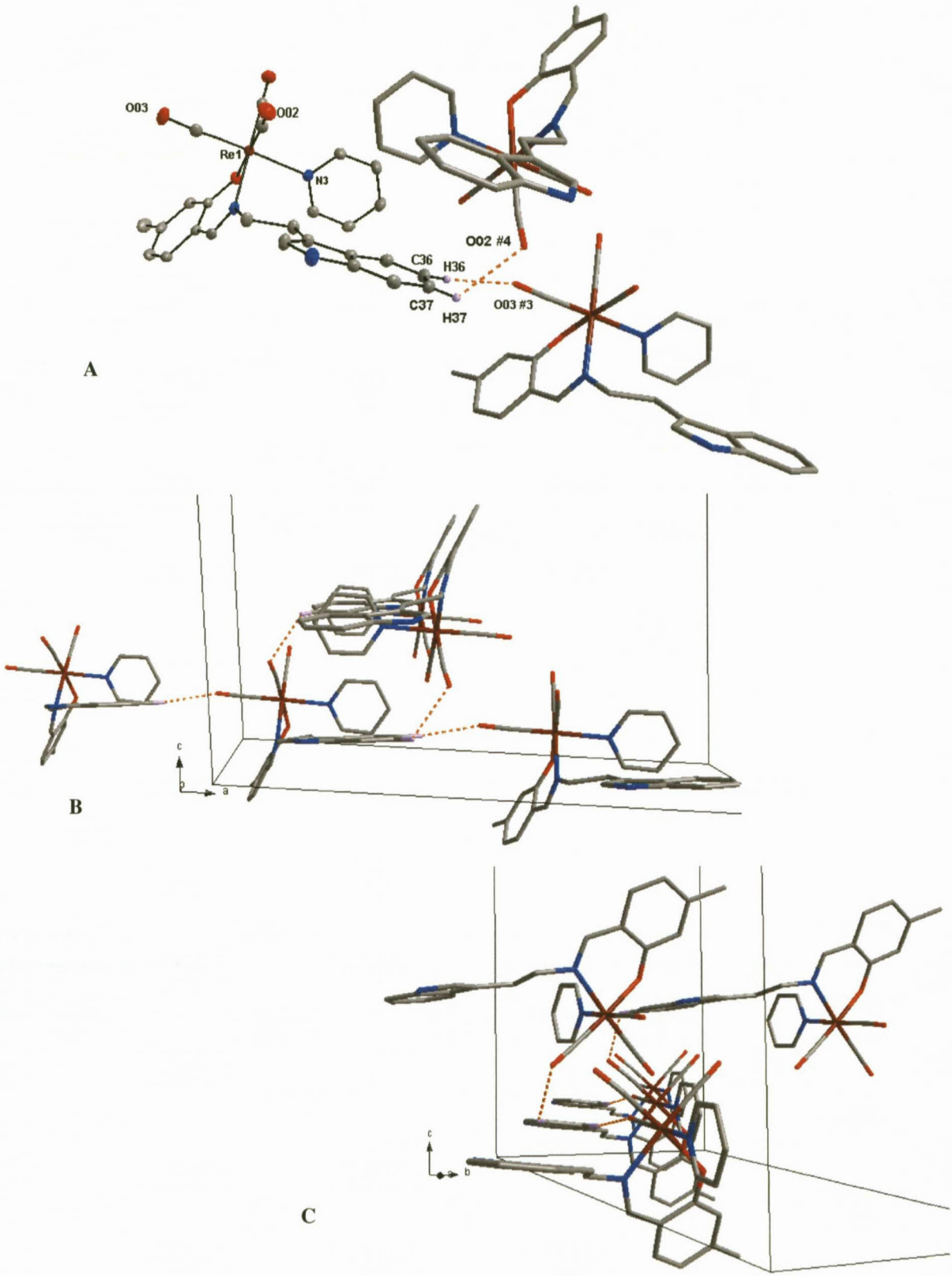

Figure 7.14: **Graphical representation of intermolecular hydrogen bond interaction between atoms (A) C36-H36...O03$^{\#3}$ and C37-H37...O02$^{\#4}$. (B & C) Two viewing angles of the infinite one dimensional chains formed by the generation of symmetry related molecules. Hydrogen interaction indicated by orange dotted lines. Certain H atoms omitted for the sake of clarity. (Symmetry operation: #3 x+1/2, y-1/2, z; #4 -x+1/2, y-1/2, -z+1/2).**

Table 7.7: Hydrogen bonds for *fac*-[Re(5Me-Sal-Trypt)(CO)$_3$(NC$_5$H$_5$)] [Å and °].

D-H...A	d(D-H)	d(H...A)	d(D...A)	<(DHA)
N(2)-H(2)...O(1)#1	0.88	2.08	2.873(2)	150.4
C(141)-H(14C)...O(01)#2	0.98	2.54	3.522(3)	176.0
C(36)-H(36)...O(03)#3	0.95	2.55	3.474(3)	165.1
C(37)-H(37)...O(02)#4	0.95	2.57	3.151(3)	119.7

Symmetry transformations used to generate equivalent atoms:
#1 x,y-1,z #2 x,-y+2,z-1/2 #3 x+1/2,y-1/2,z
#4 -x+1/2,y-1/2,-z+1/2

No π-π interaction occurs between neighboring molecules, however the molecular packing is stabilized by C-H…π interactions between several molecules as indicated in Figure 7.15 by the green dotted lines and Table 7.8.

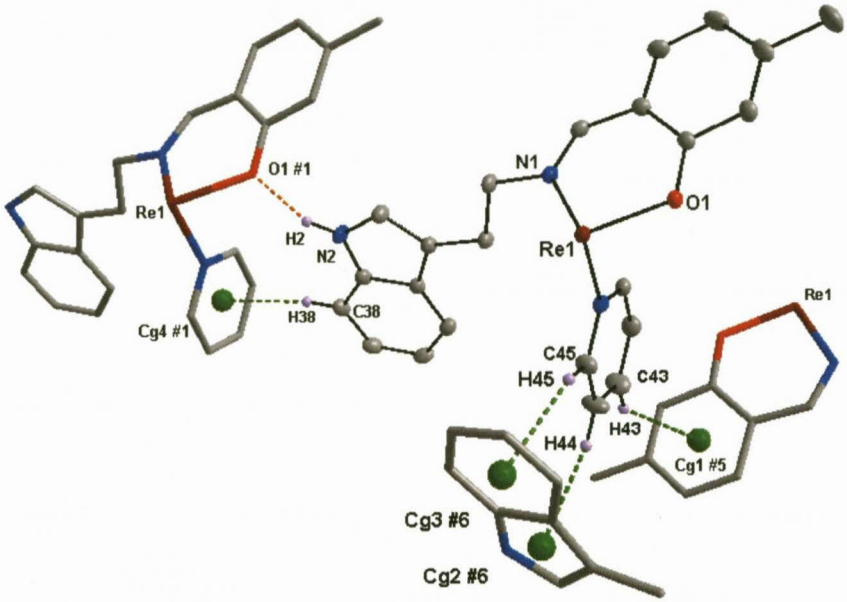

Figure 7.15: Graphical representation of the C-H…π interactions indicated by green dotted lines (Cg = centroid atom of aromatic rings). Hydrogen bonding indicated by orange dotted lines. Only partial structures are indicated for the sake of clarity.

Table 7.8: C-H…π Interaction between aromatic rings of rhenium complex.

C-H...Cg	Centroid atom (Cg)	d(H...Cg) (Å)	d(C...Cg) (Å)	< (C-H...Cg) (°)
C38-H38	Cg4 #1	2.6129(1)	3.543(2)	166.1(1)
C43-H43	Cg1 #5	2.8972(1)	3.711(2)	144.3(1)
C44-H44	Cg2 #6	2.8215(1)	3.662(2)	148.0(1)
C45-H45	Cg3 #6	2.6540(1)	3.484(2)	146.3(1)

Symmetry transformations:
#1 x, y-1, z; #5 1/2-x, 3/2-y, -z; #6 1/2-x, 1/2+y, 1/2-z
Cg1 = centroid atom of C11, C12, C13, C14, C15, C16; Cg2 = centroid atom of C31, C32, N2, C33, C34
Cg3 = centroid atom of C33, C34, C35, C36, C37, C38; Cg4 = N3, C41, C42, C43, C44, C45

The sum of the total intermolecular interactions, results in the molecules in the unit cell packing in a "head-to-head" manner to form cubic tunnels when viewed along the *b*-axis (Figure 7.16).

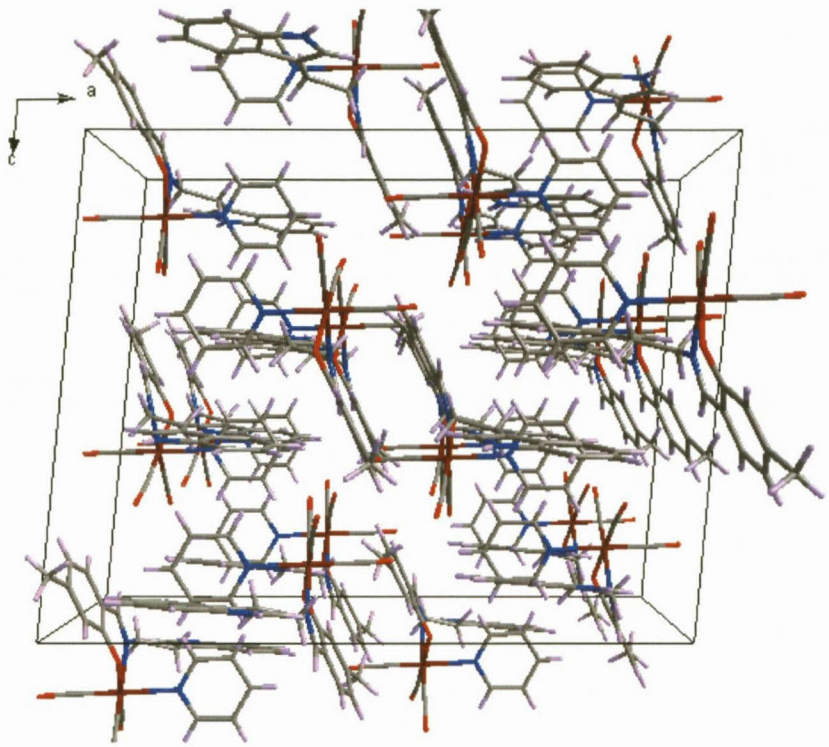

Figure 7.16: Molecular packing of the unit cell as viewed along the *b*-axis.

Structural comparisons and illustrative overlays between the coordinated rhenium tricarbonyl complex crystal structures are discussed in Section 7.8.

7.5 CRYSTAL STRUCTURE OF

fac-[Re(5Me-Sal-Carba)(CO)$_3$(NC$_5$H$_5$)]

The complex, *fac*-[Re(5Me-Sal-Carba)(CO)$_3$(NC$_5$H$_5$)] (**20**), (5Me-Sal-Carba = 2-(9-ethyl carbazol-3-yliminomethyl)-5-methylphenolato) crystallizes in a triclinic crystal system in the $P\bar{1}$ space group with two formula units per unit cell (Z = 2). The asymmetric unit contains one independent molecule. The molecular structure of (**20**) is represented in Figure 7.17 along with the atom numbering scheme. Important bond lengths and angles are given in Table 7.9.

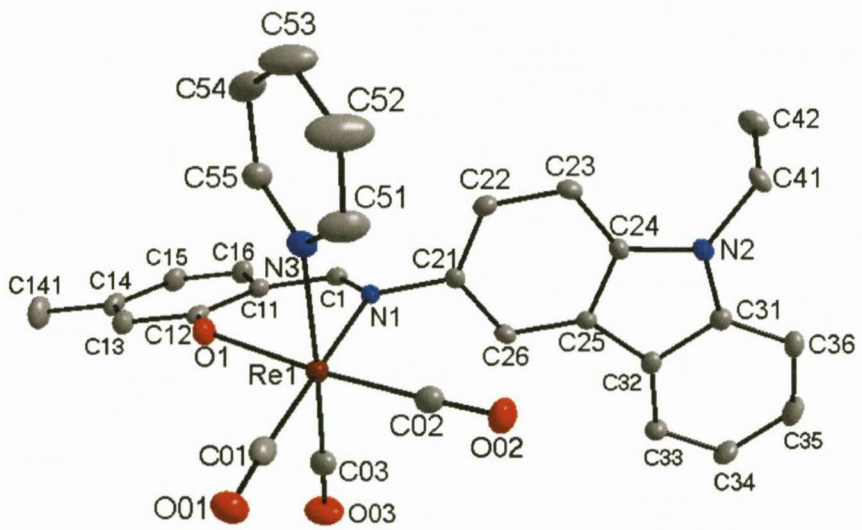

Figure 7.17: **Molecular structure of *fac*-[Re(5Me-Sal-Carba)(CO)$_3$(NC$_5$H$_5$)] (20) showing the atom numbering system. For the aromatic rings, the first digit refers to the ring number, while the second digit refers to the specific C-atom in the ring. Displacement ellipsoids are drawn at 50% probability level. H atoms are omitted for the sake of clarity.**

Table 7.9: **Selected bond distances and angles of *fac*-[Re(5Me-Sal-Carba)(CO)$_3$(NC$_5$H$_5$)] (20) [Å and °].**

Atoms	Distance	Atoms	Angle
Re1-N1	2.171(2)	N1-Re1-O1	83.49(9)
Re1-O1	2.107(2)	N3-Re1-C03	173.63(11)
Re1-N3	2.222(3)	N1-Re1-C02	92.81(11)
Re1-C01	1.925(3)	O1-Re1-C01	96.66(10)
Re1-C02	1.900(3)	O1-Re1-C02	175.26(10)
Re1-C03	1.913(3)	N1-Re1-N3	86.01(9)
N1-C1	1.289(4)	Re1-C02-O02	178.3(3)
C1-C11	1.436(4)	C1-N1-C21	116.8(2)
N1-C21	1.448(3)	N1-C1-C12-O1	7.1(3)
O1-C12	1.315(3)	C22-C21-N1-C1	98.1(3)

The central rhenium atom is coordinated to the nitrogen and oxygen atoms of the salicylidene bidentate ligand to form a six-membered ring. Three carbonyl ligands are facially coordinated to the metal centre while the sixth position of the octahedron is occupied by pyridine. The Re(I) octahedron is distorted as indicated by the N1-Re1-O1 bite angle of 83.49(9)° and the C03-Re1-N3 bond angle of 173.63(11)°. The N1-Re1-N3 bond angle is near perpendicular with an angle of 86.01(9)°. The Re1-N1 and Re1-O1 bond distances (2.171(2) Å and 2.107(2) Å) are comparable to other N,O ligand-to-metal bond distances which are in the range of 2.162 – 2.186 Å for Re-N and 2.099 – 2.184 Å for Re-O.[10,13,14,15] The bond distance of rhenium to N3, the coordinated pyridine molecule, is 2.222(3) Å and compares well with similar complexes where bond distances between 2.203 – 2.230 Å were observed.[12,15] The C1-N1 bond distance (1.289(4) Å) is indicative of a double bond. The O1-C12 (1.315(3) Å), N1-C21 (1.448(3) Å) and C1-C11 (1.436(4) Å) are consistent for single bonds for the respective atoms.[16]

The plane formed by the salicylidene C1 aromatic backbone (Plane 1: C11, C12, C13, C14, C15, C16) is tilted relative to the Re1 equatorial plane (Plane 2: Re1, N1, O1, C01, C02) with a dihedral angle of 21.84(8)° (Figure 7.18). The pyridine molecule lies above Plane 1 whereas the carbazole substituent lies partially below Plane 1.

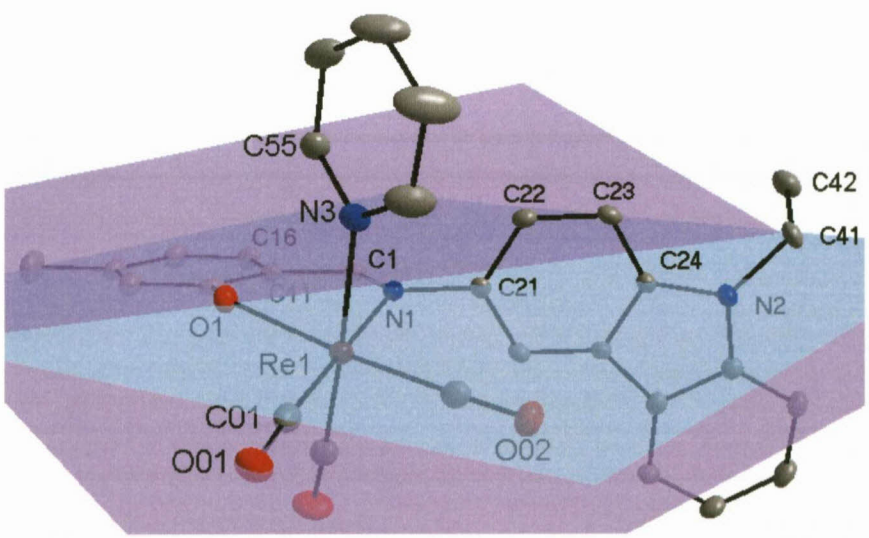

Figure 7.18: **Graphical representation of the tilting salicylidene aromatic backbone (Plane 1 indicated in blue, Plane 2 indicated in purple). H atoms are omitted for clarity.**

The thirteen member ring of the carbazole substituent is planar. It is rotated significantly to the C1 aromatic backbone relative to the non-coordinated free ligand. The dihedral angle between the C1 backbone ring (Plane 1) and the carbazole substituent (Plane 3: C21, C22, C23, C24, C25, C26, N2, C31, C32, C33, C34, C35, C36) is 78.56(7)° compared to the related dihedral angle (4.37(4)°) for the free ligand.

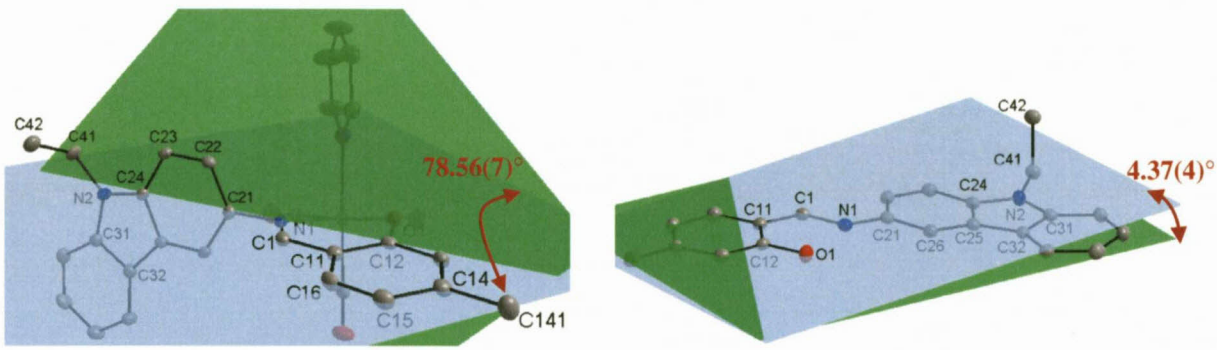

A: Coordinated ligand **B: Free ligand**

Figure 7.19: **Graphical representation of the rotation of the carbazole substituent of the (A) coordinated ligand, (B) the free ligand. H atoms are omitted for clarity.**

The carbazole substituent is orientated with a dihedral angle of 82.20(6)° to the Re1 equatorial plane (Plane 2). The pyridine molecule (Plane 4: N3, C51, C52, C53, C54, C55) is rotated closer to perpendicular relative to the Re1 equatorial plane (Plane 2) (86.74(9)°) than to the carbazole Plane 3 (52.61(9)°).

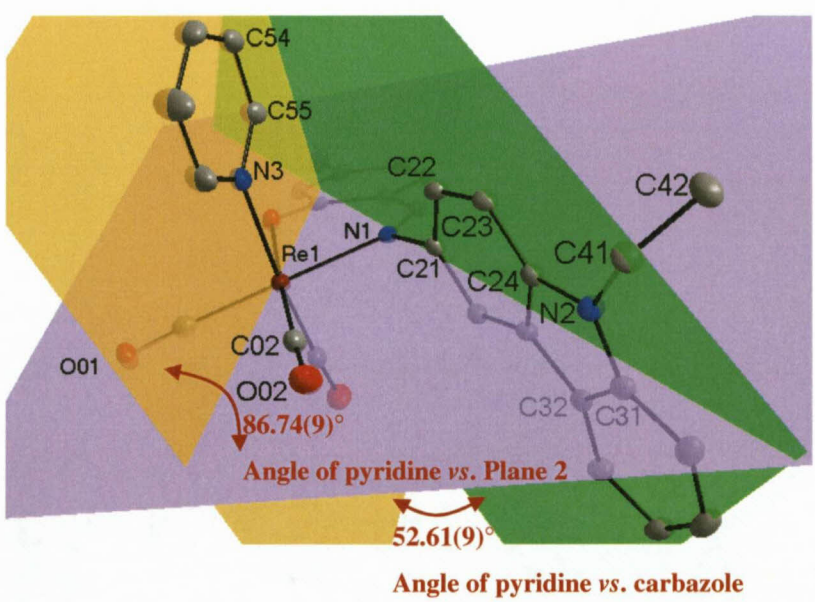

Figure 7.20: **Graphical representation of the orientation of the carbazole substituent (Plane 3 indicated in green). Re1 equatorial plane (Plane 2) indicated in purple and pyridine ring (Plane 4) indicated in yellow. H atoms are omitted for clarity.**

A few hydrogen bond interactions occur within the crystal structure. Intramolecular bonding occurs between the pyridine atoms of C55-H55 and O1 atom of the bidentate ligand. Intermolecular bonding occurs between C42-H42B...O1$^{\#2}$ and C36-H36...O02$^{\#3}$ of neighbouring molecules as indicated in Figure 7.21 and Table 7.10. An equivalent interaction occurs between C36$^{\#3}$-H36$^{\#3}$...O02 to form rectangular tubes (Figure 7.22).

Due to the intermolecular H-bonding C36-H36...O02$^{\#3}$, π-π interaction occurs between carbazole substituents. A centroid to centroid distance of 4.265(3) Å (Cg1...Cg1; Cg1 = centroid atom of N2, C24, C25, C32, C31) occurs with an interplanar angle of 0.3(1)°.

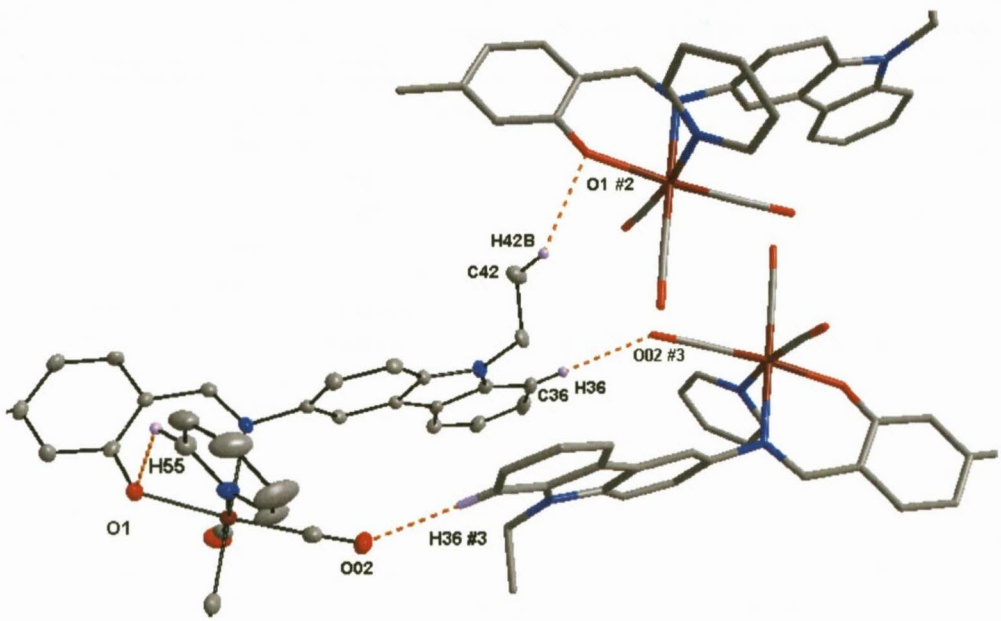

Figure 7.21: **Graphical representation of Complex 20, illustrating H-bond interactions (orange dotted lines). Certain atoms are omitted for clarity.**

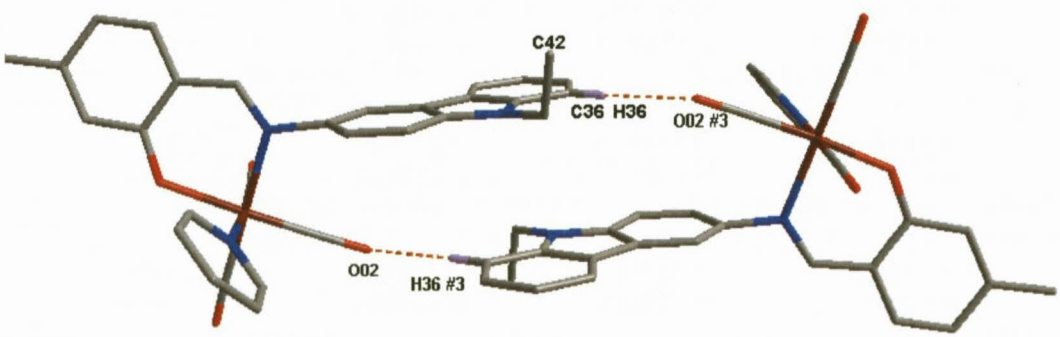

Figure 7.22: **Graphical representation of Complex 20, illustrating rectangular tubes formed by H-bonding (orange dotted lines). Certain atoms are omitted for clarity.**

Table 7.10: Hydrogen bonds for *fac*-[Re(5Me-Sal-Carba)(CO)$_3$(NC$_5$H$_5$)] [Å and °].

D-H...A	d(D-H)	d(H...A)	d(D...A)	<(DHA)
C(42)-H(42B)...O(1)#2	0.98	2.54	3.311(4)	135.6
C(55)-H(55)...O(1)#1	0.95	2.38	2.926(4)	116.2
C(36)-H(36)...O(02)#3	0.95	2.50	3.447(4)	177.4

Symmetry transformations used to generate equivalent atoms:
#1 x,y,z #2 x+1,y-1,z #3 -x+3,-y+1,-z+1

The crystal packing in the unit cell is further stabilized by soft van der Waal, O…O interactions between O02…O03$^{\#4}$ and O03…O02$^{\#4}$ (O…O = 2.910(4) Å; symmetry operation #4: 2-x, 2-y, 1-z). The interaction forms a six-membered cyclic diamer in the chair confirmation as indicated in Figure 7.23.

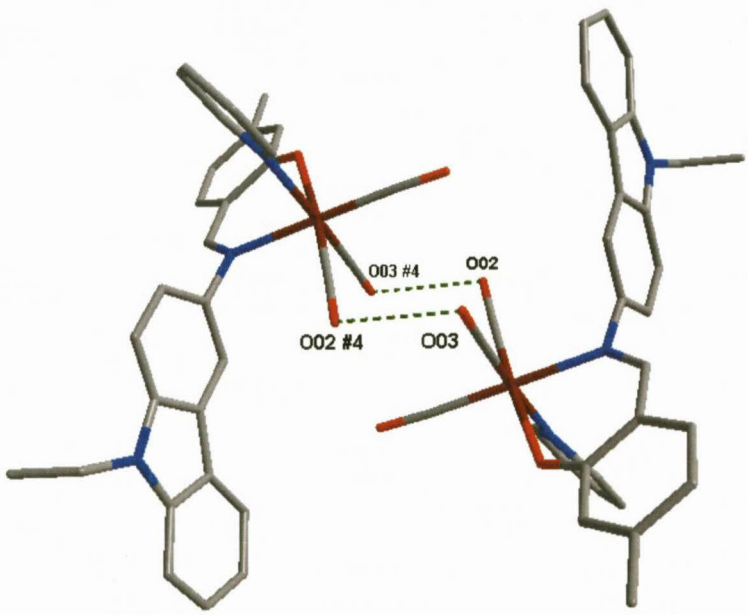

Figure 7.23: O…O interactions between neighbouring molecules to form hexacyclic diamer.

A few C-H… π interactions occur between the aromatic rings of the neighbouring rhenium complexes as illustrated in Figure 7.24 and Table 7.11 below.

Table 7.11: C-H…π Interaction between aromatic rings of rhenium complex.

C-H...Cg	Centroid atom (Cg)	d(H...Cg) (Å)	d(C...Cg) (Å)	< (C-H...Cg) (°)
C23-H23	Cg4 #5	2.947(1)	3.838(4)	156.9(2)
C41-H41B	Cg6 #3	2.917(1)	3.503(4)	118.8(2)
C54-H54	Cg5 #5	2.905(1)	3.606(4)	131.6(2)

Symmetry transformations:
#3 3-x, 1-y, 1-z; #5 2-x, 1-y, 2-z
Cg4 = centroid atom of C11, C12, C13, C14, C15, C16; Cg5 = centroid atom of C21, C22, C23, C24, C25, C26;
Cg6 = centroid atom of C31, C32, C33, C34, C35, C36

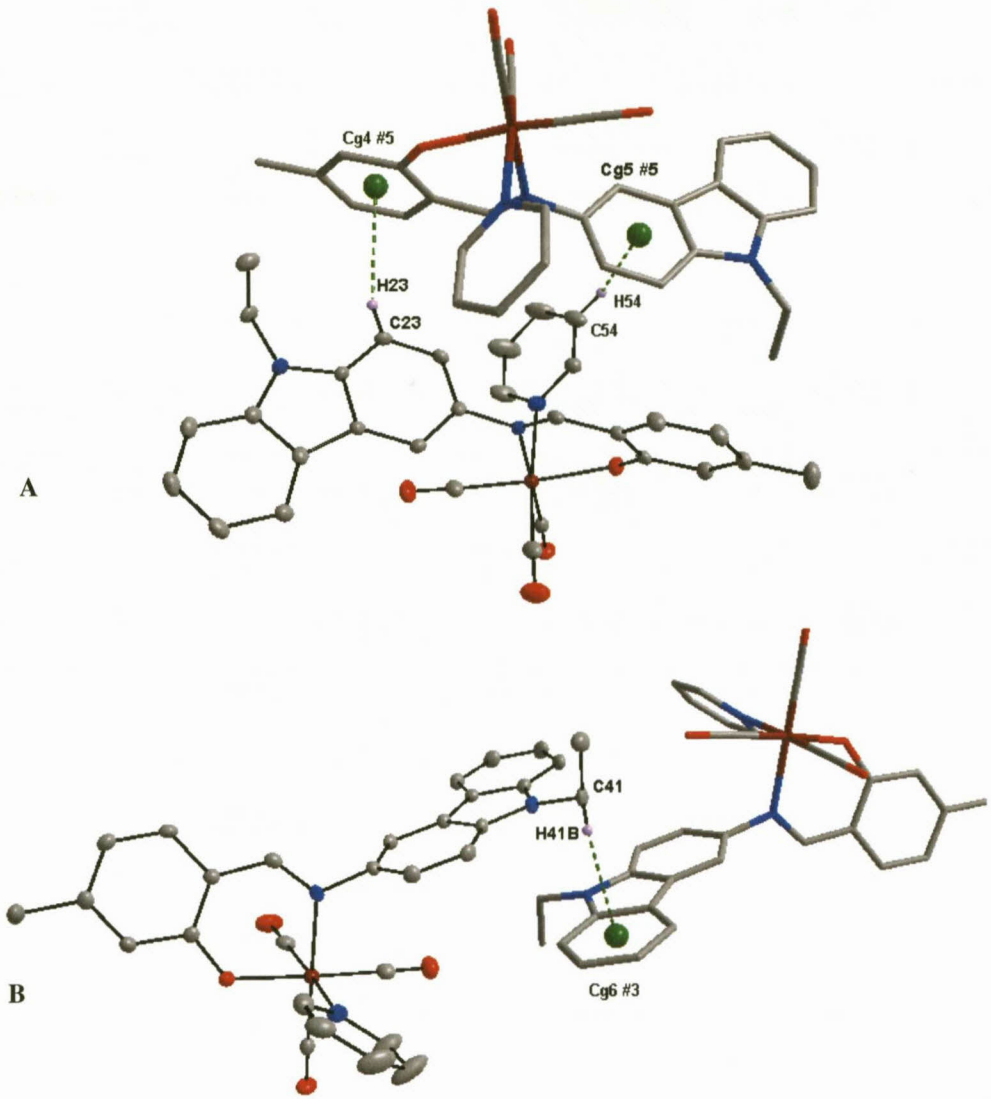

Figure 7.24: **Graphical representation of the C-H…π ring interactions indicated by green dotted lines (Cg = centroid atom of aromatic rings).**

The final interaction observed is an intramolecular C-O...π interaction between C02-O02 and first six-membered aromatic ring of the carbazole substituent as illustrated in Figure 7.25

Table 7.12: **C-O…π Interaction between aromatic rings of rhenium complex.**

C-O...Cg	Centroid atom (Cg)	d(O...Cg) (Å)	d(C...Cg) (Å)	< (C-O...Cg) (°)
C02-O02	Cg5 #1	3.502(3)	3.501(4)	80.4(2)

Symmetry transformations:
#1 x, y, z
Cg5 = centroid atom of C21, C22, C23, C24, C25, C26

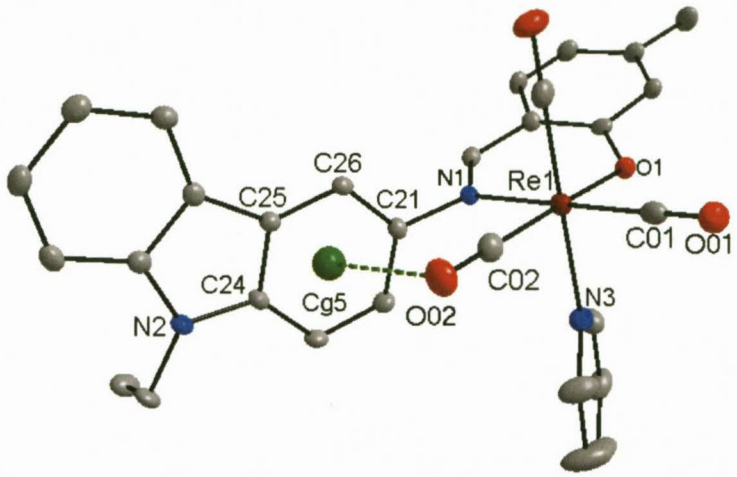

Figure 7.25: **Graphical representation of the C-O…π ring interactions indicated by green dotted lines (Cg = centroid atom of aromatic rings). H-atoms omitted for clarity**

The molecules pack in a "face-to-face" manner relative to the carbazole substituent as illustrated in Figure 7.26. Structural comparisons and illustrative overlays between the coordinated rhenium tricarbonyl complex crystal structures are discussed in Section 7.8.

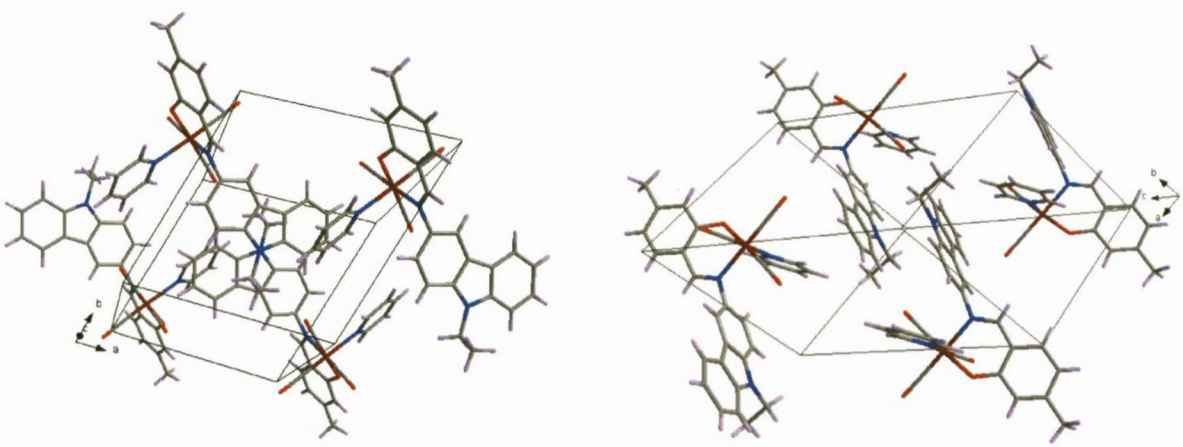

Figure 7.26: **Molecular packing of unit cell viewed from two different perspectives.**

7.6 CRYSTAL STRUCTURE OF

fac-[Re(5Me-Sal-*m*Tol)(CO)$_3$(HOCH$_3$)]

The complex, *fac*-[Re(5Me-Sal-*m*Tol)(CO)$_3$(HOCH$_3$)] (**21**), (5Me-Sal-*m*Tol = 5-methyl-2-(*m*-tolyliminomethyl)phenolato) crystallizes in a orthorhombic crystal system in the *Pbcn* space group with eight formula units per unit cell (Z = 8). The asymmetric unit contains one independent molecule. The molecular structure of (**21**) is represented in Figure 7.27 along with the atom numbering scheme. Important bond lengths and angles are given in Table 7.13.

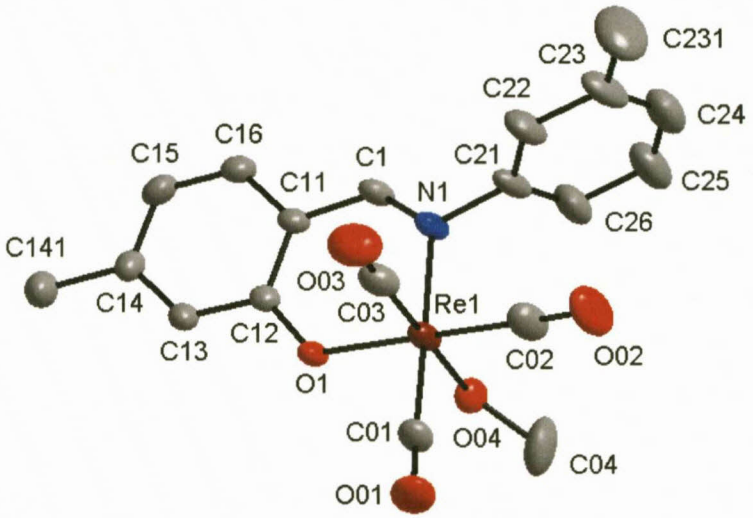

Figure 7.27: **Molecular structure of *fac*-[Re(5Me-Sal-*m*Tol)(CO)$_3$(HOCH$_3$)] (21) showing the atom numbering system. For the aromatic rings, the first digit refers to the ring number, while the second digit refers to the specific C-atom in the ring. Displacement ellipsoids are drawn at 30% probability level. H atoms are omitted for the sake of clarity.**

Table 7.13: **Selected bond distances and angles of *fac*-[Re(5Me-Sal-*m*Tol)(CO)$_3$(HOCH$_3$)] (21) [Å and °].**

Atoms	Distance	Atoms	Angle
Re1-N1	2.157(5)	N1-Re1-O1	83.77(19)
Re1-O1	2.123(4)	O04-Re1-C03	175.7(3)
Re1-C01	1.914(7)	N1-Re1-C02	94.2(3)
Re1-C02	1.895(9)	O1-Re1-C01	94.8(3)
Re1-C03	1.901(11)	O1-Re1-C02	175.5(3)
Re1-O04	2.189(5)	N1-Re1-O04	84.2(2)
N1-C1	1.278(9)	Re1-C02-O02	178.7(8)
C1-C11	1.443(10)	C1-N1-C21	116.8(6)
N1-C21	1.481(10)	Re1-O04-C04	126.4(5)
O1-C12	1.325(7)	N1-C1-C12-O1	11.1(6)
		C22-C21-N1-C1	91.4(1)

The *fac*-Re(I) tricarbonyl metal centre is coordinated to three carbonyl ligands, one methanol molecule and to the N,O bidentate ligand. The octahedron is distorted as indicated by the N1-Re1-O1 bite angle of 83.77(19)° and the C03-Re1-O04 bond angle of 175.7(3)°. The Re1-N1 and Re1-O1 bond distances (2.157(5) Å and 2.123(4) Å) are comparable to other N,O ligand-to-metal bond distances which are in the range of 2.162 – 2.186 Å for Re-N and 2.099 – 2.184 Å for Re-O.[10,13,14,15]

The bond angle of the coordinated methanol was found to be 126.4(5)° for Re1-O04-C04. The bond distance of rhenium to O04, the methanol oxygen, was calculated as 2.189(5) Å, which is slightly longer than that found for Re-OH_2 bonds, where the distances to the water oxygen range between 2.153 – 2.170 Å for related Re(N-O) complexes. [17,18,19]

The plane formed by the salicylidene C1 aromatic backbone (Plane 1: C11, C12, C13, C14, C15, C16) is tilted relative to the Re1 equatorial plane (Plane 2: Re1, N1, O1, C01, C02) with a dihedral angle of 16.8(2)° (Figure 7.28).

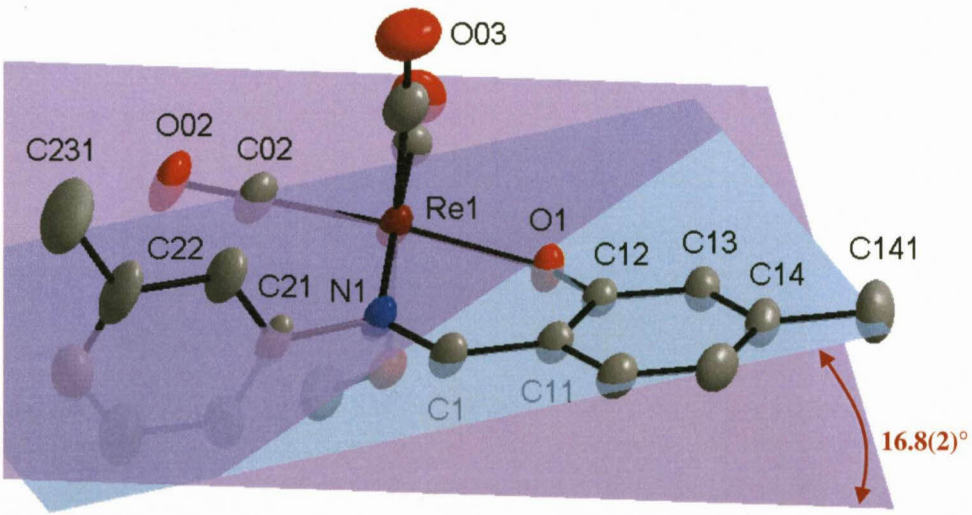

Figure 7.28: **Graphical representation of the tilting aromatic backbone (Plane 1 indicated in blue, Plane 2 indicated in purple). H atoms are omitted for clarity.**

The *m*-tolyl substituent bonded to the imine N atom is rotated significantly to the C1 aromatic ring relative to the non-coordinated free ligand. The dihedral angle between the C1 backbone

[17] M. Schutte, G. Kemp, H.G. Visser, A. Roodt, *Inorg. Chem.*, 2011, publication accepted
[18] M. Schutte, H.G. Visser, *Acta Cryst.*, 2008, E64, m1226
[19] M. Schutte, H.G. Visser, A. Roodt, *Acta Cryst.*, 2008, E64, m1610

(Plane 1) and the *m*-tolyl ring (Plane 3: C21, C22, C23, C24, C25, C26) is 80.5(3)° compared to the related dihedral angle (1.76(9)°) for the free ligand (Figure 7.29). The *m*-tolyl ring is rotated nearly perpendicular to the Re1 equatorial plane (Plane 2) with a dihedral angle of 86.4(3)°. The methyl moiety points above the plane in the opposite direction as the coordinated methanol molecule (Figure 7.28).

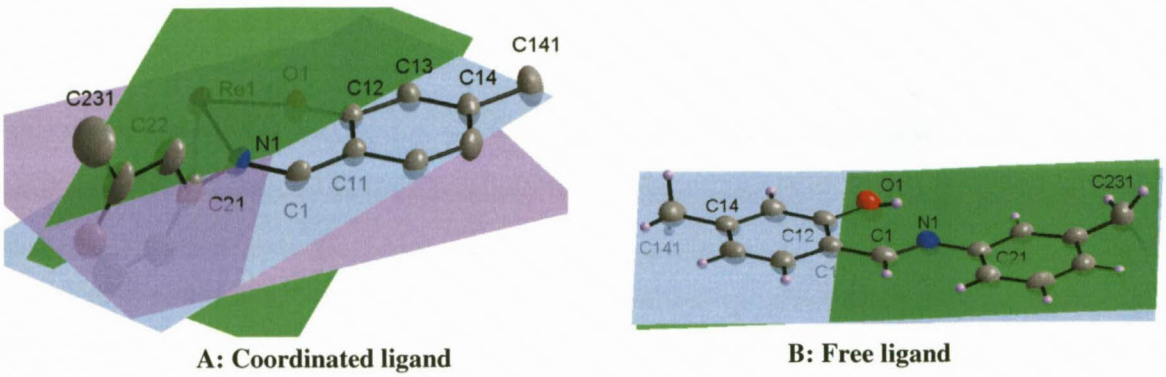

A: Coordinated ligand **B: Free ligand**

Figure 7.29: **Graphical representation of the rotation of the *m*-tolyl substituent of the (A) coordinated ligand, (B) the free ligand. Certain atoms are omitted for clarity.**

Two classical intermolecular hydrogen bonding occurs between neighbouring molecules. The interaction between atoms O04-H04...O1$^{\#1}$ and the symmetry generated molecule forms a six-membered hexacylic ring with a boat conformation (Figure 7.30). A π-π interaction between the C1 aromatic rings of the salicylidene backbone, occurs between the same two molecules.

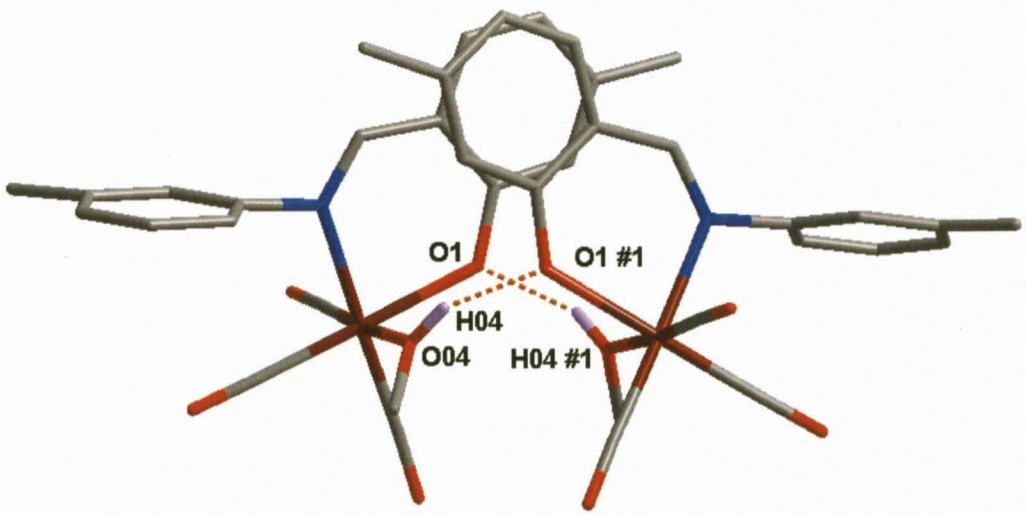

Figure 7.30: **Graphical representation of hydrogen bond and π-π interaction between neighboring molecules. H atoms are omitted for the sake of clarity.**

Table 7.14: **Hydrogen bonds for *fac*-[Re(5Me-Sal-*m*Tol)(CO)$_3$(HOCH$_3$)] [Å and °].**

D-H...A	d(D-H)	d(H...A)	d(D...A)	<(DHA)
O(04)-H(04)...O(1)#1	0.84	1.82	2.598(7)	154.4
C(1)-H(1)...O(02)#2	0.95	2.41	3.253(9)	147.5

Symmetry transformations used to generate equivalent atoms:
#1 -x+1,y,-z+1/2 #2 -x+3/2,y-1/2,z

Table 7.15: **π-π Interaction between aromatic rings of rhenium complexes.**

Centroid atom	Centroid atom	Distance between centroid atoms (Å)	Interplanar angle (°)
Cg1	Cg1 #1	3.728(4)	1.3(2)

Symmetry transformations used to generate equivalent atoms:
#1 1-x, y, 0.5-z
Cg1 = centroid atom of C11, C12, C13, C14, C15, C16

The second hydrogen bond interaction occurs between C1-H1…O02$^{\#2}$, which is further stabilized by the weak H-bond interaction between C231-H23A…O01$^{\#2}$ (C231…O01$^{\#2}$ = 3.665(16) Å, < C-H…O = 140.2(8)°) indicated by the green dotted line.

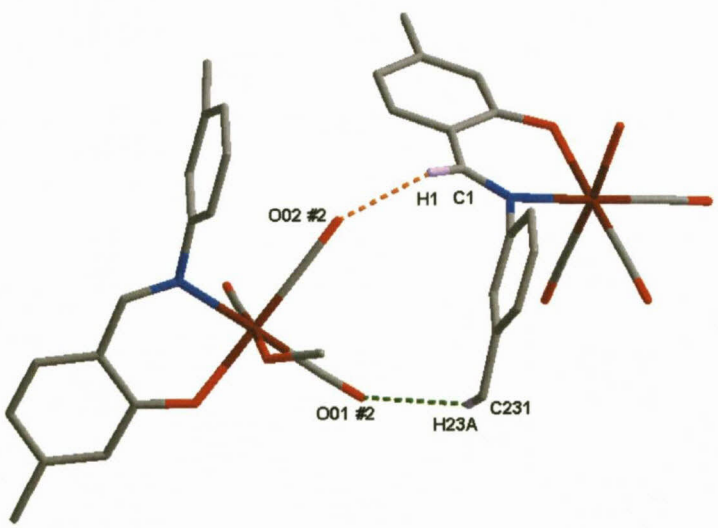

Figure 7.31: **Graphical representation of hydrogen bond interaction between neighboring molecules. Weak H-bond interaction indicated in green. H atoms are omitted for the sake of clarity.**

The molecular structure contains one C-H…π interaction between C24-H24 and the C1$^{\#3}$ aromatic salicylidene backbone as indicated in Figure 7.32 by the green dotted line. An intramolecular C-O…π interaction occurs between one carbonyl ligand and the coordinated *m*-tolyl substituent.

Table 7.16: C-X…π Interaction between aromatic rings of rhenium complex.

C-X...Cg	Centroid atom (Cg)	d(X...Cg) (Å)	d(C...Cg) (Å)	< (C-X...Cg) (°)
C24-H24	Cg1 #3	2.75(1)	3.67(1)	166.0(7)
C02-O02	Cg2 #4	3.530(8)	3.521(9)	79.9(6)

Symmetry transformations:
#3 1.5-x, 0.5-y, 0.5+z; #4 x, y, z
Cg1 = centroid atom of C11, C12, C13, C14, C15, C16; Cg2 = centroid atoms of C21, C22, C23, C24, C25, C26

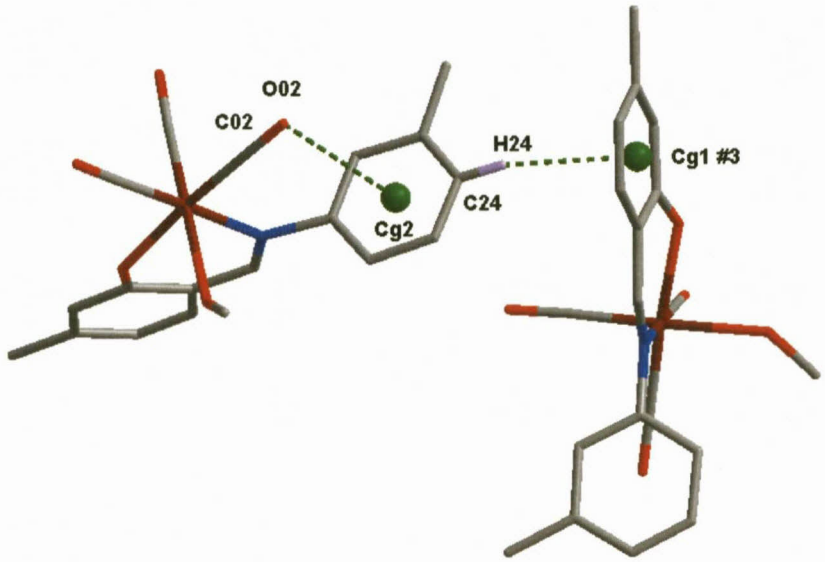

Figure 7.32: Graphical representation of C-X…π interactions between neighboring molecules indicated by green dotted lines. H atoms are omitted for the sake of clarity.

The molecular packing of the unit cell, as indicated in Figure 7.33, illustrates the π-π interactions between the salicylidene backbone. Structural comparisons and illustrative overlays between the coordinated rhenium tricarbonyl complex crystal structures are discussed in Section 7.8.

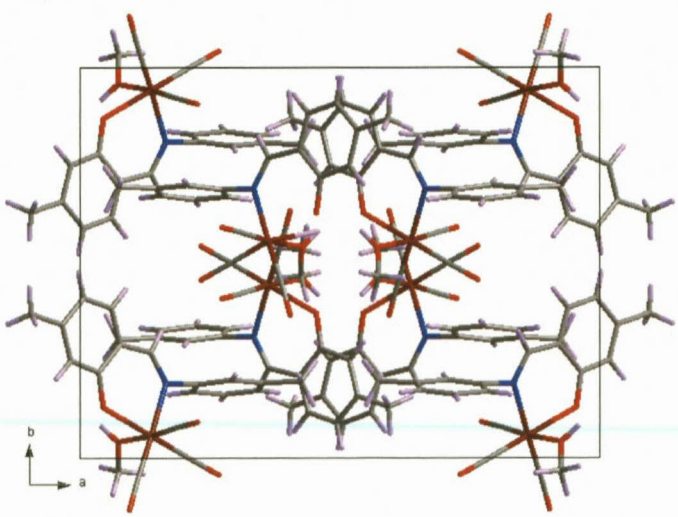

Figure 7.33: Molecular packing of the unit cell as viewed along the *c*-axis.

7.7 CRYSTAL STRUCTURE OF

fac-[Re(5Me-Sal-3Me2Bu)(CO)$_3$(HOCH$_3$)]

The complex, *fac*-[Re(5Me-Sal-3Me2Bu(CO)$_3$(HOCH$_3$)] (**22**), (5Me-Sal-3Me2Bu = 5-methyl-2-(1,2-dimethylpropyliminomethyl)phenolato) crystallizes in a monoclinic crystal system in the *C2/c* space group with eight formula units per unit cell (Z = 8). The asymmetric unit contains one independent molecule. The molecular structure of (**22**) is represented in Figure 7.34 along with the atom numbering scheme. Important bond lengths and angles are given in Table 7.17.

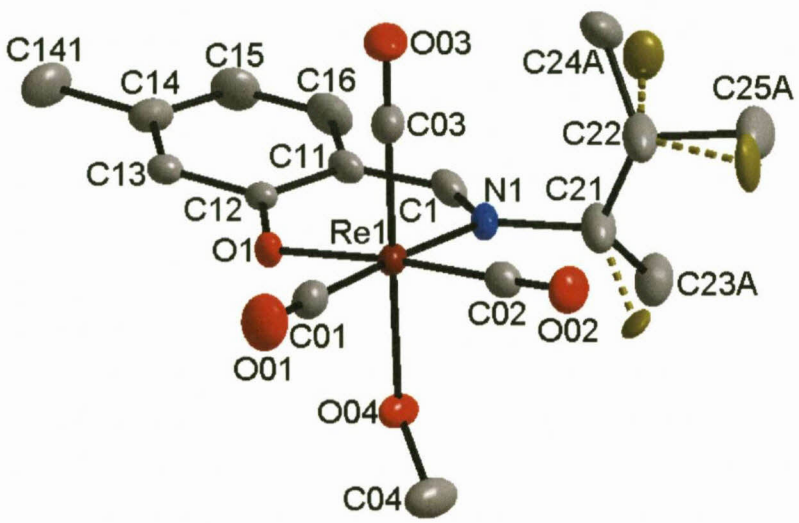

Figure 7.34: **Molecular structure of *fac*-[Re(5Me-Sal-3Me2Bu)(CO)$_3$(HOCH$_3$)] (22) showing the atom numbering system. For the aromatic rings, the first digit refers to the ring number, while the second digit refers to the specific C-atom in the ring. Displacement ellipsoids are drawn at 50% probability level. H atoms are omitted for the sake of clarity.**

Table 7.17: **Selected bond distances and angles of *fac*-[Re(5Me-Sal-3Me2Bu)(CO)$_3$(HOCH$_3$)] (22) [Å and °].**

Atoms	Distance	Atoms	Angle
Re1-N1	2.179(4)	N1-Re1-O1	85.47(11)
Re1-O1	2.117(3)	O04-Re1-C03	176.03(16)
Re1-C01	1.916(5)	N1-Re1-C02	95.68(16)
Re1-C02	1.903(4)	O1-Re1-C01	93.24(15)
Re1-C03	1.896(5)	O1-Re1-C02	175.45(15)
Re1-O04	2.180(3)	N1-Re1-O04	82.37(12)
N1-C1	1.285(6)	Re1-C02-O02	177.4(4)
C1-C11	1.438(6)	C1-N1-C21	115.6(4)
N1-C21	1.509(6)	Re1-O04-C04	123.1(3)
O1-C12	1.328(4)	N1-C1-C12-O1	10.7(3)
		C22-C21-N1-C1	100.3(6)

The 3Me2Bu imino group contains two disorders. Atoms C24 and C25 are substitutionally disordered over two positions with a 0.63(3) : 0.37(3) ratio. Atom C23 is also substitutionally disordered over two positions with a 0.59(1) : 0.41(1) ratio. Refinement of the crystal structure assuming only one type of disorder with a 0.60(1) : 0.40(1) ratio, results in an increase in the goodness of fit value (GOOF = 1.295 for two disorders *vs.* 1.296 for one disorder). The disorder of the coordinated substituent is illustrated in Figure 7.35 below.

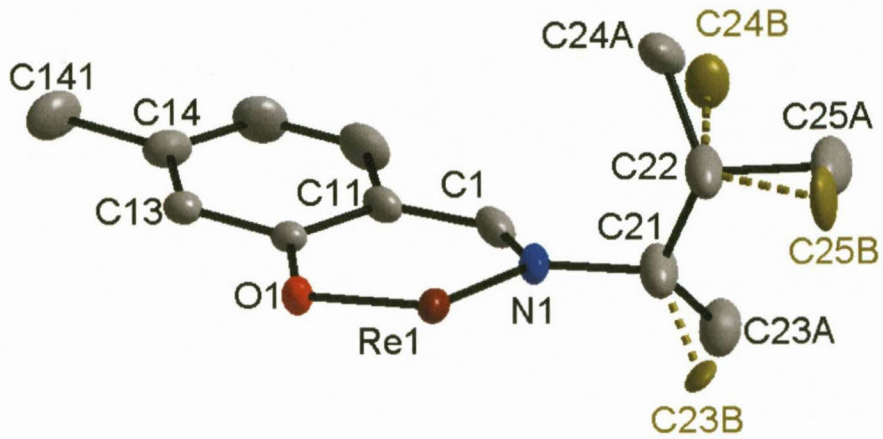

Figure 7.35: Molecular structure indicating the disorder on the 3Me2Bu substituent of 22. H atoms are omitted for clarity.

The *fac*-Re(I) tricarbonyl metal centre is coordinated to three carbonyl ligands, one methanol molecule as well as to the N,O donor atoms of the bidentate ligand. The octahedron is distorted as indicated by the N1-Re1-O1 bite angle of 85.47(11)° and the C03-Re1-O04 bond angle of 176.03(16)°. The Re1-N1 and Re1-O1 bond distances (2.179(4) Å and 2.117(3) Å) are comparable to other N,O ligand-to-metal bond distances which are in the range of 2.162 – 2.186 Å for Re-N and 2.099 – 2.184 Å for Re-O.[10,13,14,15]

The bond angle of the coordinated methanol was found to be 123.1(3)° for Re1-O04-C04. The bond distance of rhenium to O04, the methanol oxygen, was calculated as 2.180(3) Å, which is slightly longer than that found for Re-OH_2 bonds, where the distances to the water oxygen range between 2.153 – 2.170 Å for related Re(N-O) complexes.[17,18,19]

The plane formed by the salicylidene C1 aromatic backbone (Plane 1: C11, C12, C13, C14, C15, C16) is tilted relative to the Re1 equatorial plane (Plane 2: Re1, N1, O1, C01, C02) with a dihedral angle of 18.3(1)° (Figure 7.36).

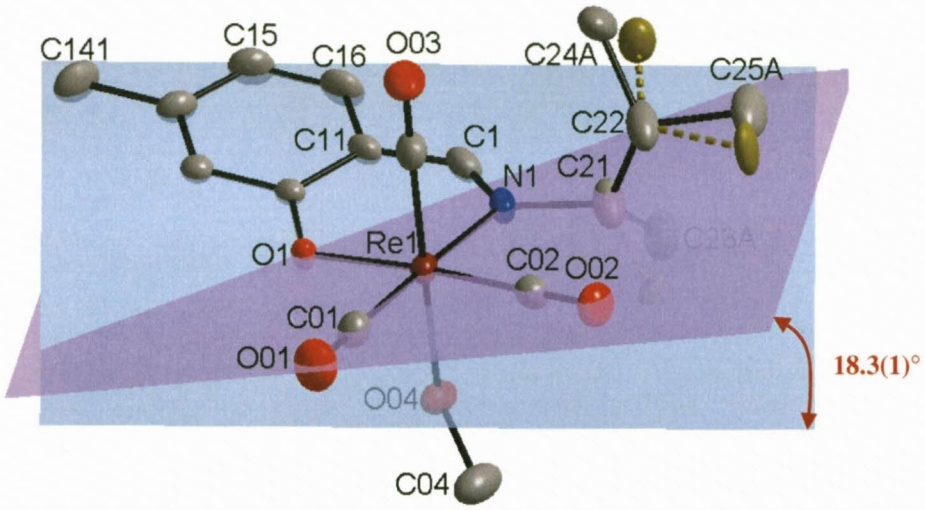

Figure 7.36: **Graphical representation of the tilting salicylidene aromatic backbone (Plane 1 indicated in blue, Plane 2 indicated in purple). H atoms are omitted for clarity.**

Two classical intermolecular hydrogen bonds occur between neighbouring molecules. The interaction between atoms O04-H04…O1$^{\#1}$ and the symmetry generated molecule forms a six-membered hexacylic ring with a boat conformation (Figure 7.37). A π-π interaction between the C1 aromatic rings of the salicylidene backbone, occurs between the same two molecules. The second hydrogen bond interaction occurs between atoms C1-H1…O02$^{\#2}$ as illustrated in Figure 7.38.

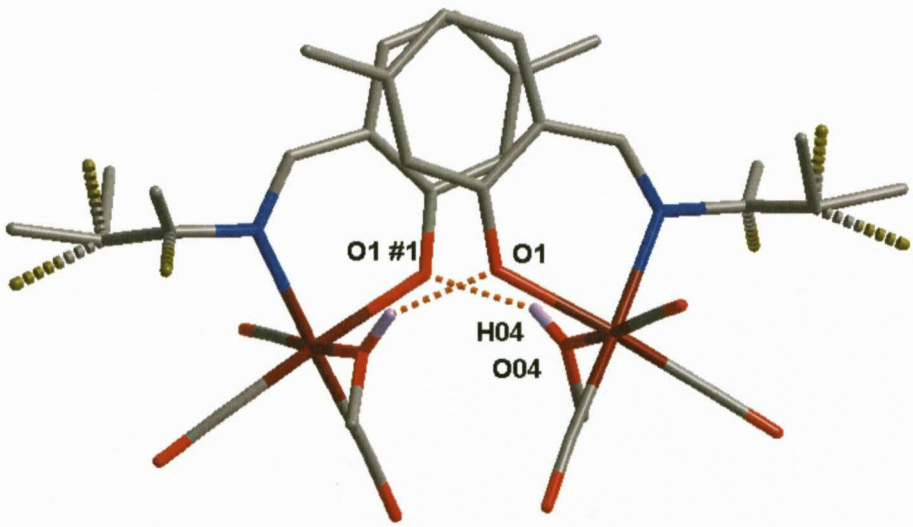

Figure 7.37: **Graphical representation of the hydrogen bond interaction (orange dotted line) between neighbouring molecules. H-atoms are omitted for the sake of clarity.**

Table 7.18: Hydrogen bonds for *fac*-[Re(5Me-Sal-3Me2Bu)(CO)$_3$(HOCH$_3$)] [Å and °].

D-H...A	d(D-H)	d(H...A)	d(D...A)	<(DHA)
O(04)-H(04)...O(1)#1	0.84	1.85	2.579(4)	144.4
C(1)-H(1)...O(02)#2	0.95	2.50	3.438(5)	170.9

Symmetry transformations used to generate equivalent atoms:
#1 -x+1,y,-z+1/2 #2 -x+1/2,y+1/2,-z+1/2

Table 7.19: π-π Interaction between aromatic rings of rhenium complexes.

Centroid atom	Centroid atom	Distance between centroid atoms (Å)	Interplanar angle (°)
Cg1	Cg1 #1	3.730(1)	4.5(2)

Symmetry transformations used to generate equivalent atoms:
#1 -x+1,y,-z+1/2
Cg1 = centroid atom of C11, C12, C13, C14, C15, C16

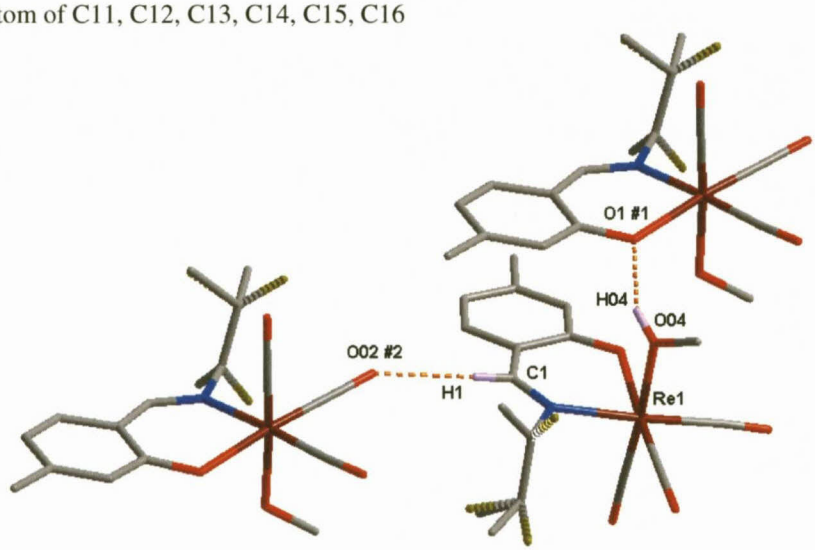

Figure 7.38: Graphical representation of the all hydrogen bond interactions (orange dotted line) between neighbouring molecules. H-atoms are omitted for the sake of clarity.

The molecular structure contains one C-H…π interaction between the 3Me2Bu substituent, atoms C24A-H24A and a neighbouring C1 aromatic salicylidene backbone as indicated in Figure 7.39 by the green dotted line.

Table 7.20: C-H…π Interaction between aromatic rings of rhenium complex.

C-H...Cg	Centroid atom (Cg)	d(H...Cg) (Å)	d(C...Cg) (Å)	< (C-H...Cg) (°)
C24A-H24A	Cg1 #3	2.5701(1)	3.478(15)	154.2(8)

Symmetry transformations:
#3 0.5-x, 0.5-y, -z;
Cg1 = centroid atom of C11, C12, C13, C14, C15, C16

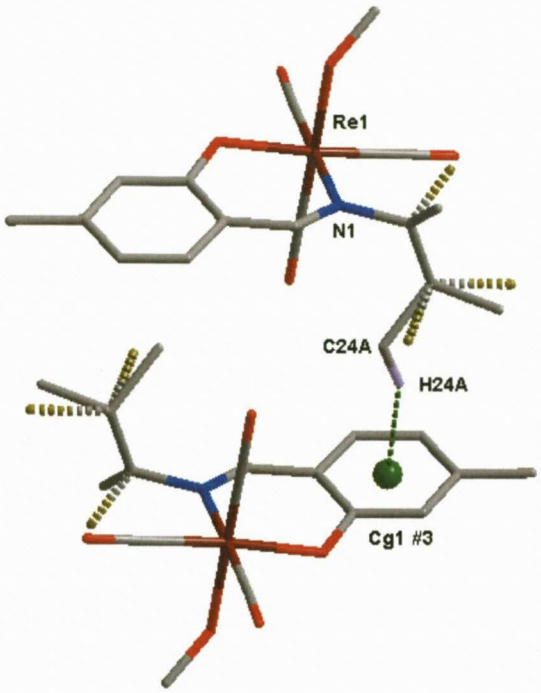

Figure 7.39: **Graphical representation of the C-H…π interaction (green dotted line) between neighbouring molecules. H-atoms are omitted for the sake of clarity.**

Structural comparisons and illustrative overlays between the various coordinated rhenium tricarbonyl complex crystal structures are discussed in Section 7.8.

7.8 INTERPRETATION AND CORRELATION OF STRUCTURAL PARAMETERS

The following subsection correlates structural data from the various functionalized *fac*-$[Re(CO)_3]^+$ complexes. The general crystallographic parameters, bond distances and angles of interest of the crystal structures are given in Tables 7.21 and 7.22.

Table 7.21: **Cell dimension overview of presented functionalized *fac*-[Re(L,L'-Bid)$(CO)_3$(S)] complexes (L,L'-Bid = 5Me-Sal-T, T = coordinated substituent, S = coordinated methanol or pyridine).**

L,L'-Bid	**5Me-Sal-Hist**	**5Me-Sal-Trypt**	**5Me-Sal-Carba**	**5Me-Sal-*m*Tol**	**5Me-Sal-3Me2Bu**
	(18)	**(19)**	**(20)**	**(21)**	**(22)**
S	**-**	**Pyridine**	**Pyridine**	**$HOCH_3$**	**$HOCH_3$**
Crystal System	Triclinic	Monoclinic	Triclinic	Orthorhombic	Monoclinic
Space Group	*P*ī	*C2/c*	*P*ī	*Pbcn*	*C2/c*
Unit Cell Dimensions					
a (Å)	7.3705(1)	23.5078(7)	10.705(5)	18.9720(7)	18.1040(4)
b (Å)	9.1241(2)	10.9385(3)	10.711(5)	14.2191(5)	15.1508(4)
c (Å)	12.8797(2)	18.4481(5)	13.305(5)	14.2316(5)	13.8715(4)
α (°)	107.597(1)	90	66.469(5)	90	90
β (°)	103.111(1)	95.355(2)	67.663(5)	90	102.896(2)
γ (°)	94.297(1)	90	72.708(5)	90	90
Volume ($Å^3$)	794.43(2)	4723.0(2)	1274.6(1)	3839.2(2)	3708.8(2)
Z	2	8	2	8	8

Five salicylidene rhenium tricarbonyl complexes were presented in this chapter. The backbone of the N,O bidentate ligand had been modified by the addition of a methyl moiety in the fifth position. Complex **18**, containing the histamine substituent bonded to the imine N atom, is the only complex whereby the amino substituent has rotated to coordinate as a N,N,O tridentate ligand. Complexes **19** and **20** contain biologically active amines coordinated to the imine N atom and have successfully substituted the methanol solvent for pyridine. The last two *fac*-rhenium tricarbonyl complexes (**21**, **22**) contain aromatic and aliphatic substituents coordinated to the imine nitrogen. A methanol solvento ligand is coordinated directly to the rhenium metal centre of these last two complexes.

Complexes **18** and **20** both crystallize in the triclinic *P*ī crystal system with two molecules per unit cell. Complex **19** and **22** crystallize in the monoclinic *C2/c* crystal system, with eight molecules per unit cell. These two crystal structures are isostructural to the five *fac*-[Re(Sal-

T)$(CO)_3(HOCH_3)$] complexes (**11** – **15**) reported in Chapter 6 which crystallized in the same space group but contain significantly different unit cell dimensions.

Table 7.22: **Selected geometrical parameters of the presented *fac*-[Re(L,L'-Bid)$(CO)_3$(S)] complexes (S = coordinated methanol or pyridine) tabulated for comparison [Å, °].**

L,L'-Bid	5Me-Sal-Hist (18)	5Me-Sal-Trypt (19)	5Me-Sal-Carba (20)	5Me-Sal-*m*Tol (21)	5Me-Sal-3Me2Bu (22)
S	-	Pyridine	Pyridine	$HOCH_3$	$HOCH_3$
Bonds Distance (Å)					
Re1-N1	2.1599(19)	2.1795(16)	2.171(2)	2.157(5)	2.179(4)
Re1-O1	2.1454(16)	2.1232(13)	2.107(2)	2.123(4)	2.117(3)
Re1-C01	1.924(2)	1.929(2)	1.925(3)	1.914(7)	1.916(5)
Re1-C02	1.905(2)	1.906(2)	1.900(3)	1.895(9)	1.903(4)
Re1-C03	1.911(2)	1.907(2)	1.913(3)	1.901(11)	1.896(5)
Re1-O04	-	-	-	2.189(5)	2.180(3)
Re-N32	2.1875(19)	-	-	-	-
Re-N3	-	2.2267(16)	2.222(3)	-	-
N1-C1	1.285(3)	1.289(2)	1.289(4)	1.278(9)	1.285(6)
Bond angle (°)					
N1-Re1-O1	80.11(7)	84.47(6)	83.49(9)	83.77(19)	85.47(11)
O04-Re1-C03	-	-	-	175.7(3)	176.03(16)
N32-Re1-C03	174.63(9)	-	-	-	-
N3-Re1-C03	-	178.86(7)	173.63(11)	-	-
Re1-O04-C04	-	-	-	126.4(5)	123.1(3)
Re1-C02-O02	178.64(19)	174.31(18)	178.3(3)	178.7(8)	177.4(4)
C1-N1-C21	117.91(19)	115.35(16)	116.8(2)	116.8(6)	115.6(4)
Torsion angle (°)					
N1-C1-C12-O1	19.5(2)	13.4(2)	7.1(3)	11.1(6)	10.7(3)

Bond distances and angles of the respective rhenium tricarbonyl complexes are all within normal range. Few significant differences are found within the tabulated values. Complex **20** containing the large carbazole substituent has the shortest Re1-O1 bond distance and the longest Re-C03 bond distance. The carbazole substituent is significantly rotated to the C1 aromatic backbone relative to the orientation of the free ligand (dihedral angle of 78.56(7)° *vs.* 4.37(4)°). However the N1-C1-C12-O1 torsion angle is the smallest of the five complexes (**18** – **22**).

Overlay diagrams of the various rhenium tricarbonyl complexes have been drawn to indicate the similarity in coordination between the various complexes. The solid state free ligand is compared to the rhenium coordinated ligand to investigate the flexibility of the ligand around the C=N double bond of the imine functionality. Please note that several of the overlays are only drawn through the salicylidene backbone to allow free rotation of the substituent bonded to the imine N atom and therefore yield low RMS values.

The free ligand, 5Me-SalH-Hist (**6**) contains two independent molecules in the asymmetric unit, both with similar dihedral angles between the two aromatic ring systems. Overlay diagrams of each molecule of the free ligand and *fac*-[Re(5Me-Sal-Hist)$(CO)_3$] (**18**) illustrates the flexible nature of the ligand.

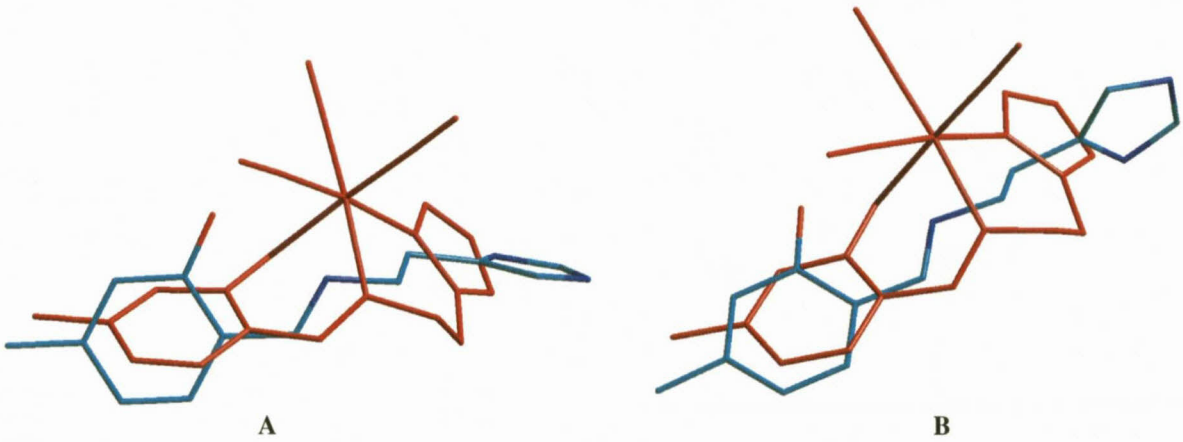

Figure 7.40: **Overlay of crystal structures, Ligand 6 and Complex 18 (red). (A) First molecule of free ligand contained in the asymmetric unit is illustrated (RMS error of = 1.736 Å). (B) Second molecule of free ligand is illustrated (RMS = 1.800 Å). Overlay is drawn through all ligand atoms.**

The overlay between the crystal structures of the free ligand 5Me-SalH-Trypt (**7**) and the rhenium coordinated complex *fac*-[Re(5Me-Sal-Trypt)$(CO)_3(NC_5H_5)$] (**19**) similarly illustrates the flexible nature of the coordinating ligand. Unlike **18**, no tridentate formation occurred by the coordination of the N2 atom in the indole ring system to the rhenium metal centre.

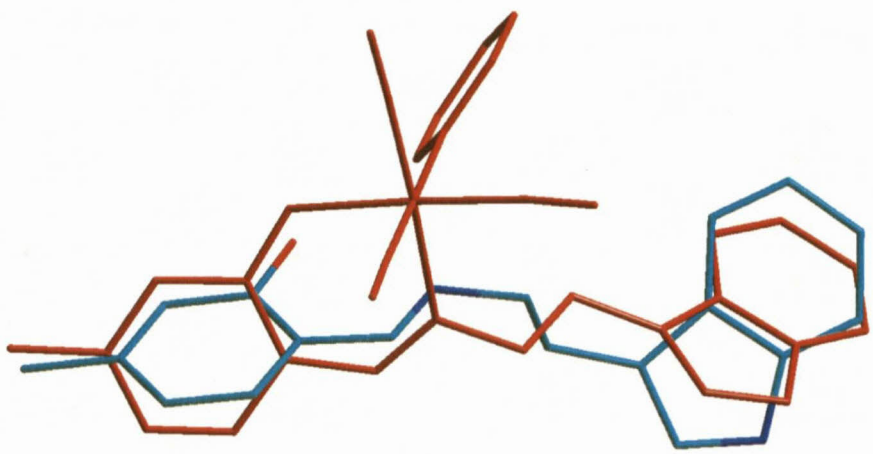

Figure 7.41: **Overlay of crystal structures, Ligand 7 and Complex 19 (red). (RMS = 1.058 Å). Overlay is drawn through all ligand atoms.**

The overlay between the crystal structures of the free ligand 5Me-SalH-Carba (**8**) and the rhenium coordinated complex *fac*-[Re(5Me-Sal-Carba)$(CO)_3(NC_5H_5)$] (**20**) indicates the significant rotation of the carbazole functionality bonded to the imine N atom.

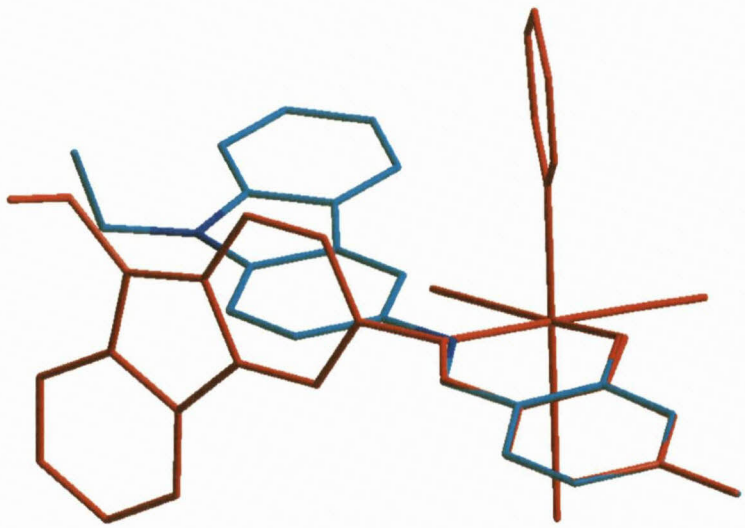

Figure 7.42: **Overlay of crystal structures, Ligand 8 and Complex 20 (red). (RMS = 6.974 x 10^{-2} Å). Overlay drawn through the salicylidene backbone only, to allow free rotation of carbazole substituent. (True RMS value determined from overlay through all atoms is 1.124 Å)**

To directly compare the influence of the addition of a methyl moiety in the fifth position on the salicylidene backbone, complexes *fac*-[Re(Sal-*m*Tol)$(CO)_3(HOCH_3)$] (**11**) and *fac*-[Re(5Me-Sal-*m*Tol)$(CO)_3(HOCH_3)$] (**21**) were overlain. Complex **11** crystallizes in the monoclinic *C*2/c space group, whereas **21** crystallizes in the orthorhombic *Pbcn* spacegroup. The only significant difference is the orientation of the *m*-tolyl moiety which lies with the methyl functionality pointing in reverse directions.

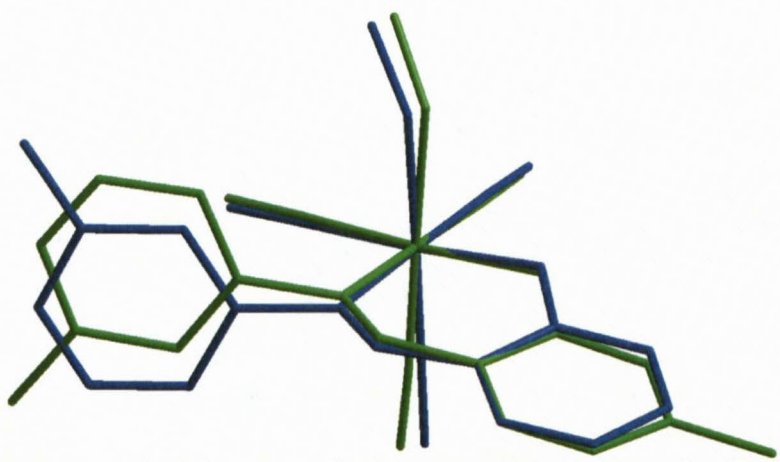

Figure 7.43: **Overlay of crystal structures, 11 (blue) and 21 (green, crystal structure inverted). (Overlay drawn through all atoms, RMS = 1.300 Å).**

A comparison between two rhenium tricarbonyl complexes containing aliphatic substituents is indicated by *fac*-[Re(Sal-3MeBu)$(CO)_3(HOCH_3)$] (**15**) and *fac*-[Re(5Me-Sal-3Me2Bu)$(CO)_3(HOCH_3)$] (**22**). The two complexes both illustrate the imino substituent in a similar orientation.

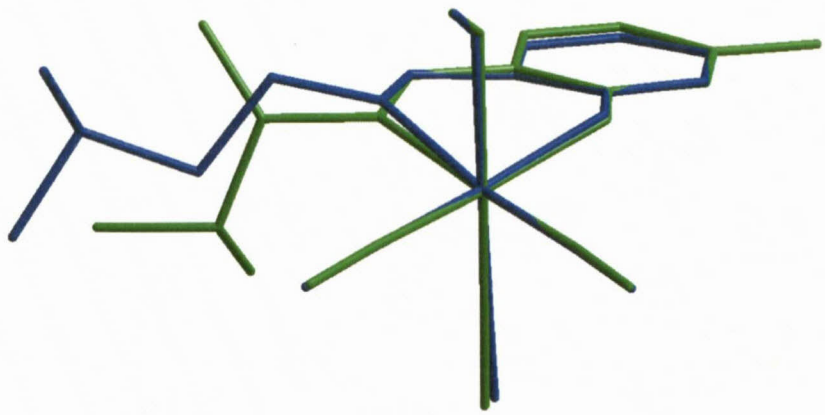

Figure 7.44: **Overlay of crystal structures, 15 (blue) and 22 (green). (Overlay drawn through all atoms, excluding the imino substituent, RMS = 0.105 Å). The disordered minor occupied atoms for the 3MeBu and 3Me2Bu substituents are omitted for clarity.**

The two complexes, *fac*-[Re(Sal-Ph)$(CO)_3(NC_5H_5)$] (**16**) and *fac*-[Re(5Me-Sal-Carba)$(CO)_3(NC_5H_5)$] (**20**), further illustrates the tendency for the rhenium salicylidene complexes to crystallize with the imino substituent in a similar position. The ligand 5Me-SalH-Carba contains a 13 membered ring system coordinated to the imine N atom, whereas the SalH-Ph ligand only has a 6 membered aromatic ring. Despite the significant differences in size, the amino substituents crystallize in near identical orientation as indicated by Figure 7.45.

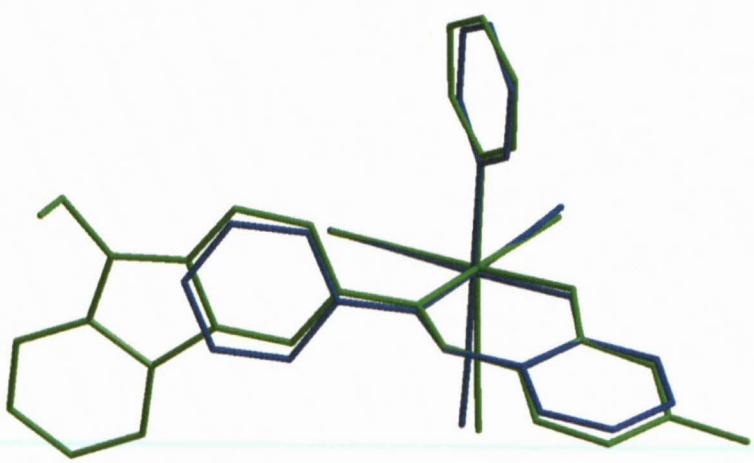

Figure 7.45: **Overlay of crystal structures, 16 (blue, crystal structure inverted) and 20 (green). (Overlay drawn through all atoms, excluding the imino substituent, RMS = 0.213 Å).**

7.9 CONCLUSION

The crystal structures of five rhenium tricarbonyl complexes (**18** - **22**) containing various coordinated substituents bonded to the imine N atom, were analyzed and discussed in this section. The crystal structures display similar unit cell parameters, molecular packing, intermolecular hydrogen bonding as well as π-π stacking.

The coordination of salicylidene to *fac*-rhenium(I) tricarbonyl moieties is rare and only four chemically related crystal structures have been reported to date.[10,11,20] A crystallographic investigation of the complexes synthesized in this study was considered important to fully understand the coordination mode and packing effects. Various substituents were coordinated to the imine N atom of the bidentate ligand *via* the Schiff-base reaction. Initially the focus was aimed at aromatic and aliphatic substituents in order to understand the bonding mode and the effects which steric and electronic parameters may have on the crystal packing. It is easier to define the steric and electronic parameters of a phenyl substituent compared to a 13-membered carbazole aromatic ring structure. Added to the fact, that it is nonsensical to spend significant research time synthesizing salicylidene ligands containing complex biological substituents when it was initially uncertain why the ligand could not be coordinated to rhenium(I) metal centre in high yields, in an aqueous medium, as described in Chapter 3. Following the successful crystallization of the *fac*-[Re(Sal)$(CO)_3$(S)] complexes, including three which contained biologically active substituents, several interesting features have been noticed. Seven *fac*-[Re(Sal)$(CO)_3$(**HOCH$_3$**)] complexes containing a coordinated methanol solvent were crystallized. Five of the seven complexes (**11-15**, **22**) are isostructural and crystallize in the *C*2/*c* space group. Four *fac*-[Re(Sal)$(CO)_3$(**NC$_5$H$_5$**)] complexes containing a coordinated pyridine were crystallized. Two of the four complexes (**16**, **17**) crystallize in the $P2_1/c$ space group, while one of the complexes (**19**) crystallizes in the *C*2/*c* space group. There is a significant tendency of the Re(I) salicylidene tricarbonyl complexes to crystallize in the monoclinic space group.

A second interesting feature is the rotation of the substituent, coordinated to the imine N atom, around the C=N double bond. In the crystallographic section describing the structural effects of the crystallized free SalH ligands, the planarity of the salicylidene molecules was

[20] Cambridge Structural Database (CSD), Version 5.32, February 2011 update. F.H. Allen, *Acta Cryst.*, 2002, B58, 380

discussed. The planarity of the free ligands is of interest due to the potential thermochromic and photochromic properties as described in Section 4.1. The imine substituents in the *fac*-[Re(Sal)$(CO)_3$(S)] complexes, all indicated significant ability to rotate around the C=N bond allowing sufficient space for the bidentate ligand to coordinate to the Re(I) metal centre. This illustrates the ability of the ligand to adapt and holds potential for the future coordination of ligands containing large bulky substituents.

The properties of an organometallic complex are determined not only by the nature of the metal centre but also on the steric and electronic demands of the coordinated ligands. A chemical kinetic study on the effects induced by the various substituents is considered an integral part of this study as few reaction kinetic studies have been conducted on Re(I) and Tc(I) tricarbonyl complexes. Furthermore, little attention has been made to the substitution of other coordinated solvents besides water. To further understand the effects which the salicylidene bidentate ligand may have on the solvent substitution reaction, a kinetic study on selected Re(I) tricarbonyl complexes will be discussed in Chapter 9.

8 THEORETICAL STUDY OF NON-COORDINATED SalH LIGANDS AND *fac*-[Re(Sal)(CO)$_3$(S)] COMPLEXES

8.1 INTRODUCTION

Computational chemistry is a technique whereby the chemical properties of a molecule can be investigated by computational software to determine amongst other, molecular geometry, transition states, energies of molecules and chemical reactivity. Several calculation methods exist and can be classified into a few broad classes beginning from the simplest, molecular mechanics to the advanced *ab initio* methods.[1,2,3]

- Molecular mechanics (MM)
- Semi-empirical methods (SE)
- Density functional theory (DFT)
- *Ab initio* calculations

Midway between the classes is the density functional theory (DFT). The calculations are based on electron density function rather than wave function and are known for its reasonable results, accuracy and reasonable computational requirements.

Computational calculations are increasingly being used to understand the behavior of metal ions in coordination and organometallic chemistry.[4,5,6] To compare the factors which determine the crystal structures in the solid state, theoretical structures for both the organic

---

[1] E. Lewars, *Computation Chemistry: Introduction to the theory and applications of molecular and quantum mechanics*, Kluwer Academic, New York, USA, 2004

[2] F. Jensen, *Introduction to Computational Chemistry*, 2nd Ed., John Wiley & Sons Ltd., England, UK, 2007

[3] J.B. Foresman, Æ. Frisch, *Exploring Chemistry with Electronic Structure Methods,* 2nd Ed., Gaussian, Inc. Pittsburgh, PA, USA, 1993

[4] R.D. Adams, B. Captain, C.B. Hollandsworth, M. Johannsson, J.L. Smith Jnr. *Organometallics*, 2006, 25, 3848

[5] K.P. Gable, A. AbuBaker, K. Zientara, A.M. Wainwright, *Organometallics*, 1999, 18, 173

[6] D.V. Partyka, N. Deligonul, M.P. Washington, T.G. Gray, *Organometallics*, 2009, 28, 5837

ligands as well as the coordinated rhenium complexes were optimized and verified to be a global minimum through frequency calculations.

Due to the interest in the various possible conformations which the non-coordinated salicylidene ligands can adopt in the solid state, a computational study of the molecules in the gas phase was conducted to analyze the variation of planarity between the salicylidene backbone and the imine bonded substituent. The rotation of the Schiff-base ligands around the C=N double bond is suspected to influence the photochromic and thermochromic properties of the organic molecules.[7,8] The following non-coordinated SalH ligands were chosen for the theoretical calculations in this section of the study: SalH-*m*Tol, 5Me-SalH-*m*Tol and 5Me-SalH-Carba.

The coordination of the functionalized salicylidene bidentate ligands to the *fac*-$[M(CO)_3]^+$ moiety is one of the research aspects of this study. During the crystallographic study, the flexibility of the coordinated ligands was observed. Similarly, significant rotation of the C=N double bond of the Schiff-base ligand occurred, which allowed for the coordination to the metal centre. To determine the extent to which the orientation of the complexes are influenced by packing effects, computational calculations in the gas phase were conducted on several *fac*-[Re(Sal-T)$(CO)_3$(S)] complexes. The following rhenium coordinated complexes were chosen for the theoretical calculations: *fac*-[Re(Sal-*m*Tol)$(CO)_3$(S)], *fac*-[Re(Sal-Ph)$(CO)_3$(S)] and *fac*-[Re(5Me-Sal-Carba)$(CO)_3$(S)] (S = $HOCH_3$, NC_5H_5).

Only a few salicylidene ligands and corresponding rhenium complexes have been selected to investigate the geometrical comparison between solid state and theoretical structures. The compounds all contain aromatic substituents bonded to the imine N atom, however the size of the substituents differ significantly (*i.e.* 6 member cyclic ring *vs.* 13 member cyclic ring). The theoretical effect induced by the substitution of methanol by pyridine on the 'open third position' of the rhenium tricarbonyl octahedral will be included in the study.

The theoretical optimized structures with the lowest relative energy were compared to the crystal structures of the corresponding non-coordinated free ligand, SalH, as well as the

---

[7] F. Arod, M. Gardon, P. Pattison, G. Chapuis, *Acta Cryst.*, 2005, C61, o317
[8] F. Arod, P. Pattison, K.J. Schenk, G. Chapuis, *Crystal Growth and Design*, 2007, 7, 1679

coordinated *fac*-[Re(Sal-T)$(CO)_3$(S)] complexes. The structural differences between the solid state and the theoretical optimized structures can be graphically represented by overlay diagrams. The structural differences can also be mathematically described by the root mean square (RMS) value, which is a measure of how far the average is from zero, providing information on the variations of bond lengths and angles. The study is based on DFT calculations utilizing the B3LYP/6-311G++(d,p) basis set for the organic ligands and the LanL2DZ for the metal complexes.

8.2 EXPERIMENTAL

The DFT molecular orbital calculations were determined using the Gaussian-03W software package.[9] DFT calculations were done at the B3LYP[10,11] level of theory with the 6-311G++(d,p) basis set[12,13,14] for the main group elements and LanL2DZ[15] for rhenium, using the High Performance Computing Facility of the University of the Free State. Optimized structures were verified as minima through frequency analysis. Molecular graphics were obtained using DIAMOND[16] while graphical representations of overlays were obtained with Hyperchem 7.52.[17]

The crystal structures are denoted with numerical values, for example SalH-*m*Tol, *fac*-[Re(Sal-*m*Tol)$(CO)_3$($HOCH_3$)] or *fac*-[Re(Sal-*m*Tol)$(CO)_3$(NC_5H_5)] are indicated as **L_1**, **Re_1a** or **Re_1b**, where **L**, **R** = ligand or rhenium molecules, **a** = methanol coordinated

---

[9] M.J. Frisch, G.W. Trucks, H.B. Schlegel, G.E. Scuseria, M.A. Robb, J.R. Cheeseman, J.A Montgomery Jr., T. Vreven, K.N. Kudin, J.C. Burant, J.M. Millam, S.S. Iyengar, J. Tomasi, V. Barone, B. Mennucci, M. Cossi, G. Scalmani, N. Rega, G.A. Petersson, H. Nakatsuji, M. Hada, M. Ehara, K. Toyota, R. Fukuda, J. Hasegawa, M. Ishida, T. Nakajima, Y. Honda, O. Kitao, H. Nakai, M. Klene, X. Li, J.E. Knox, H.P. Hratchian, J.B. Cross, V. Bakken, C. Adamo, J. Jaramillo, R. Gomperts, R.E. Stratmann, O. Yazyev, A.J. Austin, R. Cammi, C. Pomelli, J.W. Ochterski, P.Y. Ayala, K. Morokuma, G.A. Voth, P. Salvador, J.J. Dannenberg, V.G. Zakrzewski, S. Dapprich, A.D. Daniels, M.C. Strain, O. Farkas, D.K. Malick, A.D. Rabuck, F. Raghavachari, J.B. Foresman, J.V. Ortiz, Q. Cui, A.G. Baboul, S. Clifford, J. Cioslowski, B.B. Stefanov, G. Liu, A. Liashenko, P. Piskorz, I. Komaromi, R.L. Martin, D.J. Fox, T. Keith, M.A. Al-Laham, C.Y. Peng, A. Nanayakkara, M. Challacombe, P.M.W. Gill, B. Johnson, W. Chen, M.W. Wong, C. Gonzalez, J.A. Pople. *GAUSSIAN-03*, 2004, Revision C.01, Gaussian, Inc., Wallingford, CT

[10] A.D. Becke. *J. Chem. Phys.*, 1993, 98, 5648

[11] C. Lee, W. Yang, R.G. Parr, *Phys. Rev. B*, 1988, 37, 785

[12] P.C. Hariharan, J.A. Pople. *Theoret. Chim. Acta*, 1973, 28, 213

[13] M.M. Francl, W.J. Petro, W.J. Hehre, J.S. Binkley, M.S. Gordon, D.J. DeFrees, J.A. Pople. *J. Chem. Phys.*, 1982, 77, 3654

[14] L.A. Curtiss, P.C. Redfern, K. Raghavachari, *WIREs Comput. Mol. Sci.*, 2011, 1, 810

[15] P.J Hay, W.R. Wadt, *J. Chem. Phys.*, 1985, 82, 299

[16] K. Brandenburg, H. Putz, DIAMOND, Release 3.0c, Crystal Impact GbR, Bonn, Germany, 2005

[17] Hyperchem ^{TM} Release 7.52, Windows Molecular Modeling System, Hypercube, Inc., 2002

complex and **b** = pyridine coordinated complex. The corresponding optimized structures are indicated as **L_1***, **Re_1a*** or **Re_1b*** respectively.

8.3 THEORETICAL CALCULATIONS ON NON-COORDINATED SalH LIGANDS

8.3.1 2-(*m*-Tolyliminomethyl)phenol - SalH-*m*Tol

The non-coordinated free ligand SalH-*m*Tol (**L_1**) (Figure 8.1A) where SalH-*m*Tol = 2-(*m*-tolyliminomethyl)phenol, is compared to the corresponding DFT optimized structure (**L_1***) in Figure 8.1B.

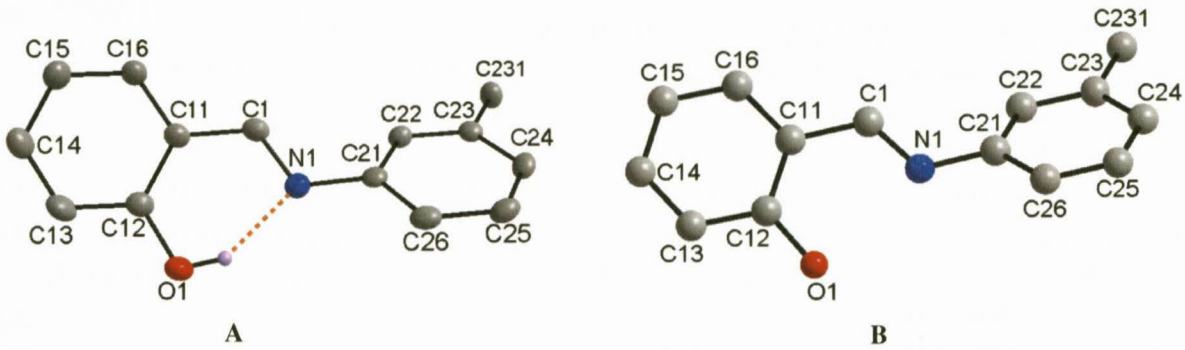

Figure 8.1: **(A) Graphical representation of the crystal structure of SalH-*m*Tol (L_1). Displacement ellipsoids are drawn at 50% probability level. Intramolecular hydrogen bond indicated by orange dotted line. (B) Graphical representation of DFT optimized structure SalH-*m*Tol (L_1*). Hydrogen atoms are omitted for clarity.**

Table 8.1: **Comparison of selected ligand geometrical parameters of crystal structure SalH-*m*Tol (L_1) with the optimized structure L_1* [Å and °].**

	$L\_1_{Crystal}$	L_1*_{DFT}
N1-C1	1.289(3)	1.288
N1-C21	1.426(3)	1.409
N1...O1	2.595(2)	2.635
C1-C11	1.444(3)	1.450
O1-C12	1.355(2)	1.341
C11-C1-N1	121.2(2)	122.5
O1-C12-C11	120.9(1)	121.9
C1-N1-C21	119.5(2)	121.3
O1-C12-C11-N1	3.2(2)	0.16
Dihedral angle between aromatic rings	47.03(8)	39.6

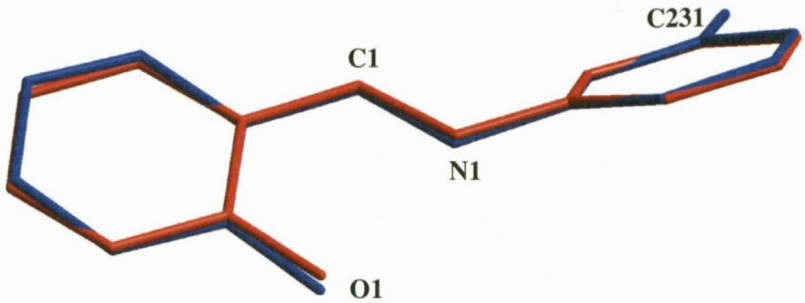

Figure 8.2: **Graphical representation of an overlay of crystal structure (blue) and DFT optimized structure (red) (RMS value = 0.096 Å). Overlay fit excludes all hydrogen atoms.**

The crystal structure and the DFT optimized structure both contain a non-planar orientation with similar rotation around the C=N double bond. The torsion angle (O1-C12-C11-N1) of the crystal structure is greater than for the optimized structure (3.2(2)° *vs.* 0.16°). The intramolecular hydrogen bond interaction causes the N1...O1 bond distance to be shorter for the crystal structure than for the optimized structure which experiences no hydrogen bond in the gas phase. The N1-C21 and O1-C12 bond distances for **L_1** is longer than for the optimized structure and is likely caused by the effects of the intramolecular hydrogen bond. The overlay diagram show good correlation between the theoretical and solid state structure with a RMS value of 0.096 Å.

8.3.2 5-Methyl-2-(*m*-tolyliminomethyl)phenol - 5Me-SalH-*m*Tol

The non-coordinated free ligand 5Me-SalH-*m*Tol (**L_2**) (Figure 8.3A) where 5Me-SalH-*m*Tol = 5-methyl-2-(*m*-tolyliminomethyl)phenol, is compared to the corresponding DFT optimized structure (**L_2***) in Figure 8.3B.

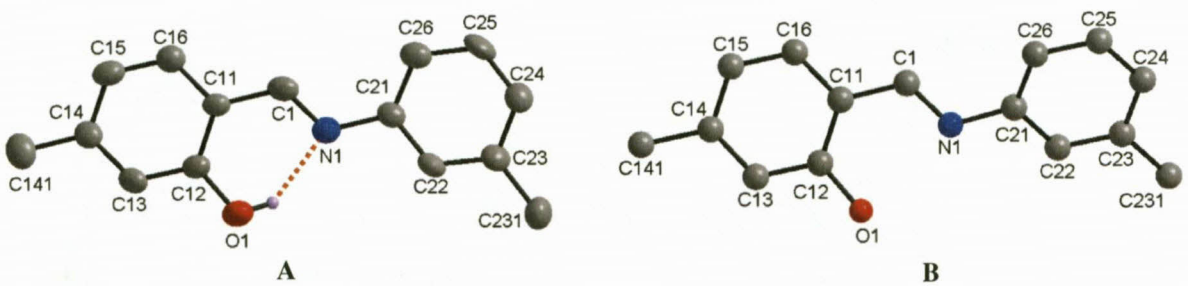

Figure 8.3: **(A) Graphical representation of the crystal structure of 5Me-SalH-*m*Tol (L_2). Displacement ellipsoids are drawn at 50% probability level. (B) Graphical representation of DFT optimized structure 5Me-SalH-*m*Tol (L_2*). Hydrogen atoms are omitted for clarity.**

Table 8.2: **Comparison of selected ligand geometrical parameters of crystal structure 5Me-SalH-*m*Tol (L_2) with the theoretical structure L_2* [Å and °].**

	$L\_2_{Crystal}$	$L\_2^*_{DFT}$
N1-C1	1.282(3)	1.289
N1-C21	1.425(4)	1.341
N1...O1	2.590(3)	2.636
C1-C11	1.451(4)	1.447
O1-C12	1.350(4)	1.341
C11-C1-N1	121.6(4)	122.5
O1-C12-C11	120.9(4)	121.8
C1-N1-C21	122.1(3)	121.2
O1-C12-C11-N1	1.5(3)	0.043
Dihedral angle between aromatic rings	1.8(1)	38.6

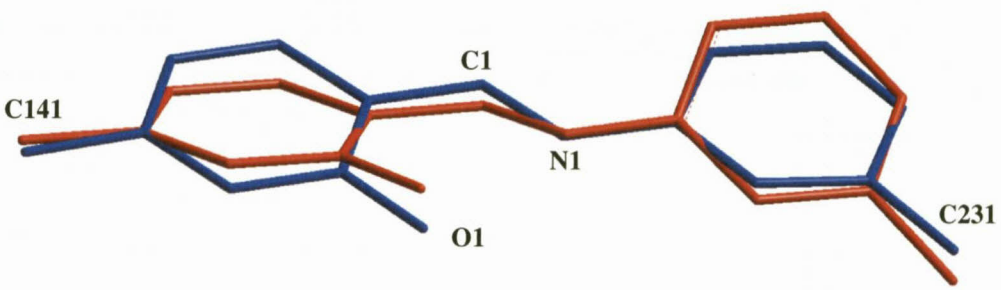

Figure 8.4: **Graphical representation of the overlay of crystal structure (blue) and DFT optimized structure (red) (RMS value = 0.379 Å). Overlay fit excludes all hydrogen atoms.**

The solid state structure is planar with a dihedral angle of 1.8(1)° between the salicylidene C1 aromatic backbone and the *m*-tolyl substituent. The DFT theoretical structure, which has been optimized to a global minimum, is non-planar with a calculated dihedral angle of 38.6°. A reasonable overlay is obtained between the two structures with a RMS value of 0.379 Å. The N...O length of the crystal structure is 0.046 Å shorter than for **L_2*** which is likely caused by the intramolecular hydrogen bond. In general, the bond angles and distances are similar within experimental error.

The crystal structures of both Sal-*m*Tol (**L_1**) and 5Me-Sal-*m*Tol (**L_2**) crystallize in the orthorhombic $P2_12_12_1$ space group and experience no hydrogen bond interactions besides the O1-H...N1 intramolecular interaction (§ 4.3 and 4.4). However, the solid state structures indicate significant differences between the dihedral angle of the aromatic rings (47.03(8)° *vs.* 1.8(1)°). The diffraction data for **L_1** was collected at 100 K where as the data for **L_2** was determined at 298 K. The DFT optimized structures (**L_1*** and **L_2***) for these chemically similar molecules have near identical dihedral angles (39.6° *vs.* 38.6°). It is important to

remember that theoretical optimizations do not take intra- and intermolecular interactions into account when calculating the compounds and therefore would not be influence by crystal packing effects. A X-ray diffraction temperature study would be of considerable interest as a future investigation to determine whether these complexes contain thermochromic properties.

8.3.3 2-(9-Ethylcarbazol-3-yliminomethyl)-5-methylphenol - 5Me-SalH-Carba

The non-coordinated free ligand 5Me-SalH-Carba (**L_3**) (Figure 8.5A) where 5Me-SalH-Carba = 2-(9-ethylcarbazol-3-yliminomethyl)-5-methylphenol, is compared to the corresponding DFT optimized structure (**L_3***) in Figure 8.5B.

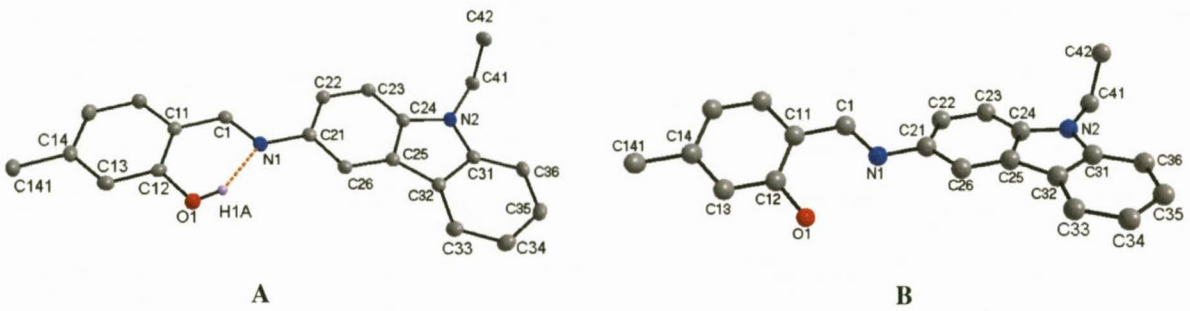

Figure 8.5: **(A) Graphical representation of the crystal structure of 5Me-SalH-Carba (L_3). Displacement ellipsoids are drawn at 50% probability level. Intramolecular hydrogen bond indicated by orange dotted line. (B) Graphical representation of DFT optimized structure 5Me-SalH-Carba (L_3*). Hydrogen atoms are omitted for clarity.**

Table 8.3: **Comparison of selected ligand geometrical parameters of crystal structure 5Me-SalH-Carba (L_3) with the optimized structure L_3* [Å and °].**

	$L\_3_{Crystal}$	$L\_3^*_{DFT}$
N1-C1	1.290(2)	1.289
N1-C21	1.422(2)	1.409
N1...O1	2.607(2)	2.634
C1-C11	1.453(2)	1.449
O1-C12	1.355(2)	1.342
C11-C1-N1	121.2(1)	122.4
O1-C12-C11	121.7(1)	121.7
C1-N1-C21	122.6(1)	122.0
O1-C12-C11-N1	3.1(2)	0.122
Dihedral angle between aromatic rings	4.37(4)	32.5

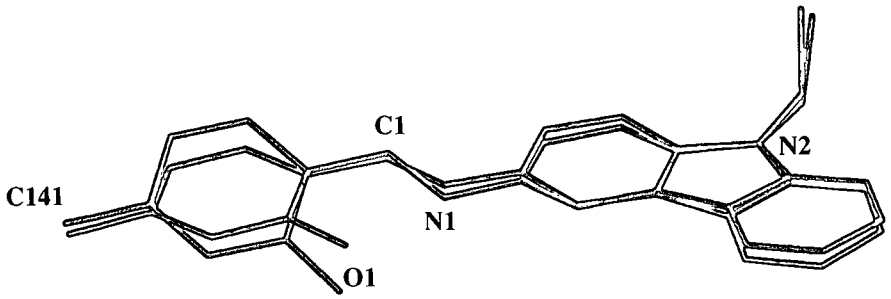

Figure 8.6: **Graphical representation of the overlay of crystal structure (blue) and DFT optimized structure (red) (RMS value = 0.372 Å). Overlay fit excludes all hydrogen atoms.**

The organic ligand consists of a carbazole substituent, a thirteen member aromatic ring system, which is coordinated to the imine nitrogen atom of the salicylidene backbone. The crystal structure of **L_3** (diffraction data acquired at 100 K) crystallises in the same space group as **L_1** and **L_2** namely $P2_12_12_1$. The crystal structure of **L_3** is essential planar with a dihedral angle of 4.37(4)° between the aromatic systems of the salicylidene ligand, compared to the non-planar DFT optimized structure (**L_3***) with a dihedral angle of 32.5°. A reasonable overlay is obtained between the two structures with a RMS value of 0.372 Å. The N...O length of the crystal structure is 0.027 Å shorter than for **L_3*** which is likely caused by the intramolecular hydrogen bond. The crystal structure of **L_3** experiences π-π interaction as well as intermolecular hydrogen bonding by the ethyl moiety on the carbazole substituent. The various packing effects and atomic interactions may explain the orientation of the coordinated substituent relative to the optimized structure. In general, the bond angles and distances are similar within experimental error.

8.4 THEORETICAL CALCULATIONS ON *fac*-[Re(Sal-T)(CO)$_3$(S)] COMPLEXES

8.4.1 *fac*-[Re(Sal-*m*Tol)(CO)$_3$(HOCH$_3$)]

The coordinated rhenium complex, *fac*-[Re(Sal-*m*Tol)(CO)$_3$(HOCH$_3$)] (**Re_1a**) (Figure 8.7A) where Sal-*m*Tol = 2-(*m*-tolyliminomethyl)phenolato is compared to the corresponding DFT optimized structure (**Re_1a***) in Figure 8.7B.

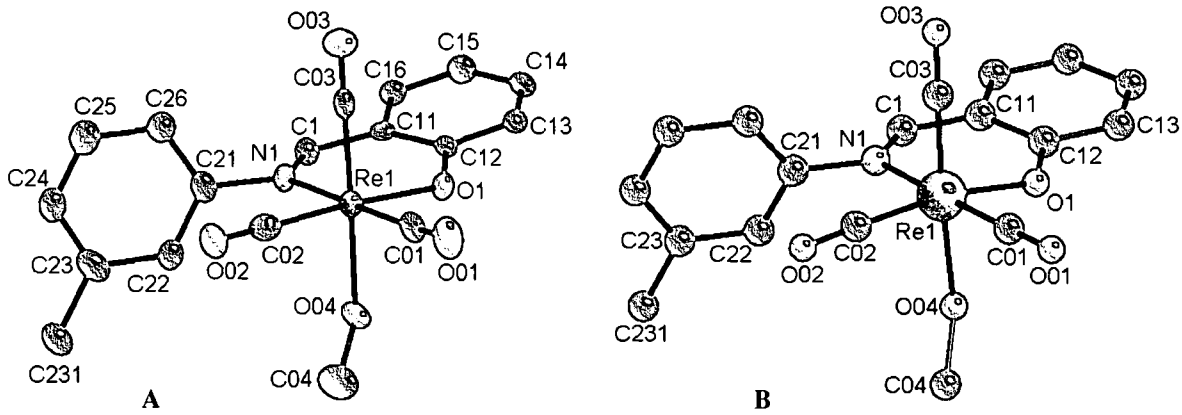

Figure 8.7: **(A) Graphical representation of the crystal structure of *fac*-[Re(Sal-*m*Tol)(CO)$_3$(HOCH$_3$)] (Re_1a). Displacement ellipsoids are drawn at 50% probability level. (B) Graphical representation of DFT optimized structure *fac*-[Re(Sal-*m*Tol)(CO)$_3$(HOCH$_3$)] (Re_1a*). Hydrogen atoms are omitted for clarity.**

Table 8.4: **Comparison of selected geometrical parameters of crystal structure *fac*-[Re(Sal-*m*Tol)(CO)$_3$(HOCH$_3$)] (Re_1) with the optimized structure Re_1* [Å and °].**

	Re_1a $_{Crystal}$	**Re_1a*$_{DFT}$**
Re1-N1	2.157(4)	2.181
Re1-O1	2.119(3)	2.121
Re1-O04	2.179(3)	2.245
N1-C1	1.290(6)	1.321
N1-C21	1.456(6)	1.459
N1...O1	2.878(6)	2.878
C1-C11	1.449(7)	1.444
O1-C12	1.339(6)	1.344
N1-Re1-O1	84.6(1)	84.0
Re1-O04-C04	122.1(4)	127.1
O04-Re1-C03	175.4(2)	172.1
C11-C1-N1	126.4(5)	128.4
O1-C12-C11	122.7(4)	122.7
C1-N1-C21	115.7(4)	115.4
O1-C12-C11-N1	8.6(6)	4.2
Dihedral angle between aromatic rings	81.9(2)	82.3

The optimized structure of **Re_1a*** adopted a distorted octahedral geometry similar to the corresponding crystal structure with a N1-Re1-O1 bite angle of 84.0° *vs.* 84.6(1)° and a O04-Re1-C03 bond angle of 172.1° *vs.* 175.4(2)°. The coordinated methanol ligand has a greater bond angle in the optimized structure relative to the solid state structure with a Re1-O04-C04 bond angle of 127.1° *vs.* 122.1(4)°. The difference is likely due to the two intermolecular hydrogen bonding experienced by both the O04 and C04 atoms in the solid state structure

between neighbouring molecules (§ 6.3). Slightly longer bond lengths are predicted for the optimized **Re_1a*** structure in comparison to the corresponding bond lengths of the crystal structure (Table 8.4).

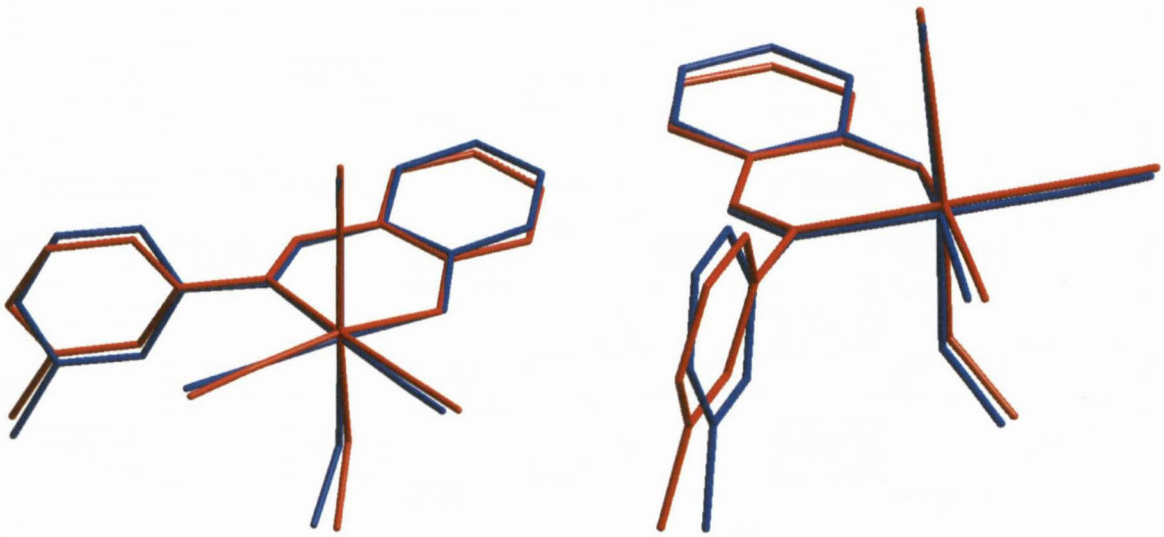

Figure 8.8: **Two perspectives for the overlay of crystal structure (blue) and DFT optimized structure (red) (RMS value = 0.275 Å). Overlay fit excludes all hydrogen atoms.**

The visual comparison of the two structures yields a reasonable overlay with a RMS value of 0.275 Å. Slight deviation is observed in the orientation of the salicylidene C1 aromatic backbone with the crystal structure tilted upwards above the optimized structure (O1-C12-C11-N1 torsion angle of 4.2° *vs.* 8.6(6)°). The rotation of the two aromatic rings (C1 backbone relative to the *m*-tolyl substituent) is similar within experimental error 82.3° *vs.* 81.9(2)°.

8.4.2 *fac*-[Re(Sal-Ph)(CO)$_3$(S)]

The coordinated rhenium complexes, *fac*-[Re(Sal-Ph)(CO)$_3$(HOCH$_3$)] (**Re_2a**) (Figure 8.9A) where Sal-Ph = 2-(phenyliminomethyl)phenolato is compared to the corresponding DFT optimized structure (**Re_2a***) in Figure 8.9B.

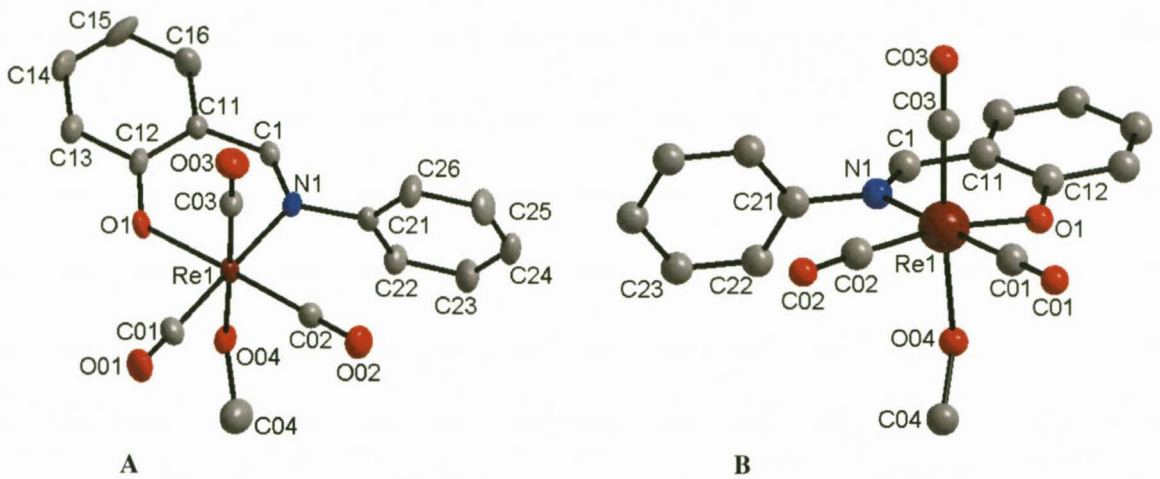

Figure 8.9: **(A) Graphical representation of the crystal structure of *fac*-[Re(Sal-Ph)$(CO)_3(HOCH_3)$] (Re_2a) (crystal structure inverted). Displacement ellipsoids are drawn at 50% probability level. (B) Graphical representation of DFT optimized structure *fac*-[Re(Sal-Ph)$(CO)_3(HOCH_3)$] (Re_2a*). Hydrogen atoms are omitted for clarity.**

For the sake of comparison, the pyridine substituted rhenium complexes, *fac*-[Re(Sal-Ph)$(CO)_3(NC_5H_5)$] (**Re_2b**) (Figure 8.10A) (NC_5H_5 = pyridine) is compared to the corresponding DFT optimized structure (**Re_2b***) in Figure 8.10B.

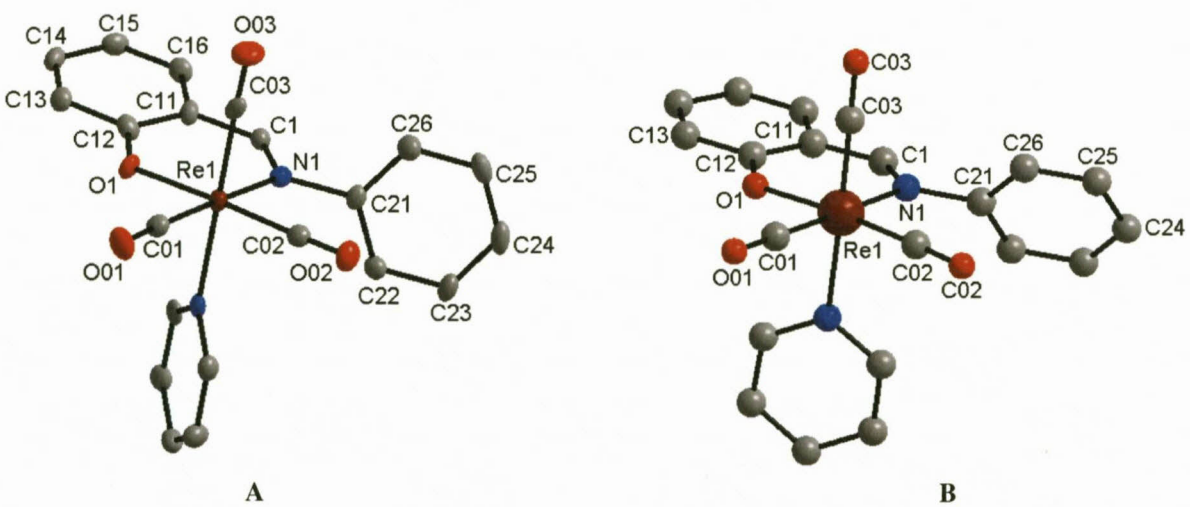

Figure 8.10: **(A) Graphical representation of the crystal structure of *fac*-[Re(Sal-Ph)$(CO)_3(NC_5H_5)$] (Re_2b). Displacement ellipsoids are drawn at 50% probability level. (B) Graphical representation of DFT optimized structure *fac*-[Re(Sal-Ph)$(CO)_3(NC_5H_5)$] (Re_2b*). Hydrogen atoms are omitted for clarity.**

Table 8.5: **Comparison of selected geometrical parameters of crystal structure *fac*-[Re(Sal-Ph)(CO)$_3$(HOCH$_3$)] (Re_2a) and *fac*-[Re(Sal-Ph)(CO)$_3$(NC$_5$H$_5$)] (Re_2b) with the optimized structures of Re_2a* and Re_2b* [Å and °].**

	Re_2a $_{Crystal}$	Re_2a*$_{DFT}$	Re_2b $_{Crystal}$	Re_2b*$_{DFT}$
Re1-N1	2.164(6)	2.183	2.152(5)	2.197
Re1-O1	2.121(5)	2.119	2.114(3)	2.121
Re1-O04 / N_{py}	2.188(5)	2.245	2.207(5)	2.238
N1-C1	1.288(9)	1.322	1.298(7)	1.326
N1-C21	1.459(8)	1.457	1.448(7)	1.455
N1...O1	2.878(9)	2.878	2.870(5)	2.923
C1-C11	1.460(9)	1.443	1.428(7)	1.439
O1-C12	1.326(8)	1.343	1.302(6)	1.331
N1-Re1-O1	84.4(2)	84.0	84.5(2)	85.2
Re1-O04-C04	121.2(5)	127.5	-	-
C03-Re1-O04 / N_{py}	174.9(3)	172.1	178.4(2)	175.9
C11-C1-N1	126.1(6)	128.4	126.4(5)	129.2
O1-C12-C11	124.3(6)	122.6	124.5(5)	123.4
C1-N1-C21	115.6(6)	115.3	114.4(5)	115.0
O1-C12-C11-N1	9.6(8)	4.1	1.3(6)	2.5
Dihedral angle between salicylidene aromatic rings	88.5(3)	80.0	75.1(2)	64.9

O04 = oxygen atom of coordinated methanol; N_{py} = nitrogen atom of coordinated pyridine

The DFT optimized structure of **Re_2a*** has a distorted octahedral geometry around the rhenium metal centre similar to the solid state structure **Re_2a**. The N1-Re1-O1 bite angles are identical within experimental error. The bond distance to the coordinated methanol ligand is significantly shorter in the solid state relative to the optimized structure with a Re1-O04 bond distance of 2.188(5) Å for **Re_2a** *vs.* 2.245 Å. The Re1-O04-C04 bond angle for the solid state structure is less than for the optimized structure 121.2(5)° *vs.* 127.5°. In general the bond lengths and angles compare well for the corresponding **Re_2a** and **Re_2a*** structures.

The DFT optimized structure of the pyridine coordinated complex, **Re_2b***, has a similar distorted octahedral geometry to the **Re_2b** complex. The N1-Re1-O1 bite angle of the four structures **Re_2a**, **Re_2a***, **Re_2b** and **Re_2b*** are the same within experimental error. The bond lengths in Table 8.5 reveals longer bond lengths for the optimized **Re_2b*** complex in comparison with the corresponding lengths of the **Re_2b** crystal structure. The dihedral angle between the C1 aromatic backbone and the phenyl substituent is larger for both the solid state structures relative to the theoretical analogues. The difference between the dihedral angle is 8.5° for the methanol complexes and 10.2° for the pyridine complexes.

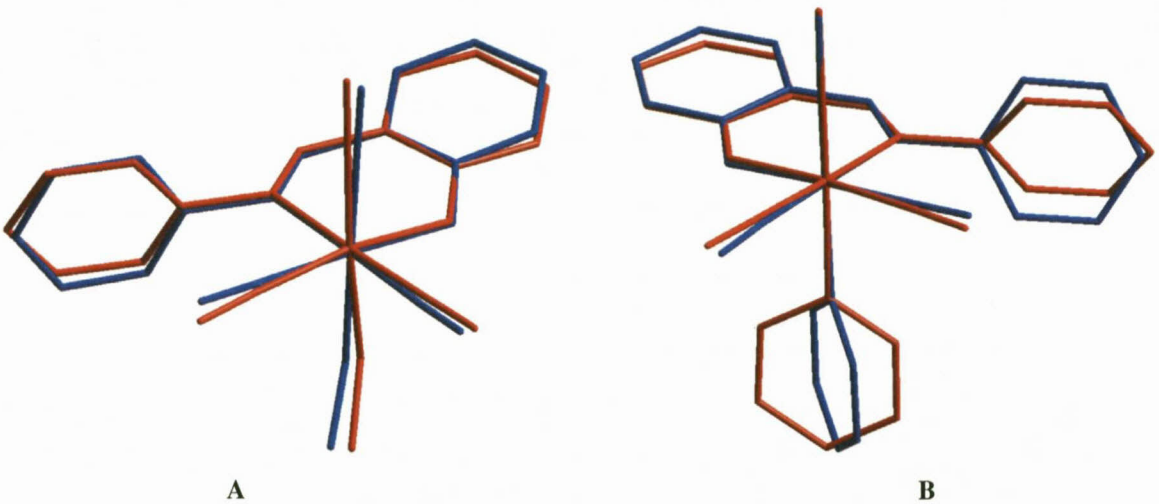

A B

Figure 8.11: **Graphical representation of the overlay of crystal structure (blue) and DFT optimized structure (red). (A) Overlay of Re_2a *vs.* Re_2a* (RMS value = 0.210 Å). (B) Overlay of Re_2b vs. Re_2b* (RMS value = 0.544 Å). Overlay fit excludes all hydrogen atoms.**

The visual comparison between the crystal and optimized structure is seen in Figure 8.11. A reasonable overlay for the methanol complex **Re_2a** and **Re_2a*** was obtained with an RMS value of 0.210 Å. The overlay for the pyridine complex **Re_2b** and **Re_2b*** shows significant deviation in the orientation of the coordinated pyridine ligand and the phenyl substituent yielding an RMS value of 0.544 Å.

8.4.3 *fac*-[Re(5Me-Sal-Carba)(CO)$_3$(S)]

The coordinated rhenium complex, *fac*-[Re(5Me-Sal-Carba)(CO)$_3$(NC_5H_5)] (**Re_3b**) (Figure 8.12A) where 5Me-Sal-Carba = 2-(9-ethylcarbazol-3-yliminomethyl)-5-methylphenolato, is compared to the corresponding DFT optimized structure (**Re_3b***) in Figure 8.12B. The crystal structure of the methanol coordinated complex *fac*-[Re(5Me-Sal-Carba)(CO)$_3$(**HOCH$_3$**)] could not be obtained. In order to observe any geometrical trends within the complexes, the DFT optimized structure (**Re_3a***) was determined and is included for the sake of comparison.

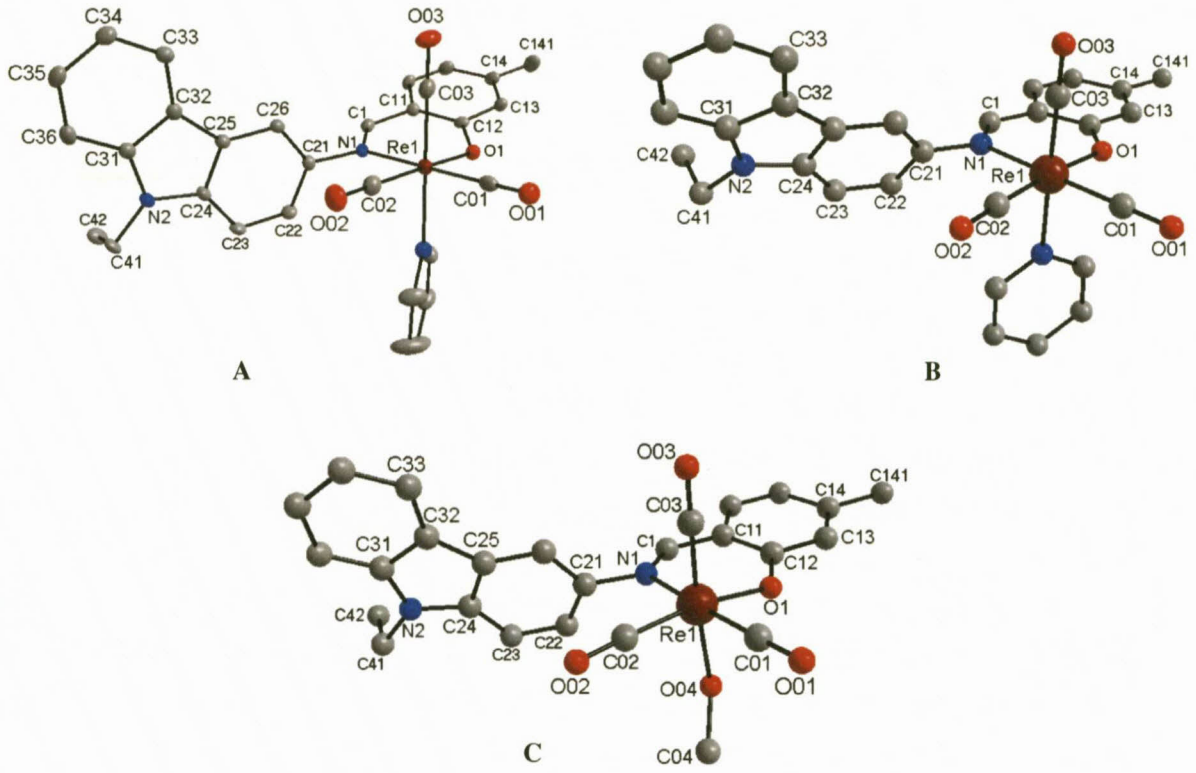

Figure 8.12: **(A) Graphical representation of the crystal structure of *fac*-[Re(5Me-Sal-Carba)$(CO)_3(NC_5H_5)$] (Re_3b). Displacement ellipsoids are drawn at 50% probability level. (B) DFT optimized structure of *fac*-[Re(5Me-Sal-Carba)$(CO)_3(NC_5H_5)$] (Re_3b*). (C) DFT optimized structure of *fac*-[Re(5Me-Sal-Carba)$(CO)_3(HOCH_3)$] (Re_3a*). Hydrogen atoms are omitted for clarity.**

Table 8.6: **Comparison of selected geometrical parameters of crystal structure *fac*-[Re(5Me-Sal-Carba)$(CO)_3(NC_5H_5)$] (Re_3b) with the DFT structures of Re_3b* and Re_3a* [Å and °].**

	Re_3b $_{Crystal}$	Re_3b*$_{DFT}$	Re_3a*$_{DFT}$
Re1-N1	2.171(2)	2.195	2.182
Re1-O1	2.107(2)	2.122	2.122
Re1-O04 / N_{py}	2.222(3)	2.237	2.247
N1-C1	1.289(4)	1.326	1.322
N1-C21	1.448(3)	1.458	1.460
N1...O1	2.849(3)	2.931	2.883
C1-C11	1.436(4)	1.438	1.442
O1-C12	1.315(3)	1.332	1.345
N1-Re1-O1	83.49(9)	85.5	84.1
Re1-O04-C04	-	-	126.7
C03-Re1-O04 / N_{py}	173.6(1)	176.2	172.1
C11-C1-N1	126.2(3)	129.2	128.5
O1-C12-C11	124.3(2)	123.3	122.5
C1-N1-C21	116.8(2)	115.0	115.3
O1-C12-C11-N1	4.6(3)	2.7	4.3
Dihedral angle between salicylidene aromatic rings	78.56(7)	65.2	80.3

O04 = oxygen atom of coordinated methanol; N_{py} = nitrogen atom of coordinated pyridine

The DFT optimized structures of **Re_3a*** (methanol complex) and **Re_3b*** (pyridine complex) has a distorted octahedral geometry around the rhenium metal similar to the solid state structure **Re_3b**. The N1-Re1-O1 bite angle of **Re_3b**, **Re_3b*** and **Re_3a*** are similar. In general the bond lengths and angles compare well for the corresponding **Re_3b** and **Re_3b*** structures with the solid state structure containing shorter bond lengths.

The visual comparison between the crystal and optimized structure is seen in Figure 8.13. The overlay of the pyridine complex **Re_3b** and **Re_3b*** indicate poor correlation between the DFT optimized structure and its crystallographic counterpart with an RMS value of 0.864 Å. The orientation of the pyridine ring, carbazole substituent and salicylidene backbone of the crystal structure show significant deviation from the DFT optimized structure.

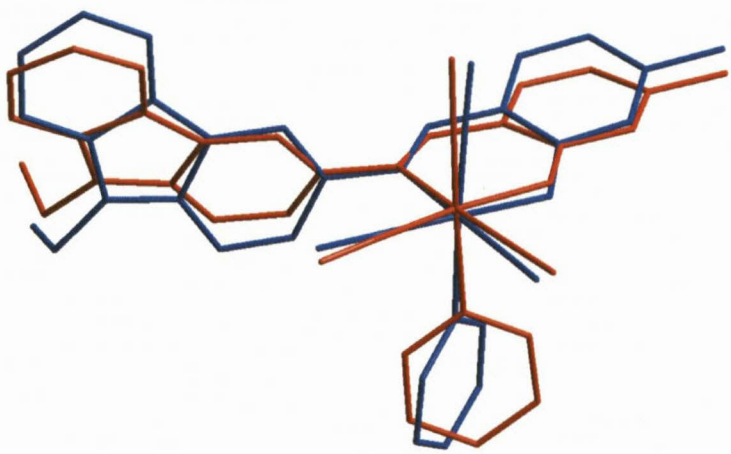

Figure 8.13: **Graphical representation of the overlay of crystal structure Re_3b (blue) and DFT optimized structure Re_3b* (red) (RMS value = 0.864 Å). Overlay fit excludes all hydrogen atoms.**

8.5 CONCLUSION

The structures of various aromatic salicylidene ligands, SalH, and rhenium tricarbonyl complexes *fac*-[Re(Sal-T)$(CO)_3$(S)] (T = aromatic substituent, S = methanol or pyridine) were successfully calculated and optimized.

The optimized bond lengths and angles of the non-coordinated ligands as well as the coordinated rhenium tricarbonyl complexes compare well to the corresponding crystal structures as indicated in the tables below. In general the N1=C1 bond lengths for the

optimized ligands are nearly identical, differing only in the third decimal value. Similarly for the tabulated bond angles (Table 8.7 and 8.8). The N1...O1 distance of the crystallized structures is significantly shorter than the optimized structures due to the intramolecular hydrogen bond. The dihedral angle between the C1 backbone and the aromatic substituent, bonded to the imine N atom, range between 32.5° and 39.6° for the optimized structures. The dihedral angle for the corresponding crystal structures has a significant wider range from 1.8° to 47.0° (Table 8.8).

Table 8.7: **Selected bond lengths for optimized and crystallographic structures of the non-coordinated SalH-T ligand (Å).**

Bond length SalH-T	N1-C1 (Crystal)	N1-C1 (DFT)	N1...O1 (Crystal)	N1...O1 (DFT)	O1-C12 (Crystal)	O1-C12 (DFT)
SalH-*m*Tol	1.289(3)	1.288	2.595(2)	2.635	1.355(2)	1.341
5Me-SalH-*m*Tol	1.282(3)	1.289	2.590(3)	2.636	1.350(4)	1.341
5Me-SalH-Carba	1.290(2)	1.289	2.607(2)	2.634	1.355(2)	1.342

Table 8.8: **Selected bond angles for optimized and crystallographic structures of the non-coordinated SalH-T ligand (°).**

Bond angle SalH-T	C11-C1-N1 (Crystal)	C11-C1-N1 (DFT)	C1-N1-C21 (Crystal)	C1-N1-C21 (DFT)	Dihedral angle (Crystal)	Dihedral angle (DFT)
SalH-*m*Tol	121.2(2)	122.5	119.5(2)	121.3	47.03(8)	39.6
5Me-SalH-*m*Tol	121.6(4)	122.5	122.1(3)	121.2	1.8(1)	38.6
5Me-SalH-Carba	121.2(1)	122.4	122.6(1)	122.0	4.37(4)	32.5

The variations between the optimized rhenium tricarbonyl complexes and the crystallographic structures are summarised in Table 8.9 and 8.10. The Re1-N1 bond length is approximate ~2.182 Å for all three optimized rhenium complexes consisting of a coordinated methanol ligand. The optimized pyridine coordinated complexes have a longer average Re1-N1 bond length of 2.196 Å. Despite the theoretical tendency for the Re1-N1 bond length to increase with the substitution of methanol for pyridine, the crystallographic bond length for **Re_2a** and **Re_2b** decreases from 2.164(6) Å to 2.152(5) Å. The optimized bond length of Re1-O1 has a small range between 2.119 Å – 2.122 Å for both methanol and pyridine coordinated complexes. However the equivalent crystallographic Re1-O1 bond lengths range between 2.107(2) Å – 2.121(5) Å. The optimized bond angles for the rhenium complexes approximate closely to the crystallographic determined values. The dihedral angle between the C1 backbone and the aromatic substituent, for the optimized structures, range between

80.0° - 82.3° (methanol complexes) and 64.9° - 65.2° (pyridine structures). The dihedral angle of the crystallographic complex *fac*-[Re(Sal-Ph)$(CO)_3$(S)] follows a similar decrease in value from 88.5(3)° to 75.1(2)° for complexes **Re_2a** to **Re_2b**.

Table 8.9: **Selected bond lengths for optimized and crystallographic structures of the *fac*-[Re(Sal-T)$(CO)_3$(S)] complexes (Å).**

Bond length		Re1-N1	Re1-N1	Re1-O1	Re1-O1	Re-O04/N_{Py}	Re-O04/N_{Py}
Sal-T	S	(Crystal)	(DFT)	(Crystal)	(DFT)	(Crystal)	(DFT)
Sal-*m*Tol	$HOCH_3$	2.157(4)	2.181	2.119(3)	2.121	2.179(3)	2.245
Sal-Ph	$HOCH_3$	2.164(6)	2.183	2.121(5)	2.119	2.188(5)	2.245
5Me-Sal-Carba	$HOCH_3$	-	2.182	-	2.122	-	2.247
Sal-Ph	NC_5H_5	2.152(5)	2.197	2.114(3)	2.121	2.207(5)	2.238
5Me-Sal-Carba	NC_5H_5	2.171(2)	2.195	2.107(2)	2.122	2.222(3)	2.237

O04 = oxygen atom of coordinated methanol; N_{py} = nitrogen atom of coordinated pyridine

Table 8.10: **Selected bond angles for optimized and crystallographic structures of the *fac*-[Re(Sal-T)$(CO)_3$(S)] complexes (°).**

Bond angle		N1-Re1-O1	N1-Re1-O1	C03-Re1-O04/N_{Py}	C03-Re1-O04/N_{Py}	Dihedral angle	Dihedral angle
Sal-T	S	(Crystal)	(DFT)	(Crystal)	(DFT)	(Crystal)	(DFT)
Sal-*m*Tol	$HOCH_3$	84.6(1)	84.0	175.4(2)	172.1	81.9(2)	82.3
Sal-Ph	$HOCH_3$	84.4(2)	84.0	174.9(3)	172.1	88.5(3)	80.0
5Me-Sal-Carba	$HOCH_3$	-	84.1	-	172.1	-	80.3
Sal-Ph	NC_5H_5	84.5(2)	85.2	178.4(2)	175.9	75.1(2)	64.9
5Me-Sal-Carba	NC_5H_5	83.49(9)	85.5	173.6(1)	176.2	78.56(7)	65.2

O04 = oxygen atom of coordinated methanol; N_{py} = nitrogen atom of coordinated pyridine

Overlay diagrams of the theoretical molecules with their experimental solid state counterparts have provided a visual means to compare the structures. Reasonable overlay diagrams and RMS values were obtained for the ligand compounds as well as for methanol coordinated rhenium complexes. However, the DFT optimized structures for the pyridine coordinated rhenium complexes, indicate a poorer correlation relative to the crystallographic counterpart.[18]

A better approximation to determine the possible orientation of the crystalline pyridine coordinated complex may be found by utilizing the DFT optimized structure of the methanol complex. The overlay diagrams which compares the crystallographic pyridine complex with

[18] A. Brink, H.G. Visser, A. Roodt, *J. Coord. Chem.*, 2011, 64, 122

the DFT methanol complex yields reasonable RMS values, as illustrated in Figures 8.14 and 8.15 below.

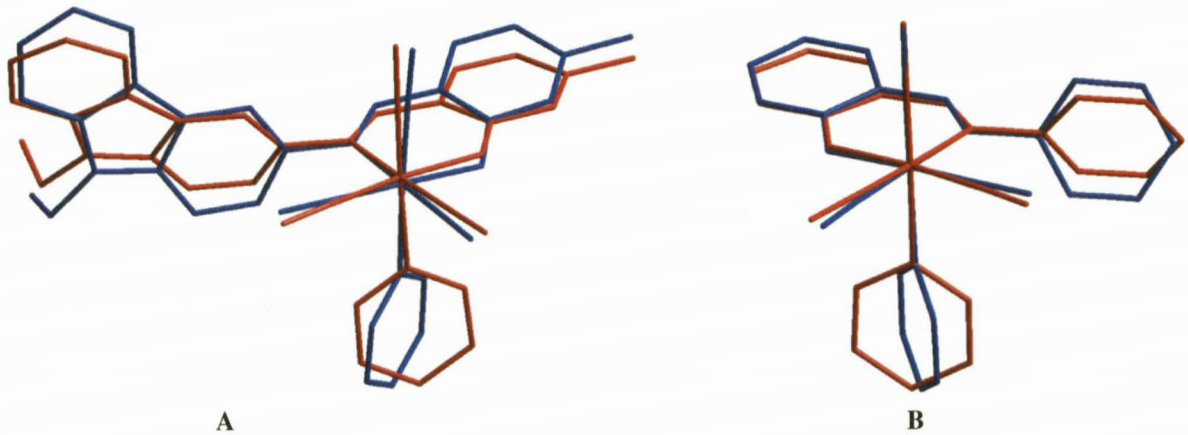

A B

Figure 8.14: **Graphical representation of the overlay of *pyridine* coordinated crystal structure (blue) and *pyridine* coordinated DFT optimized structure (red). (A) Overlay of Re_3b *vs.* Re_3b* (RMS value = 0.864 Å). (B) Overlay of Re_2b *vs.* Re_2b* (RMS value = 0.544 Å). Overlay fit excludes all hydrogen atoms.**

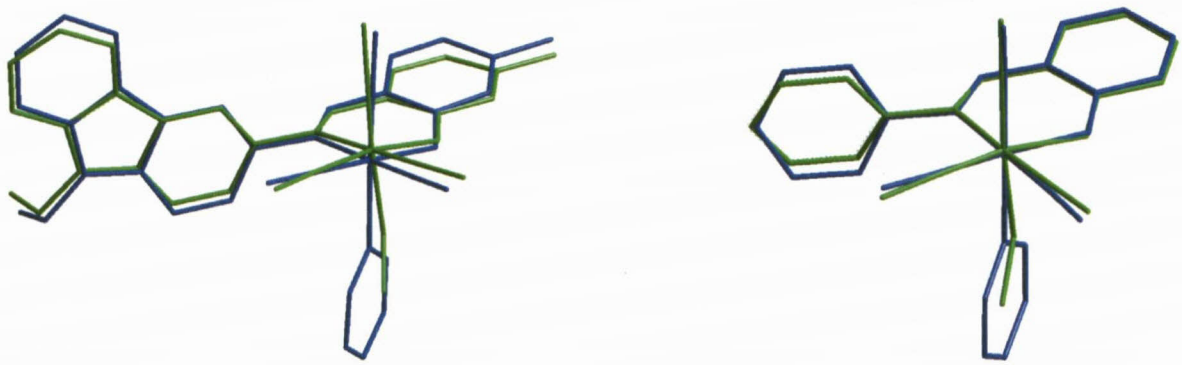

A B

Figure 8.15: **Graphical representation of the overlay of *pyridine* coordinated crystal structure (blue) and *methanol* coordinated DFT optimized structure (green). (A) Overlay of Re_3b *vs.* Re_3a* (RMS value = 0.362 Å). (B) Overlay of Re_2b (crystal structure inverted) *vs.* Re_2a* (RMS value = 0.244 Å). Overlay fit excludes all hydrogen atoms.**

Although the structural conformations in the crystal and DFT optimized structures are similar, some deviations between the corresponding DFT/solid state structures have been found. The differences between the crystallographic data and the corresponding DFT optimized structures illustrate the net impact of packing effects and intermolecular bonds on the geometrical parameters of the solid state structures. However the DFT approximations are reasonable and can be utilized if the coordination mode of a specific complex is required but which cannot be crystallized for some reason or other.

9 METHANOL SUBSTITUTION KINETIC STUDY OF *fac*-[Re(Sal)(CO)$_3$(S)] COMPLEXES

9.1 INTRODUCTION

Chemical kinetics focuses on the observed characteristics of a chemical reaction, the manner in which a specific system changes from one state to another and the time required for the transition. Kinetics considers all the factors which may affect the reaction rate, as well as how the rate can be described by a reaction mechanism.[1] Various factors such as concentration, temperature and pressure variations, sensitivity to light, water and air *etc.*, can affect the reaction mechanism and rate. Importantly, it must be remembered that chemical kinetics only reflects a statistical average state of the molecules participating in the chemical reaction.[2] In order to make a useful interpretation of a reaction study, the system can be simplified by using a closed constant-volume, isothermal or isobaric system. The chemical reaction rate[3] is now defined as the rate of change with time of the concentration of any of the reactants or products.

To ensure the development of methods by which radionuclides (^{99m}Tc, $^{186/188}$Re) can be included into useful radiopharmaceuticals, a knowledge of kinetics and reaction mechanisms of *fac*-[M(CO)$_3$(S)$_3$]$^{n+}$ (S = coordinated solvent ligands) should be explored in order to characterize the complexes and understand the factors which may affect biodistribution.[4] Few reaction kinetic studies have been conducted on Re(I) and Tc(I) tricarbonyl complexes,[5,6,7,8,9] as previously discussed in Chapter 2. A detailed kinetic study investigated the water

---

[1] K.A. Connors, *Chemical Kinetics: The Study of Reaction Rates Solution*, VCH Publishers, New York, 1990
[2] J.W. Moore, R.G. Pearson, *Kinetics and Mechanism*, 3rd Ed., John Wiley & Sons, Inc., New York, 1981
[3] G.G. Hammes, *Principles of Chemical Kinetics*, Academic Press, Inc., New York, 1978
[4] A. Roodt, A. Abou-Hamdan, H.P. Engelbrecht, A.E. Merbach, *Advances in Inorganic Chemistry*, 2000, 49, 59
[5] B. Salignac, P.V. Grundler, S. Cayemittes, U. Frey, R. Scopelliti, A.E. Merbach, *Inorg. Chem.*, 2003, 42, 3516
[6] L. Helm, *Coord. Chem. Rev.*, 2008, 252, 2346
[7] R. Alberto, R. Schibli, R. Waibel, U. Abram, A.P. Schubiger, *Coord. Chem. Rev.*, 1999, 192, 901
[8] G. Kemp, *Ph.D. Thesis*, University of Johannesburg, Johannesburg, South Africa, 2006
[9] M. Schutte, *M.Sc. Dissertation*, University of the Free State, Bloemfontein, South Africa, 2008

exchange[5,6] of *fac*-$[Re(CO)_3(H_2O)_3]^+$ (k_{ex} = 6.3(1) x 10^{-3} s^{-1}) as well as the monohydroxo species $[Re(CO)_3(OH)(H_2O)_2]$ (k_{OH} = 27(1) s^{-1}). Activation parameters for the water exchange process indicate a dissociative interchange mechanism ($\Delta H^{\neq}$ = 90(3) kJ mol^{-1}, $\Delta S^{\neq}$ = 14(10) J.K.mol^{-1}). The activation parameters for the water substitution reactions[5,6,10,11] of *fac*-$[Re(CO)_3(H_2O)_3]^+$ indicate a mechanism change-over from I_d for the harder ligands to I_a for softer ligands, such as dimethylsulfide (DMS) and tetrahydrothiophene (THT) which are better nucleophiles. The substitution reaction of *fac*-$[Re(L,L'\text{-Bid})(CO)_3(H_2O)]^{n+}$ (L,L'-Bid = N-O, N-N', O-O' bidentate ligands, n = -1, 0, +1) have been investigated[8,9] whereby the bidentate ligand blocks two of the reactive water sites, leaving the third site open for substitution. Both studies indicate that substitution occurs *via* an associative type mechanism. The reactivity effects introduced by the various bidentate ligands on the rhenium metal centre were of prime interest. An interesting complex studied by Schutte,[9] *fac*-$[Re(Flav)(CO)_3(H_2O)]$ (Flav = anion of 3-hydroxyflavone) whereby the biological active ligand is coordinated directly onto the metal centre, underwent aqua substitution reactions with DMAP, nearly 150 times faster than an analogous O-O' bidentate Re complex. Whether this is due to the close proximity of the biological ligand to the metal centre or the internal properties of the ligand itself will lead to attractive future investigations.

A chemical kinetic study on the effects induced by various donor bidentate ligands on the rhenium metal centre is considered an integral part of this study, as the properties of an organometallic complex is determined not only by the nature of the metal centre but also on the steric and electronic demands of the coordinated ligands. Little attention thus far has been paid to the substitution of other coordinated solvents besides water. The possibility of various solvents that may increase the stability of the rhenium complexes or have greater lability and be substituted more rapidly than aqua ligands holds potential for future drug design as these *fac*-$[M(CO)_3(S)_3]^{n+}$ may react differently than the aqua substituted complexes and therefore could be an interesting prospect for future kit design in radiopharmacy. This study deals with a kinetic investigation of the reaction between *fac*-$[Re(L,L'\text{-Bid})(CO)_3(S)]$ and various entering monodentate ligands, to examine the mechanism under controlled chemical environments.

---

[10] P.V. Grundler, L. Helm, R. Alberto, A.E. Merbach, *Inorg. Chem.*, 2006, 45, 10378
[11] P.V. Grundler, B. Salignac, S. Cayemittes, R. Alberto, A.E. Merbach, *Inorg. Chem.*, 2004, 43, 865

9.2 REAGENTS AND EQUIPMENT

All reagents and chemicals were of analytical grade. All organic solvents were freshly dried and distilled before use. The pyridine reagents were dried according to literature procedures over CaH_2.[12,13] Initial kinetic measurements were performed on a Varian Cary 50 Conc UV-Visible Spectrophotometer, equipped with a Julabo F12-mV temperature cell regulator (accurate within 0.1 °C) in a 1.000 ± 0.001 cm quartz cuvette cell. Fast kinetic reactions were performed on a Hi-Tech SF-61DX2 Stopped-flow instrument equipped with a Julabo F12-mV temperature regulator. The dead time of the mixing unit is estimated to be less than 2.0 ms. The Stopped-flow instrument is a multiple wavelength apparatus in the Diode-Array mode in which the initial reactions were collected in order to find the appropriate wavelength of the absorbance change. After the specific wavelength was selected, the Stopped-flow system was changed to the more sensitive Photo-Multiplier setup in order to study the kinetic reactions. The Hi-Tech Stopped-flow instrument is Microsoft Windows operated with Kinet Asyst Stopped-Flow Kinetic Studio software[14] for the acquisition and analysis of kinetic data. All kinetic measurements were performed under pseudo first-order conditions in which the ligand concentration is at least ten times greater than the total concentration of the rhenium complexes. The data was fitted to selected functions using the Scientist MicroMath, Version 2.01 program.[15] The solid lines in the figures represent computer least squares fits of data, while experimental values are represented as individual points, denoted by selected symbols.

9.3 GENERAL RATE LAWS & EQUILIBRIUM STUDIES

Substitution involves the replacement of a ligand coordinated to a metal by a free ligand in solution or the replacement of a coordinated metal ion by a free metal ion. No change in the oxidation state of the metal occurs during the reaction, however a change may occur as a result of the substitution. The systems of interest for this study are the substitution reactions of *fac*-$[Re(L,L'\text{-Bid})(CO)_3(S)]^{n+}$, where the coordinated solvento ligand (S) is replaced by

[12] W.L.F. Armarego, C.L.L. Chai, *Purification of Laboratory Chemicals*, 5th Ed., Elsevier Science, 2003
[13] D.R. Burfield, R.H. Smithers, A.S.C. Tan, *J. Org. Chem.*, 1981, 46, 629
[14] TgK Scientific Kinetic Studio, Version 1.0.8.32278, Copyright © TgK Scientific, 2008.
[15] MicroMath Scientist for Windows, Version 2.01, Copyright © 1986 – 1995, MicroMath, Inc.

various neutrally charged entering ligands (L). The following simple reaction scheme is useful for depicting the reaction (Scheme 9.1).

$$[Re(S)] + [L] \underset{k_{-1}}{\overset{k_1, K}{\rightleftharpoons}} [Re(L)] + [S]$$

Scheme 9.1: **Suggested reaction scheme for solvento substitution reactions of *fac*-[Re(N-O)(CO)$_3$(S)] complexes.**

Preliminary results made it very difficult to ascertain whether an associative, a dissociative or an interchange type mechanism can be proposed for these substitution processes. As a result, a short discussion of the three types of mechanism, of importance to this study, is first discussed here. The results from our kinetic studies were then fitted to the respective equations and by a process of elimination, we were able to determine the intimate mechanism for the *fac*-[Re(L,L'-Bid)(CO)$_3$(S)]$^{n+}$ complexes which were investigated.

9.3.1 Associative Activated Mechanism

For an associatively activated mechanism, in which a seven-coordinated transition state is formed during a rate determining step, followed by the fast dissociation of the leaving group, the following mechanism is applied:

$$[Re(S)] + [L] \underset{k_{-1}}{\overset{k_1, K}{\rightleftharpoons}} [Re(S)(L)]^{\neq} \quad \text{Rate determining step}$$

$$[Re(S)(L)]^{\neq} \longrightarrow [Re(L)] + [S] \quad \text{Fast}$$

Scheme 9.2: **Suggested mechanism for associative reactions of *fac*-[Re(N-O)(CO)$_3$(S)] complexes.**

Here k_1 represents the forward reaction, k_{-1} the reverse reaction rate constant, [Re(S)] is the *fac*-[Re(N-O)(CO)$_3$(S)] starting complex, S is the coordinated solvento ligand, L is the entering ligand and [Re(L)] is the final substitution product, *fac*-[Re(N-O)(CO)$_3$(L)]. For a typical one-step reaction (Scheme 9.1) under pseudo first-order conditions with [L] >> [Re(S)] and [Re(L)], the pseudo first-order rate constant can be determined by Equation 9.1.

$$k_{obs} = k_1[L] + k_{-1} \quad \text{... 9.1}$$

where k_{obs} is the observed rate constant. The plot of k_{obs} *vs.* [L] should yield a straight line with a slope of k_1 and an intercept of k_{-1}. The equilibrium constant of the reaction can be determined by the following equation:

$$K_1 = \frac{k_1}{k_{-1}} \quad \text{... 9.2}$$

If the mechanism is associatively activated, *A*, then the reaction characteristics (steric and electronic effects, activation parameters, *etc.*) are more sensitive to any change in the entering group, than they are to the leaving group.[16,17]

9.3.2 Interchange Mechanism

An interchange mechanism, *I*, whereby there is an interchange of S and L perhaps within the outer-sphere complex (Re(S) ··· L) to form a rapid pre-equilibrium, followed by a slower, rate-determining second reaction.

$$[Re(S)] + [L] \underset{}{\overset{K_2}{\rightleftharpoons}} [Re(S)\cdots(L)]^{\neq} \qquad \text{Fast}$$

$$[Re(S)\cdots(L)]^{\neq} \underset{k_{-3}}{\overset{k_3}{\rightleftharpoons}} [Re(L)] + [S] \qquad \text{Rate determining step}$$

Scheme 9.3: Suggested mechanism for interchange reactions of *fac*-[Re(N-O)(CO)$_3$(S)] complexes.

The extent of the influence of the entering ligand (L) will determine whether the correct mechanism is I_d, *I* or I_a. The rate equation for this scheme can be defined as:

$$k_{obs} = k_3K_2[L] / (1 + K_2[L]) + k_{-3} \quad \text{... 9.3}$$

---

[16] T.W. Swaddle, *Adv. Inorg. Bioinorg. Mech.*, 1983, 2, 95.
[17] R.G. Wilkins, *Kinetics and Mechanism of Reactions of Transition Metal Complexes*, 2nd Ed., VCH Publishers, Inc., New York, 2002

Here K_2 is the pre-equilibrium constant, k_3 is the observed second-order limiting rate constant and k_{-3} is the reverse reaction indicated by the intercept.[17]

9.3.3 Dissociative Mechanism

The dissociative mechanism, *D*, for an octahedral coordinated complex, can be represented by the following scheme:

$$[Re(S)] \underset{k_{-4}}{\overset{k_4,\ K_4}{\rightleftharpoons}} [Re] + [S] \qquad \text{Rate determining step}$$

$$[Re] + [L] \underset{k_{-5}}{\overset{k_5,\ K_5}{\rightleftharpoons}} [Re(L)] \qquad \text{Fast}$$

Scheme 9.4: Suggested mechanism for dissociative reactions of *fac*-[Re(N-O)(CO)$_3$(S)] complexes.

Here k_4 is the rate-determining step and the five-coordinated intermediate, [Re], is generated with a sufficient lifetime to discriminate between (S) and (L). If [L] is used in sufficient excess over [Re(S)] and the 2nd reaction becomes irreversible *ie.* $k_{-5} \approx 0$, then the rate equation becomes:

$$k_{obs} = k_4k_5[L] / (k_{-4}[S] + k_5[L]) \qquad \text{... 9.4}$$

Equation 9.4 can be rewritten in the following form:

$$k_{obs} = k_4[L] / ((k_{-4}/k_5)[S] + [L]) \qquad \text{... 9.5}$$

Here $k_{-4}/k_5 = k_s$ is called the discriminatory factor, which measures the efficiency with which the entering ligand (L) captures the reactive five-coordinate intermediate in competition with the re-entry of the leaving solvent ligand (S). The dissociation constant k_4 measures the rates at which the solvent ligands leave the coordination sphere of the metal and can be related to the steric and electronic properties of the leaving group.[18,19,20,21]

---

[18] G. Alibrandi, G. Bruno, S. Lanza, D. Minniti, R. Romeo, M.L. Tobe, *Inorg. Chem.*, 1987, 26, 185

9.3.4 Distinguishing Between the Three Mechanisms

The assignment of the mechanisms based on the rate laws can be difficult. If the reactions are studied under pseudo first-order conditions ([L] >> [Re(S)]), then the second-order rate law for an associative mechanism will hold for *all* concentrations of (L). At low [L], all three mechanisms will give linear second-order rate behaviour (Table 9.1).

For dissociative and interchange mechanisms, the linear dependence of k_{obs} on [L] at low [L] concentrations will be replaced by an independence at high [L]. An interchange mechanism will however still be influenced by the electronic and steric nature of the incoming ligand, where as dissociative mechanisms will reach similar saturation limits at high concentrations irrespective of the nature of the ligand. In the case of high [L] (Table 9.1), the limiting rate constants will be k_4 for the breakage of the [Re(S)] bond or k_3 for the interchange within the outer-sphere complex. Under pseudo first-order conditions the following approximations, as illustrated in Table 9.1, can be made for various concentrations of (L) for the dissociative and interchange mechanisms.[17]

Table 9.1: Rate laws for substitution mechanisms under different conditions

	Low [L]	Medium [L]	High [L]
Dissociative	$k_5[L] < k_{-4}[S]$ Re is scavenged by S preferentially	$k_5[L] \sim k_{-4}[S]$	$k_5[L] > k_{-4}[S]$ Re scavenged by [L] preferentially
	$k_{obs} = k_4k_5[L] / (k_{-4}[S])$	$k_{obs} = k_4k_5[L] / (k_{-4}[S] + k_5[L])$	$k_{obs} = k_4$
Interchange	$K_2[L] < 1$ Small build up of outer-sphere complex	$K_2[L] \sim 1$	$K_2[L] > 1$ Formation of outer-sphere complex complete
	$k_{obs} = k_3K_2[L]$	$k_{obs} = k_3K_2[L] / (1 + K_2[L])$	$k_{obs} = k_3$

[19] G. Alibrandi, D. Minniti, L.M. Scolaro, R. Romeo, *Inorg. Chem.*, 1989, 28, 1939
[20] R. Romeo, A. Grassi, L.M. Scolaro, *Inorg. Chem.*, 1992, 31, 4383
[21] O.F. Wendt, *Ph.D. Thesis*, Lund University, Lund, Sweden, 1997

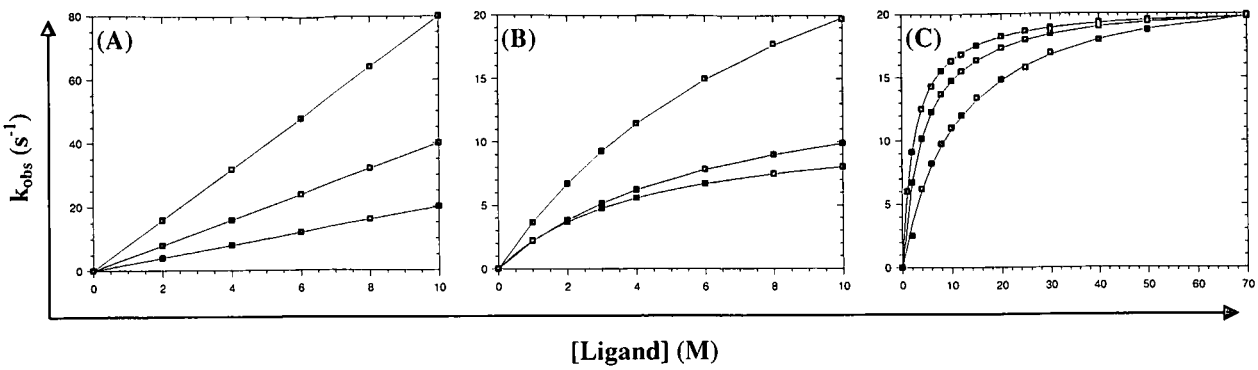

Figure 9.1: **Theoretical plots for the various substitution mechanisms under different ligand concentrations. (A) Associative mechanism, (B) Interchange mechanism, (C) Dissociative mechanism.**

9.3.5 General Reaction Conditions

All reactions, monitored in this study, were performed under pseudo first-order conditions. The observed pseudo first-order rate constants for such substitution reactions may be obtained from fitting experimental data obtained as a function of time to Eq. 9.6:

$$A_{obs}=A_{\infty}-(A_{\infty}-A_0)e^{-k_{obs}t} \qquad \text{... 9.6}$$

where A_{obs} = observed absorbance, A_{∞} = final absorbance, A_0 = initial absorbance, k_{obs} = pseudo first-order rate constant and t = time.

The activation parameters $\Delta H^{\neq}$ (enthalpy of activation) and $\Delta S^{\neq}$ (entropy of activation) were important indicators used to assign the intimate mechanisms for the reactions studied. The logarithmic form of the Eyring equation (Eq. 9.7) was used to obtain values of the activation parameters.

$$\ln\frac{k}{T}=\ln\frac{k_B}{h}-\frac{\Delta H^{\neq}}{RT}+\frac{\Delta S^{\neq}}{R} \qquad \text{... 9.7}$$

where k_B = Boltzmann constant and h = Planck constant. The value of $(-\Delta H^{\neq}/R)$ can be determined from the slope of the graph of ln(k/T) *vs.* (1/T). The value of $\Delta S^{\neq}$ can be calculated from the intercept.

The equilibrium constant (denoted by K_1) for the reaction between the *fac*-[Re(L,L'-Bid)$(CO)_3$(S)]$^{n+}$ complex and monodentate entering ligands (L) was determined kinetically using the definition $K_1 = k_1/k_{-1}$ (Eq. 9.2). It was alternatively obtained by non-linear least-squares analysis using the established relationship based on UV-Vis data:

$$A_{obs} = (A_M + A_{ML}K_1[L])/(1 + K_1[L]) \quad \text{... 9.8}$$

The above equation, as reported previously,[22] is derived from Beer's law, mass balance and the definition of K_1 for the overall reaction, where A_M and A_{ML} are the observed absorbance of the *fac*-[Re(L,L'-Bid)$(CO)_3$(S)]$^{n+}$ and *fac*-[Re(L,L'-Bid)$(CO)_3$(L)]$^{n+}$ complexes, A_{obs} = the observed absorbance and [L] = the concentration of the entering ligand, respectively.[23]

9.4 MOTIVATIONS AND RESULTS FOR KINETIC EXPERIMENTAL CONDITIONS

The axial methanol substitution reaction in neutral *fac*-[Re^{I}(N-O)$(CO)_3$$(HOCH_3)$] complexes were investigated (where Re^{I} complexes = *fac*-[Re(Sal-*m*Tol)$(CO)_3$$(HOCH_3)$] (**1**), *fac*-[Re(Sal-*p*Tol)$(CO)_3$$(HOCH_3)$] (**2**), *fac*-[Re(Sal-Ph)$(CO)_3$$(HOCH_3)$] (**3**), *fac*-[Re(Sal-CyHex)$(CO)_3$$(HOCH_3)$] (**4**), *fac*-[Re(Sal-3MeBu)$(CO)_3$$(HOCH_3)$] (**5**) with Sal-mTol = 2-(*m*-tolyliminomethyl)phenolato, Sal-*p*Tol = 2-(*p*-tolyliminomethyl)phenolato, Sal-Ph = 2-(phenyliminomethyl)phenolato, Sal-CyHex = 2-(cyclohexyliminomethyl)phenolato and Sal-3MeBu = 2-(3-methylbutyliminomethyl)phenolato). The five complexes were selected to investigate the possible influence which a range of aromatic and aliphatic substituents could have on the kinetics. The conscious choice of complexes **1** – **3** was to investigate the subtle variations of substituents on the phenyl ring, whereas the inclusion of **4** and **5** allows the evaluation of electronic effects on the ligand backbone.

[22] H.J. van der Westhuizen, R. Meijboom, A. Roodt, M. Schutte, *Inorg. Chem.*, 2010, 49, 9599
[23] A. Roodt, J.G. Leipoldt, E.A. Deutsch, J.C. Sullivan, *Inorg. Chem.*, 1992, 31, 1080

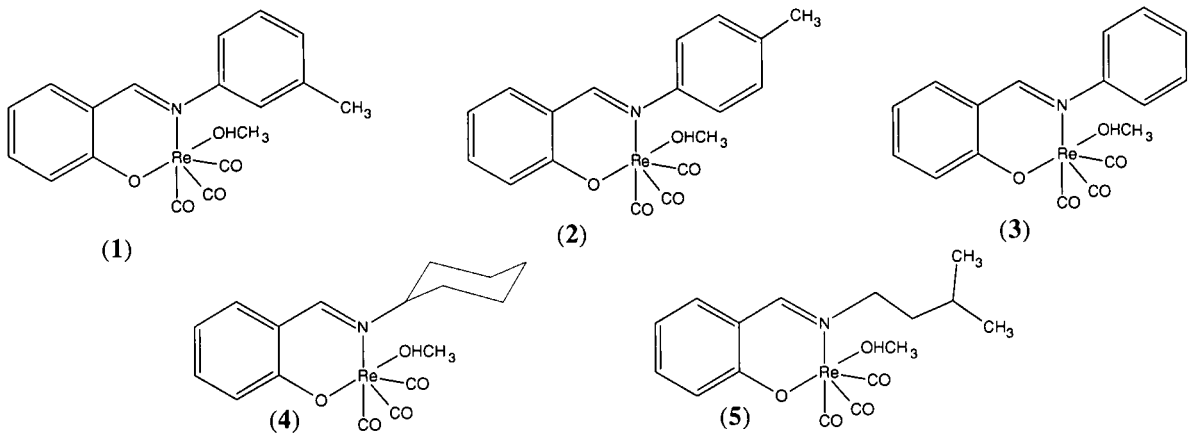

Scheme 9.5: **Line structures of various *fac*-[Re(N-O)(CO)$_3$(HOCH$_3$)] complexes used for kinetic investigations.**

The methanol substitution of rhenium(I) tricarbonyl complexes has only recently been reported[24] and it was considered essential to understand systems whose electronic and steric properties could be easily determined before studying the kinetics on ligands containing complex biological substituents. Various substituted pyridines (3-chloropyridine, pyridine, 4-picoline and 4-dimethylaminopyridine) were selected as the monodentate entering ligands due to their range of pKa values.[25,26]

The synthesis and characterisation of both starting reagents and substitution products, *fac*-[Re(L,L'-Bid)(CO)$_3$(S)] (L,L'-Bid = Sal ligand, S = coordinating methanol or pyridine) were reported in Section 3.3.3. The substitution products were also confirmed unambiguously and characterised by X-ray diffraction. Stability tests of the *fac*-[Re(L,L'-Bid)(CO)$_3$(HOCH$_3$)] reagent in methanol solutions were the first performed kinetic studies. The solutions were scanned over a longer period of time (72 h) than the studied reactions to ensure that the reagents do not undergo any changes such as decomposition, polymerisation or coordination. No significant decomposition or interactions were observed. Fresh solutions were however prepared for separate days of kinetic experiments even though the stability of solutions was confirmed. Preliminary kinetic studies were conducted using Br^- (in the form of NaBr or

[24] M. Schutte, G. Kemp, H.G. Visser, A. Roodt, *Inorg. Chem.*, 2011, *manuscript accepted*
[25] D.D. Perrin, *Dissociation Constants of Organic Bases in Aqueous Solution*, Butterworths, London, 1965; Supplement, 1972
[26] David R. Lide, ed., *CRC, Handbook of Chemistry and Physics*, 88th Edition (CD-ROM, Version 2008), CRC Press/Taylor and Francis, Boca Raton, Florida.

$[Et_4N]Br$) as entering ligand, however no reaction was observed. From synthetic experiments, it is known that the reaction of $[Et_4N]_2[Re(CO)_3(Br)_3]$ (ReAA) with the SalH ligands results in methanol replacing bromide in the 3rd position (Chapter 3). Therefore it should be unsurprising that an excess of bromide ions do not re-enter the coordination sphere due to the fact that the stability constants of the *fac*-[Re(L,L'-Bid)$(CO)_3$(Br)] species were much lower than that of the range of ligands selected here.[24] All five complexes have stable chelating ligand systems. The SalH ligand remains coordinated to the Re metal centre even in the presence of excess pyridine. The ligand is only liberated if Br^- ions and excess pyridine is present to form the *fac*-$[Re(Py)_2(CO)_3Br]$ complex. Other preliminary studies with imidazole were conducted, however the spectral changes (despite increasing the Re complex concentration) were considered too small to yield accurate results and were not pursued further.

All kinetic experiments were performed in methanol due to the poor solubility of *fac*-[Re(Sal-*m*Tol)$(CO)_3(HOCH_3)$] in water. Initial kinetic experiments with substituted pyridine were conducted in analytical grade methanol. Two reactions, a fast initial reaction and a secondary much slower reaction, were observed. The second slower reaction was confirmed to be a water substitution reaction. Preliminary kinetic studies indicated that the observed rate for the 2nd reaction increased with increasing concentration of water and was the only reaction present in the absence of pyridine. When dry, freshly distilled methanol was used, the second reaction was not observed, confirming our suspicions of the water substitution. The 1st reaction rate was unaffected by changing water concentrations. All kinetic experiments were then conducted in dry methanol to eliminate the possibility of interference from water substitution. The water substitution reaction was considered beyond the scope of this present study but will be pursued in the future.

Kinetic studies were first attempted on a slow UV-Vis Spectrophotometer, however due to the fast rates most of the reaction was lost as the first 20 seconds of the reaction is spent on manually mixing the samples. Therefore all kinetic measurements were monitored on a Stopped-Flow Spectrophotometer and were reproducible both on the Diode-Array and Photo-Multiplier mode.

Under pseudo first-order conditions with [L] >> [Re(L,L'-Bid)$(CO)_3$(S)] (in dry methanol) only one reaction was observed for all the reagents under the reaction conditions described. The k_{obs} versus [Ligand] plots, determined for the range of complexes and entering ligands used, in general produced linear plots in some cases, and non-linear plots in others. This obviously complicated the determination of the intimate mechanism, therefore fits of the rate data were applied to Equations 9.1, 9.2, 9.3 and 9.5 (as for Associative, Interchange and Dissociative mechanisms). The reverse reaction rates (k_{-3}) for Eq. 9.3 were initially determined for all reactions, however the near zero values (approximates to zero within standard deviation) were considered insignificant and therefore are not included in tables listed below. From the above preliminary kinetic observations and the information which will be discussed in Sections 9.5 and 9.6, the proposed mechanism for the substitution reactions is explained in the rest of this chapter.

9.5 KINETIC STUDY OF MeOH SUBSITUTION IN *fac*-[Re(Sal-*m*Tol)(CO)$_3$(HOCH$_3$)]

9.5.1 *fac*-[Re(Sal-*m*Tol)(CO)$_3$(HOCH$_3$)] + 3-Chloropyridine

The synthesis of the *fac*-[Re(Sal-*m*Tol)(CO)$_3$(HOCH$_3$)] complex is described in Section 3.3.3. Preliminary studies indicated that the complex is stable in methanol for several hours as long as no water is present. The spectral changes observed in a typical UV-Vis scan, for the reaction of *fac*-[Re(Sal-*m*Tol)(CO)$_3$(HOCH$_3$)] with 3-chloropyridine, are shown in Figure 9.2. The observed rate constants, calculated at two wavelengths (395, 436 nm), were determined for the various ligand concentrations and are identical within experimental error. Only one reaction was observed, under our experimental conditions, for the substitution reaction and the k_{obs} *vs.* [3-ClPy] data were obtained at four different temperatures (Figure 9.3). The observed rate data were fitted to Equations 9.1, 9.3 and 9.5 and the calculated rate constants are found in Table 9.2. The linear plots obtained from k_{obs} *vs.* [3-ClPy] data indicate that any of the three equations for an *A*, *I* or *D* mechanism could hold. As expected, the second-order rate constants (k_1) generally increase by a factor of two for each 10 °C increase of temperature.

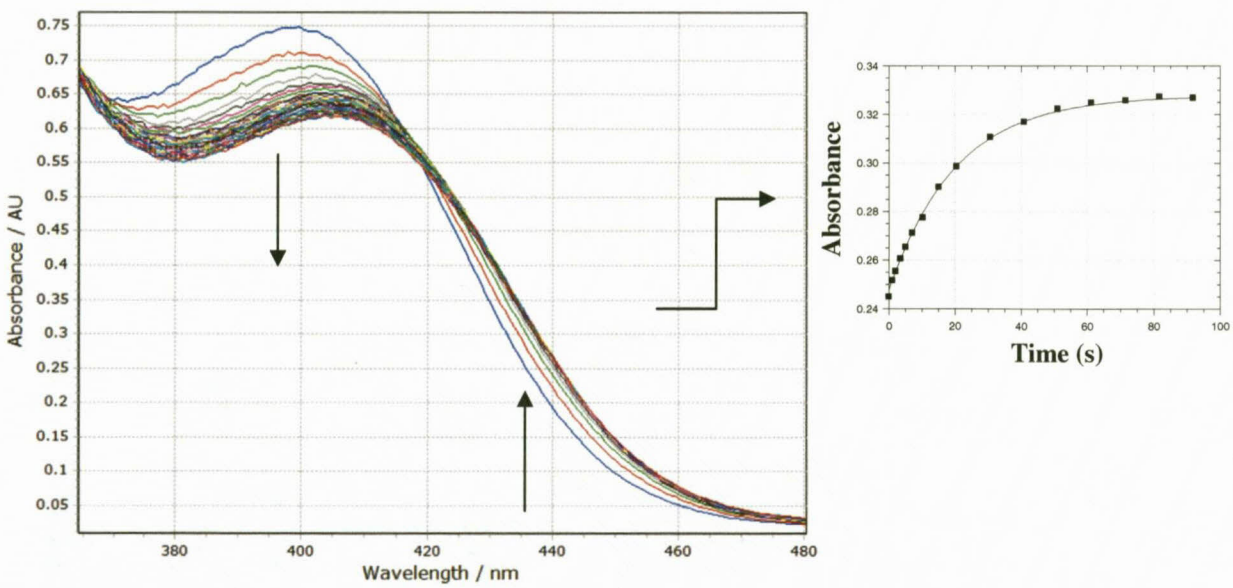

Figure 9.2: **Typical UV-Vis spectral change for the methanol substitution reaction of *fac*-[Re(Sal-*m*Tol)(CO)$_3$(HOCH$_3$)] with 3-chloropyridine in methanol at 15.0 °C, [Re complex] = 4.38 x 10^{-4} M, [3-ClPy] = 0.04 M, Δt = 1 s.**

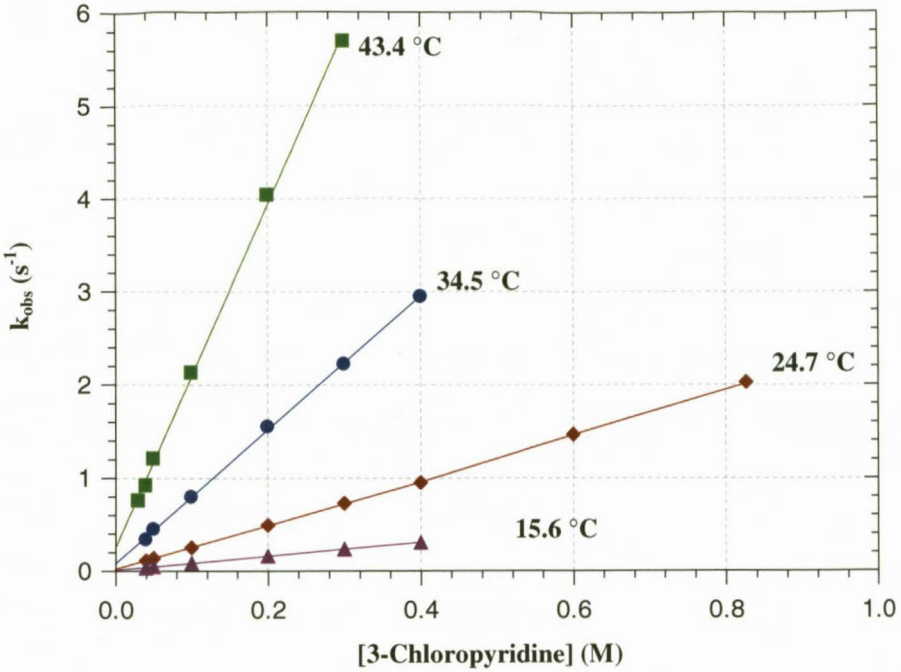

Figure 9.3: **Plot of k_{obs} *vs.* [Ligand] for the reaction between *fac*-[Re(Sal-*m*Tol)$(CO)_3(HOCH_3)$] and 3-chloropyridine at various temperatures in methanol, yielding linear plots, [Re complex] = 4.38 x 10^{-4} M, (λ = 436 nm), (Appendix C, Table C.1).**

The equilibrium constant, K_1, for the reactions are large for all four temperatures indicating favourability towards the forward reaction. The large standard deviation on the k_{-1} value increases the uncertainty of the equilibrium constant, therefore the equilibrium constant was determined individually from the absorbance *vs.* ligand concentration plots (Figure 9.4) (K_1 = 153(17) M^{-1}) and is comparable, within experimental error, with the kinetically determined value of 91(11) M^{-1} as obtained for the data fits to the Eq. 9.2 for *A* mechanism.

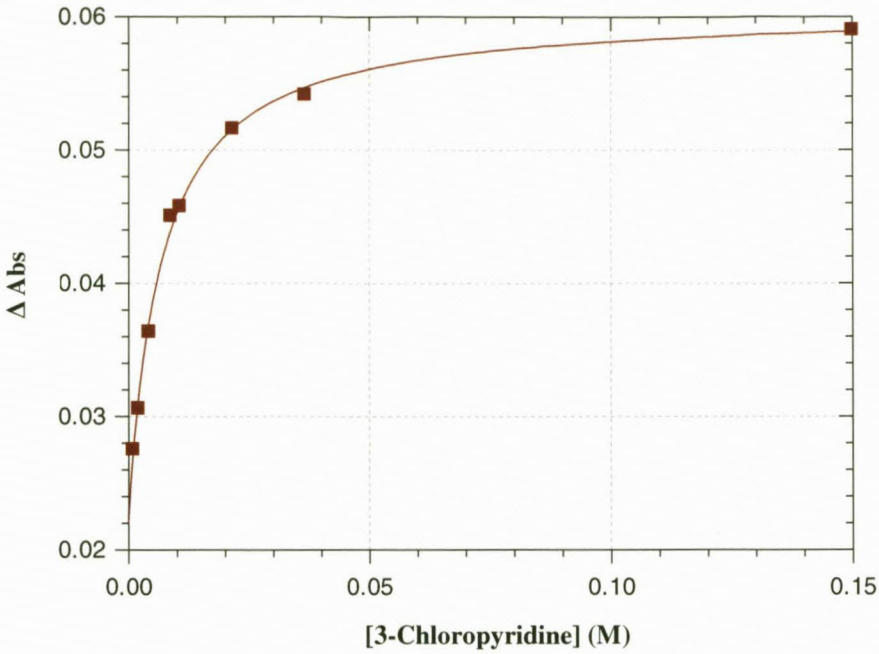

Figure 9.4: **Equilibrium constant determined by the plot of ΔAbsorbance *vs.* [Ligand] for the reaction between *fac*-[Re(Sal-*m*Tol)(CO)$_3$(HOCH$_3$)] and 3-chloropyridine at 25.5 °C in methanol (Eq. 9.8), [Re complex] = 4.33 x 10^{-4} M, (λ = 436 nm), [3-ClPy] = 0.001 M – 0.15 M, (Appendix C, Table C.2).**

Table 9.2: **Kinetic data of the rate constants for the reaction between *fac*-[Re(Sal-*m*Tol)(CO)$_3$(HOCH$_3$)] and 3-chloropyridine at various temperatures, [Re complex] = 4.38 x 10^{-4} M, [3-ClPy] = 0.04 M – 0.8 M.**

	Temperature (°C)	15.6	24.7	34.5	43.4	Equilibrium determination at 25.5 °C
Associative	k_1 ($M^{-1}s^{-1}$) [a]	0.743(8)	2.33(1)	7.18 (7)	18.4(3)	-
	k_{-1} (s^{-1})	0.014(2)	0.026(3)	0.08(2)	0.25(5)	-
	K_1 (M^{-1}) [b]	52(6)	91(11)	88(18)	74(16)	153(17) [c]
Interchange	k_3 (s^{-1}) [d]	1.6(3)	9(2)	25(7)	28(3)	-
	K_2 (M^{-1})	0.6(1)	0.30(8)	0.3(1)	0.9(1)	-
	$k_f = k_3K_2$	0.9(3)	3(1)	8(3)	24(5)	-
Dissociative	k_4 (s^{-1}) [e]	1.6(3)	9(2)	25(7)	28(3)	-
	k_{-4}/k_5	0.07(2)	0.13(4)	0.12(4)	0.047(7)	-

[a] Eq. 9.1; [b] Eq. 9.2; [c] Eq. 9.8, Figure 9.4; [d] Eq. 9.3; [e] Eq. 9.5

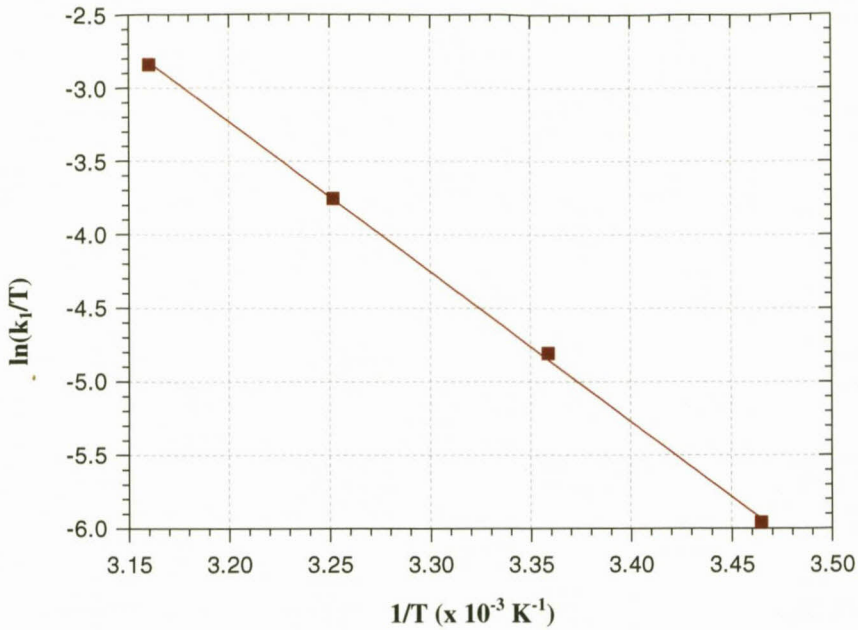

Figure 9.5: **Eyring plots of the k_1 rate constant for the reaction of *fac*-[Re(Sal-*m*Tol)(CO)$_3$(HOCH$_3$)] with 3-chloropyridine in methanol (Appendix C, Table C.6)**

The activation parameters of the reaction between *fac*-[Re(Sal-*m*Tol)(CO)$_3$(HOCH$_3$)] and [3-ClPy] were determined by fitting the data to Eq. 9.7 (Figure 9.5). The standard enthalpy and entropy of the first mechanism (Scheme 9.1) were determined as $\Delta H_1^{\neq}$ = +85.1(6) kJ.mol^{-1} and $\Delta S_1^{\neq}$ = +48(2) J.K^{-1}.mol^{-1}.

The positive value of the standard entropy, $\Delta S_1^{\neq}$, suggests that a *D* or I_d mechanism would be more correctly assigned. Furthermore, it is considered less likely for a six-coordinated metal complex to adopt a seven-coordinate intermediate as per Associative mechanism, although it is known that the 3rd row transition metals may expand their coordination spheres.[17,27,28,29] However, by extrapolating the fits of the k_{obs} *vs.* [Ligand] data to Eq. 9.3 (*I* mechanism), the following figure is obtained (Figure 9.6), which is as expected for a typical I_d type mechanism. The possible ligand concentration at which saturation limits may be achieved for an I_d type mechanism can also be estimated from Figure 9.6. At low ligand concentrations the interchange and dissociative mechanisms will give a linear second-order rate behaviour *i.e.*

---

[27] B.P. Sullivan, R.S. Lumpkin, T.J. Meyers, *Inorg. Chem.*, 1987, 26, 1247

[28] R.H. Crabtree, *The Organometallic Chemistry of the Transition Metals*, 4th Ed., John Wiley & Sons, Inc., New York, 2005

[29] A. Roodt, H.G. Visser, A. Brink, *Crystallography Reviews,* 2011, 17, 241

$k_f = k_1 = k_3K_2$. From Table 9.2, the forward rate constant (k_f) for an interchange mechanism is similar to the second-order rate constant (k_1) within experimental error.

Although not evident from these experimental results, Figure 9.6 illustrates that as previously mentioned; the data sets do not exclude an interchange mechanism. A comparative discussion of the proposed rate law and data will be undertaken in later paragraphs.

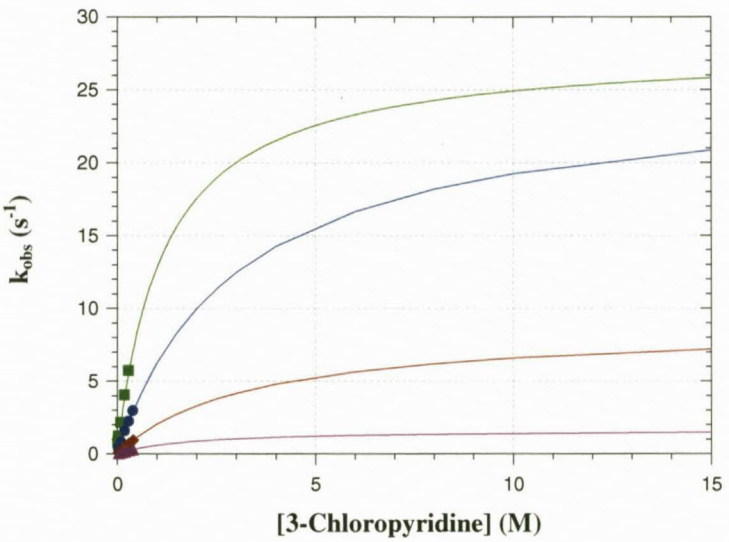

Figure 9.6: **Extrapolated plot of k_{obs} *vs.* [Ligand] for the reaction between *fac*-[Re(Sal-*m*Tol)(CO)$_3$(HOCH$_3$)] and 3-chloropyridine at various temperatures in methanol, assuming an interchange mechanism.**

9.5.2 *fac*-[Re(Sal-*m*Tol)(CO)$_3$(HOCH$_3$)] + Pyridine

The methanol substitution reaction of *fac*-[Re(Sal-*m*Tol)(CO)$_3$(HOCH$_3$)] with pyridine was investigated at four different temperatures. The k_{obs} *vs.* [Py] rate data were fitted to Equations 9.1, 9.3, and 9.5 and the observed rate constants are tabulated in Table 9.3. Linear plots for the k_{obs} *vs.* [Py] data were obtained at all four temperatures, indicating that any of the three equations for an *A*, *I* or *D* mechanism could hold. Higher concentration values were re-determined at 25.0 °C to ensure that line curvature, which may indicate saturation levels, did not start within measureable concentration values.

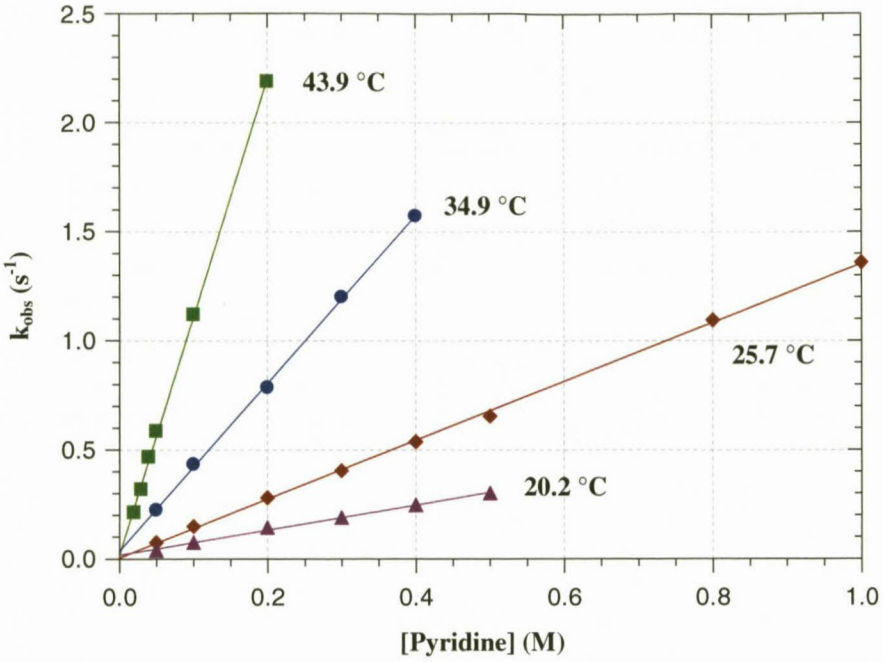

Figure 9.7: **Plot of k_{obs} *vs.* [Ligand] for the reaction between *fac*-[Re(Sal-*m*Tol)$(CO)_3(HOCH_3)$] and pyridine at various temperatures in methanol, yielding a linear plot, [Re complex] = 3.62 x 10^{-4} M, (λ = 440 nm), (Appendix C, Table C.3)**

Table 9.3: **Kinetic data of the rate constants for the reaction between *fac*-[Re(Sal-*m*Tol)$(CO)_3(HOCH_3)$] and pyridine at various temperatures, [Re complex] = 3.62 x 10^{-4} M, [Py] = 0.02 M – 1.0 M.**

	Temperature (°C)	20.2	25.7	34.9	43.9
Associative	k_1 ($M^{-1}s^{-1}$) [a]	0.57(2)	1.29(2)	3.85(5)	10.81(7)
	k_{-1} (s^{-1})	0.018(6)	0.019(5)	0.04(1)	0.032(6)
	K_1 (M^{-1}) [b]	32(10)	67(18)	106(36)	337(68)
Interchange	k_3 (s^{-1}) [c]	1.3(2)	5.5(9)	23(14)	31(5)
	K_2 (M^{-1})	0.6(2)	0.27(5)	0.2(1)	0.38(7)
	$k_f = k_3K_2$	0.8(2)	1.5(4)	4(4)	12(3)
Dissociative	k_4 (s^{-1}) [d]	1.3(2)	5.5(9)	23(14)	31(5)
	k_{-4}/k_5	0.07(2)	0.15(3)	0.2(1)	0.11(2)

[a] Eq. 9.1; [b] Eq. 9.2; [c] Eq. 9.3; [d] Eq. 9.5

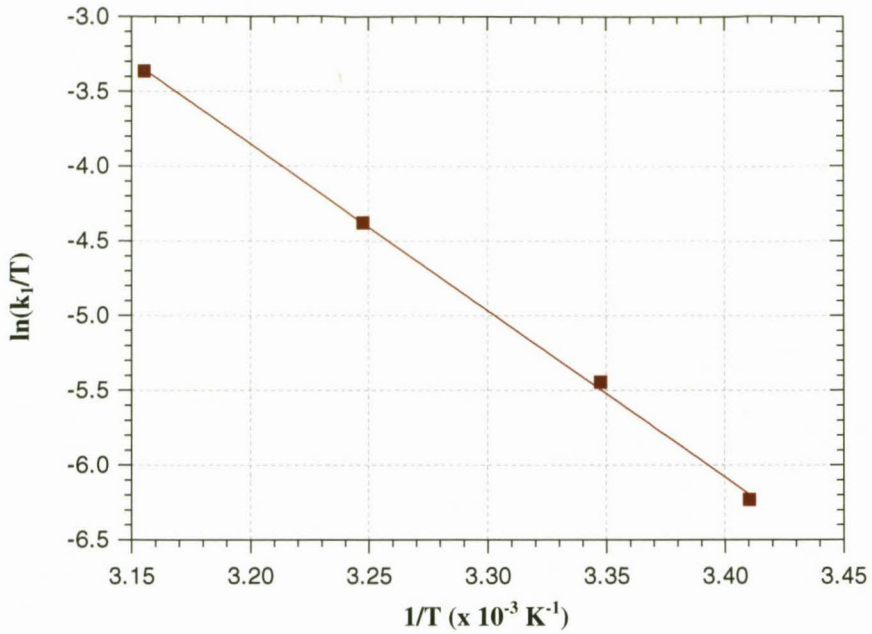

Figure 9.8: **Eyring plots of the k_1 rate constant for the reaction of *fac*-[Re(Sal-*m*Tol)(CO)$_3$(HOCH$_3$)] with pyridine in methanol (Appendix C, Table C.6).**

The second-order rate constant, k_1, increases systematically with increasing temperature. The reverse reaction rate (k_{-1}) obtained from the data plots are near zero within experimental error and are considered negligible. The activation parameters, enthalpy and entropy of the first mechanism (Scheme 9.1) were determined as $\Delta H_1^{\neq}$ = +92(2) kJ.mol^{-1} and $\Delta S_1^{\neq}$ = +66(7) J. K^{-1}.mol^{-1}. The positive value of the standard entropy, $\Delta S_1^{\neq}$, indicates a *D* or I_d mechanism would be more correctly assigned.

If an interchange mechanism is assumed, an extrapolated plot can be calculated to indicate at which possible ligand concentration a saturation limit may be achieved (Figure 9.9). At low ligand concentrations the interchange and dissociative mechanisms will give a linear second-order rate behaviour *i.e.* $k_f = k_1 = k_3K_2$. From Table 9.3, the forward rate constant (k_f) for an interchange mechanism is similar to the second-order rate constant (k_1) within experimental error. A comparative discussion of the proposed rate law and data will be undertaken in later paragraphs.

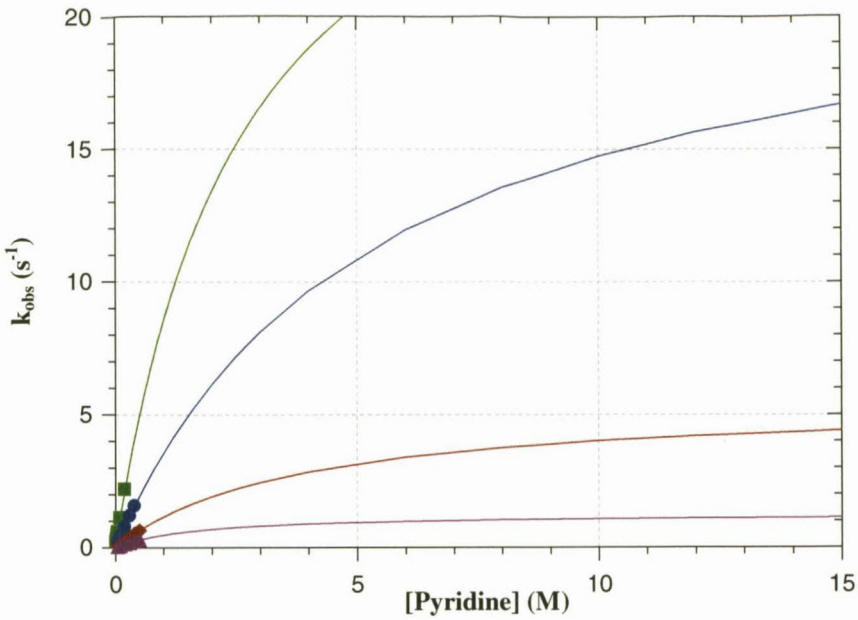

Figure 9.9: **Extrapolated plot of k_{obs} *vs.* [Ligand] for the reaction between *fac*-[Re(Sal-*m*Tol)(CO)$_3$(HOCH$_3$)] and pyridine at various temperatures in methanol, assuming a interchange mechanism.**

9.5.3 *fac*-[Re(Sal-*m*Tol)(CO)$_3$(HOCH$_3$)] + 4-Picoline

The methanol substitution reaction of *fac*-[Re(Sal-*m*Tol)(CO)$_3$(HOCH$_3$)] with various concentrations of 4-picoline (pKa = 5.99) was investigated at four different temperatures and fitted to Equations 9.1, 9.3, and 9.5. The pseudo first-order rate constants were determined for the three mechanisms and summarised in Table 9.4. Data was initially fitted to linear plots obtained for the four temperatures, however the data does not suitably fit a linear equation (Figure 9.10). A more accurate plot was determined for the interchange mechanism (Figure 9.11). The forward rate constant (k_f) for an interchange mechanism better approximates the second-order rate constant (k_1) (within experimental error) than the data found for the reaction with pyridine. Higher concentration values were re-analysed at 25.0 °C to determine the saturation limit of the line curvature.

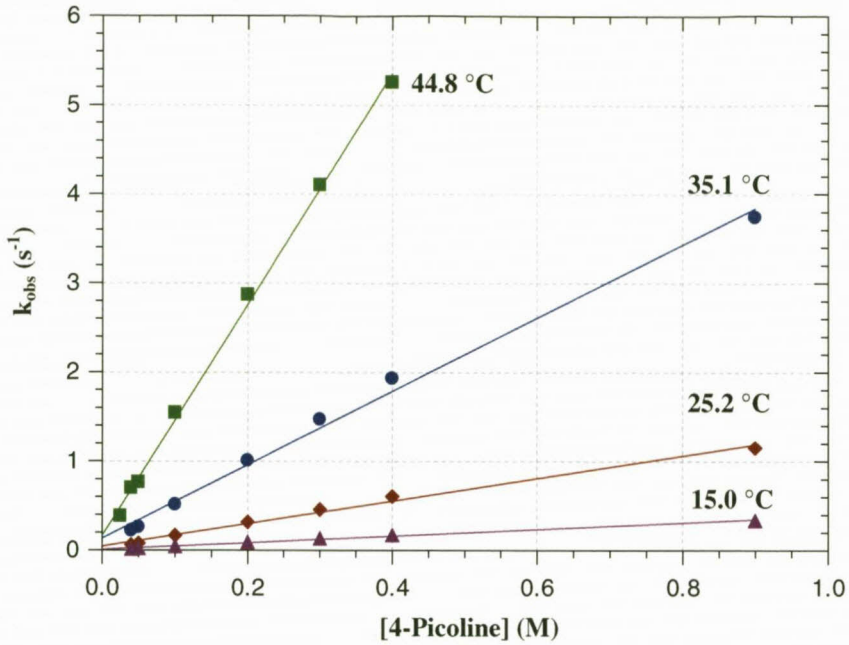

Figure 9.10: **Plot of k_{obs} *vs.* [Ligand] for the reaction between *fac*-[Re(Sal-*m*Tol)$(CO)_3(HOCH_3)$] and 4-picoline, assuming an associative mechanism, at various temperatures in methanol, [Re complex] = 4.65 x 10^{-4} M, (λ = 438 nm).**

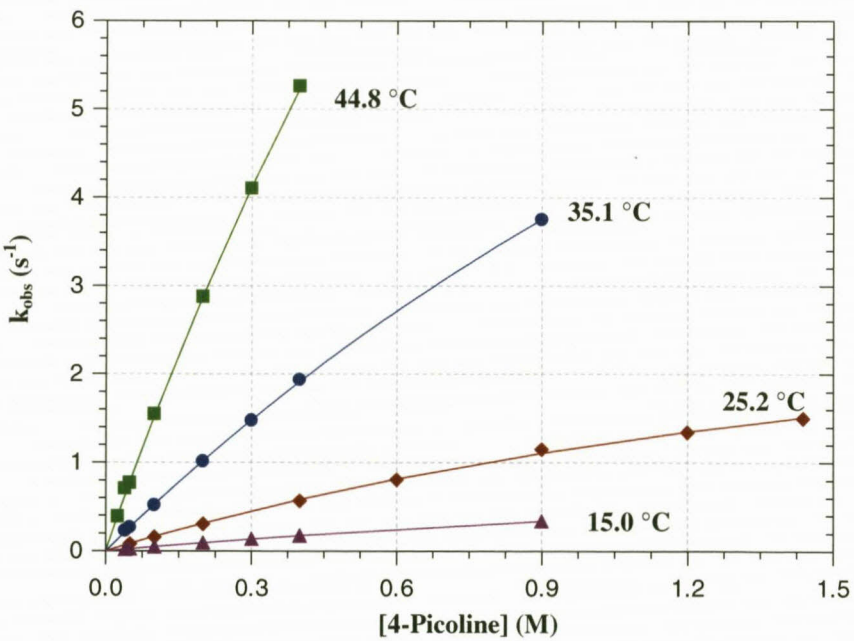

Figure 9.11: **Plot of k_{obs} *vs.* [Ligand] for the reaction between *fac*-[Re(Sal-*m*Tol)$(CO)_3(HOCH_3)$] and 4-picoline at various temperatures in methanol, yielding a limiting plot, [Re complex] = 4.65 x 10^{-4} M, (λ = 438 nm), (Appendix C, Table C.4).**

Table 9.4: **Kinetic data of the rate constants for the reaction between *fac*-[Re(Sal-*m*Tol)(CO)$_3$(HOCH$_3$)] and 4-picoline at various temperatures, [Re complex] = 4.65 x 10^{-4} M, [4-Picoline] = 0.02 M – 1.5 M.**

	Temperature (°C)	15.0	25.2	35.1	44.8
Associative	k_1 ($M^{-1}s^{-1}$) [a]	0.37(1)	1.27(5)	4.1(1)	13.0(3)
	k_{-1} (s^{-1})	0.014(6)	0.05(2)	0.14(6)	0.17(5)
	K_1(M^{-1}) [b]	27(11)	25(10)	29(12)	78(26)
Interchange	k_3 (s^{-1}) [c]	1.36(2)	3.9(3)	16.1(5)	28(3)
	K_2 (M^{-1})	0.373(8)	0.44(4)	0.34(1)	0.57(2)
	$k_f = k_3K_2$	0.51(1)	1.7(2)	5.4(3)	16(3)
Dissociative	k_4 (s^{-1}) [d]	1.36(2)	3.9(3)	16.1(5)	28(3)
	k_{-4}/k_5	0.109(2)	0.093(9)	0.120(5)	0.071(8)

[a] Eq. 9.1; [b] Eq. 9.2; [c] Eq. 9.3; [d] Eq. 9.5

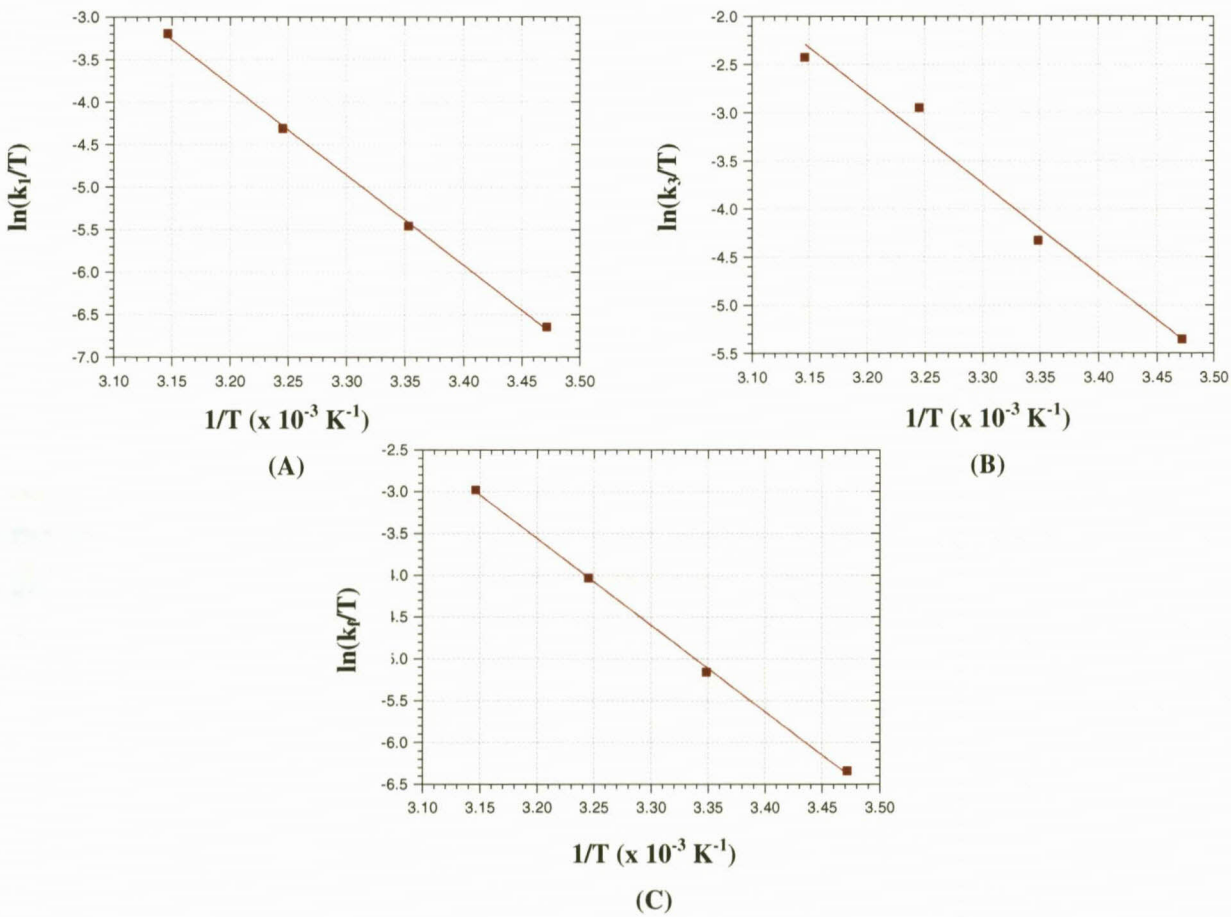

Figure 9.12: **Eyring plots of the rate constant for the reaction of *fac*-[Re(Sal-*m*Tol)(CO)$_3$(HOCH$_3$)] with 4-picoline in methanol. (A) Assuming a linear, associative mechanism (k_1), (B) assuming an interchange mechanism (k_3), (C) assuming an interchange mechanism utilizing the forward rate constant (k_f), (Appendix C, Table C.6).**

Eyring plots for both the associative mechanism (k_1) and the interchange mechanism (k_3, k_f) were determined in order to compare the activation parameters obtained for the two mechanisms. The enthalpy and entropy of activation for the first mechanism (Scheme 9.1) was determined as $\Delta H_1^{\neq}$ = +88(2) kJ.mol^{-1} and $\Delta S_1^{\neq}$ = +53(6) J.K^{-1}.mol^{-1}. The activation parameters for the second mechanism (Scheme 9.3) were calculated as $\Delta H_3^{\neq}$ = +78(8) kJ.mol^{-1} and $\Delta S_3^{\neq}$ = +30(27) J.K^{-1}.mol^{-1}. The large ESD values of the activation parameters for $\Delta H_3^{\neq}$ and $\Delta S_3^{\neq}$ are due to a 'combination of uncertainties'. Therefore the activation parameters for the second mechanism utilizing the forward rate constant (k_f) were calculated as $\Delta H_f^{\neq}$ = +86(2) kJ.mol^{-1} and $\Delta S_f^{\neq}$ = +49(6) J.K^{-1}.mol^{-1} yielding better approximations (within experimental error) to the activation parameters determined for the first mechanism.

The positive value of the entropy of activation as well as the appearance of non-linear plots for k_{obs} *vs.* [Ligand] data, with curvature is an indication that an interchange- or dissociative-type mechanism is a better mechanistic approximation than an associative-type mechanism. If an interchange mechanism is assumed, an extrapolated plot can be calculated to indicate at which possible ligand concentration a saturation limit may be achieved (Figure 9.13). A comparative discussion of the proposed rate law and data will be undertaken in later paragraphs.

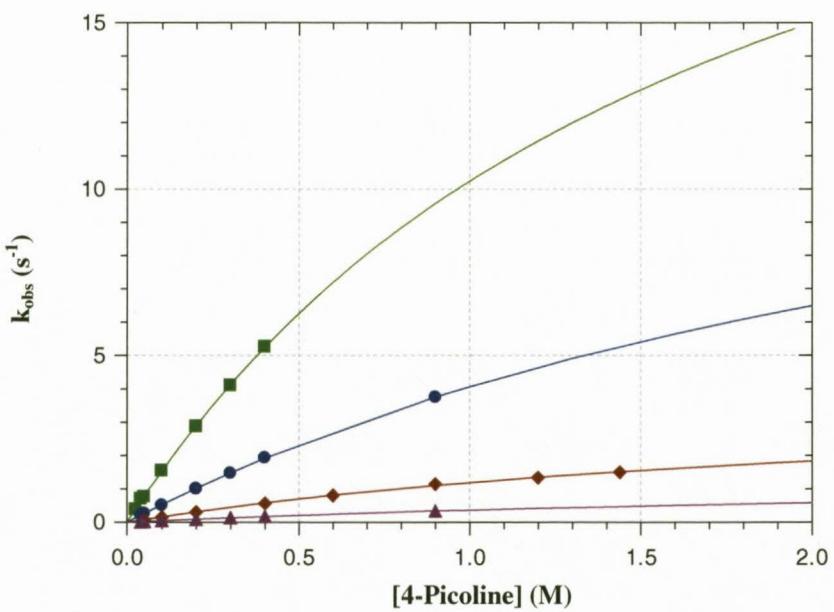

Figure 9.13: **Extrapolated plot of k_{obs} *vs.* [Ligand] for the reaction between *fac*-[Re(Sal-*m*Tol)(CO)$_3$(HOCH$_3$)] and 4-picoline at various temperatures in methanol, assuming a interchange mechanism.**

9.5.4 *fac*-[Re(Sal-*m*Tol)(CO)$_3$(HOCH$_3$)] + DMAP

The methanol substitution reaction of *fac*-[Re(Sal-*m*Tol)(CO)$_3$(HOCH$_3$)] with various concentrations of 4-dimethylaminopyridine, DMAP (pKa = 9.8) was investigated at four different temperatures and fitted to Equations 9.1, 9.3, and 9.5. The pseudo first-order rate constants were determined for the three mechanisms and summarised in Table 9.5. The k_1, k_{-1}, K_1 values were calculated using the four lowest concentrations to yield values with very high standard deviations. The second-order rate constant (k_1) was compared to the forward rate constant, k_f. The values of k_1 at 15.0, 25.0, 35.0 °C differ too greatly to be of any experimental significance and are therefore not reported. Only the second-order rate constant determined at 46.0°C is significant when compared to k_f (k_1 = 18.3(1) $M^{-1}s^{-1}$, k_{-1} = 0.015(4) s^{-1}, K_1 = 1218(317) M^{-1}). The non-linear data obtained at four temperatures, was fitted to an interchange mechanism as illustrated in Figure 9.14. Higher concentration values were re-determined at 25.0 °C to determine the saturation limit of the line curvature.

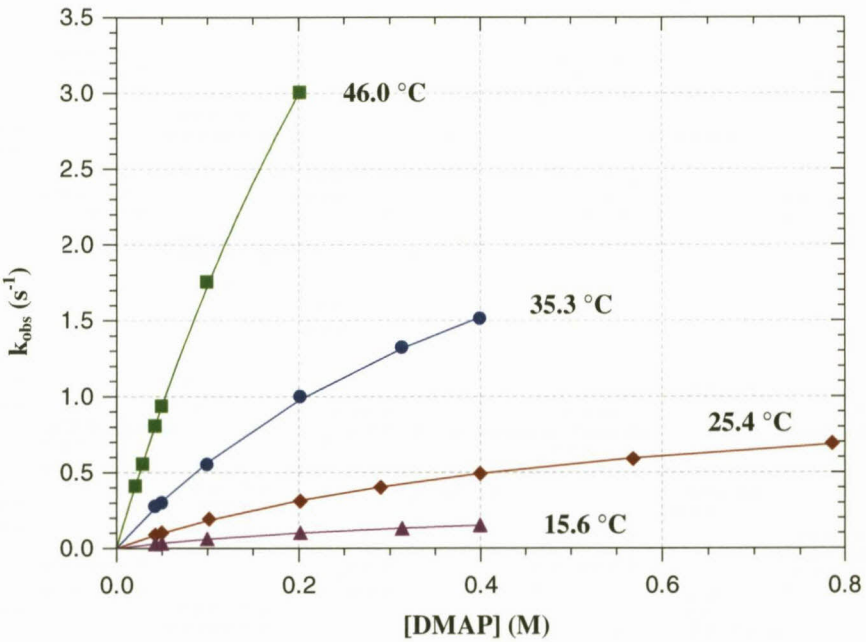

Figure 9.14: **Plot of k_{obs} *vs.* [Ligand] for the reaction between *fac*-[Re(Sal-*m*Tol)(CO)$_3$(HOCH$_3$)] and DMAP at various temperatures in methanol, [Re complex] = 5.19 x 10^{-4} M, (λ = 440 nm), (Appendix C, Table C.5)**

Table 9.5: **Kinetic data of the rate constants for the reaction between *fac*-[Re(Sal-*m*Tol)(CO)$_3$(HOCH$_3$)] and DMAP at various temperatures, [Re complex] = 5.19 x 10^{-4}M, [DMAP] = 0.04 M – 0.8 M.**

	Temperature (°C)	15.6	25.4	35.3	46.0
Interchange	k_3 (s^{-1}) [a]	0.297(7)	1.15(2)	3.5(2)	11.2(6)
	K_2 (M^{-1})	2.6(1)	1.88(7)	1.9(2)	1.8(1)
	$k_f = k_3K_2$	0.76(4)	2.16(9)	6.7(5)	20(2)
Dissociative	k_4 (s^{-1}) [b]	0.297(2)	1.15(2)	3.5(2)	11.2(6)
	k_4/k_5	0.0158(7)	0.0215(8)	0.021(1)	0.022(1)

[a] Eq. 9.3; [b] Eq. 9.5

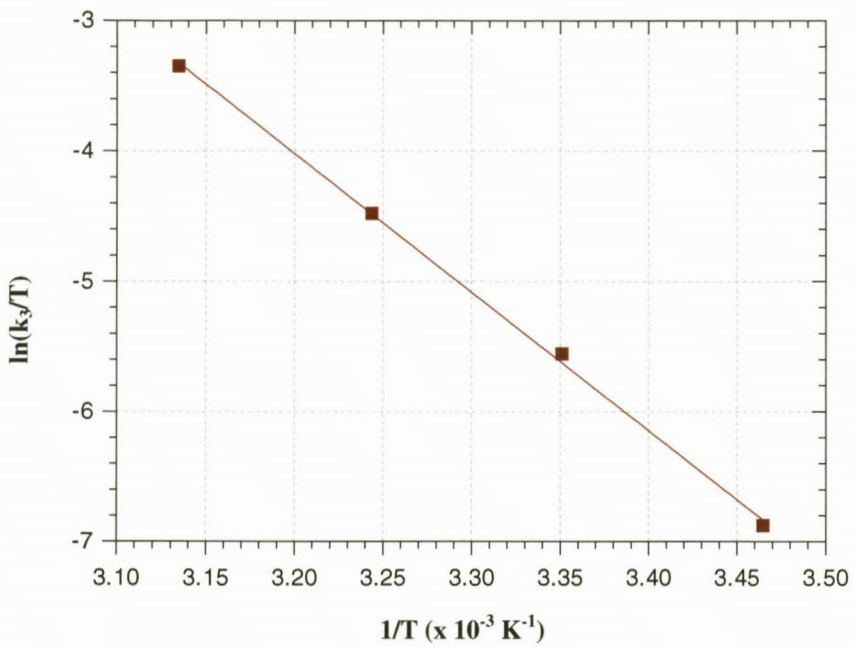

Figure 9.15: **Eyring plots of the k_3 rate constant for the reaction of *fac*-[Re(Sal-*m*Tol)(CO)$_3$(HOCH$_3$)] with DMAP in methanol (Appendix C, Table C.6)**

The activation parameters, enthalpy and entropy of the interchange mechanism (Scheme 9.3) were determined as $\Delta H_3^{\neq}$ = +88(2) kJ.mol^{-1} and $\Delta S_3^{\neq}$ = +52(7) J.K^{-1}.mol^{-1}. If an interchange mechanism is assumed, an extrapolated plot can be calculated to indicate at which possible ligand concentration a saturation limit may be achieved (Figure 9.16).

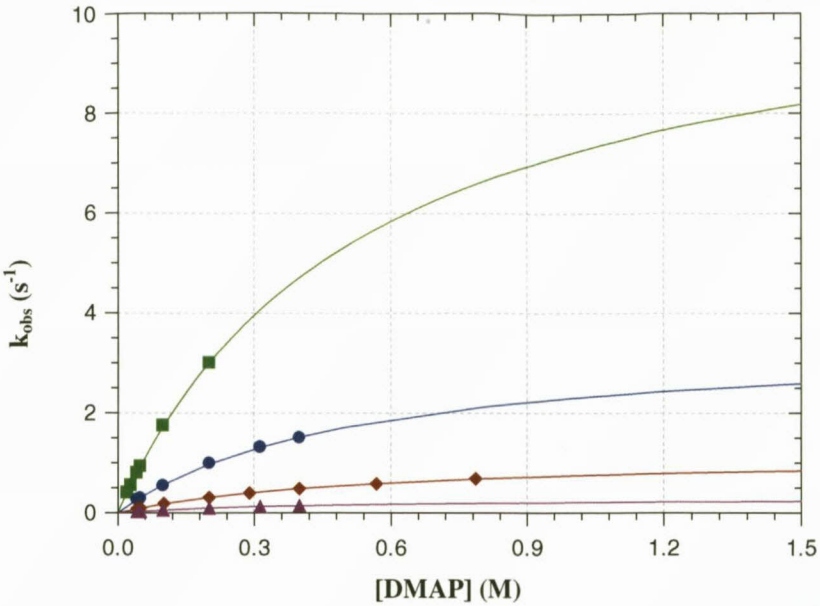

Figure 9.16: **Extrapolated plot of k_{obs} *vs.* [Ligand] for the reaction between *fac*-[Re(Sal-*m*Tol)$(CO)_3(HOCH_3)$] and DMAP at various temperatures in methanol, assuming a interchange mechanism.**

9.5.5 Summary of *fac*-[Re(Sal-*m*Tol)$(CO)_3(HOCH_3)$] kinetics

The rate data at 25.0 °C for the methanol substitution reactions between *fac*-[Re(Sal-*m*Tol)$(CO)_3(HOCH_3)$] and various monodentate entering ligands are illustrated in Figure 9.17 and summarized in Table 9.6.

Linear plots with no obvious tendency of curvature were found for 3-chloropyridine and pyridine (Figure 9.18), the ligands with the lowest pKa values (2.81, 5.23). Data obtained for 4-picoline indicates slight curvature (pKa = 5.99), whereas the reaction with DMAP (pKa = 9.8) indicates distinct curvature with near saturation limits (Figure 9.19).

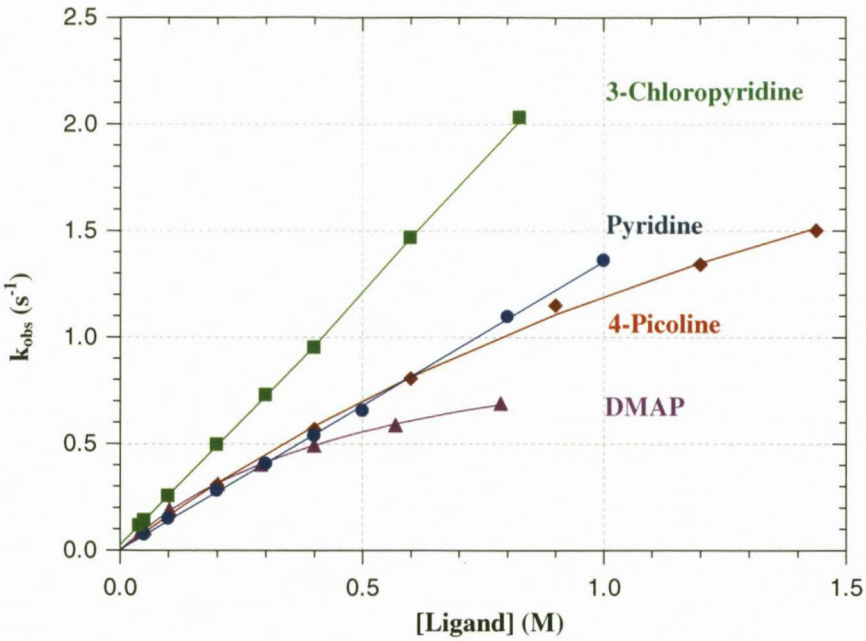

Figure 9.17: **Plot of k_{obs} *vs.* [Ligand] for the reaction between *fac*-[Re(Sal-*m*Tol)$(CO)_3(HOCH_3)$] and various entering ligands at 25.0 °C in methanol.**

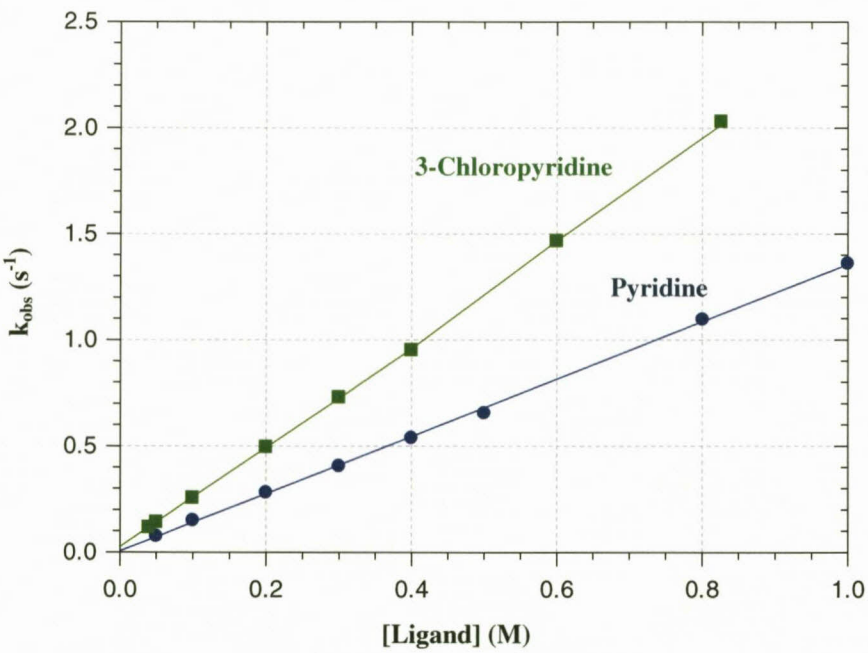

Figure 9.18: **Plot of k_{obs} *vs.* [Ligand] for the reaction between *fac*-[Re(Sal-*m*Tol)$(CO)_3(HOCH_3)$] and 3-chloropyridine and pyridine at 25.0 °C in methanol indicating linearity.**

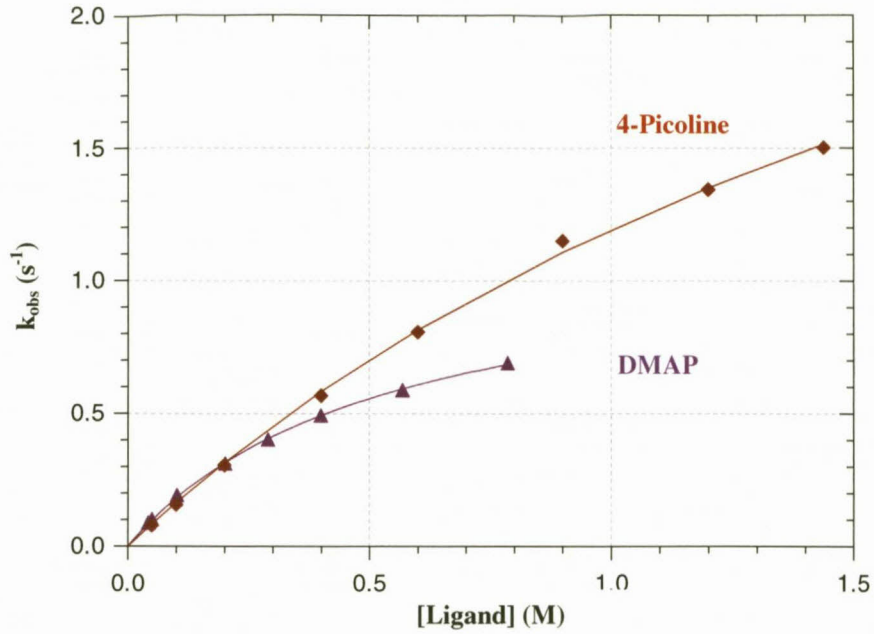

Figure 9.19: **Plot of k_{obs} *vs.* [Ligand] for the reaction between *fac*-[Re(Sal-*m*Tol)$(CO)_3(HOCH_3)$] and 4-picoline and DMAP at 25.0 °C in methanol indicating the line curvature, *i.e.* saturation kinetics.**

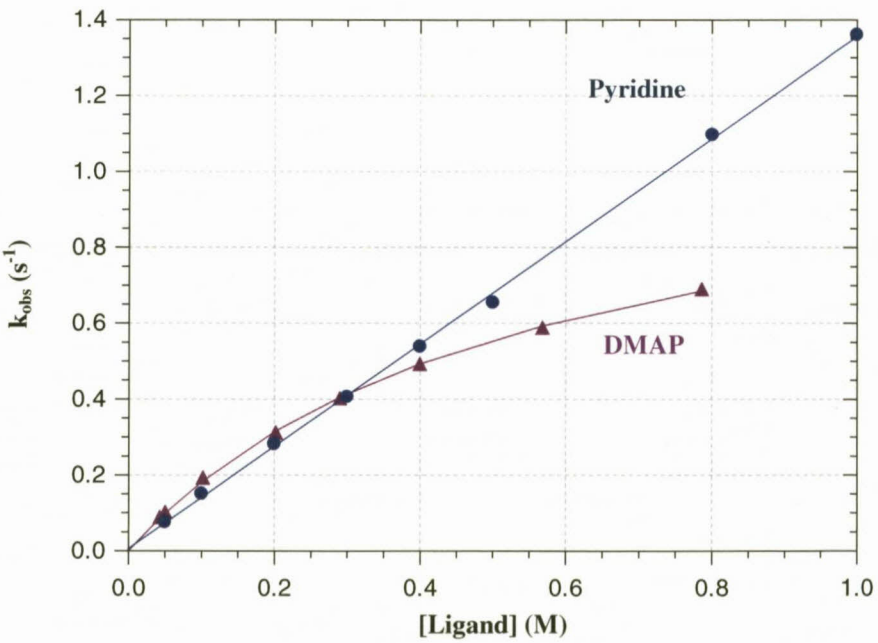

Figure 9.20: **Plot of k_{obs} *vs.* [Ligand] for the reaction between *fac*-[Re(Sal-*m*Tol)$(CO)_3(HOCH_3)$] and pyridine and DMAP at 25.0 °C in methanol.**

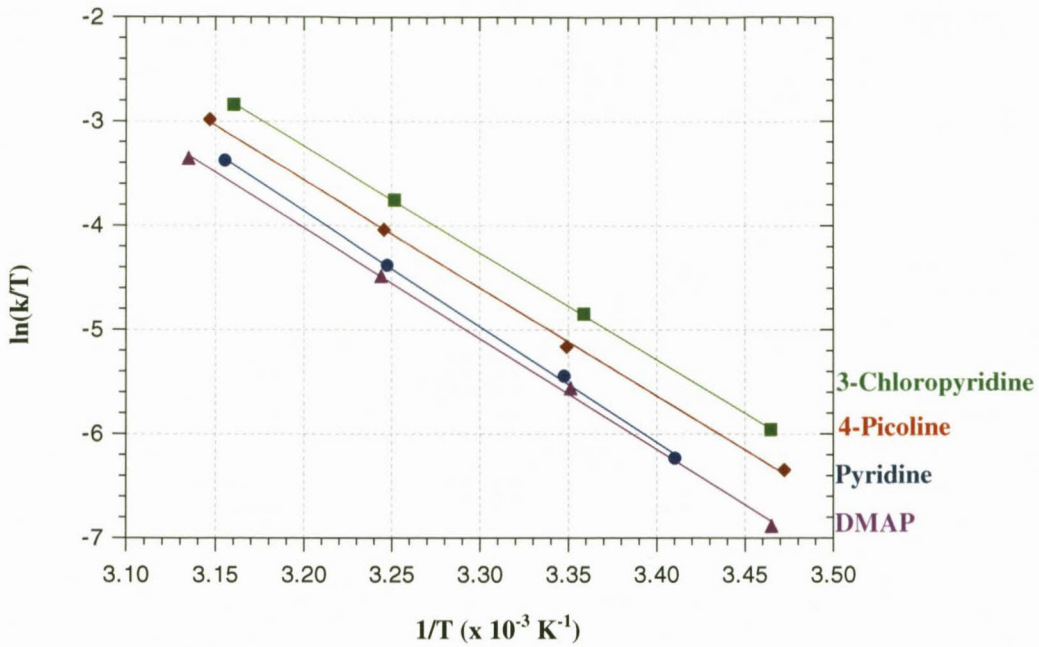

Figure 9.21: **Eyring plots of the rate constant for the reaction of *fac*-[Re(Sal-*m*Tol)(CO)$_3$(HOCH$_3$)] with various ligands in methanol.**

All calculated second-order rate constants determined from Eq. 9.1, 9.3 and 9.5 for an associative-, interchange- and dissociative-type mechanism, decrease in value from 3-ClPy > Py > 4-Pic > DMAP. This tendency is inversely proportional to the pKa values of the ligands, which is contrary to what is expected for an associative type mechanism. The linear plots for 3-ClPy and Py could indicate an associative (*A*) or interchange associative (I_a) mechanism, however the positive values for entropy of activation $\Delta S^{\neq}$ point to a dissociative or I_d type mechanism.

The second order rate constant (k_1) obtained for the reaction of *fac*-[Re(Sal-*m*Tol)(CO)$_3$(HOCH$_3$)] with pyridine (k_1 = 1.29(2) $M^{-1}s^{-1}$) is faster than values determined by Kemp[8] and Schutte[9] for other analogous (N-O) bidentate ligands (*fac*-[Re(Pico)(CO)$_3$(H$_2$O)] k_1 = 1.6(1) x 10^{-3} $M^{-1}s^{-1}$; *fac*-[Re(Quin)(CO)$_3$(H$_2$O)] k_1 = 3.9(1) x 10^{-3} $M^{-1}s^{-1}$; *fac*-[Re(2,4-PicoH)(CO)$_3$(H$_2$O)] k_1 = 1.641(8) x 10^{-3} $M^{-1}s^{-1}$; *fac*-[Re(2,4-QuinH)(CO)$_3$(H$_2$O)] k_1 = 3.31(2) x 10^{-3} $M^{-1}s^{-1}$), where Pico = 2-picolinate, Quin = 2-quinolinate, 2,4-PicoH = 2,4-pyridinedicarboxylate, 2,4-QuinH = 2,4-quinolinedicarboxylate.

A very important observation for these results, assuming an I_d mechanism is manifested in the stepwise increase in the pre-equilibrium constant (K_2), in direct agreement with the Bronsted acid-base properties, *i.e.* electron density on the entering N-atom of the pyridine type ligand. This is considerable good supporting evidence for an I_d mechanism.

Table 9.6: **Summary of kinetic data obtained for the reaction of *fac*-[Re(Sal-*m*Tol)(CO)$_3$(HOCH$_3$)] with various entering ligands at 25.0 °C in methanol.**

Ligand	k_1 ($M^{-1}s^{-1}$)	k_{-1} (s^{-1})	K_1 (M^{-1})	k_3 (s^{-1})	K_2 (M^{-1})	k_4 (s^{-1})	k_{-4}/k_5	pK
3-ClPy	2.33(1)	0.026(3)	91(11)	9(2)	0.30(8)	9(2)	0.13(4)	2.8
Pyridine	1.29(2)	0.019(5)	67(18)	5.5(9)	0.27(5)	5.5(9)	0.15(3)	5.2
4-Picoline	1.27(5)	0.05(2)	25(10)	3.9(3)	0.44(4)	3.9(3)	0.093(9)	5.9
DMAP	-	-	-	1.15(2)	1.88(7)	1.15(2)	0.0215(8)	9.8

Table 9.7: **Kinetic data obtained from the Eyring equation for the reaction of *fac*-[Re(Sal-*m*Tol)(CO)$_3$(HOCH$_3$)] with various entering ligands at 25.0 °C in methanol.**

Ligand	k_1 ($M^{-1}s^{-1}$)	k_3 (s^{-1})	K_2 (M^{-1})	$k_f = k_3K_2$	k_4 (s^{-1})	$\Delta H^{\neq}$ ($kJ.mol^{-1}$)	$\Delta S^{\neq}$ ($J.K^{-1}mol^{-1}$)
3-Cl-Py	2.33(1)	9(2)	0.30(8)	3(1)	9(2)	85.1(6) (k_1)	48(2) (k_1)
Pyridine	1.29(2)	5.5(9)	0.27(5)	1.5(4)	5.5(9)	92(2) (k_1)	66(7) (k_1)
4-Picoline	1.27(5)	3.9(3)	0.44(4)	1.7(2)	3.9(3)	88(2) (k_1) 78(8) (k_3) 86(2) (k_f)	53(6) (k_1) 30(27) (k_3) 49(6) (k_f)
DMAP	-	1.15(2)	1.88(7)	2.16(9)	1.15(2)	88(2) (k_3)	52(7) (k_3)

9.6 KINETIC STUDY OF MeOH SUBSITUTION IN *fac*-[Re(Sal-T)(CO)$_3$(HOCH$_3$)]

9.6.1 *fac*-[Re(Sal-*p*Tol)(CO)$_3$(HOCH$_3$)] + DMAP, Py

Following the results obtained in Section 9.5, only two ligands (DMAP and Py) were selected to continue the kinetic study, to enable the comparison of ligand backbone substituents on the rate constants and the mechanism. The methanol substitution reaction of *fac*-[Re(Sal-*p*Tol)(CO)$_3$(HOCH$_3$)] with various concentrations of 4-dimethylaminopyridine, DMAP (pKa = 9.8) and pyridine, Py (pKa = 5.23) were investigated at 25.0 °C and fitted to Equations 9.1, 9.3, and 9.5. The pseudo first-order rate constants, applicable for the three mechanisms, were determined and are summarised in Table 9.8. Non-linear data plots were obtained for the reaction with DMAP and therefore the linear second-order rate constant k_1, could not be obtained within reasonable error. Due to the linearity of the reaction with pyridine, rate constants with large experimental errors were determined for the interchange and dissociative mechanism. The values (indicated in *italics*) were determined for completeness of the study and should be considered with caution.

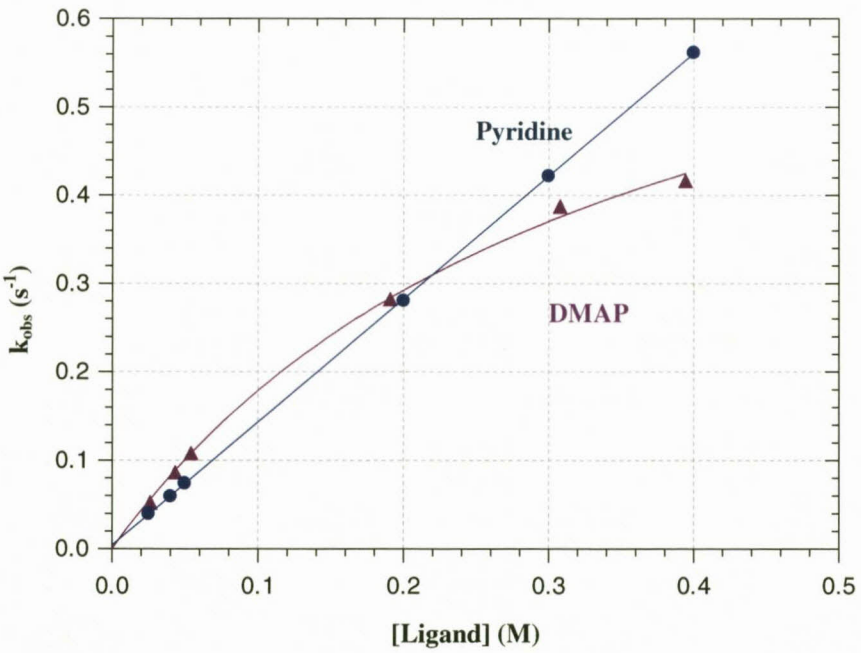

Figure 9.22: **Plot of k_{obs} *vs.* [Ligand] for the reaction between *fac*-[Re(Sal-*p*Tol)(CO)$_3$(HOCH$_3$)] and pyridine and DMAP at 25.0 °C in methanol, [Re complex] = 2.84 x 10^{-4} M, (Pyridine λ = 437 nm, DMAP λ = 438), (Appendix C, Table C.7).**

Table 9.8: **Kinetic data of the rate constants for the reaction between *fac*-[Re(Sal-*p*Tol)(CO)$_3$(HOCH$_3$)] and pyridine and DMAP at 25.0 °C, [Re complex] = 2.84 x 10^{-4} M, [Pyridine] = 0.02 M – 0.4 M, [DMAP] = 0.02 M – 0.4 M.**

Ligand	k_1 ($M^{-1}s^{-1}$)	k_{-1} (s^{-1})	K_1 (M^{-1})	k_3 (s^{-1})	K_2 (M^{-1})	k_4 (s^{-1})	k_{-4}/k_5	Temperature (°C)
Pyridine	1.393(3)	0.0037(7)	372(73)	*31(32)*	*0.05(5)*	*31(32)*	*0.9(9)*	25.1
DMAP	-	-	-	0.80(5)	2.9(3)	0.80(5)	0.014(2)	25.1

9.6.2 *fac*-[Re(Sal-Ph)(CO)$_3$(HOCH$_3$)] + DMAP, Py

Following the results obtained in sections 9.5 and 9.6.1, only two ligands (DMAP and Py) were selected to continue the kinetic study, to enable the comparison of ligand backbone substituents on the rate constants and the mechanism.

The methanol substitution reaction of *fac*-[Re(Sal-Ph)(CO)$_3$(HOCH$_3$)] with various concentrations of 4-dimethylaminopyridine, DMAP (pKa = 9.8) and pyridine, Py (pKa = 5.23) were investigated at 25.0 °C and fitted to Equations 9.1, 9.3, and 9.5. The pseudo first-order rate constants, applicable for the three mechanisms, were determined and are summarised in Table 9.9. Non-linear data plots were obtained for the reaction with DMAP and therefore the linear second-order rate constant k_1, could not be obtained within reasonable error. Due to the linearity of the reaction with pyridine, rate constants with large experimental errors were determined for the interchange and dissociative mechanism. The values (indicated in *italics*) were determined for completeness of the study and should be considered with caution.

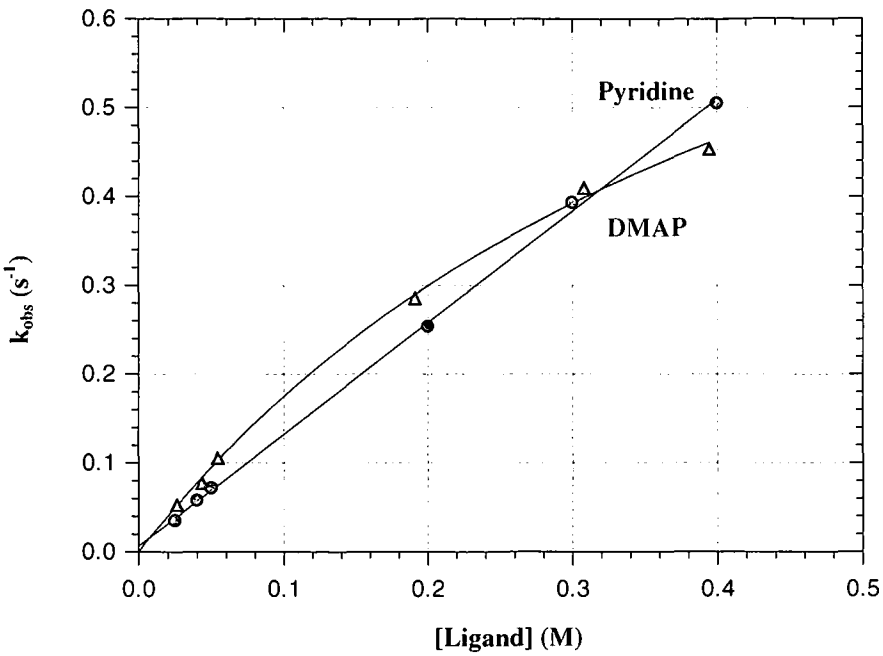

Figure 9.23: **Plot of k_{obs} *vs.* [Ligand] for the reaction between *fac*-[Re(Sal-Ph)$(CO)_3(HOCH_3)$] and pyridine and DMAP at 25.0 °C in methanol, [Re complex] = 2.90 x 10^{-4} M, (Pyridine λ = 442 nm, DMAP λ = 442), (Appendix C, Table C.8).**

Table 9.9: **Kinetic data of the rate constants for the reaction between *fac*-[Re(Sal-Ph)$(CO)_3(HOCH_3)$] and pyridine and DMAP at 25.0 °C, [Re complex] = 2.90 x 10^{-4} M, [Pyridine] = 0.02 M – 0.4 M, [DMAP] = 0.02 M – 0.4 M.**

Ligand	k_1 ($M^{-1}s^{-1}$)	k_{-1} (s^{-1})	K_1 (M^{-1})	k_3 (s^{-1})	K_2 (M^{-1})	k_4 (s^{-1})	k_{-4}/k_5	Temperature (°C)
Pyridine	1.26(2)	0.006(4)	196(117)	*8(5)*	*0.2(1)*	*8(5)*	*0.2(2)*	25.7
DMAP	-	-	-	1.03(8)	2.0(2)	1.03(8)	0.020(3)	25.7

9.6.3 *fac*-[Re(Sal-3MeBu)$(CO)_3(HOCH_3)$] + DMAP, Py

Following the results obtained in sections 9.5 and 9.6.1, only two ligands (DMAP and Py) were selected to continue the kinetic study, to enable the comparison of ligand backbone substituents on the rate constants and the mechanism.

The methanol substitution reaction of an aliphatic complex *fac*-[Re(Sal-3MeBu)$(CO)_3(HOCH_3)$], with various concentrations of 4-dimethylaminopyridine, DMAP (pKa = 9.8) and pyridine, Py (pKa = 5.23) were investigated at 25.0 °C and fitted to

Equations 9.1, 9.3, and 9.5. The pseudo first-order rate constants, applicable for the three mechanisms, were determined and summarised in Table 9.10. Non-linear data plots were obtained for the reaction with DMAP and therefore the linear second-order rate constant k_1, could not be obtained within reasonable error. Due to the linearity of the reaction with pyridine, rate constants with large experimental errors were determined for the interchange and dissociative mechanism. The values (indicated in *italics*) were determined for completeness of the study and should be considered with caution.

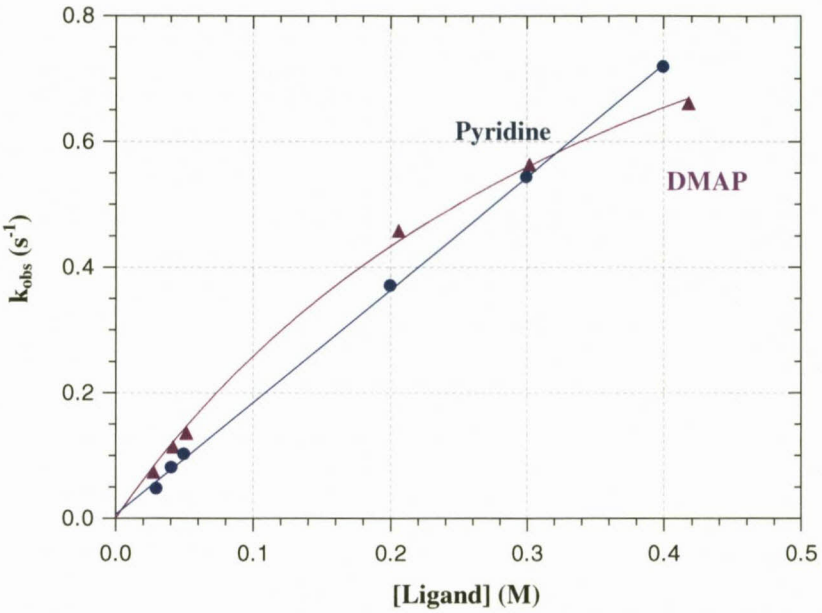

Figure 9.24: **Plot of k_{obs} *vs.* [Ligand] for the reaction between *fac*-[Re(Sal-3MeBu)$(CO)_3(HOCH_3)$] and pyridine and DMAP at 25.0 °C in methanol, [Re complex] = 3.22 x 10^{-4} M, (Pyridine λ = 416 nm, DMAP λ = 422), (Appendix C, Table C.9).**

Table 9.10: **Kinetic data of the rate constants for the reaction between *fac*-[Re(Sal-3MeBu)$(CO)_3(HOCH_3)$] and pyridine and DMAP at 25.0 °C, [Re complex] = 3.22 x 10^{-4} M, [Pyridine] = 0.02 M – 0.4 M, [DMAP] = 0.02 M – 0.4 M.**

Ligand	k_1 ($M^{-1}s^{-1}$)	k_{-1} (s^{-1})	K_1 (M^{-1})	k_3 (s^{-1})	K_2 (M^{-1})	k_4 (s^{-1})	k_{-4}/k_5	Temperature (°C)
Pyridine	1.79(2)	0.006(5)	301(256)	*11(6)*	*0.17(9)*	*11(6)*	*0.2(1)*	25.3
DMAP	-	-	-	1.34(9)	2.4(3)	1.34(9)	0.017(2)	25.1

9.6.4 *fac*-[Re(Sal-CyHex)(CO)$_3$(HOCH$_3$)] + 3-ClPy, Py, 4-Pic, DMAP

The methanol substitution reaction of a cyclic aliphatic complex *fac*-[Re(Sal-CyHex)(CO)$_3$(HOCH$_3$)] was investigated at 25.0 °C initially with pyridine and DMAP. Unexpectedly, line curvature was found for pyridine which till this point has always given linear plots with various *fac*-[Re(L,L'-Bid)(CO)$_3$(HOCH$_3$)] complexes even at high ligand concentrations. Therefore the reactions were studied with all four substituted pyridine ligands as described in Section 9.5.5 for the Sal-*m*Tol complex and fitted to Equations 9.1, 9.3, and 9.5. The pseudo first-order rate constants were determined for the three mechanisms (*A*, *I* and *D*) and are summarised in Table 9.11. Non-linear data plots were obtained for all four ligand reactions. The second-order rate constants are inversely proportional to the pKa values of the entering ligands, the same tendency was observed for *fac*-[Re(Sal-*m*Tol)(CO)$_3$(HOCH$_3$)] kinetic studies.

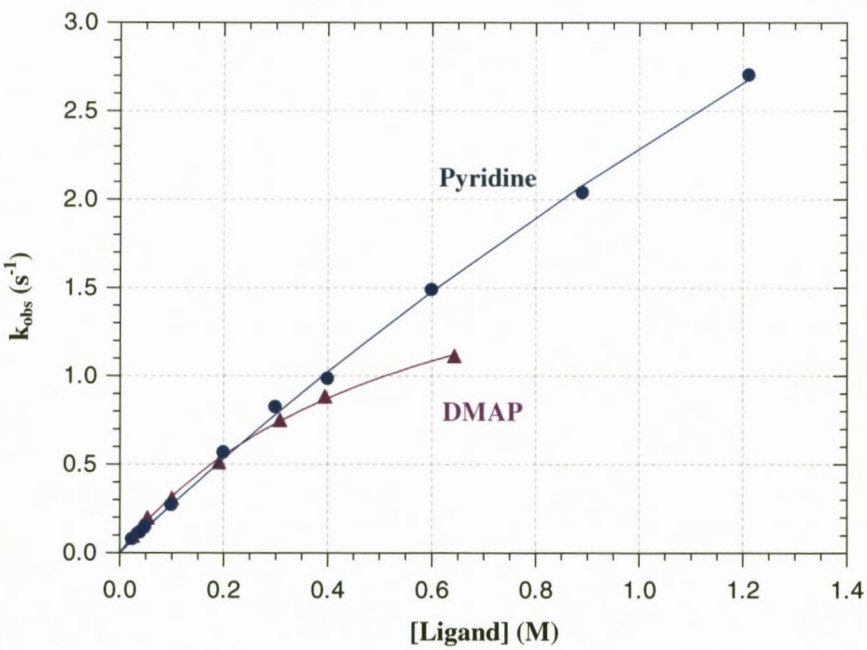

Figure 9.25: **Plot of k_{obs} *vs.* [Ligand] for the reaction between *fac*-[Re(Sal-CyHex)(CO)$_3$(HOCH$_3$)] and pyridine and DMAP at 25.0 °C in methanol, assuming a interchange mechanism, [Re complex] = 1.83 x 10^{-4} M, (Pyridine λ = 417 nm, DMAP λ = 420 nm).**

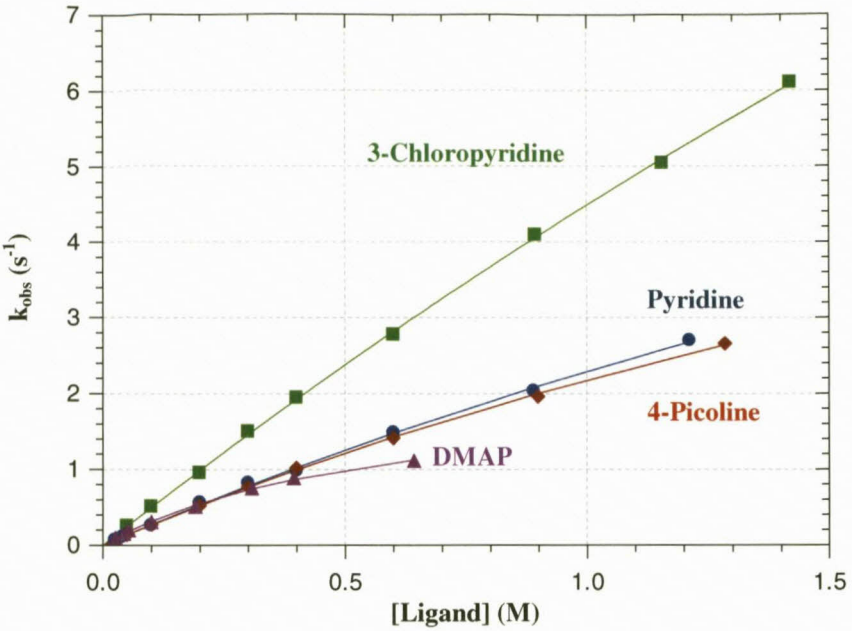

Figure 9.26: **Plot of k_{obs} *vs.* [Ligand] for the reaction between *fac*-[Re(Sal-CyHex)$(CO)_3(HOCH_3)$] and various entering ligands at 25.0 °C in methanol, [Re complex] = 1.83 x 10^{-4} M, (3-ClPy λ = 419 nm, pyridine λ = 417 nm, 4-picoline λ = 418 nm, DMAP λ = 420 nm), (Appendix C, Table C.10).**

Table 9.11: **Kinetic data of the rate constants for the reaction between *fac*-[Re(Sal-CyHex)$(CO)_3(HOCH_3)$] and entering ligands at 25.0 °C, [Re complex] = 1.83 x 10^{-4} M, [3-ClPy] = 0.05 M – 1.5 M, [Pyridine] = 0.02 M – 1.2 M, [4-Picoline] = 0.05 M – 1.3 M [DMAP] = 0.02 M – 0.7 M.**

Ligand	k_1 ($M^{-1}s^{-1}$)	k_{-1} (s^{-1})	k_3 (s^{-1})	K_2 (M^{-1})	$k_f = k_3K_2$	k_4 (s^{-1})	k_{-4}/k_5	Temp. (°C)	pKa
3-ClPy	4.30(6)	0.14(5)	40(4)	0.13(1)	5.1(8)	40(4)	0.32(4)	24.8	2.81
Pyridine	2.22(5)	0.07(3)	13(2)	0.21(3)	2.8(6)	13(2)	0.19(3)	25.2	5.23
4-Picoline	2.03(6)	0.13(4)	10.4(7)	0.26(2)	2.8(3)	10.4(7)	0.15(1)	25.0	5.99
DMAP	1.7(1)	0.13(4)	2.11(9)	1.8(1)	3.7(3)	2.11(9)	0.023(2)	25.2	9.8

To further emphasize the tendency, in conjunction with the observations made in Section 9.5.5, the increase in the pre-equilibrium constant (K_2) (assuming an I_d mechanism) very nicely follows the Bronsted acid-base properties of the entering pyridine ligand. The K_2 constant increases by more than an order-or magnitude from 3-ClPy to DMAP (Table 9.11).

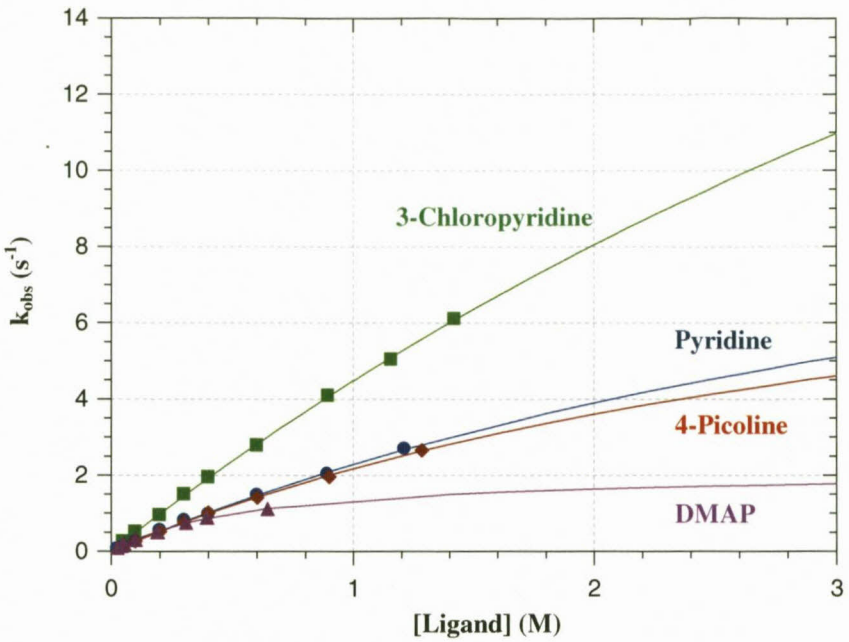

Figure 9.27: **Extrapolated plot of k_{obs} *vs.* [Ligand] for the reaction between *fac*-[Re(Sal-CyHex)$(CO)_3(HOCH_3)$] and various entering ligands at 25.0 °C in methanol, assuming an interchange mechanism.**

9.7 DISCUSSION OF *fac*-[Re(Sal-T)$(CO)_3(HOCH_3)$] KINETICS

Five neutral rhenium(I) tricarbonyl complexes were selected for this study, three of which contained N-O aromatic and two with N-O aliphatic donor bidentate ligands. The methanol coordinated in the axial position on the Re(I) metal centre was available for substitution. The rate data for the substitution reactions are summarised in Tables 9.12 - 9.13 and graphically illustrated in Figures 9.28 and 9.29 (for DMAP and pyridine only). Very fast reactions occurred for all five rhenium complexes. The second-order rate constants for the N-O complexes are significantly faster that that found for N-O, N-N' and O-O' bidentate rhenium complexes studied by Kemp and Schutte,[24] which the exception of *fac*-[Re(Flav)$(CO)_3(H_2O)$] (Flav = 3-hydroxyflavonate) whose rate constant (k_1) with pyridine is of similar magnitude. The activation parameters determined by these authors indicated that the reactions, most probably proceed *via* an associative type mechanism.

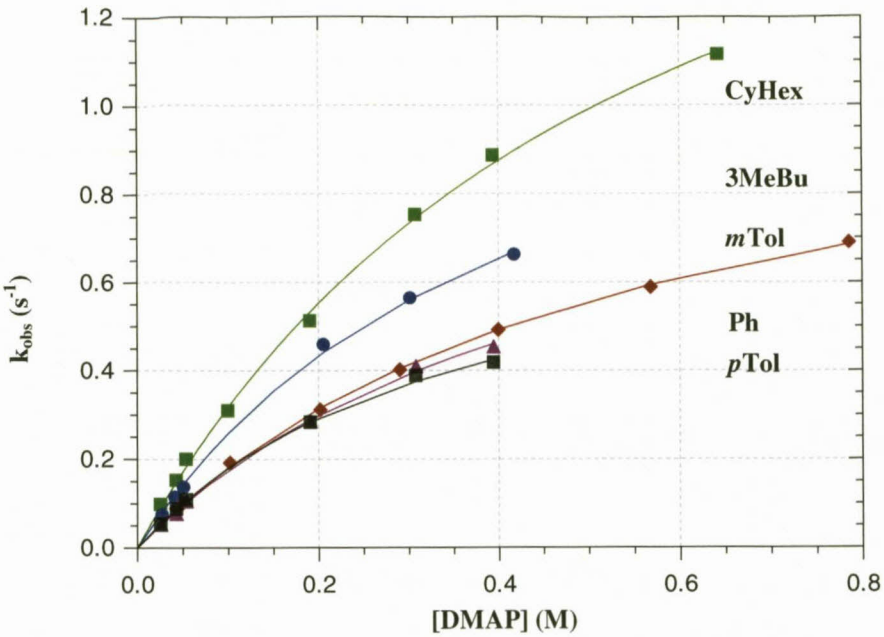

Figure 9.28: **Plot of k_{obs} *vs.* [DMAP] for the reaction between *fac*-[Re(Sal-T)(CO)$_3$(HOCH$_3$)] and DMAP at 25.0 °C in methanol (T = coordinated substituent).**

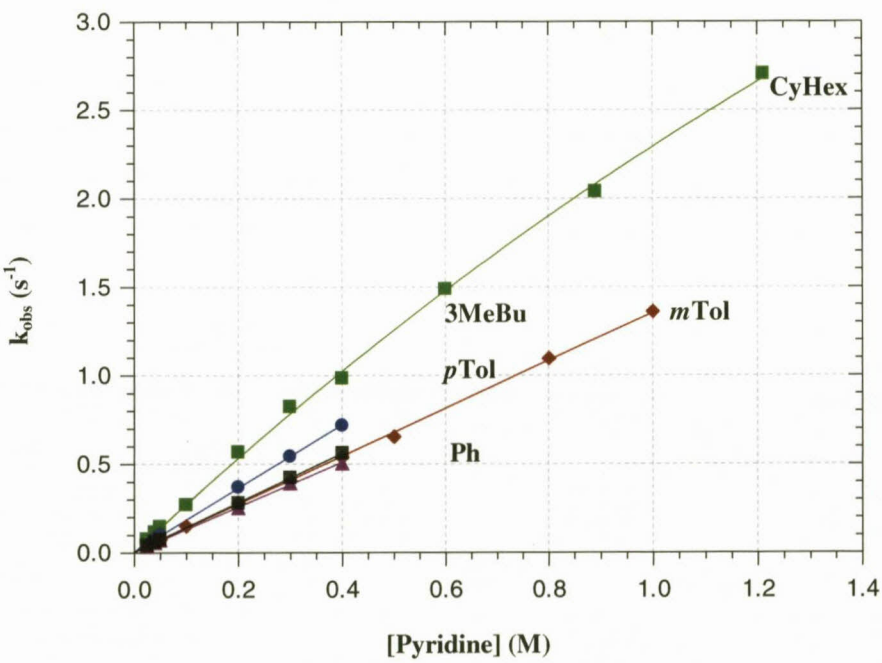

Figure 9.29: **Plot of k_{obs} *vs.* [Pyridine] for the reaction between *fac*-[Re(Sal-T)(CO)$_3$(HOCH$_3$)] and pyridine at 25.0 °C in methanol (T = coordinated substituent).**

Table 9.12: **Kinetic data obtained for the reaction of *fac*-[Re(Sal-T)(CO)$_3$(HOCH$_3$)] with Pyridine at 25.0 °C in methanol.**

Tail	IR (ν_{CO}, cm^{-1})	k_1 ($M^{-1}s^{-1}$)	K_1 (M^{-1})	k_3 (s^{-1})	K_2 (M^{-1})	$k_f = k_3K_2$	k_4 (s^{-1})	k_{-4}/k_5
*m*Tol	2002.0, 1968.8	1.29(2)	67(18)	5.5(9)	0.27(5)	1.5(4)	5.5(9)	0.15(3)
*p*Tol	2015.6, 1878.3	1.393(3)	372(73)	*31(32)*	*0.05(5)*	*1.4(2.1)*	*31(32)*	*0.9(9)*
Ph	2020.5, 1892.5	1.26(2)	196(117)	*8(5)*	*0.2(1)*	*1.4(1.3)*	*8(5)*	*0.2(2)*
3MeBu	2001.4, 1876.5	1.79(2)	301(256)	*11(6)*	*0.17(9)*	*1.9(1.4)*	*11(6)*	*0.2(1)*
CyHex	2014.9, 1871.6	2.22(5)	30(11)	13(2)	0.21(3)	2.8(6)	13(2)	0.19(3)

* Values with large ESD's (*indicated in italics*) are given for completeness of study.

Table 9.13: **Kinetic data obtained for the reaction of *fac*-[Re(Sal-T)(CO)$_3$(HOCH$_3$)] with DMAP at 25.0 °C in methanol.**

Tail	IR (ν_{CO}, cm^{-1})	k_1 ($M^{-1}s^{-1}$)	K_1 (M^{-1})	k_3 (s^{-1})	K_2 (M^{-1})	$k_f = k_3K_2$	k_4 (s^{-1})	k_{-4}/k_5
*m*Tol	2002.0, 1968.8	-	-	1.15(2)	1.88(7)	2.16(9)	1.15(2)	0.0215(8)
*p*Tol	2015.6, 1878.3	-	-	0.80(5)	2.9(3)	2.3(3)	0.80(5)	0.014(2)
Ph	2020.5, 1892.5	-	-	1.03(8)	2.0(2)	2.1(3)	1.03(8)	0.020(3)
3MeBu	2001.4, 1876.5	-	-	1.34(9)	2.4(3)	3.2(5)	1.34(9)	0.017(2)
CyHex	2014.9, 1871.6	1.7(1)	13(5)	2.11(9)	1.8(1)	3.7(3)	2.11(9)	0.023(2)

From previous paragraphs it is obvious that assigning the mechanism is difficult. However, in our opinion, these results convincingly point towards an I_d mechanism. The reasons for this are discussed systematically in the following paragraphs.

- The range of entering ligands used do not differ substantially, *i.e.* the donor groups are similar, all the pyridines used are aromatic. Therefore one would expect that the intimate mechanism for all the reactions studied should be similar or at the very least only point to a subtle changeover *e.g.* $I_a \rightarrow I_d$.
- All the reactions studied are very fast, the slowest of which is completed in ~ 60 s. This places limitations on the concentration range that could be used to evaluate the effect of ligand concentrations on k_{obs} in many cases, since our Stopped-flow device can only accurately measure reactivities of 1 s and slower.
- The above fact could be a reason why straight lines for plots of k_{obs} *vs.* [Ligand] were obtained in some cases as higher ligand concentrations resulted in reactions which were complete in under 1 s.
- The extrapolated plots of k_{obs} *vs.* [Ligand] for the reactions where straight lines were obtained all reach saturation points at different saturation levels, thus excluding a Dissociative mechanism (see Figure 9.1).
- Non-linear plots were found for the reaction of DMAP with all the rhenium complexes.
- The reaction of *fac*-[Re(Sal-*m*Tol)$(CO)_3(HOCH_3)$] with DMAP and 4-picoline and the reaction of *fac*-[Re(Sal-CyHex)$(CO)_3(HOCH_3)$] with all entering ligands yield non-linear plots. Line curvature is an indication of a dissociative or an interchange mechanism.
- The mechanism type can therefore not be associatively activated.
- In a dissociative type mechanism, increasing the electron density on the metal centre would increase the rate with which saturation limits are reached. The rate constant for the dissociative mechanism (k_4, DMAP reactions) increase in general for Cy > *m*Tol > Ph.
- The dissociation constant, k_4, for a pure dissociative mechanism should be constant and independent on the nature of the entering ligand (see Figure 9.1). The values of k_4 for the substitution reaction of *fac*-[Re(Sal-CyHex)$(CO)_3(HOCH_3)$] with 3-

chloropyridine is nineteen times faster than for DMAP (k_4 = 40(4) >> 2.11(9) s^{-1}) and eight times for *fac*-[Re(Sal-mTol)$(CO)_3(HOCH_3)$] (k_4 = 9(2) >> 1.15(2) s^{-1}).

- Thus, the most likely mechanism is considered to be an interchange dissociative mechanism (I_d) (Scheme 9.3) which is further confirmed by the positive values determined for the entropy of activation ($\Delta S^{\neq}$), whereby there is an interchange of S and L within the outer-sphere complex (Re(S) ··· L) to form a rapid pre-equilibrium, followed by a slower, rate-determining second reaction.
- In general, the I_d stability constant (K_2) increases as the electron density of the entering ligand increases as indicated for the reactions of *fac*-[Re(Sal-*m*Tol)$(CO)_3(HOCH_3)$] and *fac*-[Re(Sal-CyHex)$(CO)_3(HOCH_3)$].

$$[Re(S)] + [L] \underset{}{\overset{K_2}{\rightleftharpoons}} [Re(S)\cdots(L)]^{\neq}$$

$$[Re(S)\cdots(L)]^{\neq} \underset{k_{-3}}{\overset{k_3}{\rightleftharpoons}} [Re(L)] + [S]$$

Scheme 9.3: Suggested mechanism for interchange reactions of *fac*-[Re(N-O)$(CO)_3$(S)] complexes.

A discrepancy occurs in the reaction of *fac*-[Re(Sal-*p*Tol)$(CO)_3(HOCH_3)$] with DMAP which cannot be explained at the moment. A methyl functionality in the *meta* position provides less electron density than the *para* position, therefore *fac*-[Re(Sal-*p*Tol)$(CO)_3(HOCH_3)$] should be more electron rich than *fac*-[Re(Sal-*m*Tol)$(CO)_3(HOCH_3)$], however the rate constant (k_3) for *fac*-[Re(Sal-*p*Tol)$(CO)_3(HOCH_3)$] is the slower of the two complexes. However, upon consideration of the overall rate reaction ($k_f = k_3K_2$) the *p*Tol complex is faster. This suggests that the electron density variation is probably too small to induce an observable effect. From the crystallographic data there is no significant difference in the Re-O_{04} bond distance which could explain the kinetic results (*p*Tol complex Re-O_{04} = 2.17(3) Å *vs.* *m*Tol complex Re-O_{04} = 2.179(3) Å).

Although the complexes show prominent IR stretching frequencies, there is no systematic dependence on the bidentate ligand properties. The Re-OH-CH_3 bond angle (determined from crystallographic studies) is not significantly different when comparing the aromatic and aliphatic complexes (*p*Tol (123.6(19)°), Ph (121.2(5)°) and *m*Tol (122.1(3)°) *vs.* CyHex (123.8(7)°) and 3MeBu (124.3(4)°). It is clear that the Sal-type ligands activate the Re(I)

metal centre significantly, allowing the novel opportunity to evaluate substitution reactions under limiting conditions, *i.e.* by exhibiting non-linear reaction rate profiles.

More detailed crystallographic and kinetic studies, particularly with regards to high-pressure kinetic studies, are necessary to further confirm the intimate mechanism in the substitution kinetics.

10 *IN VITRO* CANCER SCREENING OF SELECTED COMPOUNDS

10.1 INTRODUCTION

The growth inhibitory effects of selected non-coordinated salicylidene ligands, SalH-T (T = coordinated substituent) and *fac*-[Re(Sal-T)$(CO)_3$(S)] complexes (S = methanol / pyridine) were investigated. The compounds were tested in the 3-cell line panel consisting of TK10 (renal), UACC62 (melanoma) and MCF7 (breast) cancer cells using a Sulforhodamine B (**SRB**) assay.

The SRB assay was developed by Skehan *et al.*[1] to measure drug-induced cytotoxity and cell proliferation for large-scale drug screening applications. SRB is an anionic bright pink aminoxanthene protein dye with two sulfonic groups ($C_{27}H_{30}N_2O_7S_2$).

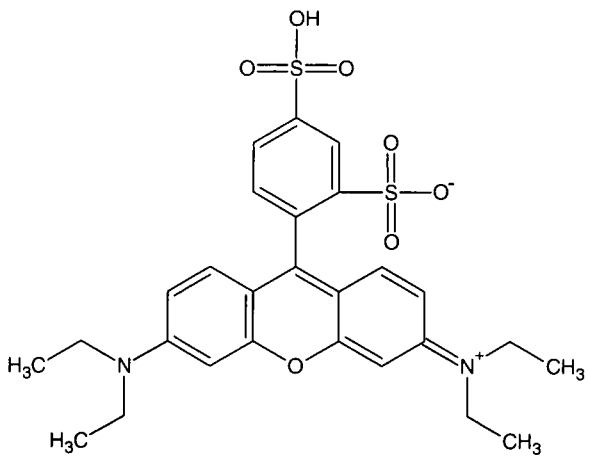

Figure 10.1: Chemical structure of Sulforhodamine B.

The SRB assay method is rapid, inexpensive and sensitive for measuring the cellular protein content of adherent and suspension cultures in 96-well microtiter plates. The method was designed to be suitable for laboratory purposes as well as for very large-scale applications such as the National Cancer Institute's disease-oriented *in vitro* anticancer-drug discovery

[1] P. Skehan, R. Storeng, D. Scudiero, A. Monks, J. McMahon, D. Vistica, J.T. Warren, H. Bokesch, S. Kenney, M.R. Boyd, *J. Natl. Cancer Inst.*, 1990, 82, 1107

screen, which requires the use of several million culture wells per year. The end-point of the SRB assay is colorimetric, non-destructive and indefinitely stable. It provides a sensitive and appropriate assay to measure drug-induced cytoxicity.[2]

The assay is based on the ability of the protein dye sulforhodamine B to bind electrostatically in a pH-dependent manner to protein basic amino acid residues of trichloroacetic acid (TCA)-fixed cells. The dye binds to the fixed cellular protein under mild acidic conditions. It can then be extracted from the cells and solubilized for measurement under mild basic conditions.

The three cell line panel is recommended by the National Cancer Institute for preliminary screens. The SRB Assay, for this study, was performed by the Council for Scientific and Industrial Research (CSIR), South Africa,[3,4] in accordance with the protocol of the Drug Evaluation Branch of the National Cancer Institute.

10.2 EXPERIMENTAL

The human cell lines TK10, UACC62 and MCF7 were obtained from National Cancer Institute (NCI) in the framework of a collaborative research program between CSIR and NCI. Cell lines were routinely maintained as monolayer cell cultures in RPMI containing 5% fetal bovine serum, 2 mM L-glutamine and 50μg/ml gentamicin. For the screening experiment, the cells (3-19 passages) were inoculated in 96-well microtiter plates at plating densities of 7-10 000 cells/well and were incubated for 24 h. After 24 h one plate was fixed with trichloroacetic acid (TCA) to represent a measurement of the cell population for each cell line at the time of drug addition (T_0). The other plates with cells were treated with the experimental compounds which were previously dissolved in DMSO as 10mM stocks and diluted in medium to a final concentration 10μM. Cells without compounds served as controls. Blank wells contained complete medium without cells. Emetine was used as a reference standard (concentration = 10 μM). The plates were incubated for 48 h after addition of the compounds. At the end of the incubation period, the cells were fixed to the bottom of

[2] R.D. Blumenthal, *Chemosensitivity: In Vitro Assays*, Vol. 1, Humana Press Inc., Totawa, NJ., USA, 2005
[3] N. Kolesnikova, H. Hoppe, CSIR Biosciences Pharmacology Group, *In Vitro Cancer Screening Report*, South Africa, reported 2011-01-17
[4] N. Kolesnikova, D. Koot, H. Hoppe, CSIR Biosciences Pharmacology Group, *In Vitro Cancer Screening Report*, South Africa, reported 2011-07-19

each well with cold 50% trichloroacetic acid, washed, dried and dyed with SRB. Unbound dye was removed and protein-bound dye was extracted with 10mM Tris base for optical density determination at a wavelength 540 nm using a multiwell spectrophotometer. Optical density measurements were used to calculate the net percentage cell growth:

The optical density of the test wells after 48 h period of exposure to test compound is T_i, the optical density at time zero is T_0, and the control (untreated cells) optical density is C.

Percentage cell growth was calculated as:
$[(T_i-T_0)/(C-T_0)]$ x 100 for concentrations at which $T_i \geq T_0$
$[(T_i-T_0)/T_0]$ x 100 for concentrations at which $T_i < T_0$.

10.3 *IN VITRO* CANCER SCREENING RESULTS

The % growth is the total growth of cells in the treated wells compared to untreated controls over a 48 h experimental period. In other words a 100% growth indicates there are the same amount of cells in treated wells as in untreated control wells, after 48 h. 0% Growth indicates no increase in cell number as the treated wells contain the same number of cells as at the start of the incubation period, time zero (T_0). -100% Growth indicates no cells remain after the 48 h incubation period.

The growth inhibitory effects of selected non-coordinated salicylidene ligands, SalH-T are listed in Table 10.1 while the results for the rhenium tricarbonyl complexes are listed in Table 10.2. Graphical representations of the results are listed in Figures 10.2 – 10.3.

Table 10.1: **Net growth of renal, melanoma and breast cancer cells analysed according a sulforhodamine B assay against SalH-T ligands.**

	Compound	Chemical Structure	Conc. (μM)	Renal Cells TK10 Growth (%)	Melanoma Cells UACC62 Growth (%)	Breast Cells MCF7 Growth (%)
1	4F-SalH-*m*Tol	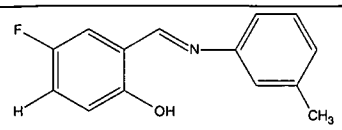	10	82.01(2)	91.03(1)	77.49(2)
2	SalH-*m*Tol	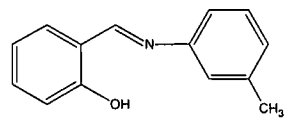	10	92.64(1)	97.29(3)	78.42(4)
3	SalH-Carba	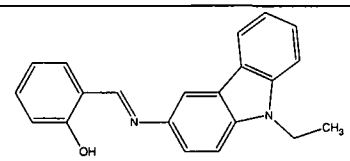	10	80.69(2)	98.12(4)	75.43(1)
4	5Me-SalH-Carba	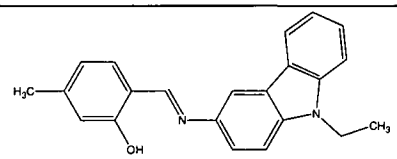	10	81.08(2)	101.45(2)	77.07(5)
5	5Me-SalH-Trypt	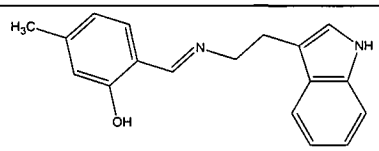	10	86.47(1)	93.31(2)	68.63(2)
6	5Me-SalH-Tyra	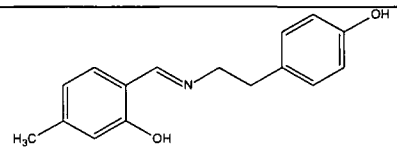	10	71.83(2)	97.27(5)	83.77(2)
7	5Me-SalH-Triaz	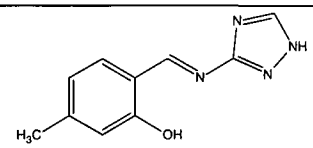	10	79.60(1)	101.65(8)	76.15(1)
8	5Me-SalH-Hist	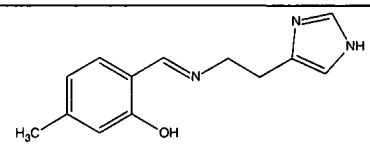	10	76.25(1)	100.58(2)	82.14(8)
9	5Me-SalH-Pen	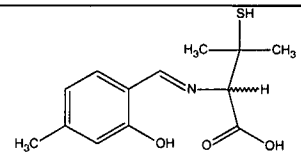	10	85.45(1)	96.21(92)	78.35(6)
10	5Me-SalH-4OHPh	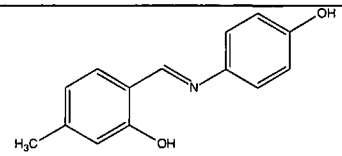	10	65.87(1)	73.24(1)	74.29(9)
E	Emetine (Positive control)	-	10	-61.980(2)	-94.230(5)	-47.24(1)

Table 10.2: **Net growth of renal, melanoma and breast cancer cells analysed according a sulforhodamine B assay against *fac*-[Re(Sal-T)(CO)$_3$(S)] complexes.**

	Sal-T	S	Chemical Structure	Conc (μM)	Renal Cells TK10 Growth (%)	Melanoma Cells UACC62 Growth (%)	Breast Cells MCF7 Growth (%)
11	5Me-Sal-Carba	$HOCH_3$	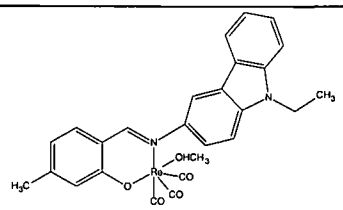	10	102.01(4)	93.23(5)	93.84(1)
12	5Me-Sal-Carba	NC_5H_5	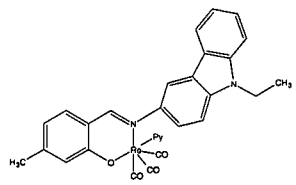	10	78.68(8)	70.30(2)	70.68(15)
13	5Me-Sal-Hist	-	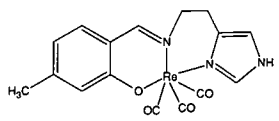	10	106.11(4)	84.65(4)	93.49(3)
14	Sal-4NitroPh	$HOCH_3$	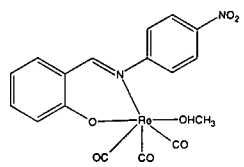	10	92.38(4)	51.03(27)	73.11(4)
15	Sal-Ph	NC_5H_5	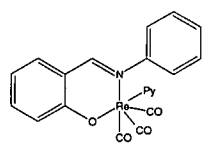	10	43.66(2)	38.35(4)	58.05(11)
E	Emetine (Positive control)	-	-	10	-61.35(1)	-86.66(1)	-46.41(1)

Py = NC_5H_5 = pyridine

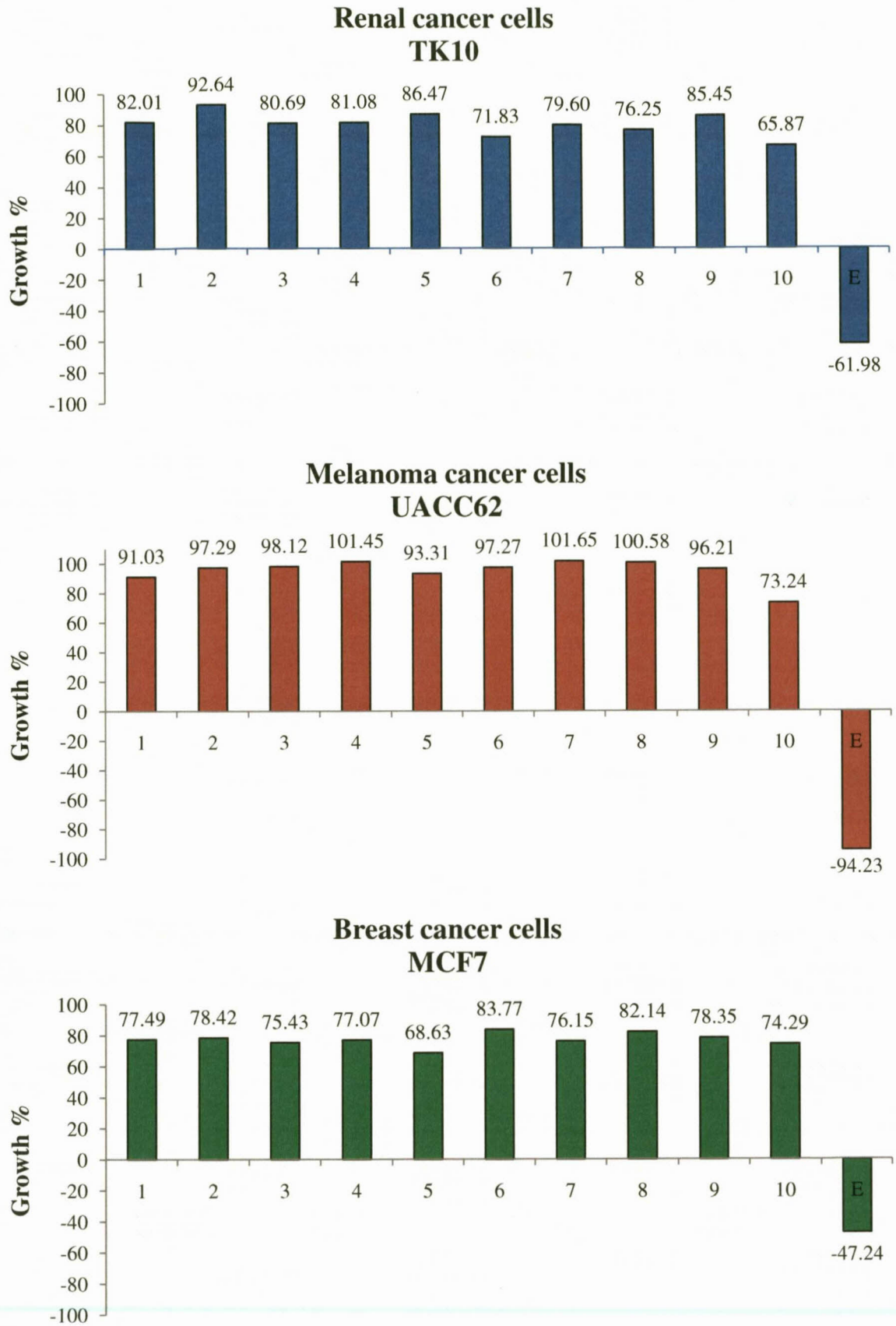

Figure 10.2: **Graphical representation of net growth of renal, melanoma and breast cancer cells analysed according a sulforhodamine B assay against SalH-T ligands.**

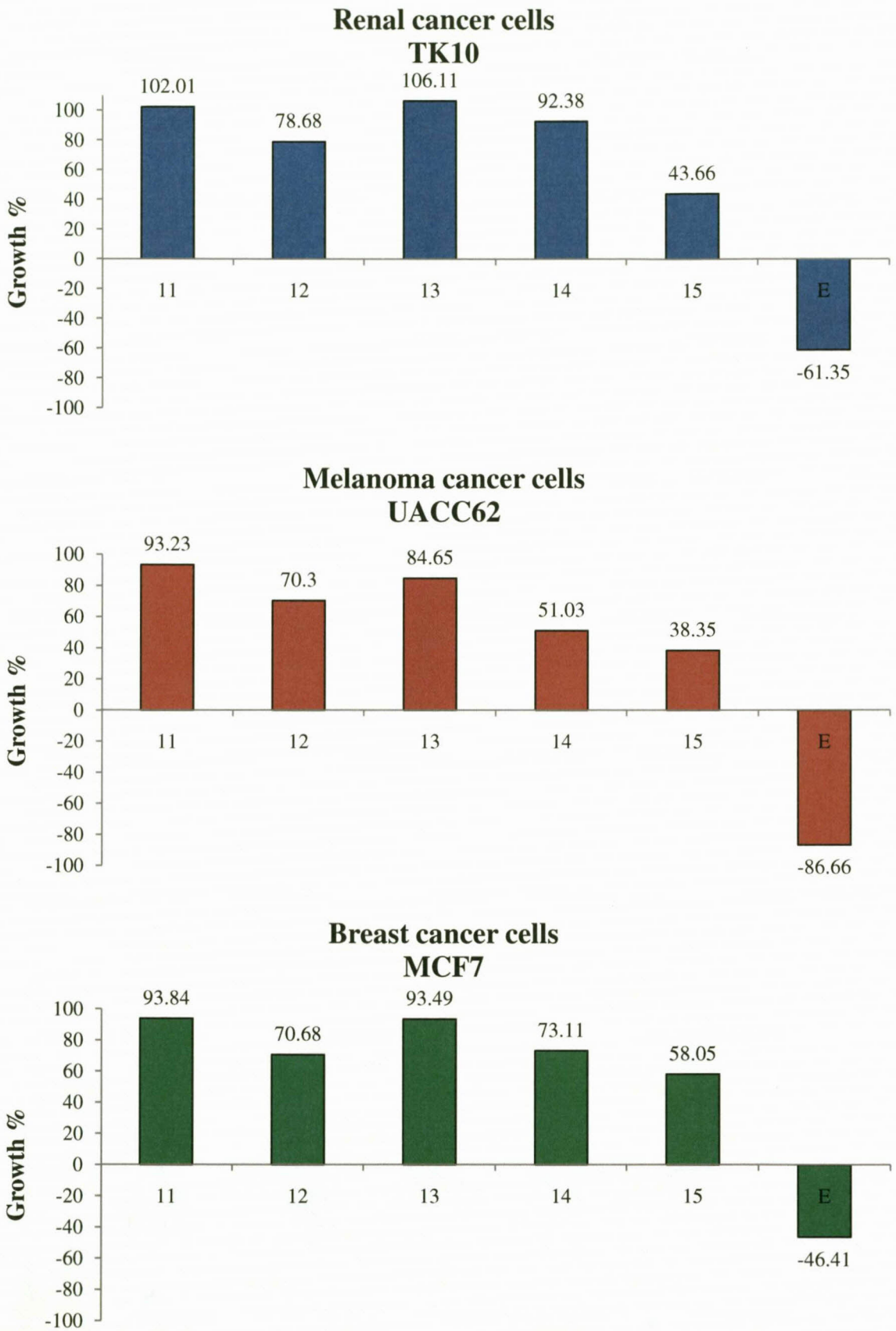

Figure 10.3: **Graphical representation of net growth of renal, melanoma and breast cancer cells analysed according a sulforhodamine B assay against *fac*-[Re(Sal-T)(CO)$_3$(S)] complexes (T = substituent, S = methanol/pyridine).**

10.4 CONCLUSION

It can be seen from the tabulated results, that none of the organic free SalH ligands show any significant toxicity / activity (percentage cell growth of ≤ 0) to the three cancer types selected, however some inhibition on cell growth did occur. 5Me-SalH-Trypt and 5Me-SalH-4OHPh have the highest inhibition of cell growth for breast cells and renal cells respectively, of the compounds tested.

No significant cell activity (percentage cell growth of ≤ 0) was found for the selected *fac*-[Re(Sal-T)$(CO)_3$(S)] complexes. Limited cell growth inhibition was however observed for a few complexes. *fac*-[Re(Sal-4NitroPh)$(CO)_3(HOCH_3)$] (**15**) has the highest inhibition of cell growth for all three types of cancer cells. *fac*-[Re(5Me-Sal-Hist)$(CO)_3$] (**14**) has a greater selectivity of growth inhibition for melanoma cancer cells. The cell selectivity may be advantageous, as it affords the possibility of developing compounds that are specific for particular types of cancer, as opposed to having outright toxicity for all dividing cells.

The biological activity of the compounds is still under investigation as the *in vitro* cancer screen of the remaining ligands and Re-Sal complexes will still be conducted. The IC50 values of any active compounds must be determined as well as biological distribution studies. Further experiments will include the use of radiorhenium to evaluate the combined effects of chemo- and radio-activity on selected cell lines.

11 EVALUATION OF STUDY

11.1 INTRODUCTION

One of the original motivations of this study was to gain further insight into the coordinative and chemical properties of the *fac*-$[M(CO)_3]^+$ (M = Tc, Re) complexes used as potential imaging and the therapeutic radiopharmaceutical agents. The design of a range of ligands which would allow convenient coordination of selected directing molecules to a common coordinative ligand backbone was an integral part of the study. Finally, the coordination of the functionalized organic ligand backbone to the *fac*-$[M(CO)_3]^+$ metal centre was explored and the chemical, kinetic and biological properties of the new complexes were investigated. The findings of this investigation are briefly discussed below.

11.2 EVALUATION

11.2.1 Synthesis and single crystal X-ray crystallographic study

The organic ligands synthesised in this study were made according to the Schiff-base reaction. The Schiff-base ligands are widely utilised due to the relative ease of formation and wide versatility whereby the individual chemical properties (steric and electronic parameters, denticity, donor atoms *etc.*) may be altered. Only a few Re(I) and Tc(I) tricarbonyl complexes containing salicylidene bidentate ligands have been reported. The salicylidene ligand originates from the aldehyde, salicylaldehyde, which reacts with various amines to form the salicylidene backbone containing various amino substituents bonded to the imine nitrogen atom. The prime focus of this study was therefore to explore the synthesis of a range of N,O bidentate salicylidene ligands which could then be further utilized to evaluate their coordinating ability to the *fac*-$[M(CO)_3]^+$ core. This lead to the successful synthesis and characterization of a range of salicylidene ligands **SalH,** containing aromatic, aliphatic and biological active imino substituents.

The aromatic and aliphatic substituents were selected for their various steric and electronic parameters which would affect the properties of the coordinated organometallic tricarbonyl complex. They were also selected as a prototype to determine whether the salicylidene ligands could be coordinated to the rhenium tricarbonyl complexes in high yield and purity. The biological amines which were chosen for the continuation of the ligand study, were selected for their known diverse biological activities. A further aspect of interest was whether these biological compounds, varying in structure and size, could be synthesised in high yield and purity. All the Schiff-base ligands were readily synthesised and several crystals suitable for single crystal X-ray diffraction were obtained. The crystallographic study illustrated the various packing effects of the salicylidene compounds including the rotation of the C=N imine double bond which results in various orientations of the coordinated substituents. The synthesis of the aliphatic SalH ligands often yielded oils or crystals at -40 °C. Diffraction data of these compounds could not be obtained. A computational study was therefore conducted to determine whether theoretical optimizations (DFT calculations) could yield reasonable approximations of the orientation of the synthesised compounds (§ 11.2.2).

Ideally the synthesis of radiopharmaceuticals designed for routine clinical application should be prepared in a saline solution (0.9% NaCl in water or buffer).[1] The synthesis of the aqua specie *fac*-[Re(Sal-T)(CO)$_3$(**H$_2$O**)] from an aqueous medium proved unsuccessful as the reactions yielded impure oils. The solubility of certain ligands in water was low and therefore a small amount of methanol was added. In general the dominant specie formation, in the aqueous/methanol solution, was the rhenium-methanol complex *fac*-[Re(Sal-T)(CO)$_3$(**HOCH$_3$**)]. These results lead to the synthetic procedure utilizing methanol as the solvent to yield Re(I)-methanol complexes. The decision to use methanol proved successful for several reasons. Firstly, crystallographically pure products were obtained opposed to impure oils from an aqueous medium. The coordinated methanol is easily substituted by other neutral monodentate ligands, to yield pure product in satisfactory yields. Several *fac*-[Re(Sal-T)(CO)$_3$(HOCH$_3$)] complexes were soluble in water and a water substitution reaction was identified during the kinetic substitution study. The synthesis of the Re(I)-methanol tricarbonyl complexes adds an additional dimension to the development of radiopharmaceutical kit design utilising the [2+1] approach.

---

[1] R. Alberto, R. Schibli, R. Waibel, U. Abram, A.P. Schubiger, *Coord. Chem. Rev.*, 1999, 192, 901

The coordination mode of the *fac*-[Re(Sal-T)$(CO)_3(HOCH_3)$] complexes were investigated by single crystal X-ray diffraction studies. The methanol crystal structures were often difficult to determine due to the sensitivity of the crystals to temperature. The crystalline complexes readily lost crystallinity at temperatures above 30 °C and therefore had to be grown and stored at 4 °C, otherwise the formation of oils occurred. The purity of the complexes were unaffected by the loss of crystallinity as determined by NMR. The crystallographic studies indicated that bond angles and bond lengths were not significantly affected by the different nitrogen-coordinated substituents. Methanol crystal structures showed a tendency to crystallise in the *C2/c* space group. The various substituents contained similar orientation, not withstanding varied steric size or changing aromaticity.

11.2.2 Computational study

A computational study of the molecules in the gas phase was conducted to better understand the variation of planarity of the aromatic rings in the salicylidene molecule. DFT calculations for rhenium complexes were performed at the B3LYP/LanL2DZ level of theory, where the optimized structure (indicated by no imaginary frequencies) with the lowest energy was obtained. The organic ligands containing C, H, O, N, F atoms were calculated at a higher level of theory (B3LYP/6-311G++(d,p)). The theoretical optimized structures with the lowest relative energy was compared to the crystal structures of the corresponding non-coordinated free ligand, SalH, as well as the coordinated *fac*-[Re(Sal-T)$(CO)_3$(S)] complexes. A good correlation was observed between the conformations adopted in the solid state and the predicted conformations, with comparable bond lengths and angles. The theoretical optimized structures were reasonable approximations and therefore DFT calculations can be utilized if the coordination mode of a specific complex is required but which cannot be determined by crystallographic studies.

11.2.3 Substitution kinetic study

The reactivity of the complexes was evaluated by a detailed kinetic study and was considered an integral part of the research as few reaction kinetic studies have been conducted on Re(I) and Tc(I) tricarbonyl complexes. A kinetic study of the methanol substitution by various entering monodentate ligands were successfully investigated on selected *fac*-[Re(Sal-

T)$(CO)_3(HOCH_3)$] complexes. The substitution reaction of methanol by water was observed in analytical grade solvents after which all kinetic studies had to be conducted in dry solvents. Only one reaction was observed for the substitution reaction in dry solvents. The reaction was very rapid and had to be measured with the use of a Stopped-flow Spectrophotometer in the millisecond range. The mechanism was determined as an interchange dissociative mechanism (I_d) whereby there is an interchange between the coordinated methanol ligand and the free mondentate ligand in solution, within the outer-sphere complex to form a rapid pre-equilibrium, followed by a slower, rate-determining second reaction. The dissociative-type mechanism was further confirmed by positive values of the entropy of activation ($\Delta S^{\neq}$).

11.2.4 *In vitro* cancer screening

The growth inhibitory effects of selected non-coordinated salicylidene ligands and *fac*-[Re(Sal-T)$(CO)_3$(S)] complexes were tested in the 3-cell line panel consisting of TK10 (renal), UACC62 (melanoma) and MCF7 (breast) cancer cells using a Sulforhodamine B (SRB) assay. The three cell line panel is recommended by the National Cancer Institute for preliminary anti-cancer screens. None of the organic free ligands showed any significant toxicity / activity (percentage cell growth of ≤ 0) to the three cancer types selected. No significant cell activity was found for the selected *fac*-[Re(Sal-T)$(CO)_3$(S)] complexes however limited cell growth inhibition was observed for a few complexes. The study concerning the biological activity of all the ligand and rhenium compounds is currently underway as the IC50 values of any active compounds as well as their toxicity against normal cell cultures must still be determined.

11.3 FUTURE WORK

A large range of Schiff-base ligands could be synthesized containing various imino substituents coordinated to the imine nitrogen atom. The aqueous solubility of the ligands should be addressed, perhaps by functionalising the salicylidene backbone with carboxyl groups or other hydrophilic substituents. Further research into the synthesis of ligands containing a fluoride moiety would allow for the development of dual radiopharmaceuticals such as combining ^{18}F for PET imaging with $^{186/188}$ Re for radiotherapy.

The synthesis of the *fac*-[Re(Sal-T)$(CO)_3$(S)] must be expanded to develop a rapid, synthetic route in an aqueous medium. Other solvents, compatible with routine clinical applications, such as ethanol or dimethylsulphoxide, should be explored. The coordination of the SalH-T ligands to ^{99m}Tc(I) must still be investigated and a detailed kinetic study on the substitution of the coordinated solvent in the third position should be conducted.

The substitution kinetic study should be expanded by investigating additional rhenium coordinated Schiff-base ligands. The water substitution reaction would provide additional information on how tightly bound is the solvent molecule, in the third position, to the rhenium metal centre. The kinetic behaviour of five-member Schiff-base ligands could be explored and compared to the behaviour of the six-member Salicylidene ligand. High-pressure kinetic studies will provide additional information on the intimate mechanism of the substitution reactions.

In vitro cancer screening as well as biological distribution studies must be conducted on the remaining SalH ligands and Re(I)-Sal complexes. The biological effects induced by varying the compound coordinated in the third position, according to the [2+1] approach, shall be explored in future studies. This should include the evaluation of the combined effect (chemo- as well as radio-activity) on cancer cells.

SUMMARY

Rhenium(I) and technetium(I) tricarbonyl complexes hold significant potential as model radiopharmaceuticals which could be utilized as therapeutic and imaging agents. ^{99m}Technetium in particular, is one radionuclide which is used in more than 80% of radiopharmaceuticals as a diagnostic agent. The biodistribution of a potential radiopharmaceutical can in principle be manipulated by the coordination of a biologically active molecule to the radionuclide.

The principle aim of this study was to gain further insight into the chemistry, coordination and kinetic behaviour of *fac*-$[M(CO)_3]^+$ (M = Tc, Re) complexes. With this idea in mind, a range of salicylidene ligands, SalH, were synthesised according to the Schiff-base reaction. These organic ligands were synthesized as potential bifunctional chelators between the tricarbonyl radionuclide and the biologically active directing molecule. The ligands contain various amine compounds which were coordinated to the imine nitrogen atom on the salicyclidene "backbone". The imino substituents consisted of aromatic, aliphatic and biologically active moieties with varying steric, electronic and biological properties and included amines such as *m*-toluidine, 3-methylbutylamine, aniline, histamine, tryptamine, tyramine *etc*. The ligands were characterized *via* NMR and IR spectroscopy. A single crystal X-ray diffraction study of the ligands was reported and revealed the various orientations of the substituents relative to the salicylidene backbone. The reported X-ray crystallographic structure determinations included the following ligands: 2-(*m*-tolyliminomethyl)phenol, 5-methyl-2-(*m*-tolyliminomethyl)phenol, 4-fluoro-2-(*m*-tolyliminomethyl)phenol, 2-(4-nitro-phenyliminomethyl)phenol, 2-[(4-hydroxyphenyl)iminomethyl]-5-methylphenol, 2-[(2-imidazol-4-yl)ethyliminomethyl]-5-methylphenol, 2-[(2-indol-3-yl-ethyl)iminomethyl]-5-methylphenol, 2-(9-ethylcarbazol-3-yliminomethyl)-5-methylphenol, 2-[2-(4-hydroxy-phenyl)ethyliminomethyl]-5-methylphenol, 5-methyl-2-(1,2,4-triazol-3-yliminomethyl)-phenol.

A further important part of this investigation was concerned with the synthesis and evaluation of the solid state characteristics of the SalH ligands coordinated to the rhenium(I) metal centre. The advantage of the *fac*-$[M^I(CO)_3(S)_3]^+$ complex (M = Tc or Re; S = H_2O or other

coordinated solvents) is the high stability of the classic low spin d^6 $[M(CO)_3]^+$ core in water and the potential of exchanging the labile solvent ligands. The SalH bidentate ligands were bonded to the *fac*-$[M(CO)_3]^+$ core according to the [2+1] approach, thus leaving an 'open' third position occupied by either a solvent or by a neutral monodentate ligand. The complexes were also characterized *via* NMR and IR spectroscopy. The solid state behaviour of these *fac*-[Re(Sal)$(CO)_3$(S)] complexes were investigated by X-ray crystallography, and included the complexes: *fac*-[Re(Sal-*m*Tol)$(CO)_3(HOCH_3)$], *fac*-[Re(Sal-Ph)$(CO)_3(HOCH_3)$], *fac*-[Re(Sal-*p*Tol)$(CO)_3(HOCH_3)$], *fac*-[Re(Sal-CyHex)$(CO)_3(HOCH_3)$], *fac*-[Re(Sal-3MeBu)$(CO)_3(HOCH_3)$], *fac*-[Re(Sal-Ph)$(CO)_3(NC_5H_5)$], *fac*-[Re(Sal-3MeBu)$(CO)_3(NC_5H_5)$], *fac*-[Re(5Me-Sal-Hist)$(CO)_3$], *fac*-[Re(5Me-Sal-Trypt)$(CO)_3$ (NC_5H_5)], *fac*-[Re(5Me-Sal-Carba)$(CO)_3(NC_5H_5)$], *fac*-[Re(5Me-Sal-*m*Tol)$(CO)_3(HOCH_3)$], *fac*-[Re(5Me-Sal-3Me2Bu)$(CO)_3(HOCH_3)$]. The coordination geometry around the Re(I) metal centre in the crystal structures was a distorted octahedron. The imino substituents crystallize in similar orientations despite various steric sizes, while the bond angles and lengths were not significantly affected by the different nitrogen-coordinated substituents.

The study of the solid state coordination of the complexes was further supplemented with a theoretical DFT (density functional theory) study for specifically the 2-(*m*-tolyliminomethyl)phenol, 5-methyl-2-(*m*-tolyliminomethyl)phenol, 2-(9-ethylcarbazol-3-yliminomethyl)-5-methylphenol, *fac*-[Re(Sal-*m*Tol)$(CO)_3$(S)], *fac*-[Re(Sal-Ph)$(CO)_3$(S)], *fac*-[Re(5Me-Sal-Carba)$(CO)_3$(S)] compounds. The comparison between the optimised structure and the crystal data reveal small differences, illustrating that predictions can be made in terms of the coordination of the bidentate ligands to the rhenium metal centre utilising DFT techniques.

A kinetic study of substitution of the coordinated solvent ligand of *fac*-[Re(Sal)$(CO)_3$(S)] complexes was done. The following complexes were evaluated: *fac*-[Re(Sal-*m*Tol)$(CO)_3(HOCH_3)$], *fac*-[Re(Sal-*p*Tol)$(CO)_3(HOCH_3)$], *fac*-[Re(Sal-Ph)$(CO)_3(HOCH_3)$], *fac*-[Re(Sal-3MeBu)$(CO)_3(HOCH_3)$], *fac*-[Re(Sal-CyHex)$(CO)_3(HOCH_3)$] for entering ligands 3-chloropyridine, pyridine, 4-picoline and 4-dimethylaminopyridine in methanol as solvent. The rates were quite fast and varied from seconds to minutes under the conditions studied. Only one reaction was observed under dry conditions. The Sal-Re ligand systems allowed the unique opportunity to confirm non-associative behaviour since for selected ligands, pyridine and DMAP, limiting kinetic profiles were obtained; clear evidence of either

I or *D* intimate mechanisms. An interchange dissociative (I_d) mechanism was proposed for the substitution reaction with positive activation entropy and enthalpy values.

An *in vitro* cancer screen was conducted on selected non-coordinated ligands and *fac*-[Re(Sal)$(CO)_3$(S)] complexes in a 3-cell line panel consisting of TK10 (renal), UACC62 (melanoma) and MCF7 (breast) cancer cells using a Sulforhodamine B (SRB) assay. No significant cell activity was found but limited cell growth inhibition was observed.

Keywords: Radiopharmaceutical, radionuclide, cancer activity, rhenium, technetium, tricarbonyl complexes, salicylidene, bidentate ligands, crystallography, kinetic study.

OPSOMMING

Renium(I) en tegnesium(I) trikarbonielkomplekse het betekenisvolle potensiaal as model kerngeneesmiddels wat gebruik sou kon word as terapeutiese- en beeldingsagente. ^{99m}Tegnesium word spesifiek in meer as 80% van alle radiofarmaseutiese middels as diagnostiese middel gebruik. Die bioverspreiding van `n potensiële radiofarmaseutiese middel kan in beginsel gemanipuleer word deur die koördinasie van `n biologies-aktiewe verbinding aan die radionuklied.

'n Primêre doel van hierdie studie was om beter insig in die chemiese, koördinatiewe en kinetiese gedrag van *fac*-$[M(CO)_3]^+$ (M = Tc, Re) komplekse te verkry. Met hierdie as uitgangspunt, is daar eerstens `n reeks salisielidien vry ligande, SalH, met behulp van die Schiff-basis reaksie gesintetiseer. Hierdie organiese ligandstukture is gesintetiseer om potensieel as multifunksionele groepe tussen die trikarboniel radionuklied en die biologies aktiewe molekuul op te tree. Die ligande bevat verskeie amienverbindings wat aan die imien stikstofatoom op die salisielidien 'ruggraat' gekoördineer is. Die iminosubstituente bestaan uit aromatiese, alifatiese en biologies aktiewe onderdele met verskillende steriese, elektroniese en biologiese eienskappe en het die volgende ingesluit: *m*-toluïdien, 3-metielbutielamien, anilien, histamien, triptamien, tiramien ens. Die ligande is gekarakteriseer deur middel van KMR en IR spektroskopie. Enkelkristal X-straaldiffraksiestudies is uitgevoer en het gefokus op die verskeie oriëntasies van die substituente ten opsigte van die salisielidienruggraat. Die verbindings wat met behulp van enkelkristal X-straalkristallografie ondersoek is, sluit die volgende ligande in: 2-(*m*-tolieliminometiel)fenol, 5-metiel-2-(*m*-tolieliminometiel)fenol, 4-fluoro-2-(*m*-tolieliminometiel)fenol, 2-(4-nitrofenieliminometiel)-fenol, 2-[(4-hydroksifenyl)iminometiel]-5-metielfenol, 2-[(2-imidasol-4-iel)etielimino-metiel]-5-metielfenol, 2-[(2-indol-3-iel-etiel)iminometiel]-5-metielfenol, 2-(9-etielkarbasol-3-ieliminometiel)-5-metielfenol, 2-[2-(4-hydroksifenyl)etieliminometiel]-5-metielfenol, 5-metiel-2-(1,2,4-triasol-3-ieliminometiel)fenol.

`n Verdere belangrike doelstelling van hierdie ondersoek was die sintese en evaluasie van die vastetoestand eienskappe van die SalH ligande wanneer dit aan die renium(I) metaalkern gekoördineer is. 'n Voordeel van die *fac*-$[M^I(CO)_3(S)_3]^+$ komplekse (M = Tc of Re; S = H_2O

of ander koördinerende oplosmiddel) is die hoë stabiliteit van die klassieke laespin d^6 $[M(CO)_3]^+$ kerne in water en die potensiële uitruiling van die labiele oplosmiddelligande. Die SalH bidentate ligande is aan die *fac*-$[M(CO)_3]^+$ volgens die [2+1] benadering gekoppel en laat dus `n derde posisie oop wat deur `n oplosmiddel of `n neutrale monodentate ligand beset kan word. Die komplekse is ook deur middel van KMR en IR spektroskopie gekarakteriseer. Die vastetoestand gedrag van *fac*-$[Re(Sal)(CO)_3(S)]$ komplekse is deur middel van X-straal kristallografie bestudeer, en het die volgende ingesluit: *fac*-$[Re(Sal\text{-}m\text{Tol})(CO)_3(HOCH_3)]$, *fac*-$[Re(Sal\text{-}Ph)(CO)_3(HOCH_3)]$, *fac*-$[Re(Sal\text{-}p\text{Tol})(CO)_3(HOCH_3)]$, *fac*-$[Re(Sal\text{-}CyHex)(CO)_3(HOCH_3)]$, *fac*-$[Re(Sal\text{-}3MeBu)(CO)_3(HOCH_3)]$, *fac*-$[Re(Sal\text{-}Ph)(CO)_3(NC_5H_5)]$, *fac*-$[Re(Sal\text{-}3MeBu)(CO)_3(NC_5H_5)]$, *fac*-$[Re(5Me\text{-}Sal\text{-}Hist)(CO)_3]$, *fac*-$[Re(5Me\text{-}Sal\text{-}Trypt)(CO)_3(NC_5H_5)]$, *fac*-$[Re(5Me\text{-}Sal\text{-}Carba)(CO)_3(NC_5H_5)]$, *fac*-$[Re(5Me\text{-}Sal\text{-}m\text{Tol})(CO)_3(HOCH_3)]$, *fac*-$[Re(5Me\text{-}Sal\text{-}3Me2Bu)(CO)_3(HOCH_3)]$. Die koördinasiegeometrie rondom die Re(I) is in die vorm van 'n verwronge oktaheder en die iminosubstituente kristalliseer in soortgelyke oriëntasies ten spyte van verskille in steriese groottes. Die bindingshoeke en -afstande word nie sigbaar deur die verskillende stikstof-gekoördineerde substituente beïnvloed nie.

Die studie van die vastetoestand koördinasiechemie van die komplekse is verder aangevul met `n teoretiese DFT (digtheidsfunksieteorie) studie vir spesifiek die 2-(*m*-tolieliminometiel)fenol, 5-metiel-2-(*m*-tolieliminometiel)fenol, 2-(9-etielkarbasol-3-iel-iminometiel)-5-metielfenol, *fac*-$[Re(Sal\text{-}m\text{Tol})(CO)_3(S)]$, *fac*-$[Re(Sal\text{-}Ph)(CO)_3(S)]$, *fac*-$[Re(5Me\text{-}Sal\text{-}Carba)(CO)_3(S)]$ verbindings. 'n Vergelyking tussen die geoptimiseerde strukture en die vanaf die kristaldata toon slegs geringe verskille. Dit bevestig gevolglik dat hierdie teoretiese studies gebruik kan word om voorspellings te maak ten opsigte van koördinasie van soortgelyke bidentate ligande aan die renium metaalkern.

`n Kinetiese studie van die substitusie van die gekoördineerde oplosmiddel ligand van 'n reeks *fac*-$[Re(Sal)(CO)_3(S)]$ komplekse is ook onderneem. Die volgende komplekse is geëvalueer: *fac*-$[Re(Sal\text{-}m\text{Tol})(CO)_3(HOCH_3)]$, *fac*-$[Re(Sal\text{-}p\text{Tol})(CO)_3(HOCH_3)]$, *fac*-$[Re(Sal\text{-}Ph)(CO)_3(HOCH_3)]$, *fac*-$[Re(Sal\text{-}3MeBu)(CO)_3(HOCH_3)]$, *fac*-$[Re(Sal\text{-}CyHex)(CO)_3(HOCH_3)]$, met 3-chloropiridien, piridien, 4-pikolien en 4-dimetielaminopiridien as inkomende ligande in metanol as oplosmiddel. Die tempo's was redelik vinnig en het van sekondes tot minute gewissel en slegs een reaksie is onder droë toestande waargeneem. Die Sal-Re ligandsisteme het die unieke geleentheid gebied om die nie-assosiatiewe gedrag met

piridien en 4-dimetielaminopiridien as inkomende ligande te bestudeer, en het beperkende kinetiese gedrag geopenbaar, wat goeie getuienis ten gunste van 'n *I* of selfs 'n *D* intieme meganisme is. `n Uitruilings dissosiatiewe (I_d) meganisme is gevolglik voorgestel vir hierdie substitusiereaksies, met positiewe aktiveringsentropie- en entalpie waardes.

In vitro kankeraktiwiteit van geselekteerde vry ligande en *fac*-[Re(Sal)$(CO)_3$(S)] komplekse is ondersoek in `n 3-sellynpaneel bestaande uit TK10 (renale), UACC62 (melanomiese) en MCF7 (bors) kankerselle met `n Sulforodamien B (SRB) toets. Geen noemenswaardige selakiwiteit is gevind nie, maar beperkte selgroei-inhibering is tog waargeneem.

APPENDIX A

APPENDIX A

Supplementary data of SalH-mTol for the atomic coordinates, bond distances and angles and anisotropic displacement parameters are given in appendix tables A.

Table A.1: Atomic coordinates (x 10^4) and equivalent isotropic displacement parameters ($Å^2$ x 10^3) for SalH-*m*Tol. U(eq) is defined as one third of the trace of the orthogonalized U^{ij} tensor.

	x	y	z	U(eq)
C(1)	-45(3)	-1758(2)	7089(2)	22(1)
C(231)	245(3)	-3461(2)	3094(2)	27(1)
C(11)	389(3)	-1545(2)	8215(2)	21(1)
C(12)	1066(3)	-493(2)	8566(2)	23(1)
C(13)	1401(3)	-308(2)	9663(2)	26(1)
C(14)	1038(3)	-1137(2)	10413(2)	28(1)
C(15)	366(3)	-2180(2)	10092(2)	29(1)
C(16)	68(3)	-2375(2)	9001(2)	24(1)
C(21)	-390(3)	-1214(2)	5267(2)	21(1)
C(22)	117(3)	-2209(2)	4752(2)	21(1)
C(23)	-336(3)	-2400(2)	3671(2)	22(1)
C(24)	-1310(3)	-1586(2)	3115(2)	24(1)
C(25)	-1806(3)	-591(2)	3628(2)	26(1)
C(26)	-1332(3)	-394(2)	4698(2)	24(1)
N(1)	79(2)	-974(1)	6367(1)	21(1)
O(1)	1369(2)	353(1)	7849(1)	28(1)

Table A.2: Bond distances (Å) and angles (°) for SalH-*m*Tol.

Bond	Distance (Å)	Bond Angle	Angle (°)
C(1)-N(1)	1.289(3)	N(1)-C(1)-C(11)	121.17(18)
C(1)-C(11)	1.444(3)	N(1)-C(1)-H(1A)	119.5(11)
C(1)-H(1A)	1.04(2)	C(11)-C(1)-H(1A)	119.3(11)
C(231)-C(23)	1.509(3)	C(23)-C(231)-H(2A)	109.5
C(231)-H(2A)	0.9800	C(23)-C(231)-H(2B)	109.5
C(231)-H(2B)	0.9800	H(2A)-C(231)-H(2B)	109.5
C(231)-H(2C)	0.9800	C(23)-C(231)-H(2C)	109.5
C(11)-C(16)	1.401(3)	H(2A)-C(231)-H(2C)	109.5
C(11)-C(12)	1.415(3)	H(2B)-C(231)-H(2C)	109.5

C(12)-O(1)	1.355(2)	C(16)-C(11)-C(12)	118.16(19)
C(12)-C(13)	1.389(3)	C(16)-C(11)-C(1)	119.94(18)
C(13)-C(14)	1.377(3)	C(12)-C(11)-C(1)	121.85(18)
C(13)-H(13)	0.9500	O(1)-C(12)-C(13)	118.97(19)
C(14)-C(15)	1.394(3)	O(1)-C(12)-C(11)	120.99(18)
C(14)-H(14)	0.9500	C(13)-C(12)-C(11)	120.0(2)
C(15)-C(16)	1.380(3)	C(14)-C(13)-C(12)	120.2(2)
C(15)-H(15)	0.9500	C(14)-C(13)-H(13)	119.9
C(16)-H(16)	0.9500	C(12)-C(13)-H(13)	119.9
C(21)-C(26)	1.392(3)	C(13)-C(14)-C(15)	121.1(2)
C(21)-C(22)	1.392(3)	C(13)-C(14)-H(14)	119.5
C(21)-N(1)#1	1.426(3)	C(15)-C(14)-H(14)	119.5
C(21)-N(1)	1.426(3)	C(16)-C(15)-C(14)	118.9(2)
C(22)-C(23)	1.391(3)	C(16)-C(15)-H(15)	120.5
C(22)-H(22)	0.9500	C(14)-C(15)-H(15)	120.5
C(23)-C(24)	1.391(3)	C(15)-C(16)-C(11)	121.6(2)
C(24)-C(25)	1.389(3)	C(15)-C(16)-H(16)	119.2
C(24)-H(24)	0.9500	C(11)-C(16)-H(16)	119.2
C(25)-C(26)	1.382(3)	C(26)-C(21)-C(22)	120.14(19)
C(25)-H(25)	0.9500	C(26)-C(21)-N(1)	117.58(17)
C(26)-H(26)	0.9500	C(22)-C(21)-N(1)	122.24(18)
N(1)-N(1)#1	0.000(5)	C(23)-C(22)-C(21)	120.44(19)
O(1)-H(1B)	0.8400	C(23)-C(22)-H(22)	119.8
		C(21)-C(22)-H(22)	119.8
		C(24)-C(23)-C(22)	119.0(2)
		C(24)-C(23)-C(231)	119.94(19)
		C(22)-C(23)-C(231)	121.04(19)
		C(25)-C(24)-C(23)	120.5(2)
		C(25)-C(24)-H(24)	119.8
		C(23)-C(24)-H(24)	119.8
		C(26)-C(25)-C(24)	120.5(2)
		C(26)-C(25)-H(25)	119.8
		C(24)-C(25)-H(25)	119.8
		C(25)-C(26)-C(21)	119.4(2)
		C(25)-C(26)-H(26)	120.3
		C(21)-C(26)-H(26)	120.3
		C(1)-N(1)-C(21)	119.45(16)
		C(12)-O(1)-H(1B)	109.5

Table A.3: **Anisotropic displacement parameters ($Å^2 x\ 10^3$) for SalH-*m*Tol. The anisotropic displacement factor exponent takes the form: $-2\pi^2[\ h^2a^{*2}U^{11} + ... + 2\ h\ k\ a^*\ b^*\ U^{12}\ ]$**

	U11	U22	U33	U23	U13	U12
C(1)	18(1)	20(1)	27(1)	-1(1)	2(1)	1(1)
C(231)	28(1)	29(1)	26(1)	-3(1)	-4(1)	4(1)
C(11)	21(1)	18(1)	25(1)	-2(1)	1(1)	3(1)
C(12)	18(1)	21(1)	28(1)	-2(1)	2(1)	2(1)
C(13)	20(1)	23(1)	34(1)	-7(1)	-2(1)	0(1)
C(14)	27(1)	31(1)	26(1)	-5(1)	-3(1)	3(1)
C(15)	34(1)	27(1)	26(1)	2(1)	1(1)	3(1)
C(16)	28(1)	21(1)	25(1)	-2(1)	2(1)	0(1)
C(21)	18(1)	22(1)	23(1)	4(1)	4(1)	-5(1)
C(22)	19(1)	21(1)	24(1)	3(1)	0(1)	1(1)
C(23)	16(1)	24(1)	24(1)	2(1)	1(1)	-4(1)
C(24)	18(1)	32(1)	21(1)	6(1)	1(1)	-3(1)
C(25)	22(1)	25(1)	31(1)	11(1)	1(1)	1(1)
C(26)	20(1)	19(1)	34(1)	3(1)	3(1)	0(1)
N(1)	21(1)	22(1)	22(1)	0(1)	2(1)	1(1)
O(1)	32(1)	21(1)	30(1)	-1(1)	0(1)	-4(1)

Supplementary data of 5Me-SalH-mTol for the atomic coordinates, bond distances and angles and anisotropic displacement parameters are given in appendix tables B.

Table B.1: **Atomic coordinates ($x\ 10^4$) and equivalent isotropic displacement parameters ($Å^2\ x\ 10^3$) for 5Me-SalH-*m*Tol. U(eq) is defined as one third of the trace of the orthogonalized U^{ij} tensor.**

	x	y	z	U(eq)
C(1)	2616(6)	1330(5)	4074(2)	61(1)
C(11)	3572(7)	694(5)	4532(2)	53(1)
C(12)	5705(6)	-94(5)	4551(2)	56(1)
C(13)	6515(6)	-738(5)	4994(1)	61(1)
C(14)	5315(7)	-578(5)	5424(2)	62(1)

C(15)	3213(7)	233(5)	5406(2)	67(1)
C(16)	2376(7)	846(5)	4973(1)	66(1)
C(21)	2745(7)	1788(5)	3212(2)	56(1)
C(22)	4111(6)	1544(5)	2802(1)	59(1)
C(23)	3404(7)	2015(5)	2332(2)	64(1)
C(24)	1344(8)	2862(5)	2289(2)	69(1)
C(25)	-24(7)	3130(5)	2692(2)	76(1)
C(26)	653(7)	2585(5)	3154(2)	68(1)
C(141)	6223(6)	-1301(6)	5897(1)	88(1)
C(231)	4895(7)	1692(6)	1890(1)	89(1)
N(1)	3684(5)	1195(4)	3665(1)	63(1)
O(1)	6981(4)	-258(4)	4141(1)	83(1)

Table B.2: Bond distances (Å) and angles (°) for 5Me-SalH-*m*Tol.

Bond	Distance (Å)	Bond Angle	Angle (°)
C(1)-N(1)	1.282(3)	N(1)-C(1)-C(11)	121.6(4)
C(1)-C(11)	1.451(4)	N(1)-C(1)-H(1)	119.2
C(1)-H(1)	0.9300	C(11)-C(1)-H(1)	119.2
C(11)-C(16)	1.398(4)	C(16)-C(11)-C(12)	117.4(4)
C(11)-C(12)	1.399(4)	C(16)-C(11)-C(1)	120.7(4)
C(12)-O(1)	1.350(4)	C(12)-C(11)-C(1)	121.9(4)
C(12)-C(13)	1.387(4)	O(1)-C(12)-C(13)	119.3(4)
C(13)-C(14)	1.375(4)	O(1)-C(12)-C(11)	120.9(4)
C(13)-H(13)	0.9300	C(13)-C(12)-C(11)	119.8(4)
C(14)-C(15)	1.390(5)	C(14)-C(13)-C(12)	121.9(4)
C(14)-C(141)	1.499(4)	C(14)-C(13)-H(13)	119.0
C(15)-C(16)	1.359(4)	C(12)-C(13)-H(13)	119.0
C(15)-H(15)	0.9300	C(13)-C(14)-C(15)	118.0(4)
C(16)-H(16)	0.9300	C(13)-C(14)-C(141)	120.8(4)
C(21)-C(22)	1.390(4)	C(15)-C(14)-C(141)	121.2(4)
C(21)-C(26)	1.388(5)	C(16)-C(15)-C(14)	120.8(4)
C(21)-N(1)	1.425(4)	C(16)-C(15)-H(15)	119.6
C(22)-C(23)	1.392(4)	C(14)-C(15)-H(15)	119.6
C(22)-H(22)	0.9300	C(15)-C(16)-C(11)	122.0(4)
C(23)-C(24)	1.385(5)	C(15)-C(16)-H(16)	119.0
C(23)-C(231)	1.510(4)	C(11)-C(16)-H(16)	119.0

C(24)-C(25)	1.376(4)	C(22)-C(21)-C(26)	119.1(4)
C(24)-H(24)	0.9300	C(22)-C(21)-N(1)	115.1(4)
C(25)-C(26)	1.385(4)	C(26)-C(21)-N(1)	125.8(4)
C(25)-H(25)	0.9300	C(21)-C(22)-C(23)	121.8(4)
C(26)-H(26)	0.9300	C(21)-C(22)-H(22)	119.1
C(141)-H(14A)	0.9600	C(23)-C(22)-H(22)	119.1
C(141)-H(14B)	0.9600	C(24)-C(23)-C(22)	117.6(5)
C(141)-H(14C)	0.9600	C(24)-C(23)-C(231)	121.5(4)
C(231)-H(23A)	0.9600	C(22)-C(23)-C(231)	120.8(4)
C(231)-H(23B)	0.9600	C(25)-C(24)-C(23)	121.3(5)
C(231)-H(23C)	0.9600	C(25)-C(24)-H(24)	119.4
O(1)-H(1A)	0.8200	C(23)-C(24)-H(24)	119.4
		C(24)-C(25)-C(26)	120.5(4)
		C(24)-C(25)-H(25)	119.8
		C(26)-C(25)-H(25)	119.8
		C(25)-C(26)-C(21)	119.6(4)
		C(25)-C(26)-H(26)	120.2
		C(21)-C(26)-H(26)	120.2
		C(14)-C(141)-H(14A)	109.5
		C(14)-C(141)-H(14B)	109.5
		H(14A)-C(141)-H(14B)	109.5
		C(14)-C(141)-H(14C)	109.5
		H(14A)-C(141)-H(14C)	109.5
		H(14B)-C(141)-H(14C)	109.5
		C(23)-C(231)-H(23A)	109.5
		C(23)-C(231)-H(23B)	109.5
		H(23A)-C(231)-H(23B)	109.5
		C(23)-C(231)-H(23C)	109.5
		H(23A)-C(231)-H(23C)	109.5
		H(23B)-C(231)-H(23C)	109.5
		C(1)-N(1)-C(21)	122.1(3)
		C(12)-O(1)-H(1A)	109.5

Table B.3: **Anisotropic displacement parameters ($Å^2$x 10^3) for 5Me-SalH-*m*Tol. The anisotropic displacement factor exponent takes the form: $-2\pi^2[h^2a^{*2}U^{11} + ... + 2\ h\ k\ a^*\ b^*\ U^{12}]$**

	U11	U22	U33	U23	U13	U12
C(1)	43(2)	63(3)	77(3)	-15(2)	-2(3)	0(2)
C(11)	40(2)	58(3)	60(3)	-8(2)	1(2)	0(2)
C(12)	45(3)	61(3)	63(3)	-15(3)	0(2)	-1(2)
C(13)	45(3)	67(3)	70(3)	-13(3)	-12(3)	5(3)
C(14)	67(3)	57(3)	62(3)	-15(2)	-10(3)	1(3)
C(15)	56(3)	68(3)	76(3)	-11(3)	11(3)	-1(3)
C(16)	55(3)	71(3)	71(3)	-6(3)	-1(3)	-2(3)
C(21)	52(3)	46(3)	70(3)	-5(2)	-7(3)	1(3)
C(22)	50(3)	54(3)	73(3)	3(3)	-6(2)	7(3)
C(23)	65(3)	51(3)	76(3)	4(3)	-1(3)	7(3)
C(24)	79(4)	55(3)	72(3)	2(3)	-6(3)	1(3)
C(25)	59(3)	63(3)	104(4)	3(3)	-20(3)	20(3)
C(26)	58(3)	67(3)	79(3)	-11(3)	-7(3)	2(3)
C(141)	103(3)	78(3)	81(3)	-5(3)	-19(3)	-3(3)
C(231)	93(3)	108(3)	65(3)	9(3)	2(3)	8(4)
N(1)	52(2)	73(2)	64(2)	-9(2)	-3(2)	1(2)
O(1)	59(2)	121(2)	70(2)	-15(2)	2(2)	20(2)

Supplementary data of 4F-SalH-mTol for the atomic coordinates, bond distances and angles and anisotropic displacement parameters are given in appendix tables C.

Table C.1: **Atomic coordinates (x 10^4) and equivalent isotropic displacement parameters ($Å^2$ x 10^3) for 4F-SalH-*m*Tol. U(eq) is defined as one third of the trace of the orthogonalized U^{ij} tensor.**

	x	y	z	U(eq)
N(1)	5168(2)	7931(4)	5161(2)	17(1)
O(1)	6248(2)	5330(3)	7167(1)	23(1)
F(1)	9578(1)	-665(3)	5408(1)	28(1)
C(1)	5962(2)	6410(4)	4795(2)	18(1)

C(11)	6955(2)	4372(4)	5556(2)	16(1)
C(12)	7069(2)	3900(4)	6713(2)	18(1)
C(13)	8048(2)	1934(5)	7418(2)	21(1)
C(14)	8897(2)	416(5)	6980(2)	22(1)
C(15)	8756(2)	873(4)	5839(2)	20(1)
C(16)	7817(2)	2812(5)	5123(2)	18(1)
C(21)	4220(2)	9970(4)	4414(2)	17(1)
C(22)	3265(2)	11211(4)	4830(2)	17(1)
C(23)	2280(2)	13232(5)	4173(2)	19(1)
C(24)	2290(2)	14038(5)	3088(2)	21(1)
C(25)	3257(2)	12853(5)	2678(2)	22(1)
C(26)	4219(2)	10818(4)	3326(2)	21(1)
C(231)	1250(2)	14526(5)	4626(2)	23(1)

Table C.2: Bond distances (Å) and angles (°) for 4F-SalH-*m*Tol.

Bond	Distance (Å)	Bond Angle	Angle (°)
N(1)-C(1)	1.287(3)	C(1)-N(1)-C(21)	120.69(16)
N(1)-C(21)	1.422(3)	C(12)-O(1)-H(1B)	109.5
O(1)-C(12)	1.353(3)	N(1)-C(1)-C(11)	121.23(18)
O(1)-H(1B)	0.8400	N(1)-C(1)-H(1A)	119.4
F(1)-C(15)	1.361(2)	C(11)-C(1)-H(1A)	119.4
C(1)-C(11)	1.450(3)	C(16)-C(11)-C(12)	119.11(19)
C(1)-H(1A)	0.9500	C(16)-C(11)-C(1)	118.98(18)
C(11)-C(16)	1.401(3)	C(12)-C(11)-C(1)	121.91(18)
C(11)-C(12)	1.407(3)	O(1)-C(12)-C(13)	118.70(18)
C(12)-C(13)	1.396(3)	O(1)-C(12)-C(11)	121.31(19)
C(13)-C(14)	1.385(3)	C(13)-C(12)-C(11)	119.99(19)
C(13)-H(13)	0.9500	C(14)-C(13)-C(12)	120.27(19)
C(14)-C(15)	1.377(3)	C(14)-C(13)-H(13)	119.9
C(14)-H(14)	0.9500	C(12)-C(13)-H(13)	119.9
C(15)-C(16)	1.373(3)	C(15)-C(14)-C(13)	118.9(2)
C(16)-H(16)	0.9500	C(15)-C(14)-H(14)	120.5
C(21)-C(22)	1.395(3)	C(13)-C(14)-H(14)	120.5
C(21)-C(26)	1.401(3)	F(1)-C(15)-C(16)	118.91(19)
C(22)-C(23)	1.396(3)	F(1)-C(15)-C(14)	118.57(19)
C(22)-H(22)	0.9500	C(16)-C(15)-C(14)	122.5(2)

C(23)-C(24)	1.397(3)	C(15)-C(16)-C(11)	119.17(19)
C(23)-C(231)	1.499(3)	C(15)-C(16)-H(16)	120.4
C(24)-C(25)	1.389(3)	C(11)-C(16)-H(16)	120.4
C(24)-H(24)	0.9500	C(22)-C(21)-C(26)	119.44(19)
C(25)-C(26)	1.386(3)	C(22)-C(21)-N(1)	116.25(17)
C(25)-H(25)	0.9500	C(26)-C(21)-N(1)	124.30(18)
C(26)-H(26)	0.9500	C(21)-C(22)-C(23)	121.53(18)
C(231)-H(23A)	0.9800	C(21)-C(22)-H(22)	119.2
C(231)-H(23B)	0.9800	C(23)-C(22)-H(22)	119.2
C(231)-H(23C)	0.9800	C(22)-C(23)-C(24)	118.16(18)
		C(22)-C(23)-C(231)	120.94(18)
		C(24)-C(23)-C(231)	120.90(19)
		C(25)-C(24)-C(23)	120.63(19)
		C(25)-C(24)-H(24)	119.7
		C(23)-C(24)-H(24)	119.7
		C(26)-C(25)-C(24)	120.94(19)
		C(26)-C(25)-H(25)	119.5
		C(24)-C(25)-H(25)	119.5
		C(25)-C(26)-C(21)	119.3(2)
		C(25)-C(26)-H(26)	120.4
		C(21)-C(26)-H(26)	120.4
		C(23)-C(231)-H(23A)	109.5
		C(23)-C(231)-H(23B)	109.5
		H(23A)-C(231)-H(23B)	109.5
		C(23)-C(231)-H(23C)	109.5
		H(23A)-C(231)-H(23C)	109.5
		H(23B)-C(231)-H(23C)	109.5

Table C.3: Anisotropic displacement parameters ($Å^2 x\ 10^3$) for 4F-SalH-*m*Tol. The anisotropic displacement factor exponent takes the form: $-2\pi^2[\ h^2a^{*2}U^{11} + ... + 2\ h\ k\ a^*\ b^*\ U^{12}\ ]$

	U11	U22	U33	U23	U13	U12
N(1)	16(1)	17(1)	17(1)	1(1)	6(1)	0(1)
O(1)	26(1)	27(1)	18(1)	3(1)	12(1)	8(1)
F(1)	28(1)	26(1)	32(1)	1(1)	15(1)	9(1)

C(1)	20(1)	17(1)	16(1)	1(1)	7(1)	-2(1)
C(11)	17(1)	14(1)	16(1)	-1(1)	5(1)	-2(1)
C(12)	19(1)	19(1)	17(1)	-1(1)	7(1)	-2(1)
C(13)	23(1)	23(1)	16(1)	3(1)	5(1)	-1(1)
C(14)	20(1)	21(1)	21(1)	2(1)	4(1)	1(1)
C(15)	17(1)	19(1)	24(1)	-2(1)	10(1)	0(1)
C(16)	19(1)	19(1)	18(1)	-1(1)	10(1)	-1(1)
C(21)	17(1)	15(1)	18(1)	-1(1)	6(1)	-2(1)
C(22)	18(1)	16(1)	16(1)	-1(1)	7(1)	-2(1)
C(23)	17(1)	19(1)	20(1)	-3(1)	6(1)	-2(1)
C(24)	18(1)	19(1)	22(1)	1(1)	4(1)	2(1)
C(25)	24(1)	25(1)	19(1)	4(1)	9(1)	3(1)
C(26)	21(1)	22(1)	21(1)	0(1)	10(1)	2(1)
C(231)	19(1)	24(1)	25(1)	-2(1)	9(1)	2(1)

Supplementary data of SalH-4NitroPh for the atomic coordinates, bond distances and angles and anisotropic displacement parameters are given in appendix tables D.

Table D.1: Atomic coordinates (x 10^4) and equivalent isotropic displacement parameters ($Å^2$ x 10^3) for SalH-4NitroPh. U(eq) is defined as one third of the trace of the orthogonalized U^{ij} tensor.

	x	y	z	U(eq)
N(1)	6148(1)	-867(2)	-554(1)	19(1)
N(241)	10201(1)	1354(3)	1360(1)	26(1)
O(1)	4507(1)	-3835(2)	-826(1)	24(1)
O(2)	10545(1)	59(3)	1974(1)	35(1)
O(3)	10670(1)	3145(3)	1171(1)	38(1)
C(1)	5577(1)	578(3)	-1070(1)	19(1)
C(11)	4534(1)	-66(3)	-1540(1)	17(1)
C(12)	4041(1)	-2254(3)	-1416(1)	19(1)
C(13)	3044(1)	-2793(3)	-1905(1)	20(1)
C(14)	2540(1)	-1200(3)	-2502(1)	20(1)
C(15)	3018(1)	964(3)	-2635(1)	22(1)
C(16)	4004(1)	1508(3)	-2154(1)	20(1)
C(21)	7184(1)	-226(3)	-119(1)	19(1)
C(22)	7674(1)	-1830(3)	491(1)	20(1)

C(23)	8668(1)	-1346(3)	979(1)	23(1)
C(24)	9174(1)	754(3)	828(1)	21(1)
C(25)	8728(1)	2344(3)	202(1)	22(1)
C(26)	7729(1)	1862(3)	-272(1)	23(1)

Table D.2: Bond distances (Å) and angles (°) for SalH-4NitroPh.

Bond	Distance (Å)	Bond Angle	Angle (°)
N(1)-C(1)	1.289(2)	C(1)-N(1)-C(21)	121.10(15)
N(1)-C(21)	1.418(2)	O(3)-N(241)-O(2)	123.51(16)
N(241)-O(3)	1.229(2)	O(3)-N(241)-C(24)	117.92(16)
N(241)-O(2)	1.230(2)	O(2)-N(241)-C(24)	118.57(16)
N(241)-C(24)	1.462(2)	C(12)-O(1)-H(1B)	109.5
O(1)-C(12)	1.353(2)	N(1)-C(1)-C(11)	121.94(16)
O(1)-H(1B)	0.8400	N(1)-C(1)-H(1A)	119.0
C(1)-C(11)	1.445(2)	C(11)-C(1)-H(1A)	119.0
C(1)-H(1A)	0.9500	C(16)-C(11)-C(12)	118.87(16)
C(11)-C(16)	1.401(2)	C(16)-C(11)-C(1)	118.97(15)
C(11)-C(12)	1.414(2)	C(12)-C(11)-C(1)	122.15(15)
C(12)-C(13)	1.396(2)	O(1)-C(12)-C(13)	119.01(15)
C(13)-C(14)	1.382(2)	O(1)-C(12)-C(11)	121.60(15)
C(13)-H(13)	0.9500	C(13)-C(12)-C(11)	119.39(15)
C(14)-C(15)	1.397(3)	C(14)-C(13)-C(12)	120.37(16)
C(14)-H(14)	0.9500	C(14)-C(13)-H(13)	119.8
C(15)-C(16)	1.380(2)	C(12)-C(13)-H(13)	119.8
C(15)-H(15)	0.9500	C(13)-C(14)-C(15)	120.91(17)
C(16)-H(16)	0.9500	C(13)-C(14)-H(14)	119.5
C(21)-C(22)	1.391(2)	C(15)-C(14)-H(14)	119.5
C(21)-C(26)	1.404(3)	C(16)-C(15)-C(14)	119.01(16)
C(22)-C(23)	1.386(2)	C(16)-C(15)-H(15)	120.5
C(22)-H(22)	0.9500	C(14)-C(15)-H(15)	120.5
C(23)-C(24)	1.386(3)	C(15)-C(16)-C(11)	121.45(16)
C(23)-H(23)	0.9500	C(15)-C(16)-H(16)	119.3
C(24)-C(25)	1.384(3)	C(11)-C(16)-H(16)	119.3
C(25)-C(26)	1.381(2)	C(22)-C(21)-C(26)	119.49(16)
C(25)-H(25)	0.9500	C(22)-C(21)-N(1)	115.96(15)
C(26)-H(26)	0.9500	C(26)-C(21)-N(1)	124.55(16)

		C(23)-C(22)-C(21)	120.93(16)
		C(23)-C(22)-H(22)	119.5
		C(21)-C(22)-H(22)	119.5
		C(24)-C(23)-C(22)	118.17(16)
		C(24)-C(23)-H(23)	120.9
		C(22)-C(23)-H(23)	120.9
		C(25)-C(24)-C(23)	122.27(16)
		C(25)-C(24)-N(241)	118.39(16)
		C(23)-C(24)-N(241)	119.33(16)
		C(26)-C(25)-C(24)	119.09(16)
		C(26)-C(25)-H(25)	120.5
		C(24)-C(25)-H(25)	120.5
		C(25)-C(26)-C(21)	119.97(17)
		C(25)-C(26)-H(26)	120.0
		C(21)-C(26)-H(26)	120.0

Table D.3: Anisotropic displacement parameters ($Å^2 x\ 10^3$) for SalH-4NitroPh. The anisotropic displacement factor exponent takes the form: $-2\pi^2[\ h^2 a^{*2} U^{11} + ... + 2\ h\ k\ a^*\ b^*\ U^{12}\ ]$

	U11	U22	U33	U23	U13	U12
N(1)	19(1)	19(1)	20(1)	-2(1)	2(1)	0(1)
N(241)	21(1)	28(1)	29(1)	-3(1)	-1(1)	2(1)
O(1)	25(1)	19(1)	27(1)	5(1)	-4(1)	-1(1)
O(2)	31(1)	32(1)	39(1)	2(1)	-11(1)	4(1)
O(3)	28(1)	38(1)	44(1)	3(1)	-5(1)	-12(1)
C(1)	20(1)	18(1)	20(1)	-2(1)	5(1)	-2(1)
C(11)	18(1)	17(1)	18(1)	-1(1)	4(1)	0(1)
C(12)	21(1)	16(1)	19(1)	0(1)	4(1)	2(1)
C(13)	22(1)	16(1)	22(1)	-1(1)	4(1)	-2(1)
C(14)	19(1)	23(1)	20(1)	-4(1)	1(1)	-1(1)
C(15)	22(1)	22(1)	21(1)	2(1)	3(1)	2(1)
C(16)	21(1)	17(1)	22(1)	2(1)	6(1)	0(1)
C(21)	19(1)	20(1)	17(1)	-3(1)	4(1)	0(1)
C(22)	22(1)	16(1)	23(1)	0(1)	2(1)	1(1)
C(23)	25(1)	20(1)	24(1)	0(1)	1(1)	5(1)

C(24)	17(1)	25(1)	21(1)	-5(1)	2(1)	1(1)
C(25)	20(1)	24(1)	24(1)	0(1)	4(1)	-4(1)
C(26)	22(1)	24(1)	22(1)	3(1)	2(1)	-1(1)

Supplementary data of 5Me-SalH-4OHPh for the atomic coordinates, bond distances and angles and anisotropic displacement parameters are given in appendix tables E.

Table E.1: Atomic coordinates (x 10^4) and equivalent isotropic displacement parameters ($Å^2$ x 10^3) for 5Me-SalH-4OHPh. U(eq) is defined as one third of the trace of the orthogonalized U^{ij} tensor.

	x	y	z	U(eq)
C(1)	2738(2)	1406(2)	8741(3)	53(1)
C(11)	1782(2)	1902(2)	8818(3)	45(1)
C(12)	1680(2)	3073(2)	8830(3)	48(1)
C(13)	721(2)	3529(2)	8792(3)	55(1)
C(14)	-128(2)	2888(2)	8791(3)	56(1)
C(15)	-22(2)	1739(2)	8825(3)	61(1)
C(16)	912(2)	1266(2)	8841(3)	59(1)
C(21)	4525(2)	1556(2)	8597(3)	46(1)
C(22)	4658(2)	595(2)	7661(3)	52(1)
C(23)	5625(2)	260(2)	7495(3)	53(1)
C(24)	6471(2)	873(2)	8245(3)	52(1)
C(25)	6342(2)	1831(2)	9202(3)	58(1)
C(26)	5378(2)	2172(2)	9364(3)	56(1)
C(141)	-1164(2)	3393(2)	8736(4)	81(1)
N(1)	3556(1)	1991(2)	8775(2)	51(1)
O(1)	2491(1)	3720(1)	8862(2)	65(1)
O(2)	7445(1)	586(1)	8115(2)	72(1)

Table E.2: Bond distances (Å) and angles (°) for 5Me-SalH-4OHPh.

Bond	Distance (Å)	Bond Angle	Angle (°)
C(1)-N(1)	1.297(2)	N(1)-C(1)-C(11)	121.8(2)
C(1)-C(11)	1.420(3)	N(1)-C(1)-H(1A)	119.1

C(1)-H(1A)	0.9300	C(11)-C(1)-H(1A)	119.1
C(11)-C(16)	1.394(3)	C(16)-C(11)-C(1)	121.5(2)
C(11)-C(12)	1.421(3)	C(16)-C(11)-C(12)	117.96(19)
C(12)-O(1)	1.331(2)	C(1)-C(11)-C(12)	120.54(19)
C(12)-C(13)	1.387(3)	O(1)-C(12)-C(13)	120.5(2)
C(13)-C(14)	1.372(3)	O(1)-C(12)-C(11)	120.50(18)
C(13)-H(13)	0.9300	C(13)-C(12)-C(11)	119.0(2)
C(14)-C(15)	1.395(3)	C(14)-C(13)-C(12)	122.2(2)
C(14)-C(141)	1.504(3)	C(14)-C(13)-H(13)	118.9
C(15)-C(16)	1.369(3)	C(12)-C(13)-H(13)	118.9
C(15)-H(15)	0.9300	C(13)-C(14)-C(15)	118.8(2)
C(16)-H(16)	0.9300	C(13)-C(14)-C(141)	121.6(2)
C(21)-C(22)	1.374(3)	C(15)-C(14)-C(141)	119.6(2)
C(21)-C(26)	1.385(3)	C(16)-C(15)-C(14)	120.3(2)
C(21)-N(1)#1	1.423(2)	C(16)-C(15)-H(15)	119.8
C(21)-N(1)	1.423(2)	C(14)-C(15)-H(15)	119.8
C(22)-C(23)	1.379(3)	C(15)-C(16)-C(11)	121.8(2)
C(22)-H(22)	0.9300	C(15)-C(16)-H(16)	119.1
C(23)-C(24)	1.373(3)	C(11)-C(16)-H(16)	119.1
C(23)-H(23)	0.9300	C(22)-C(21)-C(26)	118.8(2)
C(24)-O(2)	1.365(2)	C(22)-C(21)-N(1)	124.14(19)
C(24)-C(25)	1.378(3)	C(26)-C(21)-N(1)	117.0(2)
C(25)-C(26)	1.377(3)	C(21)-C(22)-C(23)	120.1(2)
C(25)-H(25)	0.9300	C(21)-C(22)-H(22)	120.0
C(26)-H(26)	0.9300	C(23)-C(22)-H(22)	120.0
C(141)-H(14A)	0.9600	C(24)-C(23)-C(22)	121.2(2)
C(141)-H(14B)	0.9600	C(24)-C(23)-H(23)	119.4
C(141)-H(14C)	0.9600	C(22)-C(23)-H(23)	119.4
O(1)-H(1B)	0.8200	O(2)-C(24)-C(23)	123.7(2)
O(2)-H(2)	0.8200	O(2)-C(24)-C(25)	117.3(2)
		C(23)-C(24)-C(25)	118.9(2)
		C(26)-C(25)-C(24)	120.1(2)
		C(26)-C(25)-H(25)	119.9
		C(24)-C(25)-H(25)	119.9
		C(25)-C(26)-C(21)	120.8(2)
		C(25)-C(26)-H(26)	119.6
		C(21)-C(26)-H(26)	119.6
		C(14)-C(141)-H(14A)	109.5

		C(14)-C(141)-H(14B)	109.5
		H(14A)-C(141)-H(14B)	109.5
		C(14)-C(141)-H(14C)	109.5
		H(14A)-C(141)-H(14C)	109.5
		H(14B)-C(141)-H(14C)	109.5
		C(1)-N(1)-C(21)	124.8(2)
		C(12)-O(1)-H(1B)	109.5
		C(24)-O(2)-H(2)	109.5

Table E.3: Anisotropic displacement parameters ($Å^2 x\ 10^3$) for 5Me-SalH-4OHPh. The anisotropic displacement factor exponent takes the form: $-2\pi^2[h^2a^{*2}U^{11} + ... + 2\ h\ k\ a^*\ b^*\ U^{12}]$

	U11	U22	U33	U23	U13	U12
C(1)	56(2)	53(2)	54(1)	2(1)	18(1)	-5(1)
C(11)	43(1)	50(2)	44(1)	1(1)	12(1)	-4(1)
C(12)	40(1)	60(2)	46(1)	2(1)	11(1)	-7(1)
C(13)	47(2)	53(2)	66(2)	3(1)	12(1)	0(1)
C(14)	44(1)	74(2)	50(1)	5(1)	11(1)	-2(1)
C(15)	45(1)	75(2)	65(2)	5(1)	18(1)	-14(1)
C(16)	58(2)	55(2)	65(2)	0(1)	17(1)	-13(1)
C(21)	43(1)	48(1)	47(1)	-2(1)	11(1)	0(1)
C(22)	47(1)	51(1)	60(1)	-2(1)	13(1)	-5(1)
C(23)	51(2)	45(1)	67(2)	-4(1)	18(1)	1(1)
C(24)	39(1)	53(2)	64(2)	3(1)	13(1)	2(1)
C(25)	46(2)	54(2)	72(2)	-10(1)	10(1)	-7(1)
C(26)	52(2)	52(1)	64(2)	-12(1)	9(1)	-2(1)
C(141)	47(2)	97(2)	99(2)	9(2)	17(1)	1(1)
N(1)	42(1)	63(1)	50(1)	2(1)	14(1)	0(1)
O(1)	45(1)	53(1)	96(1)	-1(1)	16(1)	-5(1)
O(2)	47(1)	74(1)	96(1)	-12(1)	18(1)	2(1)

Supplementary data of 5Me-SalH-Hist for the atomic coordinates, bond distances and angles and anisotropic displacement parameters are given in appendix tables F.

Table F.1: Atomic coordinates (x 10^4) and equivalent isotropic displacement parameters ($Å^2$ x 10^3) for 5Me-SalH-Hist. U(eq) is defined as one third of the trace of the orthogonalized U^{ij} tensor.

	x	y	z	U(eq)
C(2)	2190(2)	5250(2)	1278(1)	21(1)
C(3)	1557(2)	4636(2)	1734(1)	21(1)
C(5)	6208(2)	4791(2)	1034(1)	20(1)
C(6)	6623(2)	4448(2)	1701(1)	24(1)
C(31)	1026(2)	5681(2)	2072(1)	18(1)
C(33)	-152(2)	6495(2)	2613(1)	22(1)
C(35)	1264(2)	7038(2)	2120(1)	21(1)
C(61)	6029(2)	5402(2)	2056(1)	19(1)
C(63)	4886(2)	6077(2)	2639(1)	23(1)
C(65)	6103(2)	6777(2)	2079(1)	23(1)
C(141)	2891(2)	-179(2)	-1156(1)	30(1)
C(441)	8674(2)	-74(2)	-1180(1)	26(1)
N(32)	129(1)	5344(1)	2386(1)	23(1)
N(34)	506(1)	7542(1)	2467(1)	20(1)
N(62)	5253(1)	4963(1)	2411(1)	22(1)
N(64)	5373(1)	7192(1)	2452(1)	21(1)
C(1)	1973(2)	4118(2)	365(1)	20(1)
C(11)	2236(1)	3049(2)	-16(1)	19(1)
C(12)	3142(2)	2008(2)	222(1)	19(1)
C(13)	3341(2)	975(2)	-151(1)	22(1)
C(14)	2671(2)	959(2)	-760(1)	22(1)
C(15)	1786(2)	2004(2)	-999(1)	24(1)
C(16)	1567(2)	3025(2)	-632(1)	23(1)
N(1)	2570(1)	4176(1)	928(1)	21(1)
O(1)	3839(1)	1984(1)	811(1)	24(1)
C(4)	6274(2)	3420(2)	213(1)	20(1)
C(41)	6908(2)	2592(2)	-145(1)	19(1)
C(42)	8279(2)	2301(2)	49(1)	20(1)
C(43)	8846(2)	1456(2)	-292(1)	21(1)
C(44)	8077(2)	898(2)	-827(1)	21(1)

C(45)	6725(2)	1221(2)	-1032(1)	22(1)
C(46)	6157(2)	2051(2)	-692(1)	22(1)
N(2)	6928(1)	3960(1)	710(1)	21(1)
O(2)	9070(1)	2828(1)	570(1)	25(1)

Table F.2: Bond distances (Å) and angles (°) for 5Me-SalH-Hist.

Bond	Distance (Å)	Bond Angle	Angle (°)
C(2)-N(1)	1.4590(18)	N(1)-C(2)-C(3)	109.58(12)
C(2)-C(3)	1.5260(19)	N(1)-C(2)-H(2C)	109.8
C(2)-H(2C)	0.9900	C(3)-C(2)-H(2C)	109.8
C(2)-H(2D)	0.9900	N(1)-C(2)-H(2D)	109.8
C(3)-C(31)	1.4979(19)	C(3)-C(2)-H(2D)	109.8
C(3)-H(3A)	0.9900	H(2C)-C(2)-H(2D)	108.2
C(3)-H(3B)	0.9900	C(31)-C(3)-C(2)	112.73(12)
C(5)-N(2)	1.4607(18)	C(31)-C(3)-H(3A)	109.0
C(5)-C(6)	1.5222(19)	C(2)-C(3)-H(3A)	109.0
C(5)-H(5A)	0.9900	C(31)-C(3)-H(3B)	109.0
C(5)-H(5B)	0.9900	C(2)-C(3)-H(3B)	109.0
C(6)-C(61)	1.499(2)	H(3A)-C(3)-H(3B)	107.8
C(6)-H(6A)	0.9900	N(2)-C(5)-C(6)	110.86(12)
C(6)-H(6B)	0.9900	N(2)-C(5)-H(5A)	109.5
C(31)-C(35)	1.365(2)	C(6)-C(5)-H(5A)	109.5
C(31)-N(32)	1.3832(18)	N(2)-C(5)-H(5B)	109.5
C(33)-N(32)	1.3230(19)	C(6)-C(5)-H(5B)	109.5
C(33)-N(34)	1.3412(19)	H(5A)-C(5)-H(5B)	108.1
C(33)-H(33)	0.9500	C(61)-C(6)-C(5)	111.89(12)
C(35)-N(34)	1.3757(18)	C(61)-C(6)-H(6A)	109.2
C(35)-H(35)	0.9500	C(5)-C(6)-H(6A)	109.2
C(61)-C(65)	1.364(2)	C(61)-C(6)-H(6B)	109.2
C(61)-N(62)	1.3814(18)	C(5)-C(6)-H(6B)	109.2
C(63)-N(62)	1.3265(19)	H(6A)-C(6)-H(6B)	107.9
C(63)-N(64)	1.3391(19)	C(35)-C(31)-N(32)	109.38(13)
C(63)-H(63)	0.9500	C(35)-C(31)-C(3)	129.46(13)
C(65)-N(64)	1.3709(18)	N(32)-C(31)-C(3)	121.14(13)
C(65)-H(65)	0.9500	N(32)-C(33)-N(34)	112.23(13)
C(141)-C(14)	1.512(2)	N(32)-C(33)-H(33)	123.9

C(141)-H(14A)	0.9800	N(34)-C(33)-H(33)	123.9
C(141)-H(14B)	0.9800	C(31)-C(35)-N(34)	106.35(13)
C(141)-H(14C)	0.9800	C(31)-C(35)-H(35)	126.8
C(441)-C(44)	1.510(2)	N(34)-C(35)-H(35)	126.8
C(441)-H(44A)	0.9800	C(65)-C(61)-N(62)	109.12(13)
C(441)-H(44B)	0.9800	C(65)-C(61)-C(6)	128.53(14)
C(441)-H(44C)	0.9800	N(62)-C(61)-C(6)	122.33(13)
N(34)-H(34)	0.8800	N(62)-C(63)-N(64)	112.22(13)
N(64)-H(64)	0.8800	N(62)-C(63)-H(63)	123.9
C(1)-N(1)	1.2823(18)	N(64)-C(63)-H(63)	123.9
C(1)-C(11)	1.453(2)	C(61)-C(65)-N(64)	106.79(13)
C(1)-H(1A)	0.9500	C(61)-C(65)-H(65)	126.6
C(11)-C(16)	1.4030(19)	N(64)-C(65)-H(65)	126.6
C(11)-C(12)	1.406(2)	C(14)-C(141)-H(14A)	109.5
C(12)-O(1)	1.3565(16)	C(14)-C(141)-H(14B)	109.5
C(12)-C(13)	1.393(2)	H(14A)-C(141)-H(14B)	109.5
C(13)-C(14)	1.390(2)	C(14)-C(141)-H(14C)	109.5
C(13)-H(13)	0.9500	H(14A)-C(141)-H(14C)	109.5
C(14)-C(15)	1.397(2)	H(14B)-C(141)-H(14C)	109.5
C(15)-C(16)	1.382(2)	C(44)-C(441)-H(44A)	109.5
C(15)-H(15)	0.9500	C(44)-C(441)-H(44B)	109.5
C(16)-H(16)	0.9500	H(44A)-C(441)-H(44B)	109.5
O(1)-H(1B)	0.8400	C(44)-C(441)-H(44C)	109.5
C(4)-N(2)	1.2802(18)	H(44A)-C(441)-H(44C)	109.5
C(4)-C(41)	1.4550(19)	H(44B)-C(441)-H(44C)	109.5
C(4)-H(4)	0.9500	C(33)-N(32)-C(31)	105.16(12)
C(41)-C(46)	1.398(2)	C(33)-N(34)-C(35)	106.88(12)
C(41)-C(42)	1.411(2)	C(33)-N(34)-H(34)	126.6
C(42)-O(2)	1.3621(17)	C(35)-N(34)-H(34)	126.6
C(42)-C(43)	1.395(2)	C(63)-N(62)-C(61)	105.14(12)
C(43)-C(44)	1.389(2)	C(63)-N(64)-C(65)	106.73(12)
C(43)-H(43)	0.9500	C(63)-N(64)-H(64)	126.6
C(44)-C(45)	1.401(2)	C(65)-N(64)-H(64)	126.6
C(45)-C(46)	1.383(2)	N(1)-C(1)-C(11)	122.00(14)
C(45)-H(45)	0.9500	N(1)-C(1)-H(1A)	119.0
C(46)-H(46)	0.9500	C(11)-C(1)-H(1A)	119.0
O(2)-H(2B)	0.8400	C(16)-C(11)-C(12)	118.40(13)
		C(16)-C(11)-C(1)	120.29(14)

		C(12)-C(11)-C(1)	121.30(13)
		O(1)-C(12)-C(13)	118.65(13)
		O(1)-C(12)-C(11)	121.43(13)
		C(13)-C(12)-C(11)	119.92(13)
		C(14)-C(13)-C(12)	121.20(14)
		C(14)-C(13)-H(13)	119.4
		C(12)-C(13)-H(13)	119.4
		C(13)-C(14)-C(15)	118.94(14)
		C(13)-C(14)-C(141)	120.36(14)
		C(15)-C(14)-C(141)	120.70(13)
		C(16)-C(15)-C(14)	120.36(14)
		C(16)-C(15)-H(15)	119.8
		C(14)-C(15)-H(15)	119.8
		C(15)-C(16)-C(11)	121.17(14)
		C(15)-C(16)-H(16)	119.4
		C(11)-C(16)-H(16)	119.4
		C(1)-N(1)-C(2)	117.89(13)
		C(12)-O(1)-H(1B)	109.5
		N(2)-C(4)-C(41)	122.24(14)
		N(2)-C(4)-H(4)	118.9
		C(41)-C(4)-H(4)	118.9
		C(46)-C(41)-C(42)	118.34(13)
		C(46)-C(41)-C(4)	120.14(14)
		C(42)-C(41)-C(4)	121.52(13)
		O(2)-C(42)-C(43)	118.85(14)
		O(2)-C(42)-C(41)	121.06(13)
		C(43)-C(42)-C(41)	120.08(13)
		C(44)-C(43)-C(42)	120.78(14)
		C(44)-C(43)-H(43)	119.6
		C(42)-C(43)-H(43)	119.6
		C(43)-C(44)-C(45)	119.30(13)
		C(43)-C(44)-C(441)	120.80(14)
		C(45)-C(44)-C(441)	119.89(13)
		C(46)-C(45)-C(44)	120.07(13)
		C(46)-C(45)-H(45)	120.0
		C(44)-C(45)-H(45)	120.0
		C(45)-C(46)-C(41)	121.38(14)
		C(45)-C(46)-H(46)	119.3

		C(41)-C(46)-H(46)	119.3
		C(4)-N(2)-C(5)	118.32(13)
		C(42)-O(2)-H(2B)	109.5

Table F.3: Anisotropic displacement parameters ($Å^2 x\ 10^3$) for 5Me-SalH-Hist. The anisotropic displacement factor exponent takes the form: $-2\pi^2[\ h^2a^{*2}U^{11} + ... + 2\ h\ k\ a^*\ b^*\ U^{12}\ ]$

	U11	U22	U33	U23	U13	U12
C(2)	25(1)	18(1)	23(1)	-1(1)	11(1)	1(1)
C(3)	26(1)	17(1)	22(1)	0(1)	10(1)	0(1)
C(5)	23(1)	19(1)	21(1)	-2(1)	9(1)	1(1)
C(6)	32(1)	19(1)	23(1)	1(1)	11(1)	6(1)
C(31)	20(1)	17(1)	17(1)	1(1)	6(1)	1(1)
C(33)	27(1)	19(1)	25(1)	1(1)	14(1)	1(1)
C(35)	23(1)	18(1)	23(1)	0(1)	10(1)	0(1)
C(61)	23(1)	18(1)	18(1)	2(1)	6(1)	2(1)
C(63)	29(1)	17(1)	24(1)	2(1)	13(1)	2(1)
C(65)	29(1)	20(1)	24(1)	1(1)	13(1)	0(1)
C(141)	39(1)	27(1)	25(1)	-5(1)	12(1)	-3(1)
C(441)	33(1)	22(1)	27(1)	-3(1)	15(1)	1(1)
N(32)	28(1)	18(1)	25(1)	0(1)	13(1)	-1(1)
N(34)	25(1)	15(1)	21(1)	-2(1)	9(1)	0(1)
N(62)	28(1)	17(1)	23(1)	1(1)	10(1)	1(1)
N(64)	29(1)	14(1)	21(1)	-1(1)	10(1)	1(1)
C(1)	19(1)	19(1)	24(1)	3(1)	9(1)	1(1)
C(11)	18(1)	20(1)	21(1)	1(1)	9(1)	-3(1)
C(12)	19(1)	21(1)	19(1)	2(1)	7(1)	-2(1)
C(13)	24(1)	19(1)	24(1)	2(1)	10(1)	1(1)
C(14)	26(1)	21(1)	23(1)	-2(1)	12(1)	-6(1)
C(15)	22(1)	30(1)	19(1)	0(1)	7(1)	-5(1)
C(16)	20(1)	26(1)	23(1)	3(1)	7(1)	0(1)
N(1)	23(1)	19(1)	23(1)	-1(1)	11(1)	-1(1)
O(1)	30(1)	23(1)	19(1)	-1(1)	5(1)	5(1)
C(4)	22(1)	18(1)	22(1)	2(1)	9(1)	0(1)

C(41)	23(1)	15(1)	20(1)	1(1)	9(1)	0(1)
C(42)	24(1)	16(1)	19(1)	1(1)	8(1)	-2(1)
C(43)	22(1)	19(1)	24(1)	2(1)	10(1)	1(1)
C(44)	30(1)	15(1)	22(1)	1(1)	13(1)	-1(1)
C(45)	29(1)	19(1)	19(1)	-1(1)	7(1)	-2(1)
C(46)	24(1)	20(1)	22(1)	1(1)	7(1)	0(1)
N(2)	24(1)	19(1)	21(1)	-2(1)	10(1)	0(1)
O(2)	24(1)	26(1)	24(1)	-7(1)	6(1)	2(1)

Supplementary data of 5Me-SalH-Trypt for the atomic coordinates, bond distances and angles and anisotropic displacement parameters are given in appendix tables G.

Table G.1: Atomic coordinates (x 10^4) and equivalent isotropic displacement parameters ($Å^2$ x 10^3) for 5Me-SalH-Trypt. U(eq) is defined as one third of the trace of the orthogonalized U^{ij} tensor.

	x	y	z	U(eq)
C(1)	2587(2)	2195(2)	3276(1)	14(1)
C(2)	2062(2)	3564(2)	4807(1)	16(1)
C(3)	1553(2)	2355(2)	5492(1)	15(1)
C(11)	3804(2)	1179(2)	2625(1)	13(1)
C(12)	5940(2)	754(2)	2948(1)	14(1)
C(13)	6997(2)	-329(2)	2338(1)	15(1)
C(14)	5992(2)	-975(2)	1406(1)	15(1)
C(15)	3886(2)	-530(2)	1083(1)	16(1)
C(16)	2816(2)	520(2)	1688(1)	16(1)
C(31)	68(2)	2891(2)	6230(1)	14(1)
C(32)	-2017(2)	2176(2)	6267(1)	16(1)
C(33)	-1276(2)	4062(2)	7599(1)	14(1)
C(34)	588(2)	4119(2)	7081(1)	13(1)
C(35)	2454(2)	5233(2)	7470(1)	16(1)
C(36)	2426(2)	6215(2)	8349(1)	17(1)
C(37)	569(2)	6110(2)	8854(1)	18(1)
C(38)	-1308(2)	5047(2)	8484(1)	17(1)
C(141)	7146(2)	-2154(2)	764(1)	20(1)
N(1)	3470(2)	2785(1)	4140(1)	16(1)
N(2)	-2852(2)	2886(1)	7076(1)	17(1)

O(1)	6985(2)	1343(1)	3842(1)	18(1)

Table G.2: Bond distances (Å) and angles (°) for 5Me-SalH-Trypt.

Bond	Distance (Å)	Bond Angle	Angle (°)
C(1)-N(1)	1.2817(17)	N(1)-C(1)-C(11)	120.94(12)
C(1)-C(11)	1.4615(17)	N(1)-C(1)-H(1A)	119.5
C(1)-H(1A)	0.9500	C(11)-C(1)-H(1A)	119.5
C(2)-N(1)	1.4622(16)	N(1)-C(2)-C(3)	106.99(10)
C(2)-C(3)	1.5334(18)	N(1)-C(2)-H(2A)	110.3
C(2)-H(2A)	0.9900	C(3)-C(2)-H(2A)	110.3
C(2)-H(2B)	0.9900	N(1)-C(2)-H(2B)	110.3
C(3)-C(31)	1.4995(17)	C(3)-C(2)-H(2B)	110.3
C(3)-H(3A)	0.9900	H(2A)-C(2)-H(2B)	108.6
C(3)-H(3B)	0.9900	C(31)-C(3)-C(2)	116.16(10)
C(11)-C(16)	1.3971(18)	C(31)-C(3)-H(3A)	108.2
C(11)-C(12)	1.4114(18)	C(2)-C(3)-H(3A)	108.2
C(12)-O(1)	1.3462(15)	C(31)-C(3)-H(3B)	108.2
C(12)-C(13)	1.3994(17)	C(2)-C(3)-H(3B)	108.2
C(13)-C(14)	1.3923(18)	H(3A)-C(3)-H(3B)	107.4
C(13)-H(13)	0.9500	C(16)-C(11)-C(12)	118.55(11)
C(14)-C(15)	1.4015(19)	C(16)-C(11)-C(1)	120.57(11)
C(14)-C(141)	1.5065(17)	C(12)-C(11)-C(1)	120.75(11)
C(15)-C(16)	1.3845(18)	O(1)-C(12)-C(13)	118.64(11)
C(15)-H(15)	0.9500	O(1)-C(12)-C(11)	121.59(11)
C(16)-H(16)	0.9500	C(13)-C(12)-C(11)	119.76(12)
C(31)-C(32)	1.3661(18)	C(14)-C(13)-C(12)	121.05(12)
C(31)-C(34)	1.4422(17)	C(14)-C(13)-H(13)	119.5
C(32)-N(2)	1.3770(16)	C(12)-C(13)-H(13)	119.5
C(32)-H(32)	0.9500	C(13)-C(14)-C(15)	118.98(12)
C(33)-N(2)	1.3732(17)	C(13)-C(14)-C(141)	120.26(12)
C(33)-C(38)	1.3927(18)	C(15)-C(14)-C(141)	120.75(12)
C(33)-C(34)	1.4215(17)	C(16)-C(15)-C(14)	120.26(12)
C(34)-C(35)	1.4066(18)	C(16)-C(15)-H(15)	119.9
C(35)-C(36)	1.3844(18)	C(14)-C(15)-H(15)	119.9
C(35)-H(35)	0.9500	C(15)-C(16)-C(11)	121.38(12)
C(36)-C(37)	1.4082(19)	C(15)-C(16)-H(16)	119.3

C(36)-H(36)	0.9500	C(11)-C(16)-H(16)	119.3
C(37)-C(38)	1.3838(19)	C(32)-C(31)-C(34)	106.16(11)
C(37)-H(37)	0.9500	C(32)-C(31)-C(3)	125.40(12)
C(38)-H(38)	0.9500	C(34)-C(31)-C(3)	128.19(12)
C(141)-H(14A)	0.9800	C(31)-C(32)-N(2)	110.52(11)
C(141)-H(14B)	0.9800	C(31)-C(32)-H(32)	124.7
C(141)-H(14C)	0.9800	N(2)-C(32)-H(32)	124.7
N(2)-H(2C)	0.8800	N(2)-C(33)-C(38)	130.14(12)
O(1)-H(1B)	0.8400	N(2)-C(33)-C(34)	107.39(11)
		C(38)-C(33)-C(34)	122.46(12)
		C(35)-C(34)-C(33)	118.66(11)
		C(35)-C(34)-C(31)	134.34(12)
		C(33)-C(34)-C(31)	106.98(11)
		C(36)-C(35)-C(34)	118.99(12)
		C(36)-C(35)-H(35)	120.5
		C(34)-C(35)-H(35)	120.5
		C(35)-C(36)-C(37)	121.03(12)
		C(35)-C(36)-H(36)	119.5
		C(37)-C(36)-H(36)	119.5
		C(38)-C(37)-C(36)	121.47(12)
		C(38)-C(37)-H(37)	119.3
		C(36)-C(37)-H(37)	119.3
		C(37)-C(38)-C(33)	117.38(12)
		C(37)-C(38)-H(38)	121.3
		C(33)-C(38)-H(38)	121.3
		C(14)-C(141)-H(14A)	109.5
		C(14)-C(141)-H(14B)	109.5
		H(14A)-C(141)-H(14B)	109.5
		C(14)-C(141)-H(14C)	109.5
		H(14A)-C(141)-H(14C)	109.5
		H(14B)-C(141)-H(14C)	109.5
		C(1)-N(1)-C(2)	118.48(11)
		C(33)-N(2)-C(32)	108.93(11)
		C(33)-N(2)-H(2C)	125.5
		C(32)-N(2)-H(2C)	125.5
		C(12)-O(1)-H(1B)	109.5

Table G.3: Anisotropic displacement parameters ($Å^2 x\ 10^3$) for 5Me-SalH-Trypt. The anisotropic displacement factor exponent takes the form: $-2\pi^2[\ h^2a^{*2}U^{11} + ... + 2\ h\ k\ a^*\ b^*\ U^{12}\ ]$

	U11	U22	U33	U23	U13	U12
C(1)	14(1)	13(1)	16(1)	4(1)	4(1)	2(1)
C(2)	19(1)	16(1)	15(1)	1(1)	7(1)	4(1)
C(3)	17(1)	15(1)	14(1)	2(1)	3(1)	3(1)
C(11)	14(1)	13(1)	13(1)	2(1)	4(1)	0(1)
C(12)	15(1)	13(1)	12(1)	3(1)	2(1)	-1(1)
C(13)	13(1)	16(1)	16(1)	4(1)	4(1)	3(1)
C(14)	19(1)	14(1)	14(1)	3(1)	6(1)	2(1)
C(15)	19(1)	17(1)	12(1)	1(1)	2(1)	1(1)
C(16)	14(1)	17(1)	16(1)	4(1)	2(1)	3(1)
C(31)	15(1)	14(1)	12(1)	3(1)	2(1)	3(1)
C(32)	18(1)	15(1)	13(1)	1(1)	2(1)	2(1)
C(33)	14(1)	14(1)	16(1)	4(1)	3(1)	2(1)
C(34)	15(1)	14(1)	13(1)	4(1)	2(1)	4(1)
C(35)	16(1)	15(1)	17(1)	3(1)	3(1)	2(1)
C(36)	17(1)	15(1)	18(1)	1(1)	0(1)	0(1)
C(37)	23(1)	16(1)	14(1)	0(1)	3(1)	4(1)
C(38)	18(1)	19(1)	16(1)	3(1)	6(1)	5(1)
C(141)	25(1)	22(1)	15(1)	1(1)	5(1)	8(1)
N(1)	18(1)	14(1)	15(1)	1(1)	6(1)	2(1)
N(2)	13(1)	20(1)	16(1)	2(1)	4(1)	-1(1)
O(1)	18(1)	22(1)	14(1)	-2(1)	1(1)	4(1)

Supplementary data of 5Me-SalH-Carba for the atomic coordinates, bond distances and angles and anisotropic displacement parameters are given in appendix tables H.

Table H.1: Atomic coordinates (x 10^4) and equivalent isotropic displacement parameters ($Å^2$ x 10^3) for 5Me-SalH-Carba. U(eq) is defined as one third of the trace of the orthogonalized U^{ij} tensor.

	x	y	z	U(eq)
C(13)	2462(2)	6894(2)	1785(1)	18(1)
C(14)	1795(2)	7660(2)	1294(1)	18(1)
C(15)	2687(2)	8747(2)	1103(1)	20(1)
C(16)	4220(2)	9039(2)	1396(1)	19(1)
C(31)	13608(2)	7366(2)	4153(1)	18(1)
C(32)	12115(2)	6659(2)	4046(1)	16(1)
C(33)	11837(2)	5549(2)	4404(1)	19(1)
C(34)	13027(2)	5181(2)	4871(1)	23(1)
C(35)	14484(2)	5904(2)	4980(1)	23(1)
C(36)	14807(2)	7004(2)	4623(1)	20(1)
C(41)	14809(2)	9459(2)	3768(1)	18(1)
C(42)	14203(2)	10520(2)	4218(1)	21(1)
C(141)	116(2)	7328(2)	986(1)	23(1)
C(1)	6578(2)	8554(2)	2151(1)	16(1)
C(11)	4916(2)	8265(2)	1884(1)	17(1)
C(12)	4004(2)	7186(2)	2085(1)	16(1)
C(21)	8939(2)	8053(2)	2829(1)	16(1)
C(22)	9944(2)	9110(2)	2656(1)	18(1)
C(23)	11516(2)	9309(2)	2934(1)	17(1)
C(24)	12103(2)	8426(2)	3393(1)	16(1)
C(25)	11140(2)	7347(2)	3561(1)	16(1)
C(26)	9541(2)	7172(2)	3280(1)	16(1)
N(1)	7295(2)	7818(1)	2573(1)	17(1)
N(2)	13603(2)	8417(1)	3744(1)	18(1)
O(1)	4603(1)	6393(1)	2553(1)	21(1)

Table H.2: Bond distances (Å) and angles (°) for 5Me-SalH-Carba.

Bond	Distance (Å)	Bond Angle	Angle (°)
C(13)-C(14)	1.389(2)	C(14)-C(13)-C(12)	120.99(15)
C(13)-C(12)	1.397(2)	C(14)-C(13)-H(13)	119.5
C(13)-H(13)	0.9500	C(12)-C(13)-H(13)	119.5
C(14)-C(15)	1.404(2)	C(13)-C(14)-C(15)	119.09(14)
C(14)-C(141)	1.508(2)	C(13)-C(14)-C(141)	119.76(15)
C(15)-C(16)	1.385(2)	C(15)-C(14)-C(141)	121.14(15)
C(15)-H(15)	0.9500	C(16)-C(15)-C(14)	120.17(15)
C(16)-C(11)	1.399(2)	C(16)-C(15)-H(15)	119.9
C(16)-H(16)	0.9500	C(14)-C(15)-H(15)	119.9
C(31)-N(2)	1.388(2)	C(15)-C(16)-C(11)	121.28(15)
C(31)-C(36)	1.398(2)	C(15)-C(16)-H(16)	119.4
C(31)-C(32)	1.414(2)	C(11)-C(16)-H(16)	119.4
C(32)-C(33)	1.397(2)	N(2)-C(31)-C(36)	129.05(15)
C(32)-C(25)	1.446(2)	N(2)-C(31)-C(32)	109.18(13)
C(33)-C(34)	1.393(2)	C(36)-C(31)-C(32)	121.75(15)
C(33)-H(33)	0.9500	C(33)-C(32)-C(31)	119.63(14)
C(34)-C(35)	1.400(2)	C(33)-C(32)-C(25)	133.86(14)
C(34)-H(34)	0.9500	C(31)-C(32)-C(25)	106.47(13)
C(35)-C(36)	1.394(2)	C(34)-C(33)-C(32)	118.93(15)
C(35)-H(35)	0.9500	C(34)-C(33)-H(33)	120.5
C(36)-H(36)	0.9500	C(32)-C(33)-H(33)	120.5
C(41)-N(2)	1.4574(19)	C(33)-C(34)-C(35)	120.72(15)
C(41)-C(42)	1.524(2)	C(33)-C(34)-H(34)	119.6
C(41)-H(41A)	0.9900	C(35)-C(34)-H(34)	119.6
C(41)-H(41B)	0.9900	C(36)-C(35)-C(34)	121.56(15)
C(42)-H(42A)	0.9800	C(36)-C(35)-H(35)	119.2
C(42)-H(42B)	0.9800	C(34)-C(35)-H(35)	119.2
C(42)-H(42C)	0.9800	C(35)-C(36)-C(31)	117.39(15)
C(141)-H(14A)	0.9800	C(35)-C(36)-H(36)	121.3
C(141)-H(14B)	0.9800	C(31)-C(36)-H(36)	121.3
C(141)-H(14C)	0.9800	N(2)-C(41)-C(42)	111.76(12)
C(1)-N(1)	1.290(2)	N(2)-C(41)-H(41A)	109.3
C(1)-C(11)	1.453(2)	C(42)-C(41)-H(41A)	109.3
C(1)-H(1A)	0.9500	N(2)-C(41)-H(41B)	109.3
C(11)-C(12)	1.409(2)	C(42)-C(41)-H(41B)	109.3

C(12)-O(1)	1.3549(18)	H(41A)-C(41)-H(41B)	107.9
C(21)-C(26)	1.391(2)	C(41)-C(42)-H(42A)	109.5
C(21)-C(22)	1.415(2)	C(41)-C(42)-H(42B)	109.5
C(21)-N(1)	1.4215(18)	H(42A)-C(42)-H(42B)	109.5
C(22)-C(23)	1.381(2)	C(41)-C(42)-H(42C)	109.5
C(22)-H(22)	0.9500	H(42A)-C(42)-H(42C)	109.5
C(23)-C(24)	1.398(2)	H(42B)-C(42)-H(42C)	109.5
C(23)-H(23)	0.9500	C(14)-C(141)-H(14A)	109.5
C(24)-N(2)	1.3845(19)	C(14)-C(141)-H(14B)	109.5
C(24)-C(25)	1.413(2)	H(14A)-C(141)-H(14B)	109.5
C(25)-C(26)	1.399(2)	C(14)-C(141)-H(14C)	109.5
C(26)-H(26)	0.9500	H(14A)-C(141)-H(14C)	109.5
O(1)-H(1B)	0.8400	H(14B)-C(141)-H(14C)	109.5
		N(1)-C(1)-C(11)	121.22(14)
		N(1)-C(1)-H(1A)	119.4
		C(11)-C(1)-H(1A)	119.4
		C(16)-C(11)-C(12)	118.50(14)
		C(16)-C(11)-C(1)	119.81(14)
		C(12)-C(11)-C(1)	121.64(14)
		O(1)-C(12)-C(13)	118.32(14)
		O(1)-C(12)-C(11)	121.70(14)
		C(13)-C(12)-C(11)	119.96(14)
		C(26)-C(21)-C(22)	120.02(14)
		C(26)-C(21)-N(1)	115.88(14)
		C(22)-C(21)-N(1)	124.10(14)
		C(23)-C(22)-C(21)	121.54(14)
		C(23)-C(22)-H(22)	119.2
		C(21)-C(22)-H(22)	119.2
		C(22)-C(23)-C(24)	118.02(14)
		C(22)-C(23)-H(23)	121.0
		C(24)-C(23)-H(23)	121.0
		N(2)-C(24)-C(23)	129.20(14)
		N(2)-C(24)-C(25)	109.33(13)
		C(23)-C(24)-C(25)	121.47(13)
		C(26)-C(25)-C(24)	119.61(14)
		C(26)-C(25)-C(32)	133.81(15)
		C(24)-C(25)-C(32)	106.53(13)
		C(21)-C(26)-C(25)	119.31(14)

		C(21)-C(26)-H(26)	120.3
		C(25)-C(26)-H(26)	120.3
		C(1)-N(1)-C(21)	122.63(14)
		C(24)-N(2)-C(31)	108.45(13)
		C(24)-N(2)-C(41)	124.96(13)
		C(31)-N(2)-C(41)	125.66(13)
		C(12)-O(1)-H(1B)	109.5

Table H.3: Anisotropic displacement parameters ($Å^2 x\ 10^3$) for 5Me-SalH-Carba. The anisotropic displacement factor exponent takes the form: $-2\pi^2[h^2a^{*2}U^{11} + ... + 2\ h\ k\ a^*\ b^*\ U^{12}]$

	U11	U22	U33	U23	U13	U12
C(13)	17(1)	17(1)	22(1)	-1(1)	3(1)	-1(1)
C(14)	15(1)	21(1)	19(1)	-4(1)	2(1)	2(1)
C(15)	19(1)	23(1)	20(1)	3(1)	-2(1)	2(1)
C(16)	18(1)	18(1)	21(1)	2(1)	1(1)	-2(1)
C(31)	19(1)	17(1)	17(1)	-3(1)	0(1)	1(1)
C(32)	17(1)	17(1)	14(1)	-2(1)	1(1)	2(1)
C(33)	20(1)	18(1)	20(1)	0(1)	2(1)	2(1)
C(34)	26(1)	21(1)	21(1)	3(1)	2(1)	2(1)
C(35)	25(1)	24(1)	18(1)	0(1)	-5(1)	5(1)
C(36)	20(1)	21(1)	20(1)	-4(1)	-5(1)	1(1)
C(41)	17(1)	19(1)	20(1)	-1(1)	1(1)	-2(1)
C(42)	20(1)	19(1)	24(1)	-3(1)	-1(1)	-2(1)
C(141)	16(1)	23(1)	29(1)	-3(1)	-3(1)	1(1)
C(1)	16(1)	15(1)	18(1)	-2(1)	1(1)	0(1)
C(11)	16(1)	16(1)	17(1)	-2(1)	2(1)	2(1)
C(12)	18(1)	14(1)	16(1)	0(1)	2(1)	3(1)
C(21)	16(1)	17(1)	16(1)	-3(1)	1(1)	1(1)
C(22)	19(1)	17(1)	17(1)	0(1)	1(1)	2(1)
C(23)	19(1)	16(1)	17(1)	-1(1)	2(1)	-1(1)
C(24)	16(1)	17(1)	16(1)	-3(1)	0(1)	0(1)
C(25)	17(1)	16(1)	15(1)	-2(1)	2(1)	1(1)
C(26)	17(1)	16(1)	17(1)	-1(1)	1(1)	0(1)
N(1)	16(1)	18(1)	17(1)	-3(1)	1(1)	1(1)

N(2)	17(1)	18(1)	18(1)	0(1)	-3(1)	-1(1)
O(1)	21(1)	19(1)	24(1)	5(1)	-4(1)	-1(1)

Supplementary data of 5Me-SalH-Tyra for the atomic coordinates, bond distances and angles and anisotropic displacement parameters are given in appendix tables I.

Table I.1: Atomic coordinates (x 10^4) and equivalent isotropic displacement parameters ($Å^2$ x 10^3) for 5Me-SalH-Tyra. U(eq) is defined as one third of the trace of the orthogonalized U^{ij} tensor.

	x	y	z	U(eq)
C(441)	3911(3)	9938(2)	1197(1)	24(1)
O(2)	3986(2)	9602(1)	4316(1)	19(1)
O(6)	1316(2)	12646(1)	10444(1)	23(1)
C(4)	1195(3)	11624(2)	4760(1)	17(1)
C(5)	1631(3)	11889(2)	6256(1)	19(1)
C(6)	1175(3)	11094(2)	7014(1)	19(1)
C(41)	1758(2)	11108(2)	3904(1)	16(1)
C(42)	3231(2)	10111(1)	3703(1)	15(1)
C(43)	3865(2)	9747(2)	2808(1)	16(1)
C(44)	3141(3)	10322(2)	2144(1)	17(1)
C(45)	1663(3)	11284(2)	2358(1)	17(1)
C(46)	988(3)	11658(2)	3217(1)	17(1)
C(61)	1208(2)	11563(2)	7909(1)	16(1)
C(62)	1601(3)	12646(2)	8059(1)	18(1)
C(63)	1655(3)	13033(2)	8893(1)	17(1)
C(64)	1299(3)	12333(2)	9610(1)	17(1)
C(65)	889(3)	11251(2)	9473(1)	21(1)
C(66)	856(3)	10876(2)	8639(1)	21(1)
N(2)	1987(2)	11277(1)	5407(1)	18(1)
C(1)	6453(3)	3249(2)	-378(1)	17(1)
C(2)	6528(3)	3080(2)	1187(1)	20(1)
C(3)	6908(3)	3889(2)	1851(1)	18(1)
C(11)	6867(3)	3792(2)	-1196(1)	16(1)
C(12)	7677(3)	4825(2)	-1263(1)	17(1)
C(13)	8130(3)	5287(2)	-2112(1)	18(1)
C(14)	7827(2)	4777(2)	-2849(1)	18(1)

C(15)	7023(3)	3760(2)	-2769(1)	18(1)
C(16)	6566(2)	3289(2)	-1960(1)	18(1)
C(31)	6655(2)	3495(2)	2784(1)	16(1)
C(32)	6891(2)	4235(2)	3431(1)	17(1)
C(33)	6714(3)	3928(2)	4302(1)	18(1)
C(34)	6290(2)	2848(2)	4554(1)	16(1)
C(35)	6010(2)	2106(2)	3930(1)	17(1)
C(36)	6188(2)	2431(2)	3055(1)	17(1)
C(141)	8331(3)	5292(2)	-3743(1)	22(1)
N(1)	6819(2)	3632(1)	333(1)	19(1)
O(1)	7983(2)	5302(1)	-573(1)	22(1)
O(3)	6198(2)	2568(1)	5413(1)	22(1)

Table I.2: Bond distances (Å) and angles (°) for 5Me-SalH-Tyra.

Bond	Distance (Å)	Bond Angle	Angle (°)
C(441)-C(44)	1.501(2)	C(44)-C(441)-H(44A)	109.5
C(441)-H(44A)	0.9800	C(44)-C(441)-H(44B)	109.5
C(441)-H(44B)	0.9800	H(44A)-C(441)-H(44B)	109.5
C(441)-H(44C)	0.9800	C(44)-C(441)-H(44C)	109.5
O(2)-C(42)	1.297(2)	H(44A)-C(441)-H(44C)	109.5
O(2)-H(2)	0.8400	H(44B)-C(441)-H(44C)	109.5
O(6)-C(64)	1.355(2)	C(42)-O(2)-H(2)	109.5
O(6)-H(6C)	0.8400	C(64)-O(6)-H(6C)	109.5
C(4)-N(2)	1.298(2)	N(2)-C(4)-C(41)	123.88(17)
C(4)-C(41)	1.415(2)	N(2)-C(4)-H(4)	118.1
C(4)-H(4)	0.9500	C(41)-C(4)-H(4)	118.1
C(5)-N(2)	1.461(2)	N(2)-C(5)-C(6)	111.14(15)
C(5)-C(6)	1.514(2)	N(2)-C(5)-H(5A)	109.4
C(5)-H(5A)	0.9900	C(6)-C(5)-H(5A)	109.4
C(5)-H(5B)	0.9900	N(2)-C(5)-H(5B)	109.4
C(6)-C(61)	1.510(2)	C(6)-C(5)-H(5B)	109.4
C(6)-H(6A)	0.9900	H(5A)-C(5)-H(5B)	108.0
C(6)-H(6B)	0.9900	C(61)-C(6)-C(5)	115.28(15)
C(41)-C(46)	1.415(2)	C(61)-C(6)-H(6A)	108.5
C(41)-C(42)	1.437(2)	C(5)-C(6)-H(6A)	108.5
C(42)-C(43)	1.413(2)	C(61)-C(6)-H(6B)	108.5

C(43)-C(44)	1.382(2)	C(5)-C(6)-H(6B)	108.5
C(43)-H(43)	0.9500	H(6A)-C(6)-H(6B)	107.5
C(44)-C(45)	1.412(3)	C(46)-C(41)-C(4)	118.90(16)
C(45)-C(46)	1.368(2)	C(46)-C(41)-C(42)	119.63(16)
C(45)-H(45)	0.9500	C(4)-C(41)-C(42)	121.16(16)
C(46)-H(46)	0.9500	O(2)-C(42)-C(43)	122.01(16)
C(61)-C(62)	1.390(3)	O(2)-C(42)-C(41)	120.94(16)
C(61)-C(66)	1.392(3)	C(43)-C(42)-C(41)	117.00(16)
C(62)-C(63)	1.390(2)	C(44)-C(43)-C(42)	122.38(16)
C(62)-H(62)	0.9500	C(44)-C(43)-H(43)	118.8
C(63)-C(64)	1.387(2)	C(42)-C(43)-H(43)	118.8
C(63)-H(63)	0.9500	C(43)-C(44)-C(45)	119.66(16)
C(64)-C(65)	1.390(3)	C(43)-C(44)-C(441)	120.78(16)
C(65)-C(66)	1.381(3)	C(45)-C(44)-C(441)	119.56(16)
C(65)-H(65)	0.9500	C(46)-C(45)-C(44)	119.92(16)
C(66)-H(66)	0.9500	C(46)-C(45)-H(45)	120.0
C(1)-N(1)	1.296(2)	C(44)-C(45)-H(45)	120.0
C(1)-C(11)	1.415(2)	C(45)-C(46)-C(41)	121.34(17)
C(1)-H(1)	0.9500	C(45)-C(46)-H(46)	119.3
C(2)-N(1)	1.464(2)	C(41)-C(46)-H(46)	119.3
C(2)-C(3)	1.513(3)	C(62)-C(61)-C(66)	116.63(16)
C(2)-H(2A)	0.9900	C(62)-C(61)-C(6)	124.27(16)
C(2)-H(2B)	0.9900	C(66)-C(61)-C(6)	119.09(16)
C(3)-C(31)	1.503(2)	C(61)-C(62)-C(63)	122.28(17)
C(3)-H(3A)	0.9900	C(61)-C(62)-H(62)	118.9
C(3)-H(3B)	0.9900	C(63)-C(62)-H(62)	118.9
C(11)-C(16)	1.410(2)	C(64)-C(63)-C(62)	120.02(16)
C(11)-C(12)	1.437(2)	C(64)-C(63)-H(63)	120.0
C(12)-O(1)	1.296(2)	C(62)-C(63)-H(63)	120.0
C(12)-C(13)	1.416(2)	O(6)-C(64)-C(63)	123.72(16)
C(13)-C(14)	1.377(2)	O(6)-C(64)-C(65)	117.82(16)
C(13)-H(13)	0.9500	C(63)-C(64)-C(65)	118.45(16)
C(14)-C(15)	1.417(3)	C(66)-C(65)-C(64)	120.78(17)
C(14)-C(141)	1.507(2)	C(66)-C(65)-H(65)	119.6
C(15)-C(16)	1.366(2)	C(64)-C(65)-H(65)	119.6
C(15)-H(15)	0.9500	C(65)-C(66)-C(61)	121.83(17)
C(16)-H(16)	0.9500	C(65)-C(66)-H(66)	119.1
C(31)-C(36)	1.394(3)	C(61)-C(66)-H(66)	119.1

C(31)-C(32)	1.397(2)	C(4)-N(2)-C(5)	124.94(16)
C(32)-C(33)	1.385(2)	N(1)-C(1)-C(11)	122.49(17)
C(32)-H(32)	0.9500	N(1)-C(1)-H(1)	118.8
C(33)-C(34)	1.394(3)	C(11)-C(1)-H(1)	118.8
C(33)-H(33)	0.9500	N(1)-C(2)-C(3)	107.48(15)
C(34)-O(3)	1.363(2)	N(1)-C(2)-H(2A)	110.2
C(34)-C(35)	1.385(3)	C(3)-C(2)-H(2A)	110.2
C(35)-C(36)	1.394(2)	N(1)-C(2)-H(2B)	110.2
C(35)-H(35)	0.9500	C(3)-C(2)-H(2B)	110.2
C(36)-H(36)	0.9500	H(2A)-C(2)-H(2B)	108.5
C(141)-H(14A)	0.9800	C(31)-C(3)-C(2)	116.28(15)
C(141)-H(14B)	0.9800	C(31)-C(3)-H(3A)	108.2
C(141)-H(14C)	0.9800	C(2)-C(3)-H(3A)	108.2
O(1)-H(1A)	0.8400	C(31)-C(3)-H(3B)	108.2
O(3)-H(3)	0.8400	C(2)-C(3)-H(3B)	108.2
		H(3A)-C(3)-H(3B)	107.4
		C(16)-C(11)-C(1)	119.89(16)
		C(16)-C(11)-C(12)	119.57(16)
		C(1)-C(11)-C(12)	120.48(16)
		O(1)-C(12)-C(13)	122.02(16)
		O(1)-C(12)-C(11)	120.92(16)
		C(13)-C(12)-C(11)	117.06(16)
		C(14)-C(13)-C(12)	122.23(17)
		C(14)-C(13)-H(13)	118.9
		C(12)-C(13)-H(13)	118.9
		C(13)-C(14)-C(15)	119.84(16)
		C(13)-C(14)-C(141)	120.75(17)
		C(15)-C(14)-C(141)	119.41(16)
		C(16)-C(15)-C(14)	119.63(16)
		C(16)-C(15)-H(15)	120.2
		C(14)-C(15)-H(15)	120.2
		C(15)-C(16)-C(11)	121.67(17)
		C(15)-C(16)-H(16)	119.2
		C(11)-C(16)-H(16)	119.2
		C(36)-C(31)-C(32)	117.17(16)
		C(36)-C(31)-C(3)	124.27(16)
		C(32)-C(31)-C(3)	118.56(16)
		C(33)-C(32)-C(31)	122.05(17)

		C(33)-C(32)-H(32)	119.0
		C(31)-C(32)-H(32)	119.0
		C(32)-C(33)-C(34)	119.75(17)
		C(32)-C(33)-H(33)	120.1
		C(34)-C(33)-H(33)	120.1
		O(3)-C(34)-C(35)	122.97(16)
		O(3)-C(34)-C(33)	117.65(16)
		C(35)-C(34)-C(33)	119.37(16)
		C(34)-C(35)-C(36)	120.13(16)
		C(34)-C(35)-H(35)	119.9
		C(36)-C(35)-H(35)	119.9
		C(31)-C(36)-C(35)	121.50(17)
		C(31)-C(36)-H(36)	119.2
		C(35)-C(36)-H(36)	119.2
		C(14)-C(141)-H(14A)	109.5
		C(14)-C(141)-H(14B)	109.5
		H(14A)-C(141)-H(14B)	109.5
		C(14)-C(141)-H(14C)	109.5
		H(14A)-C(141)-H(14C)	109.5
		H(14B)-C(141)-H(14C)	109.5
		C(1)-N(1)-C(2)	125.42(16)
		C(12)-O(1)-H(1A)	109.5
		C(34)-O(3)-H(3)	109.5

Table I.3: Anisotropic displacement parameters ($Å^2 x\ 10^3$) for 5Me-SalH-Tyra. The anisotropic displacement factor exponent takes the form: $-2\pi^2[h^2 a^{*2} U^{11} + ... + 2\ h\ k\ a^*\ b^*\ U^{12}]$

	U11	U22	U33	U23	U13	U12
C(441)	28(1)	30(1)	13(1)	-1(1)	-5(1)	-1(1)
O(2)	23(1)	19(1)	13(1)	0(1)	-6(1)	1(1)
O(6)	38(1)	22(1)	13(1)	0(1)	-6(1)	-12(1)
C(4)	17(1)	18(1)	16(1)	-1(1)	-2(1)	-1(1)
C(5)	23(1)	21(1)	12(1)	-2(1)	-2(1)	-1(1)
C(6)	24(1)	22(1)	11(1)	-1(1)	-2(1)	-7(1)
C(41)	16(1)	19(1)	13(1)	1(1)	-3(1)	-4(1)

C(42)	17(1)	14(1)	14(1)	0(1)	-4(1)	-4(1)
C(43)	17(1)	17(1)	15(1)	-2(1)	-3(1)	-2(1)
C(44)	18(1)	20(1)	14(1)	-1(1)	-3(1)	-7(1)
C(45)	20(1)	19(1)	14(1)	3(1)	-7(1)	-4(1)
C(46)	17(1)	18(1)	17(1)	1(1)	-4(1)	-2(1)
C(61)	14(1)	19(1)	14(1)	-1(1)	-2(1)	-2(1)
C(62)	23(1)	19(1)	13(1)	2(1)	-3(1)	-4(1)
C(63)	21(1)	15(1)	16(1)	0(1)	-4(1)	-4(1)
C(64)	19(1)	22(1)	12(1)	-2(1)	-4(1)	-5(1)
C(65)	30(1)	21(1)	14(1)	3(1)	-5(1)	-10(1)
C(66)	26(1)	18(1)	18(1)	0(1)	-3(1)	-9(1)
N(2)	21(1)	22(1)	11(1)	0(1)	-2(1)	-3(1)
C(1)	18(1)	17(1)	16(1)	-1(1)	-4(1)	-1(1)
C(2)	27(1)	20(1)	13(1)	2(1)	-5(1)	-5(1)
C(3)	19(1)	21(1)	13(1)	2(1)	-4(1)	-3(1)
C(11)	18(1)	17(1)	13(1)	0(1)	-4(1)	-2(1)
C(12)	18(1)	17(1)	17(1)	-2(1)	-5(1)	-1(1)
C(13)	19(1)	18(1)	16(1)	1(1)	-5(1)	-4(1)
C(14)	14(1)	21(1)	16(1)	1(1)	-3(1)	0(1)
C(15)	18(1)	22(1)	14(1)	-4(1)	-5(1)	-3(1)
C(16)	18(1)	17(1)	18(1)	-2(1)	-4(1)	-3(1)
C(31)	14(1)	20(1)	13(1)	2(1)	-3(1)	-1(1)
C(32)	18(1)	16(1)	16(1)	2(1)	-4(1)	-3(1)
C(33)	19(1)	18(1)	17(1)	-2(1)	-4(1)	-2(1)
C(34)	15(1)	22(1)	13(1)	2(1)	-3(1)	-2(1)
C(35)	18(1)	18(1)	15(1)	2(1)	-4(1)	-4(1)
C(36)	18(1)	20(1)	13(1)	-1(1)	-4(1)	-3(1)
C(141)	23(1)	30(1)	14(1)	3(1)	-5(1)	-7(1)
N(1)	24(1)	20(1)	12(1)	1(1)	-4(1)	-2(1)
O(1)	35(1)	21(1)	13(1)	1(1)	-8(1)	-10(1)
O(3)	31(1)	23(1)	12(1)	3(1)	-5(1)	-10(1)

APPENDIX A

Supplementary data of 5Me-SalH-Triaz for the atomic coordinates, bond distances and angles and anisotropic displacement parameters are given in appendix tables J.

Table J.1: Atomic coordinates (x 10^4) and equivalent isotropic displacement parameters ($Å^2$ x 10^3) for 5Me-SalH-Triaz. U(eq) is defined as one third of the trace of the orthogonalized U^{ij} tensor.

	x	y	z	U(eq)
N(1)	6887(1)	4271(5)	7644(2)	15(1)
N(22)	7631(1)	7655(6)	6762(2)	16(1)
N(23)	8094(1)	9588(5)	7158(2)	19(1)
N(25)	7645(1)	7299(6)	8938(2)	17(1)
O(1)	6134(1)	1178(5)	6120(2)	22(1)
C(1)	6622(1)	3028(6)	8663(2)	16(1)
C(11)	6111(1)	916(6)	8512(3)	16(1)
C(12)	5878(1)	81(6)	7245(3)	16(1)
C(13)	5370(1)	-1883(6)	7145(3)	18(1)
C(14)	5068(1)	-3010(6)	8269(3)	18(1)
C(15)	5304(1)	-2214(6)	9524(3)	19(1)
C(16)	5816(2)	-316(6)	9640(3)	18(1)
C(21)	7372(1)	6333(6)	7822(3)	15(1)
C(24)	8087(1)	9275(6)	8463(3)	18(1)
C(141)	4494(1)	-5013(7)	8156(3)	22(1)

Table J.2: Bond distances (Å) and angles (°) for 5Me-SalH-Triaz.

Bond	Distance (Å)	Bond Angle	Angle (°)
N(1)-C(1)	1.294(3)	C(1)-N(1)-C(21)	120.0(2)
N(1)-C(21)	1.388(3)	C(21)-N(22)-N(23)	109.8(2)
N(22)-C(21)	1.337(4)	C(24)-N(23)-N(22)	102.5(2)
N(22)-N(23)	1.364(3)	C(24)-N(23)-H(23)	128.8
N(23)-C(24)	1.323(4)	N(22)-N(23)-H(23)	128.8
N(23)-H(23)	0.8800	C(21)-N(25)-C(24)	101.9(2)
N(25)-C(21)	1.335(4)	C(12)-O(1)-H(1B)	109.5
N(25)-C(24)	1.371(4)	N(1)-C(1)-C(11)	121.3(2)
O(1)-C(12)	1.348(3)	N(1)-C(1)-H(1A)	119.4

O(1)-H(1B)	0.8400	C(11)-C(1)-H(1A)	119.4
C(1)-C(11)	1.440(4)	C(16)-C(11)-C(12)	118.1(2)
C(1)-H(1A)	0.9500	C(16)-C(11)-C(1)	120.1(2)
C(11)-C(16)	1.408(4)	C(12)-C(11)-C(1)	121.8(2)
C(11)-C(12)	1.418(4)	O(1)-C(12)-C(13)	118.5(2)
C(12)-C(13)	1.389(4)	O(1)-C(12)-C(11)	121.6(2)
C(13)-C(14)	1.394(4)	C(13)-C(12)-C(11)	119.9(2)
C(13)-H(13)	0.9500	C(12)-C(13)-C(14)	121.4(3)
C(14)-C(15)	1.405(4)	C(12)-C(13)-H(13)	119.3
C(14)-C(141)	1.508(4)	C(14)-C(13)-H(13)	119.3
C(15)-C(16)	1.378(4)	C(13)-C(14)-C(15)	118.6(2)
C(15)-H(15)	0.9500	C(13)-C(14)-C(141)	121.3(2)
C(16)-H(16)	0.9500	C(15)-C(14)-C(141)	120.2(3)
C(24)-H(24)	0.9500	C(16)-C(15)-C(14)	120.7(3)
C(141)-H(14A)	0.9800	C(16)-C(15)-H(15)	119.6
C(141)-H(14B)	0.9800	C(14)-C(15)-H(15)	119.6
C(141)-H(14C)	0.9800	C(15)-C(16)-C(11)	121.2(3)
		C(15)-C(16)-H(16)	119.4
		C(11)-C(16)-H(16)	119.4
		N(25)-C(21)-N(22)	110.8(2)
		N(25)-C(21)-N(1)	129.8(3)
		N(22)-C(21)-N(1)	119.4(2)
		N(23)-C(24)-N(25)	115.0(3)
		N(23)-C(24)-H(24)	122.5
		N(25)-C(24)-H(24)	122.5
		C(14)-C(141)-H(14A)	109.5
		C(14)-C(141)-H(14B)	109.5
		H(14A)-C(141)-H(14B)	109.5
		C(14)-C(141)-H(14C)	109.5
		H(14A)-C(141)-H(14C)	109.5
		H(14B)-C(141)-H(14C)	109.5

Table J.3: **Anisotropic displacement parameters ($Å^2 x\ 10^3$) for 5Me-SalH-Triaz. The anisotropic displacement factor exponent takes the form: $-2\pi^2[\ h^2a^{*2}U^{11} + ... + 2\ h\ k\ a^*\ b^*\ U^{12}\ ]$**

	U11	U22	U33	U23	U13	U12
N(1)	18(1)	16(1)	13(1)	-1(1)	1(1)	1(1)
N(22)	20(1)	17(1)	11(1)	0(1)	1(1)	0(1)
N(23)	20(1)	22(1)	15(1)	1(1)	2(1)	-4(1)
N(25)	19(1)	19(1)	12(1)	-2(1)	1(1)	1(1)
O(1)	24(1)	29(1)	12(1)	-2(1)	1(1)	-8(1)
C(1)	22(1)	18(1)	10(1)	-1(1)	-2(1)	2(1)
C(11)	19(1)	16(1)	13(1)	0(1)	1(1)	3(1)
C(12)	18(1)	16(1)	14(1)	-1(1)	2(1)	2(1)
C(13)	24(1)	17(1)	14(1)	0(1)	0(1)	4(1)
C(14)	20(1)	16(1)	19(1)	-1(1)	0(1)	2(1)
C(15)	23(2)	19(1)	15(1)	0(1)	3(1)	1(1)
C(16)	24(2)	19(1)	11(1)	1(1)	1(1)	2(1)
C(21)	19(1)	17(1)	11(1)	0(1)	-1(1)	5(1)
C(24)	18(1)	23(1)	15(1)	-2(1)	0(1)	-1(1)
C(141)	26(2)	18(1)	23(2)	-1(1)	0(1)	-1(1)

APPENDIX B

Supplementary data of fac-[Re(Sal-mTol)(CO)$_3$(HOCH$_3$)] for the atomic coordinates, bond distances and angles and anisotropic displacement parameters are given in appendix tables A.

Table A.1: Atomic coordinates (x 10^4) and equivalent isotropic displacement parameters (Å^2 x 10^3) for *fac*-[Re(Sal-*m*Tol)(CO)$_3$(HOCH$_3$)]. U(eq) is defined as one third of the trace of the orthogonalized U^{ij} tensor.

	x	y	z	U(eq)
Re(1)	8551(1)	4480(1)	1458(1)	22(1)
N(1)	8175(2)	3097(3)	1894(3)	23(1)
O(01)	9104(2)	6410(3)	798(3)	44(1)
O(1)	9509(2)	3669(3)	1378(3)	24(1)
O(02)	7204(2)	5630(3)	1756(3)	35(1)
O(03)	7632(2)	4216(3)	-662(3)	41(1)
O(04)	9202(2)	4553(3)	2986(2)	26(1)
C(01)	8919(3)	5685(4)	1074(4)	29(1)
C(1)	8470(3)	2238(4)	1887(4)	25(1)
C(02)	7713(3)	5201(4)	1649(4)	28(1)
C(03)	7983(3)	4308(4)	143(4)	28(1)
C(04)	9182(4)	5392(6)	3580(5)	58(2)
C(11)	9108(3)	2000(4)	1531(3)	19(1)
C(12)	9580(3)	2700(4)	1265(3)	20(1)
C(13)	10165(3)	2367(4)	906(4)	25(1)
C(14)	10290(3)	1380(4)	831(4)	32(1)
C(15)	9839(3)	683(4)	1095(4)	32(1)
C(16)	9256(3)	1001(4)	1436(4)	26(1)
C(21)	7488(3)	3124(4)	2197(4)	28(1)
C(22)	7527(3)	3291(4)	3158(4)	30(1)
C(23)	6859(4)	3364(4)	3444(4)	35(1)
C(24)	6180(3)	3276(4)	2724(5)	37(2)
C(25)	6141(4)	3113(5)	1773(5)	45(2)
C(26)	6800(3)	3039(5)	1494(5)	38(2)
C(231)	6896(3)	3540(5)	4487(4)	38(2)

Table A.2: Bond distances (Å) and angles (°) for *fac*-[Re(Sal-*m*Tol)(CO)$_3$(HOCH$_3$)].

Bond	Distance (Å)	Bond Angle	Angle (°)
Re(1)-C(03)	1.890(6)	C(03)-Re(1)-C(01)	87.9(2)
Re(1)-C(01)	1.913(6)	C(03)-Re(1)-C(02)	87.7(2)
Re(1)-C(02)	1.919(6)	C(01)-Re(1)-C(02)	88.3(2)
Re(1)-O(1)	2.119(3)	C(03)-Re(1)-O(1)	96.94(18)
Re(1)-N(1)	2.157(4)	C(01)-Re(1)-O(1)	93.36(18)
Re(1)-O(04)	2.179(3)	C(02)-Re(1)-O(1)	175.10(19)
N(1)-C(1)	1.290(6)	C(03)-Re(1)-N(1)	92.6(2)
N(1)-C(21)	1.456(6)	C(01)-Re(1)-N(1)	177.91(19)
O(01)-C(01)	1.150(6)	C(02)-Re(1)-N(1)	93.7(2)
O(1)-C(12)	1.339(6)	O(1)-Re(1)-N(1)	84.58(14)
O(02)-C(02)	1.154(6)	C(03)-Re(1)-O(04)	175.51(19)
O(03)-C(03)	1.157(6)	C(01)-Re(1)-O(04)	96.2(2)
O(04)-C(04)	1.429(7)	C(02)-Re(1)-O(04)	94.26(18)
O(04)-H(04)	0.9500	O(1)-Re(1)-O(04)	80.99(13)
C(1)-C(11)	1.449(7)	N(1)-Re(1)-O(04)	83.21(15)
C(1)-H(1)	0.9500	C(1)-N(1)-C(21)	115.6(4)
C(04)-H(04A)	0.9800	C(1)-N(1)-Re(1)	128.0(4)
C(04)-H(04B)	0.9800	C(21)-N(1)-Re(1)	116.3(3)
C(04)-H(04C)	0.9800	C(12)-O(1)-Re(1)	129.1(3)
C(11)-C(16)	1.401(7)	C(04)-O(04)-Re(1)	122.1(3)
C(11)-C(12)	1.414(7)	C(04)-O(04)-H(04)	118.9
C(12)-C(13)	1.399(7)	Re(1)-O(04)-H(04)	118.9
C(13)-C(14)	1.370(8)	O(01)-C(01)-Re(1)	176.1(5)
C(13)-H(13)	0.9500	N(1)-C(1)-C(11)	126.4(5)
C(14)-C(15)	1.385(8)	N(1)-C(1)-H(1)	116.8
C(14)-H(14)	0.9500	C(11)-C(1)-H(1)	116.8
C(15)-C(16)	1.373(7)	O(02)-C(02)-Re(1)	179.3(5)
C(15)-H(15)	0.9500	O(03)-C(03)-Re(1)	179.1(5)
C(16)-H(16)	0.9500	O(04)-C(04)-H(04A)	109.5
C(21)-C(22)	1.373(8)	O(04)-C(04)-H(04B)	109.5
C(21)-C(26)	1.385(8)	H(04A)-C(04)-H(04B)	109.5
C(22)-C(23)	1.412(8)	O(04)-C(04)-H(04C)	109.5
C(22)-H(22)	0.9500	H(04A)-C(04)-H(04C)	109.5
C(23)-C(24)	1.386(8)	H(04B)-C(04)-H(04C)	109.5

C(23)-C(231)	1.492(8)	C(16)-C(11)-C(12)	118.3(5)
C(24)-C(25)	1.359(8)	C(16)-C(11)-C(1)	116.8(5)
C(24)-H(24)	0.9500	C(12)-C(11)-C(1)	124.9(5)
C(25)-C(26)	1.391(8)	O(1)-C(12)-C(13)	118.4(5)
C(25)-H(25)	0.9500	O(1)-C(12)-C(11)	122.7(4)
C(26)-H(26)	0.9500	C(13)-C(12)-C(11)	118.8(5)
C(231)-H(23A)	0.9800	C(14)-C(13)-C(12)	120.7(5)
C(231)-H(23B)	0.9800	C(14)-C(13)-H(13)	119.6
C(231)-H(23C)	0.9800	C(12)-C(13)-H(13)	119.6
		C(13)-C(14)-C(15)	121.4(5)
		C(13)-C(14)-H(14)	119.3
		C(15)-C(14)-H(14)	119.3
		C(16)-C(15)-C(14)	118.5(5)
		C(16)-C(15)-H(15)	120.8
		C(14)-C(15)-H(15)	120.8
		C(15)-C(16)-C(11)	122.3(5)
		C(15)-C(16)-H(16)	118.8
		C(11)-C(16)-H(16)	118.9
		C(22)-C(21)-C(26)	121.2(5)
		C(22)-C(21)-N(1)	119.8(5)
		C(26)-C(21)-N(1)	118.9(5)
		C(21)-C(22)-C(23)	119.9(5)
		C(21)-C(22)-H(22)	120.1
		C(23)-C(22)-H(22)	120.1
		C(24)-C(23)-C(22)	117.6(5)
		C(24)-C(23)-C(231)	122.1(5)
		C(22)-C(23)-C(231)	120.3(6)
		C(25)-C(24)-C(23)	122.5(6)
		C(25)-C(24)-H(24)	118.8
		C(23)-C(24)-H(24)	118.8
		C(24)-C(25)-C(26)	119.7(6)
		C(24)-C(25)-H(25)	120.1
		C(26)-C(25)-H(25)	120.1
		C(21)-C(26)-C(25)	119.1(6)
		C(21)-C(26)-H(26)	120.5
		C(25)-C(26)-H(26)	120.5
		C(23)-C(231)-H(23A)	109.5
		C(23)-C(231)-H(23B)	109.5

		H(23A)-C(231)-H(23B)	109.5
		C(23)-C(231)-H(23C)	109.5
		H(23A)-C(231)-H(23C)	109.5
		H(23B)-C(231)-H(23C)	109.5

Table A.3: Anisotropic displacement parameters ($Å^2$x 10^3) for *fac*-[Re(Sal-*m*Tol)$(CO)_3(HOCH_3)$].. The anisotropic displacement factor exponent takes the form: $-2\pi^2[h^2a^{*2}U^{11} + ... + 2 h k a^* b^* U^{12}]$

	U11	U22	U33	U23	U13	U12
Re(1)	22(1)	20(1)	26(1)	0(1)	9(1)	2(1)
N(1)	20(2)	24(2)	27(2)	3(2)	10(2)	-1(2)
O(01)	50(3)	29(2)	61(3)	10(2)	30(2)	1(2)
O(1)	20(2)	21(2)	33(2)	-1(2)	10(2)	0(2)
O(02)	30(2)	35(2)	42(2)	1(2)	16(2)	13(2)
O(03)	36(2)	52(3)	32(2)	-7(2)	2(2)	5(2)
O(04)	33(2)	25(2)	22(2)	3(2)	7(2)	13(2)
C(01)	29(3)	27(3)	33(3)	1(3)	14(3)	7(3)
C(1)	25(3)	25(3)	26(3)	3(2)	10(2)	-2(2)
C(02)	34(3)	22(3)	25(3)	2(2)	5(3)	0(3)
C(03)	24(3)	27(3)	37(3)	0(3)	16(3)	-1(2)
C(04)	42(4)	76(6)	52(4)	-18(4)	6(3)	24(4)
C(11)	20(3)	22(3)	13(2)	-1(2)	0(2)	0(2)
C(12)	18(3)	25(3)	16(3)	-2(2)	4(2)	1(2)
C(13)	24(3)	33(3)	19(3)	-2(2)	6(2)	-4(2)
C(14)	24(3)	46(4)	26(3)	-11(3)	7(2)	4(3)
C(15)	32(3)	29(3)	37(3)	-7(3)	11(3)	2(3)
C(16)	28(3)	21(3)	29(3)	-5(2)	8(2)	-2(2)
C(21)	31(3)	22(3)	36(3)	1(3)	16(3)	3(2)
C(22)	27(3)	28(3)	36(3)	0(3)	11(3)	-2(2)
C(23)	51(4)	25(3)	36(3)	-1(3)	21(3)	4(3)
C(24)	32(3)	37(4)	46(4)	-2(3)	17(3)	-1(3)
C(25)	35(4)	45(4)	57(5)	-12(3)	19(3)	-1(3)
C(26)	31(3)	43(4)	39(4)	-6(3)	11(3)	-1(3)
C(231)	44(4)	38(4)	37(3)	-3(3)	20(3)	3(3)

Supplementary data of fac-[Re(Sal-Ph)(CO)$_3$(HOCH$_3$)]for the atomic coordinates, bond distances and angles and anisotropic displacement parameters are given in appendix tables B.

Table B.1: Atomic coordinates (x 10^4) and equivalent isotropic displacement parameters (Å^2 x 10^3) for *fac*-[Re(Sal-Ph)(CO)$_3$(HOCH$_3$)]. U(eq) is defined as one third of the trace of the orthogonalized U^{ij} tensor.

	x	y	z	U(eq)
Re(1)	3501(1)	5376(1)	6379(1)	22(1)
N(1)	3167(3)	6773(4)	6877(4)	22(1)
O(1)	4485(3)	6170(4)	6353(4)	26(1)
O(01)	4009(3)	3397(4)	5710(4)	39(1)
O(02)	2113(3)	4226(4)	6535(4)	39(1)
O(03)	2598(3)	5703(4)	4148(4)	42(1)
O(04)	4187(3)	5274(4)	7986(4)	26(1)
C(01)	3844(4)	4140(5)	5996(5)	27(2)
C(1)	3476(4)	7631(5)	6887(5)	22(1)
C(02)	2639(4)	4663(5)	6491(5)	26(1)
C(03)	2937(4)	5584(5)	4990(6)	28(2)
C(04)	4225(5)	4356(8)	8554(8)	52(2)
C(11)	4101(4)	7861(5)	6498(5)	22(1)
C(12)	4548(4)	7137(5)	6228(5)	23(1)
C(13)	5122(4)	7461(6)	5836(6)	30(2)
C(14)	5246(4)	8456(6)	5730(6)	33(2)
C(15)	4811(5)	9180(6)	6008(6)	37(2)
C(16)	4240(4)	8876(6)	6390(6)	33(2)
C(21)	2520(4)	6744(5)	7259(6)	26(2)
C(22)	2634(4)	6714(6)	8268(6)	31(2)
C(23)	2022(5)	6648(6)	8633(7)	38(2)
C(24)	1286(4)	6632(6)	7949(6)	34(2)
C(25)	1163(4)	6674(7)	6927(7)	39(2)
C(26)	1782(4)	6726(6)	6559(6)	37(2)

Table B.2: Bond distances (Å) and angles (°) for *fac*-[Re(Sal-Ph)(CO)$_3$(HOCH$_3$)].

Bond	Distance (Å)	Bond Angle	Angle (°)
Re(1)-C(03)	1.895(7)	C(03)-Re(1)-C(02)	87.8(3)
Re(1)-C(02)	1.909(7)	C(03)-Re(1)-C(01)	88.0(3)
Re(1)-C(01)	1.920(7)	C(02)-Re(1)-C(01)	86.9(3)
Re(1)-O(1)	2.121(5)	C(03)-Re(1)-O(1)	95.6(3)
Re(1)-N(1)	2.164(6)	C(02)-Re(1)-O(1)	176.5(3)
Re(1)-O(04)	2.188(5)	C(01)-Re(1)-O(1)	94.0(3)
N(1)-C(1)	1.288(9)	C(03)-Re(1)-N(1)	94.6(3)
N(1)-C(21)	1.459(9)	C(02)-Re(1)-N(1)	94.6(3)
O(1)-C(12)	1.326(8)	C(01)-Re(1)-N(1)	177.1(3)
O(01)-C(01)	1.155(9)	O(1)-Re(1)-N(1)	84.38(19)
O(02)-C(02)	1.155(9)	C(03)-Re(1)-O(04)	174.9(3)
O(03)-C(03)	1.148(9)	C(02)-Re(1)-O(04)	96.1(2)
O(04)-C(04)	1.459(10)	C(01)-Re(1)-O(04)	95.5(2)
O(04)-H(04)	0.9500	O(1)-Re(1)-O(04)	80.48(18)
C(1)-C(11)	1.460(9)	N(1)-Re(1)-O(04)	81.84(19)
C(1)-H(1)	0.9500	C(1)-N(1)-C(21)	115.6(6)
C(04)-H(04A)	0.9800	C(1)-N(1)-Re(1)	127.9(5)
C(04)-H(04B)	0.9800	C(21)-N(1)-Re(1)	116.5(4)
C(04)-H(04C)	0.9800	C(12)-O(1)-Re(1)	127.6(4)
C(11)-C(12)	1.408(9)	C(04)-O(04)-Re(1)	121.2(5)
C(11)-C(16)	1.409(10)	C(04)-O(04)-H(04)	119.4
C(12)-C(13)	1.410(9)	Re(1)-O(04)-H(04)	119.4
C(13)-C(14)	1.377(11)	O(01)-C(01)-Re(1)	175.5(7)
C(13)-H(13)	0.9500	N(1)-C(1)-C(11)	126.0(6)
C(14)-C(15)	1.397(12)	N(1)-C(1)-H(1)	117.0
C(14)-H(14)	0.9500	C(11)-C(1)-H(1)	117.0
C(15)-C(16)	1.390(11)	O(02)-C(02)-Re(1)	178.4(6)
C(15)-H(15)	0.9500	O(03)-C(03)-Re(1)	179.5(7)
C(16)-H(16)	0.9500	O(04)-C(04)-H(04A)	109.5
C(21)-C(22)	1.352(10)	O(04)-C(04)-H(04B)	109.5
C(21)-C(26)	1.395(10)	H(04A)-C(04)-H(04B)	109.5
C(22)-C(23)	1.385(10)	O(04)-C(04)-H(04C)	109.5
C(22)-H(22)	0.9500	H(04A)-C(04)-H(04C)	109.5
C(23)-C(24)	1.383(11)	H(04B)-C(04)-H(04C)	109.5
C(23)-H(23)	0.9500	C(12)-C(11)-C(16)	120.1(7)

C(24)-C(25)	1.368(12)	C(12)-C(11)-C(1)	123.8(6)
C(24)-H(24)	0.9500	C(16)-C(11)-C(1)	116.1(6)
C(25)-C(26)	1.398(11)	O(1)-C(12)-C(11)	124.3(6)
C(25)-H(25)	0.9500	O(1)-C(12)-C(13)	117.7(6)
C(26)-H(26)	0.9500	C(11)-C(12)-C(13)	118.0(6)
		C(14)-C(13)-C(12)	121.1(7)
		C(14)-C(13)-H(13)	119.5
		C(12)-C(13)-H(13)	119.5
		C(13)-C(14)-C(15)	121.3(7)
		C(13)-C(14)-H(14)	119.3
		C(15)-C(14)-H(14)	119.3
		C(16)-C(15)-C(14)	118.5(7)
		C(16)-C(15)-H(15)	120.7
		C(14)-C(15)-H(15)	120.7
		C(15)-C(16)-C(11)	121.0(7)
		C(15)-C(16)-H(16)	119.5
		C(11)-C(16)-H(16)	119.5
		C(22)-C(21)-C(26)	120.8(7)
		C(22)-C(21)-N(1)	120.7(6)
		C(26)-C(21)-N(1)	118.5(6)
		C(21)-C(22)-C(23)	120.9(7)
		C(21)-C(22)-H(22)	119.5
		C(23)-C(22)-H(22)	119.5
		C(24)-C(23)-C(22)	119.0(8)
		C(24)-C(23)-H(23)	120.5
		C(22)-C(23)-H(23)	120.5
		C(25)-C(24)-C(23)	120.7(7)
		C(25)-C(24)-H(24)	119.7
		C(23)-C(24)-H(24)	119.7
		C(24)-C(25)-C(26)	120.3(7)
		C(24)-C(25)-H(25)	119.9
		C(26)-C(25)-H(25)	119.9
		C(21)-C(26)-C(25)	118.4(7)
		C(21)-C(26)-H(26)	120.8
		C(25)-C(26)-H(26)	120.8

Table B.3: **Anisotropic displacement parameters ($Å^2$x 10^3) for *fac*-[Re(Sal-Ph)$(CO)_3(HOCH_3)$]. The anisotropic displacement factor exponent takes the form: $-2\pi^2[h^2a^{*2}U^{11} + ... + 2 h k a^* b^* U^{12}]$**

	U11	U22	U33	U23	U13	U12
Re(1)	15(1)	23(1)	29(1)	0(1)	8(1)	0(1)
N(1)	16(3)	27(3)	25(3)	3(2)	9(2)	-1(2)
O(1)	13(2)	28(2)	39(3)	0(2)	10(2)	1(2)
O(01)	39(3)	36(3)	50(3)	-3(3)	24(3)	7(3)
O(02)	28(3)	38(3)	51(4)	0(3)	15(3)	-6(2)
O(03)	35(3)	48(3)	36(3)	8(3)	3(3)	3(3)
O(04)	19(2)	31(3)	30(3)	-2(2)	10(2)	-6(2)
C(01)	21(3)	32(4)	29(4)	0(3)	7(3)	3(3)
C(1)	17(3)	26(3)	23(3)	0(3)	7(3)	3(3)
C(02)	22(3)	23(3)	32(4)	0(3)	9(3)	-1(3)
C(03)	23(4)	36(4)	27(4)	5(3)	9(3)	2(3)
C(04)	37(5)	61(6)	56(6)	12(5)	13(4)	-2(4)
C(11)	16(3)	25(3)	25(3)	2(3)	6(3)	0(3)
C(12)	16(3)	31(4)	23(3)	-1(3)	8(3)	-3(3)
C(13)	20(4)	40(4)	31(4)	4(3)	10(3)	-2(3)
C(14)	19(4)	47(4)	36(4)	6(4)	10(3)	-9(3)
C(15)	42(5)	41(4)	30(4)	3(3)	15(4)	-23(4)
C(16)	27(4)	26(4)	44(4)	-4(3)	12(3)	0(3)
C(21)	20(3)	22(3)	39(4)	4(3)	14(3)	2(3)
C(22)	20(4)	40(4)	30(4)	2(3)	8(3)	-2(3)
C(23)	31(4)	51(5)	38(4)	3(4)	19(3)	6(4)
C(24)	27(4)	32(4)	52(5)	-2(4)	24(4)	-3(3)
C(25)	17(4)	53(5)	46(5)	-1(4)	8(3)	-3(3)
C(26)	25(4)	52(5)	36(4)	4(4)	16(3)	-1(4)

Supplementary data of fac-[Re(Sal-pTol)(CO)$_3$(HOCH$_3$)] for the atomic coordinates, bond distances and angles and anisotropic displacement parameters are given in appendix tables C.

Table C.1: Atomic coordinates (x 10^4) and equivalent isotropic displacement parameters (Å^2 x 10^3) for *fac*-[Re(Sal-*p*Tol)(CO)$_3$(HOCH$_3$)]. U(eq) is defined as one third of the trace of the orthogonalized U^{ij} tensor.

	x	y	z	U(eq)
Re(1)	6480(1)	4598(1)	8669(1)	55(1)
N(1)	6779(9)	3272(17)	8163(13)	54(5)
O(1)	5531(8)	3835(14)	8681(13)	62(5)
O(01)	5937(11)	6440(16)	9288(15)	82(6)
O(02)	7784(10)	5731(17)	8522(15)	88(7)
O(03)	7444(11)	4312(17)	10962(13)	90(7)
C(01)	6137(12)	5760(20)	9047(17)	62(8)
C(1)	6507(13)	2440(20)	8165(17)	62(8)
C(02)	7296(12)	5350(20)	8559(17)	58(7)
C(03)	7072(12)	4410(20)	10085(16)	71(9)
O(04A)	5750(60)	4890(90)	7020(80)	90(7)
C(04A)	5700(40)	5850(60)	6640(40)	55(11)
O(04B)	5777(13)	4620(20)	7040(20)	39(7)
C(04B)	5817(16)	5340(30)	6347(17)	55(11)
C(11)	5915(13)	2210(20)	8570(18)	62(7)
C(12)	5499(13)	2900(20)	8842(18)	60(7)
C(13)	4948(14)	2580(30)	9210(20)	77(9)
C(14)	4841(17)	1640(30)	9330(20)	90(11)
C(15)	5260(20)	900(30)	9060(20)	109(11)
C(16)	5775(14)	1240(20)	8680(20)	69(7)
C(24A)	8474(15)	3466(15)	6940(20)	78(9)
C(21A)	7351(12)	3263(17)	7733(17)	64(7)
C(22A)	7140(20)	3060(40)	6640(20)	64(7)
C(23A)	7730(20)	3170(40)	6240(40)	100(30)
C(25A)	8620(30)	3630(40)	7910(40)	100(20)
C(26A)	8100(40)	3550(50)	8360(60)	100(20)
C(241)	9010(30)	3550(30)	6450(50)	121(17)
C(22B)	7240(30)	3570(50)	6810(50)	64(7)
C(23B)	7770(30)	3660(50)	6420(50)	90(30)

C(25B)	8630(40)	3130(50)	7940(60)	78(9)
C(26B)	8060(30)	3040(50)	8340(50)	48(17)
C(242)	9070(60)	3610(40)	6420(90)	121(17)

Table C.2: Bond distances (Å) and angles (°) for *fac*-[Re(Sal-*p*Tol)(CO)$_3$(HOCH$_3$)].

Bond	Distance (Å)	Bond Angle	Angle (°)
Re(1)-C(03)	1.89(2)	C(03)-Re(1)-C(01)	87.7(11)
Re(1)-C(01)	1.90(3)	C(03)-Re(1)-C(02)	88.3(11)
Re(1)-C(02)	1.95(2)	C(01)-Re(1)-C(02)	86.7(11)
Re(1)-O(1)	2.133(16)	C(03)-Re(1)-O(1)	95.9(10)
Re(1)-N(1)	2.15(2)	C(01)-Re(1)-O(1)	91.9(9)
Re(1)-O(04B)	2.17(3)	C(02)-Re(1)-O(1)	175.5(8)
Re(1)-O(04A)	2.24(10)	C(03)-Re(1)-N(1)	95.5(10)
N(1)-C(1)	1.28(3)	C(01)-Re(1)-N(1)	175.6(9)
N(1)-C(21A)	1.45(2)	C(02)-Re(1)-N(1)	96.4(9)
O(1)-C(12)	1.34(3)	O(1)-Re(1)-N(1)	84.8(7)
O(01)-C(01)	1.13(3)	C(03)-Re(1)-O(04B)	173.0(12)
O(02)-C(02)	1.11(3)	C(01)-Re(1)-O(04B)	97.7(10)
O(03)-C(03)	1.17(3)	C(02)-Re(1)-O(04B)	96.4(8)
C(1)-C(11)	1.50(3)	O(1)-Re(1)-O(04B)	79.5(7)
C(1)-H(1)	0.9500	N(1)-Re(1)-O(04B)	78.8(9)
O(04A)-C(04A)	1.44(12)	C(03)-Re(1)-O(04A)	176(3)
O(04A)-H(04G)	0.9500	C(01)-Re(1)-O(04A)	89(3)
C(04A)-H(04A)	0.9800	C(02)-Re(1)-O(04A)	92(3)
C(04A)-H(04B)	0.9800	O(1)-Re(1)-O(04A)	84(3)
C(04A)-H(04C)	0.9800	N(1)-Re(1)-O(04A)	88(3)
O(04B)-C(04B)	1.420(18)	O(04B)-Re(1)-O(04A)	10(4)
O(04B)-H(04I)	0.9500	C(1)-N(1)-C(21A)	112(2)
C(04B)-H(04D)	0.9800	C(1)-N(1)-Re(1)	128.7(14)
C(04B)-H(04E)	0.9800	C(21A)-N(1)-Re(1)	119.3(17)
C(04B)-H(04F)	0.9800	C(12)-O(1)-Re(1)	126.1(12)
C(11)-C(16)	1.40(4)	O(01)-C(01)-Re(1)	178.9(19)
C(11)-C(12)	1.40(3)	N(1)-C(1)-C(11)	125(2)
C(12)-C(13)	1.42(3)	N(1)-C(1)-H(1)	117.3
C(13)-C(14)	1.36(4)	C(11)-C(1)-H(1)	117.3
C(13)-H(13)	0.9500	O(02)-C(02)-Re(1)	176(3)

C(14)-C(15)	1.45(5)	O(03)-C(03)-Re(1)	179(3)
C(14)-H(14)	0.9500	C(04A)-O(04A)-Re(1)	119(8)
C(15)-C(16)	1.38(3)	C(04A)-O(04A)-H(04G)	120.7
C(15)-H(15)	0.9500	Re(1)-O(04A)-H(04G)	120.7
C(16)-H(16)	0.9500	O(04A)-C(04A)-H(04A)	109.5
C(24A)-C(25A)	1.29(5)	O(04A)-C(04A)-H(04B)	109.5
C(24A)-C(23B)	1.30(6)	H(04A)-C(04A)-H(04B)	109.5
C(24A)-C(25B)	1.40(8)	O(04A)-C(04A)-H(04C)	109.5
C(24A)-C(241)	1.445(19)	H(04A)-C(04A)-H(04C)	109.5
C(24A)-C(23A)	1.46(2)	H(04B)-C(04A)-H(04C)	109.5
C(24A)-C(242)	1.60(8)	C(04B)-O(04B)-Re(1)	123.6(19)
C(21A)-C(22B)	1.30(6)	C(04B)-O(04B)-H(04I)	118.2
C(21A)-C(26B)	1.34(6)	Re(1)-O(04B)-H(04I)	118.2
C(21A)-C(26A)	1.43(8)	O(04B)-C(04B)-H(04D)	109.5
C(21A)-C(22A)	1.449(19)	O(04B)-C(04B)-H(04E)	109.5
C(22A)-C(23A)	1.47(6)	H(04D)-C(04B)-H(04E)	109.5
C(22A)-H(22A)	0.9500	O(04B)-C(04B)-H(04F)	109.5
C(23A)-H(23A)	0.9500	H(04D)-C(04B)-H(04F)	109.5
C(25A)-C(26A)	1.38(6)	H(04E)-C(04B)-H(04F)	109.5
C(25A)-H(25A)	0.9500	C(16)-C(11)-C(12)	119(2)
C(26A)-H(26A)	0.9500	C(16)-C(11)-C(1)	118(2)
C(241)-H(24A)	0.9800	C(12)-C(11)-C(1)	123(3)
C(241)-H(24B)	0.9800	O(1)-C(12)-C(11)	124.4(19)
C(241)-H(24C)	0.9800	O(1)-C(12)-C(13)	117(2)
C(22B)-C(23B)	1.33(8)	C(11)-C(12)-C(13)	118(3)
C(22B)-H(22B)	0.9500	C(14)-C(13)-C(12)	121(3)
C(23B)-H(23B)	0.9500	C(14)-C(13)-H(13)	119.4
C(25B)-C(26B)	1.43(6)	C(12)-C(13)-H(13)	119.4
C(25B)-H(25B)	0.9500	C(13)-C(14)-C(15)	122(2)
C(26B)-H(26B)	0.9500	C(13)-C(14)-H(14)	118.9
C(242)-H(24D)	0.9800	C(15)-C(14)-H(14)	118.9
C(242)-H(24E)	0.9800	C(16)-C(15)-C(14)	114(3)
C(242)-H(24F)	0.9800	C(16)-C(15)-H(15)	122.9
		C(14)-C(15)-H(15)	122.9
		C(15)-C(16)-C(11)	125(3)
		C(15)-C(16)-H(16)	117.4
		C(11)-C(16)-H(16)	117.4
		C(25A)-C(24A)-C(23B)	108(4)

		C(25A)-C(24A)-C(25B)	30(3)
		C(23B)-C(24A)-C(25B)	114(4)
		C(25A)-C(24A)-C(241)	125(4)
		C(23B)-C(24A)-C(241)	120(4)
		C(25B)-C(24A)-C(241)	126(4)
		C(25A)-C(24A)-C(23A)	121(3)
		C(23B)-C(24A)-C(23A)	29(3)
		C(25B)-C(24A)-C(23A)	111(4)
		C(241)-C(24A)-C(23A)	114(2)
		C(25A)-C(24A)-C(242)	124(5)
		C(23B)-C(24A)-C(242)	120(6)
		C(25B)-C(24A)-C(242)	126(6)
		C(241)-C(24A)-C(242)	3(2)
		C(23A)-C(24A)-C(242)	115(6)
		C(22B)-C(21A)-C(26B)	117(4)
		C(22B)-C(21A)-C(26A)	105(3)
		C(26B)-C(21A)-C(26A)	30(3)
		C(22B)-C(21A)-N(1)	123(3)
		C(26B)-C(21A)-N(1)	119(3)
		C(26A)-C(21A)-N(1)	120(3)
		C(22B)-C(21A)-C(22A)	31(2)
		C(26B)-C(21A)-C(22A)	116(3)
		C(26A)-C(21A)-C(22A)	121(4)
		N(1)-C(21A)-C(22A)	119(2)
		C(21A)-C(22A)-C(23A)	115(3)
		C(21A)-C(22A)-H(22A)	122.3
		C(23A)-C(22A)-H(22A)	122.3
		C(24A)-C(23A)-C(22A)	119(4)
		C(24A)-C(23A)-H(23A)	120.3
		C(22A)-C(23A)-H(23A)	120.3
		C(24A)-C(25A)-C(26A)	124(6)
		C(24A)-C(25A)-H(25A)	118.0
		C(26A)-C(25A)-H(25A)	118.0
		C(25A)-C(26A)-C(21A)	119(6)
		C(25A)-C(26A)-H(26A)	120.4
		C(21A)-C(26A)-H(26A)	120.4
		C(24A)-C(241)-H(24A)	109.5
		C(24A)-C(241)-H(24B)	109.5

		H(24A)-C(241)-H(24B)	109.5
		C(24A)-C(241)-H(24C)	109.5
		H(24A)-C(241)-H(24C)	109.5
		H(24B)-C(241)-H(24C)	109.5
		C(21A)-C(22B)-C(23B)	125(5)
		C(21A)-C(22B)-H(22B)	117.6
		C(23B)-C(22B)-H(22B)	117.6
		C(24A)-C(23B)-C(22B)	124(5)
		C(24A)-C(23B)-H(23B)	118.0
		C(22B)-C(23B)-H(23B)	118.0
		C(24A)-C(25B)-C(26B)	121(5)
		C(24A)-C(25B)-H(25B)	119.5
		C(26B)-C(25B)-H(25B)	119.5
		C(21A)-C(26B)-C(25B)	119(5)
		C(21A)-C(26B)-H(26B)	120.4
		C(25B)-C(26B)-H(26B)	120.4
		C(24A)-C(242)-H(24D)	109.5
		C(24A)-C(242)-H(24E)	109.5
		H(24D)-C(242)-H(24E)	109.5
		C(24A)-C(242)-H(24F)	109.5
		H(24D)-C(242)-H(24F)	109.5
		H(24E)-C(242)-H(24F)	109.5

Table C.3: Anisotropic displacement parameters ($Å^2$x 10^3) for *fac*-[Re(Sal-*p*Tol)$(CO)_3(HOCH_3)$]. The anisotropic displacement factor exponent takes the form: $-2\pi^2[h^2a^{*2}U^{11} + ... + 2 h k a^* b^* U^{12}]$

	U11	U22	U33	U23	U13	U12
Re(1)	17(1)	116(1)	33(1)	12(1)	12(1)	15(1)
N(1)	32(9)	95(17)	42(9)	23(10)	22(8)	15(10)
O(1)	29(7)	96(14)	69(10)	31(10)	29(7)	20(8)
O(01)	68(12)	117(18)	75(12)	23(12)	43(11)	43(12)
O(02)	41(10)	150(20)	83(13)	-48(13)	33(9)	-30(11)
O(03)	76(13)	150(20)	46(9)	21(11)	19(9)	69(13)
C(01)	34(11)	120(20)	44(12)	17(13)	28(10)	26(13)
C(1)	51(14)	100(20)	52(13)	32(13)	35(11)	42(14)

C(02)	33(10)	100(20)	45(11)	-13(12)	25(9)	-17(12)
C(03)	44(12)	140(30)	35(11)	23(13)	23(10)	51(15)
O(04A)	76(13)	150(20)	46(9)	21(11)	19(9)	69(13)
C(04A)	28(13)	100(30)	31(14)	-5(16)	7(11)	-27(17)
O(04B)	10(9)	70(20)	33(9)	5(13)	6(7)	-11(12)
C(04B)	28(13)	100(30)	31(14)	-5(16)	7(11)	-27(17)
C(11)	47(13)	100(20)	53(13)	25(13)	38(11)	29(13)
C(12)	46(13)	100(20)	57(13)	12(14)	42(11)	6(13)
C(13)	54(15)	130(30)	65(16)	20(17)	48(14)	12(16)
C(14)	80(20)	130(30)	100(20)	20(20)	70(20)	0(20)
C(15)	110(20)	170(30)	78(17)	47(18)	66(17)	-30(20)
C(16)	66(15)	90(20)	73(15)	31(14)	55(13)	13(14)
C(24A)	55(14)	100(20)	110(20)	44(17)	67(16)	35(14)
C(21A)	38(9)	110(20)	63(11)	29(13)	38(9)	31(12)
C(22A)	38(9)	110(20)	63(11)	29(13)	38(9)	31(12)
C(23A)	140(60)	110(50)	100(50)	30(40)	110(50)	60(40)
C(25A)	40(20)	180(60)	110(30)	80(40)	60(20)	60(30)
C(26A)	40(20)	180(60)	110(30)	80(40)	60(20)	60(30)
C(241)	120(30)	120(30)	210(40)	60(30)	150(30)	40(20)
C(22B)	38(9)	110(20)	63(11)	29(13)	38(9)	31(12)
C(23B)	40(30)	210(100)	30(30)	40(40)	20(20)	70(40)
C(25B)	55(14)	100(20)	110(20)	44(17)	67(16)	35(14)
C(26B)	20(20)	90(50)	40(30)	30(30)	20(20)	10(30)
C(242)	120(30)	120(30)	210(40)	60(30)	150(30)	40(20)

Supplementary data of fac-[Re(Sal-CyHex)(CO)$_3$(HOCH$_3$)] for the atomic coordinates, bond distances and angles and anisotropic displacement parameters are given in appendix tables D.

Table D.1: **Atomic coordinates (x 10^4) and equivalent isotropic displacement parameters (Å^2 x 10^3) for *fac*-[Re(Sal-CyHex)(CO)$_3$(HOCH$_3$)]. U(eq) is defined as one third of the trace of the orthogonalized U^{ij} tensor.**

	x	y	z	U(eq)
Re(1)	6529(1)	5512(1)	8541(1)	20(1)
N(1)	6815(5)	6859(6)	7993(6)	19(2)
O(01)	6038(5)	3636(6)	9195(6)	34(2)
O(1)	5507(4)	6196(5)	8630(6)	24(2)
O(02)	7917(5)	4395(6)	8372(7)	34(2)
O(03)	7451(5)	5870(6)	10744(6)	31(2)
O(04)	5817(5)	5368(5)	6972(6)	23(2)
C(01)	6204(7)	4363(8)	8942(9)	24(2)
C(1)	6467(6)	7619(6)	8060(8)	17(2)
C(02)	7391(7)	4839(8)	8405(9)	29(3)
C(03)	7101(7)	5739(7)	9891(8)	19(2)
C(04)	5793(8)	4549(7)	6377(10)	30(3)
C(11)	5852(7)	7781(7)	8522(8)	23(2)
C(12)	5416(6)	7088(8)	8791(8)	23(2)
C(13)	4844(7)	7326(7)	9247(8)	25(2)
C(14)	4684(7)	8260(7)	9367(8)	28(2)
C(15)	5108(8)	8947(8)	9099(9)	33(3)
C(16)	5675(7)	8698(8)	8659(9)	32(3)
C(21)	7470(7)	6973(8)	7539(8)	32(3)
C(22)	7378(8)	6345(8)	6628(9)	32(3)
C(23)	8051(7)	6513(10)	6182(9)	36(3)
C(24)	8833(8)	6372(11)	6978(10)	42(4)
C(25)	8901(8)	6993(9)	7882(10)	38(3)
C(26)	8248(7)	6863(8)	8358(9)	28(3)

Table D.2: Bond distances (Å) and angles (°) for *fac*-[Re(Sal-CyHex)(CO)$_3$(HOCH$_3$)].

Bond	Distance (Å)	Bond Angle	Angle (°)
Re(1)-C(03)	1.869(10)	C(03)-Re(1)-C(02)	87.6(5)
Re(1)-C(02)	1.894(13)	C(03)-Re(1)-C(01)	89.6(5)
Re(1)-C(01)	1.896(11)	C(02)-Re(1)-C(01)	85.1(5)
Re(1)-O(1)	2.131(7)	C(03)-Re(1)-O(1)	95.5(4)
Re(1)-O(04)	2.172(8)	C(02)-Re(1)-O(1)	176.0(4)
Re(1)-N(1)	2.202(9)	C(01)-Re(1)-O(1)	92.3(4)
N(1)-C(1)	1.282(12)	C(03)-Re(1)-O(04)	174.9(3)
N(1)-C(21)	1.502(12)	C(02)-Re(1)-O(04)	96.7(4)
O(01)-C(01)	1.173(13)	C(01)-Re(1)-O(04)	93.5(4)
O(1)-C(12)	1.324(12)	O(1)-Re(1)-O(04)	80.3(3)
O(02)-C(02)	1.159(15)	C(03)-Re(1)-N(1)	93.9(4)
O(03)-C(03)	1.173(13)	C(02)-Re(1)-N(1)	97.8(4)
O(04)-C(04)	1.431(11)	C(01)-Re(1)-N(1)	175.5(4)
O(04)-H(04)	0.8400	O(1)-Re(1)-N(1)	84.6(3)
C(1)-C(11)	1.453(14)	O(04)-Re(1)-N(1)	82.8(3)
C(1)-H(1)	0.9500	C(1)-N(1)-C(21)	113.6(9)
C(04)-H(04A)	0.9800	C(1)-N(1)-Re(1)	124.2(6)
C(04)-H(04B)	0.9800	C(21)-N(1)-Re(1)	122.2(7)
C(04)-H(04C)	0.9800	C(12)-O(1)-Re(1)	127.9(7)
C(11)-C(16)	1.389(15)	C(04)-O(04)-Re(1)	123.8(7)
C(11)-C(12)	1.391(15)	C(04)-O(04)-H(04)	109.5
C(12)-C(13)	1.403(14)	Re(1)-O(04)-H(04)	126.8
C(13)-C(14)	1.399(14)	O(01)-C(01)-Re(1)	176.8(10)
C(13)-H(13)	0.9500	N(1)-C(1)-C(11)	128.7(9)
C(14)-C(15)	1.370(16)	N(1)-C(1)-H(1)	115.7
C(14)-H(14)	0.9500	C(11)-C(1)-H(1)	115.7
C(15)-C(16)	1.384(16)	O(02)-C(02)-Re(1)	175.8(10)
C(15)-H(15)	0.9500	O(03)-C(03)-Re(1)	178.8(10)
C(16)-H(16)	0.9500	O(04)-C(04)-H(04A)	109.5
C(21)-C(22)	1.516(15)	O(04)-C(04)-H(04B)	109.5
C(21)-C(26)	1.530(17)	H(04A)-C(04)-H(04B)	109.5
C(21)-H(21)	1.0000	O(04)-C(04)-H(04C)	109.5
C(22)-C(23)	1.537(15)	H(04A)-C(04)-H(04C)	109.5
C(22)-H(22A)	0.9900	H(04B)-C(04)-H(04C)	109.5

C(22)-H(22B)	0.9900	C(16)-C(11)-C(12)	118.6(10)
C(23)-C(24)	1.53(2)	C(16)-C(11)-C(1)	116.8(10)
C(23)-H(23A)	0.9900	C(12)-C(11)-C(1)	124.6(9)
C(23)-H(23B)	0.9900	O(1)-C(12)-C(11)	123.1(9)
C(24)-C(25)	1.508(17)	O(1)-C(12)-C(13)	117.3(10)
C(24)-H(24A)	0.9900	C(11)-C(12)-C(13)	119.6(10)
C(24)-H(24B)	0.9900	C(14)-C(13)-C(12)	119.7(10)
C(25)-C(26)	1.523(15)	C(14)-C(13)-H(13)	120.2
C(25)-H(25A)	0.9900	C(12)-C(13)-H(13)	120.2
C(25)-H(25B)	0.9900	C(15)-C(14)-C(13)	121.0(11)
C(26)-H(26A)	0.9900	C(15)-C(14)-H(14)	119.5
C(26)-H(26B)	0.9900	C(13)-C(14)-H(14)	119.5
		C(14)-C(15)-C(16)	118.4(11)
		C(14)-C(15)-H(15)	120.8
		C(16)-C(15)-H(15)	120.8
		C(15)-C(16)-C(11)	122.6(11)
		C(15)-C(16)-H(16)	118.7
		C(11)-C(16)-H(16)	118.7
		N(1)-C(21)-C(22)	111.8(9)
		N(1)-C(21)-C(26)	110.5(8)
		C(22)-C(21)-C(26)	113.5(10)
		N(1)-C(21)-H(21)	106.9
		C(22)-C(21)-H(21)	106.9
		C(26)-C(21)-H(21)	106.9
		C(21)-C(22)-C(23)	109.2(10)
		C(21)-C(22)-H(22A)	109.8
		C(23)-C(22)-H(22A)	109.8
		C(21)-C(22)-H(22B)	109.8
		C(23)-C(22)-H(22B)	109.8
		H(22A)-C(22)-H(22B)	108.3
		C(24)-C(23)-C(22)	111.7(10)
		C(24)-C(23)-H(23A)	109.3
		C(22)-C(23)-H(23A)	109.3
		C(24)-C(23)-H(23B)	109.3
		C(22)-C(23)-H(23B)	109.3
		H(23A)-C(23)-H(23B)	107.9
		C(25)-C(24)-C(23)	110.2(11)
		C(25)-C(24)-H(24A)	109.6

		C(23)-C(24)-H(24A)	109.6
		C(25)-C(24)-H(24B)	109.6
		C(23)-C(24)-H(24B)	109.6
		H(24A)-C(24)-H(24B)	108.1
		C(24)-C(25)-C(26)	113.3(11)
		C(24)-C(25)-H(25A)	108.9
		C(26)-C(25)-H(25A)	108.9
		C(24)-C(25)-H(25B)	108.9
		C(26)-C(25)-H(25B)	108.9
		H(25A)-C(25)-H(25B)	107.7
		C(25)-C(26)-C(21)	109.5(10)
		C(25)-C(26)-H(26A)	109.8
		C(21)-C(26)-H(26A)	109.8
		C(25)-C(26)-H(26B)	109.8
		C(21)-C(26)-H(26B)	109.8
		H(26A)-C(26)-H(26B)	108.2

Table D.3: Anisotropic displacement parameters ($Å^2x\ 10^3$) for *fac*-[Re(Sal-CyHex)$(CO)_3(HOCH_3)$]. The anisotropic displacement factor exponent takes the form: $-2\pi^2[\ h^2a^{*2}U^{11} + ... + 2\ h\ k\ a^*\ b^*\ U^{12}\ ]$

	U11	U22	U33	U23	U13	U12
Re(1)	20(1)	15(1)	27(1)	0(1)	7(1)	1(1)
N(1)	9(4)	24(5)	25(4)	-3(3)	6(4)	-2(4)
O(01)	33(5)	24(5)	46(5)	6(4)	15(4)	-2(4)
O(1)	21(4)	16(4)	35(4)	-5(3)	10(4)	-3(3)
O(02)	28(5)	30(5)	47(5)	3(4)	17(4)	5(4)
O(03)	21(5)	27(4)	42(5)	-7(4)	5(4)	-2(4)
O(04)	26(5)	14(4)	32(4)	-5(3)	12(4)	5(3)
C(01)	14(6)	27(6)	29(6)	-1(4)	3(5)	5(4)
C(1)	15(5)	7(4)	28(5)	2(4)	5(4)	-3(4)
C(02)	31(7)	23(6)	35(6)	-3(5)	12(6)	-6(5)
C(03)	25(6)	10(5)	18(5)	-1(3)	1(5)	1(4)
C(04)	34(7)	11(5)	44(7)	-8(4)	7(6)	5(5)
C(11)	22(6)	12(5)	30(6)	5(4)	-1(5)	3(4)
C(12)	15(6)	22(6)	31(6)	-3(4)	6(5)	6(4)
C(13)	37(7)	14(5)	27(5)	1(4)	13(5)	-1(5)

C(14)	28(7)	20(6)	33(6)	-1(4)	6(5)	10(5)
C(15)	43(8)	18(6)	39(6)	-12(5)	14(6)	-1(5)
C(16)	29(7)	20(6)	47(7)	-4(5)	11(6)	0(5)
C(21)	30(7)	33(7)	36(7)	4(5)	16(6)	-3(5)
C(22)	35(7)	27(6)	38(6)	-4(5)	16(6)	-8(5)
C(23)	37(8)	46(8)	35(6)	-6(5)	26(6)	-6(6)
C(24)	24(7)	73(11)	33(6)	-3(6)	13(6)	8(7)
C(25)	26(7)	40(7)	54(8)	-9(6)	19(7)	-14(6)
C(26)	18(6)	32(6)	34(6)	-3(5)	10(5)	-5(5)

Supplementary data of fac-[Re(Sal-3MeBu)(CO)$_3$(HOCH$_3$)] for the atomic coordinates, bond distances and angles and anisotropic displacement parameters are given in appendix tables E.

Table E.1: Atomic coordinates (x 10^4) and equivalent isotropic displacement parameters (Å^2 x 10^3) for *fac*-[Re(Sal-3MeBu)(CO)$_3$(HOCH$_3$)]. U(eq) is defined as one third of the trace of the orthogonalized U^{ij} tensor.

	x	y	z	U(eq)
Re(1)	3553(1)	5441(1)	6387(1)	29(1)
O(1)	4504(2)	6180(3)	6348(3)	26(1)
O(02)	2233(2)	4313(4)	6562(4)	49(1)
O(01)	3970(3)	3541(4)	5602(5)	68(2)
O(03)	2625(3)	5860(5)	4156(5)	82(2)
O(04)	4259(2)	5259(3)	7996(3)	42(1)
C(02)	2736(3)	4749(5)	6511(5)	38(2)
C(1)	3596(4)	7614(6)	6915(7)	62(2)
C(01)	3827(4)	4258(5)	5916(5)	39(2)
C(03)	2972(4)	5707(5)	4997(6)	49(2)
C(04)	4281(5)	4421(8)	8586(7)	90(4)
C(11)	4132(3)	7827(4)	6428(5)	31(1)
C(12)	4569(3)	7121(4)	6187(4)	25(1)
C(13)	5111(3)	7423(5)	5796(5)	37(1)
C(14)	5224(4)	8388(5)	5662(6)	58(2)
C(15)	4796(5)	9086(6)	5891(7)	69(3)
C(16)	4265(4)	8806(5)	6286(6)	51(2)

N(1A)	3369(4)	6740(5)	7119(6)	20(1)
C(21A)	2901(5)	6746(7)	7761(7)	27(2)
C(22A)	2075(5)	6787(8)	7109(9)	41(2)
C(23A)	1637(6)	6998(10)	7869(11)	62(2)
C(24A)	1761(17)	6410(20)	8830(20)	123(7)
C(25A)	800(6)	6877(9)	7156(11)	62(2)
N(1B)	3198(8)	6911(12)	6668(12)	20(1)
C(21B)	2462(13)	6970(18)	6870(20)	62(2)
C(22B)	2515(11)	6653(15)	7868(17)	43(5)
C(23B)	1697(8)	6338(17)	7776(15)	41(2)
C(24B)	1920(40)	6670(50)	8910(30)	123(7)
C(25B)	941(10)	6202(19)	7126(19)	62(1)

Table E.2: Bond distances (Å) and angles (°) for *fac*-[Re(Sal-3MeBu)(CO)$_3$(HOCH$_3$)].

Bond	Distance (Å)	Bond Angle	Angle (°)
Re(1)-C(03)	1.891(8)	C(03)-Re(1)-C(01)	87.6(3)
Re(1)-C(01)	1.900(6)	C(03)-Re(1)-C(02)	88.3(3)
Re(1)-C(02)	1.902(6)	C(01)-Re(1)-C(02)	86.4(3)
Re(1)-O(1)	2.117(4)	C(03)-Re(1)-O(1)	95.5(2)
Re(1)-N(1A)	2.148(7)	C(01)-Re(1)-O(1)	93.4(2)
Re(1)-O(04)	2.179(4)	C(02)-Re(1)-O(1)	176.2(2)
Re(1)-N(1B)	2.219(16)	C(03)-Re(1)-N(1A)	100.2(3)
O(1)-C(12)	1.331(7)	C(01)-Re(1)-N(1A)	172.0(3)
O(02)-C(02)	1.165(7)	C(02)-Re(1)-N(1A)	95.7(3)
O(01)-C(01)	1.152(7)	O(1)-Re(1)-N(1A)	84.0(2)
O(03)-C(03)	1.139(8)	C(03)-Re(1)-O(04)	175.1(2)
O(04)-C(04)	1.406(9)	C(01)-Re(1)-O(04)	95.7(2)
O(04)-H(04)	0.8400	C(02)-Re(1)-O(04)	95.5(2)
C(1)-N(1B)	1.212(18)	O(1)-Re(1)-O(04)	80.78(14)
C(1)-N(1A)	1.346(11)	N(1A)-Re(1)-O(04)	76.4(2)
C(1)-C(11)	1.447(9)	C(03)-Re(1)-N(1B)	83.6(5)
C(1)-H(1)	0.9500	C(01)-Re(1)-N(1B)	170.3(4)
C(04)-H(05A)	0.9800	C(02)-Re(1)-N(1B)	97.3(4)
C(04)-H(05B)	0.9800	O(1)-Re(1)-N(1B)	83.5(4)

C(04)-H(05C)	0.9800	N(1A)-Re(1)-N(1B)	16.7(3)
C(11)-C(12)	1.402(8)	O(04)-Re(1)-N(1B)	92.8(4)
C(11)-C(16)	1.403(9)	C(12)-O(1)-Re(1)	127.4(3)
C(12)-C(13)	1.398(7)	C(04)-O(04)-Re(1)	124.5(4)
C(13)-C(14)	1.374(9)	C(04)-O(04)-H(04)	109.5
C(13)-H(13)	0.9500	Re(1)-O(04)-H(04)	126.0
C(14)-C(15)	1.376(10)	O(02)-C(02)-Re(1)	178.1(5)
C(14)-H(14)	0.9500	N(1B)-C(1)-N(1A)	28.3(6)
C(15)-C(16)	1.373(9)	N(1B)-C(1)-C(11)	121.2(10)
C(15)-H(15)	0.9500	N(1A)-C(1)-C(11)	128.0(7)
C(16)-H(16)	0.9500	N(1B)-C(1)-H(1)	114.4
N(1A)-C(21A)	1.469(10)	N(1A)-C(1)-H(1)	116.0
C(21A)-C(22A)	1.537(12)	C(11)-C(1)-H(1)	116.0
C(21A)-H(21A)	0.9900	O(01)-C(01)-Re(1)	177.6(7)
C(21A)-H(21B)	0.9900	O(03)-C(03)-Re(1)	179.3(8)
C(22A)-C(23A)	1.584(14)	O(04)-C(04)-H(05A)	109.5
C(22A)-H(22A)	0.9900	O(04)-C(04)-H(05B)	109.5
C(22A)-H(22B)	0.9900	H(05A)-C(04)-H(05B)	109.5
C(23A)-C(24A)	1.50(3)	O(04)-C(04)-H(05C)	109.5
C(23A)-C(25A)	1.582(16)	H(05A)-C(04)-H(05C)	109.5
C(23A)-H(23A)	1.0000	H(05B)-C(04)-H(05C)	109.5
C(24A)-H(24A)	0.9800	C(12)-C(11)-C(16)	118.9(5)
C(24A)-H(24B)	0.9800	C(12)-C(11)-C(1)	123.7(6)
C(24A)-H(24C)	0.9800	C(16)-C(11)-C(1)	117.1(6)
C(25A)-H(25A)	0.9800	O(1)-C(12)-C(13)	118.8(5)
C(25A)-H(25B)	0.9800	O(1)-C(12)-C(11)	122.7(5)
C(25A)-H(25C)	0.9800	C(13)-C(12)-C(11)	118.5(5)
N(1B)-C(21B)	1.54(3)	C(14)-C(13)-C(12)	121.1(6)
C(21B)-C(22B)	1.41(3)	C(14)-C(13)-H(13)	119.5
C(21B)-H(21C)	0.9900	C(12)-C(13)-H(13)	119.5
C(21B)-H(21D)	0.9900	C(13)-C(14)-C(15)	120.8(6)
C(22B)-C(23B)	1.599(17)	C(13)-C(14)-H(14)	119.6
C(22B)-H(22C)	0.9900	C(15)-C(14)-H(14)	119.6
C(22B)-H(22D)	0.9900	C(16)-C(15)-C(14)	119.0(7)
C(23B)-C(25B)	1.436(17)	C(16)-C(15)-H(15)	120.5
C(23B)-C(24B)	1.54(2)	C(14)-C(15)-H(15)	120.5
C(23B)-H(23B)	1.0000	C(15)-C(16)-C(11)	121.7(6)
C(24B)-H(24D)	0.9800	C(15)-C(16)-H(16)	119.2

C(24B)-H(24E)	0.9800	C(11)-C(16)-H(16)	119.2
C(24B)-H(24F)	0.9800	C(1)-N(1A)-C(21A)	115.7(7)
C(25B)-H(25D)	0.9800	C(1)-N(1A)-Re(1)	122.2(5)
C(25B)-H(25E)	0.9800	C(21A)-N(1A)-Re(1)	121.6(6)
C(25B)-H(25F)	0.9800	N(1A)-C(21A)-C(22A)	112.2(7)
		N(1A)-C(21A)-H(21A)	109.2
		C(22A)-C(21A)-H(21A)	109.2
		N(1A)-C(21A)-H(21B)	109.2
		C(22A)-C(21A)-H(21B)	109.2
		H(21A)-C(21A)-H(21B)	107.9
		C(21A)-C(22A)-C(23A)	107.7(9)
		C(21A)-C(22A)-H(22A)	110.2
		C(23A)-C(22A)-H(22A)	110.2
		C(21A)-C(22A)-H(22B)	110.2
		C(23A)-C(22A)-H(22B)	110.2
		H(22A)-C(22A)-H(22B)	108.5
		C(24A)-C(23A)-C(25A)	107.9(13)
		C(24A)-C(23A)-C(22A)	121.8(16)
		C(25A)-C(23A)-C(22A)	103.5(10)
		C(24A)-C(23A)-H(23A)	107.6
		C(25A)-C(23A)-H(23A)	107.6
		C(22A)-C(23A)-H(23A)	107.6
		C(23A)-C(24A)-H(24A)	109.5
		C(23A)-C(24A)-H(24B)	109.5
		H(24A)-C(24A)-H(24B)	109.5
		C(23A)-C(24A)-H(24C)	109.5
		H(24A)-C(24A)-H(24C)	109.5
		H(24B)-C(24A)-H(24C)	109.5
		C(23A)-C(25A)-H(25A)	109.5
		C(23A)-C(25A)-H(25B)	109.5
		H(25A)-C(25A)-H(25B)	109.5
		C(23A)-C(25A)-H(25C)	109.5
		H(25A)-C(25A)-H(25C)	109.5
		H(25B)-C(25A)-H(25C)	109.5
		C(1)-N(1B)-C(21B)	116.1(15)
		C(1)-N(1B)-Re(1)	125.3(11)
		C(21B)-N(1B)-Re(1)	116.1(12)
		C(22B)-C(21B)-N(1B)	114(2)

		C(22B)-C(21B)-H(21C)	108.8
		N(1B)-C(21B)-H(21C)	108.8
		C(22B)-C(21B)-H(21D)	108.8
		N(1B)-C(21B)-H(21D)	108.8
		H(21C)-C(21B)-H(21D)	107.7
		C(21B)-C(22B)-C(23B)	105.7(18)
		C(21B)-C(22B)-H(22C)	110.6
		C(23B)-C(22B)-H(22C)	110.6
		C(21B)-C(22B)-H(22D)	110.6
		C(23B)-C(22B)-H(22D)	110.6
		H(22C)-C(22B)-H(22D)	108.7
		C(25B)-C(23B)-C(24B)	122(3)
		C(25B)-C(23B)-C(22B)	147.9(19)
		C(24B)-C(23B)-C(22B)	86(2)
		C(25B)-C(23B)-H(23B)	96.2
		C(24B)-C(23B)-H(23B)	96.2
		C(22B)-C(23B)-H(23B)	96.2
		C(23B)-C(24B)-H(24D)	109.5
		C(23B)-C(24B)-H(24E)	109.5
		H(24D)-C(24B)-H(24E)	109.5
		C(23B)-C(24B)-H(24F)	109.5
		H(24D)-C(24B)-H(24F)	109.5
		H(24E)-C(24B)-H(24F)	109.5
		C(23B)-C(25B)-H(25D)	109.5
		C(23B)-C(25B)-H(25E)	109.5
		H(25D)-C(25B)-H(25E)	109.5
		C(23B)-C(25B)-H(25F)	109.5
		H(25D)-C(25B)-H(25F)	109.5
		H(25E)-C(25B)-H(25F)	109.5

Table E.3: Anisotropic displacement parameters ($Å^2 x\ 10^3$) for *fac*-[Re(Sal-3MeBu)$(CO)_3(HOCH_3)$]. The anisotropic displacement factor exponent takes the form: $-2\pi^2[\ h^2 a^{*2} U^{11} + ... + 2\ h\ k\ a^*\ b^*\ U^{12}\ ]$

	U11	U22	U33	U23	U13	U12
Re(1)	24(1)	29(1)	35(1)	-9(1)	13(1)	-4(1)
O(1)	26(2)	26(2)	29(2)	0(2)	13(2)	2(2)
O(02)	40(2)	51(3)	64(3)	-18(2)	26(2)	-21(2)
O(01)	103(4)	41(3)	93(4)	-19(3)	74(4)	-8(3)
O(03)	50(3)	117(6)	53(4)	25(4)	-15(3)	-25(3)
O(04)	39(2)	53(3)	32(2)	-4(2)	13(2)	-22(2)
C(02)	36(3)	39(4)	40(4)	-16(3)	14(3)	-7(3)
C(1)	53(3)	56(4)	96(5)	-15(3)	51(3)	-4(3)
C(01)	48(4)	36(4)	46(4)	-5(3)	31(3)	-5(3)
C(03)	32(3)	48(4)	60(5)	3(4)	10(3)	-10(3)
C(04)	82(6)	124(9)	54(5)	21(6)	11(5)	-63(6)
C(11)	30(3)	31(3)	32(3)	2(3)	12(2)	4(2)
C(12)	23(2)	32(3)	21(3)	6(2)	8(2)	6(2)
C(13)	43(3)	40(4)	38(4)	14(3)	27(3)	9(3)
C(14)	73(5)	49(4)	74(5)	30(4)	56(5)	8(4)
C(15)	91(6)	36(4)	111(7)	29(5)	75(6)	20(4)
C(16)	63(5)	31(4)	77(5)	17(4)	46(4)	14(3)
N(1A)	22(4)	22(3)	16(4)	10(3)	9(3)	5(3)
C(21A)	25(4)	34(5)	27(5)	6(4)	15(4)	4(4)
C(22A)	33(4)	45(5)	53(6)	16(4)	26(4)	11(4)
C(23A)	53(3)	56(4)	96(5)	-15(3)	51(3)	-4(3)
C(24A)	101(16)	68(18)	265(18)	69(12)	145(13)	24(10)
C(25A)	53(3)	56(4)	96(5)	-15(3)	51(3)	-4(3)
N(1B)	22(4)	22(3)	16(4)	10(3)	9(3)	5(3)
C(21B)	53(3)	56(4)	96(5)	-15(3)	51(3)	-4(3)
C(22B)	54(14)	34(11)	49(14)	10(10)	30(12)	12(10)
C(23B)	33(4)	45(5)	53(6)	16(4)	26(4)	11(4)
C(24B)	101(16)	68(18)	265(18)	69(12)	145(13)	24(10)
C(25B)	53(1)	56(1)	96(1)	-16(1)	51(2)	-4(2)

Supplementary data of fac-[Re(Sal-Ph)(CO)$_3$(NC$_5$H$_5$)] for the atomic coordinates, bond distances and angles and anisotropic displacement parameters are given in appendix tables F.

Table F.1: Atomic coordinates (x 10^4) and equivalent isotropic displacement parameters (Å^2 x 10^3) for *fac*-[Re(Sal-Ph)(CO)$_3$(NC$_5$H$_5$)]. U(eq) is defined as one third of the trace of the orthogonalized U^{ij} tensor.

	x	y	z	U(eq)
Re(1)	2383(1)	1971(1)	8906(1)	16(1)
N(1)	2706(4)	3471(5)	9737(2)	19(1)
N(3)	4404(4)	2441(5)	8707(2)	17(1)
O(01)	2100(4)	-46(4)	7655(2)	31(1)
O(1)	1895(4)	3662(3)	8235(2)	19(1)
O(02)	3225(4)	-437(4)	9882(2)	28(1)
O(03)	-418(4)	1344(4)	9203(2)	33(1)
C(1)	2322(5)	4730(5)	9712(3)	19(1)
C(01)	2176(5)	710(5)	8122(3)	20(1)
C(02)	2920(5)	468(5)	9512(3)	20(1)
C(03)	635(6)	1615(6)	9086(3)	22(1)
C(11)	1739(5)	5444(5)	9097(3)	20(1)
C(12)	1557(6)	4889(5)	8397(3)	23(1)
C(13)	1009(5)	5757(5)	7835(3)	22(1)
C(14)	650(6)	7072(5)	7955(3)	22(1)
C(15)	828(6)	7620(6)	8648(3)	24(1)
C(16)	1359(6)	6837(5)	9202(3)	22(1)
C(21)	3284(6)	3019(5)	10433(3)	18(1)
C(22)	4635(6)	2894(5)	10573(3)	21(1)
C(23)	5196(6)	2471(6)	11246(3)	25(1)
C(24)	4407(7)	2158(5)	11760(3)	27(1)
C(25)	3060(6)	2246(5)	11619(3)	26(1)
C(26)	2493(6)	2684(6)	10952(3)	25(1)
C(31)	5274(6)	1417(6)	8651(3)	21(1)
C(32)	6550(6)	1658(6)	8520(3)	26(1)
C(33)	6961(6)	2978(5)	8441(3)	24(1)
C(34)	6080(5)	4015(6)	8493(3)	22(1)
C(35)	4823(6)	3717(5)	8625(3)	20(1)

Table F.2: Bond distances (Å) and angles (°) for *fac*-[Re(Sal-Ph)(CO)$_3$(NC$_5$H$_5$)].

Bond	Distance (Å)	Bond Angle	Angle (°)
N(1)-Re(1)	2.152(5)	C(1)-N(1)-Re(1)	127.4(4)
N(3)-Re(1)	2.207(5)	C(21)-N(1)-Re(1)	117.7(3)
O(1)-Re(1)	2.114(3)	C(35)-N(3)-C(31)	117.3(5)
C(1)-N(1)	1.298(7)	C(35)-N(3)-Re(1)	122.6(4)
C(1)-C(11)	1.428(7)	C(31)-N(3)-Re(1)	120.1(4)
C(1)-H(1)	0.9500	C(12)-O(1)-Re(1)	129.6(3)
C(01)-O(01)	1.150(6)	C(03)-Re(1)-C(02)	87.7(2)
C(01)-Re(1)	1.925(5)	C(03)-Re(1)-C(01)	90.1(2)
C(02)-O(02)	1.152(6)	C(02)-Re(1)-C(01)	87.8(2)
C(02)-Re(1)	1.910(5)	C(03)-Re(1)-O(1)	95.3(2)
C(03)-O(03)	1.164(7)	C(02)-Re(1)-O(1)	176.97(19)
C(03)-Re(1)	1.904(6)	C(01)-Re(1)-O(1)	92.72(19)
C(11)-C(12)	1.423(7)	C(03)-Re(1)-N(1)	93.4(2)
C(11)-C(16)	1.444(7)	C(02)-Re(1)-N(1)	94.8(2)
C(12)-O(1)	1.302(6)	C(01)-Re(1)-N(1)	175.7(2)
C(12)-C(13)	1.426(7)	O(1)-Re(1)-N(1)	84.54(16)
C(13)-C(14)	1.371(7)	C(03)-Re(1)-N(3)	178.44(19)
C(13)-H(13)	0.9500	C(02)-Re(1)-N(3)	93.2(2)
C(14)-C(15)	1.410(8)	C(01)-Re(1)-N(3)	91.2(2)
C(14)-H(14)	0.9500	O(1)-Re(1)-N(3)	83.85(16)
C(15)-C(16)	1.361(8)	N(1)-Re(1)-N(3)	85.23(17)
C(15)-H(15)	0.9500	N(1)-C(1)-C(11)	126.4(5)
C(16)-H(16)	0.9500	N(1)-C(1)-H(1)	116.8
C(21)-C(22)	1.389(8)	C(11)-C(1)-H(1)	116.8
C(21)-C(26)	1.390(8)	O(01)-C(01)-Re(1)	177.6(5)
C(21)-N(1)	1.448(7)	O(02)-C(02)-Re(1)	178.9(5)
C(22)-C(23)	1.395(8)	O(03)-C(03)-Re(1)	177.3(5)
C(22)-H(22)	0.9500	C(12)-C(11)-C(1)	124.4(5)
C(23)-C(24)	1.376(9)	C(12)-C(11)-C(16)	119.0(5)
C(23)-H(23)	0.9500	C(1)-C(11)-C(16)	116.5(5)
C(24)-C(25)	1.381(9)	O(1)-C(12)-C(11)	124.5(5)
C(24)-H(24)	0.9500	O(1)-C(12)-C(13)	118.1(5)
C(25)-C(26)	1.392(8)	C(11)-C(12)-C(13)	117.4(5)
C(25)-H(25)	0.9500	C(14)-C(13)-C(12)	122.0(5)
C(26)-H(26)	0.9500	C(14)-C(13)-H(13)	119.0

C(31)-N(3)	1.360(7)	C(12)-C(13)-H(13)	119.0
C(31)-C(32)	1.386(8)	C(13)-C(14)-C(15)	120.5(5)
C(31)-H(31)	0.9500	C(13)-C(14)-H(14)	119.7
C(32)-C(33)	1.378(7)	C(15)-C(14)-H(14)	119.7
C(32)-H(32)	0.9500	C(16)-C(15)-C(14)	119.7(5)
C(33)-C(34)	1.376(8)	C(16)-C(15)-H(15)	120.2
C(33)-H(33)	0.9500	C(14)-C(15)-H(15)	120.2
C(34)-C(35)	1.379(8)	C(15)-C(16)-C(11)	121.3(5)
C(34)-H(34)	0.9500	C(15)-C(16)-H(16)	119.4
C(35)-N(3)	1.341(7)	C(11)-C(16)-H(16)	119.4
C(35)-H(35)	0.9500	C(22)-C(21)-C(26)	120.2(5)
		C(22)-C(21)-N(1)	119.5(5)
		C(26)-C(21)-N(1)	120.4(5)
		C(21)-C(22)-C(23)	119.6(6)
		C(21)-C(22)-H(22)	120.2
		C(23)-C(22)-H(22)	120.2
		C(24)-C(23)-C(22)	119.8(6)
		C(24)-C(23)-H(23)	120.1
		C(22)-C(23)-H(23)	120.1
		C(23)-C(24)-C(25)	120.9(5)
		C(23)-C(24)-H(24)	119.5
		C(25)-C(24)-H(24)	119.5
		C(24)-C(25)-C(26)	119.6(6)
		C(24)-C(25)-H(25)	120.2
		C(26)-C(25)-H(25)	120.2
		C(21)-C(26)-C(25)	119.8(5)
		C(21)-C(26)-H(26)	120.1
		C(25)-C(26)-H(26)	120.1
		N(3)-C(31)-C(32)	122.3(5)
		N(3)-C(31)-H(31)	118.8
		C(32)-C(31)-H(31)	118.8
		C(33)-C(32)-C(31)	119.4(6)
		C(33)-C(32)-H(32)	120.3
		C(31)-C(32)-H(32)	120.3
		C(34)-C(33)-C(32)	118.4(6)
		C(34)-C(33)-H(33)	120.8
		C(32)-C(33)-H(33)	120.8
		C(33)-C(34)-C(35)	119.8(5)

		C(33)-C(34)-H(34)	120.1
		C(35)-C(34)-H(34)	120.1
		N(3)-C(35)-C(34)	122.8(5)
		N(3)-C(35)-H(35)	118.6
		C(34)-C(35)-H(35)	118.6
		C(1)-N(1)-C(21)	114.4(5)

Table F.3: **Anisotropic displacement parameters ($Å^2$x 10^3) for *fac*-[Re(Sal-Ph)$(CO)_3(NC_5H_5)$]. The anisotropic displacement factor exponent takes the form: $-2\pi^2[h^2a^{*2}U^{11} + ... + 2 h k a^* b^* U^{12}]$**

	U11	U22	U33	U23	U13	U12
C(1)	19(3)	24(3)	15(3)	1(2)	2(2)	1(2)
C(01)	18(3)	23(3)	19(3)	-2(2)	-1(2)	0(2)
C(02)	18(3)	22(3)	19(3)	-3(2)	1(2)	-1(2)
C(03)	22(3)	26(3)	15(3)	-6(2)	-4(2)	9(2)
C(11)	22(3)	22(3)	15(3)	3(2)	-1(2)	-1(2)
C(12)	25(3)	25(3)	19(3)	-1(2)	6(2)	-5(2)
C(13)	22(3)	27(3)	17(3)	0(2)	-1(2)	-1(2)
C(14)	19(3)	27(3)	20(3)	8(2)	-1(2)	1(2)
C(15)	22(3)	19(3)	32(3)	3(2)	6(3)	4(2)
C(16)	25(3)	21(3)	20(3)	-5(2)	3(2)	-2(2)
C(21)	23(3)	15(2)	15(3)	-2(2)	-2(2)	1(2)
C(22)	21(3)	23(3)	17(3)	-4(2)	2(2)	-1(2)
C(23)	30(3)	27(3)	16(3)	0(2)	-5(2)	6(3)
C(24)	43(4)	22(3)	14(3)	1(2)	-2(3)	2(2)
C(25)	40(4)	22(3)	15(3)	-1(2)	8(3)	0(2)
C(26)	24(3)	30(3)	20(3)	-3(2)	1(2)	-1(2)
C(31)	26(3)	20(2)	18(3)	3(2)	2(2)	3(2)
C(32)	22(3)	26(3)	29(3)	7(2)	3(3)	4(2)
C(33)	20(3)	34(3)	19(3)	4(2)	3(2)	-3(2)
C(34)	26(3)	25(3)	14(3)	-5(2)	1(2)	-2(2)
C(35)	27(3)	25(3)	8(2)	-4(2)	1(2)	2(2)
N(1)	17(2)	20(2)	19(2)	1(2)	2(2)	1(2)
N(3)	21(2)	22(2)	8(2)	-2(2)	-1(2)	1(2)
O(01)	42(3)	30(2)	20(2)	-8(2)	6(2)	-3(2)

O(1)	21(2)	15(2)	19(2)	2(2)	-4(2)	4(2)
O(02)	34(2)	24(2)	25(2)	5(2)	-1(2)	1(2)
O(03)	20(2)	39(2)	41(3)	-1(2)	4(2)	-4(2)
Re(1)	18(1)	18(1)	12(1)	-1(1)	-1(1)	0(1)

Supplementary data of fac-[Re(Sal-3MeBu)(CO)$_3$(NC$_5$H$_5$)] for the atomic coordinates, bond distances and angles and anisotropic displacement parameters are given in appendix tables G.

Table G.1: Atomic coordinates (x 10^4) and equivalent isotropic displacement parameters (Å^2 x 10^3) for *fac*-[Re(Sal-3MeBu)(CO)$_3$(NC$_5$H$_5$)]. U(eq) is defined as one third of the trace of the orthogonalized U^{ij} tensor.

	x	y	z	U(eq)
Re(1)	1575(1)	1635(1)	9538(1)	42(1)
N(1)	1332(2)	2949(3)	8518(1)	42(1)
C(11)	3039(2)	2309(4)	8240(2)	47(1)
O(1)	2961(2)	740(2)	9293(1)	52(1)
C(12)	3443(2)	1195(3)	8798(2)	46(1)
N(3)	2709(2)	3511(3)	10020(1)	51(1)
O(02)	-319(2)	3127(3)	9971(2)	74(1)
O(01)	2088(2)	-144(3)	11011(1)	82(1)
O(03)	137(2)	-1004(3)	8757(1)	71(1)
C(1)	2011(2)	3036(3)	8121(2)	45(1)
C(03)	672(3)	-19(4)	9056(2)	50(1)
C(21)	315(2)	3814(3)	8234(2)	48(1)
C(15)	4616(3)	2008(5)	7773(2)	77(1)
C(31)	2491(3)	5011(4)	9887(2)	64(1)
C(02)	397(3)	2554(4)	9811(2)	51(1)
C(01)	1887(2)	515(4)	10456(2)	54(1)
C(14)	5009(3)	926(5)	8320(2)	72(1)
C(22)	-611(2)	2766(4)	7859(2)	54(1)
C(13)	4453(2)	519(4)	8821(2)	60(1)
C(35)	3686(3)	3162(5)	10459(2)	70(1)
C(16)	3641(3)	2673(4)	7736(2)	60(1)
C(34)	4439(4)	4241(7)	10756(2)	89(1)

C(23)	-1683(3)	3591(4)	7569(2)	62(1)
C(32)	3219(4)	6175(5)	10162(3)	87(1)
C(25)	-2093(4)	4289(6)	8189(2)	101(2)
C(33)	4218(4)	5761(7)	10608(3)	95(2)
C(24)	-2498(3)	2481(5)	7097(3)	104(2)

Table G.2: Bond distances (Å) and angles (°) for *fac*-[Re(Sal-3MeBu)$(CO)_3(NC_5H_5)$].

Bond	Distance (Å)	Bond Angle	Angle (°)
Re(1)-C(02)	1.901(3)	C(02)-Re(1)-C(03)	90.51(13)
Re(1)-C(03)	1.917(4)	C(02)-Re(1)-C(01)	88.07(13)
Re(1)-C(01)	1.919(3)	C(03)-Re(1)-C(01)	90.04(13)
Re(1)-O(1)	2.1075(19)	C(02)-Re(1)-O(1)	175.50(12)
Re(1)-N(1)	2.172(2)	C(03)-Re(1)-O(1)	93.90(10)
Re(1)-N(3)	2.213(3)	C(01)-Re(1)-O(1)	91.07(10)
N(1)-C(1)	1.290(4)	C(02)-Re(1)-N(1)	94.29(10)
N(1)-C(21)	1.482(4)	C(03)-Re(1)-N(1)	92.80(10)
C(11)-C(16)	1.405(4)	C(01)-Re(1)-N(1)	176.29(11)
C(11)-C(12)	1.416(4)	O(1)-Re(1)-N(1)	86.35(8)
C(11)-C(1)	1.433(4)	C(02)-Re(1)-N(3)	94.20(12)
O(1)-C(12)	1.305(3)	C(03)-Re(1)-N(3)	174.62(10)
C(12)-C(13)	1.419(4)	C(01)-Re(1)-N(3)	92.71(12)
N(3)-C(31)	1.340(4)	O(1)-Re(1)-N(3)	81.42(9)
N(3)-C(35)	1.344(4)	N(1)-Re(1)-N(3)	84.27(9)
O(02)-C(02)	1.156(3)	C(1)-N(1)-C(21)	115.8(2)
O(01)-C(01)	1.152(3)	C(1)-N(1)-Re(1)	124.9(2)
O(03)-C(03)	1.146(4)	C(21)-N(1)-Re(1)	119.32(17)
C(1)-H(1)	0.9500	C(16)-C(11)-C(12)	119.1(3)
C(21)-C(22)	1.517(4)	C(16)-C(11)-C(1)	116.8(3)
C(21)-H(21A)	0.9900	C(12)-C(11)-C(1)	124.0(3)
C(21)-H(21B)	0.9900	C(12)-O(1)-Re(1)	129.34(19)
C(15)-C(16)	1.369(5)	O(1)-C(12)-C(11)	125.2(3)
C(15)-C(14)	1.381(6)	O(1)-C(12)-C(13)	117.3(3)
C(15)-H(15)	0.9500	C(11)-C(12)-C(13)	117.4(3)
C(31)-C(32)	1.383(5)	C(31)-N(3)-C(35)	116.7(3)

C(31)-H(31)	0.9500	C(31)-N(3)-Re(1)	123.5(2)
C(14)-C(13)	1.368(5)	C(35)-N(3)-Re(1)	119.8(3)
C(14)-H(14)	0.9500	N(1)-C(1)-C(11)	128.8(3)
C(22)-C(23)	1.524(4)	N(1)-C(1)-H(1)	115.6
C(22)-H(22A)	0.9900	C(11)-C(1)-H(1)	115.6
C(22)-H(22B)	0.9900	O(03)-C(03)-Re(1)	178.9(3)
C(13)-H(13)	0.9500	N(1)-C(21)-C(22)	112.2(2)
C(35)-C(34)	1.357(6)	N(1)-C(21)-H(21A)	109.2
C(35)-H(35)	0.9500	C(22)-C(21)-H(21A)	109.2
C(16)-H(16)	0.9500	N(1)-C(21)-H(21B)	109.2
C(34)-C(33)	1.360(7)	C(22)-C(21)-H(21B)	109.2
C(34)-H(34)	0.9500	H(21A)-C(21)-H(21B)	107.9
C(23)-C(25)	1.521(5)	C(16)-C(15)-C(14)	118.4(3)
C(23)-C(24)	1.524(5)	C(16)-C(15)-H(15)	120.8
C(23)-H(23)	1.0000	C(14)-C(15)-H(15)	120.8
C(32)-C(33)	1.386(7)	N(3)-C(31)-C(32)	123.3(4)
C(32)-H(32)	0.9500	N(3)-C(31)-H(31)	118.3
C(25)-H(25A)	0.9800	C(32)-C(31)-H(31)	118.3
C(25)-H(25B)	0.9800	O(02)-C(02)-Re(1)	179.2(3)
C(25)-H(25C)	0.9800	O(01)-C(01)-Re(1)	178.9(3)
C(33)-H(33)	0.9500	C(13)-C(14)-C(15)	121.7(3)
C(24)-H(24A)	0.9800	C(13)-C(14)-H(14)	119.1
C(24)-H(24B)	0.9800	C(15)-C(14)-H(14)	119.1
C(24)-H(24C)	0.9800	C(21)-C(22)-C(23)	114.5(3)
		C(21)-C(22)-H(22A)	108.6
		C(23)-C(22)-H(22A)	108.6
		C(21)-C(22)-H(22B)	108.6
		C(23)-C(22)-H(22B)	108.6
		H(22A)-C(22)-H(22B)	107.6
		C(14)-C(13)-C(12)	121.0(4)
		C(14)-C(13)-H(13)	119.5
		C(12)-C(13)-H(13)	119.5
		N(3)-C(35)-C(34)	123.4(4)
		N(3)-C(35)-H(35)	118.3
		C(34)-C(35)-H(35)	118.3
		C(15)-C(16)-C(11)	122.3(4)
		C(15)-C(16)-H(16)	118.8
		C(11)-C(16)-H(16)	118.8

		C(35)-C(34)-C(33)	119.7(5)
		C(35)-C(34)-H(34)	120.2
		C(33)-C(34)-H(34)	120.2
		C(25)-C(23)-C(22)	112.4(3)
		C(25)-C(23)-C(24)	111.5(4)
		C(22)-C(23)-C(24)	109.5(3)
		C(25)-C(23)-H(23)	107.8
		C(22)-C(23)-H(23)	107.8
		C(24)-C(23)-H(23)	107.8
		C(31)-C(32)-C(33)	117.9(4)
		C(31)-C(32)-H(32)	121.0
		C(33)-C(32)-H(32)	121.0
		C(23)-C(25)-H(25A)	109.5
		C(23)-C(25)-H(25B)	109.5
		H(25A)-C(25)-H(25B)	109.5
		C(23)-C(25)-H(25C)	109.5
		H(25A)-C(25)-H(25C)	109.5
		H(25B)-C(25)-H(25C)	109.5
		C(34)-C(33)-C(32)	119.0(4)
		C(34)-C(33)-H(33)	120.5
		C(32)-C(33)-H(33)	120.5
		C(23)-C(24)-H(24A)	109.5
		C(23)-C(24)-H(24B)	109.5
		H(24A)-C(24)-H(24B)	109.5
		C(23)-C(24)-H(24C)	109.5
		H(24A)-C(24)-H(24C)	109.5
		H(24B)-C(24)-H(24C)	109.5

Table G.3: Anisotropic displacement parameters ($Å^2 x\ 10^3$) for *fac*-[Re(Sal-3MeBu)$(CO)_3(NC_5H_5)$]. The anisotropic displacement factor exponent takes the form: $-2\pi^2[\ h^2a^{*2}U^{11} + ... + 2\ h\ k\ a^*\ b^*\ U^{12}\ ]$

	U11	U22	U33	U23	U13	U12
Re(1)	39(1)	47(1)	44(1)	8(1)	17(1)	6(1)
N(1)	40(1)	43(1)	44(1)	7(1)	13(1)	0(1)
C(11)	39(2)	58(2)	47(2)	-9(2)	16(1)	-10(2)
O(1)	45(1)	55(1)	60(1)	10(1)	23(1)	15(1)
C(12)	38(2)	50(2)	53(2)	-14(1)	16(1)	-6(1)
N(3)	47(2)	61(2)	50(1)	-7(1)	18(1)	-1(1)
O(02)	68(2)	81(2)	88(2)	21(1)	45(2)	30(1)
O(01)	72(2)	108(2)	63(1)	40(2)	16(1)	8(2)
O(03)	83(2)	65(2)	70(2)	-2(1)	29(1)	-23(2)
C(1)	46(2)	47(2)	43(2)	1(1)	13(1)	-7(1)
C(03)	54(2)	54(2)	48(2)	14(2)	24(1)	8(2)
C(21)	52(2)	42(2)	52(2)	12(1)	17(1)	12(1)
C(15)	55(2)	116(3)	71(2)	-26(2)	39(2)	-25(2)
C(31)	63(2)	65(2)	70(2)	-16(2)	26(2)	3(2)
C(02)	57(2)	47(2)	53(2)	11(2)	20(2)	9(2)
C(01)	43(2)	63(2)	57(2)	12(2)	17(2)	7(2)
C(14)	42(2)	93(3)	87(3)	-32(2)	27(2)	-5(2)
C(22)	46(2)	48(2)	65(2)	12(2)	12(2)	7(2)
C(13)	39(2)	70(2)	72(2)	-17(2)	18(2)	3(2)
C(35)	54(2)	91(3)	59(2)	2(2)	6(2)	-5(2)
C(16)	55(2)	77(2)	53(2)	-7(2)	21(2)	-16(2)
C(34)	68(3)	127(4)	65(2)	-14(3)	7(2)	-23(3)
C(23)	49(2)	65(2)	73(2)	26(2)	16(2)	12(2)
C(32)	105(4)	65(3)	101(3)	-38(2)	44(3)	-21(3)
C(25)	82(3)	137(4)	98(3)	44(3)	47(3)	60(3)
C(33)	86(4)	122(4)	79(3)	-45(3)	26(3)	-38(3)
C(24)	53(3)	86(3)	154(4)	24(3)	-7(3)	1(2)

Supplementary data of fac-[Re(5Me-Sal-Hist)(CO)$_3$] for the atomic coordinates, bond distances and angles and anisotropic displacement parameters are given in appendix tables H.

Table H.1: **Atomic coordinates (x 10^4) and equivalent isotropic displacement parameters (Å^2 x 10^3) for *fac*-[Re(5Me-Sal-Hist)(CO)$_3$]. U(eq) is defined as one third of the trace of the orthogonalized U^{ij} tensor.**

	x	y	z	U(eq)
Re(1)	6922(1)	7080(1)	7961(1)	12(1)
N(1)	5086(3)	7258(2)	6452(2)	13(1)
N(32)	6446(3)	9477(2)	8660(2)	14(1)
N(34)	6491(3)	11734(2)	9928(2)	18(1)
O(01)	9268(3)	6804(2)	10178(2)	29(1)
O(1)	4233(2)	6396(2)	8194(1)	14(1)
O(02)	10679(2)	8059(2)	7537(1)	19(1)
O(03)	7141(3)	3638(2)	6840(1)	21(1)
C(01)	8379(4)	6930(3)	9357(2)	19(1)
C(1)	3562(3)	6304(3)	5883(2)	15(1)
C(02)	9251(3)	7705(3)	7695(2)	14(1)
C(2)	5493(3)	8628(3)	6122(2)	15(1)
C(3)	4785(4)	9998(3)	6852(2)	19(1)
C(03)	7096(3)	4942(3)	7270(2)	16(1)
C(11)	2792(3)	5067(3)	6218(2)	14(1)
C(12)	3110(3)	5190(3)	7371(2)	14(1)
C(13)	2171(3)	4021(3)	7638(2)	16(1)
C(14)	1043(3)	2710(3)	6806(2)	18(1)
C(15)	762(3)	2601(3)	5673(2)	19(1)
C(16)	1584(3)	3778(3)	5389(2)	18(1)
C(31)	5632(3)	10452(3)	8104(2)	16(1)
C(33)	6943(3)	10308(3)	9756(2)	16(1)
C(35)	5664(4)	11850(3)	8896(2)	19(1)
C(141)	155(4)	1431(3)	7127(2)	24(1)

Table H.2: Bond distances (Å) and angles (°) for *fac*-[Re(5Me-Sal-Hist)(CO)$_3$].

Bond	Distance (Å)	Bond Angle	Angle (°)
Re(1)-C(02)	1.905(2)	C(02)-Re(1)-C(03)	90.55(10)
Re(1)-C(03)	1.911(2)	C(02)-Re(1)-C(01)	87.19(10)
Re(1)-C(01)	1.924(2)	C(03)-Re(1)-C(01)	87.65(10)
Re(1)-O(1)	2.1454(16)	C(02)-Re(1)-O(1)	177.41(7)
Re(1)-N(1)	2.1599(19)	C(03)-Re(1)-O(1)	89.83(8)
Re(1)-N(32)	2.1875(19)	C(01)-Re(1)-O(1)	95.38(8)
N(1)-C(1)	1.285(3)	C(02)-Re(1)-N(1)	97.31(8)
N(1)-C(2)	1.467(3)	C(03)-Re(1)-N(1)	93.90(8)
N(32)-C(33)	1.333(3)	C(01)-Re(1)-N(1)	175.22(9)
N(32)-C(31)	1.390(3)	O(1)-Re(1)-N(1)	80.11(7)
N(34)-C(33)	1.332(3)	C(02)-Re(1)-N(32)	93.24(8)
N(34)-C(35)	1.370(3)	C(03)-Re(1)-N(32)	174.63(9)
N(34)-H(34)	0.8800	C(01)-Re(1)-N(32)	96.33(9)
O(01)-C(01)	1.153(3)	O(1)-Re(1)-N(32)	86.22(7)
O(1)-C(12)	1.334(3)	N(1)-Re(1)-N(32)	81.85(7)
O(02)-C(02)	1.157(3)	C(1)-N(1)-C(2)	117.91(19)
O(03)-C(03)	1.157(3)	C(1)-N(1)-Re(1)	123.49(15)
C(1)-C(11)	1.446(3)	C(2)-N(1)-Re(1)	118.31(14)
C(1)-H(1)	0.9500	C(33)-N(32)-C(31)	105.93(19)
C(2)-C(3)	1.526(3)	C(33)-N(32)-Re(1)	124.68(16)
C(2)-H(2A)	0.9900	C(31)-N(32)-Re(1)	129.39(15)
C(2)-H(2B)	0.9900	C(33)-N(34)-C(35)	107.7(2)
C(3)-C(31)	1.505(3)	C(33)-N(34)-H(34)	126.2
C(3)-H(3A)	0.9900	C(35)-N(34)-H(34)	126.2
C(3)-H(3B)	0.9900	C(12)-O(1)-Re(1)	116.71(14)
C(11)-C(16)	1.403(3)	O(01)-C(01)-Re(1)	178.1(2)
C(11)-C(12)	1.418(3)	N(1)-C(1)-C(11)	124.5(2)
C(12)-C(13)	1.399(3)	N(1)-C(1)-H(1)	117.8
C(13)-C(14)	1.394(3)	C(11)-C(1)-H(1)	117.8
C(13)-H(13)	0.9500	O(02)-C(02)-Re(1)	178.64(19)
C(14)-C(15)	1.398(3)	N(1)-C(2)-C(3)	108.75(18)
C(14)-C(141)	1.504(3)	N(1)-C(2)-H(2A)	109.9
C(15)-C(16)	1.376(3)	C(3)-C(2)-H(2A)	109.9
C(15)-H(15)	0.9500	N(1)-C(2)-H(2B)	109.9
C(16)-H(16)	0.9500	C(3)-C(2)-H(2B)	109.9

C(31)-C(35)	1.366(3)	H(2A)-C(2)-H(2B)	108.3
C(33)-H(33)	0.9500	C(31)-C(3)-C(2)	115.7(2)
C(35)-H(35)	0.9500	C(31)-C(3)-H(3A)	108.4
C(141)-H(14A)	0.9800	C(2)-C(3)-H(3A)	108.4
C(141)-H(14B)	0.9800	C(31)-C(3)-H(3B)	108.4
C(141)-H(14C)	0.9800	C(2)-C(3)-H(3B)	108.4
		H(3A)-C(3)-H(3B)	107.4
		O(03)-C(03)-Re(1)	177.9(2)
		C(16)-C(11)-C(12)	119.4(2)
		C(16)-C(11)-C(1)	119.1(2)
		C(12)-C(11)-C(1)	121.3(2)
		O(1)-C(12)-C(13)	119.9(2)
		O(1)-C(12)-C(11)	121.9(2)
		C(13)-C(12)-C(11)	118.2(2)
		C(14)-C(13)-C(12)	121.8(2)
		C(14)-C(13)-H(13)	119.1
		C(12)-C(13)-H(13)	119.1
		C(13)-C(14)-C(15)	119.0(2)
		C(13)-C(14)-C(141)	120.2(2)
		C(15)-C(14)-C(141)	120.7(2)
		C(16)-C(15)-C(14)	120.2(2)
		C(16)-C(15)-H(15)	119.9
		C(14)-C(15)-H(15)	119.9
		C(15)-C(16)-C(11)	121.2(2)
		C(15)-C(16)-H(16)	119.4
		C(11)-C(16)-H(16)	119.4
		C(35)-C(31)-N(32)	108.1(2)
		C(35)-C(31)-C(3)	126.6(2)
		N(32)-C(31)-C(3)	125.2(2)
		N(34)-C(33)-N(32)	111.2(2)
		N(34)-C(33)-H(33)	124.4
		N(32)-C(33)-H(33)	124.4
		C(31)-C(35)-N(34)	107.0(2)
		C(31)-C(35)-H(35)	126.5
		N(34)-C(35)-H(35)	126.5
		C(14)-C(141)-H(14A)	109.5
		C(14)-C(141)-H(14B)	109.5
		H(14A)-C(141)-H(14B)	109.5

		C(14)-C(141)-H(14C)	109.5
		H(14A)-C(141)-H(14C)	109.5
		H(14B)-C(141)-H(14C)	109.5

Table H.3: Anisotropic displacement parameters ($Å^2$x 10^3) for *fac*-[Re(5Me-Sal-Hist)$(CO)_3$]. The anisotropic displacement factor exponent takes the form: $-2\pi^2[h^2a^{*2}U^{11} + ... + 2 h k a^* b^* U^{12}]$

	U11	U22	U33	U23	U13	U12
Re(1)	12(1)	12(1)	10(1)	2(1)	3(1)	1(1)
N(1)	16(1)	12(1)	10(1)	3(1)	6(1)	3(1)
N(32)	15(1)	13(1)	12(1)	2(1)	5(1)	0(1)
N(34)	19(1)	16(1)	15(1)	-3(1)	8(1)	-1(1)
O(01)	29(1)	39(1)	19(1)	14(1)	1(1)	3(1)
O(1)	14(1)	14(1)	12(1)	0(1)	4(1)	-1(1)
O(02)	16(1)	20(1)	22(1)	6(1)	7(1)	1(1)
O(03)	24(1)	15(1)	22(1)	3(1)	7(1)	4(1)
C(01)	18(1)	20(1)	17(1)	4(1)	7(1)	0(1)
C(1)	17(1)	18(1)	9(1)	2(1)	5(1)	5(1)
C(02)	20(1)	10(1)	10(1)	3(1)	2(1)	3(1)
C(2)	15(1)	16(1)	13(1)	5(1)	4(1)	1(1)
C(3)	23(1)	15(1)	19(1)	7(1)	5(1)	3(1)
C(03)	14(1)	20(1)	14(1)	7(1)	4(1)	1(1)
C(11)	12(1)	13(1)	16(1)	2(1)	4(1)	2(1)
C(12)	10(1)	14(1)	15(1)	1(1)	4(1)	4(1)
C(13)	16(1)	16(1)	16(1)	4(1)	7(1)	3(1)
C(14)	16(1)	14(1)	25(1)	5(1)	9(1)	4(1)
C(15)	15(1)	16(1)	20(1)	-1(1)	4(1)	0(1)
C(16)	15(1)	20(1)	13(1)	0(1)	2(1)	4(1)
C(31)	13(1)	16(1)	16(1)	2(1)	6(1)	2(1)
C(33)	14(1)	17(1)	15(1)	3(1)	6(1)	0(1)
C(35)	20(1)	16(1)	21(1)	6(1)	7(1)	4(1)
C(141)	24(2)	16(1)	30(1)	5(1)	10(1)	-1(1)

Supplementary data of fac-[Re(5Me-Sal-Trypt)(CO)$_3$(NC$_5$H$_5$)] for the atomic coordinates, bond distances and angles and anisotropic displacement parameters are given in appendix tables I.

Table I.1: **Atomic coordinates (x 10^4) and equivalent isotropic displacement parameters (Å^2 x 10^3) for *fac*-[Re(5Me-Sal-Trypt)(CO)$_3$(NC$_5$H$_5$)]. U(eq) is defined as one third of the trace of the orthogonalized U^{ij} tensor.**

	x	y	z	U(eq)
Re(1)	1020(1)	6491(1)	1427(1)	13(1)
N(1)	937(1)	5243(1)	503(1)	16(1)
O(1)	1078(1)	7864(1)	624(1)	17(1)
C(01)	1108(1)	7673(2)	2206(1)	18(1)
C(2)	1021(1)	3910(2)	615(1)	20(1)
C(02)	970(1)	5197(2)	2111(1)	20(1)
C(3)	1643(1)	3570(2)	821(1)	19(1)
C(03)	213(1)	6611(2)	1447(1)	20(1)
C(31)	1719(1)	2215(2)	915(1)	18(1)
C(32)	1314(1)	1328(2)	926(1)	21(1)
C(33)	2151(1)	347(2)	1092(1)	18(1)
C(34)	2262(1)	1611(2)	1018(1)	17(1)
C(35)	2831(1)	2017(2)	1059(1)	20(1)
C(36)	3264(1)	1164(2)	1168(1)	23(1)
C(37)	3142(1)	-85(2)	1239(1)	24(1)
C(38)	2588(1)	-511(2)	1206(1)	21(1)
C(41)	2203(1)	6353(2)	751(1)	18(1)
C(42)	2788(1)	6244(2)	721(1)	23(1)
C(43)	3142(1)	6160(2)	1361(1)	29(1)
C(44)	2897(1)	6181(2)	2018(1)	31(1)
C(45)	2312(1)	6275(2)	2009(1)	23(1)
C(141)	112(1)	10290(2)	-1334(1)	31(1)
N(2)	1570(1)	192(2)	1044(1)	22(1)
N(3)	1962(1)	6370(1)	1383(1)	16(1)
O(01)	1157(1)	8394(1)	2660(1)	26(1)
O(02)	897(1)	4385(2)	2492(1)	31(1)
O(03)	-274(1)	6653(1)	1486(1)	30(1)
C(1)	764(1)	5568(2)	-152(1)	17(1)

C(11)	630(1)	6786(2)	-415(1)	17(1)
C(12)	777(1)	7869(2)	-20(1)	16(1)
C(13)	602(1)	8994(2)	-343(1)	19(1)
C(14)	298(1)	9062(2)	-1020(1)	22(1)
C(15)	169(1)	7988(2)	-1412(1)	24(1)
C(16)	339(1)	6879(2)	-1116(1)	21(1)

Table I.2: Bond distances (Å) and angles (°) for *fac*-[Re(5Me-Sal-Trypt)$(CO)_3(NC_5H_5)$].

Bond	Distance (Å)	Bond Angle	Angle (°)
C(01)-O(01)	1.149(2)	O(01)-C(01)-Re(1)	178.62(18)
C(01)-Re(1)	1.929(2)	N(1)-C(2)-C(3)	112.78(15)
C(2)-N(1)	1.483(2)	N(1)-C(2)-H(2A)	109.0
C(2)-C(3)	1.522(3)	C(3)-C(2)-H(2A)	109.0
C(2)-H(2A)	0.9900	N(1)-C(2)-H(2B)	109.0
C(2)-H(2B)	0.9900	C(3)-C(2)-H(2B)	109.0
C(02)-O(02)	1.156(2)	H(2A)-C(2)-H(2B)	107.8
C(02)-Re(1)	1.906(2)	O(02)-C(02)-Re(1)	174.31(18)
C(3)-C(31)	1.500(3)	C(31)-C(3)-C(2)	111.84(16)
C(3)-H(3A)	0.9900	C(31)-C(3)-H(3A)	109.2
C(3)-H(3B)	0.9900	C(2)-C(3)-H(3A)	109.2
C(03)-O(03)	1.154(3)	C(31)-C(3)-H(3B)	109.2
C(03)-Re(1)	1.907(2)	C(2)-C(3)-H(3B)	109.2
C(31)-C(32)	1.361(3)	H(3A)-C(3)-H(3B)	107.9
C(31)-C(34)	1.436(3)	O(03)-C(03)-Re(1)	177.03(19)
C(32)-N(2)	1.388(2)	C(32)-C(31)-C(34)	106.51(17)
C(32)-H(32)	0.9500	C(32)-C(31)-C(3)	129.06(18)
C(33)-N(2)	1.370(2)	C(34)-C(31)-C(3)	124.43(17)
C(33)-C(38)	1.393(3)	C(31)-C(32)-N(2)	110.33(17)
C(33)-C(34)	1.417(3)	C(31)-C(32)-H(32)	124.8
C(34)-C(35)	1.405(3)	N(2)-C(32)-H(32)	124.8
C(35)-C(36)	1.380(3)	N(2)-C(33)-C(38)	130.07(19)
C(35)-H(35)	0.9500	N(2)-C(33)-C(34)	107.85(17)
C(36)-C(37)	1.404(3)	C(38)-C(33)-C(34)	122.07(18)
C(36)-H(36)	0.9500	C(35)-C(34)-C(33)	119.19(18)

C(37)-C(38)	1.380(3)	C(35)-C(34)-C(31)	133.83(18)
C(37)-H(37)	0.9500	C(33)-C(34)-C(31)	106.97(17)
C(38)-H(38)	0.9500	C(36)-C(35)-C(34)	118.57(19)
C(41)-N(3)	1.343(3)	C(36)-C(35)-H(35)	120.7
C(41)-C(42)	1.386(3)	C(34)-C(35)-H(35)	120.7
C(41)-H(41)	0.9500	C(35)-C(36)-C(37)	121.20(19)
C(42)-C(43)	1.382(3)	C(35)-C(36)-H(36)	119.4
C(42)-H(42)	0.9500	C(37)-C(36)-H(36)	119.4
C(43)-C(44)	1.390(3)	C(38)-C(37)-C(36)	121.58(19)
C(43)-H(43)	0.9500	C(38)-C(37)-H(37)	119.2
C(44)-C(45)	1.376(3)	C(36)-C(37)-H(37)	119.2
C(44)-H(44)	0.9500	C(37)-C(38)-C(33)	117.38(19)
C(45)-N(3)	1.358(3)	C(37)-C(38)-H(38)	121.3
C(45)-H(45)	0.9500	C(33)-C(38)-H(38)	121.3
C(141)-C(14)	1.511(3)	N(3)-C(41)-C(42)	122.51(19)
C(141)-H(14A)	0.9800	N(3)-C(41)-H(41)	118.7
C(141)-H(14B)	0.9800	C(42)-C(41)-H(41)	118.7
C(141)-H(14C)	0.9800	C(43)-C(42)-C(41)	119.38(19)
N(2)-H(2)	0.8800	C(43)-C(42)-H(42)	120.3
N(3)-Re(1)	2.2267(16)	C(41)-C(42)-H(42)	120.3
C(1)-N(1)	1.289(2)	C(42)-C(43)-C(44)	118.6(2)
C(1)-C(11)	1.443(3)	C(42)-C(43)-H(43)	120.7
C(1)-H(1)	0.9500	C(44)-C(43)-H(43)	120.7
C(11)-C(16)	1.409(3)	C(45)-C(44)-C(43)	119.0(2)
C(11)-C(12)	1.416(3)	C(45)-C(44)-H(44)	120.5
C(12)-O(1)	1.325(2)	C(43)-C(44)-H(44)	120.5
C(12)-C(13)	1.412(3)	N(3)-C(45)-C(44)	122.76(19)
C(13)-C(14)	1.383(3)	N(3)-C(45)-H(45)	118.6
C(13)-H(13)	0.9500	C(44)-C(45)-H(45)	118.6
C(14)-C(15)	1.398(3)	C(14)-C(141)-H(14A)	109.5
C(15)-C(16)	1.375(3)	C(14)-C(141)-H(14B)	109.5
C(15)-H(15)	0.9500	H(14A)-C(141)-H(14B)	109.5
C(16)-H(16)	0.9500	C(14)-C(141)-H(14C)	109.5
N(1)-Re(1)	2.1795(16)	H(14A)-C(141)-H(14C)	109.5
O(1)-Re(1)	2.1232(13)	H(14B)-C(141)-H(14C)	109.5
		C(33)-N(2)-C(32)	108.33(16)
		C(33)-N(2)-H(2)	125.8
		C(32)-N(2)-H(2)	125.8

		C(41)-N(3)-C(45)	117.70(17)
		C(41)-N(3)-Re(1)	122.34(13)
		C(45)-N(3)-Re(1)	119.93(13)
		N(1)-C(1)-C(11)	127.58(17)
		N(1)-C(1)-H(1)	116.2
		C(11)-C(1)-H(1)	116.2
		C(16)-C(11)-C(12)	119.10(18)
		C(16)-C(11)-C(1)	116.53(18)
		C(12)-C(11)-C(1)	124.36(17)
		O(1)-C(12)-C(13)	119.43(17)
		O(1)-C(12)-C(11)	122.85(17)
		C(13)-C(12)-C(11)	117.71(17)
		C(14)-C(13)-C(12)	122.26(19)
		C(14)-C(13)-H(13)	118.9
		C(12)-C(13)-H(13)	118.9
		C(13)-C(14)-C(15)	119.40(19)
		C(13)-C(14)-C(141)	120.1(2)
		C(15)-C(14)-C(141)	120.54(19)
		C(16)-C(15)-C(14)	119.68(18)
		C(16)-C(15)-H(15)	120.2
		C(14)-C(15)-H(15)	120.2
		C(15)-C(16)-C(11)	121.77(19)
		C(15)-C(16)-H(16)	119.1
		C(11)-C(16)-H(16)	119.1
		C(1)-N(1)-C(2)	115.35(16)
		C(1)-N(1)-Re(1)	123.96(13)
		C(2)-N(1)-Re(1)	120.37(12)
		C(12)-O(1)-Re(1)	124.41(12)
		C(02)-Re(1)-C(03)	85.10(8)
		C(02)-Re(1)-C(01)	90.81(8)
		C(03)-Re(1)-C(01)	88.68(8)
		C(02)-Re(1)-O(1)	177.05(7)
		C(03)-Re(1)-O(1)	95.35(7)
		C(01)-Re(1)-O(1)	92.12(7)
		C(02)-Re(1)-N(1)	92.60(7)
		C(03)-Re(1)-N(1)	92.35(7)
		C(01)-Re(1)-N(1)	176.52(7)
		O(1)-Re(1)-N(1)	84.47(6)

		C(02)-Re(1)-N(3)	95.96(7)
		C(03)-Re(1)-N(3)	178.86(7)
		C(01)-Re(1)-N(3)	91.71(7)
		O(1)-Re(1)-N(3)	83.57(5)
		N(1)-Re(1)-N(3)	87.19(6)

Table I.3: Anisotropic displacement parameters ($Å^2$x 10^3) for *fac*-[Re(5Me-Sal-Trypt)$(CO)_3(NC_5H_5)$]. The anisotropic displacement factor exponent takes the form: $-2\pi^2[h^2a^{*2}U^{11} + ... + 2 h k a^* b^* U^{12}]$

	U11	U22	U33	U23	U13	U12
C(01)	16(1)	18(1)	21(1)	3(1)	2(1)	1(1)
C(2)	19(1)	11(1)	29(1)	-1(1)	0(1)	0(1)
C(02)	20(1)	19(1)	21(1)	-2(1)	1(1)	-1(1)
C(3)	18(1)	14(1)	26(1)	1(1)	1(1)	0(1)
C(03)	20(1)	14(1)	24(1)	-3(1)	0(1)	-1(1)
C(31)	18(1)	14(1)	21(1)	-1(1)	0(1)	0(1)
C(32)	17(1)	15(1)	32(1)	-1(1)	0(1)	1(1)
C(33)	20(1)	16(1)	19(1)	-2(1)	1(1)	2(1)
C(34)	18(1)	16(1)	17(1)	-1(1)	2(1)	1(1)
C(35)	21(1)	19(1)	21(1)	-3(1)	4(1)	-3(1)
C(36)	16(1)	29(1)	25(1)	-6(1)	2(1)	-1(1)
C(37)	22(1)	26(1)	22(1)	-4(1)	0(1)	9(1)
C(38)	26(1)	15(1)	22(1)	-2(1)	-1(1)	4(1)
C(41)	20(1)	14(1)	21(1)	0(1)	2(1)	-1(1)
C(42)	24(1)	23(1)	22(1)	1(1)	8(1)	1(1)
C(43)	18(1)	39(1)	31(1)	3(1)	6(1)	6(1)
C(44)	20(1)	48(1)	23(1)	4(1)	-2(1)	4(1)
C(45)	21(1)	29(1)	18(1)	3(1)	3(1)	2(1)
C(141)	34(1)	31(1)	28(1)	14(1)	6(1)	10(1)
N(2)	18(1)	13(1)	35(1)	0(1)	0(1)	-3(1)
N(3)	14(1)	13(1)	21(1)	-1(1)	2(1)	-1(1)
O(01)	29(1)	23(1)	25(1)	-7(1)	2(1)	1(1)
O(02)	37(1)	27(1)	28(1)	9(1)	2(1)	-8(1)
O(03)	15(1)	29(1)	45(1)	-8(1)	3(1)	-1(1)
C(1)	14(1)	16(1)	22(1)	-4(1)	2(1)	0(1)

C(11)	14(1)	18(1)	18(1)	0(1)	4(1)	2(1)
C(12)	13(1)	18(1)	17(1)	2(1)	4(1)	1(1)
C(13)	19(1)	17(1)	22(1)	3(1)	6(1)	2(1)
C(14)	18(1)	27(1)	21(1)	9(1)	8(1)	6(1)
C(15)	21(1)	36(1)	15(1)	5(1)	2(1)	5(1)
C(16)	19(1)	25(1)	18(1)	-2(1)	2(1)	1(1)
N(1)	13(1)	12(1)	23(1)	-1(1)	1(1)	1(1)
O(1)	19(1)	12(1)	20(1)	2(1)	-2(1)	-1(1)
Re(1)	12(1)	11(1)	16(1)	0(1)	1(1)	0(1)

Supplementary data of fac-[Re(5Me-Sal-Carba)(CO)$_3$(NC$_5$H$_5$)] for the atomic coordinates, bond distances and angles and anisotropic displacement parameters are given in appendix tables J.

Table J.1: Atomic coordinates (x 10^4) and equivalent isotropic displacement parameters (Å^2 x 10^3) for *fac*-[Re(5Me-Sal-Carba)(CO)$_3$(NC$_5$H$_5$)]. U(eq) is defined as one third of the trace of the orthogonalized U^{ij} tensor.

	x	y	z	U(eq)
Re(1)	8834(1)	8609(1)	7354(1)	15(1)
N(1)	10137(2)	7537(2)	8466(2)	14(1)
N(2)	14942(2)	4440(2)	6464(2)	16(1)
N(3)	7960(3)	6679(3)	8105(2)	19(1)
O(1)	7404(2)	9031(2)	8836(2)	16(1)
O(01)	7051(2)	10164(2)	5725(2)	24(1)
O(02)	10997(2)	7729(2)	5351(2)	28(1)
O(03)	9961(2)	11247(2)	6658(2)	33(1)
C(1)	10022(3)	7746(3)	9389(2)	15(1)
C(01)	7687(3)	9573(3)	6362(2)	19(1)
C(02)	10168(3)	8081(3)	6099(3)	21(1)
C(03)	9546(3)	10262(3)	6879(3)	21(1)
C(11)	8893(3)	8585(3)	9968(2)	14(1)
C(12)	7663(3)	9192(3)	9663(2)	14(1)
C(13)	6635(3)	9985(3)	10319(2)	16(1)
C(14)	6784(3)	10165(3)	11238(2)	18(1)

C(15)	8000(3)	9545(3)	11536(2)	19(1)
C(16)	9027(3)	8781(3)	10915(2)	17(1)
C(21)	11383(3)	6672(3)	8016(2)	14(1)
C(22)	11386(3)	5274(3)	8260(2)	16(1)
C(23)	12537(3)	4435(3)	7789(2)	16(1)
C(24)	13691(3)	5027(3)	7071(2)	14(1)
C(25)	13703(3)	6436(3)	6815(2)	13(1)
C(26)	12528(3)	7268(3)	7292(2)	14(1)
C(31)	15769(3)	5435(3)	5849(2)	16(1)
C(32)	15042(3)	6697(3)	6033(2)	15(1)
C(33)	15671(3)	7868(3)	5480(2)	18(1)
C(34)	17008(3)	7755(3)	4766(2)	21(1)
C(35)	17714(3)	6491(3)	4598(3)	23(1)
C(36)	17126(3)	5318(3)	5126(2)	19(1)
C(41)	15356(3)	2969(3)	6598(3)	19(1)
C(42)	15870(3)	2167(3)	7635(3)	25(1)
C(51)	8029(4)	5966(4)	7447(3)	33(1)
C(52)	7558(5)	4724(4)	7899(3)	48(1)
C(53)	6983(4)	4188(4)	9069(3)	40(1)
C(54)	6894(3)	4907(3)	9755(3)	29(1)
C(55)	7397(3)	6137(3)	9249(3)	22(1)
C(141)	5641(3)	11003(3)	11912(3)	26(1)

Table J.2: Bond distances (Å) and angles (°) for *fac*-[Re(5Me-Sal-Carba)$(CO)_3(NC_5H_5)$].

Bond	Distance (Å)	Bond Angle	Angle (°)
Re(1)-C(02)	1.900(3)	C(02)-Re(1)-C(03)	91.55(13)
Re(1)-C(03)	1.913(3)	C(02)-Re(1)-C(01)	87.09(13)
Re(1)-C(01)	1.925(3)	C(03)-Re(1)-C(01)	89.51(12)
Re(1)-O(1)	2.107(2)	C(02)-Re(1)-O(1)	175.25(10)
Re(1)-N(1)	2.171(2)	C(03)-Re(1)-O(1)	91.41(11)
Re(1)-N(3)	2.222(3)	C(01)-Re(1)-O(1)	96.66(10)
N(1)-C(1)	1.289(4)	C(02)-Re(1)-N(1)	92.79(11)
N(1)-C(21)	1.448(3)	C(03)-Re(1)-N(1)	90.02(11)
N(2)-C(31)	1.380(4)	C(01)-Re(1)-N(1)	179.51(10)

N(2)-C(24)	1.388(3)	O(1)-Re(1)-N(1)	83.49(8)
N(2)-C(41)	1.460(3)	C(02)-Re(1)-N(3)	93.60(12)
N(3)-C(51)	1.344(4)	C(03)-Re(1)-N(3)	173.64(11)
N(3)-C(55)	1.350(4)	C(01)-Re(1)-N(3)	94.46(11)
O(1)-C(12)	1.315(3)	O(1)-Re(1)-N(3)	83.21(9)
O(01)-C(01)	1.156(4)	N(1)-Re(1)-N(3)	86.02(9)
O(02)-C(02)	1.162(4)	C(1)-N(1)-C(21)	116.8(2)
O(03)-C(03)	1.152(4)	C(1)-N(1)-Re(1)	126.71(19)
C(1)-C(11)	1.436(4)	C(21)-N(1)-Re(1)	115.61(17)
C(1)-H(1)	0.9500	C(31)-N(2)-C(24)	108.5(2)
C(11)-C(12)	1.417(4)	C(31)-N(2)-C(41)	126.4(2)
C(11)-C(16)	1.421(4)	C(24)-N(2)-C(41)	124.6(2)
C(12)-C(13)	1.414(4)	C(51)-N(3)-C(55)	117.1(3)
C(13)-C(14)	1.383(4)	C(51)-N(3)-Re(1)	121.5(2)
C(13)-H(13)	0.9500	C(55)-N(3)-Re(1)	121.3(2)
C(14)-C(15)	1.401(4)	C(12)-O(1)-Re(1)	127.39(17)
C(14)-C(141)	1.504(4)	N(1)-C(1)-C(11)	126.2(3)
C(15)-C(16)	1.370(4)	N(1)-C(1)-H(1)	116.9
C(15)-H(15)	0.9500	C(11)-C(1)-H(1)	116.9
C(16)-H(16)	0.9500	O(01)-C(01)-Re(1)	177.0(3)
C(21)-C(26)	1.384(4)	O(02)-C(02)-Re(1)	178.3(3)
C(21)-C(22)	1.399(4)	O(03)-C(03)-Re(1)	176.1(3)
C(22)-C(23)	1.386(4)	C(12)-C(11)-C(16)	119.1(2)
C(22)-H(22)	0.9500	C(12)-C(11)-C(1)	123.8(2)
C(23)-C(24)	1.388(4)	C(16)-C(11)-C(1)	117.1(2)
C(23)-H(23)	0.9500	O(1)-C(12)-C(13)	118.3(2)
C(24)-C(25)	1.411(4)	O(1)-C(12)-C(11)	124.3(2)
C(25)-C(26)	1.399(4)	C(13)-C(12)-C(11)	117.4(2)
C(25)-C(32)	1.445(4)	C(14)-C(13)-C(12)	122.7(3)
C(26)-H(26)	0.9500	C(14)-C(13)-H(13)	118.7
C(31)-C(36)	1.406(4)	C(12)-C(13)-H(13)	118.7
C(31)-C(32)	1.409(4)	C(13)-C(14)-C(15)	119.1(3)
C(32)-C(33)	1.400(4)	C(13)-C(14)-C(141)	120.0(3)
C(33)-C(34)	1.386(4)	C(15)-C(14)-C(141)	120.8(3)
C(33)-H(33)	0.9500	C(16)-C(15)-C(14)	120.0(3)
C(34)-C(35)	1.400(4)	C(16)-C(15)-H(15)	120.0
C(34)-H(34)	0.9500	C(14)-C(15)-H(15)	120.0
C(35)-C(36)	1.378(4)	C(15)-C(16)-C(11)	121.6(3)

C(35)-H(35)	0.9500	C(15)-C(16)-H(16)	119.2
C(36)-H(36)	0.9500	C(11)-C(16)-H(16)	119.2
C(41)-C(42)	1.515(4)	C(26)-C(21)-C(22)	121.1(2)
C(41)-H(41A)	0.9900	C(26)-C(21)-N(1)	119.0(2)
C(41)-H(41B)	0.9900	C(22)-C(21)-N(1)	119.7(2)
C(42)-H(42A)	0.9800	C(23)-C(22)-C(21)	121.2(3)
C(42)-H(42B)	0.9800	C(23)-C(22)-H(22)	119.4
C(42)-H(42C)	0.9800	C(21)-C(22)-H(22)	119.4
C(51)-C(52)	1.383(5)	C(22)-C(23)-C(24)	117.8(2)
C(51)-H(51)	0.9500	C(22)-C(23)-H(23)	121.1
C(52)-C(53)	1.378(6)	C(24)-C(23)-H(23)	121.1
C(52)-H(52)	0.9500	N(2)-C(24)-C(23)	129.3(2)
C(53)-C(54)	1.374(5)	N(2)-C(24)-C(25)	109.0(2)
C(53)-H(53)	0.9500	C(23)-C(24)-C(25)	121.7(2)
C(54)-C(55)	1.384(4)	C(26)-C(25)-C(24)	119.7(2)
C(54)-H(54)	0.9500	C(26)-C(25)-C(32)	133.7(3)
C(55)-H(55)	0.9500	C(24)-C(25)-C(32)	106.6(2)
C(141)-H(14A)	0.9800	C(21)-C(26)-C(25)	118.5(2)
C(141)-H(14B)	0.9800	C(21)-C(26)-H(26)	120.7
C(141)-H(14C)	0.9800	C(25)-C(26)-H(26)	120.7
		N(2)-C(31)-C(36)	129.1(3)
		N(2)-C(31)-C(32)	109.4(2)
		C(36)-C(31)-C(32)	121.5(3)
		C(33)-C(32)-C(31)	119.7(3)
		C(33)-C(32)-C(25)	133.9(3)
		C(31)-C(32)-C(25)	106.4(2)
		C(34)-C(33)-C(32)	118.9(3)
		C(34)-C(33)-H(33)	120.6
		C(32)-C(33)-H(33)	120.6
		C(33)-C(34)-C(35)	120.5(3)
		C(33)-C(34)-H(34)	119.7
		C(35)-C(34)-H(34)	119.7
		C(36)-C(35)-C(34)	122.2(3)
		C(36)-C(35)-H(35)	118.9
		C(34)-C(35)-H(35)	118.9
		C(35)-C(36)-C(31)	117.2(3)
		C(35)-C(36)-H(36)	121.4
		C(31)-C(36)-H(36)	121.4

		N(2)-C(41)-C(42)	111.5(2)
		N(2)-C(41)-H(41A)	109.3
		C(42)-C(41)-H(41A)	109.3
		N(2)-C(41)-H(41B)	109.3
		C(42)-C(41)-H(41B)	109.3
		H(41A)-C(41)-H(41B)	108.0
		C(41)-C(42)-H(42A)	109.5
		C(41)-C(42)-H(42B)	109.5
		H(42A)-C(42)-H(42B)	109.5
		C(41)-C(42)-H(42C)	109.5
		H(42A)-C(42)-H(42C)	109.5
		H(42B)-C(42)-H(42C)	109.5
		N(3)-C(51)-C(52)	122.7(3)
		N(3)-C(51)-H(51)	118.7
		C(52)-C(51)-H(51)	118.7
		C(53)-C(52)-C(51)	119.4(4)
		C(53)-C(52)-H(52)	120.3
		C(51)-C(52)-H(52)	120.3
		C(54)-C(53)-C(52)	118.8(3)
		C(54)-C(53)-H(53)	120.6
		C(52)-C(53)-H(53)	120.6
		C(53)-C(54)-C(55)	118.9(3)
		C(53)-C(54)-H(54)	120.6
		C(55)-C(54)-H(54)	120.6
		N(3)-C(55)-C(54)	123.1(3)
		N(3)-C(55)-H(55)	118.4
		C(54)-C(55)-H(55)	118.4
		C(14)-C(141)-H(14A)	109.5
		C(14)-C(141)-H(14B)	109.5
		H(14A)-C(141)-H(14B)	109.5
		C(14)-C(141)-H(14C)	109.5
		H(14A)-C(141)-H(14C)	109.5
		H(14B)-C(141)-H(14C)	109.5

Table J.3: Anisotropic displacement parameters ($Å^2 x\ 10^3$) for *fac*-[Re(5Me-Sal-Carba)$(CO)_3(NC_5H_5)$]. The anisotropic displacement factor exponent takes the form: $-2\pi^2[\ h^2a^{*2}U^{11} + ... + 2\ h\ k\ a^*\ b^*\ U^{12}\ ]$

	U11	U22	U33	U23	U13	U12
Re(1)	15(1)	14(1)	14(1)	-4(1)	-4(1)	-2(1)
N(1)	12(1)	11(1)	15(1)	-3(1)	-2(1)	-2(1)
N(2)	17(1)	12(1)	18(1)	-7(1)	-3(1)	-2(1)
N(3)	21(1)	17(1)	20(1)	-3(1)	-9(1)	-3(1)
O(1)	15(1)	19(1)	18(1)	-9(1)	-6(1)	-2(1)
O(01)	28(1)	23(1)	24(1)	-5(1)	-14(1)	-2(1)
O(02)	26(1)	33(1)	21(1)	-11(1)	-2(1)	-1(1)
O(03)	37(1)	27(1)	39(1)	-1(1)	-18(1)	-16(1)
C(1)	14(1)	14(1)	14(1)	-1(1)	-4(1)	-4(1)
C(01)	20(1)	17(1)	19(1)	-9(1)	-2(1)	-5(1)
C(02)	20(1)	22(2)	18(1)	-3(1)	-7(1)	-4(1)
C(03)	17(1)	23(2)	22(2)	-4(1)	-9(1)	-2(1)
C(11)	15(1)	15(1)	12(1)	-2(1)	-3(1)	-4(1)
C(12)	16(1)	14(1)	12(1)	-3(1)	-1(1)	-7(1)
C(13)	13(1)	19(1)	18(1)	-7(1)	-4(1)	-3(1)
C(14)	15(1)	21(1)	16(1)	-8(1)	0(1)	-7(1)
C(15)	20(1)	25(2)	15(1)	-7(1)	-5(1)	-7(1)
C(16)	15(1)	23(1)	16(1)	-5(1)	-7(1)	-3(1)
C(21)	14(1)	14(1)	12(1)	-3(1)	-5(1)	-1(1)
C(22)	17(1)	15(1)	15(1)	-2(1)	-2(1)	-6(1)
C(23)	21(1)	10(1)	16(1)	-3(1)	-6(1)	-5(1)
C(24)	16(1)	12(1)	14(1)	-5(1)	-4(1)	-1(1)
C(25)	15(1)	12(1)	12(1)	-3(1)	-4(1)	-3(1)
C(26)	16(1)	11(1)	16(1)	-3(1)	-6(1)	-2(1)
C(31)	18(1)	16(1)	14(1)	-6(1)	-5(1)	-3(1)
C(32)	16(1)	17(1)	12(1)	-5(1)	-5(1)	-2(1)
C(33)	21(1)	16(1)	16(1)	-5(1)	-4(1)	-5(1)
C(34)	22(1)	24(2)	16(1)	-6(1)	-1(1)	-10(1)
C(35)	16(1)	32(2)	19(1)	-13(1)	2(1)	-7(1)
C(36)	18(1)	22(1)	17(1)	-11(1)	-3(1)	-1(1)
C(41)	23(1)	12(1)	24(2)	-10(1)	-7(1)	1(1)
C(42)	31(2)	17(1)	30(2)	-7(1)	-15(1)	-1(1)
C(51)	52(2)	31(2)	24(2)	-1(1)	-19(2)	-20(2)

C(52)	87(3)	37(2)	36(2)	-2(2)	-32(2)	-34(2)
C(53)	56(2)	31(2)	41(2)	6(2)	-27(2)	-27(2)
C(54)	24(2)	30(2)	25(2)	4(1)	-11(1)	-9(1)
C(55)	23(2)	19(1)	20(1)	-4(1)	-6(1)	-3(1)
C(141)	20(2)	36(2)	28(2)	-21(2)	-4(1)	-3(1)

Supplementary data of fac-[Re(5Me-Sal-mTol)(CO)$_3$(HOCH$_3$)] for the atomic coordinates, bond distances and angles and anisotropic displacement parameters are given in appendix tables K.

Table K.1: Atomic coordinates (x 10^4) and equivalent isotropic displacement parameters (Å^2 x 10^3) for *fac*-[Re(5Me-Sal-*m*Tol)(CO)$_3$(HOCH$_3$)]. U(eq) is defined as one third of the trace of the orthogonalized U^{ij} tensor.

	x	y	z	U(eq)
Re(1)	6375(1)	4437(1)	1963(1)	48(1)
N(1)	6657(3)	3094(4)	2560(5)	51(1)
O(1)	5454(2)	3713(3)	1521(4)	48(1)
O(01)	5957(4)	6335(4)	1128(5)	88(2)
O(02)	7670(4)	5432(5)	2756(6)	102(3)
O(03)	7266(4)	4083(6)	218(6)	105(2)
O(04)	5731(3)	4594(3)	3230(4)	54(1)
C(01)	6101(5)	5618(5)	1429(6)	58(2)
C(1)	6366(3)	2296(5)	2423(6)	53(2)
C(02)	7173(4)	5068(6)	2457(8)	75(2)
C(03)	6916(5)	4210(6)	861(7)	71(2)
C(04)	5752(6)	5351(8)	3869(8)	104(4)
C(11)	5779(4)	2094(5)	1811(5)	45(2)
C(12)	5362(3)	2802(5)	1368(5)	42(2)
C(13)	4820(3)	2505(5)	789(5)	50(2)
C(14)	4659(4)	1582(5)	639(5)	55(2)
C(15)	5069(4)	900(5)	1085(6)	59(2)
C(16)	5606(4)	1160(5)	1644(6)	55(2)
C(21)	7265(4)	3114(5)	3214(7)	62(2)
C(22)	7931(4)	3009(7)	2849(8)	82(2)

C(23)	8526(4)	3083(7)	3461(10)	82(2)
C(24)	8420(6)	3267(8)	4385(8)	91(3)
C(25)	7782(5)	3373(7)	4720(8)	90(2)
C(26)	7178(5)	3299(7)	4146(8)	90(2)
C(141)	4060(5)	1305(8)	-1(8)	100(3)
C(231)	9241(6)	3053(9)	3047(8)	100(3)

Table K.2: Bond distances (Å) and angles (°) for *fac*-[Re(5Me-Sal-*m*Tol)(CO)$_3$(HOCH$_3$)].

Bond	Distance (Å)	Bond Angle	Angle (°)
Re(1)-C(02)	1.895(9)	C(02)-Re(1)-C(03)	87.4(4)
Re(1)-C(03)	1.901(11)	C(02)-Re(1)-C(01)	87.1(4)
Re(1)-C(01)	1.914(7)	C(03)-Re(1)-C(01)	88.2(4)
Re(1)-O(1)	2.123(4)	C(02)-Re(1)-O(1)	175.5(3)
Re(1)-N(1)	2.157(5)	C(03)-Re(1)-O(1)	96.7(3)
Re(1)-O(04)	2.189(5)	C(01)-Re(1)-O(1)	94.8(3)
N(1)-C(1)	1.278(9)	C(02)-Re(1)-N(1)	94.3(3)
N(1)-C(21)	1.481(10)	C(03)-Re(1)-N(1)	92.3(3)
O(1)-C(12)	1.325(7)	C(01)-Re(1)-N(1)	178.6(3)
O(01)-C(01)	1.139(8)	O(1)-Re(1)-N(1)	83.77(19)
O(02)-C(02)	1.157(10)	C(02)-Re(1)-O(04)	95.3(4)
O(03)-C(03)	1.145(11)	C(03)-Re(1)-O(04)	175.9(3)
O(04)-C(04)	1.410(10)	C(01)-Re(1)-O(04)	94.9(3)
O(04)-H(04)	0.8400	O(1)-Re(1)-O(04)	80.43(19)
C(1)-C(11)	1.443(10)	N(1)-Re(1)-O(04)	84.5(2)
C(1)-H(1)	0.9500	C(1)-N(1)-C(21)	116.6(6)
C(04)-H(04A)	0.9800	C(1)-N(1)-Re(1)	128.3(5)
C(04)-H(04B)	0.9800	C(21)-N(1)-Re(1)	115.0(4)
C(04)-H(04C)	0.9800	C(12)-O(1)-Re(1)	129.1(4)
C(11)-C(16)	1.389(10)	C(04)-O(04)-Re(1)	126.4(5)
C(11)-C(12)	1.427(9)	C(04)-O(04)-H(04)	109.5
C(12)-C(13)	1.384(9)	Re(1)-O(04)-H(04)	124.2
C(13)-C(14)	1.364(9)	O(01)-C(01)-Re(1)	177.7(8)
C(13)-H(13)	0.9500	N(1)-C(1)-C(11)	127.0(7)
C(14)-C(15)	1.396(11)	N(1)-C(1)-H(1)	116.5

C(14)-C(141)	1.509(12)	C(11)-C(1)-H(1)	116.5
C(15)-C(16)	1.345(10)	O(02)-C(02)-Re(1)	178.2(9)
C(15)-H(15)	0.9500	O(03)-C(03)-Re(1)	177.1(9)
C(16)-H(16)	0.9500	O(04)-C(04)-H(04A)	109.5
C(21)-C(26)	1.363(13)	O(04)-C(04)-H(04B)	109.5
C(21)-C(22)	1.374(13)	H(04A)-C(04)-H(04B)	109.5
C(22)-C(23)	1.430(13)	O(04)-C(04)-H(04C)	109.5
C(22)-H(22)	0.9500	H(04A)-C(04)-H(04C)	109.5
C(23)-C(24)	1.355(15)	H(04B)-C(04)-H(04C)	109.5
C(23)-C(231)	1.481(14)	C(16)-C(11)-C(12)	117.9(6)
C(24)-C(25)	1.311(14)	C(16)-C(11)-C(1)	118.4(6)
C(24)-H(24)	0.9500	C(12)-C(11)-C(1)	123.7(6)
C(25)-C(26)	1.411(12)	O(1)-C(12)-C(13)	119.6(6)
C(25)-H(25)	0.9500	O(1)-C(12)-C(11)	122.9(6)
C(26)-H(26)	0.9500	C(13)-C(12)-C(11)	117.4(6)
C(141)-H(14A)	0.9800	C(14)-C(13)-C(12)	123.6(7)
C(141)-H(14B)	0.9800	C(14)-C(13)-H(13)	118.2
C(141)-H(14C)	0.9800	C(12)-C(13)-H(13)	118.2
C(231)-H(23A)	0.9800	C(13)-C(14)-C(15)	118.3(7)
C(231)-H(23B)	0.9800	C(13)-C(14)-C(141)	120.9(8)
C(231)-H(23C)	0.9800	C(15)-C(14)-C(141)	120.8(8)
		C(16)-C(15)-C(14)	120.0(7)
		C(16)-C(15)-H(15)	120.0
		C(14)-C(15)-H(15)	120.0
		C(15)-C(16)-C(11)	122.9(7)
		C(15)-C(16)-H(16)	118.6
		C(11)-C(16)-H(16)	118.6
		C(26)-C(21)-C(22)	120.0(9)
		C(26)-C(21)-N(1)	121.4(8)
		C(22)-C(21)-N(1)	118.4(9)
		C(21)-C(22)-C(23)	119.2(11)
		C(21)-C(22)-H(22)	120.4
		C(23)-C(22)-H(22)	120.4
		C(24)-C(23)-C(22)	119.3(10)
		C(24)-C(23)-C(231)	121.8(9)
		C(22)-C(23)-C(231)	118.6(12)
		C(25)-C(24)-C(23)	120.7(10)
		C(25)-C(24)-H(24)	119.6

		C(23)-C(24)-H(24)	119.6
		C(24)-C(25)-C(26)	122.1(11)
		C(24)-C(25)-H(25)	118.9
		C(26)-C(25)-H(25)	118.9
		C(21)-C(26)-C(25)	118.6(10)
		C(21)-C(26)-H(26)	120.7
		C(25)-C(26)-H(26)	120.7
		C(14)-C(141)-H(14A)	109.5
		C(14)-C(141)-H(14B)	109.5
		H(14A)-C(141)-H(14B)	109.5
		C(14)-C(141)-H(14C)	109.5
		H(14A)-C(141)-H(14C)	109.5
		H(14B)-C(141)-H(14C)	109.5
		C(23)-C(231)-H(23A)	109.5
		C(23)-C(231)-H(23B)	109.5
		H(23A)-C(231)-H(23B)	109.5
		C(23)-C(231)-H(23C)	109.5
		H(23A)-C(231)-H(23C)	109.5
		H(23B)-C(231)-H(23C)	109.5

Table K.3: Anisotropic displacement parameters ($Å^2$x 10^3) for *fac*-[Re(5Me-Sal-*m*Tol)$(CO)_3(HOCH_3)$]. The anisotropic displacement factor exponent takes the form: $-2\pi^2[h^2a^{*2}U^{11} + ... + 2 h k a^* b^* U^{12}]$

	U11	U22	U33	U23	U13	U12
Re(1)	33(1)	39(1)	73(1)	12(1)	-8(1)	-4(1)
N(1)	28(3)	40(3)	85(4)	12(3)	-10(3)	-1(2)
O(1)	34(2)	34(2)	76(3)	-1(2)	-13(2)	4(2)
O(01)	111(5)	50(3)	102(5)	26(3)	-20(4)	6(3)
O(02)	62(4)	92(5)	153(7)	27(4)	-29(5)	-40(4)
O(03)	85(5)	115(6)	116(6)	12(5)	32(5)	14(5)
O(04)	45(3)	49(3)	69(3)	-1(2)	1(2)	-14(2)
C(01)	57(5)	47(4)	69(5)	15(4)	-11(4)	-3(3)
C(1)	34(4)	43(4)	82(5)	12(4)	-7(3)	5(3)
C(02)	53(5)	55(5)	117(7)	21(5)	-14(5)	-16(4)
C(03)	50(5)	64(5)	99(7)	16(5)	-4(5)	4(4)

C(04)	97(8)	123(9)	91(7)	-35(6)	4(6)	-52(7)
C(11)	32(3)	40(4)	64(4)	1(3)	-1(3)	6(3)
C(12)	30(3)	44(4)	53(4)	-2(3)	3(3)	4(3)
C(13)	35(4)	48(4)	66(4)	-9(3)	-4(3)	5(3)
C(14)	37(4)	55(4)	74(5)	-21(4)	-1(3)	0(3)
C(15)	59(5)	37(4)	81(6)	-13(4)	3(4)	-3(4)
C(16)	42(4)	43(4)	78(5)	-1(4)	3(4)	6(3)
C(21)	33(4)	40(4)	115(7)	20(4)	-21(4)	-4(3)
C(22)	35(3)	77(5)	134(6)	19(4)	-16(4)	1(3)
C(23)	35(3)	77(5)	134(6)	19(4)	-16(4)	1(3)
C(24)	70(6)	99(8)	104(8)	22(6)	-27(6)	-6(6)
C(25)	65(4)	101(5)	104(5)	18(4)	-32(4)	-4(4)
C(26)	65(4)	101(5)	104(5)	18(4)	-32(4)	-4(4)
C(141)	60(4)	109(6)	133(7)	-30(5)	-13(4)	2(4)
C(231)	60(4)	109(6)	133(7)	-30(5)	-13(4)	2(4)

Supplementary data of fac-[Re(5Me-Sal-3Me2Bu)(CO)$_3$(HOCH$_3$)] for the atomic coordinates, bond distances and angles and anisotropic displacement parameters are given in appendix tables L.

Table L.1: Atomic coordinates (x 10^4) and equivalent isotropic displacement parameters (Å^2 x 10^3) for *fac*-[Re(5Me-Sal-3Me2Bu)(CO)$_3$(HOCH$_3$)]. U(eq) is defined as one third of the trace of the orthogonalized U^{ij} tensor.

	x	y	z	U(eq)
O(1)	4474(2)	1138(2)	1421(2)	21(1)
N(1)	3177(2)	1671(3)	2208(2)	25(1)
C(1)	3477(2)	2424(3)	2106(3)	30(1)
C(11)	4074(2)	2630(3)	1610(3)	24(1)
C(12)	4537(2)	1999(2)	1278(3)	20(1)
C(13)	5093(2)	2301(3)	795(3)	23(1)
C(14)	5204(2)	3188(3)	640(3)	30(1)
C(15)	4758(3)	3808(3)	992(4)	38(1)
C(16)	4212(3)	3535(3)	1465(4)	35(1)
O(01)	4031(2)	-1341(2)	930(3)	44(1)

O(02)	2213(2)	-675(2)	2065(2)	33(1)
O(03)	2516(2)	670(3)	-421(2)	46(1)
O(04)	4234(2)	344(2)	3126(3)	26(1)
C(01)	3862(3)	-663(3)	1203(3)	29(1)
C(02)	2708(2)	-249(3)	1928(3)	25(1)
C(03)	2898(3)	591(3)	357(4)	31(1)
C(04)	4234(3)	-396(3)	3756(4)	46(1)
C(141)	5789(3)	3492(3)	98(4)	40(1)
C(21)	2517(3)	1689(5)	2706(4)	48(1)
C(22)	1776(3)	1636(5)	1937(4)	48(1)
Re(1)	3517(1)	430(1)	1641(1)	20(1)
C(24A)	1696(6)	2348(9)	1075(12)	45(3)
C(25A)	1094(5)	1793(16)	2398(7)	59(5)
C(24B)	1600(11)	2427(11)	1515(19)	36(4)
C(25B)	1100(8)	1217(16)	2391(12)	39(4)
C(23A)	2586(5)	2102(6)	3625(6)	40(2)
C(23B)	2645(5)	1281(7)	3602(6)	23(3)

Table L.2: Bond distances (Å) and angles (°) for *fac*-[Re(5Me-Sal-3Me2Bu)(CO)$_3$(HOCH$_3$)].

Bond	Distance (Å)	Bond Angle	Angle (°)
O(1)-C(12)	1.328(4)	C(12)-O(1)-Re(1)	128.3(2)
O(1)-Re(1)	2.117(3)	C(1)-N(1)-C(21)	115.6(4)
N(1)-C(1)	1.285(6)	C(1)-N(1)-Re(1)	124.5(3)
N(1)-C(21)	1.509(6)	C(21)-N(1)-Re(1)	119.8(3)
N(1)-Re(1)	2.179(4)	N(1)-C(1)-C(11)	128.8(4)
C(1)-C(11)	1.438(6)	N(1)-C(1)-H(1)	115.6
C(1)-H(1)	0.9500	C(11)-C(1)-H(1)	115.6
C(11)-C(12)	1.415(5)	C(12)-C(11)-C(16)	118.1(4)
C(11)-C(16)	1.415(6)	C(12)-C(11)-C(1)	124.9(4)
C(12)-C(13)	1.404(5)	C(16)-C(11)-C(1)	117.0(4)
C(13)-C(14)	1.383(6)	O(1)-C(12)-C(13)	119.0(3)
C(13)-H(13)	0.9500	O(1)-C(12)-C(11)	122.6(3)
C(14)-C(15)	1.397(7)	C(13)-C(12)-C(11)	118.4(4)
C(14)-C(141)	1.503(6)	C(14)-C(13)-C(12)	122.3(4)
C(15)-C(16)	1.368(7)	C(14)-C(13)-H(13)	118.9

C(15)-H(15)	0.9500	C(12)-C(13)-H(13)	118.9
C(16)-H(16)	0.9500	C(13)-C(14)-C(15)	119.0(4)
O(01)-C(01)	1.160(5)	C(13)-C(14)-C(141)	121.3(4)
O(02)-C(02)	1.154(5)	C(15)-C(14)-C(141)	119.7(4)
O(03)-C(03)	1.151(6)	C(16)-C(15)-C(14)	120.0(4)
O(04)-C(04)	1.421(5)	C(16)-C(15)-H(15)	120.0
O(04)-Re(1)	2.180(3)	C(14)-C(15)-H(15)	120.0
O(04)-H(04)	0.8400	C(15)-C(16)-C(11)	122.1(4)
C(01)-Re(1)	1.916(5)	C(15)-C(16)-H(16)	118.9
C(02)-Re(1)	1.903(4)	C(11)-C(16)-H(16)	118.9
C(03)-Re(1)	1.896(5)	C(04)-O(04)-Re(1)	123.1(3)
C(04)-H(04A)	0.9800	C(04)-O(04)-H(04)	109.5
C(04)-H(04B)	0.9800	Re(1)-O(04)-H(04)	127.4
C(04)-H(04C)	0.9800	O(01)-C(01)-Re(1)	176.3(4)
C(141)-H(14A)	0.9800	O(02)-C(02)-Re(1)	177.4(4)
C(141)-H(14B)	0.9800	O(03)-C(03)-Re(1)	178.4(5)
C(141)-H(14C)	0.9800	O(04)-C(04)-H(04A)	109.5
C(21)-C(23B)	1.361(10)	O(04)-C(04)-H(04B)	109.5
C(21)-C(23A)	1.400(9)	H(04A)-C(04)-H(04B)	109.5
C(21)-C(22)	1.518(7)	O(04)-C(04)-H(04C)	109.5
C(21)-H(21)	1.0000	H(04A)-C(04)-H(04C)	109.5
C(22)-C(24B)	1.341(19)	H(04B)-C(04)-H(04C)	109.5
C(22)-C(25A)	1.531(11)	C(14)-C(141)-H(14A)	109.5
C(22)-C(24A)	1.592(13)	C(14)-C(141)-H(14B)	109.5
C(22)-C(25B)	1.626(15)	H(14A)-C(141)-H(14B)	109.5
C(22)-H(22)	1.0000	C(14)-C(141)-H(14C)	109.5
C(24A)-H(24A)	0.9800	H(14A)-C(141)-H(14C)	109.5
C(24A)-H(24B)	0.9800	H(14B)-C(141)-H(14C)	109.5
C(24A)-H(24C)	0.9800	C(23B)-C(21)-C(23A)	53.8(6)
C(25A)-H(25A)	0.9800	C(23B)-C(21)-N(1)	114.7(6)
C(25A)-H(25B)	0.9800	C(23A)-C(21)-N(1)	120.4(5)
C(25A)-H(25C)	0.9800	C(23B)-C(21)-C(22)	124.1(6)
C(24B)-H(24D)	0.9800	C(23A)-C(21)-C(22)	123.4(5)
C(24B)-H(24E)	0.9800	N(1)-C(21)-C(22)	110.1(4)
C(24B)-H(24F)	0.9800	C(23B)-C(21)-H(21)	44.8
C(25B)-H(25D)	0.9800	C(23A)-C(21)-H(21)	98.3
C(25B)-H(25E)	0.9800	N(1)-C(21)-H(21)	98.3
C(25B)-H(25F)	0.9800	C(22)-C(21)-H(21)	98.3

C(23A)-H(23A)	0.9800	C(24B)-C(22)-C(21)	110.2(9)
C(23A)-H(23B)	0.9800	C(24B)-C(22)-C(25A)	84.7(10)
C(23A)-H(23C)	0.9800	C(21)-C(22)-C(25A)	111.4(5)
C(23B)-H(23D)	0.9800	C(24B)-C(22)-C(24A)	25.0(8)
C(23B)-H(23E)	0.9800	C(21)-C(22)-C(24A)	114.1(6)
C(23B)-H(23F)	0.9800	C(25A)-C(22)-C(24A)	105.2(7)
		C(24B)-C(22)-C(25B)	113.0(10)
		C(21)-C(22)-C(25B)	111.8(7)
		C(25A)-C(22)-C(25B)	32.0(6)
		C(24A)-C(22)-C(25B)	127.2(8)
		C(24B)-C(22)-H(22)	130.2
		C(21)-C(22)-H(22)	108.6
		C(25A)-C(22)-H(22)	108.6
		C(24A)-C(22)-H(22)	108.6
		C(25B)-C(22)-H(22)	78.9
		C(03)-Re(1)-C(02)	86.8(2)
		C(03)-Re(1)-C(01)	88.8(2)
		C(02)-Re(1)-C(01)	85.39(18)
		C(03)-Re(1)-O(1)	97.48(17)
		C(02)-Re(1)-O(1)	175.45(15)
		C(01)-Re(1)-O(1)	93.24(15)
		C(03)-Re(1)-N(1)	94.17(17)
		C(02)-Re(1)-N(1)	95.68(16)
		C(01)-Re(1)-N(1)	176.87(16)
		O(1)-Re(1)-N(1)	85.47(11)
		C(03)-Re(1)-O(04)	176.03(16)
		C(02)-Re(1)-O(04)	95.40(15)
		C(01)-Re(1)-O(04)	94.61(16)
		O(1)-Re(1)-O(04)	80.37(11)
		N(1)-Re(1)-O(04)	82.37(12)
		C(22)-C(24A)-H(24A)	109.5
		C(22)-C(24A)-H(24B)	109.5
		H(24A)-C(24A)-H(24B)	109.5
		C(22)-C(24A)-H(24C)	109.5
		H(24A)-C(24A)-H(24C)	109.5
		H(24B)-C(24A)-H(24C)	109.5
		C(22)-C(25A)-H(25A)	109.5
		C(22)-C(25A)-H(25B)	109.5

		H(25A)-C(25A)-H(25B)	109.5
		C(22)-C(25A)-H(25C)	109.5
		H(25A)-C(25A)-H(25C)	109.5
		H(25B)-C(25A)-H(25C)	109.5
		C(22)-C(24B)-H(24D)	109.5
		C(22)-C(24B)-H(24E)	109.5
		H(24D)-C(24B)-H(24E)	109.5
		C(22)-C(24B)-H(24F)	109.5
		H(24D)-C(24B)-H(24F)	109.5
		H(24E)-C(24B)-H(24F)	109.5
		C(22)-C(25B)-H(25D)	109.5
		C(22)-C(25B)-H(25E)	109.5
		H(25D)-C(25B)-H(25E)	109.5
		C(22)-C(25B)-H(25F)	109.5
		H(25D)-C(25B)-H(25F)	109.5
		H(25E)-C(25B)-H(25F)	109.5
		C(21)-C(23A)-H(23A)	109.5
		C(21)-C(23A)-H(23B)	109.5
		H(23A)-C(23A)-H(23B)	109.5
		C(21)-C(23A)-H(23C)	109.5
		H(23A)-C(23A)-H(23C)	109.5
		H(23B)-C(23A)-H(23C)	109.5
		C(21)-C(23B)-H(23D)	109.5
		C(21)-C(23B)-H(23E)	109.5
		H(23D)-C(23B)-H(23E)	109.5
		C(21)-C(23B)-H(23F)	109.5
		H(23D)-C(23B)-H(23F)	109.5
		H(23E)-C(23B)-H(23F)	109.5

Table L.3: Anisotropic displacement parameters ($Å^2 x\ 10^3$) for *fac*-[Re(5Me-Sal-3Me2Bu)$(CO)_3(HOCH_3)$]. The anisotropic displacement factor exponent takes the form: $-2\pi^2[\ h^2 a^{*2} U^{11} + ... + 2\ h\ k\ a^*\ b^*\ U^{12}\ ]$

	U11	U22	U33	U23	U13	U12
O(1)	21(1)	19(1)	26(1)	2(1)	11(1)	4(1)
N(1)	19(2)	38(2)	19(2)	-4(1)	7(1)	4(1)
C(1)	22(2)	36(2)	29(2)	-4(2)	3(2)	9(2)

C(11)	24(2)	23(2)	24(2)	-2(2)	3(2)	7(2)
C(12)	21(2)	22(2)	17(2)	1(1)	3(1)	4(1)
C(13)	22(2)	25(2)	20(2)	2(2)	2(2)	3(2)
C(14)	33(2)	27(2)	29(2)	8(2)	3(2)	-3(2)
C(15)	43(3)	21(2)	47(3)	6(2)	7(2)	2(2)
C(16)	35(2)	22(2)	46(3)	-2(2)	5(2)	9(2)
O(01)	52(2)	33(2)	51(2)	-14(2)	19(2)	0(2)
O(02)	28(2)	33(2)	38(2)	-2(1)	9(1)	-12(1)
O(03)	36(2)	78(3)	21(2)	3(2)	1(1)	10(2)
O(04)	22(2)	31(2)	24(2)	5(1)	0(1)	-11(1)
C(01)	30(2)	33(2)	26(2)	1(2)	9(2)	-1(2)
C(02)	23(2)	26(2)	26(2)	-2(2)	3(2)	0(2)
C(03)	27(2)	41(3)	27(2)	0(2)	10(2)	3(2)
C(04)	37(3)	58(4)	37(3)	15(2)	-1(2)	-17(2)
C(141)	44(3)	35(3)	40(3)	9(2)	9(2)	-15(2)
C(21)	24(2)	89(3)	31(2)	-9(2)	8(1)	3(2)
C(22)	24(2)	89(3)	31(2)	-9(2)	8(1)	3(2)
Re(1)	17(1)	27(1)	17(1)	1(1)	5(1)	-1(1)
C(24A)	29(4)	60(6)	47(7)	20(6)	8(4)	14(4)
C(25A)	23(4)	111(15)	44(5)	2(6)	8(4)	-4(6)
C(24B)	38(8)	27(7)	46(11)	-2(7)	17(8)	-3(6)
C(25B)	24(6)	40(11)	59(9)	-6(7)	27(6)	-7(6)
C(23A)	34(4)	50(6)	38(4)	-12(4)	14(3)	-8(4)
C(23B)	25(5)	39(6)	7(4)	2(4)	7(3)	3(4)

Appendix B: Table M

CHAPTER 8

THEORETICAL STUDY OF NON-COORDINATED SalH LIGANDS AND *fac*-[Re(Sal)(CO)$_3$(S)] COMPLEXES

Table M lists the theoretically optimized compound names (see Chapter 8) and the corresponding output file names which contain the computational results.

M1: Non coordinated SalH ligands

SalH-*m*Tol (**L_1***)	– Sal-mTol.log
5Me-SalH-*m*Tol (**L_2***)	– 5MeSal-mTol.log
5Me-SalH-Carba (**L_3***)	– 5MeSal-Carba.log

M2: *fac*-[Re(Sal)(CO)$_3$(S)] complexes

[Re(Sal-*m*Tol)(CO)$_3$(HOCH$_3$)] (**Re_1a***)	– Re-Sal-mTol-MeOH.log
[Re(Sal-Ph)(CO)$_3$(HOCH$_3$)] (**Re_2a***)	– Re-Sal-Ph-MeOH.log
[Re(Sal-Ph)(CO)$_3$(NC$_5$H$_5$)] (**Re_2b***)	– Re-Sal-Ph-Py.log
[Re(5Me-Sal-Carba)(CO)$_3$(HOCH$_3$)] (**Re_3a***)	– Re-5MeSal-Carba-MeOH.log
[Re(5Me-Sal-Carba)(CO)$_3$(NC$_5$H$_5$)] (**Re_3b***)	– Re-5MeSal-Carba-Py.log

APPENDIX C

Supplementary Data for the Methanol Kinetic Substitution Reaction of *fac*-[Re(L,L'-Bid)$(CO)_3(HOCH_3)$] Complexes

Table C.1: **(Figure 9.3) Plot of k_{obs} *vs.* [Ligand] for the reaction between *fac*-[Re(Sal-*m*Tol)$(CO)_3(HOCH_3)$] and 3-chloropyridine at various temperatures in methanol, [Re complex] = 4.38 x 10^{-4} M, (λ = 436 nm).**

[3-chloropyridine] (M)	k_{obs} (s^{-1})	k_{obs} (s^{-1})	k_{obs} (s^{-1})	k_{obs} (s^{-1})
	15.6 °C	24.7 °C	34.5 °C	43.4 °C
0.02997	-	-	-	0.758(8)
0.03996	0.0408(4)	0.117(2)	0.342(3)	0.92(1)
0.05006	0.0515(6)	0.142(1)	0.453(4)	1.21(1)
0.09991	0.0905(9)	0.256(2)	0.799(7)	2.13(2)
0.2000	0.165(2)	0.495(4)	1.55(1)	4.04(5)
0.2999	0.239(4)	0.729(7)	2.22(2)	5.69(9)
0.4000	0.309(3)	0.952(7)	2.95(2)	-
0.5999	-	1.42(2)	-	-
0.8263	-	1.95(2)	-	-

Table C.2: **(Figure 9.4) Equilibrium constant determined by the plot of ΔAbsorbance *vs.* [Ligand] for the reaction between *fac*-[Re(Sal-*m*Tol)$(CO)_3(HOCH_3)$] and 3-chloropyridine at 25 °C in methanol, [Re complex] = 4.33 x 10^{-4} M, (λ = 436 nm), [3-ClPy] = 0.001 M – 0.15 M.**

[3-chloropyridine] (M)	Δ Abs
	25.5°C
0.000962	0.02755
0.00204	0.03063
0.00421	0.03638
0.00859	0.04507
0.0105	0.04581
0.0215	0.05162
0.0365	0.05415
0.1500	0.05904

Table C.3: **(Figure 9.7) Plot of k_{obs} *vs.* [Ligand] for the reaction between *fac*-[Re(Sal-*m*Tol)(CO)$_3$(HOCH$_3$)] and pyridine at various temperatures in methanol, [Re complex] = 3.62 x 10^{-4} M, (λ = 440 nm).**

[Pyridine] (M)	k_{obs} (s^{-1})	k_{obs} (s^{-1})	k_{obs} (s^{-1})	k_{obs} (s^{-1})
	20.2 °C	25.7 °C	34.9 °C	43.9 °C
0.01799	-	-	-	0.213(4)
0.02682	-	-	-	0.319(7)
0.03988	-	-	-	0.47(1)
0.05005	0.388(6)	0.076(1)	0.225(5)	0.59(1)
0.1002	0.076(1)	0.150(2)	0.435(9)	1.12(3)
0.2000	0.145(4)	0.282(4)	0.79(2)	2.19(7)
0.3002	0.190(4)	0.406(7)	1.20(3)	-
0.4000	0.248(7)	0.54(1)	1.57(4)	-
0.5002	0.30(1)	0.66(2)	-	-
0.8007	-	0.98(3)	-	-
1.000	-	1.17(3)	-	-

Table C.4: **(Figure 9.11) Plot of k_{obs} *vs.* [Ligand] for the reaction between *fac*-[Re(Sal-*m*Tol)(CO)$_3$(HOCH$_3$)] and 4-picoline at various temperatures in methanol, [Re complex] = 4.65 x 10^{-4} M, (λ = 438 nm).**

[4-Picoline] (M)	k_{obs} (s^{-1})	k_{obs} (s^{-1})	k_{obs} (s^{-1})	k_{obs} (s^{-1})
	15.0 °C	25.6 °C	35.1 °C	44.8 °C
0.02508	-	-	-	0.387(4)
0.04008	0.0199(3)	-	0.227(2)	0.701(6)
0.04994	0.0251(2)	0.0803(1)	0.265(2)	0.766(6)
0.1001	0.0485(3)	0.1582(4)	0.516(3)	1.54(1)
0.2000	0.0941(8)	0.3064(9)	1.011(9)	2.87(2)
0.3001	0.138(1)	-	1.47(2)	4.10(3)
0.4000	0.175(2)	0.569(1)	1.94(1)	5.26(5)
0.5999	-	0.808(2)	-	-
0.9000	0.341(2)	1.151(2)	3.75(3)	-
1.1998	-	1.344(4)	-	-
1.4387	-	1.502(6)	-	-

Table C.5: **(Figure 9.14) Plot of k_{obs} *vs.* [Ligand] for the reaction between *fac*-[Re(Sal-*m*Tol)(CO)$_3$(HOCH$_3$)] and DMAP at various temperatures in methanol, [Re complex] = 5.19 x 10^{-4} M, (λ = 440 nm).**

[DMAP] (M)	k_{obs} (s^{-1})	k_{obs} (s^{-1})	k_{obs} (s^{-1})	k_{obs} (s^{-1})
	15.6 °C	25.4 °C	35.3 °C	46.0 °C
0.02134	-	-	-	0.406(3)
0.02945	-	-	-	0.552(5)
0.04289	0.0261(4)	0.089(1)	0.274(4)	0.803(6)
0.05025	0.0337(3)	0.102(1)	0.296(4)	0.934(6)
0.09995	0.0612(6)	-	0.549(7)	1.75(1)
0.1020	-	0.193(3)	-	-
0.2019	-	0.312(5)	-	-
0.2021	0.102(1)	-	1.00(1)	3.00(2)
0.2901	-	0.402(8)	-	-
0.3138	0.131(3)	-	1.32(1)	-
0.3996	0.151(2)	0.49(1)	1.51(1)	-
0.5683	-	0.59(1)	-	-
0.7862	-	0.69(1)	-	-

Table C.6: **(Figure 9.21) Eyring plots of the rate constant for the reaction between *fac*-[Re(Sal-*m*Tol)(CO)$_3$(HOCH$_3$)] with various entering ligands in methanol.**

3-Chloropyridine		Pyridine		DMAP	
1/T ($x10^{-3}$ K^{-1})	ln(k_1/T)	1/T ($x10^{-3}$ K^{-1})	ln(k_1/T)	1/T ($x10^{-3}$ K^{-1})	ln(k_3/T)
3.161	-2.845	3.156	-3.378	3.135	-3.352
3.252	-3.757	3.248	-4.382	3.244	-4.481
3.359	-4.851	3.348	-5.448	3.351	-5.559
3.465	-5.962	3.411	-6.235	3.465	-6.880

4-Picoline (A)		4-Picoline (B)		4-Picoline (C)	
1/T ($x10^{-3}$ K^{-1})	ln(k_1/T)	1/T ($x10^{-3}$ K^{-1})	ln(k_3/T)	1/T ($x10^{-3}$ K^{-1})	ln(k_f/T)
3.147	-3.199	3.147	-2.427	3.147	-2.982
3.246	-4.315	3.246	-2.952	3.246	-4.037
3.353	-5.461	3.349	-4.331	3.349	-5.160
3.472	-6.648	3.472	-5.358	3.472	-6.344

Table C.7: **(Figure 9.22) Plot of k_{obs} *vs.* [Ligand] for the reaction between *fac*-[Re(Sal-*p*Tol)$(CO)_3(HOCH_3)$] and pyridine and DMAP at 25 °C in methanol, [Re complex] = 2.84 x 10^{-4} M, (Pyridine λ = 437 nm, DMAP λ = 438).**

[DMAP] (M)	k_{obs} (s^{-1})
	25.1 °C
0.02608	0.0519(9)
0.04324	0.086(1)
0.05405	0.108(2)
0.1910	0.282(6)
0.3079	0.387(7)
0.3944	0.417(9)

[Pyridine] (M)	k_{obs} (s^{-1})
	25.1 °C
0.02498	0.0394(6)
0.04006	0.0592(8)
0.04995	0.074(1)
0.2001	0.281(4)
0.3000	0.422(5)
0.4001	0.562(8)

Table C.8: **(Figure 9.23) Plot of k_{obs} *vs.* [Ligand] for the reaction between *fac*-[Re(Sal-Ph)$(CO)_3(HOCH_3)$] and pyridine and DMAP at 25 °C in methanol, [Re complex] = 2.90 x 10^{-4} M, (Pyridine λ = 442 nm, DMAP λ = 442).**

[DMAP] (M)	k_{obs} (s^{-1})
	25.7 °C
0.02608	0.053(1)
0.04324	0.077(1)
0.05405	0.106(2)
0.1910	0.286(8)
0.3079	0.410(9)
0.3944	0.45(1)

[Pyridine] (M)	k_{obs} (s^{-1})
	25.7 °C
0.02498	0.0349(5)
0.04006	0.0576(9)
0.04995	0.072(1)
0.2001	0.253(6)
0.3000	0.393(6)
0.4001	0.505(9)

Table C.9: **(Figure 9.24) Plot of k_{obs} *vs.* [Ligand] for the reaction between *fac*-[Re(Sal-3MeBu)$(CO)_3(HOCH_3)$] and pyridine and DMAP at 25 °C in methanol, [Re complex] = 3.22 x 10^{-4} M, (Pyridine λ = 416 nm, DMAP λ = 422).**

[DMAP] (M)	k_{obs} (s^{-1})
	25.1 °C
0.02767	0.074(1)
0.04185	0.11(2)
0.05140	0.136(2)
0.2060	0.458(9)
0.3020	0.56(2)
0.4178	0.66(2)

[Pyridine] (M)	k_{obs} (s^{-1})
	25.3 °C
0.02992	0.0473(9)
0.04080	0.0812(1)
0.04995	0.102(1)
0.2001	0.370(4)
0.3000	0.543(6)
0.4001	0.72(1)

Table C.10: **(Figure 9.26) Plot of k_{obs} *vs.* [Ligand] for the reaction between *fac*-[Re(Sal-CyHex)$(CO)_3(HOCH_3)$] and various entering ligands at 25 °C in methanol, [Re complex] = 1.83 x 10^{-4} M, (3-Chloropyridine λ = 419 nm, pyridine λ = 417 nm, 4-picoline λ = 418 nm, DMAP λ = 420 nm).**

[3-ClPy] (M)	k_{obs} (s^{-1})	[Pyridine] (M)	k_{obs} (s^{-1})	[4-Picoline] (M)	k_{obs} (s^{-1})	[DMAP] (M)	k_{obs} (s^{-1})
	24.8 °C		25.2 °C		25.0 °C		25.2 °C
0.05005	0.2598(7)	0.02498	0.077(3)	0.04994	0.1419(4)	0.02608	0.097(3)
0.1002	0.514(1)	0.4006	0.115(3)	0.1001	0.2777(7)	0.04324	0.152(3)
0.1998	0.957(2)	0.04995	0.147(5)	0.2000	0.528(1)	0.05405	0.199(5)
0.2999	1.500(3)	0.0999	0.2701(8)	0.3001	0.774(2)	0.1004	0.3093(7)
0.4001	1.947(8)	0.2001	0.57(1)	0.3999	1.019(3)	0.1910	0.51(1)
0.6001	2.78(1)	0.3000	0.82(2)	0.5999	1.416(4)	0.3079	0.75(2)
0.8939	4.09(1)	0.4001	0.99(3)	0.8992	1.963(6)	0.3944	0.89(3)
1.1568	5.04(1)	0.5999	1.488(5)	1.2845	2.661(8)	0.6430	1.114(5)
1.4197	6.11(2)	0.8902	2.038(8)	-	-	-	-
-	-	1.2117	2.70(1)	-	-	-	-

Rate Laws and Kinetic Activation Parameters

Rate Constant

The rate of a reaction can be defined as the change in the concentration of a reactant or product per unit time. Denoted by the rate constant (k) that relates to the change of the reagent concentration per unit time. For a simple reaction, the following reaction can be defined:

$$A + B \xrightarrow{k} C \qquad \text{... C.1}$$

The rate can be expressed by the equation:

$$\text{Rate} = \frac{-d[A]}{dt} = \frac{-d[B]}{dt} = \frac{d[C]}{dt} = k[A]^m[B]^n \qquad \text{... C.2}$$

Where [ ] indicates concentration and the negative signs indicates the disappearance of A and B. The values m and n represent the order of the reaction with regard to the concentrations of A and B, the sum of m and n is equal to the total order of the reaction. The reaction order is the way in which the rate of the reaction will vary as the concentration of both of one of the reacting species is changed. The order of the reaction can be determined experimentally, but with difficulty. This is overcome by forcing the reaction to *pseudo*-first order conditions, where the concentration of one of the species is in excess and therefore remains essentially constant. The rate equation now becomes:

$$\text{Rate} = k_{obs}[A]^m \qquad \text{... C.3}$$

The *pseudo*-first order rate constant is now given as:

$$k_{obs} = k[B]^n \qquad \text{... C.4}$$

Variation of the concentration of B, in equation C.4, the rate constant k, can be determined. If a second reaction occurs, the rate law is extended to (under *pseudo*-first order conditions):

$$\text{Rate} = k_1[A][B] + k_2[A] \qquad \text{... C.5}$$

$$k_{obs} = k_1[B] + k_2 \qquad \text{... C.6}$$

Integration of the rate equation:

$$\text{Rate} = \frac{-d[A]}{dt} = \frac{-d[B]}{dt} = \frac{d[C]}{dt} = k[A]^m[B]^n \quad \ldots \text{C.7}$$

With boundaries of $t = 0$ and t, yields an expression in terms of concentration, C, where C is the concentration change of the reactants at time t and the initial time (t_0), (C_0).

$$[C]_t = [C]_0 e^{k_{obs}\, t} \quad \ldots \text{C.8}$$

$$\text{Where } \frac{[C]_t}{[C]_0} = \frac{A_\infty - A_t}{A_\infty - A_0} \quad \ldots \text{C.9}$$

Substitution of Eq. C.9 into the Beer-Lambert law;

$$A = \varepsilon . l . C \quad \ldots \text{C.10}$$

Where A = absorbance, ε = molar extinction coefficient, C = concentration and l = light path length, yields the following equation:

$$A_t = A_\infty - (A_\infty - A_0) e^{k_{obs}\, t} \quad \ldots \text{C.11}$$

Where A_t and A_∞ are the absorbance after time t and at the time of reaction completeness. A least-squares fit utilizing absorbance *vs.* time data for a first order reaction would yield k_{obs}, the *pseudo* first-order rate constant, for the reaction.

Spectrophotometric determination of the equilibrium constant of the reaction.

Consider the following equilibrium reaction between a complex (MX) and a ligand (L):

$$MX + L \underset{}{\overset{K}{\rightleftharpoons}} ML + X$$

The equilibrium constant for the above-mentioned reaction is given by the following equation:

$$K = \frac{[ML][X]}{[MX][L]} \quad \ldots \text{C.12}$$

Equation C.13 can be applied for the observed absorbance (A_{obs}) according to the Beer-Lambert law:

$$A_{obs} = \varepsilon_{MX}[MX] + \varepsilon_{ML}[ML] \quad \ldots \text{C.13}$$

Where A_{obs} = observed absorbance, ε_{MX} = molar extinction coefficient of MX and ε_{ML} = molar extinction coefficient of ML.

Equation C.14 can be applied for the total metal concentration according to the law of conservation of mass.

$$[M]_t = [ML] + [MX] \quad \ldots C.14$$

Where $[M]_t$ = total concentration of the absorbed M, [MX] = concentration of the MX complex, [ML] = concentration of the ML complex.

[MX] and [ML] can be defined respectively, as in Eq. C.15 & C.16 by using Eq. C.12.

$$[MX] = \frac{[ML][X]}{K[L]} \quad \ldots C.15$$

$$[ML] = \frac{K[MX][L]}{[X]} \quad \ldots C.16$$

Separate substitution of Equations C.15 and C.16 in Eq. C.14 gives Equations C.17 & C.18 respectively.

$$[M]_t = \frac{[ML][X]}{K[L]} + [ML] = [ML]\left(1 + \frac{[X]}{K[L]}\right)$$

$$[ML] = \frac{[M]_t}{1 + \frac{[X]}{K[L]}} \quad \ldots C.17$$

$$[M]_t = \frac{K[MX][L]}{[X]} + [MX] = [MX]\left(1 + \frac{K[L]}{[X]}\right)$$

$$[MX] = \frac{[M]_t}{1 + \frac{K[L]}{[X]}} \quad \ldots C.18$$

In Equation C.17 and C.18, [MX] and [ML] are expressed in terms of experimental determined values. Similar substitution of the above mentioned equations in Eq. C.13 will give the result in Equation C.19.

$$A_{obs} = \frac{\varepsilon_{MX}[M]_t}{1 + \frac{K[L]}{[X]}} + \frac{\varepsilon_{ML}[M]_t}{1 + \frac{[X]}{K[L]}} \quad \ldots C.19$$

For Equation C.19 the following apply: if [L] = 0, then [ML] = 0 so that $A_{obs} = A_{MX} = \varepsilon_{MX}[M]_t$. If [L] >>$[M]_t$, then [MX] = 0 and $A_{MX} = \varepsilon_{ML}[M]_t$. Through substitution of the last mentioned absorbance in Equation C.19 and further manipulation gives the results as in Equation C.20.

$$A_{obs} = \frac{A_{MX}}{1 + K[L]} + \frac{A_{MX}\,K[L]}{1 + K[L]}$$

$$A_{obs} = \frac{A_{MX} + A_{ML}K[L]}{1 + K[L]} \quad \ldots C.20$$

Where A_{MX} = absorbance at the beginning of the reaction and A_{ML} = absorbance when the reaction is finished.

Reaction half-life

The reaction half-life is the required time to convert 50% of the reactant. For first order reactions the half-life is determined by the equation:

$$t_{1/2} = \ln(2) / k_{obs} = 0.6932 / k_{obs} \quad \ldots \text{C.21}$$

Activation enthalpy and entropy

The Transition State Theory states that an activated complex or transition state is in equilibrium with the reagents before the reaction occurs and that the rate is given by the decomposition rate, k, of the activated complex to yield the products:

$$A + B \rightleftharpoons (AB)^{\neq} \xrightarrow{k} \text{Product} \quad \ldots \text{C.22}$$

Where $K^{\neq}_c$ = equilibrium constant

The exponential form of the Eyring equation can be derived and is given as:

$$k = \frac{k_B T}{H} e^{[\Delta S^{\neq}/R - \Delta H^{\neq}/RT]} \quad \ldots \text{C.23}$$

The equation can be rewritten in the logarithmic form:

$$\ln \frac{k}{T} = \ln \frac{k_B}{h} - \frac{\Delta H^{\neq}}{RT} + \frac{\Delta S^{\neq}}{R} \quad \ldots \text{C.24}$$

where k_B = Boltzmann constant and h = Planck constant. The value of $(-\Delta H^{\neq}/R)$ can be determined from the slope of the graph of ln(k/T) *vs.* (1/T). The value of $\Delta S^{\neq}$ can be calculated from the Y-intercept.

APPENDIX C